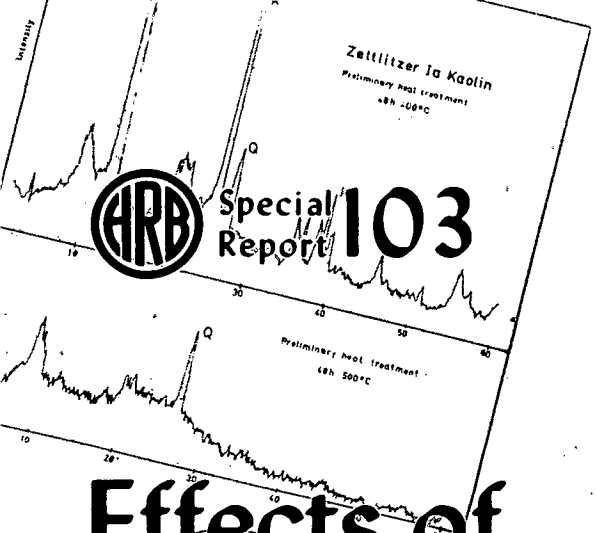

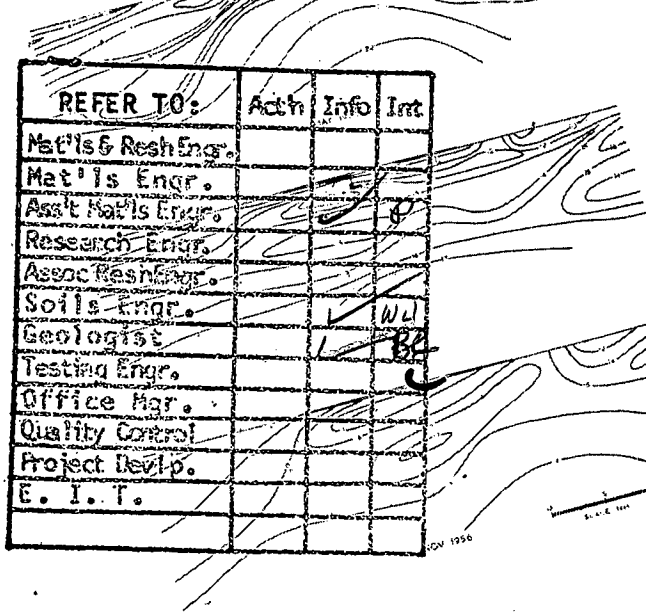

Special Report 103

Effects of Temperature and Heat on Engineering Behavior of Soils

Proceedings of an International Conference

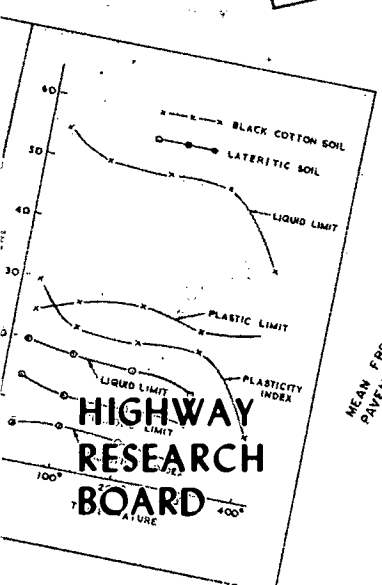

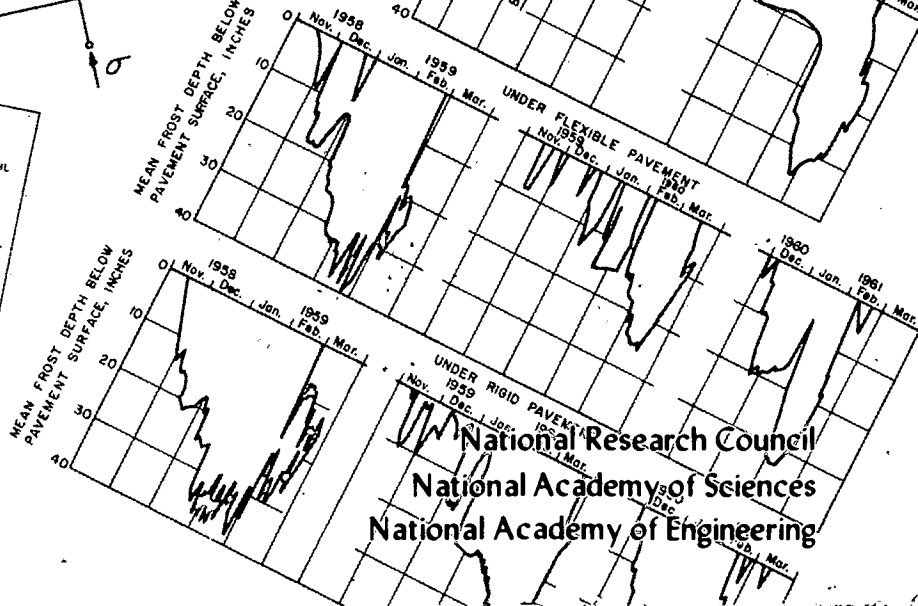

HIGHWAY RESEARCH BOARD

National Research Council
National Academy of Sciences
National Academy of Engineering

Special Report 103

Effects of Temperature and Heat on Engineering Behavior of Soils

Proceedings of an International Conference
Held at Washington, D.C., January 16, 1969
With the Support of the National Science Foundation

Subject Area
64 Soil Science

HIGHWAY RESEARCH BOARD
DIVISION OF ENGINEERING NATIONAL RESEARCH COUNCIL
NATIONAL ACADEMY OF SCIENCES—NATIONAL ACADEMY OF ENGINEERING

Washington, D. C., 1969 Publication 1641

Price: $ 8.00, Paper Cover
$10.00, Hard Cover

Available from

Highway Research Board
National Academy of Sciences
2101 Constitution Avenue
Washington, D.C. 20418

HIGHWAY RESEARCH BOARD

Officers and Members of the Executive Committee
1969

OFFICERS

OSCAR T. MARZKE
Chairman

D. GRANT MICKLE
First Vice Chairman

CHARLES E. SHUMATE
Second Vice Chairman

W. N. CAREY, JR.
Executive Director

Executive Committee

FRANCIS C. TURNER, *Federal Highway Administrator, U.S. Department of Transportation* (ex officio)

A. E. JOHNSON, *Executive Director, American Association of State Highway Officials* (ex officio)

GEORGE C. SPONSLER, *Executive Secretary, Division of Engineering, National Research Council* (ex officio)

EDWARD G. WETZEL, *Associate Consultant, Edwards and Kelcey, Newark, New Jersey* (ex officio, Past Chairman 1967)

DAVID H. STEVENS, *Chairman, Maine State Highway Commission* (ex officio, Past Chairman 1968)

DONALD S. BERRY, *Chairman, Department of Civil Engineering, Northwestern University*

CHARLES A. BLESSING, *Director, Detroit City Planning Commission*

JAY W. BROWN, *Chairman, State Road Department of Florida*

J. DOUGLAS CARROLL, JR., *Executive Director, Tri-State Transportation Commission, New York City*

HARMER E. DAVIS, *Director, Institute of Transportation and Traffic Engineering, University of California*

WILLIAM L. GARRISON, *Director, Center for Urban Studies, University of Illinois at Chicago Circle Campus*

SIDNEY GOLDIN, *Vice President of Marketing, Asiatic Petroleum Corporation, New York City*

WILLIAM J. HEDLEY, *Consultant, Federal Railroad Administration, U. S. Department of Transportation*

GEORGE E. HOLBROOK, *Vice President, E. I. du Pont de Nemours and Company*

EUGENE M. JOHNSON, *Chief Engineer, Mississippi State Highway Department*

THOMAS F. JONES, JR., *President, University of South Carolina*

LOUIS C. LUNDSTROM, *Director, Automotive Safety Engineering, General Motors Technical Center*

OSCAR T. MARZKE, *Vice President, Fundamental Research, U. S. Steel Corporation*

J. B. MCMORRAN, *Commissioner, New York Department of Transportation*

D. GRANT MICKLE, *President, Automotive Safety Foundation*

LEE LAVERNE MORGAN, *Executive Vice President, Caterpillar Tractor Company*

RICHARD L. PEYTON, *State Highway Engineer, State Highway Commission of Kansas*

CHARLES E. SHUMATE, *Chief Engineer, Colorado Department of Highways*

R. G. STAPP, *Superintendent, Wyoming State Highway Commission*

ALAN M. VOORHEES, *Alan M. Voorhees and Associates, Inc.*

Editorial Staff

EARLE W. JACKSON
Senior Editor

STEPHEN MONTGOMERY
Assistant Editor

BEATRICE G. CROFOOT
Production Manager

DR. HANS F. WINTERKORN

Professor of Geophysics and Civil Engineering
Director, Soil Physics Laboratory
Princeton University

Dr. Winterkorn came to this country in 1931, the same year he received his doctorate in physical chemistry from Heidelberg University. Born November 24, 1905, in Mannheim, Baden, Germany, he became a naturalized citizen of the United States in 1938. His early work in Missouri during the 1930's, as a researcher, engineer, and consultant to the Missouri State Highway Department and as researcher and professor at the University of Missouri, was dedicated to helping Missouri "get out of the mud." This battle cry of the highway department focused his attention on the waterproofing of clays and enabled him to develop the basic principles of soil stabilization that he has promoted through the years.

Moving to Princeton University in 1943, he established the first soil physics laboratory and started the first course ever given on the chemical behavior of soils and their possible stabilizers. During and after World War II his knowledge helped the Army and Navy stabilize military bases, roads, and ocean beaches.

His broad interest in physicochemical phenomena in soils led to extended research and theoretical developments relating to water conduction in soil, thermoelectric effects, thermo-osmotic effects, macromeritic systems, and granulometric principles, among many others. These developments have become increasingly important with the necessity for understanding and solving lunar soils problems, and some of his most recent works have been along these lines. Problems in the closely related fields of bituminous-soil stabilization and adhesion between bitumen and mineral surfaces have also been successfully overcome by the application of the basic physicochemical principles.

No contribution can be singled out as most important, but perhaps the most lasting will be the philosophical approach to the art of soil science and soil engineering. This philosophy has led him to seek out the basic and fundamental causes he has transmitted to his students as a professor, to his employers as a consultant, and to his fellow workers around the world as a dedicated scientist and engineer.

As Chairman of the Committee on Physico-Chemical Phenomena in Soils he has organized several international symposia and sponsored many sessions. Notably, the symposia on soil stabilization and on water and its conduction in soil received worldwide acclaim. His 30 years of service as Chairman have been invaluable to the Highway Research Board and to the fields of soil science, soil stabilization, and soil physics. These contributions have been evident in many phases of highway and soil engineering

practices. He currently serves on the Executive Committee of the Department of Soils, Geology and Foundations and on its Committees on Soil-Bituminous Stabilization and Sub-Surface Drainage, as well as on the Materials and Construction Committee on Effects of Natural Elements and Chemicals on Bitumen-Aggregate Combinations. To date he has had fourteen other major committee assignments with the Highway Research Board.

DEDICATION

This Conference is dedicated to Dr. Winterkorn for those 30 years as Committee Chairman and for his outstanding contributions. Dr. Oscar T. Marzke, Chairman of the Executive Committee of the Highway Research Board, related the foregoing facts as he dedicated the Conference and introduced Dr. Winterkorn.

The Committee on Physico-Chemical Phenomena in Soils, under the Chairmanship of Dr. James K. Mitchell, organized and implemented this International Conference, for which the groundwork had been laid by Dr. Winterkorn.

These Conference Proceedings have been assembled in three parts. Part I, "Introduction and Summaries," includes the Keynote Address and General Reports. Part II, "Thermal Characteristics of Soils, Thermodynamics of Soil Systems, Fluid Flows, and Frost Action," includes the papers covered by the general reporter, moderator, and panelists in the first session of the Conference. Part III, "Temperature Effects on the Engineering Properties of Soils," includes the papers covered by the general reporter, moderator, and panelists in the second session. Descriptive forewords precede each part.

As a whole the Conference has made significant contributions to the scientific world through the exposure and open discussion of the approaches to problem solutions as well as the compilation of these outstanding papers, which will serve as a ready reference. Together they will help correlate the practically important phenomena with fundamental physical and physico-chemical factors and laws. These cannot help but stimulate understanding and research in other fields of theoretical and applied soil science.

ACKNOWLEDGMENTS

Dr. Mitchell and his committee did an outstanding job of organizing this International Conference, soliciting and reviewing the papers, and conducting the general reporter-panel discussion. The success of the Conference is due to the complete cooperation evidenced throughout by authors, moderators, panelists, and general reporters. Several years of preparation and untiring efforts are culminated in these Proceedings.

For the first session, the moderator was B. P. Warkentin, Macdonald College of McGill University, Montreal. The panelists were:

Duwayne M. Anderson, U. S. Army Terrestrial Sciences Center, Hanover, New Hampshire
Philip F. Low, Purdue University
R. Torrence Martin, Massachusetts Institute of Technology
D. H. Gray, University of Michigan
Edward Penner, National Research Council of Canada, Ottawa

For the second session, the moderator was Miles S. Kersten, University of Minnesota. The panelists were:

James K. Mitchell, University of California, Berkeley
Roy E. Olson, University of Illinois
Fred J. Sanger, U. S. Army Terrestrial Sciences Center
Ronald F. Scott, California Institute of Technology
R. N. Yong, McGill University

For their penetrating and illuminating discussions, they are sincerely thanked. Without these valuable personal contributions of insight and wisdom, the Conference would not have been such a success.

Special thanks are due to Dr. Winterkorn for his translation of two of the papers from the German, and for his excellent Keynote Address, which set the pace for the panel presentations and discussions that followed.

The Committee and the Board are grateful for financial support of the International Conference and of the publication of these Proceedings by the National Science Foundation, with special thanks to Dr. Michael P. Gaus.

Department of Soils, Geology and Foundations

Eldon J. Yoder, Chairman
Purdue University, Lafayette, Indiana

Chester McDowell, Vice Chairman
Texas Highway Department, Austin

HIGHWAY RESEARCH BOARD STAFF

J. W. Guinnee

DIVISION C

O. L. Lund, Chairman
Nebraska Department of Roads, Lincoln

L. F. Erickson, Vice Chairman
Idaho Department of Highways, Boise

COMMITTEE ON PHYSICO-CHEMICAL PHENOMENA IN SOILS
(As of December 31, 1968)

James K. Mitchell, Chairman
University of California, Berkeley

L. G. Bromwell
Turgut Demirel
Sidney Diamond
Donald H. Gray
Earl B. Kinter
Joakim G. Laguros
Mo Chih Li
Harold W. Olsen
Robert Paaswell
Elmer A. Rosauer
Mehmet A. Sherif
B. P. Warkentin
Hans F. Winterkorn
F. L. D. Wooltorton

Contents

Dedication and Acknowledgments v

Part I: Introduction and General Reports 1

FOREWORD TO PART I 2

KEYNOTE ADDRESS

Hans F. Winterkorn 3

GENERAL REPORT ON THERMAL CHARACTERISTICS OF SOILS, THERMODYNAMICS OF SOIL SYSTEMS, FLUID FLOWS, AND FROST ACTION

Duwayne M. Anderson 6

TEMPERATURE EFFECTS ON THE ENGINEERING PROPERTIES AND BEHAVIOR OF SOILS

James K. Mitchell 9

Part II: Thermal Characteristics of Soils, Thermodynamics of Soil Systems, Fluid Flows, and Frost Action 29

FOREWORD TO PART II 30

EFFECTS OF HEATING ON THE SWELLING OF CLAY MINERALS

L. A. G. Aylmore, J. P. Quirk, and I. D. Sills 31

THERMAL TRANSFER OF LIQUID IN POROUS MEDIA

A. M. Globus and B. M. Mogilevsky 39

RELATIONSHIPS BETWEEN THE DAILY TEMPERATURE WAVE AND THE DEVELOPMENT OF THE NATURAL SOIL PROFILE

R. Goetz and S. Müller 51

THERMO-OSMOTIC AND THERMOELECTRIC COUPLING IN SATURATED SOILS

Donald H. Gray 66

THE PHYSICS AND CHEMISTRY OF FROZEN SOILS

Pieter Hoekstra 78

THERMODYNAMICS OF GRANULAR SYSTEMS

Alfred Holl 91

HEAT CONDUCTION IN SATURATED GRANULAR MATERIALS

Richard McGaw 114

TEMPERATURE EFFECT ON WATER RETENTION AND SWELLING PRESSURE OF CLAY SOILS

R. N. Yong, R. K. Chang, and B. P. Warkentin 132

Part III: Temperature Effects on the Engineering Properties of Soils . . . 139

FOREWORD TO PART III 140

EFFECT OF HEATING ON BEARING CAPACITY OF HIGHWAY SUBGRADES

Fernando Emmanuel Barata 141

EXPANSION OF SOILS CONTAINING SODIUM SULFATE CAUSED BY DROP IN AMBIENT TEMPERATURES

Harold D. Blaser and Oscar J. Scherer 150

INFLUENCE OF HEAT TREATMENT ON THE PULVERIZATION AND STABILIZATION CHARACTERISTICS OF TYPICAL TROPICAL SOILS

E. C. Chandrasekharan, S. Boominathan, E. Sadayan, and K. R. Narayanaswamy Setty 161

INFLUENCE OF TEMPERATURE AND OTHER CLIMATIC FACTORS ON THE PERFORMANCE OF SOIL-PAVEMENT SYSTEMS

H. Y. Fang 173

EFFECT OF TEMPERATURE ON SOME ENGINEERING PROPERTIES OF CLAY SOILS

Joakim G. Laguros 186

EFFECT OF TEMPERATURE ON ELASTICITY OF CLAYS

Sakuro Murayama 194

EFFECT OF TEMPERATURE ON STRENGTH BEHAVIOR OF COHESIVE SOIL

Calvin A. Noble and Turgut Demirel 204

TRANSIENT TEMPERATURE INFLUENCES ON SOIL BEHAVIOR

Robert E. Paaswell 220

SOME TEMPERATURE EFFECTS ON SOIL COMPRESSIBILITY AND PORE WATER PRESSURE

Robert L. Plum and Melvin I. Esrig 231

SOIL STABILIZATION BY INCIPIENT FUSION

James L. Post and Joseph A. Paduana 243

PAVEMENT TEMPERATURES AND THEIR ENGINEERING SIGNIFICANCE IN AUSTRALIA

B. G. Richards 254

TEMPERATURE EFFECTS ON THE UNCONFINED SHEAR STRENGTH OF SATURATED, COHESIVE SOIL

Mehmet A. Sherif and Chester M. Burrous 267

INFLUENCE OF SEEPAGE STREAM ON THE JOINING OF FROZEN SOIL ZONES IN ARTIFICIAL SOIL FREEZING

Tsutomu Takashi 273

EFFECT OF PRELIMINARY HEAT TREATMENT ON THE SHEAR STRENGTH OF KAOLINITE CLAY

Herbert Wöhlbier and Dieter Henning 287

Part I

INTRODUCTION AND GENERAL REPORTS

FOREWORD TO PART I

Dr. Winterkorn's Keynote Address philosophically sets the tone of the Conference with these words: ". . . to bring to the consciousness of the soils engineer the existence of thermodynamics, not as a collection of equations from which one selects those that appear pertinent and plugs the right data into them, but as a working philosophy of both qualitative and quantitative character that combines philosophical universality with practical applicability. . . ." An important example of the application of "thermodynamic thinking" is to the solution of granular systems in terrestrial or lunar environments. More of this is needed along with the development and expanded use of "electrochemical methodology."

The general reporter-moderator-panel format was followed to handle the 22 papers included in this International Conference.

The papers covered in the first session are printed in Part II of these Proceedings. Duwayne M. Anderson, as General Reporter, brought out the main points of each paper. He posed questions to the moderator and panelists on vapor transfer in unsaturated soils on surface area as a relevant parameter in soil freezing and thermo-osmosis, and on interface intervening in heat conduction.

The papers covered in the second session are printed in Part III of these Proceedings. James K. Mitchell, as General Reporter, highlighted the contributions from the authors. Some of his queries of the panel covered the influence of temperature on secondary compression rates; changes to be made in laboratory testing, analysis, and design procedure to account for strength decrease due to temperature increase; economic outlook for thermal treatment methods; outlook for a frozen ice barrier in flowing groundwater conditions; and temperature-related chemical swelling of soils.

General Report on Thermal Characteristics of Soils, Thermodynamics of Soil Systems, Fluid Flows, and Frost Action

DUWAYNE M. ANDERSON, U.S. Army Terrestrial Sciences Center,
Hanover, New Hampshire

•PART I is devoted to a consideration of the thermodynamics of soil systems, fluid flow, frost action, and certain thermal characteristics of soils. Two papers touching upon the thermodynamics of soil systems have been contributed: the paper by A. Holl focuses on the granular nature of soils, whereas the paper by R. Yong, R. K. Chang, and B. P. Warkentin touches on the thermodynamics of soil water. Dr. Holl's thermodynamic treatment of soil compression follows by analogy to classical thermodynamics in a straightforward manner. Because of this, the approach has a certain intrinsic appeal. The potential value of a thermodynamic approach to soil mechanics is difficult to calculate. One reflects that classical thermodynamics is useful chiefly because it is a convenient, systematic method of arranging and cataloguing the results of experimental observations that permits in advance the prediction of spontaneous processes and in many cases helps in arranging conditions so that borderline processes can be accomplished in a desired manner. Equally important are the limitations of classical thermodynamics: (a) as yet, it is not designed to predict the spontaneity of processes under non-isothermal conditions, nor (b) does it furnish information on process mechanisms or process rates. One also is somewhat in awe of the enormous body of experimental data upon which the discipline rests, much of it accumulated by investigators doubtful of the conclusions derived from thermodynamic theory. Thus one is brought to the realization that a transfer of thermodynamic methods to new disciplines is likely to be widely accepted and hailed as a benefit only after a very long period of doubt and testing. Subsequently it will probably be found that the validity of the method rests as much on the results of the many experimental investigations undertaken to establish or test it as upon the intrinsic value of the thermodynamic method, itself. Perhaps this point and the problem of the selection of variables posed by this paper need further exploration. As is well known, the utility of thermodynamic theory depends crucially on the proper selection of variables of state; the degree to which this has been done successfully has yet to be determined.

For practical engineering purposes the effect of temperature on the state of soil water was found by Yong, Chang, and Warkentin to be negligible. In agreement with the findings of previous investigators, at a given soil water suction they observed that the amount of water retained decreases as the temperature increases, probably in the main because the air-water surface tension decreases as the temperature increases. In accordance with earlier investigations and in agreement with the prediction of double layer theory, swelling (imbibition of water) increased with an increase in temperature. There are difficulties in terminology and perhaps the basis for a disagreement in concept in maintaining that the matrix potential is made up of ". . . swelling and capillary forces."

Two papers on thermo-osmosis have been contributed. Again from the practical point of view both conclude that in saturated soils thermoelectric and thermo-osmotic flow is completely negligible. In unsaturated soils, water transport occurs primarily in the vapor phase and sometimes it is of practical significance. For example, the transport and collection of water under pavements and airport runways due to thermal gradients is a possibility that must always be evaluated when materials and construction methods are selected. The nature and significance of the interfacial energy and the

various types of interfaces present in soils are discussed in the paper by Gray. Another point considered is the current status of the practice of utilizing electro-osmosis to dewater frozen and unfrozen soils. The paper by Globus and Mogilevsky contributes a coherent concept of the processes involved in the thermal transfer of liquid in porous materials. They propose that the net pressure difference developed in a liquid-saturated porous substance subjected to a temperature gradient is brought about by three flow components: a thermo-osmotic component in the direction of higher temperature, a thermo-self-diffusion component in the direction of lower temperature, and a Poiseuille flow component opposing the resultant of the other two. This explains how one may observe a pressure rise at the warm end of a flow column in the early stages of a thermo-osmosis experiment with a reversal at some later time. This phenomenon and the concept advanced by Globus and Mogilevsky to explain it deserve further exploration, inasmuch as the point arises in both papers.

In contrast to most situations in unfrozen soils, the effect of temperature on the properties and behavior of frozen ground is of undisputed importance. The unfrozen water contents of frozen soils change markedly with temperature. Important soil properties also depend critically on thermal regime: shear strength, bearing capacity, rheological response, and electrical properties. The paper by Hoekstra reviews recent work bearing on these points and re-emphasizes the need, expressed by many at the International Symposium on Permafrost at Purdue University in 1963 (1), for a better understanding of frozen soils. As the artificial freezing of ground becomes a more widespread engineering practice (e.g., earth stabilization, to aid in excavations, and for cryogenic storage) the need for methods of generalizing experimental data pertaining to mechanical properties of frozen and thawing soils and the establishment of standard strength and deformation parameters becomes evident. The specific surface area of soils appears in the context of this paper as a soil parameter of fundamental importance. Globus and Mogilevsky also direct attention to its fundamental significance in thermo- and electro-osmosis. It is a soil property that has been too frequently neglected, or overlooked, in soil characterizations by engineers who have not yet become aware of the useful information that can be deduced from it.

The paper by Aylmore, Quirk, and Sills is devoted to the subtle effects of partial or complete dehydration on the subsequent swelling of illite and kaolinite. They suggest the possibility that when kaolinite is physically mixed with illite, individual particles may be cross-linked through hydrogen bonding. This is a point of some interest in view of recent work indicating that hydrogen bonding in water immediately proximate to clay surfaces is less than for water in bulk (2, 3). In certain situations, it is suggested by Goetz and Mueller that the consequence of the sinusoidal, daily temperature cycle is to aid in establishing the boundary between the A and B soil horizons. They conclude that the daily temperature wave sometimes plays a distinct role in soil genesis. One is reminded in this instance of the process of particle sorting brought about by frost action. Perhaps a relationship with paleoclimate resides in the observations reported. A new equation for heat conduction in granular materials is proposed in the paper by McGaw. An outstanding feature in his development is his recognition of the thermal resistance of interfaces separating the mineral grains from surrounding substances. The paper provides a brief but comprehensive overview and comparison of the leading formulations of thermal conduction in soils. It is pointed out that several formulations in current use are adequate in representing much of the available data. Justification for seeking other formulations lies primarily in the hope that the effect of wider ranges in value of the essential variables may be more accurately predicted.

From an engineering point of view, temperature effects on soil properties generally have been of practical significance only insofar as radically different soil properties could be achieved by the artificial heating or cooling of earth materials. Higher soil strength and resistance to the deleterious effects of water have been achieved by baking or sintering earth materials, for example. The same result is achieved in another way by artificial freezing. Processes of this kind involve large quantities of energy and yield large returns in desired effect; they are, therefore, important. On the other hand, the effect of temperature on soil water-holding capacity, on the state of soil water, in inducing water transfer, etc., has been and currently still is of marginal significance

from the practical point of view. This is largely because troublesome soils generally can be avoided or excavated and discarded. This being the case, one can sympathize with a reader who is unfamiliar with the disciplines involved as he strives to follow closely reasoned arguments encumbered by cryptic notations and strange definitions, only to find at the end of the paper that the results are inconclusive or inconsequential. However regrettable, to some extent this appears to be the case here. It is easily foreseen, however, that the situation may soon be radically different. Forced utilization of soil materials of marginal suitability, when it comes, will require that effects such as described in the papers of this part of the Symposium be predictable and manageable. The investigators are wrestling to obtain an understanding of topics recommended in the past as being vital to an improved mastery of earth materials. To this end, one can only recommend patience to those who suffer and unremitting effort to those who have succeeded in penetrating the difficult scientific problems.

REFERENCES

1. Permafrost: Proceedings of an International Conference. Building Research Advisory Board, NAS-NRC Pub. 1287, 1966, 563 pp.
2. Touillaux, R., et al. Israel Jour. of Chem., Vol. 6, p. 337-348, 1968.
3. Anderson, D. M. Nature, Vol. 216, p. 563-566, 1967.

Temperature Effects on the Engineering Properties and Behavior of Soils

JAMES K. MITCHELL, Institute of Transportation and Traffic Engineering, University of California, Berkeley

•THE 14 papers covered in this general report treat a number of aspects of temperature and heat effects on the engineering properties of soils. Collectively they provide concepts and data that make possible a greatly improved understanding of the importance of thermal influences in soil mechanics and thermal treatment of soils for property improvement. In this report the most significant aspects of each of the contributed papers are summarized and appraised, relevant supplementary data and analyses are introduced as appropriate for illustration of points under discussion, and questions are raised concerning areas needing further study.

The topics discussed in the various papers may be listed as follows:

Topic	Author(s)
1. Temperature Effects on Engineering Properties	
a. Volume change phenomena, pore pressure effects, compressibility	Plum and Esrig
b. Strength	Noble and Demirel, Sherif and Burrous, Laguros
c. Elasticity	Murayama
d. Creep and stress relaxation	Noble and Demirel, Murayama
e. Swelling—salt heave	Blaser and Scherer
2. Thermal Stabilization	
a. Effects of preliminary heat treatment	Barata, Chandrasekharan et al, Wöhlbier and Henning
b. Fusion of soils	Post and Paduana
c. Ice barriers	Takashi
3. Temperature Effects in Pavement Subgrades	
a. Field observations	Richards, Fang
b. Analysis methods	Paaswell

TEMPERATURE EFFECTS ON SOIL PROPERTIES

Volume Change Phenomena, Pore Pressure Effects

Volume and pore water pressure variations that develop in saturated soils due to temperature changes can be expressed in terms of the thermal expansion of the soil components, compressibility of the soil, and physicochemical effects, as shown recently by Campanella and Mitchell (6). They showed that under fully drained conditions and constant confining pressure a volume of water, ΔV_{DR}, will drain from a saturated soil as a result of a temperature increase, ΔT, as given by

$$(\Delta V_{DR})_{\Delta T} = \alpha_w V_w \Delta T + \alpha_s V_s \Delta T - \alpha_s V_m \Delta T - (\Delta V_{st})_{\Delta T} \quad (1)$$

where

α_s = thermal coefficient of cubical expansion of mineral solids;
α_w = thermal coefficient of expansion of soil water;
V_w = volume of pore water;
V_s = volume of mineral solids;
V_m = total volume of soil specimen; and
ΔV_{st} = change in volume of soil structure due to temperature-induced changes in interparticle forces.

Under undrained conditions and constant confining pressure, a change in temperature leads to a change in pore water pressure, Δu, given by

$$\Delta u = \frac{n\Delta T(\alpha_s - \alpha_w) + \alpha_{st}\Delta T}{m_v + nm_w} \quad (2)$$

where

n = porosity;
α_{st} = physicochemical temperature coefficient of soil structure volume change;
m_v = compressibility of soil structure; and
m_w = compressibility of water.

The results of drained triaxial tests showed that significant permanent volume decreases may occur during initial temperature increases (α_{st} is negative). This is illustrated by test results for remolded illite shown in Figure 1. It may be seen that a significant irrecoverable volume of water was drained from the sample during the first heating cycle. The data suggest also that a temperature increase under drained conditions at constant effective stress followed by cooling may have exactly the same effect as overconsolidation using a pressure increase followed by unloading.

Additional data presented by Campanella and Mitchell (6) showed that pore pressure changes accompanying temperature changes under undrained conditions can be predicted reasonably well using the concepts leading to Eq. 2. The most important factors controlling pore pressure changes appear to be the thermal expansion of the pore water, the compressibility of the soil structure, and the initial effective stress. The results of tests on several clays showed that for each 1-deg F change in temperature the pore water pressure changes by about 0.75 to 1.0 percent of the initial effective stress. For less compressible materials the pore water pressure change is considerably greater. Changes of this magnitude indicate clearly the need for temperature control in the laboratory if unambiguous results are to be obtained, and provide also some indication of possible differences in properties between soils in situ and in the laboratory where temperatures may be different.

In their paper, Plum and Esrig (25) present test results and interpretations to (a) provide further insight into the effects of heating a saturated soil on compressibility, (b) determine how stress history affects observed volume changes associated with temperature change, and (c) gain insight into the phenomenon of pore pressure development due to temperature change.

In studying the effect of temperature on consolidation characteristics, Plum and Esrig found that the compression index of two clays varied both with temperature and pressure. Figure 2 shows the void ratio vs logarithm of pressure relationship for illite at two temperatures. Each specimen was initially consolidated under a pressure of 1.7 psi at a temperature of 24 C. It may be seen that below a consolidation pressure of about 30 psi the sample tested at 50 C was more compressible than the sample tested at 24 C. At pressures greater than 30 psi little difference in compressibility is apparent.

The results of triaxial consolidation tests on illite at different temperatures have been presented by Campanella and Mitchell (6), as shown in Figure 3. Unfortunately data points were not obtained in these tests for stresses less than 2 kg per sq cm. Figure 3 shows equal compression indices for three temperatures at pressures greater than 2 kg per sq cm. Since consolidation was started from the same initial water content for all

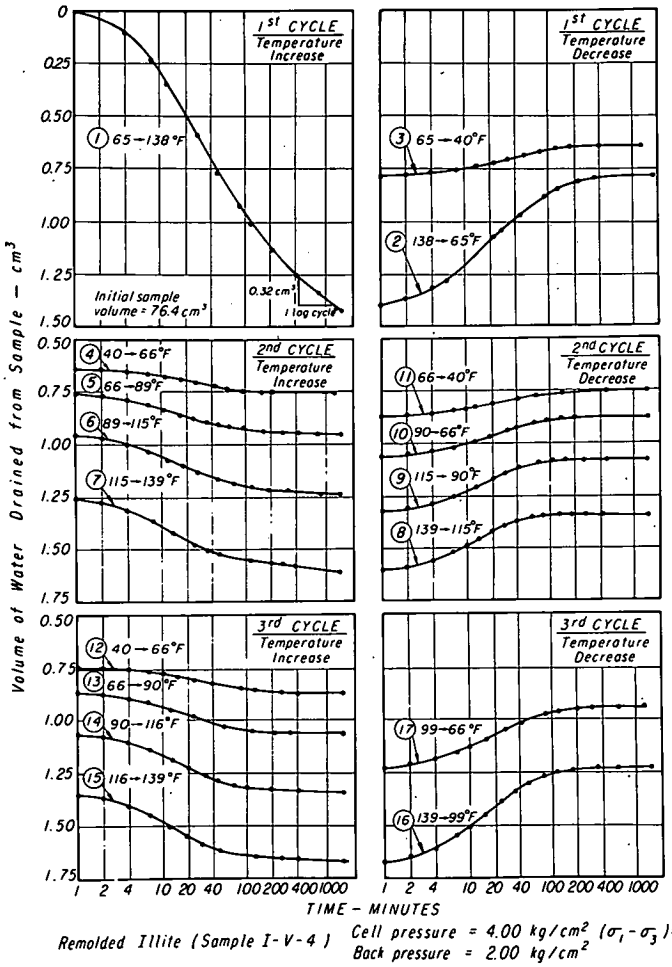

Figure 1. Relationship between volume of water drained from sample and time during temperature changes at constant stress.

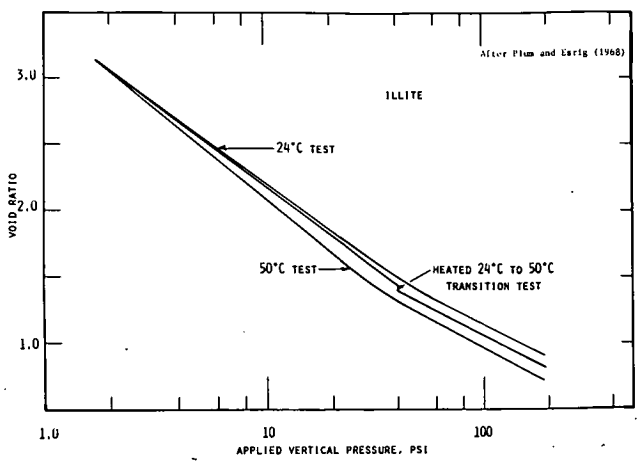

Figure 2. Influence of temperature on consolidation of illite.

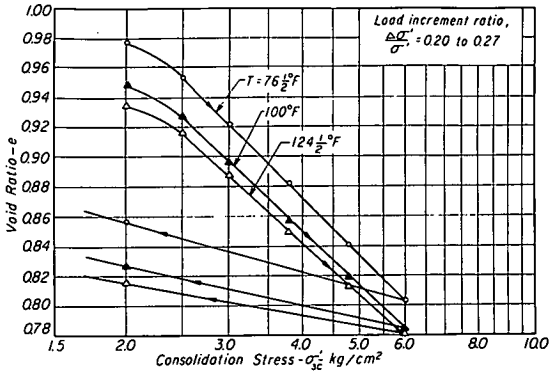

Figure 3. Effect of temperature on isotropic consolidation behavior of saturated illite.

three specimens, the specimens at the higher temperatures must have been more compressible at lower pressures to account for the void ratio differences at a pressure of 2.0 kg per sq cm. Thus the results in Figure 3 are in accordance with those of Plum and Esrig, rather than contrasting as they suggest in their paper.

The effect of heating followed by cooling and its similarity to the effects of overconsolidation may be seen in Figure 4. Plum and Esrig point out that laboratory testing of natural soils that have been heated and recooled during handling could lead to an incorrect evaluation of the maximum past pressure in the field.

The amount of temperature-induced consolidation is related to soil compressibility—the higher the compressibility the greater the consolidation for a given temperature increase. Plum and Esrig show that a given increment in temperature at constant effective stress has an effect equivalent to some increment of pressure at constant temperature. This may be seen from Figure 5, which shows the volumetric strain of illite as a function of overconsolidation ratio for a temperature increase from 24 to 50 C. For specimens with an overconsolidation ratio greater than about 1.7, this temperature increase caused no consolidation; i.e., the preconsolidation had reduced the compressibility of the soil structure sufficiently so that even after the weakening caused by the temperature increase it could still carry the applied effective stress without appreciable further consolidation.

Plum and Esrig present the results of one test conducted at quite high consolidation pressure (loading from 180 to 209 psi) and conclude that the secondary compression is only slightly affected by temperature increases. Other investigators (6, 14, 28), however, have concluded that secondary compression rates are increased significantly by temperature increases. Further consideration of this question therefore appears in order.

Temperature Sensitivity of Double Layer Repulsive Forces

Both Plum and Esrig (25) and Laguros (12) in their papers have attempted explanations of observed behavior using arguments based on changes in interparticle repulsive forces caused by temperature changes. Plum and Esrig postulate that the volume decrease associated with heating a soil results because the double layers expand, thereby increasing repulsive forces and decreasing the effective stress and strength at interparticle contacts. Contradictory statements can be found in the literature concerning the effects of heating on double layer thickness and interparticle repulsive forces.

According to the Gouy-Chapman theory the approximate double layer thickness is given by

$$\frac{1}{\chi} = \text{approximate double layer thickness} = \sqrt{\frac{\epsilon kT}{8\pi ne^2v^2}} \qquad (3)$$

where

ϵ = dielectric constant;
k = Boltzmann's constant;
T = absolute temperature;
n = electrolyte concentration;
e = electronic charge; and
v = cation valence.

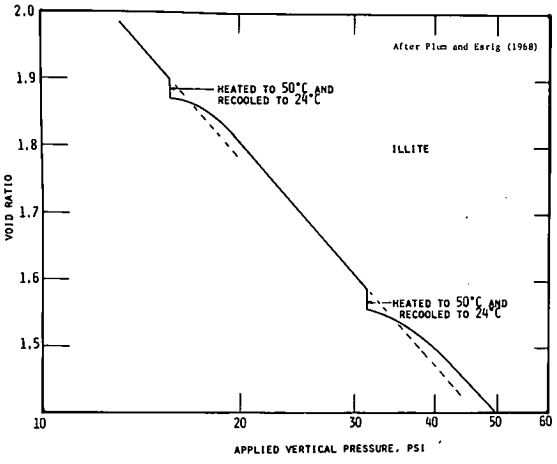

Figure 4. Effect of heating and cooling on void ratio vs pressure relationship of illite.

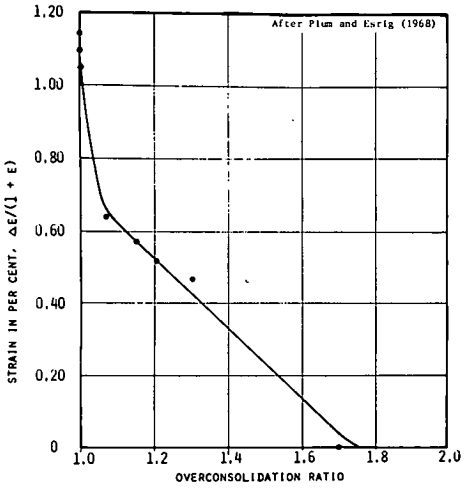

Figure 5. Effect of overconsolidation ratio on volume change of illite on heating from 24 to 50 C.

It may be seen from Eq. 3 that, for all other parameters constant, an increase in temperature should cause an expansion of the double layer. In reality, however, it is apparently impossible to vary temperature without causing a variation in the dielectric constant. If values of dielectric constant for the soil water are assumed equal to those for pure free water, then the decrease in dielectric constant with increasing temperature is sufficient to cause the quantity $1/\kappa$ to decrease with increasing temperature. Thus one might conclude that an increase in temperature should cause a depression of the double layer.

These considerations, however, neglect the fact that Eq. 3 is only an approximation of the double layer thickness. Thus direct extensions using this equation to predictions of interparticle repulsive forces may be misleading. A more refined analysis is possible using the swelling pressure equations developed by Bolt (4, 5). The concentration of cations at the mid-plane between interacting parallel particles is given by

$$v\sqrt{\beta C_o}\,(x_o + d) = 2\sqrt{C_o/C_c}\int_{\phi=0}^{\pi/2}\frac{d\phi}{\sqrt{1 - (C_o/C_c)^2\sin^2\phi}} \qquad (4)$$

where

v = valence of cation;
$\beta = \dfrac{8\pi F^2}{1000\,\epsilon RT}$;
F = Faraday constant;
R = gas constant;
d = half-distance between plates;
x_o = constant related to surface density of charge on the clay (it is generally less than 4 Å);
C_o = concentration of bulk liquid pressed out from the clay;
C_c = cation concentration at the mid-plane between particles;
ϕ = variable related to central concentration, the value of which is not needed for evaluation of the complete elliptic integral.

The swelling pressure (repulsive pressure between plates) is given by the difference between the osmotic pressures in the central plane and in the bulk solution according to

$$P_s = RT\,C_o\,(C_c/C_o + C_o/C_c - 2) \qquad (5)$$

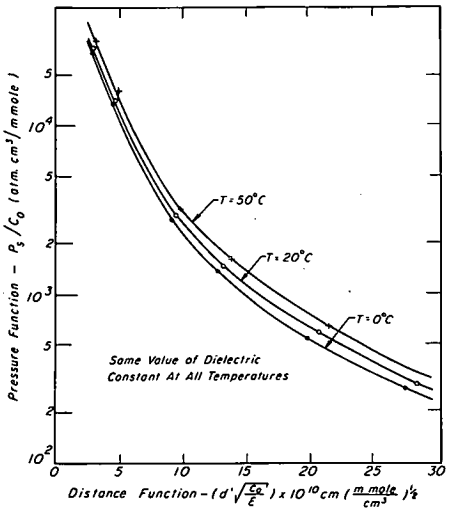

Figure 6. Effect of temperature on double layer repulsions assuming no variation in dielectric constant.

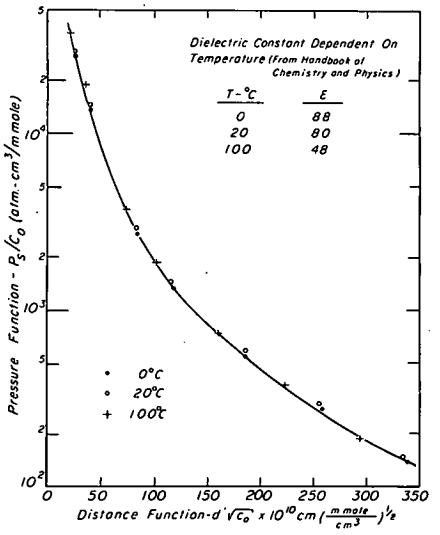

Figure 7. Effect of temperature on double layer repulsions assuming dielectric constant dependent on temperature.

The relationship between repulsive pressure and plate spacing has been evaluated for different temperatures, assuming all other quantities constant, and is shown in the form of (P_S/C_O) vs $(d'\sqrt{C_O/\epsilon})$ in Figure 6. For this analysis the quantity $(x_O + d)$ in Eq. 4 has been replaced by d', since $d' \simeq d$ at all but very small particle spacings. Figure 6 shows that an increase in temperature from 0 to 50 C causes a definite increase in repulsions for all spacings. This increase is of the order of 30 to 40 percent for the 50 C increase in temperature.

If, however, the dielectric constant is assumed to vary with temperature, then the result shown in Figure 7 is obtained, using ϵ values for pure water. It may be seen that under these conditions the repulsive pressures are unchanged over the temperature range from 0 to 100 C.

Unfortunately the dielectric constant of soil water and its variation with temperature are not known with any certainty. The presence of cations in solution and the electric field in the vicinity of particle surfaces may be expected to have an influence on the dielectric constant. Harris and O'Konski (11) present low-frequency dielectric constant data showing that as ionic concentration increases the value of ϵ decreases. For example, values at 20 C for NaCl solution are

Concentration	ϵ
0	80
2M	59.5
4M	46.0
5M	42.0

Within the double layer the concentration decreases from a very high value at the particle surface to that of the bulk solution (usually less than 1M) at large distances. Thus a varying ϵ with distance might be expected.

Van Olphen (31) suggests that the value of ϵ in the stern layer adjacent to particle surfaces may be in the range of 3-6. Low (15) cites data suggesting values of the same order in thin films on clay surfaces. Thus it would appear that the appropriate value of ϵ for use in double layer computations should be less than that for pure water.

This uncertainty in values of ϵ makes computations of the type leading to Figures 6 and 7 questionable on a quantitative basis. Regardless of the actual values, however,

an increase in temperature can be expected to decrease the dielectric constant because of the greater difficulty of ordering water molecules at higher temperatures. Thus the qualitative picture presented by Figure 7 is considered more realistic than that in Figure 6, and it is concluded that temperature variations should have little effect on interparticle double layer repulsions.

In view of these considerations it does not appear that increased double layer repulsive forces can account for the major part of the compression (through reduction of interparticle effective stresses) that occurs due to heating. It is more likely that the interparticle contact structure itself is weakened because of the increased thermal energy of the constitutent atoms.

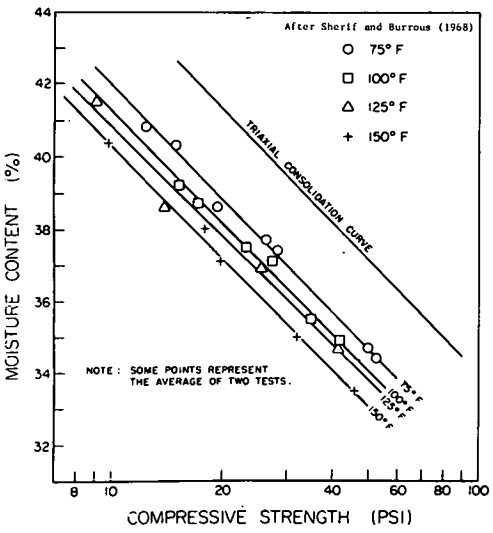

Figure 8. Effect of temperature on the undrained strength of kaolinite.

Strength

Sherif and Burrous (29) present a useful summary of previous work on the influence of temperature changes on the shearing strength of soils. While most published data indicate that an increase in temperature causes a strength reduction, not all results are in complete agreement. The data do suggest, however, that for all other factors constant (e.g., structure and water content), lower strengths are associated with higher temperatures. Test results presented by Sherif and Burrous are in accord with this.

Specimens of kaolinite were prepared by triaxial consolidation to effective stresses in the range of 20 to 98 psi. Consolidation was done at 75 C. The consolidated specimens were then tested in unconfined compression (stress-controlled) at temperatures of 75, 100, 125, and 150 F. Figure 8 shows the results of these tests in the form of the logarithm of compressive strength vs moisture content. It may be seen that the relationship is linear and unique for each temperature.

From the form of the results Sherif and Burrous concluded that a given increase in temperature has an effect on compressive strength analogous to a given increase in water content, independent of the value of the initial water content. From Figure 8 it may be seen that the strength, σ_o, at 75 F (consolidation temperature) is given by

$$\sigma_o = \exp (A - Bw) \tag{6}$$

where w is the water content and A, B are material constants.

The strength at any other temperature is given by

$$\sigma_T = \exp (A - Bw - C\Delta T) = \sigma_o \exp (-C\Delta T) \tag{7}$$

where

$T = T - T_o$ (T_o = 75 F) and
C = parameter characteristic of the strength change caused by temperature change.

Sherif and Burrous conclude that the quantity $C\Delta T/B$ might be regarded as an equivalent moisture content increase, w'. They also tested the following equation and found that it fit the data well:

$$\sigma_T = \frac{T_o}{T} \exp \left[A - B\left(\frac{\gamma_{wo}}{\gamma_w}\right) w \right] \tag{8}$$

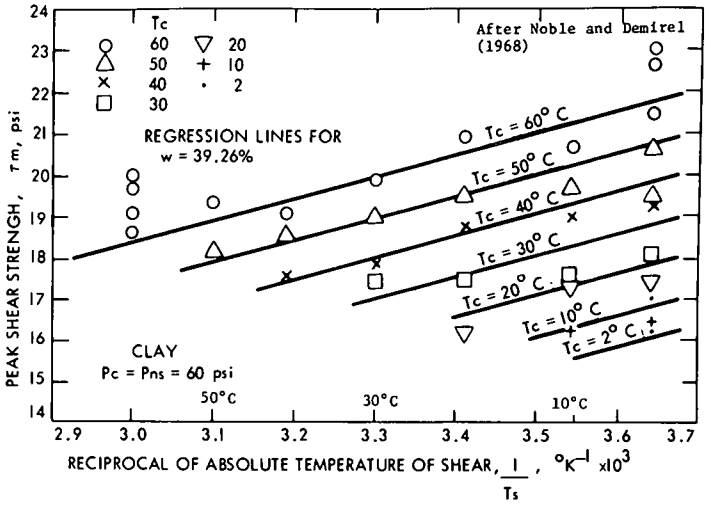

Figure 9. Effect of consolidation and test temperature on strength of alluvial clay.

where γ_{wo} and γ_w are the densities of water at T_o and T, respectively. Unfortunately they do not indicate the physical basis for this equation.

Laguros (12) indicates a progressive increase in strength as temperature is increased from 35 to 105 F for three soils. For a fourth soil, maximum strength was observed at 70 F. Although this would appear at first glance to contradict the results of Sherif and Burrous, it should be noted that in the Laguros tests specimens were compacted at the test temperature. Consequently, those compacted at the higher temperatures had significantly higher densities (and possibly different structures) than those prepared at low temperatures. As a result the strength values reflect the added variable of density. Laguros' results for liquid limit show a consistent decrease with increase in temperature, which would be expected, since the liquid limit is also a measure of strength, and at the high water contents associated with the liquid limit the initial structure and density are of little consequence.

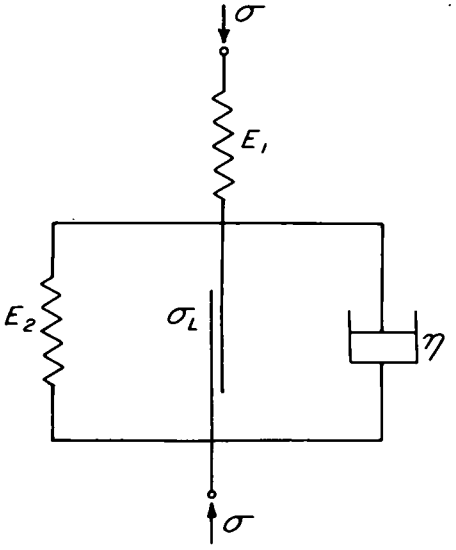

Figure 10. Mechanical model of clay skeleton proposed by Murayama.

Noble and Demirel (23) present the results of a large number of direct shear tests on a highly plastic clay that show the effects of both temperature of consolidation and temperature at test. Figure 9 summarizes the results of these tests. All specimens were tested at temperatures equal or less than the consolidation temperature. The results show clearly that the higher the consolidation temperature the greater the shear strength at any given test temperature, thus supporting the interpretation given for Laguros' results. For a given consolidation temperature, however, the strength decreases in a regular manner with increasing test temperature.

Elasticity

The elasticity properties of most engineering materials are temperature-dependent. There is no reason to believe that

the elasticity characteristics of soils should not be temperature-dependent also, although prior to the contribution by Murayama (19) specific data have not been readily available. To investigate the temperature-dependence of the elasticity of clays, Murayama has used the rheological model shown in Figure 10, which was proposed for the description of the viscoelastic behavior of soil in his earlier work (20, 21, 22).

In this model the dashpot coefficient, η, is derived using the theory of rate processes and is given by

$$\eta = \frac{\sigma_2}{2A\sigma_{20} \sinh (B\sigma_2/\sigma_{20})} \tag{9}$$

where

σ_2 = stress on dashpot;
σ_{20} = initial stress on dashpot; and
A, B = constants dependent on soil structure and temperature.

The two springs in the model are assumed linear with constants E_1 and E_2.

The purpose of the present study was to determine the effect of temperature on these two constants. Murayama proposes that the elasticity of a clay skeleton may be due partly to flexure of clay particles, but is caused mainly by physicochemical interparticle forces, and these forces should be temperature-sensitive. The stress relaxation test was used as a means for evaluating E_1 and E_2 at different temperatures. All tests were run on undisturbed specimens of the highly plastic Osaka alluvial clay tested in unconfined compression. The maximum past pressure on the undisturbed specimens was 3.8 kg per sq cm.

Solution of the rheological model shown in Figure 10 for the case of stress relaxation leads to

$$\sigma = \frac{E_1E_2}{E_1 + E_2} \left\{ \left(\epsilon_0 + \frac{\sigma_2}{E_1}\right) - \left(\epsilon_0 - \frac{\sigma_2}{E_1}\right) \frac{E_1}{BE_2} \log[AB(E_1 + E_2)t] \right\} \tag{10}$$

which holds for

$$\epsilon_0 E_1 > \sigma \geq \frac{E_1E_2}{E_1 + E_2} \left[\epsilon_0 \left(1 + \frac{2E_1}{BE_2}\right) + \frac{\sigma_2}{E_2} \left(1 - \frac{2}{B}\right) \right]$$

For very long time,

$$\sigma_{t\to\infty} = \frac{E_1E_2}{E_1 + E_2} \left(\epsilon_0 + \frac{\sigma_2}{E_2}\right) \tag{11}$$

These relationships are valid only for the range of stress where the stress vs strain relationship is linear. The rate of stress relaxation is given by

$$-\frac{d\sigma}{d \log t} = \frac{\sigma_{t\to\infty} - \sigma_L}{(E_2/E_1)B} \tag{12}$$

Although the various equations presented by Murayama can be used to compute the model parameters from the results of stress relaxation tests at different temperatures, they cannot be used directly for the prediction of the effects of temperature on stress relaxation. Whereas the parameters A and B in Eqs. 10 and 12 are known functions of temperature, the initial stress, σ_0, for a given initial strain, ϵ_0, and the final stress, $\sigma_{t\to\infty}$, are also functions of temperature, and these latter functions are unknown. The model is assumed by Murayama to be valid for stress relaxation, since the test results follow a form predicted by the derived equations.

On this basis the effect of temperature on the elastic moduli E_1 and E_2 may be examined. The test results showed that for initial strains (ϵ_0) of up to about 1.0 percent,

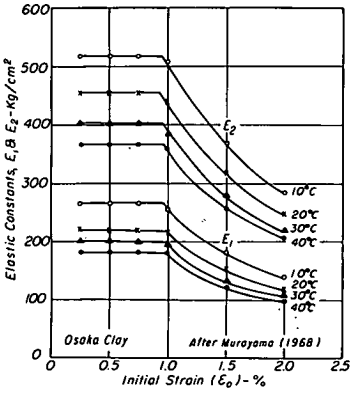

Figure 11. Influence of temperature on elastic constants in Murayama's model.

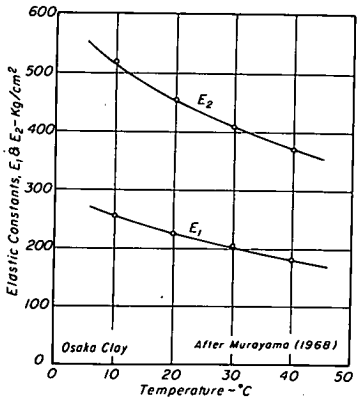

Figure 12. Elastic constants according to the Murayama model as a function of temperature.

the values of E_1 and E_2 were constant with variations in initial strain, but they decreased with further increase in initial strain, as shown in Figure 11. The results show also that as temperature increases the elastic moduli, E_1 and E_2, decrease. This temperature-sensitivity is shown more clearly in Figure 12, where values of E_1 and E_2 for $\epsilon_o <$ 1.0 percent are plotted vs temperature. Whether or not these values represent true elastic moduli, of course, depends on the validity of the rheologic model used for their evaluation.

Figure 13 shows the relationship between initial stress and initial strain in the stress relaxation tests at different temperatures. If the slopes of the straight-line portions of these curves are taken to represent the elastic modulus of the material, then it may be seen that an increase in temperature causes a significant decrease in modulus. In this case the conclusion does not depend on the validity of a rheologic model for its validity.

Creep and Stress Relaxation

A number of investigators have treated creep and stress relaxation phenomena in soils using the theory of rate processes (10) in recent years, including Murayama and Shibata (20), Mitchell (16), Christensen and Wu (8), and Andersland and Akili (1). Mitchell, Campenella and Singh (17) have provided data that substantiate the assumption that soil deformation can be considered as a thermally activated process. Noble and Demirel (23) have used a similar approach in the study of temperature effects on the deformation behavior of two soils—a highly plastic clay and a low plastic silt.

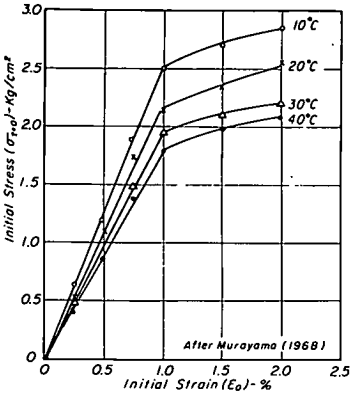

Figure 13. Effect of temperature on the stiffness of Osaka clay.

Noble and Demirel envisage that interparticle bonds form in a cohesive soil due to an oriented structure in the adsorbed water layer's adjacent clay particles. Deformation of the system then occurs by distortion and breaking of these bonds. The unstable condition that exists following the breaking of a bond is considered the "activated state" in which the "contact zone" between particles consists essentially of oriented water. This concept of the nature of bonding differs somewhat from that proposed by Mitchell, Campanella, and Singh (17), who concluded that interparticle contacts must be effectively solid-to-solid,

and subsequent considerations by Mitchell, Singh, and Campanella (18) that suggest that individual atoms in the contact structure are the activating flow units and that a contact may contain many interparticle bonds. In both cases, however, temperature would be expected to have an effect on the ease with which bonds can be broken.

The basic equation for deformation rate $\dot{\delta}$ developed by Noble and Demirel is

$$\dot{\delta} = A \exp\left(\frac{-\Delta H}{kT}\right) \exp(\beta\tau) \tag{13}$$

where

A = frequency factor, dependent on entropy of activation, but assumed independent of temperature, T;
ΔH = activation enthalpy;
k = Boltzmann's constant;
τ = applied shear stress; and
$\beta = \frac{\beta'}{kT}$ = coefficient to convert τ into an energy term.

The parameter β' is interpreted as the average volume of material containing one bond. For given values of T, $\dot{\delta}$, and A, the shear resistance is

$$\tau = \frac{1}{\beta}\left(\frac{\Delta H}{kT} + \ln \dot{\delta} - \ln A\right) \tag{14}$$

Noble and Demirel assume that the same form of relationship can be used to express the peak failure stress, τ_m, and that the consolidation stress, P_c, the normal stress during shear, P_{ns}, and the water content, w, can be accounted for by using the following equation:

$$\tau_m = \frac{1}{\beta}\left(\frac{\Delta H}{kT} + \ln \dot{\delta} - \ln M'\right) + \rho P_c + \mu P_{ns} - \gamma w \tag{15}$$

where ρ, μ, and γ are linear coefficients.

Finally, they noted that the temperature of consolidation, T_c, should be important (see Fig. 6) as well as the temperature of shear, T_s, thus leading to the following two equations:

For strength:

$$\tau_m = \frac{1}{\beta}\left(\frac{\Delta H}{kT_s} + \ln \dot{\delta} + \alpha T_c - \ln M\right) + \rho P_c + \mu P_{ns} - \gamma w \tag{16}$$

For deformation rate:

$$\ln \dot{\delta} = \ln M - \frac{\Delta H}{RT_s} + \alpha T_c + \beta\tau - \beta\rho P_c - \beta u P_{ns} + \beta\gamma w \tag{17}$$

Both constant rate of strain direct shear tests and constant stress creep tests, using stresses only slightly less than the peak strength, were run on the two soil types noted above at several different temperatures. From the results of these tests the linear coefficients in Eqs. 16 and 17 were determined by regression analysis and compared. The values of some of the coefficients deduced in this way show considerable variation (up to more than 100 percent) with variation in normal stress. Similar variations are observed when the values deduced from the creep tests are compared with those deduced from the shear tests. Nonetheless, the authors consider the values sufficiently close to tend to confirm the hypothesis of a single deformation mechanism that is independent of test procedure, and that Eqs. 16 and 17 are suitable for its description.

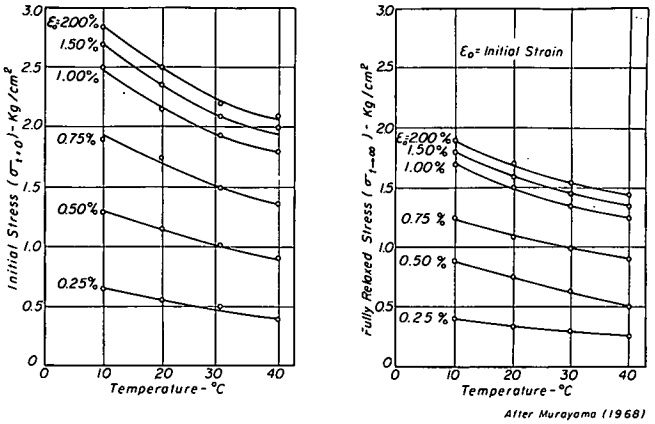

Figure 14. Influence of temperature on the initial and final stresses in stress relaxation tests on Osaka clay.

The coefficient β' was lowest at the highest normal stresses, which is consistent with the idea of increased numbers of bonds under higher stresses and a decreased volume of influence per bond. For the clay, the value of β' was determined as equivalent to a volume of 0.6711×10^{-18} cm^3, which is considered by the authors to be of the same order of size as a clay particle. This seems abnormally low, since a clay plate of dimensions $1\mu \times 1\mu \times 0.1\mu$ would have a volume of 1.0×10^{-13} cm^3. Both this fact and the observation that the equivalent volume for the silt was even smaller support the hypothesis of Mitchell, Singh, and Campanella (18) that there may be many bonds per particle contact.

Values of activation energy were found to range from 5 to 8 kcal/mole for the silt and from 12 to 21 kcal/mole for the clay. For both soils the higher values were obtained from the direct shear test results. These values are somewhat lower than those summarized by Mitchell, Singh, and Campanella (18) for a variety of soils.

The results of the stress relaxation tests presented by Murayama (19) show that for a given increment of strain both the initial stress and the fully relaxed stress decrease with increasing temperature, as may be seen from Figure 14. His results show also that the rate of stress relaxation, $-(d\sigma/d \log t)$, decreases with increasing temperature. While this may at first appear surprising, it should be noted that the relaxation process is not necessarily slower at the higher temperatures, because the difference in initial and fully relaxed stresses was greater at the lower temperatures. Since the ratio, E_2/E_1, was found to be constant and independent of temperature and the coefficient B decreased only slightly with increasing temperature, the observed behavior of $-(d\sigma/d \log t)$ is consistent with the predictions of Eq. 12.

Swelling

Mechanisms of clay swelling have been studied extensively in the past because of the many practical problems associated with construction on or with expansive soils. Attention has been focused on such causes as osmotic pressures, capillary stresses, straightening of bent particles, and ionic and particle surface hydration. Blaser and Scherer (3) provide convincing evidence that significant volume changes may also be associated with what they term "salt heave." Their study grew out of experiences with soils in the southern Nevada area that contain substantial amounts of sodium sulfate.

Blaser and Scherer have demonstrated that damage to light structures and floors was caused as a result of the influence of temperature on the hydration state of sodium sulfate. During warm weather there is an upward migration of water, evaporation, and deposition of salts. Thus the sulfate concentration may be high in the upper few feet. At temperatures above 90 F a large amount of Na_2SO_4 is soluble in water (as much as

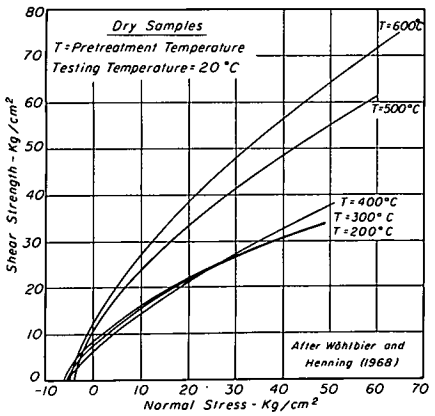

Figure 15. Effect of heat treatment on the dry strength of kaolinite.

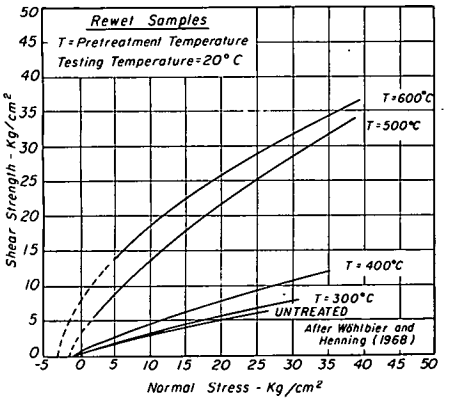

Figure 16. Effect of heat treatment on the rewet strength of kaolinite.

52 gm per 100 gm water). Temperatures below about 55 F cause crystallization of sodium sulfate, and the crystals that form can bind up to 10 H_2O molecules per molecule of Na_2SO_4. These crystallization and crystal hydration processes can cause an expansion against the soil structure and consequent heave of the ground surface.

The authors have found that soils with more than 15 percent of the particles finer than 0.005 mm and containing more than 0.2 percent Na_2SO_4 in solution are subject to salt heave, provided there is sufficient free moisture in the soil and ambient daily temperature variations range from 90 F in the daytime to below 40 F at night. These conditions are met mainly in the late fall and early spring in the Nevada area.

Methods for testing soils for determination of salt heave potential and for treating salt heave-susceptible soils are described by Blaser and Scherer in their very important contribution.

THERMAL STABILIZATION

Effects of Preliminary Heat Treatment

Three papers are concerned with the effects of heat treatment on the engineering properties of soils. Wöhlbier and Henning (32) investigated the effects of heat treatment up to 600 C on the strength and compression properties of kaolinite. Chandrasekharan et al (7) report on the effects of heat treatment on the pulverization and stabilization of two tropical soils. Barata (2) illustrates the beneficial effects of preliminary drying on the CBR of a residual weathered gneiss soil after rewetting.

Wöhlbier and Henning prepared specimens of kaolinite at an initial water content slightly less than the liquid limit by vacuum extrusion. After careful drying for 28 days the specimens were heated for a period of 48 hours to temperatures up to 600 C, using a heating rate of 60 C per hour. Although heating to 400 C had no effect on the kaolinite, heating to 500 C caused breakdown of the clay mineral structure. After heating to this temperature the clay was no longer plastic.

Some specimens were tested at the end of the heat treatment period, whereas the remainder were resaturated prior to test using a back-pressure technique. Consolidated-undrained triaxial tests were used with confining pressures up to 25 kg per sq cm. The effect of heat treatment on the strength of specimens prior to rewetting is shown in Figure 15, and after resaturation in Figure 16. It is clear from Figure 15 that the strength of the dried specimens was essentially unaffected by temperature of heat treatment in the range of 200 to 400 C. Unfortunately the authors do not present results for dried but unheated specimens for comparison purposes. It may be seen that heating above 400 C leads to a substantial increase in strength.

The results for the resaturated samples, Figure 16, are of the same form, although the curves for 300 and 400 C show a small but significant increase in strength with increase in treatment temperature. The increase in strength resulting from pretreatment

at 500 and 600 C is by comparison quite large. It is of interest to note that in all cases the failure envelopes are curved in form. Heat treatment was also observed to cause a significant increase in the stiffness of the clay, and this stiffness increase is important even for treatment temperatures less than 400 C where the strength is not significantly increased.

The beneficial effects on properties of heat treatment at temperatures sufficiently high to cause a change in the clay mineral structure are well demonstrated by the results of this study. Methods for the application of heat treatment, at the high temperatures required, to large masses of soil in the field have been developed and are described by Litvinov (13). The economics of such treatment may be unfavorable, however.

Chandrasekharan et al (7) note that insufficient pulverization and inadequate mixing often limit the effectiveness of additive stabilization in highly plastic clays. In their investigation the influences of heat treatment on the pulverization characteristics of a lateritic soil and a black cotton soil were investigated, and the effect of heat treatment and aggregate size on the effectiveness of cement stabilization of black cotton soil was studied. A range of pretreatment temperatures of 100 to 400 C was used. Among their principal findings were the following:

1. Sodium chloride addition in an amount of about 3 percent serves as an aid to pulverization.
2. Heat treatment at 250 C for two hours was found to be the optimum to facilitate easy pulverization.
3. The plasticity of black cotton soil was reduced by treatment at temperatures above 300 C.
4. Soil-cement specimens made of the heat-treated soil were stronger or weaker than the untreated soil depending on whether the coarser or finer aggregate sizes were used.

Barata (2) points out that because of the high daytime temperatures in Brazil there may be significant evaporation from compacted subgrades before paving is completed. Specimens of a weathered gneiss soil, classified as an A-4 (1) in the HRB system, were compacted using the modified AASHO procedure. The samples were then dried for 3 hours at 40 C (104 F) prior to the 4-day soaking period. The CBR was then measured and compared with the value for an identical sample not subjected to drying prior to soaking.

The results of these tests showed that the preliminary drying after compaction resulted in an increase in the CBR of about 6 percent for samples compacted dry of optimum and by about 15 percent for samples compacted wet of optimum. An explanation is given in the paper for the observed behavior in terms of the density increases that occur during drying followed by the volume increases during soaking, and the relationships between these values and contours of equal CBR on the density vs moisture content diagram.

It would appear that the results obtained from this relatively small study are significant and that further investigations should be undertaken to ascertain the full range of property changes that might be obtained using this method in practice.

Fusion of Soils

Post and Paduana (26) have discussed the melting of soils and its possible application to soil stabilization. They show how the approximate melt range of a soil may be determined using a phase equilibria approach. Most soils exhibit incongruent melt ranges rather than a single melt point. Because there are always minor constituents and trace elements in soils, the actual melt ranges will nearly always be about 100 C lower than those deduced from phase diagrams.

Melt range data are presented for several soils and are found to have values between about 1250 and 1750 C, with fat clays near the high end and feldspar-rich clays at the low end of the scale. Soils with a high alumina or lime content may have higher melt ranges. Experimental results are presented to show that melt ranges may be lowered

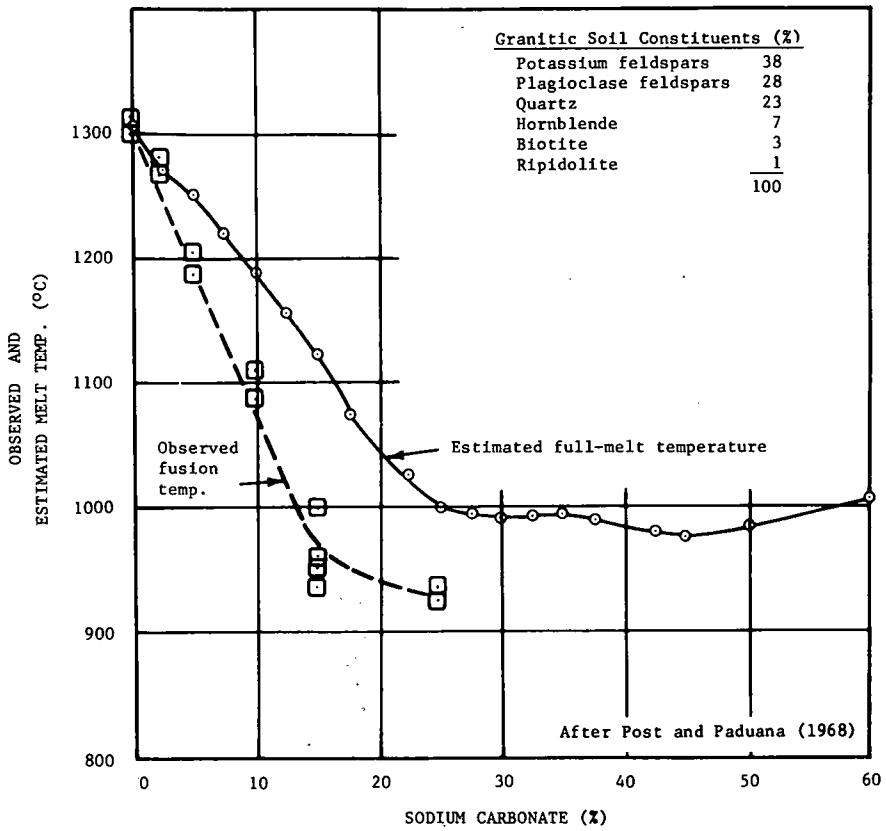

Figure 17. Effect of Na_2CO_3 additive on the melt temperature of a granitic soil.

significantly through the addition of a fluxing agent. Figure 17 shows the relationship between melt temperature and amount of sodium carbonate added to a granitic soil. It may be seen that the fusion temperature is reduced up to 350 C through the addition of Na_2CO_3. The data show also that the actual values of fusion temperature are lower than predicted values as a result of soil impurities.

Post and Paduana state that equipment is now available for producing the heat energy needed for stabilization of soils by fusion. Since soils melt incongruently over a temperature range it is only necessary to reach the initial melt range to achieve cementation of the soil mass. The authors suggest that field tests should be conducted using mobile downdraft heaters and that further studies of fluxing agents be made. Past experience with heat treatment to temperatures sufficient only to cause loss of structural water and mineral transformations (600 C±) indicates that the required quantities of heat are large and the technology is complex, however. It would appear desirable, therefore, to investigate more completely the engineering properties of fused materials, new methods for heat supply, and whether the economics of such treatment are favorable in comparison with other methods for stabilizing soils.

Ice Barriers

Takashi's paper (30) deals with the problem of forming an ice barrier to cut off groundwater flow. In the presence of flowing groundwater, completion of an ice curtain may be difficult, and in some cases impossible, because of the heat brought into the freezing zone by the flowing groundwater.

The problem of joining two frozen soil cylinders with water flowing between is considered. Equations are developed that give approximately (a) the quantity of flow

between the frozen soil cylinders, (b) the pressure distribution along a line between the cylinders in the direction of flow, (c) the flow velocity, and (d) the head difference (dam-up head) that will exist across the ice barrier at the completion of freezing. An equation is then developed that gives the temperature of flowing groundwater after its passage between the frozen cylinders.

The following equation is then derived, which gives a critical value of head drop to be expected across the completed barrier, Δp_{crit}, in terms of soil properties, temperatures of groundwater and coolant, and geometry of the freezing system:

$$\Delta p_{crit} = \frac{2\pi k}{\lambda \gamma c} \frac{\theta_f - \theta_c}{\theta_\infty - \theta_f} \cdot F\left(\frac{2a}{L}, b_{crit}\right) \tag{18}$$

where

k = thermal conductivity of frozen soil;
λ = coefficient of permeability of the unfrozen soil;
γ = density of water;
c = specific heat of groundwater;
θ_f = groundwater freezing point;
θ_∞ = initial temperature of groundwater;
θ_c = surface temperature of freezing pipe;
$F\left(\frac{2a}{L}, b_{crit}\right)$ = a nearly linear function of the freezing pipe radius and spacing = 0.6 to 1.9 for (2a/L) = 0.06 to 0.26;
a = radius of freeze pipe; and
L = distance between freeze pipes.

If the actual head drop that will develop across the barrier is less than Δp_{crit}, then completion of the ice curtain will be possible. Takashi illustrates by example the influence of each of the quantities in Eq. 18 on Δp_{crit} and shows that seepage flow has an important influence on the freezing process when the permeability is greater than about 10^{-3} m/sec. In this situation the theory presented can be used to determine whether or not an ice curtain can be completed using a given freezing system. The material in this paper should be of great value to engineers contemplating the use of ice barriers for temporary groundwater shut-off.

TEMPERATURE EFFECTS IN PAVEMENT SUBGRADES

Field Observations

Both Fang (9) and Richards (27) present data on temperatures in and beneath highway pavements and consider the influence of these temperatures on the performance of the soil-pavement system. In this review only those parts of their papers that deal with temperature effects in the subgrade will be considered.

Richards (27) describes the results of an Australia-wide study of temperature beneath sealed pavements. Eighteen field test sites were chosen as representative of the wide range of soil and climatic conditions in Australia. These sites were identical in all respects except soil type and climate. Thermistors were used for temperature measurement at a large number of points at each site. The effect of daily temperature variation was not studied, but it is known to be small below a depth of a few inches. Pavement temperatures over most of Australia range from 5 C to over 60 C.

Individual temperature readings often showed large lateral variations (5 C± near the surface) at the same depth and time. Richards suggests that this variation is due more to variations in heat gain or loss at the surface than to differences in thermal diffusivity of the materials. He does not indicate why there should be such variations across a given surface.

From the large amount of accumulated data, some of which are given in the paper, several pertinent trends have been observed. The summer temperatures and the mean temperatures at all depths are significantly greater under a bituminous seal than under natural ground surfaces. In most cases the winter temperature is slightly greater under a bituminous seal.

The maximum observed temperature gradient over distances of 10 to 15 cm was only about 0.3 C/cm. Richards concludes that a gradient of this magnitude should not cause a moisture flow in excess of about 10^{-7} cm/sec. Since gradients exist at any point for only a short time as a temperature wave moves through the soil profile, thermal moisture transfer in a lateral direction is likely to be small. If it does occur, the gradients are such to cause moisture movement down and away from the centerline. Thus the thermal contribution to overall moisture flow would be to give an increase in stability.

A point of practical importance relative to soil stabilization is brought out by Richards. The temperature of stabilized base courses may rise to 50 to 60 C during the curing period for summertime construction. Under these conditions the usual procedure of curing laboratory specimens at 20 to 25 C may be unduly conservative.

Probably the most significant conclusion Richards draws from this study in terms of the design and performance of pavements is that the major influence of temperature variations is on the load-spreading properties of bituminous layers and treated bases.

Fang (9) has summarized the pavement and subgrade temperature data accumulated during the AASHO Road Test. A brief description of the techniques used to obtain the temperature data are presented. Data are presented that show the effect of temperature on deflections of the soil-pavement system and seasonal variations in the strength characteristics of the soil-pavement system. The effect of temperature on the behavior of the subgrade soil cannot be isolated from many of these data because the measured values include either contributions from the pavement structure or from moisture content variations.

The data indicate that frost penetration was greater under rigid pavements than flexible pavements. This is attributed in part to the greater thermal conductivity of portland cement concrete. Temperature vs depth measurements confirm the earlier statement that daily air temperature variations have little effect on subgrade soil.

Analysis Methods

The paper by Paaswell (24) has been included in this section of the report since the topic treated, while potentially important in a range of problems, is particularly pertinent to the study of temperature variations beneath pavement structures. The temperature profile that develops in a soil as a result of transient temperature changes at one boundary is studied.

A series of tests on partially saturated soils showed that uniform temperature profiles will be established even when the initial moisture content variations through the sample depth varies erratically by as much as 2 percent. In general, as the saturation increased the amount of moisture movement near the points of maximum temperature gradient decreased. This would be expected since the tests were run on sealed samples and, therefore, as the saturation increases there is less vapor phase transport and less free space for water to move into. From the results of these tests Paaswell concludes that the soil-water system can be treated as a homogeneous unit for the purpose of making preliminary temperature distribution analyses.

The heat diffusion equation was solved for the case of a cylindrical volume of soil subjected to a sinusoidal temperature variation with time at the top boundary. Predicted temperatures as a function of time for different depths were compared with measured values, and the agreement was fairly good for the first pulse. Paaswell concludes with a discussion of the complex interrelationships between pore pressure, water flow, and volume change that develop during a temperature change.

CONCLUSIONS

This general report represents an attempt at summarizing the most significant concepts and conclusions advanced by the authors of the 14 papers included in Part III of this volume. The papers treat a variety of topics relating to the influences of temperature and heat on the engineering behavior of soils. A few of the main points are here singled out that, by virtue either of their great importance or because they are controversial, should be subjects of further study.

1. Evidence on the influence of temperature on secondary compression rates is conflicting, with some investigators indicating little effect and others indicating that secondary compression rates are greatly increased as temperature increases. Can this question be resolved on the basis of data already available, and if not what further work is needed?

2. Volume changes and pore pressure variations that develop when saturated soils are subjected to a temperature change are reasonably well understood. Expressions are available for their estimation in terms of the thermal expansion of the water and soil grains, the compressibility of the soil structure and water, and some type of physicochemical temperature coefficient of soil structure volume change. Arguments have been presented to account for the volume decrease (under drained conditions) of a soil structure with increased temperature based on (a) changes in double layer repulsive forces with temperature and (b) variation in the strength of the interparticle contact zone structure with strength. On the basis of the analysis presented in this paper, can we draw positive conclusions concerning the influence of temperature on double layer repulsions? What are the effects of temperature variations on other types of interparticle forces? And which of the two arguments stated above is the most reasonable to account for the behavior?

3. The preponderance of available data indicates that, for other factors constant, an increase in temperature leads to a decrease in strength. What changes, if any, should be made in laboratory testing, analysis, and design procedures for field application?

4. The temperature-dependence of deformation rates in conjunction with rate process theory has been used in a number of recent studies to draw conclusions concerning the mechanism of deformation and interparticle bonding characteristics in soils. Critical discussion of this approach is needed.

5. A "salt heave" swelling mechanism that is dependent on temperature changes has been identified by Blaser and Scherer. Further study of this phenomenon should be made. Are there other temperature-related chemical phenomena, heretofore unrecognized, that should be investigated as possible causes of volume or strength change?

6. The partial drying of compacted soil prior to soaking appears to have a beneficial effect on strength. Are there additional data beyond that presented by Barata? Are there conditions where pre-drying may be detrimental?

7. It is clear that heating soils to high temperatures can result in marked improvements in stress-deformation properties. What is the outlook for economical thermal treatment methods in the future?

8. A method has been developed by Takashi for determination of whether or not a frozen ice barrier can be successfully completed under flowing groundwater conditions. How well can this method be expected to work in practice? Have alternative approaches been developed?

9. While it has been well established that temperature variations have a significant effect on the load distributing characteristics of a pavement structure, it would appear that temperature variations in the subgrade have little influence on behavior, with the exception of frost effects. Is this a reasonable conclusion?

REFERENCES

1. Andersland, O. B., and Akili, W. Stress Effect on Creep Rates of a Frozen Clay Soil. Geotechnique, Vol. 17, p. 27-39, 1967.
2. Barata, F. E. Effect of Heating on Bearing Capacity of Highway Subgrades. HRB Spec. Rept. 103, p. 141-149, 1969.
3. Blaser, H., and Scherer, D. J. Expansion of Soils Containing Sodium Sulphate Caused by Drop in Ambient Temperature. HRB Spec. Rept. 103, p. 150-160, 1969.
4. Bolt, G. H. Analysis of the Validity of the Gouy-Chapman Theory of the Electric Double Layer. Jour. Colloid Science, Vol. 10, p. 206, 1955.
5. Bolt, G. H. Physico-Chemical Analysis of the Compressibility of Pure Clay. Geotechnique, Vol. 6, No. 2, p. 86-93, 1956.
6. Campanella, R. G., and Mitchell, J. K. Influence of Temperature Variations on Soil Behavior. Jour. Soil Mech. and Found. Div., ASCE, Vol. 94, No. SM3, Proc. Paper 5958, p. 709-734, May 1968.

7. Chandrasekharan, E. C., Boominathan, S., Sadayan, E., and Setty, K. R. Narayanaswamy. Influence of Heat Treatment on the Pulverization and Stabilization of Characteristics of Typical Tropical Soils. HRB Spec. Rept. 103, p. 161-172, 1969.
8. Christensen, R. W., and Wu, T. H. Analysis of Clay Deformation as a Rate Process. Jour. Soil Mech. and Found. Div., ASCE, Proc. Paper 4747, p. 125-157, Nov. 1964.
9. Fang, H. Y. Influence of Temperature and Other Climatic Factors on Performance of Soil-Pavement Systems. HRB Spec. Rept. 103, p. 173-185, 1969.
10. Glasstone, S., Laidler, K., and Eyring, H. The Theory of Rate Processes. McGraw-Hill, New York, 1941.
11. Harris, F. E., and O'Konski, C. T. Dielectric Properties of Aqueous Ionic Solutions at Microwave Frequencies. Jour. Phys. Chem., Vol. 61, p. 310, 1957.
12. Laguros, J. G. Effect of Temperature on Some Engineering Properties of Clay Soils. HRB Spec. Rept. 103, p. 186-193, 1969.
13. Litvinov, I. M. Stabilization of Settling and Weak Clayey Soils by Thermal Treatment. HRB Spec. Rept. 60, p. 94-112, 1960.
14. Lo, K. Y. Secondary Compression of Clays. Jour. Soil Mech. and Found. Div., ASCE, Vol. 87, No. SM4, Proc. Paper 2885, p. 61-66, 1961.
15. Low, P. F. Physical Chemistry of Clay-Water Interaction. Advances in Agronomy, Vol. 13, p. 269-327, 1961.
16. Mitchell, J. K. Shearing Resistance of Soils as a Rate Process. Jour. Soil Mech. and Found. Div., ASCE, Vol. 90, No. SM1, Proc. Paper 3773, p. 29-61, Jan. 1964.
17. Mitchell, J. J., Campanella, R. G., and Singh, A. Soil Creep as a Rate Process. Jour. Soil Mech. and Found. Div., ASCE, Vol. 94, No. SM1, Proc. Paper 5751, p. 231-253, Jan. 1968.
18. Mitchell, J. K., Singh, A., and Campanella, R. G., Bonding, Effective Stresses, and Strength of Soils. Dept. of Civil Engineering, Univ. of California, Berkeley, 1968.
19. Murayama, Sakuro. Effect of Temperature on the Elasticity of Clays. HRB Spec. Rept. 103, p. 194-203, 1969.
20. Murayama, S., and Shibata, T. On the Rheological Characters of Clay, Part I. Bull. No. 26, Disaster Prevention Research Institute, Kyoto Univ., Japan, 1958.
21. Murayama, S., and Shibata, T. Rheological Properties of Clays. Proc. Fifth Internat. Conf. on Soil Mech. and Found. Eng., Paris, Vol. I, p. 269-273, 1961.
22. Murayama, S., and Shibata, T. Flow and Stress Relaxation of Clays. Proc. Rheology and Soil Mech. Symposium of IUTAM, Grenoble, France, p. 99-129, Apr. 1964.
23. Noble, C. A., and Demirel, T. Effect of Temperature on Strength Behavior of Cohesive Soil. HRB Spec. Rept. 103, p. 204-219, 1969.
24. Paaswell, R. E. Transient Temperature Influences on Soil Behavior. HRB Spec. Rept. 103, p. 220-230, 1969.
25. Plum, R. L., and Esrig, M. I. Some Temperature Effects on Soil Compressibility and Pore Water Pressure. HRB Spec. Rept. 103, p. 231-242, 1969.
26. Post, J. L., and Paduana, J. A. Soil Stabilization by Incipient Fusion. HRB Spec. Rept. 103, p. 243-253, 1969.
27. Richards, B. G. Pavement Temperatures and Their Significance in Australia. HRB Spec. Rept. 103, p. 254-266, 1969.
28. Schiffman, R. L., Ladd, C. C., and Chen, A. T. Secondary Consolidation of Clay. Proc. Rheology and Soil Mech. Symposium, Grenoble, Springer-Verlag, 1966.
29. Sherif, M., and Burrous, C. M. Temperature Effects on the Unconfined Shear Strength of Saturated Cohesive Soil. HRB Spec. Rept. 103, p. 267-272, 1969.

30. Takashi, Tsutomu. Influence of Seepage Stream on the Joining of Frozen Soil Zones in Artificial Soil Freezing. HRB Spec. Rept. 103, 273-286, 1969.
31. Van Olphen, H. An Introduction to Clay Colloid Chemistry. Interscience Publishers, New York.
32. Wölhbier, H., and Henning, D. Effect of Preliminary Heat Treatment on the Shear Strength of Kaolinite Clay. HRB Spec. Rept. 103, 287-300, 1969.

Part II

THERMAL CHARACTERISTICS OF SOILS, THERMODYNAMICS OF SOIL SYSTEMS, FLUID FLOWS, AND FROST ACTION

FOREWORD TO PART II

The general report by Duwayne M. Anderson covers the eight papers in this part. Two of these deal mainly with the thermodynamics of soil systems touching on both the granular nature and the soil water. Thermo-osmosis is also covered by two papers, each of which raises questions about the phenomena involved and presents for consideration a solution containing a three-component flow gradient concept. Both of the papers relating to frozen soils point up the need for more data and theory on the mechanical properties of frozen and thawing soils. The importance of the specific surface area of soils as a parameter for engineering consideration is emphasized. Discussions of temperature effects on soil properties and heat conduction in granular materials include views on the thermal resistance of interfaces.

Effects of Heating on the Swelling of Clay Minerals

L. A. G. AYLMORE, J. P. QUIRK, and I. D. SILLS
Department of Soil Science and Plant Nutrition, University of Western Australia

The effects of dehydration by evacuation and heating to progressively higher temperatures up to 400 C on the subsequent hydration and swelling behavior of homoionic predominately illite clay minerals has been studied. Water vapor sorption isotherms for 200-mg tablets at 25 C were determined using a volumetric doser technique, and swelling of the clays at low water suctions was measured on ceramic suction plates.

The swelling of certain illitic clays is subject to a marked reduction (e. g., from 200 percent to 35 percent water content at 10 millibars suction) after preheating, indicating the formation of very strong binding forces between individual clay particles. Although water vapor sorption at low relative vapor pressures shows that part of the water loss on heating is irreversible, it seems unlikely that any deterioration of the crystal lattice has occurred at the temperatures used. The cation exchange capacities of the clays are unaltered, and the specific surface areas are essentially the same after heating.

The nature of the bonding mechanism is not yet clear, but there is evidence that small amounts of kaolinite impurities present may be involved. It seems likely that the formation of hydrogen bonds between silicate and aluminate surfaces can occur on complete removal of the adsorbed water molecules.

•IT HAS been known for some time that heating can markedly alter the physicochemical behavior of clay mineral systems. Such techniques have been used to some extent in road research (9, 10) and also in agriculture to increase the stability of surface soils. Heating to temperatures in excess of 600 C generally results in at least some irreversible destruction of the crystal lattice with consequent deterioration in sorptive properties. However, there is a substantial amount of data to indicate that the hydrophilic properties of certain clay minerals are modified quite appreciably by desorption long before there is any significant lattice deterioration.

The data of Mooney, Keenan, and Wood (14) and others for montmorillonite show that subsequent rehydration at low relative humidities can depend markedly on the severity of the predrying technique used to obtain an "oven-dry" weight. This is largely a result of the influence of the hydration energy of the exchangeable cations on the intercalation of water. Similarly, Martin (13) and Jurinak (11) found that the sorption of water at low relative vapor pressures by kaolinite clays was influenced by preheating to temperatures up to 300 C and attributed these effects to interparticle adhesion.

During detailed studies of water sorption and swelling by clay mineral systems it was observed that the swelling of certain clays was considerably reduced by the outgassing procedure used in the determination of specific surface area and pore size distribution by low-temperature nitrogen adsorption (3). The ability of montmorillonite clays to exhibit extensive crystalline swelling [d(001) > 40 Å] at low water suctions when sodium-saturated was found to be essentially unaltered by preheating even as high as 600 C. Similarly, the relatively small swelling exhibited by kaolinite clays even when sturated with water (2) was unaffected. In contrast, several samples of clays containing predominantly illite minerals showed large reductions in swelling after desorption. This effect has been examined in some detail in the present paper.

MATERIALS AND METHODS

The clay samples used were obtained from the following natural deposits:

•Willalooka illite—B horizon from a solonized solonetz, Hundred of Laffer, South Australia.

•Urrbrae B clay—B horizon of Urrbrae loam, a red-brown earth, Adelaide, South Australia. Clay fraction 60 percent illite and 40 percent kaolinite.

•Fithian illite—from Ward's Natural Science Establishment Inc., Illite No. 35 of the American Petroleum Institute's Research Project No. 49 (1951).

•Rocky Gully kaolinite—from pallid zone of laterite, Rocky Gully, Western Australia.

In general, samples of the clays were sodium-saturated by repeated washing with molar sodium chloride, during which the pH of the suspension was adjusted to 3.0 using hydrochloric acid. The samples were washed and finally dialyzed against distilled water using Visking cellulose casing. Initially a simple decantation process was used to remove the coarse fractions. These samples are labeled R. F. to indicate the rough fractionation used. Subsequently the $< 2\mu$ fractions were obtained by accurate sedimentation. Samples saturated with other cations were prepared from these materials using the appropriate molar chloride solution.

The air-dried clays were gently ground to a powder, equilibrated with 0.75 relative water vapor pressure, and compressed into 200-mg cores at 1200 atmospheres pressure by means of a hydraulic jack (1). This was done to facilitate subsequent experimental handling and to ensure that the clays were in an overconsolidated condition.

Heating of the clays was carried out by allowing a number of cores in weighing bottles to equilibrate for 3 days at a given temperature in a muffle furnace and cooling the ground glass stoppered bottles over phosphorus pentoxide powder before weighing.

Water content-energy data at low suctions were obtained using ceramic-perspex pressure plate systems. The cores were wet up in small stages using vacuum desiccators containing saturated salt solutions to prevent disruption of the cores by rapid differential swelling.

Surface areas were determined by application of the B. E. T. theory (7) to low-temperature nitrogen adsorption isotherms determined volumetrically in the usual way. Water vapor sorption isotherms were determined volumetrically in equipment similar to that used by Jurinak (11) incorporating a modified Pearson gage (16).

Cation exchange capacities were obtained by first saturating the clays using a neutral solution of molar strontium bromide and removing excess salt by washing with distilled water. The exchange capacities were then determined as the difference between the strontium and bromide contents of the dried clays determined using an X-ray fluorescence spectrographic method.

RESULTS AND DISCUSSION

The specific surface areas and cation-exchange capacities of the clay cores are given in Table 1. In Table 2 the decrease in weight of the Willalooka illite and Urrbrae

TABLE 1

SPECIFIC SURFACE AREAS AND CATION EXCHANGE CAPACITIES OF CLAY MATERIALS

Clay	Specific Surface Area (m^2/g)	Cation Exchange Capacity (me/100 g)
Willalooka illite (R. F.)	150	39.1
Willalooka illite ($< 2\mu$)	188	—
Urrbrae B clay (R. F.)	91	27.6
Fithian illite ($< 2\mu$)	99	—
Rocky Gully kaolinite ($< 2\mu$)	39.3	4.0

TABLE 2

WEIGHT LOSS BETWEEN SUCCESSIVE TEMPERATURES AND 400 C FOR ILLITIC CLAYS

Clay	Weight Loss (g/100 g clay at 400 C)			
	20 C	110 C	200 C	300 C
Ca^{++} Willalooka illite	16.39	4.92	2.47	1.22
Mg^{++} Willalooka illite	21.07	4.82	2.36	1.20
Na^{+} Willalooka illite	18.47	4.58	2.28	1.21
K^{+} Willalooka illite	17.36	3.89	1.87	1.10
Ca^{++} Urrbrae B clay	12.83	3.71	1.67	0.75
Mg^{++} Urrbrae B clay	13.07	3.92	1.80	0.85
Na^{+} Urrbrae B clay	13.47	3.27	1.58	0.80
K^{+} Urrbrae B clay	11.27	3.24	1.53	0.73

B clay cores between successive temperatures and 400 C has been expressed as a percentage on the basis of the weight of clay after drying to 400 C. The possible sources of weight loss on heating are surface-adsorbed water, water of hydration of the exchangeable cations, hydroxonium ions in interlayer positions normally occupied by potassium ions in unweathered micas (6), and hydroxyl groups from the clay lattice. Some weight loss may also occur from the charring of any organic matter present but this is relatively small in these materials. In general, the water contents from 110 C to higher temperatures show some relationship to the hydration energies of the exchangeable cations and the specific surface areas of the clays but the variation between different ions is not as large as might be expected if the weight losses were entirely associated with dehydration of the exchangeable cation [see Table 1 in Keenan, Mooney, and Wood (12)].

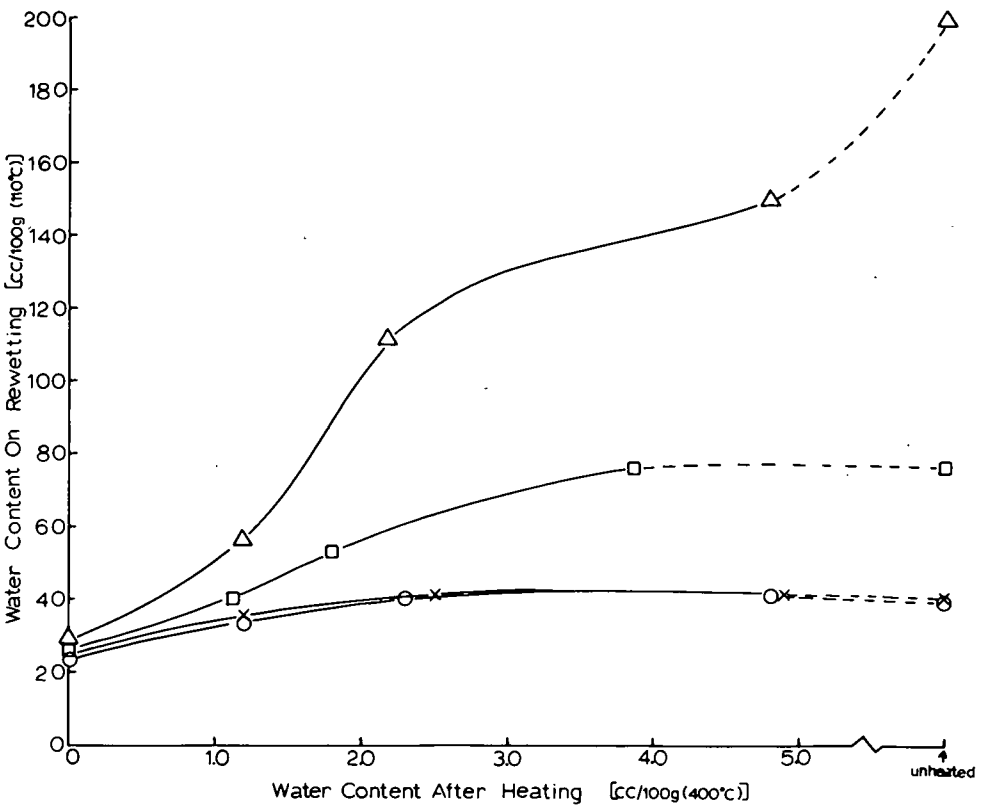

Figure 1. Water contents (cc/100 g at 110 C) for Willalooka illite cores saturated with sodium (△), potassium (□), calcium (X), and magnesium (O) cations on rewetting at 100 mB suction vs initial water content (cc/100 g at 400 C) after preheating to various temperatures.

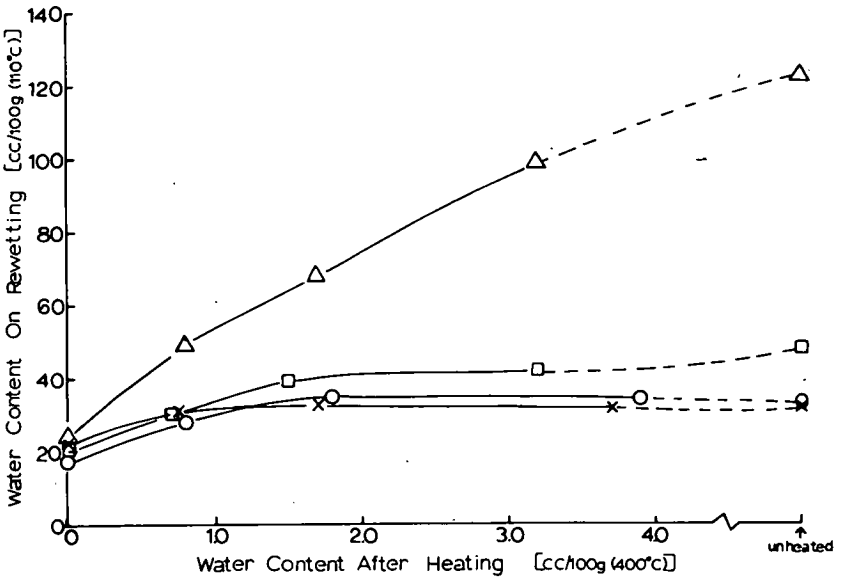

Figure 2. Water contents (cc/100 g at 110 C) for Urrbrae B cores saturated with sodium (Δ), potassium (□), calcium (X), and magnesium (O) cations on rewetting at 100 mB suction vs initial water content (cc/100 g at 400 C) after preheating to various temperatures.

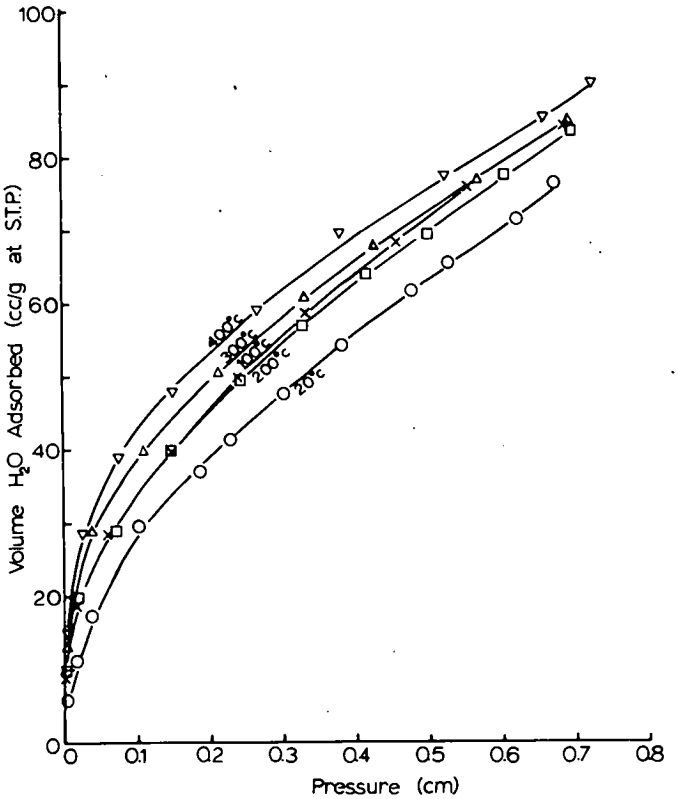

Figure 3. Water vapor adsorption isotherms at 25 C for sodium Willalooka illite degassed at various temperatures.

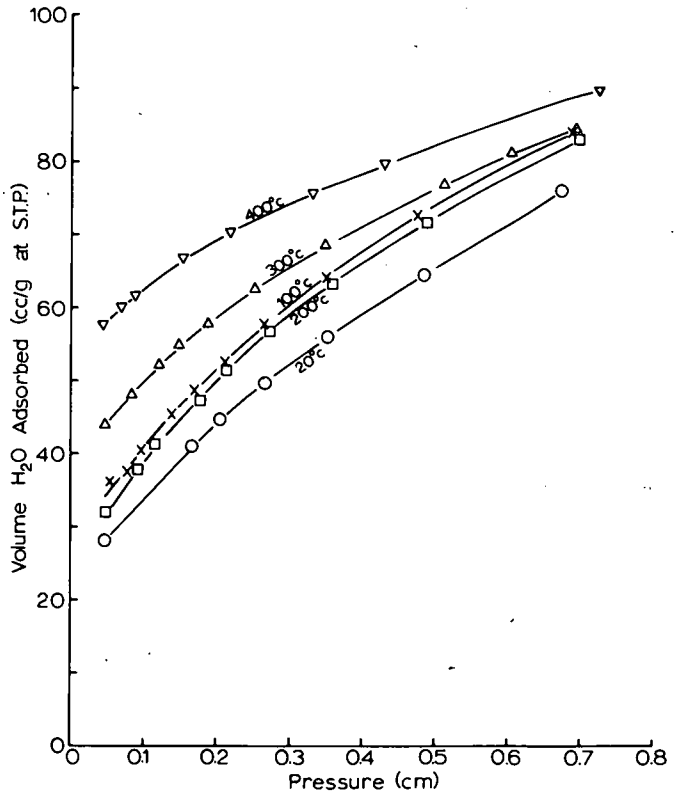

Figure 4. Water vapor desorption isotherms at 25 C for sodium Willalooka illite degassed at various temperatures.

The water contents on wetting the cores against 100 millibars (mB) suction after heating to successively higher temperatures up to 400 C, calculated on the subsequent oven-dry (110 C) basis, are shown in Figures 1 and 2 for Willalooka illite and Urrbrae B clay cores respectively when saturated with sodium, potassium, calcium, and magnesium cations. At this low suction the differences in swelling due to the exchangeable cation and increasing heat treatments become most apparent. For both clays the cores saturated with divalent magnesium and calcium cations, although unaffected by preheating to 200 C, show appreciable reductions in swelling after preheating to higher temperatures. The cores saturated with monovalent cations, and in particular those sodium-saturated, show a marked continuous reduction in swelling with increasing temperature. The large swelling of the unheated sodium clays can be attributed to the unrestrictricted development of diffuse ionic double layers. However, previous work (1) has indicated that there is an electrostatic potential barrier restricting the swelling of these clays when saturated with polyvalent ions. It is apparent that the restrictions due to the heating process either enhance or exceed these restrictions.

The cause of these restrictions is not immediately apparent. Grim (8), in reviewing the dehydration properties of illites used by numerous workers, indicates that there is no loss of structure even with the loss of hydroxyl groups until temperatures exceed 850 C. In addition, Brooks (5) found that the surface area of an illite clay was essentially constant after the loss of surface-adsorbed water and cation hydration water, until temperatures in excess of 600 C were reached. In Figures 3 and 4 are shown water sorption and desorption isotherms obtained on sodium-saturated Willalooka illite cores outgassed at various temperatures until the pressure in the volumetric system remained below 10^{-3} mm mercury after 30 minutes isolation from the pumps. Since

these isotherms were obtained on the < 2μ fraction of the clay and the clays were heated under vacuum there is of course no direct correspondence in weight loss at a particular temperature between these and the previous samples. Evacuation should result in greater dehydration at any given temperature.

The adsorption isotherms (Fig. 3) are of similar shape with the main vertical displacement occurring between outgassing at room temperature (20 C) and at 100 C. The additional water uptake obtained on the 100 C sample above the uptake after outgassing at 20 C is essentially equivalent to the additional loss of 2.7 cc at STP that occurs on heating from 20 C to 100 C. The weight loss to this stage is thus probably due largely to a reversible dehydration of the surface and cations. On further outgassing at 200 C the subsequent water uptake is slightly less and this may be attributed to a small drop in specific surface area resulting from a more intimate contact of the clay crystals on removal of the last water molecules most strongly held between regions of closest approach. Both Martin (13) and Jurinak (11) have reported such a loss of surface area. Also a decrease in B. E. T. nitrogen area of some 5 to 10 percent on desorption between 100 C and 200 C for Willalooka illite has been repeatedly observed by the authors in studies on the surface area of clays with presorbed water (4).

The weight losses on outgassing at temperatures above 100 C are far greater than those regained on subsequent water sorption. These values are given in the following table for convenience in comparing with Figures 3 and 4:

Temperature	100 C	200 C	300 C	400 C
Water loss (equivalent cc at STP/g)	2.7	16.3	25.1	47.3

The increases in subsequent water uptake observed after outgassing at 300 C and 400 C required considerably longer times for equilibration; this and the increased hysteresis effect on desorption (Fig. 4) suggest that these weight losses could be due to the loss of hydroxonium or hydroxyl ions from within the clay lattice. However, it is apparent that at least part of this loss is regained under these conditions.

Thus it seems unlikely that the reduction in swelling on heating can be attributed to deterioration of crystal structure or marked changes in the sorptive properties of the clay surfaces.

Since there is a decrease in surface area evident on vigorous outgassing it is reasonable to assume that the subsequent restrictions to swelling arise from the formation of bonds at the regions of contact of the individual clay crystals. A conceivable origin for strong electrostatic attractive forces at these points would be through the dehydrated cations sandwiched between the negatively charged clay crystals. However, this would require that the cation exchange capacity of the heated material be significantly reduced, and accurate measurements indicate that there is no such loss of exchangeable cations.

Martin (13) observed a decrease in the specific surface area and water uptake of kaolinite clays stored under a vacuum of 10^{-5} mm pressure for long periods and attributed this effect to twinning of the crystals in close juxtaposition. The mechanism of twin formation was considered to be hydrogen bonding between the oxygen surface of one crystal and the hydroxyl surface of its neighbor. Similarly, Jurinak (11) observed a degree of "coalescence" of kaolinite crystals after desorption that was related to the size of the exchangeable cation on the clay surface. The Urrbrae B clay used in the present work contains some 40 percent and the Willalooka illite about 2 percent kaolinite. Hence, it seems quite possible that the formation of interparticle hydrogen bonds on the removal of adsorbed water molecules may prevent the re-expansion of the domains of oriented clay particles despite the formation of diffuse ionic distributions on the surfaces. Such forces have been suggested by Aylmore and Quirk (2) as being responsible for the small swelling exhibited by kaolin clays.

TABLE 3

WATER CONTENTS ON WETTING TO 10 mB SUCTION FOR SODIUM FITHIAN ILLITE (< 2μ) SAMPLES

Treatment	Water Content (g/100 g)
Unheated	92.5
Preheated 300 C	133.9
Unheated plus 1 percent Rocky Gully kaolinite	92.8
1 percent Rocky Gully kaolinite added and heated to 300 C	90.8

This suggestion is strongly supported by the data in Table 3 for sodium-saturated Fithian illite that X-ray examination shows to be free of kaolinite impurity. Far from restricting the swelling of this clay, heating to 400 C results in an appreciable increase in water uptake at 10 mB suction, probably through the removal of organic binding materials. The addition of 1 percent Rocky Gully kaolinite as an impurity before heating seems to cancel this increase due to the removal of organic matter. However, it is difficult to control the intimacy of mixing of the two constituents and this would obviously influence the extent of bonding that occurs.

Dimethyl sulfoxide (DMSO) has been shown to be an effective hydrogen bond breaker (15) and hence it should be possible to at least partially restore the swelling of these clays by treatment with DMSO if hydrogen bonding is in fact responsible. This possibility was investigated by shaking samples of preheated sodium Willalooka illite with a 90 percent solution of DMSO in water for periods of two weeks and two months at 60 C. The samples were washed with distilled water, air-dried and compressed into cores as before. The water contents of these DMSO-treated cores at 10 mB suction are compared in Table 4 with control cores of the unheated clay and heated samples shaken for two weeks with distilled water.

It is apparent that the DMSO treatment is not only capable of restoring the swelling capacity of the Willalooka clay but actually increases the water uptake of the heated material beyond that of the unheated clay if carred out long enough. This may indicate the presence of some restrictions in the original clay but obviously a more detailed investigation of the DMSO treatment is warranted to establish the nature of this interaction.

From the previous results it is reasonable to conclude that the presence of the kaolinite clay is responsible for the restriction to swelling observed on heating the Willalooka and Urrbrae B clay samples. It seems very likely that the formation of hydrogen bonds between oxygen and hydroxyl surfaces on the complete removal of adsorbed water is in fact the mechanism of crosslinking that occurs. Further work is at present being undertaken in an attempt to confirm these conclusions and to determine the extent of hydrogen bonding that occurs in the different systems.

TABLE 4

EFFECT OF DMSO TREATMENT ON WATER CONTENT OF SODIUM WILLALOOKA ILLITE (< 2μ) ON WETTING TO 10 mB SUCTION

Treatment	Water Content (g/100 g)
Untreated	246
Heated 300 C, shaken with water for 2 weeks	80
Heated 300 C, shaken with 90 percent DMSO for 2 weeks	154
Heated 300 C, shaken with 90 percent DMSO for 2 months	355

REFERENCES

1. Aylmore, L. A. G., and Quirk, J. P. The Structural Status of Clay Systems. Proc. Ninth Natl. Conf. Clays and Clay Minerals, Pergamon Press, New York, 1962, p. 104.
2. Aylmore, L. A. G., and Quirk, J. P. Adsorption of Water and Electrolyte Solutions by Kaolin Clay Systems. Soil Sci., Vol. 102, p. 339, 1966.
3. Aylmore, L. A. G., and Quirk, J. P. The Micropore Size Distributions of Clay Mineral Systems. Jour. Soil Sci., Vol. 18, p. 1, 1967.
4. Aylmore, L. A. G., Quirk, J. P., and Sills, I. D. The Surface Area of Clays With Preadsorbed Water. (In preparation.)
5. Brooks, C. S. Nitrogen Adsorption Experiments on Several Clay Minerals. Soil Sci., Vol. 79, p. 331, 1955.
6. Brown, G., and Norrish, K. Hydrous Micas. Miner. Mag., Vol. 29, p. 929, 1952.
7. Brunauer, S., Emmett, P. H., and Teller, E. Adsorption of Gasses in Multimolecular Layers. Jour. Amer. Chem. Soc., Vol. 60, p. 309, 1938.
8. Grim, R. E. Clay Mineralogy. McGraw-Hill Ltd., London, 1953, 237 p.
9. Gupta, G. C., and Dutta, A. K. Water Stability of Aggregates in a Heated Black Cotton Soil. Soil Sci., Vol. 104, p. 210-216, 1967.
10. Irvine, R. H. Road Making by Heat Treatment of Soils. Jour. Inst. Eng. Australia, Vol. 11, Paper No. 332, 1930.
11. Jurinak, J. J. The Effect of Pretreatment on the Adsorption and Desorption of Water Vapour by Lithium and Calcium Kaolinite. Jour. Phys. Chem., Vol. 65, p. 62, 1961.
12. Keenan, A. G., Mooney, R. W., and Wood, L. A. The Relation Between Exchangeable Ions and Water Adsorption on Kaolinite. Jour. Phys. and Coll. Chem., Vol. 55, p. 1462, 1951.
13. Martin, R. T. Water Vapor Sorption on Lithium Kaolinite. Proc Fifth Natl. Conf. Clays and Clay Minerals, Natl. Acad. Sci.-Natl. Res. Council Pub. 566, 1958, 23 p.
14. Mooney, R. W., Keenan, A. G., and Wood, L. A. Adsorption of Water Vapour by Montmorillonite: I. Heat of Desorption and Application of B. E. T. Theory. Jour. Amer. Chem. Soc., Vol. 74, p. 1367, 1952.
15. Olejnik, S., Aylmore, L. A. G., Posner, A. M., and Quirk, J. P. Infra-Red Spectra of Kaolin Mineral-Dimethyl Sulfoxide Complexes. Jour. Phys. Chem., Vol. 72, p. 241, 1968.
16. Pearson, T. G. Uber ein Manometer zur Messung niederer Drucke leichtkondensierbarer Gase. Zeitschrift Physik. Chem., Vol. A 156, p 86, 1931.

Thermal Transfer of Liquid in Porous Media

A. M. GLOBUS and B. M. MOGILEVSKY
Agrophysical Institute, Leningrad

The time rates of thermal transfer of H_2O, C_2H_5OH, C_6H_6, CCl_4, and dibutyl phthalate ($C_{16}H_{22}O_4$) were measured at early stages of experiments with closed columns of two unsaturated porous ceramics—crushed ceramsite and crushed firebrick. The measured fluxes were shown to be higher than the calculated vapor diffusion fluxes in all cases except dibutyl phthalate, whose thermal transfer was not detected.

The differences between these values do not follow the sequence of thermo-capillary film fluxes which can be induced by surface tension gradients along the air-liquid interface. Thus thermo-capillary film flow does not play an essential role in thermal mass transfer under the conditions investigated.

The analysis of the two other possible mechanisms of thermal liquid transfer—thermo-self-diffusion and thermo-osmosis in a single capillary filled with one-component polar liquid—was accomplished on the basis of irreversible thermodynamics and kinetic theory of liquids. This analysis resulted in the expression for the steady pressure difference between the ends of a non-isothermal capillary.

•IN MANY papers reviewed by Globus (6), the time rate of thermal water transfer (TWT) in unsaturated porous media was shown to be significantly higher than vapor diffusion flux calculated according to Fick's law, with allowance for temperature-dependence of vapor pressure and diffusivity, tortuosity factor, and water-free porosity (16). Generally speaking, this is not surprising because of the existence of several mechanisms actuating thermal liquid transfer. Among these mechanisms are thermo-capillary meniscus flow due to the difference of Laplace pressure induced by temperature gradient, thermo-capillary film flow (4) due to surface tension gradients along air-liquid interface, thermo-osmosis (3, 17), and thermo-self-diffusion (1). Relative parts played by these processes in TWT are not clear, although analysis has shown (6) that thermo-capillary meniscus flow cannot explain relationships of TWT in different porous media observed experimentally.

In this paper we attempt to estimate the role of thermo-capillary film flow in TWT and discuss thermo-osmosis and thermo-self-diffusion.

THERMAL MASS TRANSFER FLUXES: TOTAL MEASURED FLUX, CALCULATED THERMAL VAPOR DIFFUSION, AND THERMO-CAPILLARY FILM FLUXES

One-dimensional thermo-capillary film flow of a liquid in porous media is described by (4)

$$q_{tf} = -\frac{\rho h^2}{2\eta}\frac{2}{3} S \frac{d\sigma}{dx} = -\frac{1}{3}\frac{\rho}{\eta}\frac{W^2}{S}\frac{\partial\sigma}{\partial T}\frac{dT}{dx} \qquad (1)$$

Here q_{tf} = time rate of thermo-capillary film flow in g/cm^2/sec; η = viscosity in g/cm/sec; $h = W/S$ = thickness of liquid film in cm; S = specific surface in cm^2/cm^3; W = moisture content on volume basis in cm^3/cm^3; T = temperature in deg C; σ = surface tension in dynes/cm; ρ = density of liquid in g/cm; and x = coordinate in cm.

TABLE 1

SOME PROPERTIES OF CERAMICS USED

Medium	Diameter of Particles, mm	Apparent Density, g/cm³	Specific Surface, cm²/cm³	Moisture-Free Porosity in Experiments cm³/cm³
Crushed ceramsite (CC)	0.5-1.0	0.60	12,400	0.71
Crushed firebrick (CB)	0.5-1.0	0.63	3,300	0.70

The temperature gradient-dependent vapor diffusion in a material, where vapor pressure is near saturation (closed system), can be described approximately by the equation

$$q_{tv} = -\alpha C D_a \frac{P}{P-p} \frac{\partial c}{\partial T} \frac{dT}{dx} \qquad (2)$$

where q_{tv} = time rate of temperature gradient-dependent vapor diffusion in g/cm²/sec; α = tortuosity factor (≈ 0.66) (12); C = liquid-free porosity in cm³/cm³; D_a = diffusivity of vapor in air in cm²/sec; P = barometric pressure in mm Hg; p = saturated vapor pressure in mm Hg; and c = vapor concentration in g/cm³.

It is evident that, for a given W (and consequently h and C) of a porous medium and equal temperature conditions, the magnitude of thermo-capillary film flow is proportional to

$$\zeta = \frac{\rho}{\eta} \frac{\partial \sigma}{\partial T}$$

and the magnitude of temperature gradient-dependent vapor diffusion relates linearly to

$$\xi = \frac{D_a}{P-p} \frac{\partial c}{\partial T}$$

Choosing substances whose ζ and ξ form different sequences and comparing calculated fluxes with the observed ones, it is possible to attempt to determine if any particular mechanism dominates in each case.

Here the results are reported concerning thermal transfer of H_2O, C_2H_5OH, C_6H_6, CCl_4 and dibutyl phthalate ($C_{16}H_{22}O_4$) in two model porous ceramic media—crushed ceramsite (CC) and crushed firebrick (CB)—investigated earlier (7).

EXPERIMENTAL

Some properties of the porous media are given in Table 1 and properties of fluid substances appropriate to their vapor and liquid transfer are given in Table 2.

TABLE 2

CHARACTERISTICS OF H_2O, C_2H_5OH, C_6H_6, CCl_4, AND $C_{16}H_{22}O_4$ INFLUENCING THEIR VAPOR DIFFUSION AND THERMO-CAPILLARY FLOW

Substance	η, g/cm/sec	ρ, g/cm³	$\partial\sigma/\partial T$, dynes/cm/deg C	$\frac{\rho}{\eta}\frac{\partial\sigma}{\partial T} \times 10^2$	P, mm Hg	$D\sigma$, cm²/sec	$\partial c/\partial T$, g/cm³ C	$\frac{DP}{P-p}\frac{\partial c}{\partial T} \times 10^7$
H_2O	0.86	1.00	0.157	18.2	27	0.27	0.13	3.62
C_2H_5OH	1.06	0.79	0.091	6.8	68	0.12	0.82	10.8
C_6H_6	0.58	0.88	0.137	20.7	105	0.09	2.06	21.5
CCl_4	0.88	1.61	0.110	20.1	131	0.09	3.60	38.9
$C_{16}H_{22}O_4$	20.0	1.05	–	–	1×10^{-4}	–		1×10^{-5}

No values of the surface tension-temperature relationship and of the vapor diffusivity of dibutyl phthalate are at our disposal, and thus no calculations have been made for this substance. However, it was felt that, because of the negligible vapor pressure, its thermal mass transfer (TMT), if it exists, can be ascribed to the liquid flow.

Experimental determinations of TMT time rates were accomplished following the method described earlier (6) for a temperature difference of 22-32 C and a steady temperature gradient of 1.0 C/cm.

Observations on the TMT kinetics in the closed horizontal cylindrical columns used in the experiments have shown that, in some range of initial moisture content W_i, the gradient of W in the middle section of a column is negligibly small at an early stage of the experiment. Transferred mass quantity increases nearly linearly with time during that period of a run. Because of constancy of W, T, and dT/dx, a mean time rate during this stage of the experiment may be taken as a true time rate of TMT at first approximation and used for comparison between the fluxes of different substances.

The TMT fluxes of H_2O, C_2H_5OH, C_6H_6, and CCl_4 were determined experimentally for a W_i of 6-8 percent. The values obtained were compared with those calculated according to Eqs. 1 and 2. When using these equations one needs to introduce some approximations. Thus, when calculating h, the authors of Eq. 1 supposed all the liquid to be distributed uniformly on the surface of solid particles. However, actually a part of the liquid is in wedges around the contacts of particles and it is impossible to compute a share of film moisture for non-ideal systems. The use of the supposition mentioned leads to overestimation of h and q_{tf}. A part of the film adjacent to the solid surface is probably more viscous than the bulk liquid, which also induces overestimation of q_{tf}. Due to a deviation of actual film surface from the direction of temperature gradient, the effective value of the latter is smaller than the overall gradient entering the equation. Further, Eq. 1 must include only the available surface, not the total surface, as a path for the liquid flow. However, we do not know any reliable method for its estimation for the media as used. In our calculations we used total specific surface measured by adsorption of water vapor (10). For h determined independently of S it leads to overestimation of q_{tf}, but for the adopted method it may cause some underestimation of q_{tf}, which probably is outweighed by the former factors. But since the initial moisture contents for all the liquids were made equal, the computed values of q_{tf} can be compared among themselves even though their absolute magnitudes are not true. Doing so, we suppose the differences in distribution of each liquid between film and wedges and in the thickness of immovable film to be insignificant.

When using Eq. 2, we accounted for the presence of dead-end pores in CC by introducing a factor calculated with the help of diffusivities of CO_2 measured experimentally.

RESULTS AND DISCUSSION

In Table 3 the time rates of TMT observed for the substances studied (q_e) are given along with those calculated according to Eqs. 1 and 2. Figure 1 shows net TMT in the closed systems as a function of W_i.

We could detect no measurable TMT of dibutyl phthalate even in very long runs (10 days).

As can be seen from Table 3, thermal transfer rates larger than those calculated according to Fick's law are appropriate not only to water but to all the substances transferred. When written in the order of their magnitudes, the values of observed TMT fluxes form a sequence similar to that of their fluxes computed according to Eq. 2, i.e., temperature gradient-dependent vapor diffusion. The ratios q_e/q_{tv} are not constant, however, and tend to decrease with the increase of q_{tv}. It may partially be explained by the fact that larger values of q_e relate to the substances whose vapor pressures in experiments could be somewhat lower than the saturated pressure. Nevertheless it is reasonable to suppose that if the excess of q_e over q_{tv} were caused by the existence of thermo-capillary film flow, the differences (q_e - q_{tv}) for all the substances should form the same sequence as the values of q_{tf} for these substances.

As Table 3 shows, this is not the case. This may be interpreted as evidence of an insignificant part played by the thermo-capillary film flow in TMT under the conditions

TABLE 3

COMPARISON BETWEEN OBSERVED (q_e) AND COMPUTED TIME RATES OF THERMAL TRANSFER OF H_2O, C_2H_5OH, C_6H_6, AND CCl_4 IN CRUSHED CERAMSITE AND CRUSHED FIREBRICK

(dT/dx = 1.0 C/cm, T = 22-32 C)

Substance	q gm/cm²/sec × 10⁶								q_e/q_{tv}		$(q_e - q_{tv}) \times 10^6$	
	Crushed Ceramsite (CC)				Crushed Firebrick (CB)							
	Eq. 1	Eq. 2	Eqs. 1 + 2	Experimental	Eq. 1	Eq. 2	Eqs. 1 + 2	Experimental	CC	CB	CC	CB
H_2O	3.14	0.14	3.28	0.70	8.18	0.18	8.36	0.89	5.0	4.9	0.56	0.71
C_2H_5OH	1.17	0.36	1.53	0.94	3.04	0.47	3.51	1.20	2.6	2.6	0.58	0.73
C_6H_6	3.56	0.75	4.31	1.27	9.29	0.98	10.27	1.76	1.7	1.8	0.52	0.78
CCl_4	3.44	1.34	4.78	1.98	9.02	1.77	10.79	3.03	1.5	1.7	0.64	1.20

of the experiment. Net TMT in closed systems depending on the ratio of thermal isothermal permeabilities of a medium increases with

$$\xi = \frac{Da}{P - p} \frac{dc}{dT}$$

and so does the range of W_i where net TMT occurs. The results suggest that, under the conditions studied (low to medium moisture content, low specific surface), vapor diffusion, probably with vapor-liquid interaction (13), is an essential element of processes which secure increased time rate of TMT, and that thermo-capillary liquid flow exerts little, if any, influence on the process investigated.

It should be noted that ratios q_e/q_{tv} are greater for H_2O and C_2H_5OH, both substances having molecules of high polarity. This property influences the degree of orientation of the liquid layer adjacent to the solid surface and thermodynamic characteristics of these layers may favor thermo-osmotic liquid flow (3).

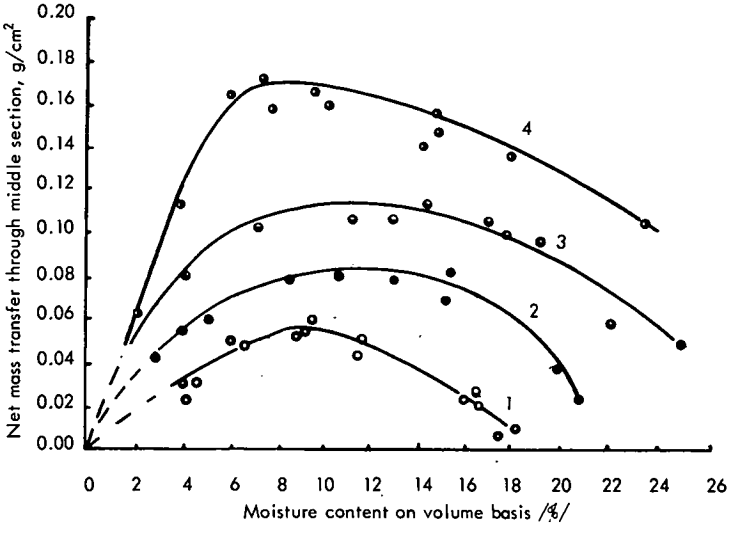

Figure 1. Net thermal transfer of several substances in granular porous ceramic (crushed firebrick): 1—H_2O, 2—C_2H_5OH, 3—C_6H_6, 4—CCl_4.

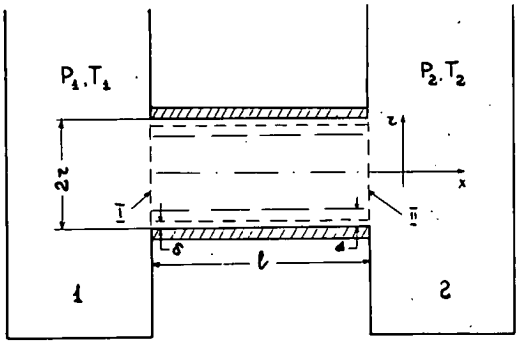

Figure 2. Capillary model.

THERMO-SELF-DIFFUSION AND THERMO-OSMOSIS OF LIQUID

In the second part of this paper we consider the thermo-osmosis and thermo-self-diffusion of liquids as probable mechanisms of TMT in porous media.

Here we consider thermo-osmosis (3) and thermo-self-diffusion in a model capillary system comprising (Fig. 2) a cylindrical capillary filled with one-component liquid and placed between two vessels, 1 and 2, where pressure P and absolute temperature T are different. In our discussion we will use the "hole theory" of liquids (5). From the point of view of this theory a liquid flow through the capillary along which there is a steady temperature field includes "molecular" (diffusion) and "bulk" components.

"Molecular" flow is due to translocations of molecules caused by the gradient of chemical potential and temperature. Considering these translocations as discrete jumps of molecules or their associates (coordinated groups) in adjacent "holes," the molecular components of the flux may be expressed with the help of the well-known equation of irreversible thermodynamics (8):

$$j_M = L_M \left(X_M + Q_M^* X_q \right) \tag{3}$$

Here L_M = the phenomenological coefficient; Q_M^* = heat of transfer of liquid per particle, which is equal to the translation movement activation energy of molecules of a liquid; and X_M and X_q = thermodynamic forces:

$$X_M = - \frac{[\text{grad } \mu]_T}{T}$$

$$X_q = - \frac{\text{grad } T}{T^2}$$

where μ_M = the chemical potential of particles of a liquid.

The "bulk" component of the flux is a well-correlated movement of particles due to the external force field. This flux is equal to

$$j_B = n_M \, u\,[r]$$

where u[r] = the radial distance-dependent velocity of liquid flow due to the pressure gradient, grad p; this velocity can be determined from the equation

$$\eta \text{ div grad } u[r] = \text{grad } p \tag{4}$$

and where n_M = concentration of particles of a liquid per unit volume and η = viscosity of a liquid. Thus, total flux is $j = j_M + j_B$, and total flow $I = I_M + I_B$ is found by integration over the section area of a capillary.

Let us consider now the influence of interaction between the liquid and capillary walls on the molecular components of mass flow. In general, energy characteristics of particles of a liquid are modified owing to such an interaction. The interaction forces weaken rapidly with the distance from the wall; thus, changed properties are appropriate to a thin layer of thickness d adjacent to the wall.

Molecular transfer of a liquid can take place both in the bulk and in the boundary layer d. Consequently, I_M may be represented approximately (taking into account the

absence of distinct boundary) as a sum of two components: one characterizing the flow in the boundary layer and the other describing the flow in the remaining volume.

Now we define Eq. 3 with the help of grad p_c and grad T only, considering μ as a function p, T, and n_h where n_h = volume concentration of holes defined in its turn by the local values of p and T. Here the pressure gradient in a capillary, grad p_c, does not equal $(P_1 - P_2)/l$ (where l = length of a capillary) because of a pressure jump in boundary zones 1 and 2 (Fig. 2) occurring due to the modified energy characteristics of a liquid in the near-wall boundary layer. We assume zones 1 and 2 degrade to flat surfaces separating a capillary from vessels 1 and 2.

At surfaces 1 and 2 the condition of equality of the particles' chemical potentials in the capillary and outer volumes is satisfied. Meantime the chemical potential in the vessels, μ_V, is defined by temperature and pressure only, whereas in a capillary the particles' chemical potential, μ_c, depends on the distance from the wall (R-r) as well.

Let us find $(p_{2c} - p_{1c})$, supposing the pressure difference to be small and using expansion of μ about P_1:

$$\text{grad } p_c = \text{grad } p + \frac{S[r]}{v_b} \text{ grad } T \tag{5}$$

where $S[r] = S_c[P_1, r] - S_b[P_1]$; S = entropy; and v_b = specific volume (per particle).

Further, using grad p_c from Eq. 5, the total molecular flow, $I_M = I_M^b + I_M^d$, is

$$I_M = - \sigma_{MP} \text{ grad } p - \sigma_{MT} \text{ grad } T \tag{6}$$

$$\sigma_{MP} = - \pi R^2 D_b \left(\frac{\partial \mu}{\partial n_h} \right)^{-1} \Psi_{MP}^b + 2 \frac{d}{R} \xi \left(\frac{\partial \mu}{\partial n_h} \right)^{-1} \Psi_{MP}^d \tag{7}$$

$$\sigma_{MT} = - \pi R^2 D_b \left[\left(\frac{\partial \mu}{\partial n_h} \right)^{-1} \left(\frac{Q_b^*}{T} + f_T^b \right) + 2 \frac{d}{R} \xi \left(\frac{\partial \mu}{\partial n_h} \right)^{-1} \left(\frac{Q_h^*}{T} + f_T^d \right) \right] \tag{8}$$

where $f_T^{b,d} = \frac{\partial \mu}{\partial n_h} \frac{\partial n_h}{\partial T} + \frac{\overline{\Delta S}}{v_b} \frac{\partial \mu}{\partial n_h} \frac{\partial n_h}{\partial p} + \frac{\overline{\Delta S}}{v_b} \frac{\partial \mu}{\partial p}$; $\xi = \frac{D_d}{D_b}$; and

$$\Psi_{MP}^{b,d} = \frac{\partial \mu}{\partial n_h} \frac{\partial n_h}{\partial p} + \frac{\partial \mu}{\partial p}$$

The first term in parentheses in Eqs. 7 and 8 was deduced as a sequence if averaging over the volume of a capillary; the second term is due to averaging over the layer d and, on the basis of the kinetic theory of liquid, the transition was accomplished from L to self-diffusivity D.

Now let us consider the bulk component of the total liquid flow in a capillary,

$$I_B = \frac{-2\pi}{v_b} \int_0^R u[r] \, dr$$

The value of u can be deduced from Eq. 4 using grad p_c from Eq. 5. The first term in the right part of Eq. 5 depends only upon P, the second one upon T; thus the total flow I_B can be split into two components:

$$I_B = I_B^P + I_B^T$$

where I_B^P = Poiseuille's flow due to the pressure difference, and I_B^T = thermo-osmotic flow due to the difference in thermodynamic properties:

$$I_B^P = -\sigma_{BP} \text{ grad } p$$
$$\sigma_{BP} = \frac{\pi R^4}{8 v_b \eta} \tag{9}$$

The component I_B^T depends upon grad T and is defined by the actual form of the relationship of $\Delta S[r]$:

$$I_B^T = -\sigma_{BT} \text{ grad } T \tag{10}$$

$$\sigma_{MT} = \frac{2\pi}{\eta v_b^2} \int_0^R r dr \int_0^R \frac{dr'}{r'} \int_0^{r'} \Delta S[r''] \, r'' \, dr'' \tag{11}$$

Considering μ = constant in the section perpendicular to capillary axis, we write

$$S[r] = \frac{\Delta h[r]}{T} \tag{12}$$

where $\Delta h[r]$ = difference of enthalpy for particles situated at (R - r) distance from the wall and particles which are sufficiently far from the layer d.

If the interaction potential changes with the distance from the wall according to $(R - r)^{-m}$, then (5)

$$\Delta h[r] = \frac{\gamma}{(R - r)^{m-3}} \tag{13}$$

Here $\gamma = \gamma_{1,2} - \gamma_{2,2}$, where γ is the force constant of the particles' interaction; $\gamma_{1,2}$ characterizes the interaction between particles of the liquid and the capillary wall, and $\gamma_{2,2}$ is the interaction between the particles themselves (we suppose the distance dependence of the particles' potential to be the same for both interactions). The maximum τ is equal to $(R - \delta)$, where δ is the minimum interparticle distance, i.e.,

$$(\Delta h)_{max} = -\frac{\gamma}{\delta^{m-3}}$$

Using Eq. 13 in Eq. 12 and inserting the result into Eq. 11, we obtain, after integration up to $(R - \delta)$ (instead of R), when neglecting terms that depend upon δ^3 and its higher powers,

$$\sigma_{BT} = \frac{\pi R^2 \delta^2 (\Delta h)_{max}}{(m - 4)(m - 5) v_b^2 \eta T} \tag{14}$$

Thus, the total flow through the capillary is

$$I = I_M + I_B = -\left(\sigma_{MP} + \sigma_{BP}\right) \text{grad } p - \left(\sigma_{MT} + \sigma_{BT}\right) \text{grad } T$$

At steady state, when I = 0, grad p and grad T are related as follows:

$$\frac{\text{grad } p}{\text{grad } T} = -\mathcal{L}$$

$$\mathcal{L} = \frac{\sigma_{MT} + \sigma_{BT}}{\sigma_{MP} + \sigma_{BP}} \tag{15}$$

Supposing each of $\frac{\partial \mu}{\partial n_h}$, $\frac{\partial n_h}{\partial T}$ and $\frac{\partial n_h}{\partial p}$ in the capillary volume to be negligibly small and adding Eqs. 7 ÷ 9 and 8 ÷ 14, we arrive at

$$\sigma_{MT} + \sigma_{BT} = -\pi R^2 k D_b \left(\frac{\partial \mu}{\partial n_b}\right)^{-1} \left[\frac{Q_e^*}{kT} - M\left(\frac{-(\Delta h)_{max}}{kT}\right)\right] \tag{16}$$

where introduction of the Boltzmann constant, k, reduces the term in brackets to a dimensionless one.

Further,

$$\sigma_{MP} + \sigma_{BP} = -\pi R^2 v_b D_b \left(\frac{\partial \mu}{\partial n_h}\right)^{-1} [1 + 2(d/R)\,\xi + N] \tag{17}$$

$$\mathcal{L} = -k/v_b \frac{\frac{Q^*}{kT} - M\left[\frac{-(\Delta h)_{max}}{kT}\right]}{1 + 2(d/R)\,\xi + N} \tag{18}$$

$$N = -\frac{R^2}{8 v_b D_b \eta} \frac{\partial \mu}{\partial n_h} \tag{19}$$

$$M = \frac{T}{(\Delta h)_{max}} \frac{\partial \mu}{\partial n_h} [1 + 2(d/R)\,\xi] + \frac{\Delta S_b}{(\Delta S_b)_{max}} + 2(d/R)\,\xi \frac{\Delta S_h}{(\Delta S_h)_{max}} + \frac{8\delta^2 N}{(m-4)(m-5)R^2} \tag{20}$$

$$Q_e^* = Q_b^* + 2(d/R)\,\xi\, Q_d^*$$

Supposing $n_M >> n_h$, we get

$$\Psi_{MP} = \frac{\partial \mu}{\partial n_h} \frac{\partial n_h}{\partial p} + \frac{\partial \mu}{\partial p} = v_b \tag{21}$$

Using the power relation of the type in Eq. 13 gives

$$\frac{\overline{\Delta S}_b}{(\Delta S)_{max}} = \frac{2}{(m-4)} d/R$$

$$\frac{\overline{\Delta S}_h}{(\Delta S)_{max}} = \frac{1}{(m-4)} \delta/d \left[1 - (\delta/d)^{m-4}\right]$$

Let us estimate $\frac{\partial \mu}{\partial n_h}$, $\frac{\partial n_h}{\partial T}$, $\frac{\partial \mu}{\partial p}$, $\frac{\partial \mu_h}{\partial p}$. Considering a liquid as a mixture of particles

of the liquid and holes we write Gibbs' free energy for liquid:

$$G = n_M g_M + n_h g_h - kT \ln \frac{(n_M + n_h)!}{n_M!\, n_h!} \tag{22}$$

where g_h = free energy of the hole.

From Eq. 22 we obtain

$$\mu_M = \frac{\partial G}{\partial n_M} = g_M + kT \ln \frac{n_M}{n_M + n_h} \tag{23}$$

$$\mu_h = \frac{\partial G}{\partial n_h} = g_h + kT \ln \frac{n_h}{n_M + n_h} \tag{24}$$

If in every microzone (in the sense of thermodynamics) there is local equilibrium in relation to the number of holes, then Eq. 22 leads to

$$n_h = \left(n_M + n_h\right) \exp\left(\frac{-g_h}{kT}\right) \tag{25}$$

$$\frac{\partial n_h}{\partial p} = -\frac{n_h v_h}{kT}$$

$$\frac{\partial n_h}{\partial T} = \frac{n_h h_h}{kT^2}$$

Here v_h is the volume of a hole, h_h is the enthalpy of the creation of a hole, and $\frac{\partial \mu}{\partial p} = v_M$ is the volume of a particle of the liquid. Then from Eq. 21,

$$\frac{\partial h}{\partial n_h} = -\frac{v_b - v_M}{v_h n_h} = -v_b kT$$

If we ascribe all the changes of the volume depending upon the changes of pressure and the temperature to the change of number of holes, then

$$dn_h = \frac{dv_b}{v_h v_b}$$

$$\frac{\partial n_h}{\partial T} = \frac{1}{v_h v_b} \frac{\partial v_b}{\partial T} = \frac{\alpha}{v_h}$$

$$\frac{\partial n_h}{\partial p} = \frac{1}{v_h v_b} \frac{\partial v_b}{\partial p} = -\frac{\beta}{v_h}$$

where α is the thermal coefficient of volume expansion, and β is the compressibility. Thus,

$$\frac{\partial \mu}{\partial n_h} \frac{\partial n_h}{\partial T} = -k \alpha T \frac{v_b}{v_h}$$

It is known (5) that $h_h = kT$ and consequently

$$\frac{\frac{\partial n_h}{\partial p}}{\frac{\partial n_h}{\partial T}} = -\frac{\beta}{\alpha} = -\frac{\upsilon_h}{\chi}$$

$$v_h = (\beta/\alpha)k$$

$$\frac{\partial \mu}{\partial n_h}\frac{\partial n_h}{\partial T} = -T\frac{\alpha^2}{\beta}v_b$$

It is possible to write

$$N = \frac{R^2 kT}{8 v_b D_b \eta} \tag{26}$$

instead of Eq. 19. Neglecting terms of order $(d/R)^3$, $(\delta/R)^3$, and higher, we have instead of Eq. 20,

$$M = \left[\frac{kT}{-(\Delta h)_{max}}\right]\frac{\alpha^2 v_b T}{k\beta} + A N \tag{27}$$

where

$$A = \frac{8\delta^2}{(m-4)(m-5)R^2}$$

in the case of Eq. 13 and

$$A = 4 d^2/R^2$$

if we consider h as a constant in the layer d, h having the value appropriate to the bulk liquid beyond this layer. Since $N >> 1$ for the majority of liquids at normal temperatures and $R \geq 10^{-6}$ cm, we can finally rewrite Eq. 18

$$\mathcal{L} = \frac{8D_b\eta}{R^2 T}\left\{\frac{Q_e^*}{kT} - M\left[\frac{-(\Delta h)_{max}}{kT}\right]\right\} \tag{28}$$

The value of $(\Delta h)_{max}$ can be estimated from the condition

$$\int_{\delta}^{\infty} \Delta h\, n_M\, dx \approx \theta \tag{29}$$

where $\theta = \theta_{la} + \theta_{ls} - \theta_{sa}$; θ_{la} and θ_{sa} are the surface tension at liquid-air and solid-air interfaces, and θ_{ls} is the same at the liquid-solid interface. For wholly wettable system $\theta < 0$.

From Eq. 29,

$$(\Delta h)_{max} = \frac{(m-4)\theta}{n_M \delta} \approx (m-4)\delta^2\theta \tag{30}$$

For $R \geq 10^{-4}$cm, $m = 6$ (Van der Waals force) $|\theta| \leq 100$ dyne/cm, $\frac{(\Delta h)_{max}}{kT} = 2 \div 3$, and consequently $M < 1$ for water.

Taking Q_e^* as equal to the activation energy of viscous flow and self-diffusion (14), i.e.,

$$Q_e^*/kT \approx 5 \div 7$$

we obtain

$$\mathcal{L} = (20 \div 40) \frac{D_b \eta}{R^2 T} \tag{31}$$

If in the system $P_1 = P_2$ at the beginning, the steady state establishes only in a certain time interval after the steady temperature gradient has set in. The magnitude of this time interval, depending on the self-diffusivity and on the characterizing dimension of a system (in this case, on the capillary length l), has the order of l^2/D. If Q_e^* and $(\Delta h)_{max}$ are of different sign—i.e. $(\Delta h)_{max} < 0$—the sign of $\mathcal{L}$ may change in the course of time, since during the first period the flow is governed by the temperature gradient-induced pressure head between the capillary ends (thermo-osmosis) and afterwards it depends mainly upon thermo-self-diffusion.

At present it is difficult to compare quantitatively the theory and experiments because of the lack of data and complexity of the systems investigated. Most of data concern polydispersed porous systems filled with electrolyte solutions, the influence of which calls for a special account in the theory. So the considerations that follow are only tentative.

Taylor and Cary (15) and Cary (2) studied thermal moisture and heat transfer in soils. They have found that in their systems Onsager's relation of reciprocity was obeyed both in saturated and unsaturated media. Habib and Soeiro (9) have found for saturated and very compacted loam $\mathcal{L}$ is of the order of 2×10^3 dynes/cm^2/grad with net thermal moisture transfer directed to a lower temperature.

One can find more details in the study by Taylor and Cary (15). During the first stage of their experiment the temperature field induced a pressure rise at the "hot" end of the column and lowering at the "cold" end. The pressure difference achieved a maximum of the order of 20 dynes/cm^2/grad; then this difference gradually changed to the opposite one having the order of 100 dynes/cm^2/grad.

Such a behavior of the system corresponds qualitatively to the theory reported, although it could be influenced by the other factors too, i.e, by the redistribution of dissolved substances.

The majority of data on the relationship between water enthalpy and moisture content of hydrophilic porous media demonstrate the lowering of h with diminishing of water film thickness (11). If this is the case, the thermo-osmotic flow must be directed to a higher temperature and induce the appropriate pressure difference. Water transfer to the lower temperature and steady state pressure difference of the reverse sign may be explained, among the other factors, by thermo-self-diffusion. Estimations with the help of Eq. 31 show that, when $R = 10^{-5}$ cm, $\mathcal{L}$ for water is of the order of 100 dynes/cm^2/grad, in semi-quantitative accordance with the data (15) if viscosity of water is assumed to be that of the bulk liquid.

The net pressure difference in the wholly filled capillary under temperature gradient is the result of a dynamic equilibrium of the three flow components: the thermo-osmotic one, I_B^T, directed to the higher temperature; the thermo-self-diffusion one, I_M^T, directed to the lower temperature; and the Poiseuille flow, I_B^P, directed opposite to the resultant of both former ones. The increased viscosity of water in the boundary layer influences mainly the thermo-osmotic component of the flow, causing its decrease.

REFERENCES

1. Ananian, A. A. The Study of Moisture Transfer and Appearance of Segregation Ice in Freezing and Frozen Soils. Tr. Gidroproekta, sb. 3, 1960, Moscow (in Russian).

2. Cary, J. W. Water Flux in Moist Soil: Thermal Versus Suction Gradients. Soil Sci., Vol. 100, No. 3, 1965.
3. Deriagin, B. V., and Sidorenkov, G. N. Thermo-Osmosis Under Normal Temperature Conditions and Its Similarity to Thermomechanical Effects in Helium—II. Doklady Akad. Nauk USSR, Vol. 32, No. 9, 1941 (in Russian).
4. Deriagin, B. V., and Melnikova, M. K. On Definition of Soil Moisture Transfer Laws. Sb. "Voprosy Agronomitcheskoi Fiziky." Selkhozizdat, Leningrad, 1956 (in Russian).
5. Frenkel, Ya. I. Kinetic Theory of Liquids. Akad. Nauk USSR, Moscow, 1945 (in Russian).
6. Globus, A. M. Study on Soil Water Movement Due to Thermal Gradient. Diss. Agrophysical Institute, Leningrad, 1962 (in Russian).
7. Globus, A. M. Influence of Apparent Density, Structure, and Nature of Solid Phase on Moisture Redistribution Due to Thermal Gradients in Closed Systems. Doklady Akad. Nauk USSR, Vol. 160, No. 1, 1965 (in Russian).
8. DeGroot, C. R., and Mazur, P. Non-Equilibrium Thermodynamics. North-Holland Publ. Co., Amsterdam, 1962.
9. Habib, P., and Soeiro, F. Migrations d'Eau dams les Sols provoquées par une Difference de Temperature. Proc. Fourth Internat. Conf. on Soil Mech. and Found. Eng., Leningrad, 1957.
10. Kutilek, M. New Method of Specific Surface Determination. Roslina Vyroba, Vol. 35, No. 6, 1962.
11. Low, P. Physical Chemistry of Clay-Water Interaction. Advances in Agronomy, Vol. 13, 1961.
12. Penman, H. L. Gas and Vapour Movement in the Soil. Jour. Agric. Sci. Vol. 31, 1940.
13. Philip, J. R., and De Vries, D. A. Moisture Movement in Porous Materials Under Temperature Gradients. Proc. Amer. Geophys. Union, Vol. 38, No. 2, 1957.
14. Robinson, R. A., and Stokes, R. H. Electrolyte Solutions. Leningrad, 1959.
15. Taylor S. A., and Cary, J. W. Analysis of the Simultaneous Flow of Water and Heat or Electricity With Thermodynamics of Irreversible Processes. Trans. Fourth Internat. Congr. Soil Sci., Amsterdam, 1961.
16. De Vries, D. A. Some Remarks on Heat Transfer by Vapour Movement in Soils. Trans. Fourth Internat. Congr. Soil Sci., Amsterdam, 1950.
17. Winterkorn, H. Fundamental Similarities Between Electro-Osmotic and Thermo-Osmotic Phenomena. HRB Proc., Vol. 27, p. 443-455, 1947.

Relationships Between the Daily Temperature Wave And the Development of the Natural Soil Profile

R. GOETZ, German Research Association, and
S. MÜLLER, State Geological Survey of Baden-Württemberg*

•IN WELL-DEVELOPED soil profiles, characterized by dislocation of clay materials, formed on loess, lime-rich moraines, and similar substrates in central and western Europe, the transition from surface to subsoil lies with impressive regularity between 30 and 40 cm below the soil surface. At the present time the question is being investigated whether causal relationships exist between this fact and the course of soil temperature. For this purpose an automatic temperature recorder has been installed in the Würmmoraine of the Rhine glacier. Measurements are made on moraine raw soil material taken from deeper unchanged layers with which sections of the natural profile on the south and north flanks of a drumlin had been replaced.

The first measurements from the 1967 growing season show a well-marked termination, at a depth of 30 to 40 cm, of the daily absorption and emission of radiant energy and of the daily march of soil temperature and circulation of soil heat. A thermally activated upper zone is differentiated at this depth from a thermally passive lower zone. In between lies an equalizing transition layer that shows a temperature maximum during the period of heat loss.

The different microclimates occurring at the northern and southern side of the drumlins and in the different seasons produce differences in degree but not in principle. According to the literature, the depth of the daily temperature wave during the summer half-year is, under otherwise comparable conditions, quite independent of soil type and vegetative cover.

THE PEDOLOGIC PROBLEM

In the transition zone between rock and atmosphere, the native rock is permeated at all joints by air and periodically also by water. A few interconnected processes transform the rock to soil. At the beginning of the weathering phase, an essential role is played by temperature changes. These cause mechanical breakup of those rocks whose mineral components have different thermal coefficients. In cold and temperate climates, mechanical comminution is achieved mostly by the expansive force of ice formation in frequent cycles of freezing and thawing. Part of the loose particles produced are transported and secondarily accumulated under the action of gravity or of glacier ice, moving water, or wind, and also through biologic processes. The latter also produce humification and biochemical transformation of the substrate. This is accompanied by an increasing contribution from solution weathering which, in humid climates, brings about a translocation of soluble bases to greater depths.

In the case of the moraines investigated by us, which are mixtures of calcareous and siliceous materials, the first phase of solution weathering is a decalcification. The remnant, left behind in the solution process, is a colloidal clayey substance that in temperate climates is at first quite mobile. This substance characterizes the fundamental process of soil formation that is of special interest in this connection: the "lessivage" or clay permeation.

*Paper translated by Hans F. Winterkorn.

The French pedologist, Duchaufour (4, p. 252ff), has for some time drawn attention to this previously little-noticed process. It occurs in central and west European soils under the influence of seepage water at neutral or slightly acid reaction of the soil solution. The lessivated colloids washed out of the surface soil layer (A-horizon), which has become impoverished in clay materials, are accumulated in the subsoil (B_t-horizon) as coatings on the granular soil constituents. Duchaufour assumes that the lessivation is due to the action of insufficiently humified, but soluble, organic substances (kryptomull) formed from vegetable residues of central European broad-leaf forests.

This process is responsible for the main soil types that we found in central and western Europe, the "sol lessivé" (Duchaufour) and the "Parabraunerde" (Mückenhausen, 9). In the nomenclature of the U.S. Soil Survey Staff (17), typical "Parabraunerde" would be a "typic Normudalf."

The lessivage is especially marked in substrates in which calcareous and silicate mineral components are mixed. Examples of these, in addition to the investigated moraines, are loess, calcareous sand stones, mixed gravels, and other mixed sediments. In soils developed on these materials, the regional soil survey in central and western Europe has encountered the interesting fact that the depth of abrupt transition, from the lessivated, mostly sandy, light grey-brown A-horizon to the underlying reddish-brown B_t-horizon with its clay enrichment, is of extraordinary constancy in all undisturbed soils and is between 30 and 40 cm. This line separates an upper soil layer that is usually poor in humus but possessed of small, loose aggregations and relatively rich in biologic activity, from a clayey subsoil, often of coarse prismatic structure, with larger water-holding capacity but with considerably less air-soil interface and consequently lesser potential for biologic activity.

During extensive mapping of forest soils in southwestern Germany, the suspicion arose that climatic factors are involved in the location of the line of separation of the two horizons, especially since it is more pronounced the warmer the regional climate. In cooler areas, the line of separation becomes an indistinct zone of transition (18). Whereas in other soil types the horizon boundaries at a depth of 30 to 40 cm are not as distinct as in the lessivated types, such boundaries are relatively frequent on loose substrates, even without lessivage—e.g., as boundary of humification on loose calcareous substrate or as boundary of brunification in the case of stunted "Braunerde" soils formed on loose rock that is poor in bases. In podsols too, the B-horizon often begins at this depth. In addition, precipitation of lime and accumulation of other substances often occur at this depth.

Because this phenomenon occurs on substrates which, though normally well-drained, may vary greatly in permeability, meteorological reasons suggested the working hypothesis that the constant thickness of the upper soil horizon could be correlated with the course of the soil temperature (11). Many soil temperature determinations from all over the globe show that the daily temperature wave reaches this depth during summer. Best evidence for this is furnished by the measurements of the Serbian meteorologist, Vujevic (19). During the years 1902-1906, he studied the course of soil temperature in a "humous soil" (probably chernozem from loess) at depth intervals of 10 cm. His results prove that the depth of penetration of the daily temperature wave during the warmest season of the year is 30 to 40 cm, and that below this, the temperature differences are damped out.

The problem is, however, complicated by the fact that a very large number of substrates are covered by allochthone layers of the same constant thickness of 30 to 40 cm. In the case of such layered substrates, the boundaries of the subsequently developed soil horizons coincide with those of the geologic strata at depth of 30 to 40 cm. This observation has caused several authors to question the existence of the lessivation process and to explain the profile of the "Parabraunerden" as a consequence of geologic stratification (14). Nobody considered the alternative and asked the question: Why do these cover strata usually have the same thicknesses?

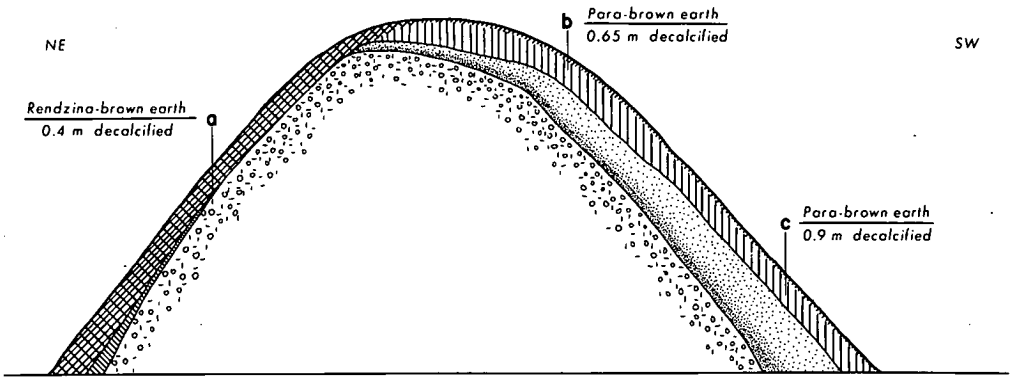

Figure 1. Cross section of a drumlin near Konstanz with asymmetric soil formation.

RESEARCH OBJECTIVE

In view of the indicated problem, it was fortunate that the forest site-mapping service of Baden-Württemberg found some "Parabraunerden" in young Wuerm glacial drumlins in the area of Konstanz on the Bodensee that were clearly formed by lessivation (12). The para-brown earths located on the narrow level crest of these hills contain no late-glacial covering layers that could have been deposited by wind action or by post-glacial soliflux. The coarse gravelly components cannot be of aeolian origin, and the preconditions necessary for soliflux are absent in the closed, level altiplains of the region.

Figure 1 shows that, depending on the exposure, different stages of soil development are observed. The pertinent relationships can be explained with great probability by the microclimate and the natural succession in the vegetative cover. One finds that in the starting stages of soil development, on the shaded NE slopes, as well as on the most extensively decalcified and developed soils of the SW flank, the surface horizons have a depth of about 40 cm. Their lower boundary is usually very sharp. The subsoils, which are enriched in clay content, often show reddish coloration in the mild vine-growing climate around the Bodensee (13, Table 95). The average yearly temperature is 8 to 9 C, the mean precipitation, 800 mm, most of which falls in summer.

The composition of the numerous drumlins of the Bodanruck of the Rhine glacier at Konstanz is quite similar. About 60 to 80 percent of the volume consists of gravel of 20 to 60 mm diameter, which is relatively loosely packed and has a high coefficient of permeability. It consists of about 60 percent alpine carbonate rock, marble, calcareous sand stones, and siliceous lime stones. The remainder is crystalline rock in which quartzites, granites, gneisses, and amphibolites prevail. The lime content varies in the finer fractions (20 to 0.6 mm) between 20 and 50 percent, which means that the content in quartz and silicates is much higher in the finely grained materials than in the gravel. The fractions below 0.6 mm amount to about 10 percent of the total weight. Their size composition is as follows:

Size Fraction (mm)	Approximate Percentage
0.6-0.1	32
0.1-0.02	48
0.02-0.002	18
<0.002	2

The fine sand fraction prevails at 20 to 30 percent lime content; these values are averages of sieve and sedimentation analyses performed at the State Geological Survey at Stuttgart.

The regularity in the variation of soil development with variation in exposure condition, and the constancy of the boundary between the upper and lower soil horizons at about 40 cm, render pairs of opposite drumlin flanks favorable objects for the study of the influence of the course of soil temperature on soil formation.

For this purpose a forest-free drumlin, named the "Walzenberg," located at the village boundary of Allensbach, was chosen. Its natural soil had been greatly changed by agri- and viniculture, and through erosion caused by these. Fertilization, employed in this soil use, produced strongly humified starting stages of soil formation (Rigosol-Pararendzina). It is interesting to note that in these stages the naturally loose moraine material is very often so well cemented, in dry condition at a depth of 30 to 40 cm, that pointed Warren hoes were required to break through this zone in digging. It is assumed that this cementation is caused by a very small amount of silicic acid that has been formed in the layer above and has been illuviated into its present location, where it forms a temporary cementing material when dry. This problem is being further investigated, but for the present, the depth location of this young hardpan is of interest.

In order to obtain useful quantitative data of the microclimatic factor acting on a drumlin, we first eliminated the many accidental variations that result from the differences in vegetative cover and from the degree of soil and humus development at a particular location. Therefore, at the test locations, raw material conditions were created that were comparable with those obtaining at the start of soil formation immediately after retreat of the ice. This could be achieved very easily by excavating, on the two drumlin flanks, pits having a cross section of 2 by 2 m down to the raw moraine material and filling these pits up to the surface with raw moraine material from the same drumlin.

The microclimatic investigations are based on the following conditions:

1. The two test areas are situated at an elevation of 450 and 500 m above sea level, in the upper third of the unforested drumlin slopes of an average slope angle of 20° toward SW(S) and NE(N), respectively.
2. The artificial filling of raw lime-rich moraine material has a single-grain structure of good permeability, and is nonplastic and hardly susceptible to erosion.
3. The surfaces of the artificial soil fills were fitted to the natural slope and were kept continuously free of vegetation.

The following microclimatic factors were determined: (a) soil temperatures at depths of 2, 5, 10, 20, 35, 50, 75 and 100 cm by continuous mechanical recording; (b) precipitation and seepage water; and (c) drainage. All microclimatic test data were evaluated in coordination with the course of the weather. For this purpose, use was made also of the measurements and records of the neighboring official climatological stations.

These investigations are financed by the German Research Association (Deutsche Forschungsgemeinschaft), and will extend over three growing seasons. At the time of this report (May 1968), only a preliminary account can be given, covering a portion of the test results obtained in 1967.

PRELIMINARY TEST RESULTS

The formulation of the problem requires average values of the course of the daily temperature in the soil over the entire growing season, April to November-December 1967. These values were obtained by adding the respective hour-values for a whole month and dividing the sum by the number of days in a month. During the recording period, we obtained a very large amount of data of variable quality. We were forced, therefore, to concentrate for a first overview on a partial evaluation of what were considered to be the most reliable data.

Suitable for this purpose appeared to be the recordings of the soil temperatures in the two months of April (mid-spring) and July (mid-summer) with their seasonally caused maximum temperature differences. For their presentation we chose the geotherms (isotherms of the soil).

Furthermore, we decided to aid in the visualization of the problem by presenting tautochrones, which show the temperature as a function of depth for a particular moment in time, from the specially suitable example of the course of the daily temperature wave in the soil on the southern flank of the moraine in the month of July (designated in the following as "July-S").

Finally, we are attempting to transmit a preliminary, comparative overview of the course of the average daily temperature for a period of six months (April 1-30; May 16-June 15; July 1-31; August 16-September 15; October 1-31; November 16-December 15, 1967). For this purpose, typical selected pairs of tautochrones are presented.

Weather During April and July

In the meteorologic characterization of the two months with respect to the long-term averages, April was classified as too cold, and July as one of the 11 hottest of this century, according to the Monthly Weather Report for Baden (published by the German Weather Service, Weather Office, Freiburg, i. Br. No. 4, April and No. 7, July 1967).

Interpretation of Results to Date

Despite the strongly contrasting starting situations with respect to weather and exposure, several common traits of the geotherms of the course of the average soil temperatures can be recognized (Figs. 2, 3, 4, 5). Most impressive—and uniquely well shown in this type of presentation—is the differentiation between an "upper zone" with more or less closely spaced geotherms and a "lower zone" with widely spaced, lightly curved or even almost rectilinear geotherms. The transition line between these two types of geotherm patterns lies with remarkable consistency at a depth of 30 to 50 cm.

We shall inspect separately the daily insolation phase ("W" = warm) in the middle of Figures 2, 3, 4 and 5, and the heat radiation phase ("C" = cold) at the left and right

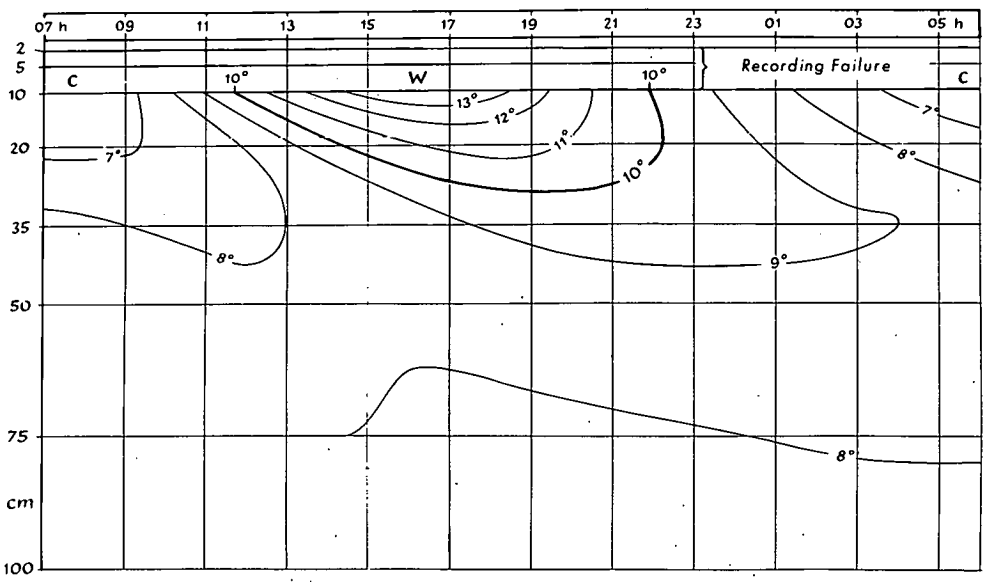

Figure 2. Geotherm of the average daily temperature course in soil for April 1967, south slope.

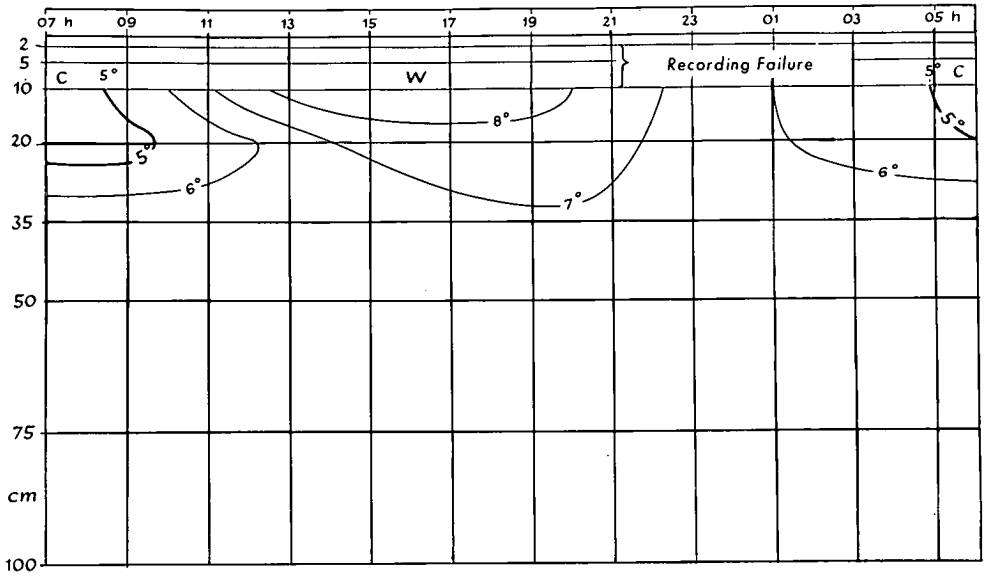

Figure 3. Geotherm of the average daily temperature course in soil for April 1967, north slope.

margins of these figures. Early in the insolation phase, the crowding toward the right hand of the geotherms in the upper zone of the north slope is indicated by the asymmetric pattern of the geotherms (Fig. 3, "W"). This crowding to the right reaches its greatest horizontal deformation in the same depth range of between 30 and 50 cm on the south slope in April as well as in the two figures for July (Figs. 2, 4, 5). We shall call this a transition layer and note the fact that in July as well as in April the dimensions of the upper zone and the depth location of the transition layer remain essentially the same. There is, however, a difference in the appearance of the zones

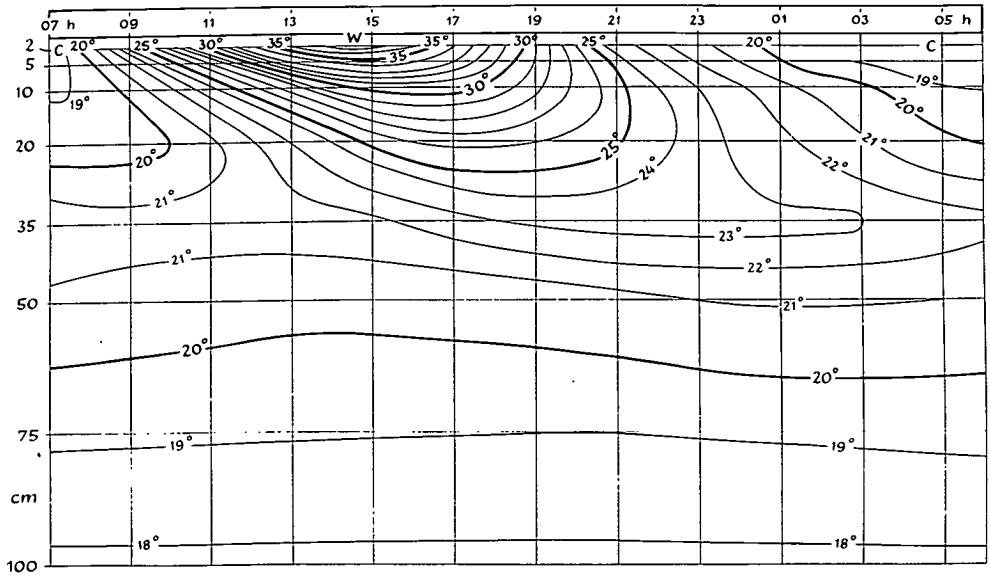

Figure 4. Geotherm of the average daily temperature course in soil for July 1967, south slope.

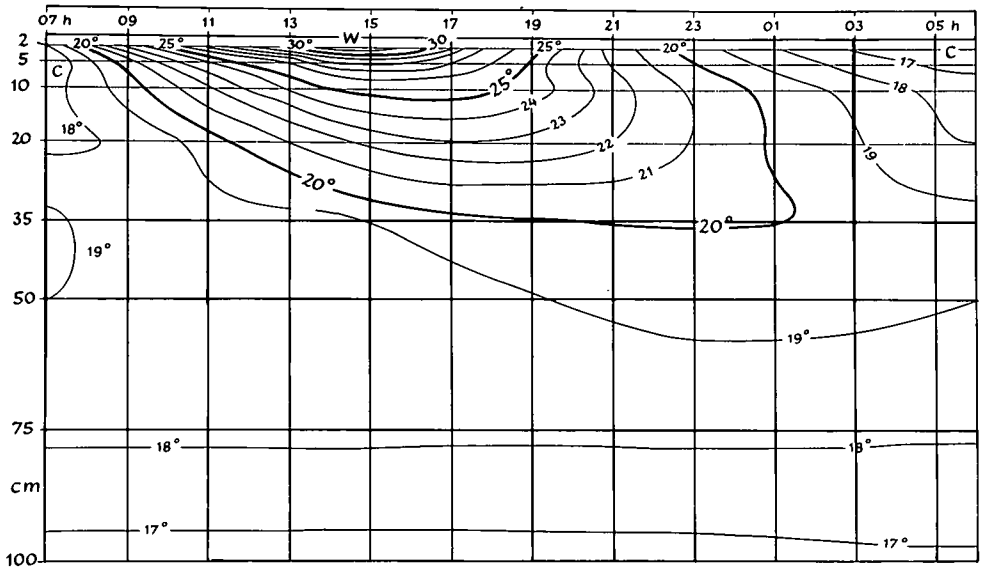

Figure 5. Geotherm of the average daily temperature course in soil for July 1967, north slope.

of maximum deformation of the July geotherms, in that this zone is strictly localized at the 35-cm depth range at the southern exposure, while it is less accentuated on the northern slope and spreads over the entire thickness of the transition layer. The geotherms for the radiation phase show the same characteristic crowding toward the right, but without reaching the same degree of deformation as shown for the insolation phase. It should be noted that all radiation phases, irrespective of season and exposure, generally move from the upper zone well into the range of the transition layer. Differences in degree between the radiation phases exist for the two slope exposures only in July; while the radiation phase loses itself gradually on the northern slope at a depth between 35 and 50 cm (Fig. 5, left margin), that on the south slope is more sharply accentuated and ends at a depth of 35 to 40 cm (Fig. 4, left). The phenomenology of the insolation and radiation phases at both exposures was quite analogous for the two months under consideration.

The daily temperature variations that express themselves in the two characteristic phases of the upper zone are noticeable in the lower zone (i.e., from about 50 to 100 cm) only as relatively weak thermal "impulses" (Figs. 2-5). Again only differences in degree can be observed between the two seasons and the two exposures.

Now our attention shall be directed to the phenomena in the "transition zone." Here in the course of the daily march of temperature—especially during the night—is developed a zone of thermal discontinuity that is connected with the marked retardation of heat penetration during the insolation period. This temperature reversal was more strictly localized on both slope sites in July than in April, and also—independent of the season—was less distinct on the north slope than on the south slope. It is, therefore, most noticeable in the horizontally-directed, strongly deformed geotherms of July-S (Fig. 4). The maximum of the daily temperature wave occurs, therefore, during the night at a depth of 35 to 40 or 50 cm, which is between the soil surface and the 1-m base line at the bottom of the test fill. This depth range can, therefore, be considered as a thermally distinct boundary layer.

Before proceeding to a general comparison of all the months in 1967 covered by this investigation, we shall treat briefly, and with the same method of presentation and analysis, the average daily temperature course obtaining in July on the south slope (Fig. 6). Tautochrones show, on the one hand, the temperatures as function of soil depth for a particular moment in time, and on the other hand, the direction of the heat flux at different depths at particular times.

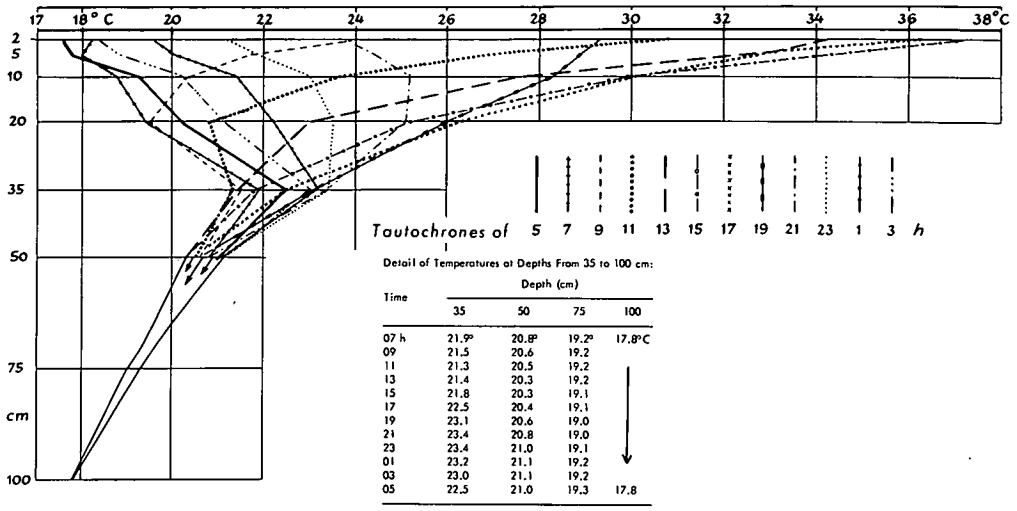

Figure 6. Tautochrones of the average daily temperature course in soil for July 1967, south slope, for all odd-numbered hours.

The main characteristic that can be observed is the relatively wide fanning out of the tautochrones between soil surface and about 35 cm depth (upper zone) and a relatively narrow bunching from there to the bottom of the pit (lower zone). This is expressive of the almost discontinuous decrease of the amplitude of the daily temperature wave at the boundary layer at about 35 cm. At a depth of 100 cm, the amplitude is completely damped out. Furthermore, in the upper zone, the two phases are characterized by the directions of the tautochrones: the tautochrones of the insolation phase run from the upper right-hand to the lower left and indicate a downward heat flux (see the 15 h [3 p.m.] tautochrone in Fig. 6), while the tautochrones of the heat radiation phase indicate an upward direction of the heat flux (see 5 h [5 a.m.] tautochrone in Fig. 6). Both follow the prevailing temperature gradient. The transition between the two phases reflects itself in several inversions in the daily course (see the 9 h and 21 h tautochrones in Fig. 6). This behavior of the tautochrones is exclusively restricted to the depth range of the upper zone. The nightly radiation phase, with temperature increase in the soil, ends at a depth of about 35 cm. This is the locus for a persistent inversion; i.e., during the nightly radiation period, the temperature maximum between soil surface and 1 m depth is localized in this boundary layer (see 01 to 07 h tautochrones in Fig. 6). The direction of the bunched tautochrones in the lower zone that run from the right top to the left bottom is expressive of the downward heat flux occurring in mid-summer (Fig. 6).

In order to obtain a first general view of the typical daily march of soil temperatures during the entire growing season, April to November-December 1967, a representative pair of tautochrones was selected for every month studied. These tautochrones were characteristic for the respective insolation and heat loss or radiation phases, and represent the respective types (Figs. 7 and 8). These two tautochrones, supplied with time (hour) notation, start from the daily maximum or minimum, respectively, at the soil surface (2 cm depth in our case). Exceptions were the tautochrone pairs from April and May-June 1967, which, because of instrument trouble, started only at depths of 10 cm.

We shall omit, for the time being, consideration of the two November-December tautochrone pairs (Figs. 7-VI and 8-VI) and also of the October pair for the north slope (Fig. 8-V). In all the other pairs—irrespective of season and slope exposure—far-reaching analogies are strikingly evident. All tautochrone forks that lie in the upper zone close themselves in the depth range of 35 cm. This means that the average

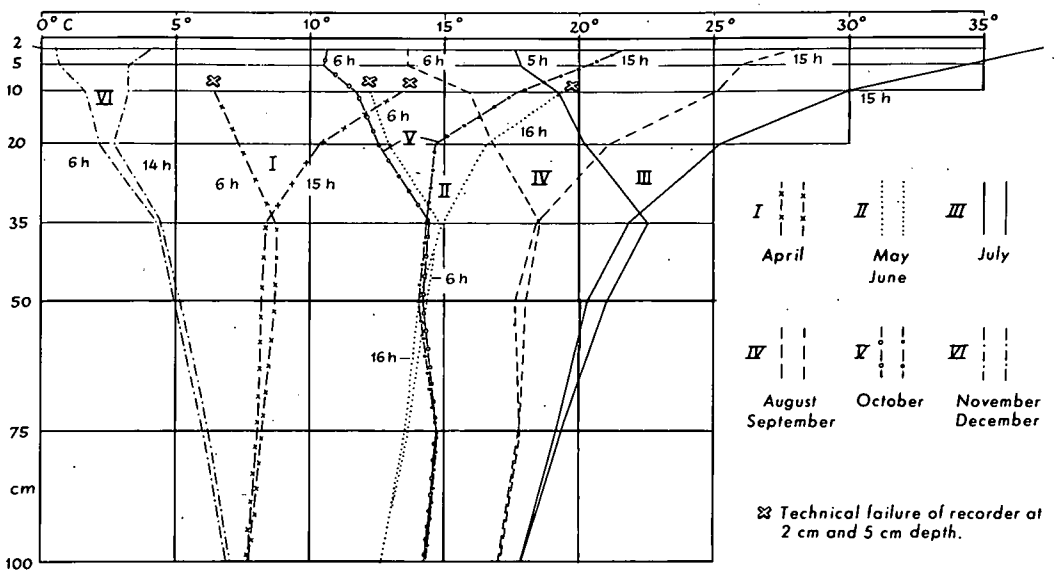

Figure 7. Selected tautochrone pairs (insolation and heat radiation types) for 6 months of the growing season of 1967, south slope.

daily temperature wave during the period from April to August-September is largely damped out in this boundary layer. Furthermore, the inversion, shown by the "radiation-loss" type in the boundary layer, is considerably less marked on the northern slope than on the southern slope. On the latter, one can observe an increasing accentuation of the inversion from April to July 1967, and thence to the fall a decrease in sharpness. The inversion of each tautochrone pair in the lower zone only reflects

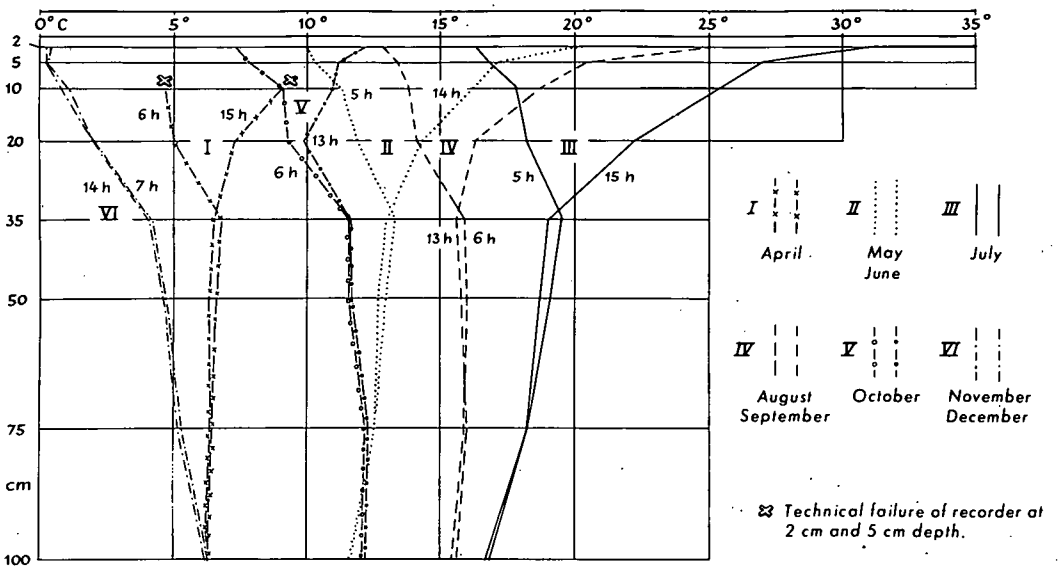

Figure 8. Selected tautochrone pairs (insolation and heat radiation types) for 6 months of the growing season of 1967, north slope.

the phase retardation of the temperature wave penetrating into the soil. Further damping and final extinction of the amplitude of the temperature wave takes place at depths from 75 to 100 cm.

The direction of the tautochrone pairs in the lower zone swings pendulum-like in the course of the growing season on both slope exposures, between practically isothermal states in April-N and August-September-N on the one hand (Fig. 8-I and IV), and a distinct downward temperature gradient in July-S and July-N on the other hand (Figs. 7-III and 8-III).

For October 1967, a fundamental difference is observed for the first time between the two tautochrone pairs deriving from the difference in exposure (Figs. 7-V and 8-V). That for the southern slope shows the general familiar features; the inversion at 35 cm depth is also still noticeable. For the northern slope, however, the insolation type (right tautochrone in Fig. 8-V) terminates at a depth of 20 cm with an inversion. Below this and down to a depth of about 75 cm a heat flux toward the soil surface predominates. Instead of the temperature inversion, hitherto observed at a depth of 35 cm, a marked change in direction of both tautochrone types is observed at the same depth. This tautochrone bent indicates a weaker heat flux in the lower zone and a relatively stronger one in the upper zone.

With a retardation of about 2 weeks, the same process takes place in the test area on the southern slope (Fig. 7-VI). Aside from the absolute temperature values, the two tautochrone pairs of October-N and November-December-S are practically congruent.

Finally, even in the upper zone there was practically no daily temperature variation on the northern exposure site during November-December 1967; i.e., differentiation between insolation and heat radiation had vanished (Fig. 8-VI). The picture is dominated by a heat flux from the bottom of the test fill to the soil surface. Instead of the previously observed formation of thermal zones, only a change in direction of the tautochrones at a depth of 35 cm is observed. This change in direction indicates a stronger heat loss flux in the upper than in the lower zone.

SUMMARY

The investigations of the soil temperatures on both slopes of the Walzenberg near Allensbach/Bodensee during the growing season 1967 have produced the following preliminary results:

1. Analysis of the 4 geotherm fields (Figs. 2-5), which represent the respective characteristic course of the daily temperature wave in the soil, renders the following thermal profile: (a) a thermally active upper zone between soil surface and about 30 cm depth, (b) a transition or boundary layer with nightly temperature reversion between 30 and 40 (50) cm, and (c) a thermally passive lower zone between 40 (50) cm and 100 cm depth (lower boundary of filled test pit).

2. With the aid of tautochrones, this division into 3 parts can be easily visualized by means of the test results for July 1967 (Fig. 6): (a) the fanning out of the tautochrones in the active upper zone, (b) the boundary layer with the localized temperature inversion during the night hours, and (c) the alignment of the tautochrones in the same direction in the passive lower zone.

3. The overview obtained with regard to the course of soil temperatures during the growing season of 1967 by means of selected tautochrone pairs leads to the recognition of subdivisions that are functions of time (Figs. 7 and 8): (a) from April (north and south slopes) to October (south slope), i.e., spring, summer, fall—the partial results enumerated in 1 and 2 are generally applicable to this time period; (b) October (north slope) and November-December (south slope), i.e., fall, winter transition—an upper zone is still active but only 20 cm thick, there is a passive lower zone from about 20 cm to the bottom of the test pit, and at the depth of the boundary layer (35 cm) temperature reversion is replaced by a change in direction of the tautochrone pair; and (c) November-December (north slope), i.e., winter—the characteristic features of the thermal profile have disappeared except for a distinct change in the direction of the tautochrone pair at the depth of the boundary layer. The results discussed under 3 are exemplified by the thermal profile sketch in Figure 9.

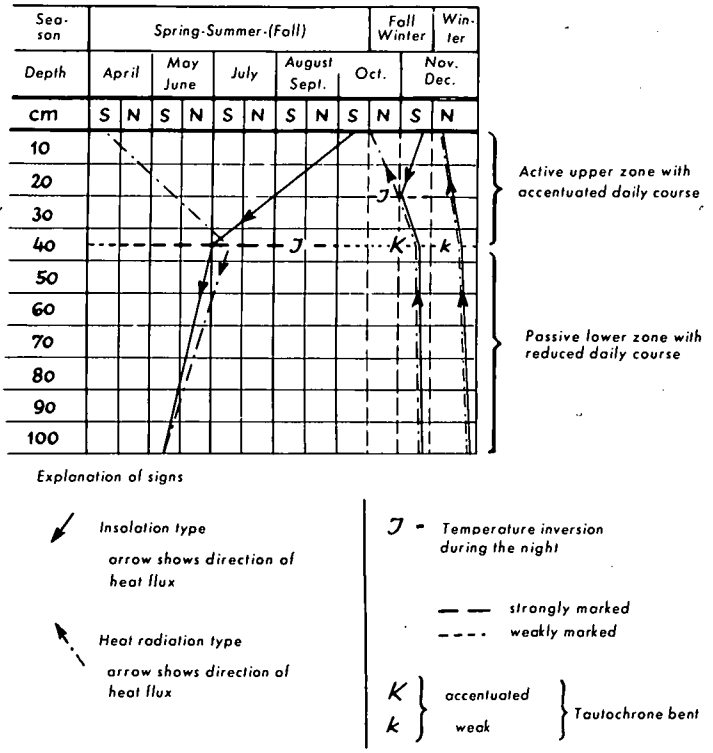

Figure 9. Comparison of the thermal profiles during the growing season of 1967.

DISCUSSION

While this research project is still in an early stage, the first results obtained are definitely significant with respect to the purpose of this study. They are in agreement with results obtained by others, especially those by Vujevic (19) and Winterkorn (22, 23).

It is brought out that the thickness of the thermally active upper zone—which from a pedologic point of view could be called the range of daily circulation of the soil heat—coincides in order of magnitude with the location of the boundary between the upper and lower soil horizons in the "Parabraunerden" of central and western Europe. The same thickness is exhibited in many locations by thin allochthone surface layers.

The following questions arise:

1. What are the causes for the constant thickness of the zone of daily heat circulation?
2. What is the effect of this thermal zone on soil genesis?

Question 1

The data show that the constant zone of the daily heat circulation in the warm months is connected with the predominance of the insolation phase. As soon as the heat loss by radiation prevails in the daily thermal picture (winter season), the zone of daily thermal circulation moves closer to the surface. An essential role seems to be played by the time rhythm in which the insolation phase and the phase of heat-loss by radiation encounter each other. On July days a temperature maximum is observed on the soil surface between 2 and 3 p.m., while at the same time the temperature at the boundary layer is still on the negative side, showing that the effect of the nightly heat loss is only now reaching the boundary layer and that, at a depth of about 40 cm, the daily minimum coincides with the maximum on the surface (see also Winterkorn and

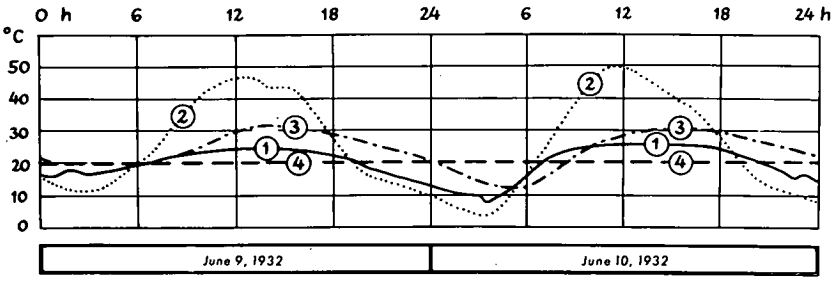

Figure 10. Daily temperature variation in air and soil, Gobi desert at Etsin Gol (after N. G. Hörner, 1933, from R. Brinkmann, Textbook of General Geology, Vol. 1, Stuttgart, 1964, p. 61): 1—temperature of air; 2—temperature of soil surface; 3—temperature of soil at 10 cm; 4—temperature of soil at 50 cm.

Eyring, 22). Since the temperature minimum on the surface occurs between 2 and 4 a.m., one could assume a twelve-hour rhythm of opposing heat impulses, which more or less compensate each other in the boundary layer. But the experimental data do not quite agree with this explanation; the influence of the soil texture, too, appears to be very small. This has already been pointed out by Chudnovskii (5), who, for soil thermal problems, differentiates only between fine, medium, and coarse granular soils (see also Winterkorn, 23). Our experimental data and those by Vujevic (19)—who very probably worked with loess-chernozem in Belgrade—show that even medium- and coarse-grained soils react in a very similar fashion. Only heavy clay soils appear to react differently, if the opposite conclusion regarding the depth of the daily heat circulation is permitted from the lesser thickness (15-20 cm) of their surface horizons. However, more experimental data are needed before a definitive statement can be made on this matter. There are two different possibilities:

1. The constant zone of thermal circulation, which in medium- and coarse-grained soils shows little dependence on environment, could follow a layer formation that is predetermined by other causes, e.g., a stratification of soil moisture. As a matter of fact, curves of average soil moisture contents show quite distinctly a boundary at about 40 cm on moist-warm summer days; this has been discussed thoroughly in a previous paper (11). But what is here cause and what is effect?

In the development of the soil profile, water is without doubt the strongest factor. But when the dimensions of the thermal circulation zone are the same in medium-grained soils with reduced permeability, and in coarse-grained soils of unhindered drainage, in arid as well as in temperate climates (Fig. 10), even in arctic thawing zones (Fig. 11), then one may justifiably doubt the primary influence of moisture stratification. With regard to this question, also, further investigations are needed.

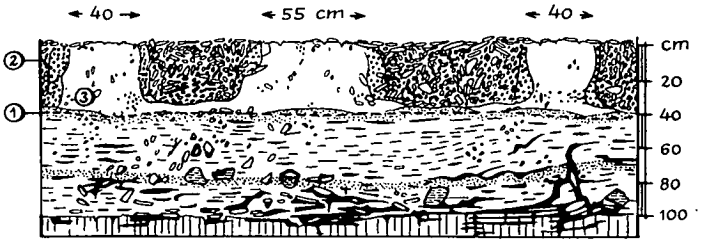

Figure 11. Kryoturbation soil on Barents Island in Spitzbergen at 402 m anove sea level (after J. Büdel, 2, p. 356): 1—surface of the permafrost soil; 2—ice pavement; 3—silt and clay cores.

Purely theoretically, other primary stratifications could be assumed which bring about stratification of the zones of thermal circulation and moisture content, e.g., a different primary electric potential in the upper and lower horizons. In this area, too, more experimental data are needed. However, it is not very probable that a primary electric potential governs soil moisture behavior since the available evidence shows a secondary dependence of the electric soil potential upon moisture content and surface area.

2. Instead of being a consequence of a preformed stratification, the constant thickness of the zone of daily heat circulation could be the combined result of thermal impulses and soil dynamic response. The general uniformity of this phenomenon is observed only on soils which, at least at the start of their development, possess a large pore space and hence a large air content. It is, therefore, easy to suspect that the soil air may play a determinant role because of its great mobility and its tendency to flow in response to even small temperature gradients. Many soils have a pore space of 30 to 60 percent, the largest part of which is occupied by air. Even though the interconnection between soil pores is often imperfect, and free interchange of soil air is often obstructed, air is still the most mobile phase in a soil. There exists, therefore, the possibility that a primary zone of daily air circulation and of consequently increased evaporation in the upper soil is responsible for the formation of the thermally active upper zone. This concept is supported by the observation that the special characteristics of the daily temperature wave on the south slope are most sharply accentuated during the driest season, i.e., at a time when the soil air dominates the behavior of the upper soil horizon.

Although a number of other questions arise at this stage, we may propose as a working hypothesis that, in porous soils, a thermally active upper zone is formed at conditions of positive heat balance and that the depth of this zone corresponds with that of the daily air circulation. An important question in this connection is whether rhythmic air pressure variations—as in the daily double air pressure wave—are playing a role in this phenomenon.

Such a primary role of the air circulation could account for the widespread constancy of the thickness of the thermally active upper zone and its lack of dependence on the magnitude of the thermal impulses received at the surface. An air circulation zone established at a positive heat balance, and of generally similar dimensions, would explain many facts in the simplest manner; the sharp bend of the tautochrones at the boundary would then correspond to the division line between the penetration of the dynamic portion of the daily wave, which is strongly accentuated by the air circulation, and the much weaker "linear" continuation of the daily wave into the subsoil, which is mainly a function of the thermal conductivity of the solid and liquid phases of the soil.

All this, however, must remain in the nature of a general discussion until more experimental data have been obtained and properly evaluated. The importance of soil thermal behavior should, however, be clearly established even though many factors and relationships are still unknown (see Winterkorn, 23).

Question 2

The second question, "How does the circulation zone affect pedogenesis?" can be answered thus:

1. In the entire thermally active zone, there is great activation of the soil biologic potential if permitted by the other environmental factors. This is shown by the distribution of heavy minerals of volcanic origin, which in relatively recent time were wind-deposited on the Roman limes in southwest Germany. Today these minerals are uniformly distributed in the approximately 40-cm thick upper soil horizon of the "Parabraunerde" that has formed on this artificial embankment since the time of the Romans (5). This means that the thermal circulation zone is also a zone of "bioturbation" in which the edaphon is so active that, with time, the entire zone becomes completely mixed up through the action of soil-burrowing animals, especially rain worms. This is also a zone of intense root development. In many raw soils, this biologically active

zone is distinguished from the underlying zone by its stronger root formation. The thermally more passive lower zone shows comparatively little life. Its boundary is often characterized by illuviation and cementation, as reported previously.

2. If the circulation zone of the estival daily heat wave also represents a zone of bioturbation in the soil, then it is easy to understand why thin allochthone surface layers often have a thickness of about 40 cm. Within the range of bioturbation, thin covering strata that possess an original thickness of perhaps 20 to 30 cm become mixed with material from the layers underneath and with newly formed organic matter. The zone of bioturbation, with its larger internal surface and finer structure, develops, with time, a distinct boundary against the underlying material. Because of the allochthone admixtures, the entire zone of bioturbation is then considered as an allochthone cover stratum. However, sedimentation and mineralogic analysis of the finer grain size materials almost always shows components from the substrate.

3. A soil genetic translocation process such as lessivation is, in undisturbed soils, restricted to the zone of thermal circulation and bioturbation. The internal surfaces of soils rich in colloidal materials undergo strong reactions within the thermally active zone of the upper soil layer. Biogenic comminution, temperature and moisture changes, and loss of bases favor decomposition of the soil colloids, while conservative tendencies prevail in the thermally passive lower layers. If this concept is correct, then elutriation of mobile soil colloids does not take place progressively from the surface down, but more or less simultaneously from the thermally active and biologically activated zone. Deposition in the thermally passive, low-porosity subsoil takes place along the narrowing seepage paths.

In southwest Germany hundreds and thousands of years are required for the formation of distinct soil profiles by these processes. A morphologic differentiation, but without translocation of clay, can be observed at a depth of about 40 cm on an embankment built of loess loam (the "Eppinger Linien") in 1695-1697, in the wine cultivation climate of North Württemberg. This can probably be considered as a structural boundary that is due to bioturbation. A "Parabraunerde," with clay translocation, was developed in the same climate on the Upper German limes, built of loess soil in the second century A.D. to denote the borders of the Roman Empire. The characteristic boundary between upper and lower soil horizon is at 40 cm depth. Obviously much time is required before the weak daily temperature wave, acting through many different processes, can produce visible proof of its role in soil genesis.

REFERENCES

1. Anlitzky, H. Die Bodentemperaturverhältnisse an einer zentralalpinen Hanglage beiderseits der Waldgrenze, Teil II-III. Archiv f. Meteorologie, Geophysik und Bioklimatologie, Serie B, Bd. 11, 1961.
2. Büdel, J. Die Abtragungsvorgänge auf Spitzbergen im Umkreis der Barentsinsel. 22. Deutscher Geographentag Köln 1961, Tagungsberichte u. wissenschaftliche Abhandlungen, p. 337-375, Verl. Franz Steiner, Wiesbaden, 1962.
3. Chudnovskii, A. F. Heat Transfer in the Soil. Translated from Russian. Israel Program for Scientific Translations, Jerusalem, 1962.
4. Duchaufour, Ph. Précis de Pédologie, Paris, 1960.
5. Dürr, F. Vulkanische Schwerminerale in Bodenprofilen Württembergs. Neues Jahrb. f. Geologie, Paläontologie, Mh. 111, p. 465-472, Stuttgart, 1953.
6. Geiger, R. Das Klima der bodennahen Luftschicht. Vieweg u. Sohn, Braunschweig, 1961.
7. Heigel, K. Über den Einfluss von Exposition und Bewuchs auf die Erdbodentemperaturen. Mitt. des Deutschen Wetterdienstes, Nr. 22, Bd. 3, Offenbach/Main, 1960.
8. Junghans, H. Zur Temperaturmessung in verschiedenen Bodenarten. Angewandte Meteorologie, Bd. 4, 1960-64, Heft 3, Okt. 1961.
9. Mückenhausen, E. Entstehung, Eigenschaften und Systematik der Böden der Bundesrepublik Deutschland. DLG-Verlag, Frankfurt/Main, 1962.

10. Müller, S. Die Unterscheidung echter Bodenhorizonte und geologischer Schichtung in Bodenprofilen Nordwürttembergs. Neues Jahrb. f. Geologie, Paläntologie, Mh. 12, p. 545-550, Stuttgart, 1952.
11. Müller, S. Thermische Sprungschichtenbildung als differenzierender Faktor im Bodenprofil. Zschr. Pflanzenernährung, Düngung, Bodenkunde 109. Bd. H. 1, S. 26-34, Weinheim, 1965.
12. Müller, S. Lessivierung in Abhängigkeit vom Kleinklima. Mittlg. der Dt. Bodenkundlichen Gesellschaft, Bd. 4, S. 65-70, Göttingen, 1965.
13. Müller, S., Schlenker, G., and Werner, J. Südwestdeutsche Waldböden im Farbbild. Schriftenreihe der Landesforstverwaltung Baden-Württemberg, Bd. 23, Stuttgart, 1967.
14. Plass, W. Braunerden und Parabraunerden in Nordhessen. Zschr. Pflanzenernährung, Düngung, Bodenkunde 114, Bd. H 1, p. 12-26, Weinheim, 1966.
15. Schäffer-Schachtschabel. Lehrbuch der Bodenkunde. Ver. F. Enke, Stuttgart, 6. Aufl., 1966.
16. Siegenthaler, J. Die Bodentemperaturen in Abhängigkeit von äusseren meteorologischen Faktoren. Gerlands Beiträge zur Geophysik, Bd. 40, 1933.
17. Soil Survey Staff. Soil Classification. A Comprehensive System. 7th Approximation. Soil Conservation Service, U.S. Dept. Agric. U.S. Govt. Print. Off., Washington, 1960.
18. Werner, J. Grundzüge einer regionalen Bodenkunde des südwestdeutschen Alpenvorlands. Schriftenreihe der Landesforstverwaltung Baden-Württemberg, Bd. 17, Stuttgart, 1964.
19. Vujevic, P. Über die Bodentemperaturen in Belgrad. Meteorologische Zeitschrift 28, H. 7, p. 289-301, Braunschweig, 1911.
20. Weyl, R. Schwermineraluntersuchungen an Böden des württembergischen Unterlandes. Neues Jahrb. f. Geologie, Paläontologie, Mh. 11, p. 482-499, Stuttgart, 1952.
21. Wetterdienst. Monatlicher Witterungsbericht für Baden. Herausgegeben vom Deutschen Wetterdienst, Wetteramt Freiburg.
22. Winterkorn, H. F., and Eyring, H. Temperature Conditions in the Surface Layer of the Earth. Appendix to Theoretical Aspects of Water Accumulation in Cohesive Subgrade Soils. HRB Proc., Vol. 25, p. 422-434, 1945.
23. Winterkorn, H. F. Behavior of Moist Soil in a Thermal Energy Field. Clays and Clay Minerals, Vol. 9, p. 85-108, Pergamon Press, 1962.

Thermo-Osmotic and Thermoelectric Coupling in Saturated Soils

DONALD H. GRAY, Department of Civil Engineering, The University of Michigan

Thermally induced flows of moisture and electricity in saturated clays were measured experimentally as the water content, exchange capacity, and pore-water electrolyte concentration were systematically varied. Prior work on thermo-osmosis in soils is reviewed, and possible coupling mechanisms are discussed in the light of new experimental results.

The clay-water systems studied exhibited characteristic thermoelectric and thermo-osmotic effects. Measureable currents on the order of 1 to 10 microamperes per deg C per cm were detected, with the warmer side having the more positive polarity. The thermoelectric current increased consistently with increasing water content, exchange capacity, or electrolyte concentration in the pore water.

Thermo-osmotic pressures on the order of a few tenths of a centimeter of water per degree Centigrade were measured with net flow occurring to either the warm or cold side. The peculiar temperature-dependence of activity coefficients of electrolytes in the pore water is suggested as a possible explanation for a given direction of moisture flow. Thermal contributions to moisture movement in saturated soils are minor compared to thermal moisture flow in partially saturated media.

•NORMALLY, we are accustomed to thinking strictly in terms of conjugate force-flux phenomena, i. e., a hydraulic gradient producing only a flow of water, an electric field producing only a flow of current, and so on. These conjugate force-flux relationships are described by well-known phenomenologic laws such as Darcy's, Ohm's, Fourier's, and Fick's. Coupling effects, on the other hand, arise when a driving force of one kind (e. g., a temperature gradient) produces a flow of another (e. g., an electruc current).

The present paper deals only with thermal coupling in clay-water systems. Results of electrokinetic studies and more general aspects of coupled flow phenomena in soils are described elsewhere by Gray and Mitchell (7), Gray (8) and Winterkorn (25).

Thermo-osmosis, a thermally induced flow of moisture in porous media, can occur under natural conditions. This phenomenon has attracted the attention of soil scientists because of its possible contribution to the net transfer of soil water and nutrients. To a lesser extent, thermo-osmosis has also been of interest to engineers because of its suspected role in problems dealing with frost heaving and moisture accumulation under pavements.

The engineering significance of thermoelectric coupling in soils is less apparent. It may be important in problems pertaining to corrosion of underground pipes carrying fluids at temperatures far above or below ground temperature. The existence of thermoelectric coupling in soils is yet another example of the extent of interaction that can occur between flows of moisture, heat, dissolved salts, and electric current in the ground.

The precise nature of thermo-osmotic flow is still not well understood. Several different transfer mechanisms have been proposed. Most of the research, both theoretical and experimental, has focused on inert, partly saturated systems where vapor phase transfer plays an important part. The nature of the thermo-osmotic process

becomes more complicated when the porous medium itself is charged or the permeant is an electrolyte. Thermal gradients then give rise to secondary electrical effects that should be taken into account.

The present paper presents results of thermo-osmosis tests with saturated, clay-water systems in which the direction of flow was contrary to results usually reported in the literature. Various hypotheses that have been used to explain the nature of thermo-osmotic flow are briefly reviewed. A new hypothesis is tentatively advanced to explain the experimental results of the study.

REVIEW OF PAST WORK

Thermo-Osmosis

In reviewing both the past work on thermo-osmosis and the results of the present study it is essential to keep in mind some important distinctions. In the first place, it is necessary to consider whether the system is inert (i.e., uncharged) and whether only single-component flow of matter (e.g., pure water) occurs. Charged membranes or clayey soils saturated with electrolyte solution do not meet these criteria. In addition, it is necessary to distinguish between partially and fully saturated systems. In the former, thermo-osmotic flow may occur in both the vapor and liquid phase.

Thermo-osmosis across inert membranes has been investigated extensively by Haas and Steinert (10) and to a lesser extent by Rastogi et al (17) and Corey and Kemper (4). Cellophane, an inert membrane with a very small pore size (from 5 to 20 Å), was used in these studies. Significant thermo-osmotic flows from hot to cold were detected in cellophane membranes, the effect becoming more pronounced as the average pore size was reduced. Rastogi observed a linear relationship between temperature gradient and osmotic flow; however, the magnitude of this flow also varied with the mean temperature in the membrane.

Carr and Sollner (2) studied thermo-osmosis across charged membranes. They reported that the rate of thermo-osmotic flow varied in proportion to the temperature difference (as observed by other investigators), but in this case the proportionality factor depended strongly on the electrolyte concentration of the outer solution. A typical plot of thermally induced flow rate against the logarithm of the concentration gave a bell-shaped curve as shown in Figure 1. They concluded, therefore, that thermo-osmosis with electrolyte solutions is an electrochemical phenomenon and is related to electro-osmosis.

In 1965, Kobatake and Fujita gave a theoretical account of Carr and Sollner's earlier experimental findings. They likewise concluded that thermo-osmotic flow in a charged membrane-electrolyte system is caused by an electrical field set up in the membrane by the applied thermal gradient. Furthermore, they argued that the dependence* of the electro-osmotic coefficient on the electrolyte concentration of the outer solution also explains the characteristic behavior of thermo-osmosis in charged membranes.

Thermo-osmosis has been studied extensively in partially saturated soils by Bouyoucos (1), Smith (18), Gowda et al (6), Gurr et al (5), Taylor et al (20, 22), and Philip and deVries (16). Although thermally induced flow of moisture in the vapor phase (from warmer to cooler areas) is widely believed to be the dominant transfer mechanism, film flow in the liquid phase cannot be ruled out (Winterkorn, 23).

Vapor phase transport is believed to result mainly from a molecular diffusion process. Convection also plays a minor role as shown by Taylor and Cavazza (20). Moisture tends to evaporate at the warmer side and condense at the colder side, thus maintaining a vapor pressure gradient.

---

*The electro-osmotic transport coefficient (i.e., the amount of water transferred per unit charge) also depends on the fixed membrane charge as described by Gray (8).

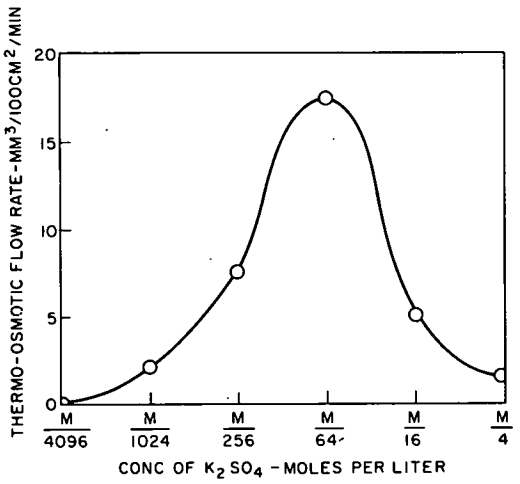

Figure 1. Typical dependence of thermo-osmotic flow on concentration of external electrolyte in a negatively charged, acidic membrane (after Carr and Sollner, 2).

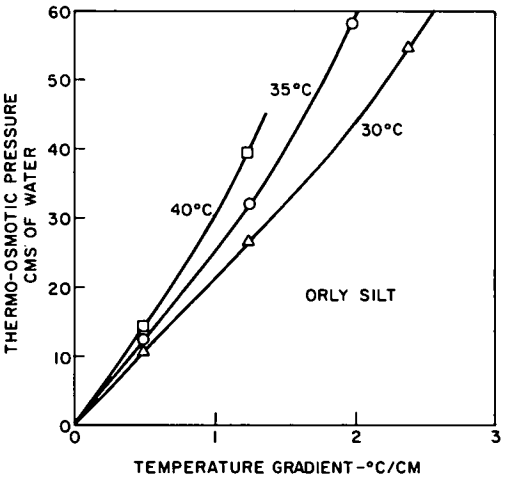

Figure 2. Thermo-osmotic pressure as a function of temperature gradient for various mean temperatures, Orly silt (after Habib and Soeiro, 9).

Transport in the liquid phase, either in thin films or small capillaries, is more complex. Cary (3) has suggested four possible mechanisms:

1. Thermally induced surface tension gradients or differences in soil moisture suction;
2. Differences between specific heat content of adsorbed water on solid surfaces and the bulk liquid in the pores;
3. Random kinetic energy changes associated with hydrogen bond distributions that develop in thermal gradients; and
4. Thermally induced osmotic or electro-osmotic gradients.

Thermo-osmosis in saturated soils has received only limited attention. The transfer mechanism in this case is poorly understood. Vapor phase transport must be ruled out, and, since there are no air-water interfaces, surface tension gradients can also be eliminated as a possible transfer mechanism.

Taylor and Cary (21) investigated thermo-osmosis in a saturated Millville silt loam, and Habib and Soeiro (9) in a saturated Orly silt. The results of the latter investigation are shown in Figure 2. Both studies report a flow of water from the higher toward the lower temperature. Habib and Soeiro reported that water movement was greatly amplified when electrolytes were mixed with the soil. Haas and Steinert (10) also reported a large increase in thermo-osmosis when a charged membrane was inserted adjacent to and in series with an inert cellophane membrane.

Cary (3) tabulated available data on the magnitude of thermally induced moisture flow in porous media. His summary included both artificial membranes and soils in various states of saturation. He was able to compare the effects of various parameters such as mean temperature, hydraulic conductivity, and initial moisture content. Cary's summary is reproduced in Table 1. All thermal moisture flows reported in Table 1 were from warm to cool.

The data in Table 1 show that thermal moisture flow is far greater in partially saturated as opposed to fully saturated soils. In unsaturated soils the relative importance of thermally induced flow rises rapidly as the moisture content decreases. Compared with moisture flow under hydraulic gradient, thermal moisture flow becomes relatively more important as the hydraulic conductivity decreases. In saturated media the thermo-osmotic pressure tends to increase with increasing mean temperature.

TABLE 1

COMPARISONS OF MOISTURE FLOW DUE TO THERMAL GRADIENTS IN VARIOUS POROUS MATERIALS[a]

Type of Porous Material	Moisture Content or Suction, bars	Thermal Flow, mm H_2O/day/ °C/cm	cm H_2O Head Equiv. to 1 C Gradient	Mean Temperature	Type of Solution Flowing	Phase of Flow
Sintered glass, 10^4 Å mean pore diameter	Saturated	0	0	25	Distilled water	Liquid
Du Pont 600 cellophane	Saturated	0.1	–	40	Double-distilled water	Liquid
Cellulose acetate, 27 Å mean pore diameter	Saturated	–	7.0	20	Distilled water	Liquid
Millipore filter, 100 Å mean pore diameter	Saturated	–	0.09	20	Distilled water	Liquid
Wyoming bentonite paste, 18 percent	Saturated	0.1	4.0	35	0.1 N NaCl	Liquid
Yolo loam soil, B = 1.4	0.06	2.0	5.5	35	0.01 N $CaSO_4$	Liquid + vapor
Houston black clay	0.66	0.7	–	38	Distilled water	Liquid + vapor
Houston black clay	1.4	0.8	–	37	Distilled water	Liquid + vapor
Millville silt loam, B = 1.5	Saturated	–	0.07	25	Water	Liquid
Millville silt loam	2.2	–	1.4×10^3	25	Water	Vapor + liquid
Millville silt loam	126	–	8.3×10^4	25	Water	Vapor
Columbia loam, B = 1.2	0.07	1.8	3	19	Distilled water	20 percent vapor, 80 percent liquid
Columbia loam, B = 1.2	0.24	0.9	13	8	Distilled water	33 percent vapor, 67 percent liquid
Columbia loam, B = 1.2	0.24	2.0	14	33	Distilled water	55 percent vapor, 45 percent liquid
Columbia loam, B = 1.2	0.45	1.6	250	25	Distilled water	Vapor + liquid
Stable air	100 percent porosity	0.4	8×10^4	27	Distilled water	vapor

[a]From Cary (3).

Thermoelectric Coupling

Electrical effects associated with thermal osmosis—particularly in charged membranes containing electrolytes—have probably not been fully appreciated. In unsaturated soils the electrical influence on thermo-osmosis can perhaps be disregarded because of the dominant role of vapor phase transfer. In saturated media, on the other hand, electrical effects become important in characterizing thermo-osmosis. Even Aubert in his early work concluded that thermo-osmosis was electrical in its origin and was related to electro-osmosis.

Thermoelectric membrane potentials are difficult to isolate because the measured emf's include electrode potentials that must be evaluated and taken into account. Nevertheless, thermoelectric potentials on the order of 0.05 mv/deg C have been reported by Ikeda (12) for dilute KCl solutions and a cation selective collodion membrane. The warmer side had the more positive potential. Thermoelectric potentials with a typical value of 0.3 mv/deg C for sandstones and shales have been reported by Madden and Marshall (15). They did not give the polarity of the potentials.

Simultaneous measurement of induced electrical current during thermo-osmosis has been carried out by Gowda et al (6) in clay soils and by Taylor and Cary (21) and Habib and Soeiro (9) in a silt loam. They detected small currents (generally decreasing with time) on the order of 1 to 5 microamps. Taylor reported a current flow from cold to warm; however, there was considerable fluctuation in the induced electrical current and potential indicating instability in the electrodes (brass screens) and the electrical properties of the system. Habib and Soeiro do not give the polarity of their measured currents; they furthermore dismiss the electric current as an electrode phenomenon. Neither of these latter investigators made provisions for the use of reversible electrodes nor were the test conditions well-suited for the detection and evaluation of electrical effects.

APPLICATION OF IRREVERSIBLE THERMODYNAMICS TO THERMAL COUPLING

As Winterkorn pointed out (25), the theory of irreversible or non-equilibrium thermodynamics is a convenient means of analyzing the simultaneous flows of water, heat, salts, and electric current in porous media. A detailed account illustrating practical applications of the theory has been given by Katchalsky (13) and Taylor (19).

Taylor and Cary (22) outlined a theoretical analysis based on the thermodynamics of irreversible processes for evaluating coupled flows of heat and water in continuous soil systems. Taylor (19) also derived the following phenomenologic equation for describing the simultaneous transfer of water and heat across a discontinuous system, viz., an inert membrane or porous soil plug:

$$J_w = \frac{L_{ww} v_w}{T} \Delta P + L_{wq} \frac{\Delta T}{T^2} \tag{1}$$

$$J_q = L_{qw} v_w \Delta P + L_{qq} \frac{\Delta T}{T^2} \tag{2}$$

where

J_w, J_q = the net fluxes of water and heat respectively;

ΔP = hydraulic pressure drop across the porous plug;

T = the absolute temperature;

L_{ww}, L_{qq} = direct transfer coefficients, e.g., the hydraulic and Fourier heat conduction coefficients respectively; and

L_{wq}, L_{qw} = coupled transfer coefficients.

The following assumptions were made in the derivation of these equations:

1. There is only single-component flow of matter, viz., pure water.
2. The system is inert and no chemical reactions occur within it.
3. External force fields are absent or cancel out.
4. The system is never too far from equilibrium, i.e., $\Delta\mu_w << RT$ and $\Delta T << T$.
5. Linearity exists between forces and fluxes.

The derived equations are in finite difference form, i.e., they have been integrated over the thickness of the membrane or porous soil plug. This is not as rigorous a formulation as it is when the phenomenologic equations are left in differential form. In this latter case, the driving forces are usually expressed as gradients and the flows are defined only locally at a point within the system (Taylor and Cary, 22). The finite difference form is probably more useful for experimental purposes. It assumes, however, that suitable "averages" can be found for the coefficients, L_{ik}, and the temperature, T, within the temperature interval, ΔT, of interest.

Equation 1 states that the net flux of water is the sum of two transfer processes that can occur simultaneously. The first is the flow of water that is controlled by the pressure difference, ΔP, and the hydraulic conductivity of the soil; the second is the flow of water that is induced by a temperature difference, ΔT.

These equations are in fact specific cases of a general relationship in irreversible thermodynamics, viz., the allowable superposition of contributions to a given flux from both conjugated and non-conjugated driving forces alike. The principle of linear superposition and the force-flux relationships are expressed in mathematical shorthand by

$$J_i = \sum_{k=1}^{n} L_{ik} X_k \quad (i,k = 1, 2, 3, \ldots n) \tag{3}$$

where the J_i and X_k are generalized fluxes and forces respectively and the L_{ik} are the phenomenologic transport coefficients previously defined.

When an external temperature gradient is applied across a soil plug the system eventually tends toward a steady-state condition. If a counter osmotic pressure is allowed to build up in response to a thermally induced flow of water, the net flux of water will vanish at the steady state, i.e., $J_w = 0$. Under these boundary conditions Eq. 1 may be written as

$$\left(\frac{\Delta P}{\Delta T}\right)_{J_w=0} = \frac{-L_{wq}}{L_{ww}V_wT} = \frac{-Q^*}{V_wT} \tag{4}$$

where Q^* is the so-called heat of transfer. Equation 4 indicates that the excess of pressure (the thermo-osmotic pressure) that will build up on the hot (or cold) side of a system in response to a unit temperature difference, $\Delta P/\Delta T$, depends on the heat of transfer, Q^*, the specific volume of water, V_w, and the average temperature of the system, T. The heat of transfer in turn is a function of the physical properties of a membrane or porous plug. In general, Q^* increases with decreasing pore size and increasing temperature.

At present there are no a priori grounds for predicting the sign of Q^* in saturated systems, i.e., which direction the thermally induced flow of water will take. The exact mechanism of coupling between matter and heat flows is not well understood. In unsaturated systems a net flow of water to the cold side has always been observed. This is understandable because of the dominant role of vapor phase transport that occurs towards the cold side. In experiments with saturated systems using cellophane (Haas and Steinert, 10), silty soils (Taylor and Cary, 21, and Habib and Soeiro, 9), and charged membranes (Carr and Sollner, 2), a flow of water to the cold side has always been reported.

One of the purposes of the present study was to determine not only the magnitude of thermo-osmotic coupling in saturated clay-water-electrolyte systems but also the direction. A clay-water system is much more complex because one is no longer dealing with an inert, single-component system (an assumption contained in Eqs. 1, 2, and 4). Applied thermal gradients will now give rise to thermoelectric and secondary electro-osmotic effects. The possibility of thermally induced osmotic gradients deserves careful consideration.

In this regard it is useful to keep in mind that temperature affects the activity coefficients of dissolved salts or ions in the pore water, and this in turn affects the chemical potential of water. The standard expression for the chemical potential of a species, "i", in terms of its activity is given by

$$\mu_i = \mu_i^\circ + RT \ln a_i \tag{5}$$

and the relationship between chemical potential of a dissolved solute, μ_s, and that of its solvent (water), μ_w, is given by a form of the Gibbs-Duhem equation,

$$d\mu_w = -\frac{n_s}{n_w}\, d\mu_s \tag{6}$$

where μ_i = chemical potential of species i,
a_i = activity potential of species i,
n_i = number of moles of species i,
R = molar gas constant, and
T = absolute temperature.

Assuming the number of moles of solute and solvent are fixed, their chemical potentials are exactly inversely related. Thus, an increase in solute activity due to temperature will produce an increase in solute chemical potential and a corresponding decrease in solvent (water) chemical potential. The dependence of solute activity on

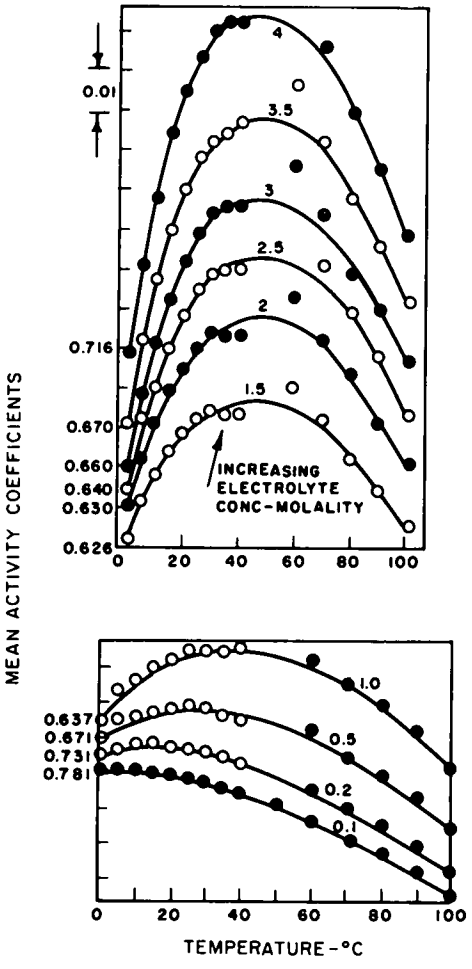

Figure 3. Mean activity coefficient of sodium chloride in 0.1 to 4.0 molal solutions as a function of temperature (after Harned and Owen, 11).

temperature (and concentration) has been measured by Harned and Owen (11). Typical response curves for sodium chloride are shown in Figure 3.

EXPERIMENTAL PROCEDURE

Thermal coupling experiments were run in conjunction with electrokinetic experiments; the latter are described elsewhere (Gray and Mitchell, 7). The effects of a systematic variation in water content, exchange capacity, and external electrolyte concentration on thermal coupling were investigated. Other variables, such as the type of counterion and the degree of saturation, were held constant by restricting the investigation to fully saturated, sodium clays. A detailed account of the experimental procedure has been given (8); salient features are summarized in the following.

Materials and Apparatus

Experimental data were obtained on three types of material: a pure kaolinite (Hydrite UF), an illitic clay (Grundite), and an artificial silty-clay comprised of equal parts by weight of kaolinite and silica flour.

The clays were made as nearly homoionic to sodium ion as possible by washing batches of clay in concentrated solutions of sodium chloride. The excess salt was then removed by leaching the clays with distilled water. The clays were subsequently dried in an oven at 230 F, lightly pulverized, and stored in sealed jars for further use. Weighed amounts of each clay were later mixed with the desired electrolyte solution into thick slurries prior to their introduction into a specially constructed flow cell.

The flow cell itself was designed so that known thermal, electrical, and hydraulic pressure gradients could be applied across the clay samples. Provisions were made to monitor the flows of electricity and water (or solution) that resulted from the application of any one of these gradients. The flow cell was bounded at two ends with retractable pistons, each with a recessed porous stone and electrode in its face. By placing the flow cell assembly in a loading frame it was possible to reduce the water content to any predetermined level. A schematic diagram of the flow cell and test layout is shown in Figure 4.

Thermo-Osmotic and Thermoelectric Tests

Internal heating and cooling coils were installed in the piston heads in order to establish a temperature gradient across the clay sample for thermal coupling tests. The heating and cooling coils in turn were connected to external constant temperature circulators. Temperatures were monitored with thermistor probes and a digital thermometer. The flow cell and test equipment were kept in a constant-temperature room maintained at 20 C.

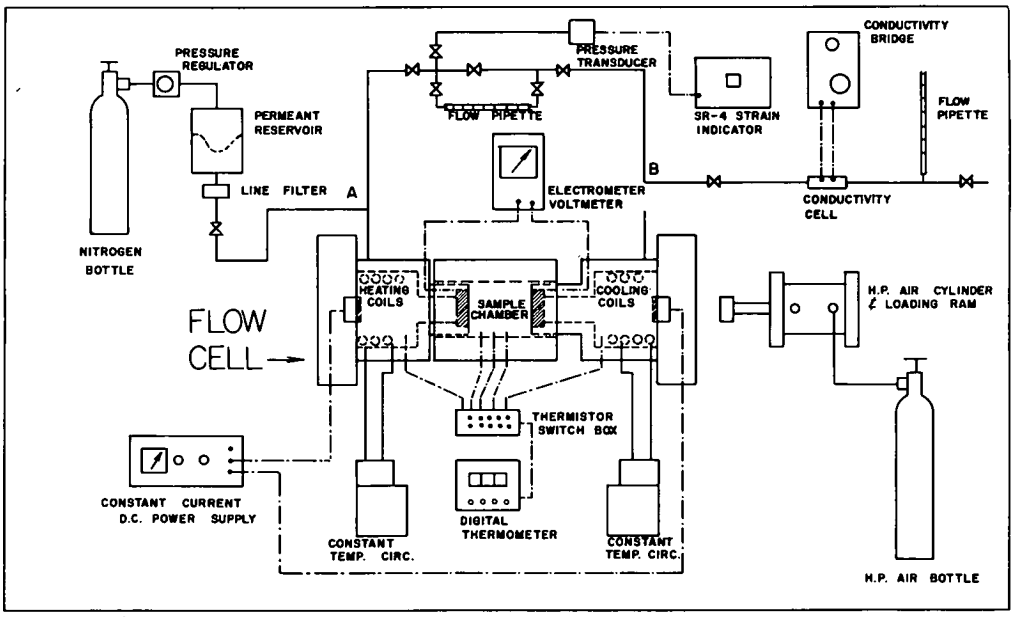

Figure 4. Schematic diagram of flow cell and test layout.

Thermo-osmotic pressures were measured in lieu of osmotic flow rates; this procedure was adopted for experimental convenience. The standard procedure was to apply a temperature gradient across a clay sample and observe the buildup in pressure as indicated by the rise or drop of water level in standpipes on either side. The ends of the clay plug were electrically short-circuited through an ammeter and the induced thermoelectric current recorded concurrently with the thermo-osmotic pressure. Reversible silver-silver chloride electrodes were used to measure the current; chloride solutions were used as the permeant in all tests.

Upon applying a temperature gradient, the water level quickly rose in the standpipes because of an initial thermometric expansion, but the two levels equalized because the standpipes were connected by an open bypass valve. Periodic temperature readings were taken to determine how quickly the system approached a steady-state distribution. Five hours proved to be an adequate time interval for temperature stabilization.

At the end of five hours, the bypass valve was closed and a temperature-induced pressure difference could develop across the clay plug. The pressure difference was directly proportional to the difference in water level in the two standpipes. The levels were read with the aid of a cathetometer. Periodic readings of the pressure difference were taken until an equilibrium pressure was reached. This was taken as the steady-state condition at which the volume flow vanishes, $J_v = 0$. The pressure difference at this point was the thermo-osmotic pressure of interest.

Simultaneous readings of the thermoelectric current were also taken. A continuous and characteristic plot of current vs time for each clay-water system was obtained in this manner.

RESULTS

A typical thermo-osmotic pressure buildup curve for kaolinite is shown in Figure 5. A gradient of approximately 1 C/cm and a mean temperature of about 26 C were common to all tests. Steady-state thermo-osmotic pressures are shown plotted vs water content in Figure 6 for the various clay-water-electrolyte systems. Except in two instances, the pressure rise always occurred at the hot side.

Typical thermoelectric behavior of the clay-water systems is shown in Figures 7 and 8. The induced thermoelectric current is shown plotted as a function of time for

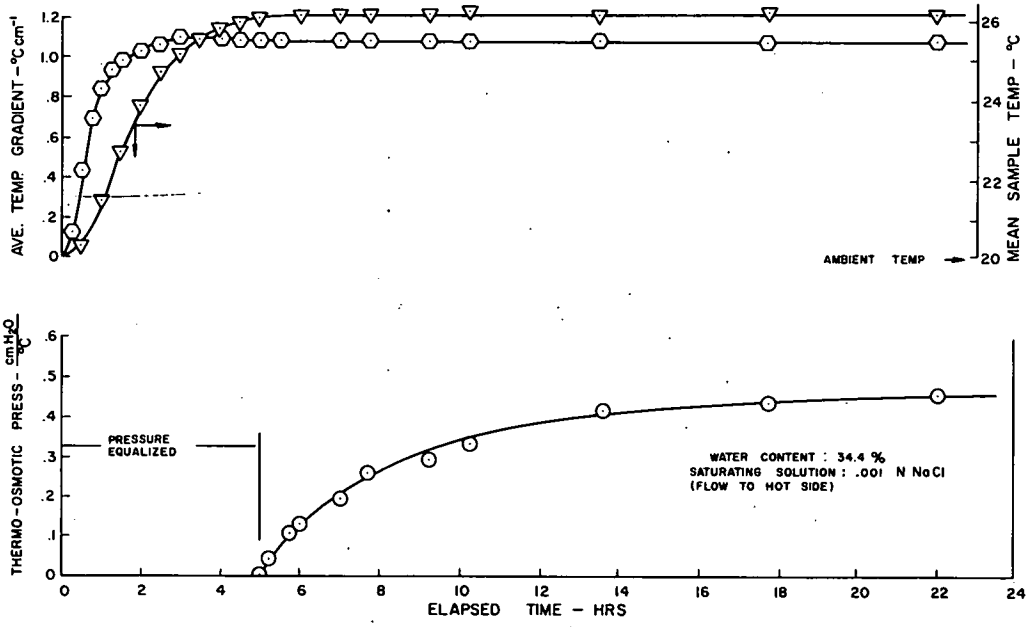

Figure 5. Thermo-osmotic pressure buildup in kaolinite.

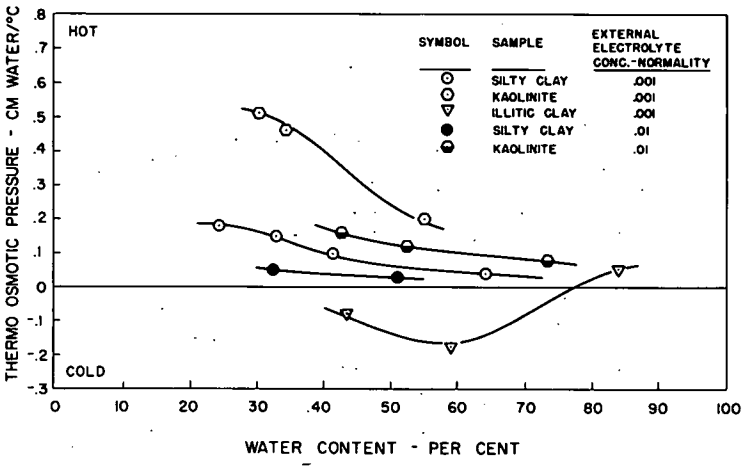

Figure 6. Thermo-osmotic pressure vs water content in clay-water-electrolyte systems.

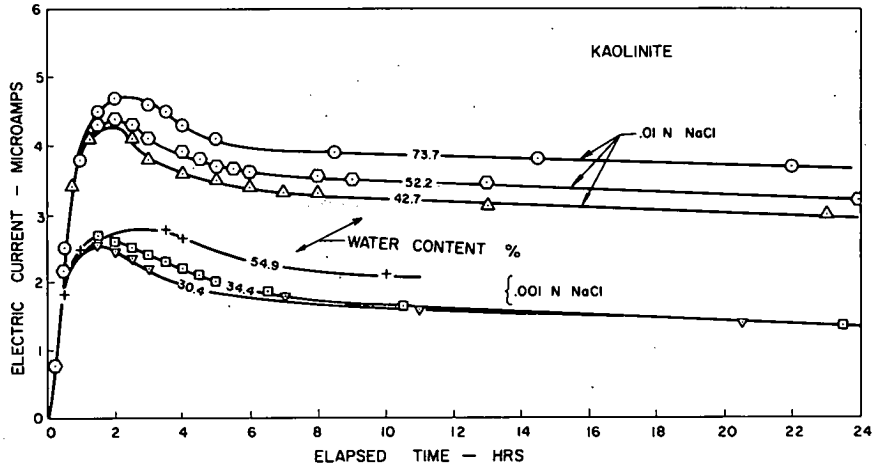

Figure 7. Thermoelectric current vs time in kaolinite for various water contents and normality of saturating solution. Average temperature gradient is 1 C/cm.

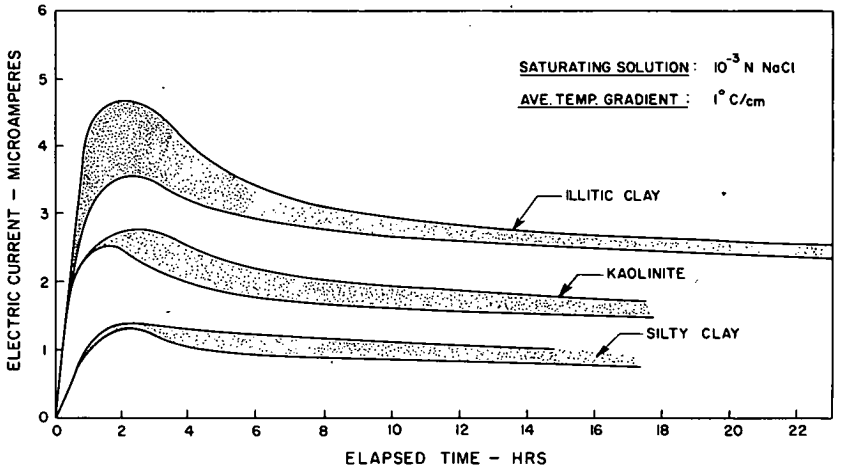

Figure 8. Comparison of thermoelectric curve envelopes for three clays.

various water contents and pore-water electrolyte concentrations in Figure 7. The electric current flow was always from hot to cold, i.e., the hot side had the more positive polarity. The current tended to increase as either the salinity of the saturating solution or the water content was increased. A comparison of the thermoelectric behavior of the three clay systems is shown by a plot of thermoelectric curve envelopes in Figure 8. For a given saturating solution and temperature gradient, the thermoelectric current increased with increasing exchange capacity of the clay.

The initial buildup in current shown in Figures 7 and 8, which reached a peak after one or two hours, is partly a streaming current effect caused by thermometric expansion and expulsion of water from the voids. This could be verified by noting an almost identical response (but with opposite polarity) when the sample was allowed to return to thermal equilibrium.

DISCUSSION AND CONCLUSIONS

Thermo-osmotic flow in saturated, clay-water systems is comparable in magnitude but opposite in direction to results reported by other investigators (see Table 1).

The polarity of the thermoelectric current in a clay-water system agrees with that observed by Ikeda (12) for a negatively charged, collodion membrane. While electrode potentials may have contributed to the induced current in the former, they cannot explain the systematic variation in thermoelectric current with exchange capacity, water content, and concentration of external electrolyte as shown in Figures 7 and 8.

A possible explanation for the direction of thermo-osmotic flow as reported herein may lie with the peculiar dependence of activity coefficients on both temperature and concentration shown in Figure 3. A difference in activity coefficient of solvent (or solute) between the warm and cold sides of a porous medium produces a difference in chemical potential. This means that a flow of solvent or salt must then occur to equalize this imbalance. The results in Figure 3 are for bulk electrolyte solutions; to test out the hypothesis further it would be necessary to determine activity coefficients for soil water electrolytes over a range of concentrations and temperatures. The concentrations shown in Figure 3 lie within the range of counterion concentrations one might expect in the interstitial water of a charged, porous medium such as a clay soil.

The preceding explanation assumes that thermally induced osmotic gradients are the dominant transfer mechanism in saturated, charged membrane systems. If secondary electro-osmotic effects are the cause, then a positive polarity is required at the cold side to produce a flow to the hot; however, the reverse was observed in the present study. Thus, an electro-osmotic explanation is apparently ruled out.

The results of this study confirm earlier investigations in suggesting that the relative magnitudes of thermally induced moisture flows are not particularly significant in saturated soils. The same is not true, it should be emphasized, in the case of partially saturated soils.

REFERENCES

1. Bouyoucos, G. J. Effect of Temperature on Movement of Water Vapor and Capillary Moisture in Soils. Jour. Agr. Res., Vol. 5, p. 141, 1915.
2. Carr, C. W., and Sollner, K. New Experiments on Thermo-Osmosis. Jour. Electrochem. Soc., Vol. 109, p. 616-22, 1962.
3. Cary, J. W. Soil Moisture Transport Due to Thermal Gradients—Practical Aspects. Proc. Soil Sci. Soc. of Amer., Vol. 30, p. 428-433, 1966.
4. Corey, A. T., and Kemper, W. D. Concept of Total Potential in Water and Its Limitations. Soil Sci., Vol. 91, p. 299-302, 1961.
5. Gurr, C. G., et al. Movement of Water in Soil Due to Temperature Gradient. Soil Sci., Vol. 74, p. 335, 1952.
6. Gowda, K. R. S., et al. Theoretical and Experimental Exploration of the Practical Possibilities of Electro-Osmosis, Part V. Rept. to U.S. Navy Dept. No. NOy15087, p. 454-564, 1949.
7. Gray, D. H., and Mitchell, J. K. Fundamental Aspects of Electro-Osmosis in Soils. Jour. Soil Mech. and Found. Eng. Div., ASCE, Vol. 93, No. SM6, p. 209-236, 1967.
8. Gray, D. H. Coupled Flow Phenomena in Clay-Water Systems. PhD thesis, University of California, Berkeley, 1966.
9. Habib, P., and Soeiro, F. Migrations d'Eau dans les Sols provoquees par une Difference de Temperature. Proc. Fourth Internat. Cong. Soil Mech., p. 40-43, 1957.
10. Haas, R., and Steinert, C. Thermo-osmose in Flussigkeiten Messungen. Zeits. Phys. Chem. Neue Folge., Vol. 21, p. 270-297, 1959.
11. Harned, H. S., and Owen, B. B. The Physical Chemistry of Electrolytic Solutions. Reinhold Publ. Co., New York, p. 359-364, 1958.

12. Ikeda, T. Non-Isothermal Membrane Potentials, Jour. Chem. Phys., Vol. 28, p. 166, 1958.
13. Katchalsky, A., and Curran, P. Non-Equilibrium Thermodynamics in Biophysics. Harvard Univ. Press, Cambridge, 1965.
14. Krischer, O., and Rohnhalter, H. Warmeleitung und Dampfdiffusion in feuchteten Guten. VDI Forschungsheft, Berlin, Vol. 402, p. 1-18, 1940.
15. Marshall, D. J., and Madden, T. R. Induced Polarization: A Study of Its Causes. Geophysics, Vol. 24, p. 790-816, 1959.
16. Philip, J. R., and deVries, D. A. Moisture Movement in Porous Materials Under Temperature Gradients. Trans. Amer. Geophys. Union, Vol. 38, p. 222-237, 1957.
17. Rastogi, R. P., et al. Cross Phenomenologic Coefficients: Part I, Studies on Thermo-Osmosis. Trans. Far. Soc., Vol. 60, p. 1386-90, 1964.
18. Smith, W. D. Thermal Transfer of Moisture in Soils. Trans. Amer. Geophy. Union, p. 511, 1943.
19. Taylor, S. A. Simultaneous Flow in Soils and Plants. Special publ., Utah State Univ., Logan, 1963.
20. Taylor, S. A., and Cavazza, L. The Movement of Soil Moisture in Response to Temperature Gradients. Proc. Soil Sci. Soc. Amer., Vol. 18, p. 351, 1954.
21. Taylor, S. A., and Cary, J. W. Analysis of the Simultaneous Flow of Water and Heat With the Thermodynamics of Irreversible Processes. Trans. Seventh Internat. Congr. Soil Sci., Madison, Vol. 1, p. 80-90, 1960.
22. Taylor, S. A., and Cary, J. W. Linear Equations for the Simultaneous Flow of Matter and Energy in a Continuous Soil System. Proc. Soil Sci. Soc. Amer., Vol. 28, p. 167-172, 1964.
23. Winterkorn, H. F. Fundamental Similarities Between Electro-Osmosis and Thermo-Osmotic Phenomena. Proc. HRB, Vol. 27, p. 443-455, 1947.
24. Winterkorn, H. F. Water Movement Through Porous Hydrophilic Systems Under Capillary, Electric, and Thermal Potentials. ASTM Symposium on Permeability of Soils, Spec. Tech. Publ. No. 163, pp. 27-35, 1955.
25. Winterkorn, H. F. Mass Transport Phenomena in Moist Porous Systems as Viewed From the Thermodynamics of Irreversible Processes. HRB Spec. Rept. 40, pp. 324-338, 1958.
26. Winterkorn, H. F. Behavior of Moist Soils in a Thermal Energy Field. Proc. Ninth National Conf. on Clays and Clay Minerals, Pergamon Press, New York, pp. 85-103, 1962.

The Physics and Chemistry of Frozen Soils

PIETER HOEKSTRA, U. S. Army Terrestrial Sciences Center, Hanover, New Hampshire

The engineering properties of frozen soils—strength, thermal conductivity, dielectric constant, and electrical conductivity—are affected by the phase composition of water in soil i. e., the ratio of unfrozen water to ice. The main factors determining the amount of unfrozen water are temperature, surface area, and salt content; minor factors are mineralogical composition, structure, and pressure. The amount of unfrozen water in frozen soils as a function of temperature and pressure can be calculated, using a thermodynamic treatment, for clays from swelling pressure data, and for granular soils from moisture characteristic curves at room temperature. The calculated data show good agreement with experimental data.

The unfrozen film conducts water and ions under the influence of temperature gradients, electrical gradients, and external pressure differences. The rate of migration depends on the surface area and the thickness of the film of unfrozen water. Since the thickness of the film decreases with decreasing temperature, the rate of migration of water through frozen soils rapidly increases as the freezing point is approached.

•THE ENGINEERING behavior of soils is strongly influenced by the interaction of mineral material with water, and the effect of naturally encountered temperatures must invariably be assigned to changes caused by temperature in the interaction of water with the mineral surface or to changes in the properties of water itself. In unfrozen soils the force systems that act on the water are capillarity and adsorption. The forces of capillarity arise from the surface tension at air-water interfaces, and the temperature effect will be proportional to the change in surface tension. For water, the surface tension changes from 75.6 dynes/cm at 0 C to 71.97 dynes/cm at 25 C. The effect of temperature on adsorption forces is more difficult to analyze. One model for physical adsorption on negatively charged surfaces that has been proposed is the theory of the diffuse electric double layer. Differentiating expressions resulting from this model with respect to temperature would be a refinement not warranted by the present accuracy of the model. In general, the effect of temperature on the value of engineering properties of unfrozen soils is neglected in practice.

In frozen ground the effect of temperature, particularly in the range of naturally encountered temperatures, is very large. The reason is that temperature changes not only the interaction of water with soil, but also the ratio of the amount of liquid water to ice. The effect of temperature in frozen ground is similar to the combined effect of change in water content and temperature in unfrozen ground. The paper reviews recent work on the phase composition of water in frozen ground and its importance to engineering properties.

PHASE COMPOSITION OF FROZEN SOILS

In a frozen soil, unfrozen adsorbed water can exist in equilibrium with ice over a large temperature range below freezing. The adsorbed water freezes gradually as the temperature is lowered, decreasing the thickness of the unfrozen film. The ice phase at each temperature is in equilibrium with an unfrozen water layer whose properties are constantly changing as the temperature is lowered. The reason for the large

freezing point depression of the unfrozen water is the presence of exchangeable ions, which are concentrated in thin films upon freezing, and specific adsorption forces emanating from a charged surface.

Figure 1 shows how the liquid water content might change in a soil column in which the temperature changes with distance. At temperatures above freezing all water is in the form of liquid water. At some temperature just below 0 C ice forms and only a certain amount of unfrozen water remains in the liquid form. By lowering the temperature further the amount of unfrozen water is reduced as more water freezes to ice.

Since the unfrozen liquid water is in equilibrium with the ice at any particular temperature and pressure, equilibrium thermodynamics is particularly well-suited to relating physical measurements on soils at above-freezing temperature, such as swelling pressure and soil water tension, to the amount of unfrozen water. Thermodynamic relations only apply to the particular soil under consideration, and cannot be used to predict changes between different soil systems. The important soil parameters are surface area and temperature. Minor variations are caused by such parameters as mineralogical composition and kind of exchangeable ions. In Figure 2 the unfrozen water content is given as a function of temperature for several soils.

The thermodynamic relationships for soils at or below the freezing point are well understood (13, 14). The physical argument is as follows: The unfrozen water exists in the presence of ice, and the two phases of water are in a stable equilibrium. The partial molar free energy of ice, $\bar{F}_i$, is equal to that of the unfrozen, $\bar{F}_{lw}$, Hence,

$$\bar{F}_i - F^\circ = \bar{F}_{lw} - F^\circ \qquad (1)$$

where F° is the free energy of the standard state, which is chosen to be bulk supercooled water at the same temperature as the sample. The ice that forms in frozen soil has been found to be ordinary ice (3), apparently not influenced by the presence of the soil surface. Thus the vapor pressure of ice in soil is the same as ice in bulk. Ice in frozen ground differs in this respect from water in unfrozen ground, where the properties and vapor pressure of water are strongly influenced by a soil surface.

The following relationship exists between $(F_l - F^\circ)$ and vapor pressure:

$$F_i - F^\circ = \bar{F}_{iw} - F^\circ = RT \ln \frac{p_{ice}}{p_o} \qquad (2)$$

where p_{ice} is the vapor pressure of ice and p_o that of bulk supercooled water. The relative humidity of frozen soil, p_{ice}/p_o, which in unfrozen ground is equal to the ratio of the vapor pressure of soil water, p_l, to bulk water, p_{lw}/p_o, is not appreciably affected by temperature at water contents of practical interest.

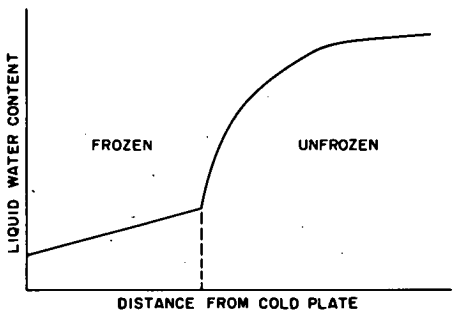

Figure 1. Liquid water content as a function of distance from the cold plate. In the frozen part ice is also present.

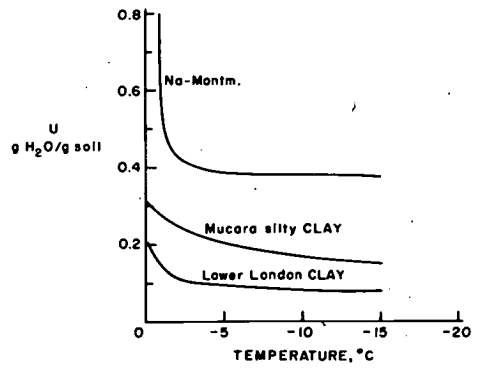

Figure 2. Unfrozen water content, U, as a function of temperature for three soils.

For a given soil the relationship between water content and soil water tension is called the moisture characteristic curve of the soil. The partial molar free energy of soil water, $\bar{F}_{lw} - F^\circ$, is related to the soil water tension, ΔP, by

$$\bar{F}_l - F^\circ = - V_l \Delta P \tag{3}$$

where V_l is the partial molar volume of liquid water. A moisture characteristic curve is usually determined at room temperature. For practical purposes the temperature effect on the moisture characteristic curve, related to the heat of wetting, can be neglected. A moisture characteristic curve can thus be considered as a relationship between partial molar free energy and water content over a fairly large temperature range.

Equations 2 and 3 are alternative expressions for the partial molar free energy of liquid water. Equation 2 is particularly useful in frozen soil when ice is also present. The unfrozen water content can be found from a moisture characteristic curve by first constructing a plot of $(\bar{F}_l - F^\circ)$ vs water content by means of Eq. 3. This curve is valid over a large temperature range. Then a curve of $(\bar{F}_l - F^\circ)$ vs temperature is constructed by means of Eq. 2, applicable strictly to frozen soil when ice and water are in equilibrium. In Figure 3 the amount of unfrozen water is plotted both as a function of $\bar{F}_l - F^\circ$ and temperature for Lower London clay.

The same relationship that exists between tension and $(\bar{F}_l - F^\circ)$ also exists between swelling pressure, π, and $(\bar{F}_{lw} - F^\circ)$. It is of the form

$$\bar{F}_{lw} - F^\circ = - \bar{V}_l \pi \tag{4}$$

Swelling pressures obtained at room temperature can thus also be used to determine amounts of unfrozen water.

For temperatures very close to freezing (0.2 C) the assumption that the free energy of ice in soil is equal to that of bulk ice may not be exactly true. If the ice consists of very small grains a correction may have to be applied for the surface energy (11). This correction becomes small below -0.5 C.

In discussing the strength of frozen ground it is important to know how the amount of unfrozen water changes with pressure (2, 13, 14, 9). Equation 1 can be used to calculate the pressure effect. Differentiating Eq. 1 with respect to pressure yields

$$\left(\frac{\delta F_i}{\delta P}\right)_T - \left(\frac{\delta F^\circ}{\delta P}\right)_T = \left(\frac{\delta \bar{F}_l}{\delta P}\right)_T - \left(\frac{\delta F^\circ}{\delta P}\right)_T \tag{5}$$

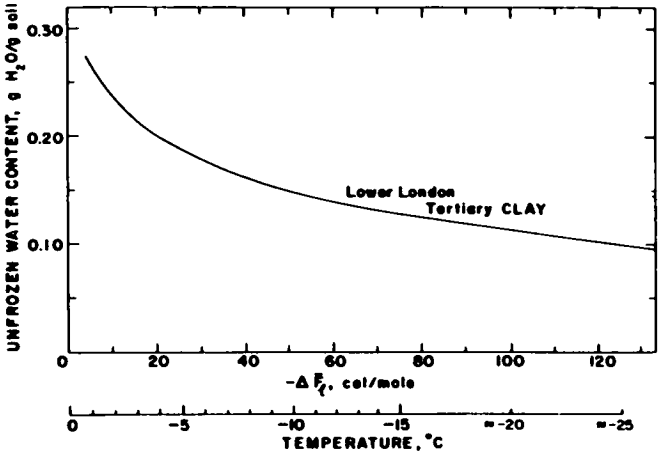

Figure 3. Liquid water content and partial molar free energy as a function of temperature for Lower London Tertiary clay.

using the relations

$$\left(\frac{\delta F_i}{\delta P}\right)_T = V_i \text{ and} \left(\frac{\delta F^\circ}{\delta P}\right)_T = \bar{V}_l$$

where V_i and V° are the molar volumes of the solid and liquid state respectively. Equation 5 can be integrated between the limits of atmospheric pressure, P_a, and any other external pressure, P, which yield

$$\left(\bar{F}_l - F^\circ\right)_{P=P} - \left(\bar{F}_l - F^\circ\right)_{P=P_a} = \left(V_i - V^\circ\right)\left(P - P_a\right) \qquad (6)$$

Equation 6 allows one to calculate the change in partial molar free energy with pressure at constant temperature, since both V_i (= 1.09 cm^3/g) and V° (= 1.0 cm^3/g) are known. Table 1 gives the change in the amount of unfrozen water caused by a pressure increase of 100 atm (1470 psi) at different temperatures for Lower London clay. The pressure effect rapidly decreases with temperature.

The phase composition of water in frozen soils thus depends first of all on temperature, and if it can be shown that the engineering properties of soils are determined by the amount of unfrozen water, one can expect the engineering properties of frozen ground to change dramatically over a relatively small temperature interval (0 to -10 C).

MASS TRANSPORT IN FROZEN SOIL

Water can be transported in frozen soils, and a study of the mechanism and rate at which this process occurs can be used to explain creep of frozen soils. Water movement can also alter the disposition of the ice phase, which often causes large changes in strength and conductance.

Frozen soils are essentially impermeable to laminar water flow and the dominant mechanism of mass transport is mainly by diffusion in the liquid phase. Diffusion can occur under the influence of temperature and external stress gradients. Mass transport occurs through the transition layer between the particle surface and the ice. Figure 4 illustrates the situation that might exist when the ice is placed in a temperature gradient field. The thickness of the film will be larger on the warm side than on the cold side, since the thickness of the transition layer is determined for a given substrate by temperature only. Thus, if there is a temperature gradient along a solid-ice interface, the thickness of the transition layer diminishes in the direction of decreasing temperature. The freezing point depression of the water in the film between a solid and an ice surface has a value equal to the negative temperature. To translate the freezing point depression into a driving force for water diffusion, the freezing point depression can perhaps be related to an equivalent osmotic pressure, π, by

$$\pi = \frac{h}{T\Delta V}\Delta T \qquad (7)$$

TABLE 1

INCREASE IN UNFROZEN WATER, ΔW, CAUSED BY A PRESSURE INCREASE OF 100 ATM IN LOWER LONDON CLAY AT DIFFERENT TEMPERATURES

Temperature, C	ΔW, g H_2O/g Clay
-1.0	0.071
-1.2	0.057
-1.4	0.034
-1.5	0.026
-2.0	0.025
-5.0	0.010
-10.0	0.005

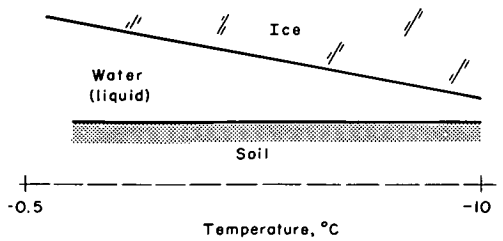

Figure 4. Change in the phase composition of water with temperature.

where h is the latent heat of freezing, T is the temperature, ΔV is the difference in partial molar volume between ice and water, and ΔT is the freezing point depression.

The equation for diffusion in an ideal solution is

$$\gamma = \frac{\lambda (T)}{RT} \Delta \pi \tag{8}$$

where γ is mass flow rate, λ (T) is the coefficient for transfer of water, and R is the gas constant.

Substituting Eq. 7 in Eq. 8 yields

$$\gamma = \frac{\lambda (T)\, h}{RT^2 \Delta V} \Delta (\Delta T) \tag{3}$$

The coefficient of transfer, λ (T), is temperature-dependent. The coefficient can be expected to decrease rapidly with decreasing temperature below freezing. Also, since the water migrates over the surfaces of the soil particles, the flow rate at a certain temperature increases with increasing surface area, and clay-type soils have a higher coefficient of transfer than a silt or sand-type soil at the same temperature below freezing. Water migration under a temperature gradient in a cylindrical column of frozen soil was measured by the attenuation of gamma radiation. In Figure 5 the rate of flow of water in frozen Fairbanks silt is plotted as a function of temperature. The water migrates through the unfrozen water layer in the direction of decreasing film thickness. It should be observed that the rate of transfer is considerable in the temperature range from 0 to -5 C. A saturated unfrozen silt soil usually has a permeability on the order of 10^{-5} cm^2/sec.

It was previously noted that an increase in pressure at constant temperature caused an increase in the amount of unfrozen water. Hence, stress gradients in soils also result in a change in unfrozen film thickness, and movement of water again will occur in the direction of decreasing film thickness. Under isothermal conditions the direction of flow is in the direction of decreasing stress.

Besides mass transport of water, ions also migrate in frozen ground. For the purpose of evaluating frozen ground for storage or ultimate disposal of radioactive waste, the self-diffusion of Na ions was measured in silts from northern Alaska (16). In Figure 6 the diffusion coefficient is given as a function of temperature. When the temperature is lowered and the film thickness decreases, the movement of the ions rapidly slows down. Nevertheless, in the temperature range from 0 to -5 C, ions have an appreciable diffusion coefficient, reduced only by a factor of 5 to 10 compared with unfrozen ground.

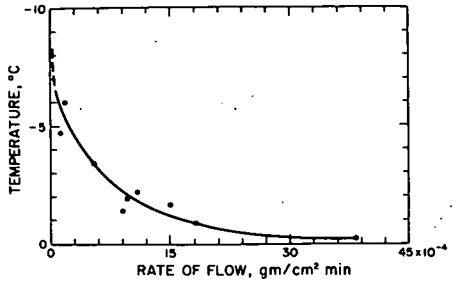

Figure 5. Rate of flow of water in frozen soil as a function of temperature below 0 C.

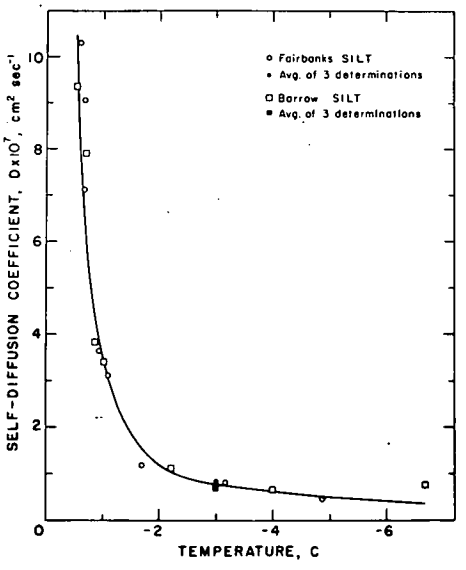

Figure 6. Apparent self-diffusion coefficient of silts from northern Alaska as a function of temperature (after Murrmann and Hoekstra, 16).

ENGINEERING PROPERTIES OF FROZEN SOILS

It has been shown that in general the engineering properties of frozen soils are very temperature-dependent in the temperature range where the phase composition of water changes appreciably. The important engineering properties for construction are strength and thermal properties.

Sections of frozen soils are sometimes used as load-bearing members of finite dimensions. The artificial freezing of a shell of ground for support during tunneling is an example. In such application both the short- and long-term strength must be considered; in particular the long-term strength is very temperature-dependent.

Serious failures occur when the permafrost degradates and frozen soil melts. The maintenance of temperature stability is, therefore, an important engineering objective. The thermal properties of soil enter into any meaningful analysis of thermal stability.

Electrical grounding of equipment and the design of broadcasting antennas require the electrical conductivity of the frozen soil as an input. The conductivity of a soil decreases rapidly when frozen. Yet, depending on the broadcasting frequency, frozen ground must be considered as a lossy dielectric. In the USSR, frozen soil sometimes is melted by passing an alternating current through a certain section.

All the engineering properties of frozen ground are influenced to a certain extent by the disposition of the ice. Different properties are encountered when ice is uniformly distributed or in lenses. These differences are not considered in this paper; here only an attempt is made to explain the temperature-dependence of the properties of frozen ground.

STRENGTH PROPERTIES OF FROZEN SOILS

In an unfrozen soil, shear stresses result from the friction between the particles in a soil skeleton. The value of the shear stress is normally expressed by Coulomb's equation:

$$\gamma = c + (\sigma - \mu) \tan \phi \tag{9}$$

where γ is the shear strength on a plane with a total normal stress σ and a pore pressure μ, and ϕ is the angle of internal friction. For wet cohesionless soil, c is zero and the soil has no unconfined compressive strength. For a clay soil, such as remolded Boston Blue clay with a water content of 29 percent, c is on the order of 3 kg/cm^2. The influence of temperature on the strength of unfrozen soil is considered small.

In frozen soil the ice forms a bond between the mineral particles, and the ice in the pores presumably can carry a stress. The shear stress of frozen soils is much higher than that of unfrozen soil, and frozen ground has been used for structural members of definite dimensions. The strength behavior of frozen ground is determined by many factors, among which are temperature, rate of stress applications, soil type, water content, and the disposition of the ice phase. The strength properties of frozen soils are highly temperature-dependent in the region of intensive phase transformations.

Figure 7 gives the ultimate unconfined compressive strength of a clay soil and sand soil at a strain rate of 0.2 in. per min. With faster rates of load application, higher ultimate strength values are observed. Many researchers found that for Ottawa sand the ultimate strength was related to the rate of stress application by

$$\sigma_{max} = A (\dot{\sigma})^b \tag{10}$$

where σ_{max} is the ultimate unconfined compressive strength and $\dot{\sigma}$ the time rate of load application.

The deformation of frozen soil under static loads has also been investigated in considerable detail. In Figure 8, the behavior of the strain with time at different levels of load application is given. In each curve several sections can be distinguished: Immediately after load application an instantaneous elastic strain arises. The strain then passes through a region of continually decreasing rate to a rate of steady creep, and finally the stage of progressive flow, characterized by an increasing rate of strain

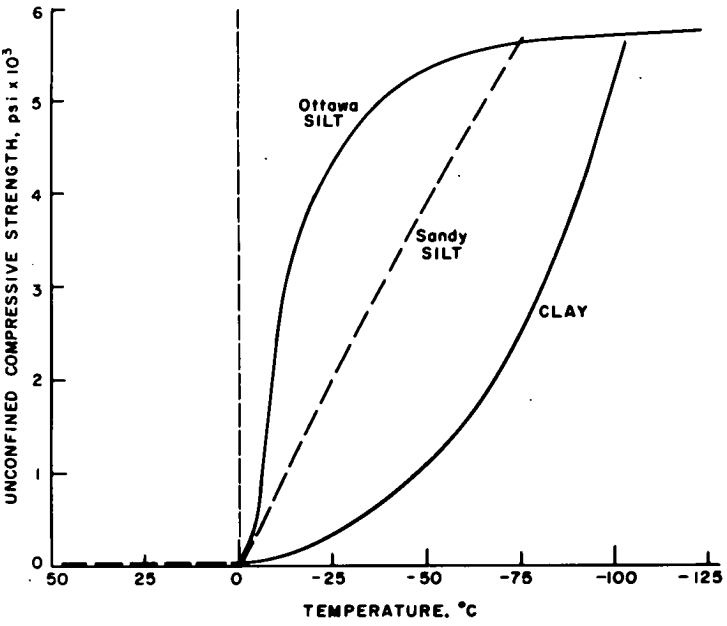

Figure 7. Ultimate compressive strength of three soils as a function of temperature (after Sayles, 19).

leading to collapse. Vialov (21) determined strain as a function of time for several temperatures, and his data are given in Figure 9. In Figure 10 the strain as a function of time at a constant load and at a temperature of -0.3 C is given for different soil types.

Frozen soil is a system of mineral particles and ice separated by films of unfrozen water. A film, even though very thin, exists at the ice-mineral particle interface down to very low temperatures. The increase in the strength of frozen soil with temperature reflects more the increased cohesive strength of the film than the temperature-dependence of the strength of ice.

The properties of the unfrozen film are also evident in the creep of frozen soil. The amount of unfrozen water was found to increase with pressure and flow of water will occur from levels of high stress to low stress. Creep is most likely the result of transport of water under stress gradients. Tsytovich postulated (22) that ice lenses can be transplaced by this mechanism. Ice will melt to replenish the films at the high-pressure end, and ice will accumulate at the low-pressure end. The transport of water under stress gradients is probably an important factor in stress relaxation in frozen ground.

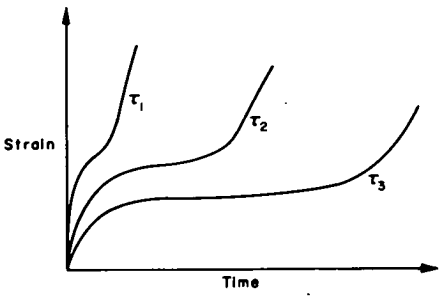

Figure 8. Behavior of strain as a function of temperature at different load levels (after Vialov, 21).

The creep rate is apparently closely related to the amount of unfrozen water. The creep rate increases rapidly with increasing temperature, as seen in Figure 9. Also, at constant temperature the creep rate increases when the soil type contains more unfrozen water (Fig. 10). This observation is a strong argument against attributing the creep to the ice phase; soils of similar ice content may have widely varying creep rates depending on soil type.

Since the phase composition of the water in frozen soils constantly changes when the temperature is lowered, it is difficult to apply the concept of activation energy to this system (4). The theory of rate processes can be applied when

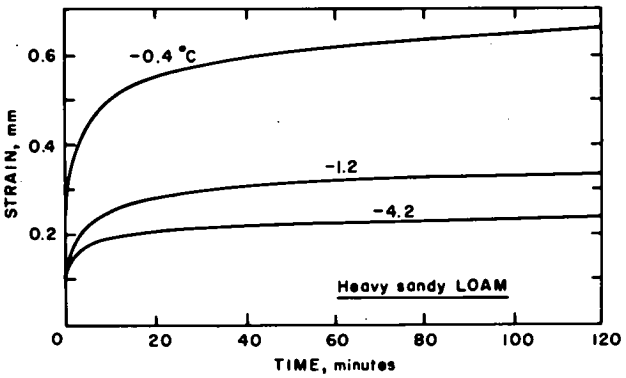

Figure 9. Strain as a function of time at constant load for a heavy sandy loam at several temperatures (after Vialov, 21).

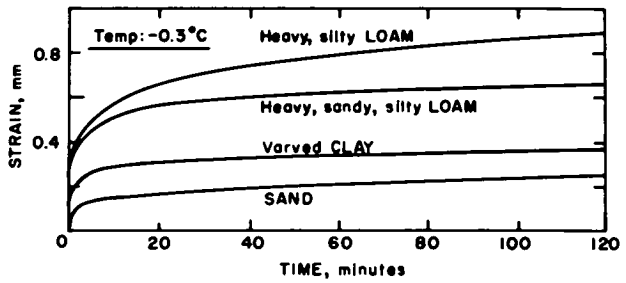

Figure 10. Strain as a function of time at constant load for several soils at a temperature of -0.3 C (after Vialov, 21).

only the thermal energy of the moving molecules changes with temperature. In frozen soil, in addition to the change in thermal energy a gradual phase change also occurs.

As a result, when the theory of rate processes is applied to creep of frozen soils, activation energies are obtained as high as as 93.4 kcal/mole, which value is clearly incompatible with either movement in ice or water. A value of 93.4 kcal/mole would be equivalent to breaking approximately 9 hydrogen bonds. In ice, activation energies for creep are on the order of 13 kcal/mole (17). Finally, Vialov (21) stresses the importance of the structure of the frozen ground on the strength of the soil. The disposition of the ice phase, e. g., in lenses or uniformly distributed, strongly affects the strength of frozen ground. The Russian literature offers many detailed accounts on this subject.

THERMAL PROPERTIES OF FROZEN SOILS

Heat is transported in frozen soils mainly by conduction, that is, the transfer of thermal energy on a molecular scale. Two independent thermal properties enter into a quantitative description of heat transfer by conduction, namely, the thermal conductivity, λ, and the heat capacity per unit weight, C. The quotient of these quantities often appears in heat flow equations; it is called the thermal diffusivity and denoted here by the symbol α.

The heat capacity per gram of unfrozen soil can be found by adding the heat capacity of the different soil constituents in one gram of soil. Thus, if X_S, X_W, and X_α denote the weight fractions of solid material, water, and air, respectively, the heat capacity is given by

$$C = X_S C_S + X_W C_W + X_\alpha C_\alpha \tag{11}$$

The third term can usually be neglected. The value of C_W is 1.00 cal/g C for water and C_S varies between 0.22 and 0.15 cal/g C depending on the mineral type.

The heat capacity of a frozen soil is somewhat more complicated (1, 2, 13, 24). The heat capacity is given by the sum of four terms, one for each phase—mineral particles, ice, and unfrozen water—plus a term that takes into account the latent heat involved when the phase composition changes with temperature. Thus, the heat required Q, to change the temperature of 1 g of frozen soil over a temperature interval ΔT, is given by (1)

$$Q = (C_S X_S + C_i X_i + C_u X_u)\,\Delta T + \int_T^{T+\Delta T} \Delta \bar{H}_f \left(\frac{\delta X_u}{\delta T}\right) \tag{12}$$

where C_s, C_i, C_u are the heat capacities of the mineral particles, the ice, and the unfrozen water respectively and likewise X_s, X_i, X_u are the weight fractions of the constituents; $\Delta\bar{H}_f$ represents the latent heat of phase change of unfrozen water in cal/g. The total weight of water, X_w, is the sum of the amount of ice and water:

$$X_w = X_i + X_u \tag{13}$$

Substituting Eq. 13 in Eq. 12 and dividing by ΔT yields

$$\frac{Q}{\Delta T} = C = C_i X_w + C_s X_\Delta + X_u (C_u - C_i) + \frac{1}{\Delta T}\int_T^{T+\Delta T} \Delta\bar{H}_f\left(\frac{\delta X_u}{\delta T}\right) dT \tag{14}$$

In Figure 11 the heat capacity of Na montmorillonite (2, 13) and Leda clay (24) is given. The heat capacity can be seen to change appreciably between 0 C and -5 C where the phase composition undergoes large changes. The amplitude of the variation in C is related to the amount of unfrozen water and will thus increase the finer the soil.

The problem of expressing the thermal conductivity of a soil as a function of the conductivities and volume fractions of the soil constituents is a very complex task. McGaw (15) has made a critical analysis of heat conduction equations for granular materials. At low water content the thermal transports across solid-liquid interfaces to a large extent determine the heat transfer from grain to grain.

The change in thermal conductivity between frozen and unfrozen soils at low water content illustrates well the importance of interfaces in heat conduction. The thermal conductivity of water at 0 C is 1.4 mcal/deg C cm sec, and the thermal conductivity of ice at 0 C is 5.0 mcal/deg C cm sec. The conductivity of ice increases with decreasing temperature and is 5.5 mcal/deg C cm sec at -9 C. Upon freezing, both parallel or series flow models would predict an increase in thermal conductivity, since liquid water is replaced by the higher conductivity material, ice. McGaw (15) measured the thermal conductivities in unsaturated frozen Ottawa sand. His data are plotted in Figure 12. One data point at -4 C was obtained from Kersten (10). Although part of the water freezes to ice with a higher conductivity, the transfer from grain to grain still has to occur through the films of liquid water. With decreasing temperature the film thickness decreases and the motion of the molecules is restricted, which apparently impedes the thermal transfer.

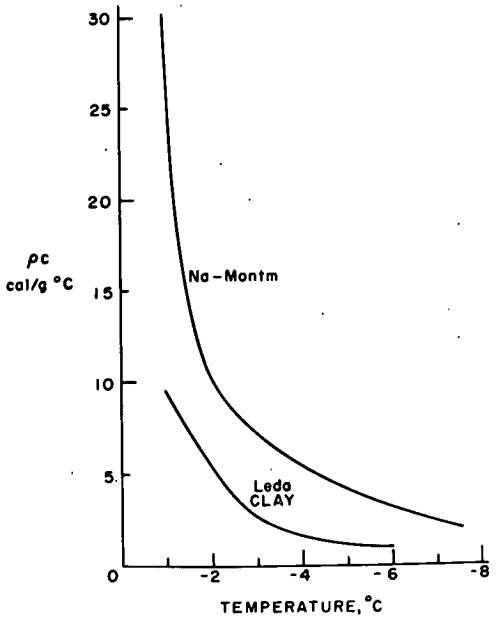

Figure 11. Apparent heat capacity of two clays as a function of temperature (from Anderson, 1, and Williams, 24).

For soils at higher water content, the thermal conductivity no longer decreases upon freezing. Perhaps the ice matrix is continuous and some heat flow paths can bypass the liquid interface. In Figure 13 the ratio of the thermal conductivity at -4 C to the thermal conductivity at +4 C according to Kersten is shown. Thermal conductivity is clearly an area in which more data are required.

When the equation for one-dimensional heat conduction,

$$q = \lambda\,(T)\,\frac{dT}{dx} \tag{15}$$

where q is heat flow in cal/cm^2 sec and λ (T) is the thermal conductivity in cal/deg C cm^2 sec, is combined with the equation describing the conservation of energy,

$$\frac{d}{dx}\,(q) = \rho\, C\, \frac{\delta T}{\delta t} \tag{16}$$

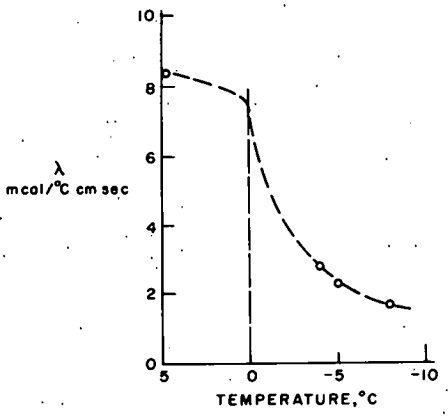

Figure 12. Thermal conductivity of unsaturated frozen Ottawa sand as a function of temperature (from McGaw, 15, and Kersten, 10).

where ρ is density of the medium in gr/cm^3 and C(T) is the heat capacity in gr/deg C, a one-dimensional heat transport equation results:

$$\rho\, C\,(T)\,\frac{\delta T}{\delta t} = \frac{S}{Sx}\left[\lambda\,(T)\,\frac{\delta T}{\delta x}\right] \qquad (17)$$

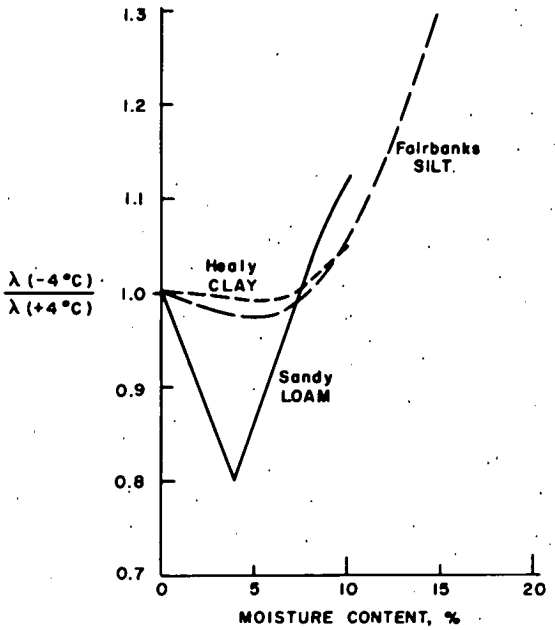

Figure 13. Ratio of thermal conductivity at -4 C to +4 C as a function of moisture content for several soils (after Kersten, 10).

In most heat flow problems both λ and C are considered independent of temperature and Eq. 17 then reduces to

$$\frac{\delta T}{\delta t} = \frac{\lambda}{\rho\, C} = \frac{\delta^2 T}{\delta\, x^2} \qquad (18)$$

and $\lambda/\rho C$ is called the diffusivity. Figure 12 and 13 illustrate that both the heat capacity, C, and the thermal conductivity, λ, are very temperature-dependent and can by no stretch of the imagination be considered as constants. Le Fur et al (12) studied the freezing of kaolinite suspensions and, by placing Eq. 17 in a finite difference form, valuated the apparent diffusivity of the medium. These data are plotted in Figure 14.

In many practical calculations one often assumes that all water freezes at the initial freezing temperature of the soil. The error of this approximation increases the finer mechanical composition of the soil.

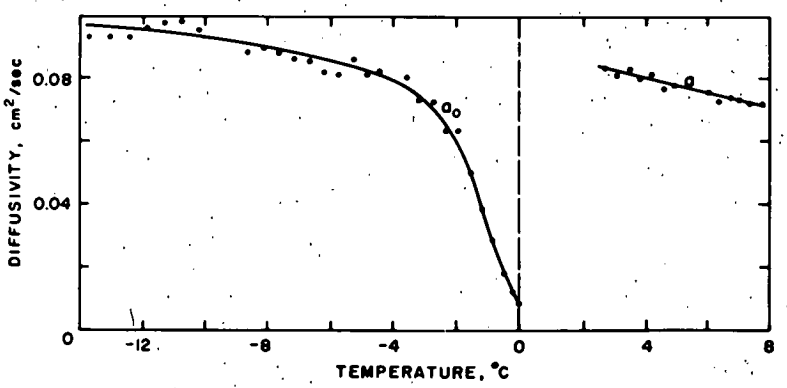

Figure 14. Thermal diffusivity of a kaolinite suspension as a function of temperature (after LeFur et al, 12).

ELECTRICAL PROPERTIES OF FROZEN GROUND

Current flow in response to an electrical gradient in a frozen soil occurs almost entirely through the unfrozen water films. Conductance measurements on a frozen soil can, therefore, be used to investigate the disposition of the unfrozen water, and are particularly useful as an indication of changes in the liquid-like films caused by variation of an external factor such as temperature or pressure.

Soil particles usually carry a negative charge, and to remain electro-neutral this charge is balanced by an excess of positive ions in the water layers close to the surface. When a soil is frozen, relatively pure ice freezes out, the ions are expelled from the ice phase, and crowded in the thin films of unfrozen water. In these thin films the ions are relatively free to move along the surface, but the mobility decreases as the thickness of the film is reduced. Self-diffusion experiments of Na ions provided further proof that at least at temperatures within 10 C from zero, the ions are the most important charge carriers. In Figure 15, the conductance of a frozen silt is shown as a function of temperature. The conductance rapidly decreases in the temperature range from 0 C to -5 C and continues to decrease at a slower rate at temperatures below -5 C.

Previously it was noted that pressure increases the amount of unfrozen water. In Figure 16, the ratio of conductance at atmospheric pressure is plotted vs the conductance at a pressure of 1500 psi. The enhanced conductance with pressure is due to an increase in the amount of unfrozen water.

In summary, one can conclude that frozen soil is not to be regarded as a good insulator. Although ice and mineral particles are relative poor conductors, the transition layer between them causes frozen soil to have a conductance factor 5 to 10 less than the same soil unfrozen.

In order to satisfy the condition of electro-neutrality, the liquid adjacent to a negatively charged surface has an excess of positively charged ions. Thus, if an electric field, E, is applied along the surface, a net force, F, is exerted on a unit volume of liquid. If the excess charge density is ρ coulombs/cm^3, and the electric field, E, is in volts/cm, then the force per unit volume of liquid in joules/cm^3 is given by

$$F = E \cdot \rho$$

A requirement for electro-osmosis is an excess of charge in the liquid layers adjacent to a charged surface. Frozen soil clearly meets these requirements. The exchangeable ions are not incorporated in the ice lattice, but are crowded in the liquid films on the particle surfaces.

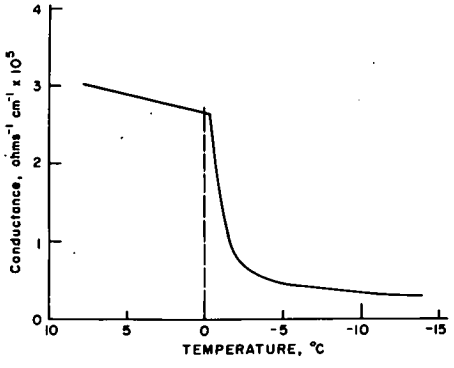

Figure 15. Conductance of a frozen silt as a function of temperature.

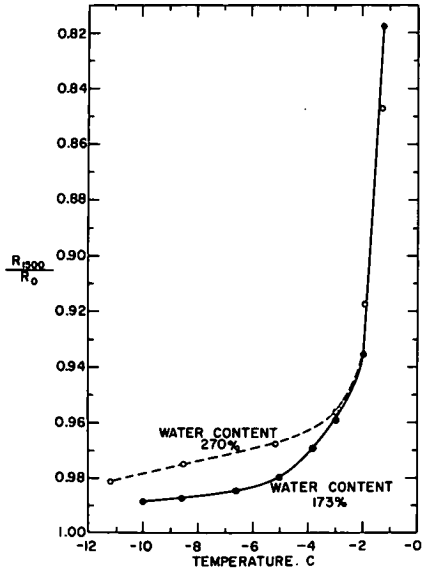

Figure 16. Relative resistance at 1500 psi for Na montmorillonite samples as a function of temperature.

TABLE 2

INITIAL AND FINAL WATER CONTENTS AFTER EXPOSING FROZEN SAMPLE TO ELECTRICAL GRADIENT OF 1 VOLT/CM FOR 24 HOURS
(Weight of Water per Weight of Clay × 100%)

Soil	Temperature C	Initial Water Content	Final Water Content	
			Within 1 cm From Anode	Within 1 cm From Cathode
Wyoming bentonite	-2.0	341	275	456
	-1.5	265	134	310
New Hampshire silt	-1.5	30	27	32
	-1.0	28	21	40

Furthermore, if these films are continuous through the frozen soil, water movement could occur by this mechanism. Verschinin et al (22) and Hoekstra and Chamberlain (6) measured electro-osmoses in frozen clays and silt. Table 2 gives the initial and final water contents after the frozen sample was exposed to an electrical gradient of 1 volt/cm for 24 hours. Water was transported in the frozen soil toward the cathode. Initially the anode area contained ice and unfrozen water, but in the final state all ice was removed from the anode region and large bodies of ice formed in the vicinity of the cathode. Shrinkage cracks might form at the anode.

The mechanism by which the ice is transported needs further discussion. The phase composition of frozen ground was found to depend on temperature and external pressure. An electrical field is not likely to influence the phase composition of frozen ground. When the film water is depleted at a certain location, some ice will melt to replenish the films and, likewise, water will freeze where the amount of liquid water exceeds the equilibrium value.

SUMMARY

The engineering properties of frozen soils are very dependent on temperature in the range from 0 C to -10 C. The temperature-dependence is related to changes in the amount of unfrozen water. The effect of temperature is most pronounced in soil types that contain large quantities of unfrozen water. The amount of unfrozen water increases in the direction sand > silt > clay.

REFERENCES

1. Anderson, D. M. Phase Composition of Frozen Montmorillonite-Water Mixtures From Heat Capacity Measurements. Soil Sci. Soc. Am. Proc., Vol. 30, p. 670, 1966.
2. Anderson, D. M. The Interface Between Ice and Silicate Surfaces. Jour. Coll. and Interface Sci., Vol. 25, p. 174, 1967.
3. Anderson, D. M., and Hoekstra, P. Crystallization of Clay-Adsorbed Water. Science, Vol. 149, p. 318, 1965.
4. Andersland, O. B., and Ahili, W. Stress Effect on Creep Rates of a Frozen Clay Soil. Geotechnique, Vol. 17, p. 27, 1967.
5. Dirksen, C., and Miller, R. D. Closed-System Freezing of Unsaturated Soils. Soil Sci. Soc. Am. Proc., Vol. 30, p. 188, 1966.
6. Hoekstra, P., and Chamberlain, E. Electro-Osmoses in Frozen Soils. Nature, Vol. 203, p. 1406, 1963.
7. Hoekstra, P. Conductance of Frozen Bentonite Suspensions. Soil Sci. Soc. Am. Proc., Vol. 29, p. 519, 1965.
8. Hoekstra, P. Moisture Movement in Soils Under Temperature Gradients With the Cold-Side Temperature Below Freezing. Water Resources Res.; Vol. 2, 1966.

9. Hoekstra, P., and Keune, R. Effect of Pressure on the Conductance of Frozen Bentonite Water Suspensions. Proc. 16th Conf. on Clay and Clay Minerals, Vol. 215, 1967.
10. Kersten, M. S. Laboratory Research for the Determination of the Thermal Properties of Soils. U. S. Engineer Division, St. Paul, Minn., 1949.
11. Koopmans, R. W. R., and Miller, R. D. Soil Freezing and Soil Water Characteristic Curves. Soil Sci. Soc. Am. Proc., Vol. 30, p. 680, 1966.
12. LeFur, B., Aquirre-Puente, J., and Szento, I. Contribution a l'etude de la congelation des argiles. CNRS, Publ. No. 160.
13. Low, P. F., Anderson D. M., and Hoekstra, P. Some Thermodynamic Relationships for Soils at or Below the Freezing Point—I. Freezing Point Depression and Heat Capacity. Water Resources Res., Vol. 4, p. 279, 1968.
14. Low, P. F., Hoekstra, P., and Anderson, D. M. Some Thermodynamic Relationships for Soils at or Below the Freezing Point—II. Effects of Temperature and Pressure on Unfrozen Soil. Water Resources Res., Vol. 4, No. 5, 1968.
15. McGaw, R. Thermal Conductivity of Compacted Sand/Ice Mixtures. Highway Research Record 215, p. 35, 1968.
16. Murrmann, R. P., and Hoekstra, P. Ion Migration in Frozen Soil. Proc. Sixth Army Science Conf., West Point, N. Y., 1968.
17. Na Kaya, U. Visco-Elastic Properties of Snow and Ice in the Greenland Ice Cap. UCCI, Publ. No. 47, p. 199, 1968.
18. Nersesova, A. A., and Tsytovich, N. A. Phase Equilibria and Transformations in Frozen Ground. Proc. Internat. Conf. on Permafrost, Purdue Univ., 1963.
19. Sayles, F. H. Low-Temperature Soil Mechanics. Tech. Note 1966, U. S. Army Cold Regions Res. and Eng. Lab.
20. Tsytovich, N. A. Bases and Foundations on Frozen Soil. HRB Spec. Rept. 58, 1959.
21. Vialov, S. S. Rheological Properties and Bearing Capacity of Frozen Soils. Translation 74, U. S. Army CRREL, Hanover, N. H.
22. Vershinin, D. V., Deriagin, B. V., and Virilenko, N. V. The Nonfreezing Water in Soil. Acad. Sci. USSR, Geograph. and Geophys. Series 13, 108, 1949; also Transl. No. 30, U. S. Army CRREL.
23. Warkentin, B. P., Bolt G. H., and Miller, R. D. Swelling Pressures of Na Montmorillonite. Soil Sci. Soc. Am. Proc., Vol. 21, p. 495, 1957.
24. Williams, P. J. Specific Heat and Apparent Specific Heat of Frozen Soil. Geotechnique, Vol. 14, p. 133, 1964.
25. Williams, P. J. Unfrozen Water in Frozen Soils. Monogian Geotechnical Institute, Publ. No. 72, 1967.
26. Williams, P. J. Unfrozen Water Content of Frozen Soils and Soil Moisture Suction. Geotechnique, Vol. 14, p. 2, 1964.

Thermodynamics of Granular Systems

ALFRED HOLL, United Asphalt and Tar Manufacturing Co., West Germany*

•GRANULAR SYSTEMS are assemblies of a very large number of grains. Winterkorn (2) was the first to recognize and utilize the analogies of such systems with molecular systems. He initiated an entirely new line of research, which proved to be very fruitful. The analogies employed by him and others with the kinetic theory of molecular systems, exemplified in the treatment of granular systems as macromeritic liquids, are ultimately a part of statistical thermodynamics.

A special branch of statistical thermodynamics of granular systems can be developed rigorously on the basis of the following axioms:

Axiom 1: A granular system consists of a finite, though very large, number of grains that are in contact with their neighbors. The individual grains possess distinct and permanent shapes.

Axiom 2: At a state of equilibrium, the grains are in positions of rest, characterized by a certain degree of order.

Axiom 3: Any movement is governed by the laws of mechanics.

From this system of axioms it is possible, in principle, to deduce all laws of a special statistical thermodynamics of granular systems, although this meets in part with very great formalistic difficulties. For this reason, this type of deduction has so far been successful only with respect to a few laws. This method, however, possesses a fundamental defect: the temperature of a granular system cannot be theoretically derived. This is perfectly obvious if one realizes that the concept of temperature is inherently alien to mechanics. The deductive process leads rather to a geometric analogue of the temperature of molecular systems. While this is useful in many respects, it cannot give a real account of the actual temperature of a granular system. For this reason, we shall forego in this paper further treatment of statistical thermodynamics, except for a few pertinent observations.

Inspired by the Winterkorn concept, we have opened up a new path in this paper: temperature and heat content are determined on the basis of the energy principle from properties of granular systems that can be measured macroscopically. For this purpose we had to derive and apply a "special classical thermodynamics of granular systems." Temperature and heat content are derived for definite work processes and general conclusions are drawn.

GRANULAR ASSEMBLIES AS THERMODYNAMIC SYSTEMS

If the volumes of the individual grains are small as compared with the total volume of the granular system, then the bulk behavior of the system will be that of a homogeneous medium. Such systems can be treated with the methods of classical thermodynamics.

Type of Thermodynamic System

Basic for the methodology developed is the definition of the volume of, or space occupied by, the granular assembly, which is then called a thermodynamic system. The system's boundaries are chosen in a manner as to render treatment of the phenomena that occur on them as simple as possible. The experiment illustrated in Figure 1 produces results that are pertinent to many problems; it will be utilized in the following

*Paper translated by Hans F. Winterkorn.

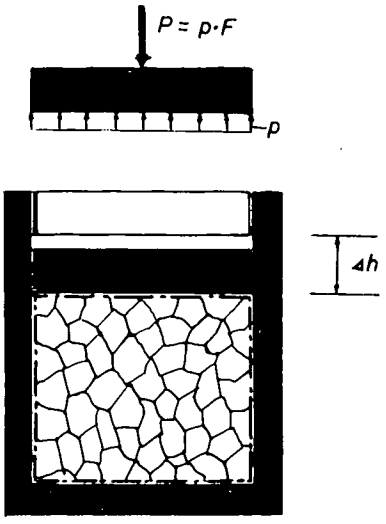

Figure 1. Grain assembly as a thermodynamic system; mechanical equilibrium at the pressure piston.

investigations. We choose as system boundaries the interior surfaces of the container (dashed lines). The container walls and the pressure piston are the environment of this system. This environment can be considered as practically rigid, since any deformation suffered by it upon load application will be very small in comparison with the deformation of the system. The space within the system boundaries represents a quasi-homogeneous closed thermodynamic system; it is considered as closed because during a process no material is allowed to pass across the system boundary.

Condition of State of the Thermodynamic System

The state of equilibrium of a system can be expressed by a few parameters. In the simplest thermodynamic system, the ideal gas, the parameters of state are the volume, v, the internal pressure, p (which for static equilibrium of the system must be equal to the external pressure), and the temperature, T. In accordance with experience, these parameters are mutually interdependent, which can be expressed by

$$f(v, p, T) = 0 \tag{1}$$

or explicitly

$$v = f(p, T) \tag{2}$$

Equation 1 or 2 is called the equation of state of this system. The simplest thermodynamic system possesses, therefore, two independent thermodynamic parameters; in Eq. 2, p and T were defined as independent, hence the third parameter, v, would have to be calculated in accordance with the equation.

An equation of state becomes more complicated as the particular thermodynamic system becomes more complicated. More complicated systems are non-ideal gases and, especially, condensed systems such as liquids and solids. In the general case of the latter, we have, instead of the volume, a strain tensor with six independent components and, instead of the uniform internal pressure, a stress tensor, also with six independent components. The rigorous treatment of such equations becomes very difficult and often even impossible.

Granular assemblies can also be considered as condensed systems. They are in a particular state of aggregation that shows partly "liquid" and partly "solid" characteristics. Representative of the liquid properties is the lack of a characteristic form or shape of the system. Maintenance of the external form under load application is possible only through the action of counter-forces. Solid properties derive from a capacity to maintain a characteristic internal order or packing. In the presence of external counter-forces, the volume of the granular systems is a function of the external loading.

The experimental arrangement shown in Figure 1 depicts an especially simple thermodynamic model of a granular system that takes into account the foregoing conditions of its particular state of aggregation. The volume of the system can be given absolutely in cubic centimeters or specifically in cubic centimeter per cubic centimeter of solids or in cubic centimeters per gram of solids. Preferred for many good reasons is the use of the specific volume, v, defined by

$$v = 1 + \epsilon \ (cm^3/cm^3) \tag{3}$$

wherein ϵ = void ratio; ϵ can be calculated from the vertical compressibility of the system. The mathematical treatment of the problem requires the use of differentials. Although the granular system does not possess a differential volume element, its formal introduction is justified by the previous assumption of quasi-homogeneity of the system. The differential of the specific volume $d(1 + \epsilon)$ is that of $d\epsilon$; therefore, the void ratio, ϵ, is sufficient for the characterization of the specific volume of a granular system.

The internal stress condition of the system shown in Figure 1 can also be very simply expressed: all section stresses are proportional to the loading stress, p. The lateral stresses can be obtained by use of the coefficient of pressure at rest, λ_0, and so on. Therefore, the loading stress, p, is ultimately sufficient for the description of the stress state of the system.

As a final parameter of state, there remains the temperature, T; accordingly, we obtain the following as an equation of state for the system exemplified in Figure 1:

$$\epsilon = f(p, T) \tag{4}$$

The Thermodynamic Process

The equation of state (Eq. 4) characterizes a special state of equilibrium of the granular system. Changing one of the parameters disturbs the system and initiates movement; in other words, a thermodynamic process takes place. The parameters become variables, and the equation of state expresses a functional relationship that indicates direction and magnitude of change resulting from variation of the independent parameters.

If the variables are changed only to a very small extent, then the state of the granular system also deviates only to a very small extent from the equilibrium state; such processes are called quasi-static. They proceed so slowly that no mass forces become mobilized within the system. The entire course of such processes can be followed by means of thermodynamic methods. If, however, the process proceeds so fast that mass forces arise, then one deals with non-static changes of state. If, as is usually the case, a system is in a state of equilibrium before and after a non-static change of state, then the initial and final states are susceptible to thermodynamic treatment while the intermediate states are not. The main thermodynamic processes in granular systems that proceed as a result of externally applied forces are mixing, separation or segregation, densification (compression and expansion), shear, and consolidation. All these processes can be investigated with thermodynamic methods. This shall be done for the densification process.

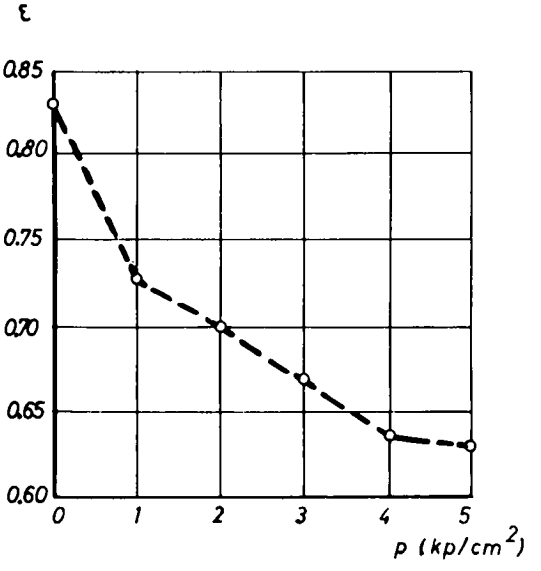

Figure 2. Experimentally determined compression function for a coarse sand.

HEAT IN THE COMPRESSION PROCESS

A complete description of the process comprises two parts: first, a statement of the changes in the parameters brought about by the process, and second, a statement of the energy changes involved in the process.

Experimental Determination of the Compression Function

The first part of the process description deals with obtaining the state

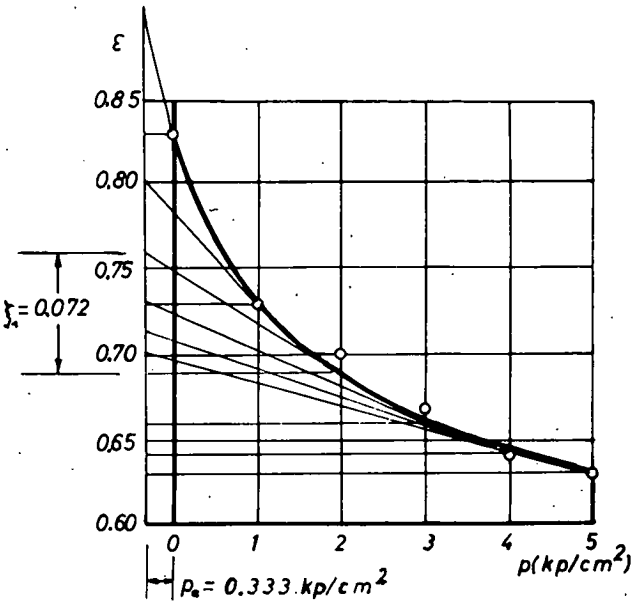

Figure 3. Logarithmic compression function for coarse sand data.

function. Equation 4 represents geometrically an area or surface in space. This makes its visual presentation quite difficult. Elimination of one of the three variables reduces the geometric presentation of the function to a curve in a plane, which can be easily visualized. Such elimination is achieved practically by keeping the parameter that is to be eliminated constant during the process. Then the relationship between the remaining variables is no longer influenced by the constant parameter.

For the quasi-static compression process, it can be assumed that the temperature, T, does not change during the process. This assumption will be justified later on. The state function for the compression process is then

$$\epsilon = f(p) \tag{5}$$

which is also called the compression function. It is determined experimentally by determination of the volume changes resulting from changes in applied pressure. From these, the void ratios, ϵ, are plotted against the pertinent pressures (Fig. 2). This method of determination is always possible, at least in principle.

Analytical Determination of the Compression Function

For many purposes, a closed mathematical form of the compression function is desirable. Since all densification processes proceed essentially in the same manner, one can use phenomenologic approaches for this purpose.

The Logarithmic Compression Function—A simple densification law can be derived from the logical assumption that the change in void ratio per change in compressive stress decreases with increasing compressive stress (at large compressive stresses the densification process is already far gone):

$$\frac{d\epsilon}{dp} = -\frac{\xi_1}{(P_a^* + P)} \tag{6}$$

in which ξ_1 and P_a^* are coefficients. This equation, which we owe to Terzaghi (1), represents the differential equation of the consolidation process. Integration gives

$$\epsilon = \epsilon_a - \xi_1 \ln \frac{P_a^* + P}{P_a^*} \tag{7}$$

in which ϵ = void ratio at static pressure p, and ϵ_a = original void ratio. Figure 3 shows the logarithmic compression law for the test series shown in Figure 2. The shaded triangle helps to visualize the geometric significance of the compression law (Eq. 6) employed and of the coefficients ξ_1 and P_a^*.

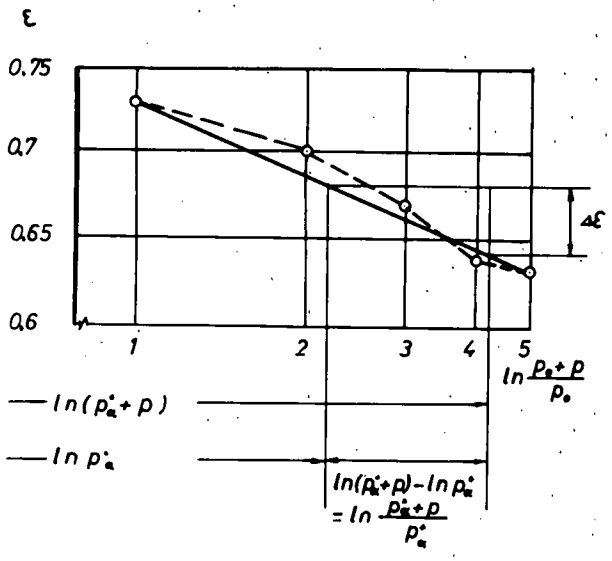

Figure 4. Densification function in semi-logarithmic presentation.

The coordinate system of Figure 4 has a linear ordinate and a logarithmic abscissa. The logarithmic function (Eq. 7) forms a straight line in this system. This method can be utilized for an approximate graphic determination of the function expressed by Eq. 7.

The Exponential Compression Function—Another densification law can be deduced from the fact that the void ratio decreases with increasing densification and tends toward a limiting value:

$$\frac{d\epsilon}{dp} = - \xi_2 (\epsilon - \epsilon_0) \tag{8}$$

The integral of this equation is

$$\epsilon = \epsilon_0 + a \cdot e^{-\xi_2 P} \tag{9}$$

in which ϵ_0 is the minimum void ratio and ξ_2 and a are coefficients. Equation 9 matches a function developed by Kezdi (3) in a different manner.

Figure 5 shows the exponential densification function for the test series shown in Figure 2. The shaded triangle allows easy visualization of the geometric meaning of the densification law employed (Eq. 8), and of the coefficients ξ_2 and ϵ_0. Figure 6 employs a coordinate system with logarithmic ordinate and linear abscissa. Accordingly, Eq. 9 is represented as a straight line.

TABLE 1

COMPARISON OF EXPERIMENTAL AND MATHEMATICAL VOIDS RATIOS

Void Ratios From:	Static Consolidation Pressure, p (ε), in kp/cm²					
	0	1	2	3	4	5
Experiments	0.83	0.73	0.70	0.67	0.64	0.63
Logarithmic function $\epsilon = 0.83 - 0.166 \log \frac{p + 0.333}{0.333}$	0.83	0.73	0.69	0.66	0.64	0.63
Exponential function $\epsilon = 0.62 + 0.21e^{-0.648p}$	0.83	0.73	0.68	0.65	0.64	0.63

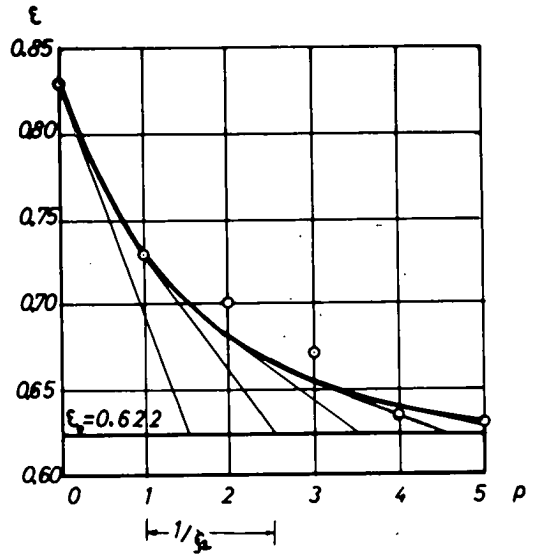

Figure 5. Exponential compression function for coarse sand data.

Other Compression Laws—Equations 7 and 9 can be made to fit a series of test data by proper choice of the respective coefficients. According to the laws of algebra, such fitting is more successful the larger the number of coefficients, i.e., the higher the powers of the independent variables that can be taken into account. This can be done very simply by the use of binomial formulations, e.g.,

$$\frac{d\epsilon}{dp} = \frac{-\xi_1}{(P + Pa)^n} \text{ or}$$

$$\frac{d\epsilon}{dp} = -\xi_2(\epsilon - \epsilon_0)^n$$

The most general manner would be a polynomial expression such as

$$\frac{d\epsilon}{dp} = \frac{\xi_1}{(a + bp + cp^2 + \ldots)}$$

Integration of such expressions is somewhat more difficult and leads to a function whose structure may be quite complicated. The question arises whether or not it is worthwhile to use such complicated expressions. Table 1 gives a comparison of void ratios determined by means of the simple compression functions (Eqs. 7 and 9) with those determined experimentally. The numerical values were determined either rigorously in accordance with statistical methods or approximately by the use of judiciously selected test data.

Table 1 shows good agreement of the analytical values with those obtained by experiment even though all calculations were based on a deliberately selected uneven test

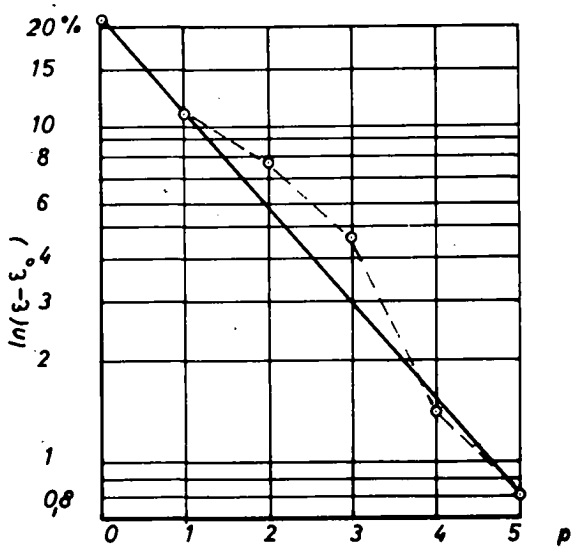

Figure 6. Plot of the logarithm of $(\epsilon - \epsilon_0)$ vs the pressure.

series. Consequently, at least for all practical purposes, there is no need for greater accuracy and refinement.

Fundamental Significance of the Exponential Compression Function—*The Complete Compression of a Granular System*—In accordance with Axioms 1 and 2, every assembly of grains possesses a particular densest state of packing which shall be designated as "zero state." This can be proved as follows: For spheres of the same size, irrespective of the actual diameter, $\epsilon_0 \simeq 0.35$. In the case of mixtures of spheres of two or more sizes, ϵ_0 is a function of the gradation or size distribution. Real grains also possess shapes that deviate from the spherical. This lends importance to their orientation in packing. As a matter of principle, though, every granular assembly possesses a minimum void ratio, ϵ_0, that defines a state of highest order and densest packing in accordance with geometrical compatibility. The exponential compression function (Eq. 9) is in harmony with this concept and, therefore, is of fundamental significance. In contrast to this, the logarithmic compression function (Eq. 7) is only able to describe the consolidation behavior within the range of actual test data and does not permit of extrapolation.

Secondary Compression Effects—Often the actual behavior of granular systems does not agree completely with the ideal assumptions made in the preceding paragraph. The deviations are caused by subsequent secondary densification effects that are superimposed on the fundamental behavior described previously. The causes for this are mainly as follows:

1. Influences of orientation: The degree of orientation depends mainly on the densification method employed. Some methods favor orientation as, for example, vibratory densification; others, like impact methods, are antagonistic to orientation. If liquid phases are present in a granular system (e.g., water in soil or hot bitumen in asphaltic mixtures), even methods that are normally antagonistic to ordering bring about a high degree of orientation. The higher this degree, the greater is the density.
2. Influences of grain fragmentation: Contrary to Axiom 1, real grains possess a finite material strength. They can be fragmented if overstressed. Limited degrees of grain fragmentation may result in increased density of the system.
3. Flow phenomena: In the presence of liquid phases in the granular system, permanent flow deformation can be observed when certain methods are employed in the compression of the system.

Practical Determination of Zero State—Despite the secondary densification effects mentioned, it is always possible to recognize the fundamental behavior of granular systems from the results of practical densification methods. The commonly used methods result in a state of very dense packing with grain fragmentation normally held within very narrow limits. Only use of excessive densification efforts results in fundamentally different internal structures having no further thermodynamic relationships with the original systems. The flow phenomena previously mentioned only change the external form of the system. Therefore, they do not interfere with the possibility of estimating the zero state void ratio that is characteristic for the system. For practical purposes, one may choose as zero state that which results from sufficient densification by such common methods as vibration-to-volume constancy, Proctor densification, or Marshall test.

Work of Compression of a Granular System

The first part of the treatment of the compression process terminates with the development of the compression function. The second and properly thermodynamic part is concerned with the energies involved. An important portion of these is the external work required for the compression. It can easily be seen that the concept of work as product of force times distance in the direction of the force used in classical stereomechanics is no longer sufficient in the case of densification, if one takes into account only the external conditions for arriving at the total work involved. Determinant is rather the work accepted by the system, which is governed by the internal state of the system. Employing the original definition of mechanical work, the work performed is

the product of the force acting at the system boundaries and the translation of the boundaries in the direction of the force. The differential of the work is then

$$dw = p \cdot F \cdot ds = p \cdot dv \tag{10}$$

where

$p \cdot F$ = force at the system boundary (p = pressure, F = area);
ds = differential of the translation of the boundary; and
dv = differential of the translation volume.

If a boundary translation process moves the system from state 1 to state 2, then the total work is represented by the integral of Eq. 10:

$$w_{12} = \int_1^2 p \cdot dv \tag{11}$$

This integral can be solved if the function $p = p(v)$ is known. This function is identical with the state function developed in the first part of the description of the densification process. For granular systems we have then, instead of Eq. 11,

$$w_{12} = \int_1^2 p(\epsilon)\, d\epsilon \tag{12}$$

Here w_{12} is the specific compression work for 1 cm^3 of material and, using the factor $1/\rho$ (ρ = density of material in g/cm^3), for 1 g of solid material. The special position of the derived thermodynamic work concept—which must be considered as an expansion of the mechanic work concept—shall be illustrated by means of an extreme example: The system is represented by a rigid body on a rigid foundation that is impacted externally by a falling mass [weight G (kp), height of fall h (m)]. The kinetic energy at the moment of impact of the falling mass on the system boundary is derived most simply from its identity with the potential energy, i.e., the product of G x h (mkp). However, the work performed on the system equals zero since the system boundary does not move in a rigid system. If, however, one considers under the same external conditions a compressible system such as a granular assembly, then this will accept work in accordance with Eq. 12. Its amount is smaller than G x h. The integral of Eq. 12 can be interpreted geometrically. It is proportional to the area between the compression line and the ϵ-axis in the case of horizontal strips. The graphic presentation of the compression line in a p/ϵ diagram shall, therefore, be called the work diagram. Its area can be determined with a planimeter or by compass addition.

By the use of mathematical compression functions, we obtain closed expressions for the compression work that can be integrated. With Eq. 7, the ln function:

$$w_{12} = \xi_1 p_e - p_a^* (\epsilon_a - \epsilon_e)\ cmp/cm^3 \tag{13}$$

With Eq. 9, the e function:

$$w_{12} = \frac{\epsilon_a - \epsilon_e}{\xi_2}\ cmp/cm^3 \tag{14}$$

The coefficient ξ_1 possesses the dimensions of a void ratio (cm^3/cm^3) while ξ_2 has the dimensions of an inverse pressure (cm^2/p). Using pertinent numerical factors, w_{12} can be expressed in other units, e.g., mkp/dm^3, mkp/kg, ft-lb/ft^3. For the numerical example given earlier, we find, for a ρ value of 2.7 g/cm^3, a w_{12} value of 1.09 mkp/kg from the ln function and 1.19 mkp/kg from the e function. The difference of 8.4 percent

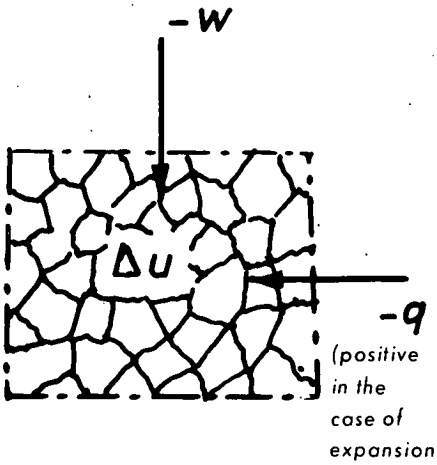

Figure 7. Sign convention.

in the calculated work finds its explanation mainly in the complete coverage of the densification range down to the zero state by the e-line. The results are influenced only to a very small degree by the slightly different course of the two functions within the measuring range.

External Friction Work

The compression work as calculated in the previous section has one shortcoming. The calculated values contain not only the compression work proper, but also the work required to overcome the external friction, i.e., the friction between the system and its surroundings (wall friction). In actual cases, this external friction work cannot be separated from the total work. It is possible, however, to give estimates of plausible values. The external friction work arises from the tangential stresses at the system boundaries. According to Coulomb, these stresses are directly proportional to the radial stresses and hence to the pressures which effect the densification. The friction work is proportional to the densification work. In specimens that possess relatively small ratios of surface to volume, the external friction may account for as much as 20 percent of the total work; less favorable specimen forms can result in much larger proportions of the external friction work. Accordingly, the wall friction influence can be taken into account in a simple manner by multiplication of the total work with an appropriate coefficient. For the calculation of limiting values and ranges, the external friction work may be neglected in first approximation in the case of specimens possessing small surface/volume ratios.

Heat in the Compression Process

It may appear astounding that heat appears this late in a treatise on thermodynamics. As a matter of fact, the heat, q, is only a particular form of energy (which crosses the system boundary together with other forms). Hence, there is nothing special about it. Both heat and work are products of a process and not parameters of state.

Energy Balance for the Compression Process—In accordance with the energy principle, all energies involved in a process are conserved. In addition to the work, w, and heat, q, mentioned previously, there exists the internal energy, u, of the system. The latter depends only on the state of the system and is, therefore, a state parameter. Employing the sign convention shown in Figure 7, the energy principle yields the following equation for a thermodynamic process:

$$\Delta u = q - w \qquad (15)$$

where

$\Delta u = u_2 - u_1$ = change in internal energy, u, during a change in state from 1 to 2;
q = heat that crosses the system boundary during the process = q_{12};
w = work that crosses the system boundary during the process = w_{12}.

Equation 15 states that the difference between the energies gained and the energies lost remains in the system as an increase in internal energy.

At this point the following comments are indicated. All three energy forms—work, w, heat, q, and internal energy, u—must be inserted in Eq. 15 in the same units. In common use are mkp/kg, kcal/kg, mkp/dm^3, kcal/dm^3, and other units. Definite conversion factors exist between the various units, such as 1 kcal $\simeq$ 427 mkp or 1 mkp $\simeq 2.34 \times 10^{-3}$ kcal.

Figure 7 shows the direction of the resultant energy fluxes during the densification processes: mechanical work is performed on the system, heat is produced. The type of energy conversion process that takes place is analogous to that in a heat pump. The efficiency of the action mechanism in the granular system is reduced as a result of secondary effects. The expended work is not entirely changed into heat (passing through internal energy), but a definite portion of it may be used in grain comminution work.

The internal energy, u, is rigorously defined by Eq. 15 for the compression process of a granular system. This emphasizes the basic assumptions made, namely, that energy amounts deriving from motion (mass effects), gravity (due to the weight of the grains), and other energy forms must be negligibly small.

The heat, q, can be determined as follows:

$$q_{12} = m \cdot c\,(T_2 - T_1) \tag{16}$$

in which

m = mass of the system;
c = specific heat per unit mass; and
T_1, T_2 = absolute temperatures of the system in degrees K; ΔT (°K) is numerically equal to ΔT (°C).

In accordance with Eq. 16,

$$q_{12} = c\Delta T \tag{17}$$

Knowledge of q_{12} and w_{12} permits calculation of Δu.

Limit Values of Temperature and Heat in the Compression Process—Maximum values for temperature change and heat production can be obtained from a type of limit calculation under the assumption that during the densification process no external friction work and no grain comminution work will be performed. The energy fluxes which obtain during the process can be divided into two components by means of a mental experiment and can be clearly presented with the aid of the following artifice. In the first part of the process, no heat is lost through the system surface. Therefore, $q_{12} = 0$ and, according to Eq. 15, the energy balance is

$$\Delta u = -w_{12} \tag{18a}$$

The increase in internal energy, Δu, of the system shows itself in a measurable increase in temperature.

In a second part of the process, the heated system is cooled to environmental temperature, whereby an amount of heat energy, $-q_{12}$ is transferred from the system to its environment. According to Eq. 15, this portion is

$$\Delta u = -q_{12} \tag{18b}$$

For the total process, the limiting value is then

$$q_{12} = +w_{12} \tag{18c}$$

Consequently, using Eq. 17, we obtain (also as limiting value) for the temperature increase

$$\Delta t = \frac{+w_{12}}{c}$$

Employing the numerical data from the example previously mentioned (hard rock particles of $c = 0.18$ kcal/kg-deg, air of $c = 0.25$ kcal/kg-deg; and for the granular system, $c = 0.2$ kcal/kg-deg):

$$\Delta t = \frac{1.19 \text{mkp/kg}}{0.2 \text{ kcal/kg-deg}} = \frac{1.19 \times 2.34 \times 10^{-3} \text{kcal/kg}}{0.2 \text{ kcal/kg-deg}} = 1.39 \times 10^{-2} \text{ deg}$$

The signs with which the energies are listed in the equations must correspond with the convention shown in Figure 7. Other granular systems will give different values for the temperature increase resulting from the compression work. According to practical experience, the order of magnitude of such temperature increases is 10^{-1} deg C or K.

Significance of Temperature and Heat for the Compression Process—The numerical example in the previous section demonstrates the fundamental difficulty of taking into account the temperature and heat changes involved in processes that take place in granular systems. All thermal effects occurring are small and cannot be measured with common thermometric devices. It can be easily calculated that the small temperature changes cause only very small thermal expansion of the individual grains and of the entire granular systems. Likewise, the resulting thermal stresses in the grains are very small compared with the compression stresses and can, therefore, be neglected. The significance of this is that, for all practical purposes, one can assume isothermal changes (T = constant) in the development of equations of state for granular systems. Granular systems are poor heat conductors, although their thermal conductivity increases with increasing density. Thermal exchange with the environment takes place only slowly. The system, after experiencing temperature increase as treated in the previous section, returns to its original temperature, which is the same as that of its environment.

A practically quasi-static compression proceeds much faster than this temperature equalization. For this reason it is sufficiently accurate for many cases to assume adiabatic processes in the development of energy equations that serve practical purposes. Temperature and heat, which are of paramount importance in the thermodynamics of molecular systems, have little influence on such simple processes experienced by granular systems as mixing, segregation, compression, expansion, and shear.

Geometric Analogue of the Temperature—As was mentioned in the introduction, thermodynamic methods are preferentially applied to molecular systems. According to the kinetic theory, the internal energy of a molecular system is the sum of the energies of molecular motion (translation, rotation, vibration, etc.), the intensity of which is greater the higher the temperature. The vibratory movement of the molecules or particles around their positions of rest requires a certain free space; this results in lesser density with increasing energy content. There exists, therefore, an analogy between the temperature of a molecular system and the relative density of a granular assembly. The "zero state" of a granular system corresponds to the zero temperature of a molecular system. These relationships and their consequences are germane to the Winterkorn concept.

Some Practical Hints for Determination of Thermodynamic Parameters

The Internal Causes of Temperature Increase—The foregoing thermodynamic considerations are silent with regard to the causes—peculiar to the granular systems—of heat production during the densification process. Only the fact of temperature increase is recorded; nevertheless, this increase is obviously due to the internal friction of the granular system.

If one makes the simplifying assumption that the work of internal friction is performed uniformly during the compression process, then it is proportional to a coefficient of internal friction, $\tan \bar{\varphi}$, and to the range of densification, $h\ (\epsilon_a - \epsilon_0)$. In the ideal case, this internal work is equal to the external work, and hence

$$\tan \bar{\varphi} = \frac{\xi_3 \times \text{area of the work diagram}}{(\epsilon_a - \epsilon_0)} \tag{19}$$

Equation 19 is of the type of the Winterkorn formula, although the individual factors do not have the same meaning; $\tan \bar{\varphi}$ is not the same as the coefficient obtained in the

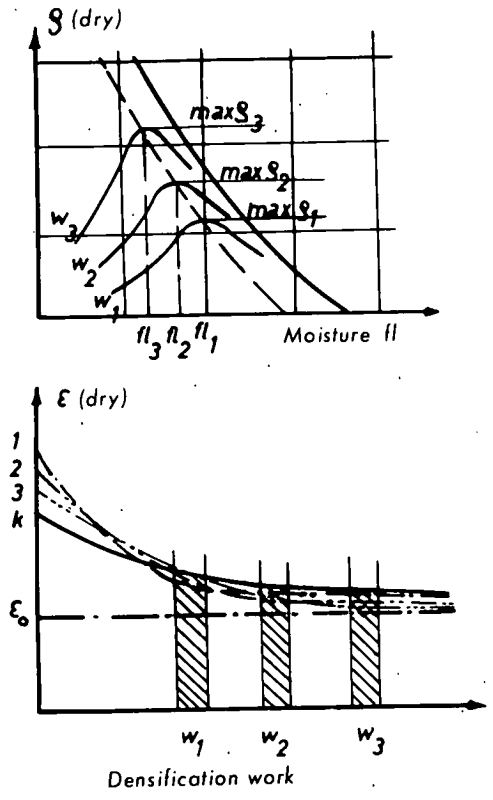

Figure 8. Dry density vs moisture content in Proctor compaction test.

shear test but instead is an average (calculated) friction coefficient that is characteristic for the compression process. It is, however, very probable that a functional relationship exists between these two coefficients of internal friction. The size of the area of the work diagram indicates the capacity of the granular system to change mechanical work into heat energy.

Determination of Work of Practical Compression Processes—Quantitative knowledge of the work involved in a compression process is of fundamental significance, not only for the determination of temperature and heat effects, but also as a measure of the economy of compression and densification processes. The term compression work, w_{12}, shall denote the specific (per unit of mass or of volume) work accepted by the system that brings about a permanent change of the granular system from state 1 (ϵ_1) to state 2 (ϵ_2). The corresponding work diagram comprises a compression and an expansion curve. In the following, we shall describe a procedure for the determination of the compression work, using as an example a granular system that is partially saturated with liquid. Such systems are of outstanding importance for the construction industry.

Thermodynamics of a Partially Saturated Granular System—Densification of a partially saturated system proceeds under squeezing of film liquid into available pore space. If the latter is large enough to accommodate the liquid phase, even at complete densification of the granular system, then no liquid will be squeezed out of the system during the compression process. We are then dealing with a closed thermodynamic system. Figure 8 shows the well-known relationships between Proctor densities and liquid contents. Plotting of the void ratios against the densification work (lower part of Fig. 8) produces monotonous curves that resemble the compression lines. Obviously, partially saturated systems show similar densification behavior as dry granular systems. They may be considered thermodynamically as quasi-homogeneous, and the equations that were derived for the dry systems may logically be applied to them. The void ratio of the dry or wet system, or the porosity, n, may serve as the volumetric parameter of state. (The densification range comprises only a certain portion of the porosity range.)

Note: Homogeneous domains in a system are called "phases" in thermodynamics. Partially saturated macromeritic systems behave in the compression process as "thermodynamically" single-phase systems. In contrast thereto are the phases as defined in molecular physics, which may be designated as "mechanical" or, better still, "physical" phases, with reference to their characterization as gaseous, liquid, or solid. In this usage (also employed by Terzaghi), the system described earlier would be composed of three phases (solid, liquid, and gas). In the field of macromeritics, systems composed of three phases may behave like solids and can be densified by pressure and impact; two-phase systems possess liquid characteristics and can be poured and pumped.

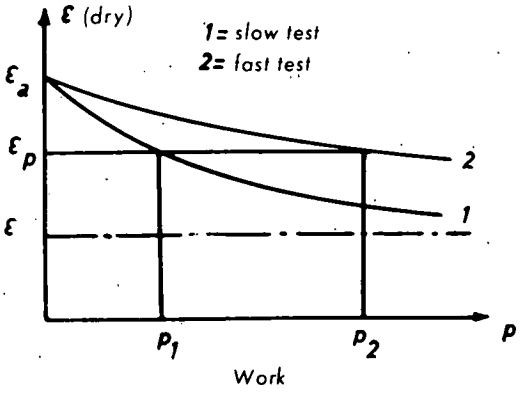

Figure 9. Influence of the rate of compression.

Internal Consolidation During the Compression Process—The consolidation mechanism of a saturated system is well known. A similar process also takes place in partially saturated systems since the flow of liquid into the free pore space requires time. Because no liquid leaves the system, this process can be designated as internal consolidation. An ideal quasi-static compression process must proceed extremely slowly and requires an infinite length of time to reach complete internal consolidation. If stepwise loading is employed, then the corresponding volume change should be read only after practical completion of the consolidation. Premature application of the next loading step leads to smaller consolidation readings than are characteristic for equilibrium conditions: The curves for incomplete compression processes lie above those for equilibrium conditions. Figure 9 shows compression curves for a slow test (practically completely consolidated) and a fast test (incomplete consolidation). The work diagram shows that attainment of a certain state of densification, ϵ_p, requires more work the faster the consolidation energy is supplied. For the determination of this work, a knowledge of the total stress condition is sufficient. Separation of the stresses into intergranular (effective) and pore water stresses is of no particular interest at this stage.

Simple Pressure Test as a Comparison Process—The densification under continuously or stepwise increased pressure—as in the test illustrated in Figure 1—lends itself especially well to simple analysis. In practice, however, densification is achieved almost exclusively by processes of repeated loadings. A loading cycle consists of loading resulting in compression of the system and unloading resulting in expansion. If this cycle is repeated many times, then the incremental consolidations become ever smaller. The system tends toward its ultimate state, i.e., the "zero" state. It should be emphasized here that, in actual repeated compression processes, secondary densification effects are superimposed on the primary reaction mechanism. This must be considered in the evaluation of the test data. Figure 10 shows a repeated and a single compression process. Both shall effect the same permanent densification, $(\epsilon_a - \epsilon_0)$. It can easily be seen that the densification work of the repeated processes is larger than that which corresponds to the area limited by the ultimate pressure, p_w, since the individual work areas of the loading cycles are partially superimposed on each other. It is also obvious that this work is not as large as corresponds to the area of the single compression process. This is because the load removal in the cyclic process returns

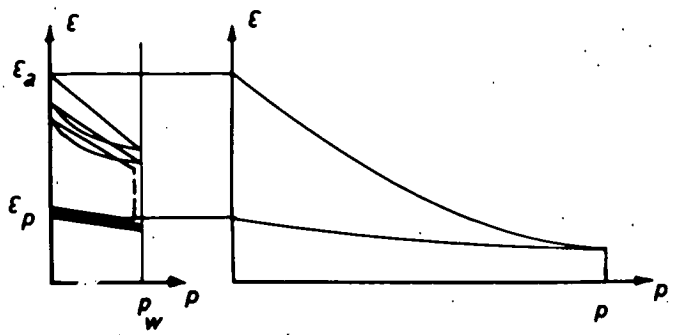

Figure 10. Comparison of effectiveness of single and repeated compression.

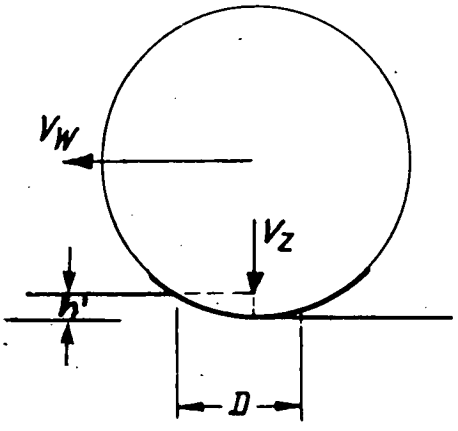

Figure 11. Mechanism of densification by rolling.

the system into the range of high initial compression response. The work required for the simple compression test represents an upper limit for the work required for repeated cyclic load applications.

Practical Application of the Comparison Process—In accordance with the contents of the two preceding sections, the compression work, sufficiently accurate for practical calculations, can be obtained from the work diagram of a simple compression process proceeding at the same rate. For the calculation of the proper rate of piston movement in the press, some very simple assumptions have been found to be adequate. If we assume, e.g., that, in the case of a rubber-tired roller, the pressure increases continuously from initial to final contact (contact pressure) (see Fig. 11), then

$$v_p = \frac{h' \cdot v_W}{D} \tag{20}$$

Numerical example: for $h' = 2$mm, $v_W = 9$ km/h, and $D = 30$ cm, we find,

$$v_p = \frac{0.2 \text{ cm} \times 150 \text{ m/min}}{30 \text{ cm}} = 1 \text{ m/min} = 1000 \text{ mm/min}$$

The comparison presupposes equal thickness of layer and test specimen. In the case of dynamic loadings, much higher action rates are found. These can be calculated from the characteristics of the vibration process, or they must be determined experimentally for impact densification. Dynamic analysis of gaseous systems shows that changes in state can be considered as quasi-static as long as the rate of progression of volume change is small compared with the velocity of sound. This is the reason why, in mechanical engineering, processes occurring in gaseous systems in motor cylinders can be treated as quasi-static up to piston velocities of 500 m/min. In the case of high-frequency vibrations, however, an increasing portion of the work is eaten up by the acceleration of component parts of the system.

Efficiency of Densification—A short reference to efficiency of densification appears to be indicated. The question may be asked why the ideal quasi-static compression process, with its comparatively low energy requirements, is not used in practice. The explanation resides in the limitations of thermodynamics as a scientific and technical tool: classical thermodynamics does not know time. (This is why an independent theory of reaction rates had to be developed.) Practical industrial processes must be completed within a certain limited time period. This leads to the concept of production efficiency as a quotient of work required to do a job and the time within which

TABLE 2

PRODUCTION EFFICIENCY OF VARIOUS DENSIFICATION PROCESSES

Type of Compression Process	Compression Work (mkp/kg)	Time Required (min)	Efficiency (mkp/min-kg)
Ideal quasi-static	small	infinite	zero
Practically quasi-static (test press; road roller)	medium	medium	small to medium
Dynamic (impact, vibration)	large	small	medium to large

it is done. Table 2 gives a qualitative listing of several processes with regard to their production efficiency.

Accordingly, it is possible to increase production efficiency by increasing the intensity of the compression process even though this also increases the total work required. This is the reason for the technical importance of practically quasi-static and dynamic compression processes. An example is the improvement of densification by roller through increase of the roller velocity. Despite decrease of the densification effect for a single roller pass, increase in number of roller passes per unit of time results in a greater densification effect for the same total time.

Additional Applications—It has been shown that, solely from the macroscopic behavior of dry or partially saturated granular systems, we could determine temperature changes and other thermal effects by the use of thermodynamic concepts. In the same manner, the specific enthalpy and entropy of a granular system can be determined. Basic for all such calculations is the exact determination of the work received by the system. It may be expected that further development of the theory of irreversible processes and its application to macromeritic systems will expand the practical usefulness of thermodynamics.

The compression of saturated granular systems involves the squeezing out of liquid; this normally takes place only with liquids of low viscosity such as water and hot or cutback bitumens. Thermodynamically, such systems must be considered as open since material flows across the system boundaries.

DEPENDENCE OF THERMODYNAMIC PARAMETERS ON THE SYSTEM COMPONENTS

Concept of Mixed-Phase Character

In a previous section the concept of a thermodynamic phase was explained. The assumed quasi-homogeneity of the granular system does not give an insight into internal conditions. Such insight may be gained, however, if one employs the concept of a thermodynamic mixed system. A mixed phase is defined as a quasi-homogeneous phase composed of several constituent physical phases that can be individually recognized. A component is defined as a physical phase necessary for the construction of the quasi-homogeneous system. For example, the components of a gas mixture are the several different types of molecules that compose the mixture.

Granular Systems as Thermodynamic Mixed Phase Systems

Granular systems represent complicated configurations in space. Hence a wide variety of geometric characteristics may be considered as "components." In Table 3, components and resulting characteristics of granular systems are coordinated and arranged in accordance with two ordering or classification principles. The horizontal subdivision takes account of the fundamental character (geometric, mechanical, thermodynamic) of the granular system. The vertical subdivision takes into account the role played by characteristic attributes (material variables, granulometric variables, system variables). This type of tabulation has proved of considerable value in many investigations.

It is significant for the physical state of granular systems that the "material" variables (e.g., the mechanical properties of different minerals) exert only a secondary influence on the system properties, or that their contributions (as in the case of heat contents but not in thermal conduction) are simply additive (see also the numerical example following Eq. 18). This shows the special nature of granular or macromeritic systems; the fact that their system properties are largely independent of the "material" properties of their granular components has its logical analogue in the properties of chemical compounds compared with their atomic constituents.

Granulometric variables describe the corpuscular characteristics of the individual grains. Of these, a necessary number is selected as "components" which must be sufficient for the characterization of the mixed phase. It would seem logical to consider all grains of the same diameter and shape as one component. However, the great

variety of diameters and forms represented in a mixture would result in a very large number of components. A simple assortment of independent variables was obtained in a previous investigation by this author in the following manner:

1. Grain diameter (symbol k) as characteristic of the individual grain.
2. Type of gradation of a mixture (symbol q) = amount of particles possessing a certain diameter k, expressed as a proportion of a standard diameter (e.g., k_{max}). The components k and q are, therefore, independent of each other. The choice of q as an independent component is especially advantageous because it is often possible to express the gradation in a closed mathematical function. A well-known method of defining a continuous gradation is by the equation

$$y = \left(\frac{k}{k_{max}}\right)^q \tag{21}$$

in which k_{max} is the maximum particle size, y is the weight portion of all particles smaller than k, and q is an exponent that is usually smaller than ½.

3. Grain form parameter (symbol f_i). It can be demonstrated that there cannot exist a universal parameter that comprises all influences of the grain form on the resulting properties of the system. It is necessary, rather, to express with special parameters, f_i, the influence of specific forms on specific properties. The statistical laws governing distribution of forms or shapes within a granular mixture render it possible to employ parameters of very simple structure.

System variables describe the type of granular system. For simple processes, as for the compression process described earlier, the simple state parameters ϵ, p, and T suffice for the description of the state of the system. Their places may be taken by others of the systems variables listed in Table 3 (derived state parameters). If one treats the granular system as a mixed system, then the equation of state must contain also the independent components:

$$f(\epsilon, p, T, k, q, f_i) = 0 \tag{22}$$

Corresponding States of Granular Systems

Equation 22 is quite complicated. Simple relationships between a parameter and a component are obtained through elimination of all the excess variables by keeping them constant. This happens if one treats the different systems always in corresponding states. The latter are defined by identical packing and orientation of the system components; therefore, only one parameter, M_i, is required for the description of a particular state of the system. Its dependence on the variable component K_k has the form

$$M_i = f(K_k) \tag{23}$$

It is obvious that zero states of granular systems are corresponding states. Correspondence between states exists when

$$\frac{1 + \epsilon_0}{1 + \epsilon_k} = \text{constant} \tag{24}$$

where ϵ_0 = void ratio of the zero state and ϵ_k = void ratio of the corresponding state. It follows from this that the so-called critical void ratio characterizes corresponding states. It should be pointed out here that, according to Eq. 24, corresponding states of liquid-containing granular systems must have the same degree of pore saturation.

Zero Diagrams and Their Analytic Treatment

A zero diagram is the graphic expression of Eq. 23 applied to zero-state systems. There exist two different types of zero diagrams, each of which may be utilized in like

TABLE 3

ARRANGEMENT OF PARAMETERS THAT ARE OF GREATEST THERMODYNAMIC SIGNIFICANCE IN GRANULAR SYSTEMS

Type of System	Geometric: Variable (a)	Mechanics: Variables (a) + (b)	Thermodynamic: Variables (a) + (b) + (c)
		Material Density (g/cm³)	
Group I: Material-Variables		Material friction tan φ (1) Strength σ_c (kp/cm²) Elasticity E (kp/cm²)	Specific heat c (kcal/kg deg) Therm. exp. coeff. α (deg^{-1}) Ther. cond. coeff. λ in J/cm s deg
Group II: Granulometric Variables	Size: grain diameter k in mm Distribution: y = f(k) Surface: 0 in mm² Specific: O_S in m²/Kg Distribution: O_S = f(k) Volume: grain volume in mm³ volume distribution — Mass Distribution Specific grain number: Z_S (St) Grain number distrib.: ΔZ_S = f(k) Shape: function for O_S: f_O Z_S: f_Z		
	Function for ϵ: f k: f_k	Function for τ: f_τ E_V: f_E	Function for w_m: f_m w_k: f_k
Group III: System Variables	Specific volume v = 1 + ϵ(1) System Density (g/cm³) Void ratio ϵ(1) Porosity n = ϵ/1 + ϵ(1) Degree of density D = 1 - n(1)	Loading p(t) in kp/cm² · s Manner of loading t Deformations and constraints Experimental variables	Temperature T (deg K)
	Relative packing D_{rel} = D/DO(1) Permeability k (cm²)	System strength τ in kp/cm² With the parameters: initial strength C(kp/cm²) friction coeff. tan φ (1) System elasticity E_v (kp/cm²)	System properties Specific heat (kcal/kg deg) Thermal expansion (deg^{-1}) Thermal conduct. (J/cm s deg K) Specific intern. energy u (kcal/kg) Specific entropy s (kcal/kg deg K) Specific enthalpy h (kcal/kg) Specific mix. work w_m (mkp/kg) Specific comp. work w_k (mkp/kg)

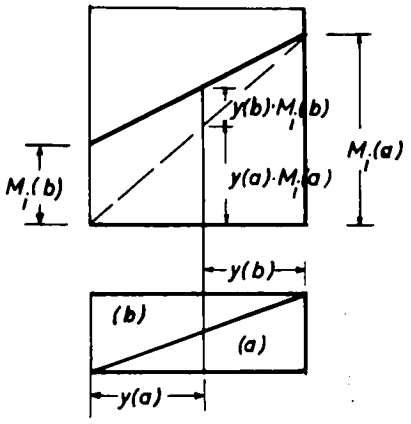

Figure 12. Pure additivity of component properties.

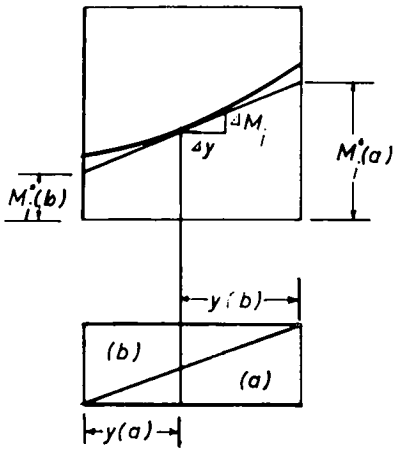

Figure 13. Partial additivity of component properties.

manner to obtain valid relationships between characteristic M_i and component K_k. Zero diagrams exist only in a few simple forms; these are susceptible to mathematical analysis.

The first type of zero diagram is defined by Eq. 23 itself. The second type represents the influence of the component K_k as a resultant of two "pure components" so that Eq. 23 becomes

$$M_i = f(M_i(a),\ M_i(b),\ y) \tag{25}$$

in which

$M_i(a)$ = characteristic of a granular system which comprises only the component (a),
$M_i(b)$ = characteristic of the "pure component" (b), and
y = general measure of the proportions of both pure components in the mixture.

Zero diagrams of the second type, corresponding with Eq. 25, show a very close relationship with the so-called phase diagrams employed in many areas of physics, such as the melting point diagrams in metallurgy and mineralogy, the boiling point diagrams, and others. Such diagrams shall be used for demonstrating the fundamental methodology of the analytic treatment of their course and information content.

Rectilinear Course of a Zero Diagram—If by experiment or by theory a rectilinear course of the zero diagram is found, this shows that the property M_i of the mixture is a purely additive function of the proportions of the components and the degree to which they possess the property of interest (Fig. 12):

$$M_{iy}(a + b) = y(a)M_i(a) + y(b)M_i(b) \tag{26}$$

Regarding the proportions, we have

$$y(a) + y(b) = 1 \tag{27}$$

Monotonous Rise of a Zero Diagram—The course of the majority of zero diagrams is not rectilinear after Eq. 26, but curvilinear. In the case of a monotonous rise, we can define a partial additivity of the desired property in the following manner:

$$M_{iy}(a + b) = y(a)M_i^*(a) + y(b)M_i^*(b) \tag{28}$$

where $M_i^*(a)$, $M_i^*(b)$ = partial properties.

For the determination of the unknown $M_i^*(a)$ and $M_i^*(b)$ of Eq. 28, we need a second independent equation, which can be obtained from a second experimentally determined point, $(y + \Delta y)$, taken in the vicinity of y:

$$M_{i(y+\Delta y)}(a + b) = [y(a) + \Delta y]\, M_i^*(a) + [y(b) - \Delta y]\, M_i^*(b) \tag{29}$$

Equations 28 and 29 yield then the desired partial values, e.g.,

$$M_i^*(a) = M_{iy}(a + b) + y(b)\,\frac{\Delta M_{iy}(a + b)}{\Delta y} \tag{30}$$

whereby

$$\Delta M_{iy}(a + b) = M_{i(y+\Delta y)}(a + b) - M_{iy}(a + b)$$

Figure 13 shows that the partial additivity is restricted to the range $y/y+\Delta y$ in which the curve can be replaced by its tangent or its secant. Other values of the particular partials hold outside of this range. Partial values are, therefore, typical thermodynamic parameters that correctly reproduce the properties of a system without necessarily reflecting an inherent reality. If the plots are only slightly curved over the entire range, then one can assume constancy of the partials in first approximation and hence, practically, pure additivity.

Extremal Course of a Zero Diagram—An extremal course of a particular physical parameter can almost always be explained by a counterplay of two oppositely acting causes. Often this can be expressed as a mathematical function. In the case of granular systems, the general situation is much simpler since extremal forms of zero diagrams always are found in similar types.

One can then establish a reference base and construct on it similar zero diagrams by addition of increments of component properties. The method is shown in Figure 14 for rectilinear zero diagrams. It can be used in a similar manner for curvilinear diagrams. We assume

$$M_i(a + b) = M_{il} + y(a)\Delta M_i(a) + y(b)\Delta M_i(b) \tag{31}$$

where M_{il} = reference base and $\Delta M_i(a)$, $\Delta M_i(b)$ = increments.

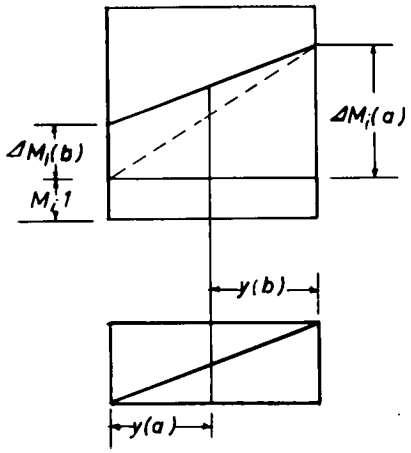

Figure 14. Additivity of increments of component properties.

Calculation of Resultant Properties of Granular Systems

Explanation of the Method—The additivity laws derived above represent an armory that permits the execution of simple, thermodynamically justified calculations of a number of properties, M_i, of a granular system. If a property of interest can be related to a reference basis, then the law expressed by Eq. 31 is used most frequently. With the chosen assortment of independent components of a granular system, we obtain very generally

$$M_i = M_{il} + \Delta M_i(k) + \Delta M_i(q) + \Delta M_i(f_i) \tag{32}$$

where

M_{il} = amount of property of reference base,

$\Delta M_i(k)$ = increment because of grain size k,
$\Delta M_i(q)$ = increment because of type of gradation q, and
$\Delta M_i(f_i)$ = increment because of grain shape.

The individual increments can themselves be additively structured.

Numerical Example: Porosity of a Granular System—In certain applications the porosity, n, is preferred over the void ratio. Both properties are functionally connected as follows:

$$n = \frac{\epsilon}{1+\epsilon} \quad ; \quad \epsilon = \frac{n}{1-n} \tag{33}$$

The relationship $n = f(\epsilon)$ represents geometrically an equilateral hyperbola whose coordinates are rotated 45 degrees and whose origins are shifted a certain amount. However, within the range of practically observed porosities, i.e., $0.1 < n < 0.4$, one may choose a linear relationship between the two properties; this is sufficiently accurate for macroscopic purposes. The relationships that have been found to hold for the void ratios can then be used, at least in first approximations, for the porosities, too. According to Eq. 32, we can then write

$$n = n_1 + \Delta n(k) + \Delta n(q) + \Delta n(f_i) \tag{34}$$

where n_1 = minimum porosity of reference system. One may choose $n = 0.26$, i.e., the minimum porosity of a system of spheres of equal size. The different increments are found by statistical or graphical evaluation of experimental data from well-planned investigations:

$\Delta n(k)$ = increment because of grain size k_{max} of system
= +0.02 for 2 mm < k_{max} < 5 mm
= ±0.00 for 8 mm < k_{max} < 12.5 mm
= -0.02 for 18 mm < k_{max} < 25 mm
= -0.05 for 35 mm < k_{max} < 45 mm

$\Delta n(q)$ = increment because of type of gradation for distribution law Eq. 21
= ±0.00 for single grain size mixtures q > 1
= -0.10 for open-graded mixtures 1 > q > 0.6
= -0.20 for dense mixtures 0.5 > q > 0.3

$\Delta n(f_n)$ = increment because of grain shape
= ±0.00 for spheres
= +0.10 for rounded grains (small surface/volume)
= +0.17 for broken grains (small surface/volume)

Intermediate values are obtained by linear extrapolation. Consider the following numerical example: A granular system, 0-12.5 mm, densely graded (q = 0.5), consists of 75 percent broken grains and 25 percent spherical grains. The porosity, n, is then:

n_1	=			0.26
$\Delta n(k)$	=			—
$\Delta n(q)$	=			-0.20
$\Delta n(f_n)$	=	0.75×0.17	= 0.13	
		0.25×0.10	= 0.03	
			0.16	= 0.16
				0.22

The porosity of this system in the zero state is found to be 0.22 or 22 percent.

It should be noted here that the degree of accuracy of this type of calculation may not be sufficient for certain applications. In such cases one should check by experiment. However, this method of calculation reflects correctly the trend of influence of the various components as determined by thermodynamic laws and represents, therefore, an irreplaceable aid for the construction of granular systems. It can be expected that a higher degree of accuracy may be attained in the future in such calculations from statistical evaluation of more extensive experimental data and as a result of greater differentiation in the assignment of increments.

Calculations for Other Properties of Granular Systems—In like manner one can obtain additive equations for permeability, shear resistance (especially the shear parameter, $\tan \varphi$), modulus of deformation, E_V, and others. In doing this, one has to keep in mind that void ratio and porosity are scalar properties, while the mechanical characteristics are vectors and functions of direction in space. The application of addition equations to vector properties, M_i, requires more severe rules of elimination. Only such states of granular systems can now be called corresponding as are obtained with the same method of densification, since only thus can they be assumed to possess the same degree of orientation. Also, in the case of changes in state, the same experimental conditions and type of deformation must be used if the behavior and properties of systems are to be compared. Thus, there exist no generally valid additive equations for the shear parameter, $\tan \varphi$. Rather, there are special addition formulae for the different types of shear tests, i.e., for direct shear, triaxial shear, etc. It is obvious that similar relationships can be established for the parameters that are more properly considered as being of thermodynamic character. For the thermal parameter of heat content—which in Table 3 is listed as a material parameter—assumption of simple additivity is sufficient. It can be considered as a scalar property.

The parameters of internal energy, u, and entropy, s, as well as specific process parameters (specific mixing work, w_m, and specific compression work, w_k) whose behavior is similar to that of state parameters, can be calculated from addition-type equations. The justification for such procedure in the case of specific process parameters derives from the system of axioms, which stipulates that the underlying processes are completely irreversible. Accordingly, only one reaction path is possible. The work required to overcome the influence of the true elasticity of the grains is so small that it can be neglected.

General Applications of the Mixed-Phase Character of Granular Systems

General Correspondence Principle for Mixed Systems—Formulation of a general correspondence principle is useful for many practical problems. This will be demonstrated on the example of the porosity, n, of a granular system. The principle holds, however, very generally for the properties of any system. In Figure 15 are plotted the porosities, n, of mixtures of two types of grains (round and fragmented). Both possess the same grain diameter and an approximately similar shape factor. The pore space of a system consists of a network of channels and cavities. The sharper the edges of the grains, the larger will be the angle spaces formed on contact of neighboring grains and the larger the porosity of the total system. This holds true for the "pure component" in which grains of the same type are in contact. In a mixed system, however, grains of the same character are no longer in direct contact; rather, in accordance with the principle of uniform distribution (axiom 2), they are well distributed and surrounded by grains of different character. However, as can be easily visualized, the shape of the

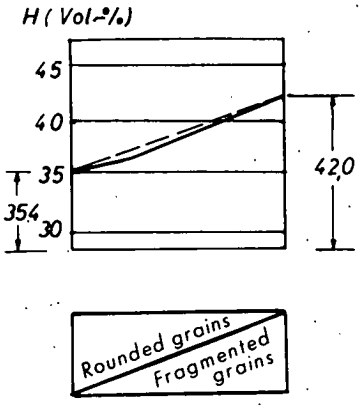

Figure 15. Porosity as a function of particle shape (binary mixture).

fragmented grains exert an influence on the size of the angle spaces even in contact with grains of other shapes. Every individual grain, therefore, makes a characteristic contribution, depending on its shape, to the total porosity of the system.

This principle can be generalized as follows: Each independent component makes a characteristic contribution to the properties of a system in accordance with its proportion in the system. The mathematical form of this correspondence principle follows Eq. 32. The present derivation, however, shows the internal relationship that, even in the case of complete separation of particles of the same kind in a mixture, their characteristic influence is maintained. Under these conditions, one cannot help being reminded of Dalton's law, which says: Each gas in a mixture of several gases behaves in a manner as if it were alone in the space of the container.

Experimental Determination of Phase Diagrams in Physics—It has already been pointed out that many phase diagrams of physics are in close agreement with zero diagrams of granular systems. The thermodynamic systems whose behavior finds expression in the phase diagrams consist of a network of ions, atoms, or molecules. It can be demonstrated that the corpuscular, rather than the "chemical," character of their elementary components determines the macroscopic behavior of such systems. One can prove a relationship between the ionic size of an element and its position in the periodic system.

The thermodynamic systems whose behavior finds expression in the zero diagrams consist of a network of grains of many different sizes and forms. Experiments on, and analysis of, granular systems disclose the conditions and reasons responsible for the various forms of zero diagrams: monotonous rise is always found in cases of good agreement in size and shape of two mixing partners. In such cases, an individual grain of one mix partner can be substituted for one of the other components without resulting change in the lattice structure. Extremal forms of zero diagrams result from great differences in shape and form of the grains of the two mix components. Substitution of a grain from one component by one from the other results in far-reaching disturbance of the lattice structure (axiom 1). Granular systems represent a singular experimental means for demonstration of analogous phenomena that occur in molecular systems.

SUMMARY AND OUTLOOK

This treatise deals with some special and some general aspects of thermodynamics. Among the special topics are the clarification of the influence of temperature and heat in work processes on granular systems. Work processes are defined as those in which the granular system receives work, as in mixing, segregation, compression, expansion, and shear. In order to determine the amount of heat produced, it is necessary to have a valid theoretical concept supported by experimental data of the macroscopic properties of granular systems and especially of the work, w_{12}, involved in the compression process. For this purpose, a method was proposed in which a simple compression test was used as comparison process. It was shown that the influence of temperature and heat in such work processes is comparatively small, and that the temperature changes are also very small.

We designate as heat processes those in which heat is adduced to the granular system, as in heating and cooling. This group of processes was not considered in the present treatise. It is obvious that, because of the large temperature differences normally employed in industrial processes of this type, the influence of heat and temperature is very significant.

Beyond the scope of these special "heat" aspects, insights of greater generality were obtained and formulated. These are of great importance for the understanding and further investigation of granular systems:

1. Granular systems can be considered as thermodynamic systems. This immediately yields more trenchant or new definitions of known phenomena. Examples of this are the system of axioms, the state of complete compression of a granular system, secondary densification effects, criterion for corresponding states, and internal consolidation.

2. The methodology that has been developed permits use of simple analytical functions for the expression of a large number of relationships existing between macroscopic parameters. Examples are the compression function, compression work, application of an analogue process, and laws of additivity. The only assumptions needed are that the chosen analytical functions yield a correct reproduction of the macroscopic behavior of the granular system. For many problems, thermodynamic methodology furnishes especially elegant solutions.

3. In accordance with classical methodology, thermodynamic parameters may be determined in two fundamentally different manners: First, they may be calculated from direct macroscopic measurements as discussed in the preceding paragraph; second, they can be calculated or estimated from the composition of the system by utilizing the concept of mixed-phase character. An example is the determination of the porosity. Hints were given for the determination of other mechanical and thermodynamic parameters. The concept of mixed-phase character permits a deep insight into the internal structure of a system; this can be expressed in a general principle of corresponding states.

4. The limitations of classical thermodynamic methodology have been pointed out. This methodology loses its power whenever the factor of time governs the physical phenomenon. Examples are production efficiency of compression processes and the time-dependence of internal consolidation. It is quite possible that the existing boundaries may be pushed back by the use of special methodologies such as the theory of irreversible processes (or by the generalized activation theory).

There can be no justifiable doubt that classical thermodynamics will become an important instrument for the treatment of problems concerned with the behavior of granular systems, since the results are of immediate practical applicability. All problems in which energy is involved, in the form of work or heat, can be treated accurately and in an interesting manner.

The theory of granular systems is made complete by the introduction of thermodynamic concepts. The structure of this theory is reflected in the arrangement of Table 3. It comprises physical disciplines of widely differing character. The geometry of granular systems (also doubling as a physical discipline) was already in the center of interest during the past century. The mechanics of granular systems was introduced by Terzaghi in 1925 (1). This resulted in a tremendously fertile expansion of the theory. Finally, we owe to Winterkorn (2) the introduction of thermodynamic methodology, whose development is proceeding very rapidly at the present time. This may be considered as the completion and crowning of the theory of granular systems.

REFERENCES

1. Terzaghi, Karl von. Erdbaumechanik auf bodenphysikalischer Grundlage. Leipzig and Wien, 1925.
2. Winterkorn, Hans F. Macromeritic Liquids. Spec. Tech. Publ. No. 156, p. 77-89, 1953.
3. Kezdi, Arpad. Grundlagen einer allgemeinen Bodenphysik. VDI Zeitschrift, Vol. 108, No. 5, p. 161, Feb. 1966.
4. Becker, R. Theorie der Wärme, Berlin, 1964.
5. Holl, Alfred. Das Kornhaufwerk, in Strassenbautechn., 1967.

Heat Conduction in Saturated Granular Materials

RICHARD McGAW, U. S. Army Terrestrial Sciences Center, Hanover, New Hampshire

Heat conduction in granular materials varies with the conductivities and volumetric proportions of the constituents. Thermal conductivities predicted by leading equations that utilize these factors are compared with reported values for quartz sand, glass beads, and lead shot, each saturated with various liquids. Only the equation of de Vries and a series/parallel flow equation proposed by Woodside and Messmer approximate the data over a range of conductivity ratio and porosity. Neither equation, however, is based on a fully rational model. An equation proposed by Kunii and Smith utilizes a better physical model but is weakened by its dependence on the regular packing of spheres.

The series/parallel approach is altered to incorporate three additional propositions: (a) the quantity of fluid that conducts heat in the series branch approaches zero at the extremes of porosity; (b) interfacial material invariably resides between this fluid and a grain, or between two grains; and (c) the possibility of contact resistance (limited surface conductance) exists at each such interface. The resulting equation is tested against the literature data and is shown to give a better understanding of heat conduction in granular materials. The equation also serves to indicate areas in which further research is needed.

•THERE IS a need for a rational theory to predict the effective thermal conductivity of granular materials found in conjunction with various fluids. Such a theory would be applicable to a wide range of engineering and geological problems, including the freezing and thawing of soils beneath highways, the dissipation of heat from building foundations or from buried utility systems, the conduction of heat through water- or oil-bearing sands, the design of insulating or refractory materials, and many others.

Many of the techniques in use at present are openly empirical, while others of a more rational development incorporate matching factors that have only a quasi-physical basis. Moreover, apparently no approach has taken into account the effect of thermal resistance between grains and fluid. A recent study (1) indicated that the thermal conductivity of a mixture of ice and sand was limited by poor thermal transfer across ice/sand boundaries. It is very likely that thermal resistance is present to some degree at all boundaries between differing materials, and particularly where foreign substances are adsorbed. A rational theory of heat conduction should make provision for the influence of this factor on overall conductivity.

Previous solutions for the thermal conductivity of granular materials have tended to fall into three major categories:

1. Empirical averaging techniques, in particular modifications built on the weighted geometric mean of the conductivities of the phases;
2. Modified parallel-flow equations based on Maxwell's electrical conductivity equation for spheres in a continuous liquid; and
3. Series/parallel flow equations.

In this paper, leading equations in each of these categories are compared with conductivity data of Woodside and Messmer (2). The data cover a large range of porosities and conductivity ratios and were obtained by means of the probe method of transient heating. This method is judged to be the most reliable technique for measuring the conductivity of multi-phase materials. All of the equations take into consideration the conductivities and volumetric proportions of the constituents, factors which together constitute the first requirement of a rational theory.

Other equations have been proposed that are not included here because they do not satisfy certain initial requirements; many of these have been reviewed elsewhere (2,3). Some have not considered the proportions of the constituents. Others have been empirically involved or based on questionable assumptions (4). Still others have utilized geometrical models that incorporate dubious estimates of the contact area between grains (5, 6).

The degree to which each equation predicts or fails to predict the experimental data is shown and the reasons analyzed. A conductance equation is then developed that attempts to correct for the inadequacies of previous solutions. This equation is based on a series/parallel flow model; however, the development differs from previous approaches in that the existence of true solid-to-solid contact between grains is discounted, while the possibility of interfacial resistance is recognized.

GEOMETRIC MEAN EQUATIONS

The basic geometric mean equation, attributed to Lichtenecker (7), is given by

$$K = K_f^n \cdot K_s^{\lambda} \tag{1}$$

or

$$\log K = n \log K_f + \lambda \log K_s$$

where K_f and K_s are the bulk conductivities of a continuous fluid phase and a dispersed granular phase, respectively; n is the porosity or volume fraction of saturating fluids; and $\lambda = (1 - n)$ is the volume fraction of solids. Asaad (8) proposed a variation to the geometric mean equation,

$$K = K_f^{pn} \cdot K_s^{1-pn} \tag{2}$$

where p varies in the neighborhood of unity and has the effect of altering the porosity corresponding to a particular value of K. Legg and Given (9) and Brown (10) proposed other variations.

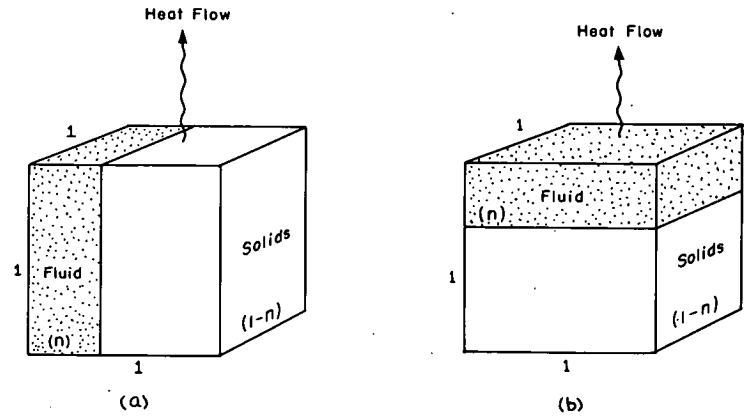

Figure 1. Schematic models of parallel flow (a) and series flow (b).

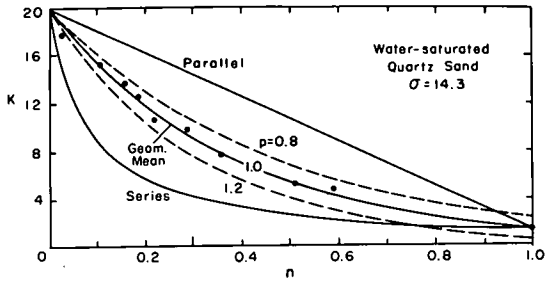

Figure 2. Conductivity (K), mcal/deg C-cm-sec, vs porosity (n); parallel, geometric mean, and series equations.

Each of these equations is an empirical compromise between two physically limiting cases, namely, parallel (maximum) flow:

$$K = nK_f + \lambda K_s \tag{3}$$

and series (minimum) flow:

$$K^{-1} = nK_f^{-1} + \lambda K_s^{-1} \tag{4}$$

Schematic diagrams of parallel and series flow are shown in Figure 1; no simple diagram representing geometric mean flow can be drawn.

A comparison of Eqs. 1 through 4 is shown in Figure 2. The curves were calculated for the case of water-saturated quartz sand (K_s = 20, K_f = 1.4 mcal/deg C-cm-sec at 20 C; $\sigma = K_s K_f^{-1} = 14.3$). The data are taken from Woodside and Messmer (2), Parts I and II, for quartz sands and quartzitic sandstones; both types of sands were found to give equal conductivities for equal porosities when water-saturated and are therefore plotted together. Equation 2 was calculated with several values of p. This equation reduces to Eq. 1 when p is unity.

Figure 2 shows the rather striking agreement of calculated geometric mean values with experimental data when the conductivity ratio ($K_s K_f^{-1}$) is less than 20. Nevertheless, the appeal of the approach is primarily based on convenience, inasmuch as little insight is provided into the physical processes involved. In a later comparison, the geometric mean equation is shown to overestimate conductivity by successively larger margins as the conductivity ratio is increased.

MODIFIED MAXWELL EQUATIONS

A second approach, and one that has received a great deal of attention, involves modifying Maxwell's electrical conductivity equation to fit presumably analogous heat conductivity situations. Maxwell's equation, rewritten in terms of conductances rather than the original specific resistances, is given by

$$K = K_f \cdot \frac{K_s + 2K_f + 2\lambda (K_s - K_f)}{K_s + 2K_f - \lambda (K_s - K_f)} \tag{5}$$

Equation 5 was derived by Maxwell to express the compound electrical conductivity of a mixture of uniform spheres dispersed in a continuous conducting fluid. An important stipulation of the derivation was that the spheres were of radii small compared with their distances, so that "their effects in disturbing the course of the current may be taken as independent of each other" (11, p. 440). Maxwell's equation is directly applicable only when the percentage of solids is well below 50 percent.

Rayleight (12) derived a similar formula for spheres arranged cubically. The derivation was extended by Burger (13) to ellipsoidal particles and by Eucken (14) to several phases dispersed in a single continuous phase. Eucken was apparently one of the first to suggest an analogy with heat flow. Most recently, de Vries (15, 16) has applied the extended equation to the thermal conductivity of soils. De Vries' equation for a fluid medium with dispersed ellipsoidal solids is

$$K = \frac{nK_f + F\lambda K_s}{n + F\lambda} \tag{6}$$

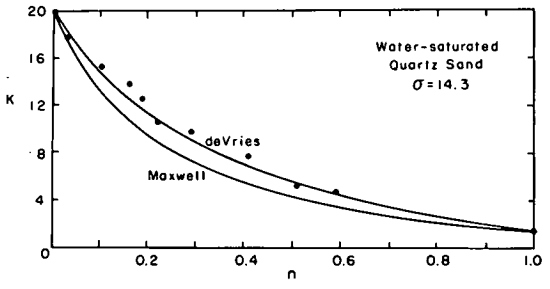

Figure 3. Conductivity (K) vs porosity (n); de Vries and Maxwell equations.

where

$$F = \frac{1}{3}\sum_{x=1}^{3}\left[1 + g_x\left(\frac{K_s}{K_f} - 1\right)\right]^{-1} \qquad (6a)$$

and

$$\sum_{x=1}^{3} g_x = 1 \qquad (6b)$$

Equation 6 has the form of Eq. 3 for parallel flow, with the exception that the factor F is different from unity. It has been suggested that F is related to the ratio of the effective temperature gradients in the continuous and dispersed phases. However, for packed granular materials, which are those to which Eq. 6 has been applied by de Vries, F is only slightly more than a weighting factor by which the equation can be fitted to a given set of data.

The empirical nature of F becomes clear when the factor g_x is considered: $g_x = g_1, g_2, g_3$ expresses the axial lengths of the ellipsoidal particle. For spherical particles, $g_x = \frac{1}{3}, \frac{1}{3}, \frac{1}{3}$, and Eq. 6 reduces to Maxwell's equation. Whereas Maxwell's equation typically underestimates experimental data for granular soils (Fig. 3), de Vries found that the assumption of $g_x = \frac{1}{8}, \frac{1}{8}, \frac{6}{8}$ results in good agreement with measured values. Nevertheless, the presumed particle, with a major axis six times the length of each minor axis, does not in reality approximate the particles of the soils to which the equation is usually applied.

It is instructive to cast Maxwell's equation into the form of Eq. 6 and to compare Maxwell's F-value with that of de Vries. When this is done, Maxwell's factor is given by

$$F(1{:}1{:}1) = \left[1 + \frac{1}{3}(\sigma - 1)\right]^{-1} = \frac{3}{\sigma + 2} \qquad (7a)$$

while de Vries' factor is

$$F(1{:}1{:}6) = \frac{4}{3}\left(\frac{11 + 13}{3\sigma^2 + 22\sigma + 7}\right) \qquad (7b)$$

As before, $\sigma = K_S K_f^{-1}$. The two F-factors are plotted against σ in Figure 4. With the exception of the point where $K_S = K_f$, de Vries' factor is everywhere larger than Maxwell's. Mineral soils fall into the lower right quadrant, where F is less than unity. For water-wet sand (σ = 14.3), F(1:1:1) is 0.184 and F(1:1:6) is 0.281. In effect, de Vries finds the solid fraction in real soils more effective in conducting heat than Maxwell's equation would predict. This result is what we would expect for particles in close association; however, the manner in which the result is obtained is to some degree arbitrary.

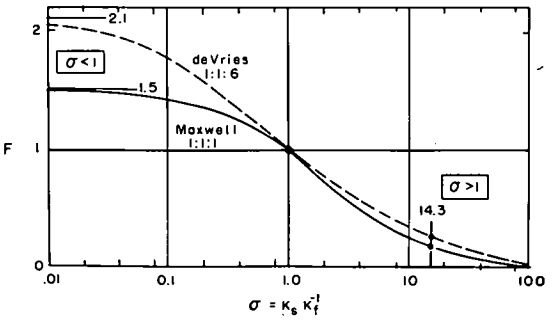

Figure 4. F-factor (F) vs conductivity ratio (σ); de Vries and Maxwell equations.

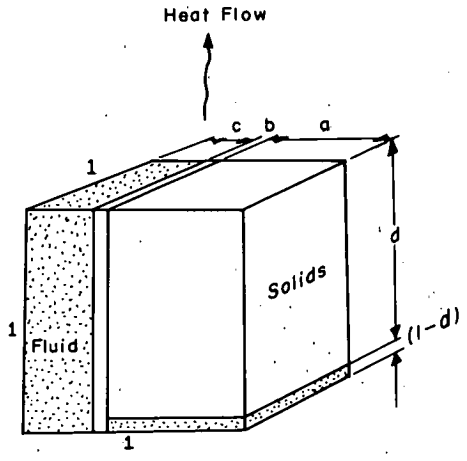

Figure 5. Schematic model of the resistor equation.

SERIES/PARALLEL EQUATIONS

A third approach accounts more directly for the mechanisms governing heat transfer from particle to particle. This approach is based on the recognition of at least two distinct paths of conduction through a granular material: a continuous path through the major portion of the fluid, and a series path through the solid particles that are thought to be bridged by a small portion of the fluid. Many investigators have postulated a third path by way of solid-to-solid connections between particles; however, as discussed later, it is unlikely that such a path actually exists except in rare instances.

The series/parallel approach differs from that of Maxwell and related equations in that a true series path is discerned. Properly applied, Maxwell's approach treats those cases where the continuous path is predominant; the series/parallel approach can potentially treat all cases from full parallel to full series flow with equal rigor.

Figure 5 shows a schematic model of series/parallel flow as proposed by Wyllie and Southwick (17). This model has been called the equivalent resistor model because it was originally proposed for electrical conductivity; the model has since been applied to the calculation of thermal conductivity. In Figure 5 fluid areas are stippled and areas representing solids are white. It will be noted that the model incorporates a continuous path through the solids in addition to the series path. As illustrated, the volumes of the various elements are expressed in terms of four ratios, a, b, c, d.

The equation for the resistor model as given by Wyllie and Southwick is

$$K = \frac{aK_sK_f}{(1-d)K_s + (d)K_f} + bK_s + cK_f \tag{8}$$

where

$$a + b + c = 1 \tag{8a}$$

Converting to the symbols used earlier for the volumetric ratios of solids and saturating fluids, we find respectively

$$\lambda = b + ad$$
$$n = 1 - b - ad = c + a(1 - d) \tag{8b}$$

In practice, it is necessary to supplement relations 8a and 8b with certain experimental measurements before the dimensions of the equivalent resistor model can be determined. To evaluate b, Wyllie and Southwick proposed evacuating the pores to make the fluid nonconducting (K_f equal to zero). Thus b was thought to be $K_VK_S^{-1}$, where K_V was the observed conductivity in a vacuum. However, the relation is not exact because, with no fluid in the pores, radiation between grains is no longer negligible; an experimentally determined value of K_V will always be higher than conduction

would account for. Thus, a small but finite K_v does not necessarily indicate the presence of a conducting path.

Since the solids could not be made nonconducting, an empirical estimate of c was necessary. Kimura (18) assumed $c = n^{1.3}$ and b = 0, but disregarded Eqs. 8b. Woodside and Messmer (2) also assumed b = 0, but calculated the value of c required to match the resistor model to experimental data. For porosities from 20 to 60 percent they found c to be virtually independent of the conductivity ratio and to take the value (n - 0.03) to a close approximation. Woodside and Messmer concluded that when the following empirical relations were incorporated,

$$\begin{aligned} b &= 0 \\ c &= n - 0.03 \\ a &= 1 - c = (1 - n) + 0.03 \\ d &= (1 - n)/a \end{aligned} \tag{8c}$$

an equation resulted that predicted the thermal conductivity of granular materials with good agreement over the range studied. With the addition of Eqs. 8c, the resistor equation becomes

$$K = (n - 0.03)K_f + (\lambda + 0.03)\left[\frac{\lambda}{\lambda + 0.03}\left(\frac{1}{K_s}\right) + \frac{0.03}{\lambda + 0.03}\left(\frac{1}{K_f}\right)\right]^{-1} \tag{9}$$

Equation 9 was termed the modified resistor equation by these investigations.

It is evident from Figure 5 that the resistor approach does not take into account the geometry of the particles or the specific arrangement of the pore fluids that enter into the series flow. Kunii and Smith (19) proposed a series/parallel equation in which they made a semi-empirical estimate of the extent of the series fluid. This equation was an updated version of an earlier one proposed by Yagi and Kunii (20) that included a term for the contact area between grains but neglected the continuous fluid path. In the later equation, Kunii and Smith sought to provide for conductive heat transfer through actual contact surfaces by introducing an empirical coefficient; nevertheless, the coefficient indirectly depended on contact area. Two other coefficients represented radiative transfer between particles and between voids. The authors took all these coefficients to be zero in a comparison with experimental data.

Kunii and Smith's equation, neglecting radiation and possible contact area, is

$$K = nK_f + \lambda\left[\frac{\varphi}{\beta}\left(\frac{1}{K_f}\right) + \frac{\gamma}{\beta}\left(\frac{1}{K_s}\right)\right]^{-1} \tag{10}$$

in which the parameters β, γ, and φ are ratios with the average diameter of a particle, D. Thus β D is the effective distance between centers of adjacent particles, γ D is the effective length of a particle, and φ D is the effective length of the series fluid. The value of each parameter was estimated through a comparison with open and close packings of uniform spheres: β was assumed to be between 0.9 and 1.0, but was taken as unity in the authors' calculations; γ was assigned the value of $^2/_3$, corresponding to the length of a cylinder having the same diameter and volume as a spherical particle; φ, as a function of porosity and conductivity ratio, was linearly interpolated between φ_1 and φ_2 calculated for the two packings. Outside the porosity range 48 to 26 percent, φ was assumed to retain the values φ_1 and φ_2.

The calculation of φ_1 and φ_2 represented an attempt to determine the amount of series fluid that would be effective in each of the reference packings. Although not wholly

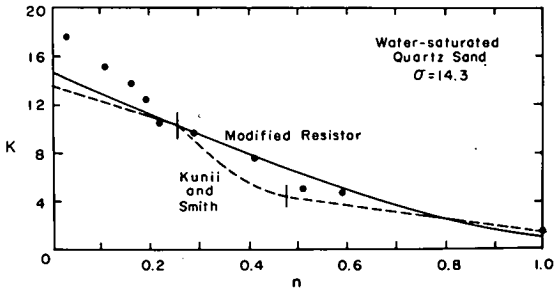

Figure 6. Conductivity (K) vs porosity (n); modified resistor and Kunii and Smith equations.

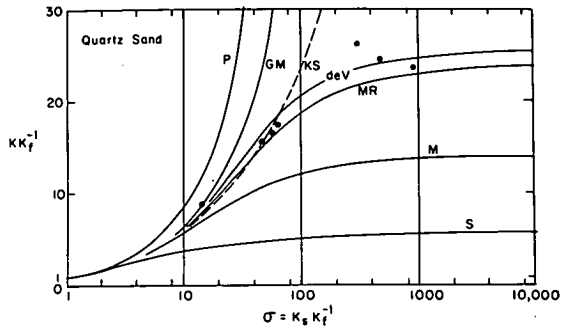

Figure 7. Comparison of conductivity equations; n = 19 percent.

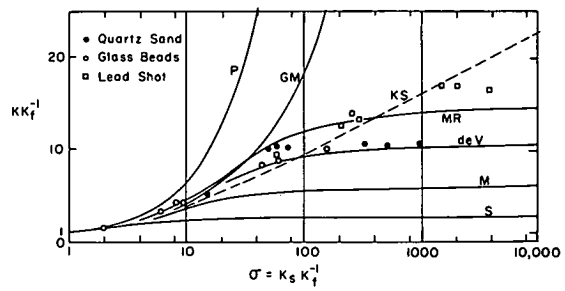

Figure 8. Comparison of conductivity equations; n = 38 percent.

rigorous, it is interesting for being the only known effort directed toward deriving such a value from basic principles. The calculation involved several steps. The first was the introduction of a conductance equation derived elsewhere [presumably by Yagi and Kunii (21), in Japanese] that represented the integral heat flow within a circular column bounded by the external surfaces of two spherical particles in contact ($\beta = 1$). In this equation the conductivity ratio was taken as a variable but apparently was used only to determine the ratio of the temperature gradients in the fluid and solid phases. The limitation placed on the extent of the conducting column by the refraction of flow lines at the spherical surfaces was not considered, inasmuch as parallel flow was assumed throughout.

The cross section of an equivalent series fluid column in each packing was estimated by weighting the total heat flow through a single hemisphere according to the number of contact points on that hemisphere, the direction of the normal to the surface at each contact point, and the total cross-sectional area of the packing perpendicular to each normal. The area of the average conducting column in the direction of general heat flow was calculated to be 70 percent of the projected area of a particle for open packing (n = 48 percent) and 15 percent for close packing (n = 26 percent). That these areas were independent of the conductivity ratio was an error arising from the assumption of parallel flow on each side of the spherical surface. The integral equation was then used to calculate the equivalent length of a cylindrical prism of series fluid having the cross-sectional area so determined, which gave the value of φ D required for each packing. Thus φ_1 and φ_2 were functions of conductivity ratio—the larger the conductivity ratio the shorter the equivalent column. According to this development, conductivity ratio altered the length of the column of series fluid but had no effect on its width.

Kunii and Smith compared their equation with experimental data reported by nine previous investigators. These data covered a broad range of materials, but porosities varied only between 38 and 50 percent. One of their figures indicated that the calculated values fell within a band extending some 15 percent on each side of the observed values.

Kunii and Smith's equation with $\beta = 1$ and $\gamma = \frac{2}{3}$ is compared in Figure 6 with Woodside and Messmer's data for water-saturated sand. The modified resistor equation is

also plotted. It is apparent that at a conductivity ratio of 14.3 neither equation closely predicts the data over a wide range of porosities. For the most part Kunii and Smith's equation underestimates the data, except at a porosity of 26 percent where there is also an abrupt change of slope. The modified resistor equation lies both above and below the data but may be said to be a fair approximation, considering the whole scale of porosities. Neither equation reproduces the value K_S at n = 0, nor does the modified resistor equation predict the value K_f at n = 1.

COMPARISON OF EQUATIONS AGAINST CONDUCTIVITY RATIO

In Figures 7, 8, and 9, the conductivity equations are compared with experimental data for quartz sand, glass beads, and lead shot, as reported by Woodside and Messmer (2). The figures show the influence of the conductivity ratio, σ, for three selected porosities: 19, 38, and 59 percent. The following equations are compared:

Geometric mean	(GM)	Eq. 1
Parallel flow	(P)	Eq. 3
Series flow	(S)	Eq. 4
Maxwell	(M)	Eq. 5
De Vries	(deV)	Eq. 6
Modified resistor	(MR)	Eq. 9
Kunii and Smith	(KS)	Eq. 10

The parallel and series results are included because they represent upper and lower limiting cases, although they do not actually approximate the data.

Several relations are immediately evident. When σ is less than 10 there is little to choose quantitatively among the equations (disregarding the limiting cases) inasmuch as they all converge to the value $K = K_S = K_f$. On the other hand, with increasing σ the geometric mean and Kunii and Smith equations are concave upward, in a manner similar to the parallel flow equation. The geometric mean equation agrees with the data up to a value of σ approximately equal to the porosity in percentage, beyond which the calculated values diverge rapidly from the observed values. Kunii and Smith's equation lies below the data at low σ, passes through at σ between 50 and 500, and continues upward. The remainder of the equations show quite a different behavior; on a semi-logarithmic plot they all have inflections beyond which they approach horizontal asymptotes. These latter equations are characterized by series-type flow at high conductivity ratios.

The series flow equation and Maxwell's equation consistently underestimate the data at all values of σ. Only the de Vries and the modified resistor equations may be said to approximate the data over a large portion of the conductivity range. Both equations fit quite well at a porosity of 19 percent. At the intermediate porosity of 38 percent, the combined data for 1.2 mm lead shot, 40/50 mesh glass beads, and 20/30 mesh quartz sand give the appearance of at least two relationships, portions of which seem to fit both equations. At a porosity of 59 percent, the de Vries equation lies well below the data when σ exceeds 20, while the modified resistor equation continues to fit fairly closely.

The reason for the failure of the de Vries equation when porosity and the conductivity ratio exceed certain limits lies with the F-factor and its dependence on g_X. Figure 3 indicated that the F-factor with g_X = 1:1:6 is essentially correct for all porosities when σ is as low as 14.3. However, at a porosity of 59 percent (Fig. 9), comparison with the position of Maxwell's equation indicates that an ellipsoidal particle even more strongly elongated would be required in order to approximate the data.

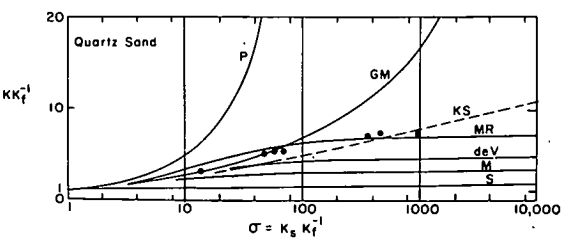

Figure 9. Comparison of conductivity equations; n = 59 percent.

Calculation gives g_x = 1:1:10, which is obviously at variance with the actual particles of sand. The conclusion is inescapable that the de Vries equivalent particle is too slender precisely because Maxwell's stipulation does not hold: the particles do indeed disturb the course of the current, even at porosities as high as 60 percent. The ellipsoidal shape is an empirical device for accounting for the large amounts of heat conducted by the fluid between adjacent grains.

De Vries, of course, has characterized his method as approximate (22). The remarkable fact is that it approximates such a large body of data with relatively small changes in the shape of the presumed particle. This circumstance leads one to speculate that the flow lines derived from a truer physical model will in some way correspond to those derived for the 1:1:6 particle.

The resistor model and the model of Kunii and Smith each take account of the series bridging fluid and its thermal effect, the first model in a qualitative way and the second in an ingenious but not wholly satisfactory quantitative way. The Kunii and Smith method results in a volume of series fluid that is variable with porosity and conductivity ratio, but which because of certain assumptions is of incorrect magnitude. The modified resistor method assumes the volume of continuous fluid to be (n - 0.03), which has the effect of assigning a constant volume (3 percent of the gross volume) to the series fluid. Except for the ambiguity in the data at n = 38 percent (Fig. 8), this equation is a good approximation for all conductivity ratios when porosity is between 19 and 59 percent. On the other hand, Figure 6 indicated that outside this porosity interval the assumption of constant series fluid volume was no longer valid, inasmuch as the end points were not reproduced. It is evident from a physical standpoint that the volume of series fluid should be zero at the porosity limits, independently of conductivity ratio. It follows, then, that if 3 percent is the approximate mean value over the entire range of porosities, there are some porosities for which the volume of series fluid will exceed this value.

THE SERIES CONDUCTING PATH

The foregoing illustrates that there is as yet no fully rational solution for the thermal conductivity of granular materials. Nevertheless, several of the equations currently in use produce strikingly close approximations to certain measured conductivities. There is therefore little purpose in proposing yet another equation that would perform the same function but in a slightly different manner. On the contrary, a new approach is needed that more closely describes the physical situation and thereby permits confident predictions over a broader range of variables; in this connection, empiricisms utilized as a temporary expedient should be of such nature that they can also be made the subject of theoretical inquiry. It is in this context that a heat conduction equation for granular materials is developed here.

It may be anticipated that such an approach will be generically similar to the series/parallel approaches of Wyllie and Southwick or Kunii and Smith, in which the series path carries a major portion of the heat flow. However, a true series path will incorporate a feature that does not appear in any of the equations previously discussed, namely, the possibility of thermal resistance across the particle interfaces bordering the series fluid.

Ingersoll, Zobel, and Ingersoll (23, p. 27) state, "In any practical consideration of heat transfer it is disastrous to overlook the contact resistance that is offered to heat flow by any discontinuity of material; here we have a phenomenon which is really a temperature discontinuity at the gas-solid boundary and which greatly increases resistance." Similarly, Van Rooyen and Winterkorn (3, p. 200) state, "In granular systems the discontinuity of energy and temperature that exists on a solid-gas interface has been recognized and experimentally proven. It is reasonable to assume that a similar phenomenon exists between a solid and a liquid phase." Birch and Clark (24) took account of contact resistance at a gas-solid interface in measuring the thermal conductivity of rock. Sakiadis and Coates (25) took account of resistance at a liquid-solid interface, stating that surface irregularities as small as 0.0005 in. (12μ) introduce considerable error in thin-liquid-layer apparatus.

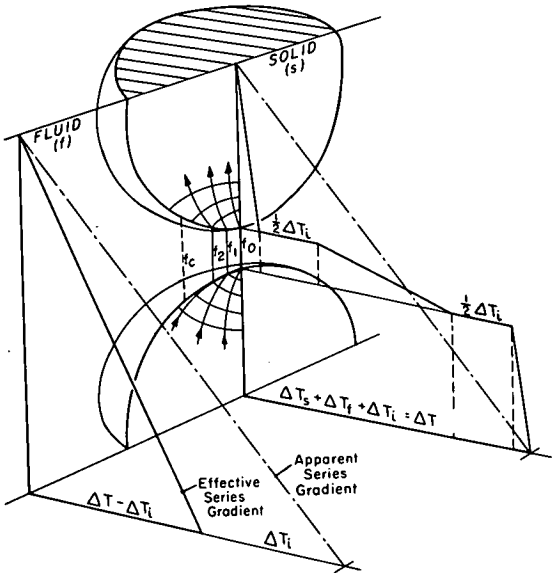

Figure 10. Series heat flow between grains.

Interfacial resistance (or equivalently, low surface-layer conductance) is caused by the molecular discontinuity that occurs at the interface where two differing materials meet. Foreign molecules adsorbed by the interfaces are also likely to reduce surface conductance. Thus, interfacial resistance and its effects must be considered a definite possibility in connection with surface-active granular solids. The outward effect is a reduction in the overall conductivity of the mixture. The previously mentioned ambiguity in the data of Figure 8 most likely arises from this cause.

A secondary result of the presence of boundaries and adsorbed layers in granular materials is that at every point of apparent contact there will remain two interfaces. Only in rare instances, such as in out-gassed sintered materials where recrystallization has progressed across crystal boundaries, will there be an obliteration of original grain surfaces leading to a true molecular matching. In the great majority of granular materials the physical reality is that there is no point at which heat can pass from grain to grain without crossing two boundaries, no matter how compact the packing may be. In other words, there is in general no solid-to-solid contact; in the resistor model equation, for example, the factor b is identically zero.

Figure 10 illustrates schematically a point of close approach between two grains in a saturated granular material. For clarity the grains are shown separated, with a finite fluid length, f_0, at the midpoint. Other fluid lengths, f_1 and f_2, occur at successively greater distances from the midpoint. Each of these lengths decreases as the particles are moved closer together, the distance f_0 eventually becoming zero. Nevertheless, because of the presence of the grain boundaries the flow path at the midpoint continues to be of the same character as each of the others. All flow paths between grains are therefore similar, the only variables being the distance across the intervening fluid and the angle at which a flow line intercepts the grain surface. No solid-to-solid connections are postulated.

A calculation made by Maxwell (11, Art. 312) indicates that currents passing through the grains will for the most part be contained by the granular boundaries, breaking through only at discrete points of high potential. Maxwell's example was that of a thin spherical shell of conductivity different from that of the media enclosed by it and surrounding it. His calculations led him to conclude that if the shell is a better conductor than the rest of the medium it tends to equalize the potential around the inner sphere; if it is a poorer conductor, it tends to prevent currents from reaching the inner sphere at all. In either case, the shell acts as a barrier to currents that would otherwise cross the space occupied by it. In the present context, the surface of the particle and the adsorbed layers constitute the shell of differing conductivity; the granular particle is analogous to the region within the shell.

Woodside and Kuzmak (26) demonstrated that the points of highest potential are precisely those where another grain comes into near contact. Using a large model composed of marble hemispheres surrounded by silica gel (simulating quartz grains in moisture-saturated air) they found that temperature gradients within a radius of ¼ grain diameter from the midpoint were more than 20 times greater than the average gradient as measured in the remote fluid. It is therefore apparent that only a small

portion of the total fluid in the system will be spatially situated to contribute to the heat flow between the grains.

The lateral extent of the series conducting fluid was considered by Kunii and Smith (19) as previously mentioned; however, these investigators failed to take into account the refracting influence of the conductivity ratio of the solids and fluid. According to the law of refraction of flow lines (11, Art. 310),

$$\frac{\tan \theta_s}{\tan \theta_f} = \frac{K_s}{K_f} = \sigma \tag{11}$$

where θ_s and θ_f are the angles that the flow lines in the solid and fluid, respectively, make with the normal to the surface of separation. With $\sigma > 1$, Eq. 11 indicates that a flow line in passing from solid to fluid to solid will be refracted as shown in Figure 10. For a given value of σ there is a flow line, f_c, for which the angle of refraction in leaving the fluid equals the inclination of the solid surface; the flow surface of which this flow line is a part does not penetrate the interior of the solid and therefore marks the lateral limit of the series fluid for that region. The higher the ratio of conductivities the closer will f_c be to the midpoint, and hence the smaller will be the total volume of fluid (for a given porosity) that can be utilized as a series connection for heat passing through the grains. With $\sigma < 1$, the reverse will be true, but this situation does not generally occur with mineral solids.

THE BASIC CONDUCTANCE EQUATION

The general condition of heat flow through a granular material saturated with fluid is taken to be as shown in Figure 11. The paths of the series flow in an internal sheet one-half grain diameter in thickness are shown by solid flow lines; the paths pass through successive points of near contact, shown schematically at the near surface of the element. The mean temperature on the upper surface of the sheet is T_2, and on the lower surface T_1; the mean temperature gradient in the direction of the general heat flow is $-(T_1 - T_2)/\Delta L$, which for ΔL sufficiently large is equal to the average temperature gradient between the remote external surfaces.

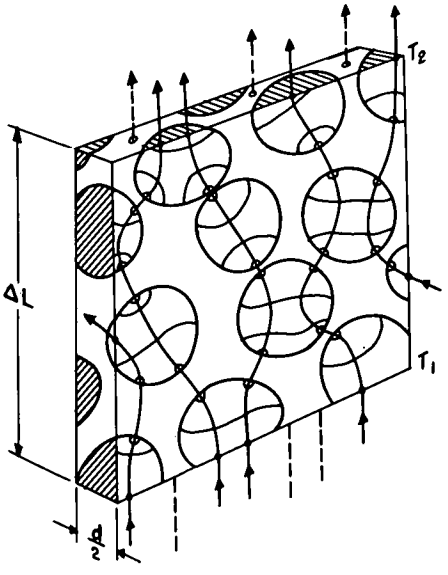

Figure 11. General heat flow through an aggregate of grains.

In addition to the series paths there are continuous paths through the fluid, indicated by dashed flow lines passing into and out of the sheet. Maxwell's analogy of the thin shell indicates that these latter paths do not intercept the particles but in all likelihood lie entirely within the fluid. There are thus two main paths for the conduction of heat through a granular material.

A general equation describing the heat flow in Figure 11 will be of the form

$$K = f(n)\, K_f + f(\lambda)\, K_{gs} \tag{12}$$

where $f(n)$ and $f(\lambda)$ are volume functions of the fluid and solids respectively, K_f is the conductivity of the bulk fluid, and K_{gs} is the apparent conductivity over the granular series path; K_{gs} will be a function of the bulk conductivities of solids and fluid, the porosity, the amount of fluid involved in

the series flow, and the interfacial resistance. An expression for K_{gs} may be derived with the aid of Figures 10 and 11.

In Figure 11, between the upper and lower surfaces and along a single flow line traversing several grains, there will be a total temperature differential ΔT_n across the solids, $\Delta T_n'$ across the intervening fluid, and $\Delta T_n''$ across the interfacial regions, such that

$$\Delta T_n + \Delta T_n' + \Delta T_n'' = T_1 - T_2 = \Delta T \tag{13}$$

Assuming steady flow with no internal sinks or sources, the heat flow in a single flow tube will be given by

$$q_n = K_s \cdot \frac{\Delta T_n}{s_n} \cdot \bar{a}_n = K_f \cdot \frac{\Delta T_n'}{f_n} \cdot \bar{a}_n' = K_i \cdot \frac{\Delta T_n''}{i_n} \cdot \bar{a}_n''$$

$$= K_{gs} \cdot \frac{\Delta T}{s_n + f_n} \cdot \frac{s_n \bar{a}_n + f_n \bar{a}_n'}{s_n + f_n} \tag{14}$$

where s_n and f_n are the actual lengths of the flow tube in the domains of the solids and fluid, respectively. The thickness of the interfacial regions, i_n, is taken to be negligible compared with the values of s_n and f_n. The mean areas of the flow tube are $\bar{a}_n$, $\bar{a}_n'$ and $\bar{a}_n''$ in the solid, fluid, and interfacial domains. With $\sigma > 1$, a_n will be generally larger than a_n', whereas $a_n' \approx a_n''$ for a single flow tube. K_i is the interfacial conductance.

The volume of the flow tube in each of the domains is given by

$$v_n = \bar{a}_n s_n \; ; \; v_n' = \bar{a}_n' f_n' \; ; \; v_n'' = \bar{a}_n'' i_n \tag{15}$$

where the series interfacial volume, v_n'', is very much smaller than v_n and v_n'. Substitution into Eq. 14 gives, for the heat flow in a single tube,

$$q_n = K_s \cdot \frac{\Delta T_n}{s_n} \cdot \frac{v_n}{s_n} = K_f \cdot \frac{\Delta T_n'}{f_n} \cdot \frac{v_n'}{f_n} = K_i \cdot \frac{\Delta T_n''}{i_n} \cdot \frac{v_n''}{i_n}$$

$$= K_{gs} \cdot \frac{\Delta T}{s_n + f_n} \cdot \frac{v_n + v_n'}{s_n + f_n} \tag{16}$$

The heat flow in the entire volume of N flow tubes is then

$$Q = \sum_{n=1}^{N} q_n = K_s \cdot \frac{\Delta T_s}{s} \cdot \frac{v_s}{s} = K_f \cdot \frac{\Delta T_f}{f} \cdot \frac{v_f}{f} = K_i \cdot \frac{\Delta T_i}{i} \cdot \frac{v_i}{i}$$

$$= K_{gs} \cdot \frac{\Delta T}{s + f} \cdot \frac{v_s + v_f}{s + f} \tag{17}$$

where ΔT_s, ΔT_f, and ΔT_i are the overall mean temperature differentials across the various phases; s, f, and i are the overall mean lengths of the flow tubes in these phases; v_s, v_f, and v_i are the actual volumes of solids, series fluid, and series interfacial material. Again, i and v_i are very small.

If ΔT_i represents the summation of the interfacial temperature differentials in the volume considered, then

$$\Delta T_s + \Delta T_f = \Delta T - \Delta T_i \tag{18}$$

which may be combined in the following way with Eq. 17 to yield an expression for K_{gs}. From Eq. 17,

$$\Delta T_f = \Delta T_s \cdot \sigma \cdot \frac{v_s}{v_f} \left(\frac{f}{s}\right)^2 \tag{19}$$

Substitution into Eq. 18 gives

$$\Delta T_s = (\Delta T - \Delta T_i) \left[1 + \sigma \cdot \frac{v_s}{v_f} \left(\frac{f}{s}\right)^2\right]^{-1} \tag{20}$$

and a combination of Eqs. 20 and 17 results in

$$K_{gs} = \left(1 - \frac{\Delta T_i}{\Delta T}\right) K_s \left(1 + \frac{f}{s}\right)^2 \left(1 + \frac{v_f}{v_s}\right)^{-1} \left[1 + \sigma \cdot \frac{v_s}{v_f} \left(\frac{f}{s}\right)^2\right]^{-1} \tag{21}$$

A comparison of the first term of Eq. 21 with Figure 10 shows that the effect of ΔT_i is to reduce the mean effective temperature gradient along the series path. When interfacial resistance is negligible owing to a high surface conductance, ΔT_i approaches zero and K_{gs} approaches its highest value as determined by the other variables. Conversely, as interfacial resistance increases, ΔT_i approaches ΔT and K_{gs} approaches zero. The quantity $(1 - \Delta T_i/\Delta T)$ thus modifies the series heat flow irrespective of K_s, K_f, or the geometry. It is convenient to specify an interfacial efficiency applicable to the series path through a granular material as follows:

$$\epsilon = 1 - \frac{\Delta T_i}{\Delta T}\,; \quad (0 \le \epsilon \le 1) \tag{22}$$

With the incorporation of this relation, Eq. 21 becomes

$$K_{gs} = \epsilon K_s \left(1 + \frac{f}{s}\right)^2 \left(1 + \frac{v_f}{v_s}\right)^{-1} \left[1 + \sigma \cdot \frac{v_s}{v_f} \left(\frac{f}{s}\right)^2\right]^{-1} \tag{23}$$

Equation 23 is the basic equation for the compound conductivity of the series path. The values of s and f are in general unknown, inasmuch as they depend on the geometry of a given system. However, the following approximation may be nearly correct in many instances:

$$\frac{f}{s} \approx \frac{v_f}{v_s} \equiv \frac{n_c}{\lambda} \tag{24}$$

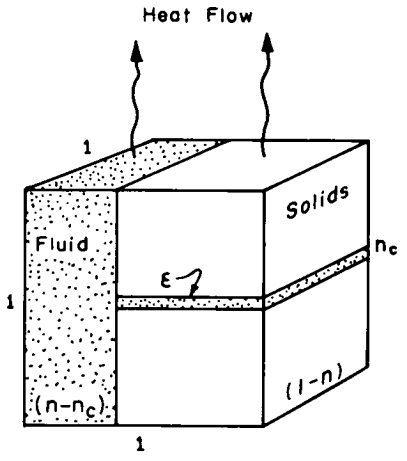

Figure 12. Schematic model of the saturated conductance equation.

where n_c is the volume fraction of fluid utilized as a series member. Substitution of Eq. 24 into Eq. 23 results in a macroscopic approximation of K_{gs} in terms of the conductivities and volumetric proportions of the constituents:

$$K_{gs} = \epsilon K_s \cdot \frac{\lambda + n_c}{\lambda + \sigma n_c} \qquad (25)$$

This expression is equivalent to a linear relation in terms of resistances,

$$\frac{1}{K_{gs}} = \frac{1}{\epsilon}\left[\frac{\lambda}{\lambda + n_c} \cdot \frac{1}{K_s} + \frac{n_c}{\lambda + n_c} \cdot \frac{1}{K_f}\right] \qquad (25a)$$

Thus, the total series resistance is increased when ϵ is less than unity.

Referring again to Eq. 12, it remains to add the contribution to overall conductivity of the continuous paths through the fluid. Equation 25a indicates that the fractional volume of material utilized in the series path is $(\lambda + n_c)$; the remainder of the fluid volume is therefore $(n - n_c)$. Hence, with the approximation of Eq. 24, Eq. 12 becomes

$$K = (n - n_c) K_f + (\lambda + n_c) K_{gs} \qquad (26)$$

Equations 25 and 26 together describe the macroscopic heat flow in the mixture. They may be combined to give the following expression for the thermal conductivity of a saturated granular material:

$$K = (n - n_c) K_f + (\lambda + n_c) \frac{\epsilon K_s (\lambda + n_c)}{\lambda + \sigma n_c} \qquad (27)$$

where $\sigma = K_s K_f^{-1}$.

Equation 27 is similar in form to the modified resistor equation with b = 0. However, there are two important differences: (a) the effects of interfacial conductance are accounted for, and (b) the volume of series fluid is as yet unspecified, being free to vary with grain size and shape, porosity, and the conductivity ratio. A prismatic model of Eq. 27 is shown in Figure 12, which may be compared with Figure 5.

Derivations of n_c and ϵ should be possible. However, the first step will be to gain some idea of their values for particular materials. The manner in which this may be accomplished is discussed in the following.

DISCUSSION

Experimental data reported by Woodside and Messmer (2) for quartz sand, glass beads, and lead shot were previously compared with selected equations for thermal conductivity. In Figures 13, 14, and 15 these data are compared with Eq. 27. The data presented are for seven different saturants at three porosity levels. In the order of increasing conductivity ratio, the saturants are water (H_2O), hydrogen (H), helium

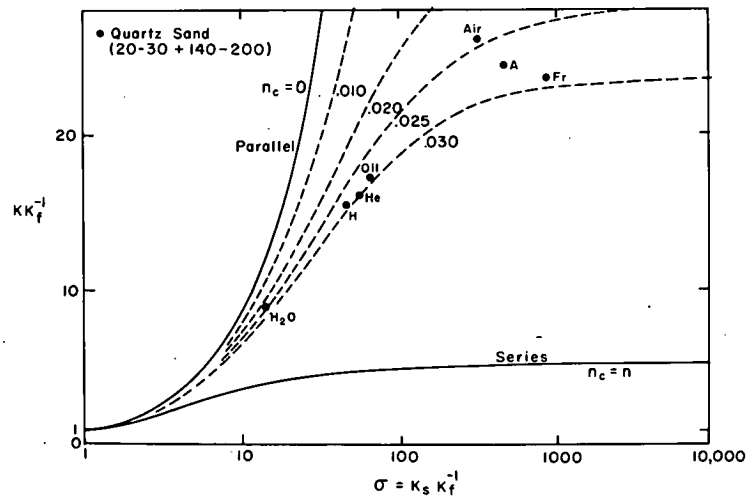

Figure 13. Comparison of the conductance equation with reported data; n = 19 percent , $\epsilon = 1$.

(He), n-heptane (Oil), dry air (Air), argon (A), and Freon-12 (Fr), all at atmospheric pressure.

The figures show familes of curves corresponding to the calculation of conductivity with two variables, n_C and σ; ϵ was taken to be unity. If in the physical system interfacial resistance is negligible, the value of n_C read from the curves is the correct value. If in reality ϵ is less than unity, the actual value of n_C is lower than the apparent value. Curves corresponding to the parallel and series combinations of the constituents are also included. These curves are the upper and lower limits of conductivity, respectively, for $\epsilon = 1$. They are also solutions to the conductance equation when $n_C = 0$ and $n_C = n$, respectively. The parallel and series relationships are therefore special cases of Eq. 27.

The curves labeled $n_C = 0.030$ are solutions to the modified resistor equation, Eq. 9. Clearly a constant value of n_C does not fit all the data. An envelope has been drawn

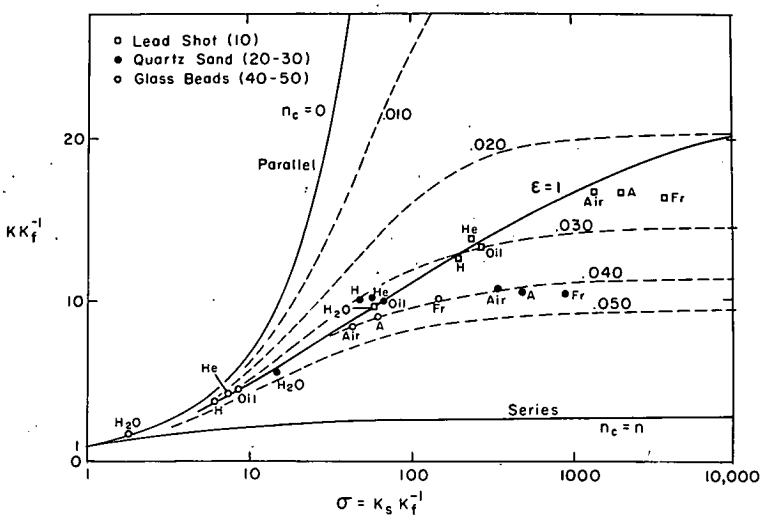

Figure 14. Comparison of the conductance equation with reported data; n = 38 percent, $\epsilon = 1$.

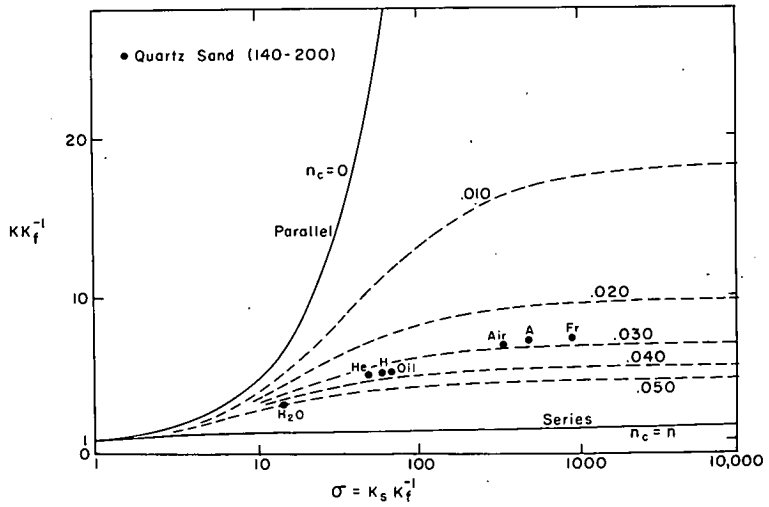

Figure 15. Comparison of the conductance equation with reported data; n = 59 percent, $\epsilon = 1$.

through the composite data of Figure 14 for 38 percent porosity. The position of this envelope is remarkably similar to the position of Kunii and Smith's estimation in Figure 8. Considering the variety of mixtures involved, it may be presumed that the envelope corresponds approximately to an efficiency of unity, and therefore to the true values of n_C. It is apparent that, at a single porosity, n_C decreases with conductivity ratio, a result that is consistent with the deduced influence of refraction. In addition, there is evidence that ϵ for dry air, argon, and Freon is less than unity; the experimental data for all three types of particles with these saturants falls below the envelope.

Envelope curves have not been drawn in Figures 13 and 15; Figure 14 illustrates that data from than one type of particle will normally be needed to define the position of the n_C-envelope for a given porosity.

Figure 16 shows the variation of n_C with n for water-saturated quartz sand (σ = 14.3). The upper curve represents the solution of Eq. 27, with $\epsilon = 1$, that fits the data shown in Figure 2. As anticipated, n_C is zero at both extremes and reaches a maximum of approximately 0.05; the mean value over the entire porosity range is very close to 0.03 for this combination of materials, as was expected. Also shown is a partial relationship for quartz sand and oil (σ = 67),

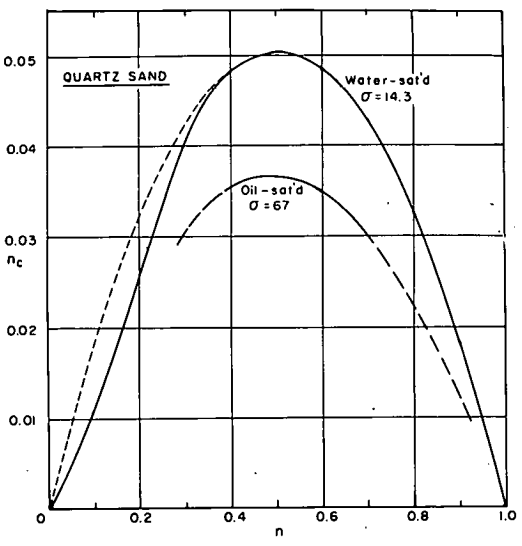

Figure 16. Volume of series fluid (n_C) vs porosity (n).

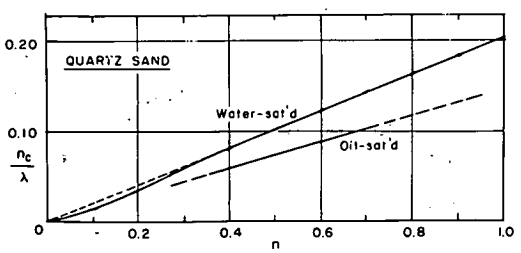

Figure 17. Volume ratio (n_C/λ) vs porosity (n).

assuming $\epsilon = 1$. For sand saturated with oil, the mean value of n_c is approximately 0.02.

Figure 17 shows the variation of the volumetric ratio, n_c/λ, with porosity. For porosities greater than 40 percent this ratio is proportional to n, being 0.20n for sand with water and 0.14n for sand with oil. The relationship is different for porosities less than 40 percent. As particles become more tightly packed, proportionately less connecting fluid is utilized.

A final remark may be made concerning the conductivity of unsaturated materials. Although Eq. 27 was derived with the assumption of full saturation, the adaptation to unsaturated conditions should require only a few additional considerations. One of the most important is the proper assessment of the volume of fluid taken up by adsorbed films at low degrees of saturation. Most of the adsorbed fluid will be part of the continuous fluid network, with only a small fraction contributing to the series connections. It may therefore be anticipated that the total volumetric water content necessary for full development of the series paths will be somewhat in excess of the actual series fluid.

SUMMARY AND CONCLUSIONS

Selected equations for calculating the thermal conductivity of granular materials have been analyzed and compared with experimental data. None of the equations was found to have a truly rational basis, although the de Vries equation and the modified resistor equation predicted the data to a fair degree. An equation by Kunii and Smith seemed to be the closest to a physical solution in form but was encumbered by empirical estimates that made it a poor approximation.

A conductance equation was then derived for saturated granular materials, based on the hypothesis that there are only two paths for heat flow through these materials: a series path through the granular network, aided by a portion of the pore fluid that acts to transfer heat from grain to grain, and a continuous path through the remainder of the fluid. A third path through continuous solid material connected at grain contact points was considered to be generally nonexistent. Every series path was assumed to cross two interfacial regions in passing from one grain to another; temperature differentials across the interfaces had the effect of reducing conductivity. The series and parallel flow equations were found to be special cases of the derived equation.

The volume of fluid brought into action as a thermal connection was found to vary with porosity and the conductivity ratio of the constituents. For systems in which the bulk conductivity of the solids exceeds that of the fluid, the maximum amount of series connecting fluid effective in any condition appeared to be approximately 5 percent by total volume.

At constant porosity, the effective volume of connecting fluid decreased with the conductivity ratio (solids to fluid). At a single conductivity ratio (14.3) the volume of connecting fluid varied from zero at porosities of 0 and 100 percent to a maximum at a porosity of 50 percent.

A transfer efficiency coefficient was defined to express the influence of thermal resistance at fluid-grain interfaces. Transfer efficiency appeared to vary with the saturating fluid. Water, hydrogen, helium, and oil had an efficiency of unity with quartz sand, glass beads, and lead shot. Dry air, argon, and Freon were less efficient with each of the three solid materials.

REFERENCES

1. McGaw, R. Thermal Conductivity of Compacted Sand/Ice Mixtures. Highway Research Record 215, pp. 35-47, 1968.
2. Woodside, W., and Messmer, J. H. Jour. Appl. Phys., Vol. 32, No. 9, pp. 1688-1699, 1961.
3. Van Rooyen, M., and Winterkorn, H. F. Theoretical and Practical Aspects of the Thermal Conductivity of Soils and Similar Granular Systems. HRB Bull. 168, pp. 143-205, 1957.

4. Webb, J. Nature, Vol. 177, p. 989, 1956.
5. Gemant, A. Jour. Appl. Phys., Vol. 21, pp. 750-754, 1950.
6. Alberts, L., Bohlmann, M., and Meiring, G. L. Brit. Jour. Appl. Phys., Vol. 17, No. 7, 1966.
7. Lichtenecker, K. Z. Physik, Vol. 27, p. 115, 1926.
8. Asaad, Y. PhD thesis, Univ. of California, 1955.
9. Legg, V. E., and Given, F. J. Bell System Tech. Jour., Vol. 19, p. 385, 1940.
10. Brown, W. F., Jr. Jour. Chem. Phys., Vol. 23, p. 1514, 1955.
11. Maxwell, J. C. A Treatise on Electricity and Magnetism, 3rd Ed., Vol. 1. Dover Publications, Inc., New York, 1954.
12. Rayleigh, W. R. Phil. Mag., Vol. 34, pp. 481-502, 1892.
13. Burger, H. C. Phys. Zeitsch., Vol. 20, pp. 73-76, 1919.
14. Eucken, A. Verein deutscher Ingenieure, Forschungsheft Nr. 353, Berlin, 1932.
15. De Vries, D. A. Thesis, Meded. Landbouhogeschool, Wageningen, Vol. 52, No. 1, pp. 1-73, 1952.
16. De Vries, D. A. In Physics of Plant Environment (W. R. van Wijk, Editor), Chap. 7. North-Holland Publ. Co., Amsterdam, 1963.
17. Wyllie, M. R. J., and Southwick, P. F. Jour. Petrol. Technol., Vol. 6, p. 44, 1954.
18. Kimura, M. Kagaka Kikai, Vol. 21, p. 750, 1957.
19. Kunii, D., and Smith, J. M. AIChE Jour., Vol. 6, No. 1, pp. 71-78, 1960.
20. Yagi, S., and Kunii, D. AIChE Jour., Vol. 3, No. 3, pp. 373-381, 1957.
21. Yagi, S., and Kunii, D. Chem. Eng. (Japan), Vol. 18, p. 576, 1954.
22. De Vries, D. A. Nature, Vol. 178, p. 1074, 1956.
23. Ingersoll, L. R., Zobel, O. J., and Ingersoll, A. C. Heat Conduction. Univ. of Wisconsin Press, Madison, 1954.
24. Birch, F., and Clark, H. Amer. Jour. Science, Vol. 238, pp. 529-558, 613-635, 1940.
25. Sakiadis, B. C., and Coates, J. AIChE Jour., Vol. 1, No. 3, pp. 275-285, 1955.
26. Woodside, W., and Kuzmak, J. M. Trans. AGU, Vol. 39, No. 4, pp. 675-680, 1958.

Temperature Effect on Water Retention and Swelling Pressure of Clay Soils

R. N. YONG and R. K. CHANG, Soil Mechanics Laboratory, McGill University, and
B. P. WARKENTIN, Department of Soil Science, Macdonald College of McGill University

Clay-water interaction in soil systems where solute effects are negligible is measured by the matric potential. The two forces contributing to the matric potential are the swelling and capillary forces. Theoretical expectation and available experimental evidence indicate that temperature changes influence the two components differently. While an exact separation of forces cannot be made because they may not necessarily be completely independent, an assessment of the specific contribution of each can be attempted through controlled experiments.

Measurements were made at 10, 25, and 45 C of soil suction on plaster of paris samples with different void-size distribution, and of soil suction and swelling pressure on kaolinite-glass bead mixtures. Soil suction was measured on the adsorption cycle. The clay-glass bead samples were precompressed to 10 bar and were then either allowed to swell (rebound) under decreasing load, or were transferred to a pressure plate apparatus and allowed to take up water under decreasing air pressure.

The results show that in the swelling pressure test, where complete saturation exists, increased temperatures resulted in slightly increased water contents for the same swelling pressure. This is consistent with qualitative predictions based on the theory of swelling due to interaction of diffuse ion-layers. For soil suction measurements, where unsaturation occurs, increased temperatures resulted in decreased water contents for the same soil water potential. This would result from decreased values of surface tension with the temperature increases. This is demonstrated more clearly with the plaster of paris samples where the capillary force is the only component of matric potential.

These measurements of temperature effects are more useful because both swelling and water uptake are measured on identical samples. The various proportions of glass beads in the clay-glass bead mixtures—from pure glass beads to pure clay systems—provide a series of results from which the temperature effect is evaluated. The purpose is to provide information on the contribution of the components of the matric potential in water retention and swelling as affected by temperature.

•THE ENERGY with which water is held in soils is referred to as the total soil water potential. Where solute effects are negligible and assuming that gravitational and gas pressure effects are insignificant, the matric potential becomes the sole component of the total potential. This situation is usually true for laboratory experimental studies. The matric potential is the component that depends upon the soil grains, i. e., the matrix of the soil (6).

The two main forces contributing to the matric potential at higher water contents are swelling and capillary forces. The former are important in clay soils while the latter are dominant in coarse-grained soils. Although it may be possible to separate the components in thermodynamic terms for theoretical considerations, it has not been possible to do so experimentally because of the interdependent behavior of the separate components. However, with the aid of controlled experiments, an assessment of the magnitude of the two forces can be made.

Several studies on the effect of temperature in the range from 5 to 50 C on water retention have been reported in the literature. The general conclusion is (a) that the effect is small and sometimes not measurable, and (b) that the amount of water retained at a given value of matric potential decreases as temperature increases (e. g., 2). These results have usually been explained as due to the decrease in surface tension, because water was considered to be held in soils primarily by surface tension forces at air-water interfaces, i. e., capillary forces. Wilkinson and Klute (4) showed that the decrease in surface tension accounted for the measured results for large sand grains, but the decrease was not large enough to explain the temperature effect in silt-size grains.

The large influence of temperature on water retention occasionally measured is thought to be due to temperature effects on the measuring instrument. The most precise measurements of matric potential are now being made with special psychrometers. Converting these measurements of vapor pressure to water potential, Klute and Richards (1) found that water content of a clay soil at constant potential did not change with temperature, but the water content of a sodium montmorillonite increased with increase in temperature. Studies of the temperature effect on swelling pressures of high-swelling sodium montmorillonite have also shown that increased temperatures resulted in increased swelling pressures for the same volume (5).

This is the temperature effect predicted from the diffuse ion-layer theory of swelling of clays (6). While this theoretical calculation of swelling pressure is based on certain assumptions that are not generally admissible for soils, and experimental confirmation of theory is limited to high-swelling soils, it is not unreasonable to expect the swelling component of the matric potential to behave in the same manner, albeit on a lesser scale. Thus, one would predict for the swelling component of matric potential that increased temperature will result in increased water content at a constant value of the matric potential.

Changes in temperature also influence the properties of adsorbed water. This is most important at lower water contents, and will not be considered here.

This paper reports measured temperature effects for water retention and swelling pressure for different clays and porous media, chosen to give both swelling and/or capillary components of matric potential. This study is part of a larger study on forces of water retention in different soils.

EXPERIMENTATION

Test samples used in this study of temperature effects on matric potential were plaster of paris blocks made with different void ratios, clay, and clay-glass bead mixtures. The clay used was a kaolin containing a small amount of mica and marketed under the name English Clay by Domtar Limited, Montreal. The glass beads used in the kaolin-glass bead mixtures were No. 14 glass beads, supplied by Potters Bros. Inc., New Jersey, with over 95 percent between 0.06 and 0.15 mm in diameter.

The plaster of paris blocks were made by mixing different proportions of plaster of paris and water to produce blocks with three different bulk densities: 0.93, 0.70 and 0.55 gm/cc. The proportions of clay to glass beads used in the different mixtures were 100 percent clay (by weight), 80, 60, 40, and 20 percent clay. The samples were wetted to saturation with water at a water potential of -1 mb. The clay and the clay-glass bead mixtures were then consolidated mechanically in the swell apparatus under a pressure of 10 bar at one of the three test temperatures, 10, 25, or 45 C. This process is similar to the consolidation process used in soil mechanics. The samples were thus always fully saturated. For the swelling pressure test, the samples were allowed to rebound

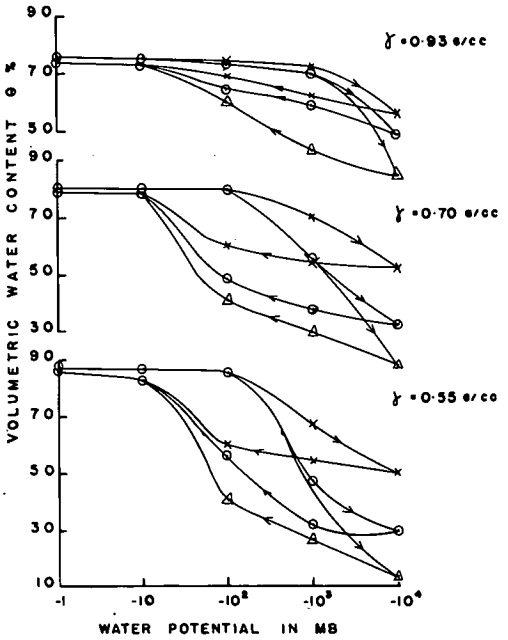

Figure 1. Temperature effect on water retention in plaster of paris (MB = millibars, γ = density).

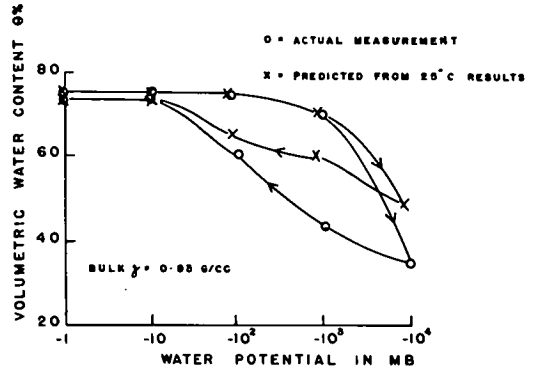

Figure 2. Predicted and measured water retention curves for plaster of paris at 45 C (MB = millibars, γ = density).

under controlled mechanical loads applied as air pressure to a flexible rubber membrane. Water content computations were made from measured values of water uptake, after drying the sample to measure the final water content.

For the water retention tests on the clay and clay-glass bead mixtures, the samples were removed from the swell chambers following equilibrium at 10 bar at one of the three test temperatures and introduced into the pressure plate apparatus at that temperature, where an air pressure of 10 bar was immediately applied directly to the sample until a new equilibrium was established. Further water expulsion occurred, possibly due to unsaturation which could occur when air pressure was applied directly to the sample. The air pressure was then lowered stepwise by a factor of 10, and the water taken up at each step measured.

The plaster of paris samples were saturated, then placed in the pressure plate apparatus at one of the three test temperatures and the equilibrium water contents measured at different air pressures on drying and rewetting.

The test results reported for the clay-glass bead mixtures are the average of two tests conducted simultaneously. Three replicates were averaged for the plaster of paris samples. The measured value agreed within 2 to 3 percent water.

DISCUSSION OF RESULTS

The three sets of results to be discussed are (a) temperature effect on water retention in plaster of paris, (b) temperature effect on swelling pressure of clay and clay-glass bead mixtures, and (c) temperature effect on water retention in clay and clay-glass bead mixtures.

The plaster of paris samples have fixed void-size distributions. The capillary force is the only means whereby water is held in the system. As would be predicted from the effect of temperature on surface tension, increasing temperatures decrease the water retention at constant potential where the sample is unsaturated (Fig. 1). The magnitude of the effect increases with decreasing bulk density. Bearing in mind that the water potential is a negative quantity, it is seen that the water potential at the point of unsaturation increases with decreasing bulk density due to increase in average void diameter. Increasing temperature increases the potential at unsaturation. These two effects, which are predicted from changes in surface tension forces, appear to result in the measured effect of bulk density.

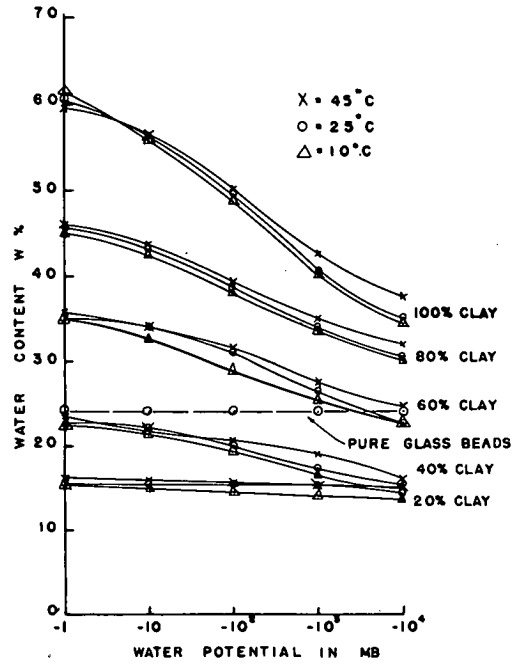

Figure 3. Temperature effect on swelling of clay and clay-glass bead mixtures (MB = millibars).

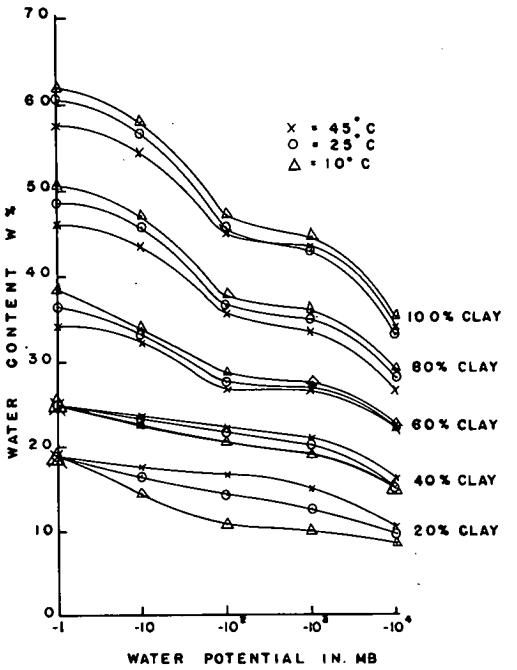

Figure 4. Temperature effect on water retention for clay and clay-glass bead mixtures (MB = millibars).

It is then interesting to determine whether the predictions from capillary theory explain the measured differences quantitatively. Calculations can be made from the equation for height of rise of water in a capillary, with surface tension and density of water having different values depending upon temperature. In Figure 2, the expected values at 45 C as calculated from measured values at 25 C are compared with measured values at 45 C.

While the effects of temperature are qualitatively as predicted, the decrease of surface tension with increasing temperature does not account for all of the measured decrease in water retention. This result is the same as found by Wilkinson and Klute (4). The calculation probably does not make an adequate correction, because it does not apply exactly to the geometry of the interconnecting voids of different sizes in the porous medium.

The measured swelling volumes for completely water-saturated samples swelling from a pressure of 10 bar are shown in Figure 3. The samples remain completely water-saturated, i. e., pores are completely filled with water, while swelling against a mechanical constraint in decreased pressure steps. Increased temperatures result in increased swelling pressures for the same water content. The effect of temperature is already established during compression where higher temperature results in higher water content at -10^4 mb potential. The amount of swelling is essentially independent of temperature with a trend at higher potential for decreasing swelling with increasing temperature. This results because more of the swelling occurs at lower potentials (3), and the temperature effect is not likely to be fully reversible.

The individual differences in pressure due to temperature changes are not large, and are about the same magnitude as the reproducibility of the measurement. However, the trends are consistent. This result is consistent with the predicted and measured influence of temperature on swelling of high-swelling montmorillonite clays. While the difuse ion-layer model for swelling cannot be applied quantitatively to the mixtures, the evidence is that the swelling component of matric potential has the op-

posite temperature coefficient to the capillary component. Temperature effects calculated from diffuse ion-layer theory show water content increases of 2 to 3 percent per 20 C—the same order of magnitude as values measured.

It has been shown from Figures 1 and 3 that opposing results occur due to temperature changes if the separate components of matric potential are considered. These results are qualitatively confirmed by the simplified theories applied to swelling and capillary retention of water. Thus measurements of water retention, where both components are known to exist, can be difficult to evaluate. In Figure 4, water retention curves for the wetting cycle are shown for samples equilibrated initially at a suction of 10 bar at the desired test temperature. Except for the 100 percent kaolinite sample, where the results for the 45 and 25 C tests appear in the reverse order, a consistent picture is presented. For clay concentrations of 60 percent and over, increased temperatures show decreased values of water retention. In the region of 40 percent clay concentration and lower, the reverse effect is seen.

The effect of the temperature changes on the two components is assumed to produce the overall change in water retention value. Thus, at proportions of clay higher than about 50 percent, the capillary component seems to dominate. Swelling within clusters or aggregates is not large enough to alter the trend produced in the large voids by the decrease in surface tension (3). At clay contents less than about 50 percent, the effect of temperature on the swelling component dominates. The clay particles tend to orient around the glass beads. One would also expect a denser packing of the beads. Swelling seems to be the dominant force in water retention.

While the effects of temperature can be predicted qualitatively with certain assumptions about fabric of the sample, it is obvious from the foregoing discussion that a number of additional factors must be evaluated before temperature effects on water retention in soils can be more completely understood. This is part of a continuing study on water retention in soils.

CONCLUSIONS

The two main components of the matric potential have been investigated in experiments designed to test their change with changes in temperature. As predicted from simplified theory, increased temperatures cause increased swelling pressures and decreased capillary water retention values in experiments where only one of the components is active. However, where the two components exist together, the two opposing trends cause different effects under temperature changes. In clay-glass bead mixtures, this may be traced to aggregate size. Where aggregate sizes are large, the swelling pressure mechanism dominates. Thus, where clay content is small, swelling of oriented clay between aggregates occurs as a dominant mechanism in water retention. On the other hand, capillary effects are dominant in the high-clay system where clay particles are irregularly aligned.

ACKNOWLEDGMENTS

This study was supported by the National Research Council of Canada.

REFERENCES

1. Klute, A., and Richards, L. A. Effect of Temperature on Relative Vapor Pressure of Water in Soils. Soil Science, Vol. 93, pp. 391-396, 1962.
2. Richards, L. A., and Weaver, L. R. Moisture Retention by Some Irrigated Soils as Related to Soil-Moisture Tension. Jour. of Agric. Research, Vol. 69, pp. 215-235, 1944.
3. Warkentin, B. P., and Chang, R. K. Swelling Component of Matric Potential of Soil Water. Submitted for publication in Soil Sci. Soc. Amer. Proc., 1968.
4. Wilkinson, G. E., and Klute, A. The Temperature Effect on the Equilibrium Energy Status of Water Held by Porous Media. Soil Sci. Soc. Amer. Proc., Vol. 26, pp. 326-329, 1962.

5. Yong, R. N. The Swelling of a Montmorillonitic Clay at Elevated Temperatures. Proc. Third Asian Regional Conf. on Soil Mech. and Found. Eng., Israel, Vol. 1, pp. 124-128, 1967.
6. Yong, R. N., and Warkentin, B. P. Introduction to Soil Behavior. Macmillan Co., New York, 1966.

Part III
TEMPERATURE EFFECTS ON THE ENGINEERING PROPERTIES OF SOILS

FOREWORD TO PART III

The General Report by James K. Mitchell covers the fourteen papers in this part. The topics treated can be divided into three groups. The first covers the temperature effects on engineering properties, volume change phenomena, pore pressure effects, compressibility, strength, elasticity, creep and stress relaxation, and swelling-salt heave. The second group concerns thermal stabilization, effects of preliminary heat treatment, and fusion of soils and ice barriers. The third group covers temperature effects in pavement subgrades relating to field observations and analysis methods.

Collectively, these provide concepts and data that make possible a greatly improved understanding of the importance of thermal influences in soil mechanics and thermal treatment of soils for improvement of properties.

Effect of Heating on Bearing Capacity of Highway Subgrades

FERNANDO EMMANUEL BARATA, School of Engineering, Federal University of Rio de Janeiro

•MOST OF Brazil's territory lies in tropical and subtropical regions. Throughout the country the soil layers compacted in highway construction are exposed—mainly in summer—to intense natural heating, frequently for prolonged periods of time. The daytime air temperature often reaches 39 to 41 C (102 to 106 F) and it is not uncommon that in some areas this temperature will remain unchanged during the night. Hence, the temperature of the bare soil attains values around 45 to 60 C (113 to 140 F) according to its composition, color, surface condition, etc. Therefore the evaporation tends to be very important (especially during the dry days) in compacted subgrades before they are covered with the pavement.

Such considerations inspired the author to investigate in the laboratory the degree of influence of preliminary drying on the future bearing capacity of compacted subgrades. It was worthwhile to study the effects of drying by heating of compacted nonsaturated soil samples and the repercussions on the strength after wetting.

In spite of some well-known shortcomings—such as the difficulty in reproducing specimens of similar characteristics, and low accuracy in the penetration test—the CBR method was selected to determine the strength because it is the most widely used procedure for pavement design in Brazil as well as abroad and because it was the most convenient method available to the author in establishing the effect of drying.

However, the author wishes to emphasize that neither the conventional CBR method chosen for carrying out the experiments nor the program of laboratory tests were able to reproduce the slow and complex phenomenon of moisture change that occurs in the subgrade from the end of construction until moisture equilibrium develops. This equilibrium probably is achieved only after several drying-wetting-drying cycles, and the traditional CBR method does not consider such a complex approach. The heating action before soaking was the only modification introduced in the CBR test by the author.

REVIEW OF THE LITERATURE

Pioneer work on the effect of heating on soaked strength was done by McDowell (1). Since 1946 McDowell has emphasized the eventual benefits of the so-called dry curing, after having tested several types of soils—coarse- and fine-grained, and from low to medium plasticity. The strength was obtained after dry-curing and subsequent soaking (by capillarity) by (a) the unconfined compression test for the coarse soils and (b) the modified bearing value (MBV, i. e., a test with equipment resembling the CBR) for the fine soils.

The coarser soils ("crushed stone-soil flexible base material mixtures," according to McDowell) were oven-dried at 60 C (140 F) for 8 hours. The finer soils ("minus 40-mesh soils") were submitted to the most severe conditions of drying, which reduced the moisture content practically to zero.

The strengths McDowell obtained for his dried-soaked samples were 2 and 1. 5 times (coarse and fine soils, respectively) the strengths that the standard test indicated. Such a large influence must have been due to the extremely severe cure conditions adopted by McDowell, specially for finer soils. Although the results may not be easily analyzed because of the great variety of parameters, McDowell has given us a general picture of dry-curing effects on soils of different types and of several energies of compaction.

TABLE 1
SOIL CHARACTERISITCS

LL	PL	PI	Percent Passing Sieve No.				Standard AASHO		CBR (55 blows)			Classification		Activity
			10	40	200	0.002 mm	γ_{dmax}	w_{opt}	γ_{dmax}	w_{opt}	Expansion, percent	HRB	Unified	
34	25	9	95.2	79.0	42.0	7.6	1,790 g/cm³	16.5	1,976 g/cm³	11.8	0.3 to 1.0	A-4(1)	SM	1.18

Even if his significant values for each type of soil at a given energy of compaction are rather few—which does not allow a detailed consideration of the heating effect—McDowell's concept, research, and conclusions have been very useful to the highway engineer.

In a more recent paper, Zalazar (2) also considered the dry-curing effect based on his experience in highway construction in Argentina. He investigated with three kinds of laboratory test: (a) CBR of statically compacted samples, (b) Hveem stabilometer, and (c) triaxial compression. His samples were also oven-dried at 60 C (140 F) and, in order to reduce the molding moisture content to pre-established values (a percentage of PL or of w_{opt}), he controlled the curing period. In the CBR test he used immersion as the means of soaking. The CBR values, in accordance with the soil type, increased between 0 and 60 percent, while the stabilometer values decreased in general and the triaxial values increased slightly.

The small number of samples used by Zalazar (two for each soil and each test—one for the standard procedure and another for dry-curing) do not encourage a deeper analysis of pre-heating effect.

EXPERIMENTATION

Soil

In order to prevent detrimental effects such as cracks during drying, the author chose a soil relatively fine-grained but of low plasticity: a purple reddish highly silty sand with clay, a residual material of weathered gneiss, found in abundance in the mountains encircling Rio de Janeiro. This soil was given preference also for its characteristics (see Table 1), which guarantee thorough soaking during the 4 days of standard CBR procedure.

Technique

After having experienced great difficulty in obtaining exact duplication (moisture content and density) of specimens, the author turned to a more feasible procedure, i. e.,

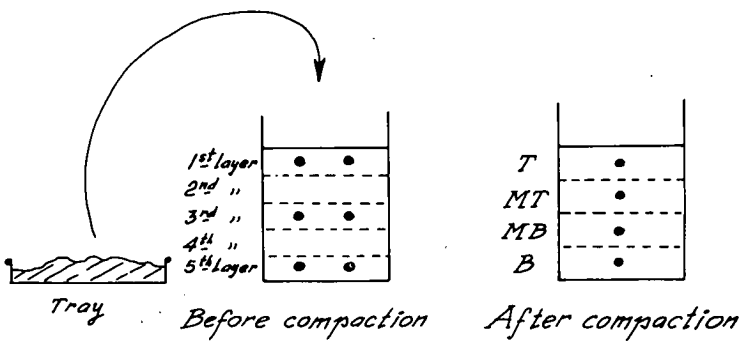

Figure 1. Location of samples for moisture content determination.

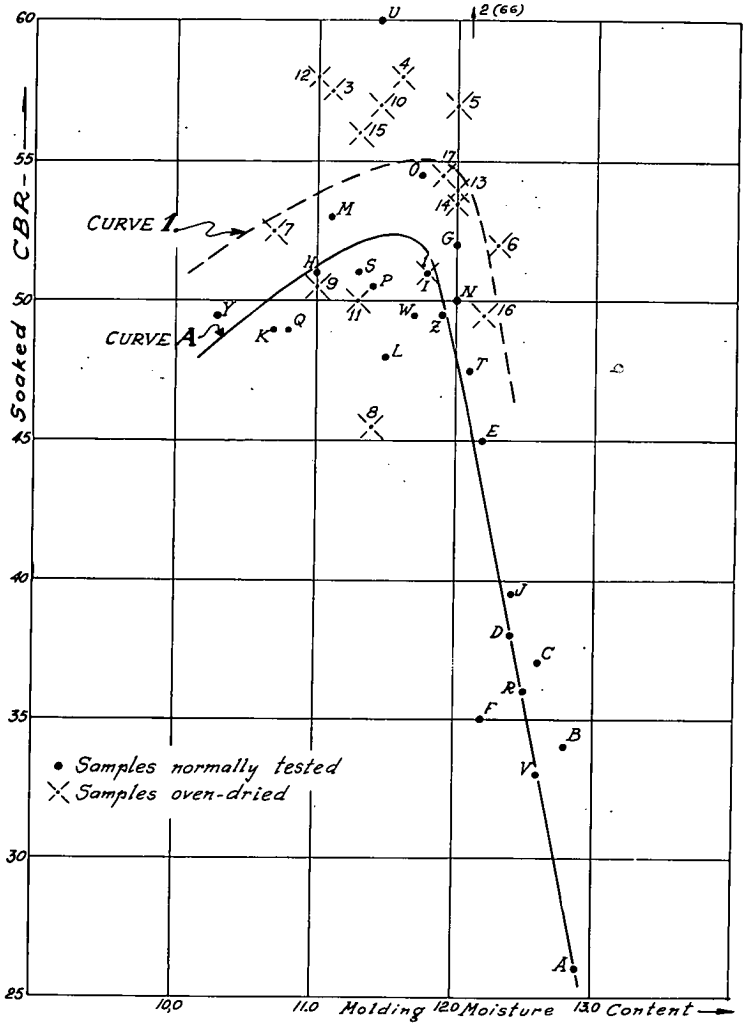

Figure 2. Variation of CBR strength with molding moisture content.

molding a large number of samples so that the desired comparison could be achieved. The step-by-step process was as follows:

1. Compaction of a great number of samples in the CBR mold, in 5 layers, 55 blows per layer, using a 10-lb hammer and stroke of 18 in.;
2. Provision of molding moisture contents from 10 to 13 percent, i. e., around the optimum value;
3. Testing of the compacted specimens in two ways: (a) employing the standard CBR method, i. e., 4 days soaking, measuring expansion subsequent to the penetration test; and (b) 3-hour oven-drying at 40 C (104 F) immediately after compaction and then testing the usual way;
4. Determination of the molding moisture content from samples taken at the exact moment of compaction when the moist soil was spread in the mold—two measurements were made from every first, third, and fifth layer, totaling six per sample (Fig. 1);
5. Determination of the after-soaking moisture content as soon as the penetration test ended, making one measurement for every quarter of each sample, i. e., four measurements per sample (Fig. 1).

The author established the temperature of 40 C as a reasonably representative value of average normal summer conditions to which the upper layers of subgrades of Brazilian roads are subjected.

Preliminary experiments indicated that 3 hours in the oven (at 40 C) was the necessary minimum to affect appreciably the initial moisture content. Moreover, a longer period of drying might have upset the routine of the laboratory where the tests were performed.

The drying of samples while in the molds was carried out in the oven, placing them with their flat surface in a vertical position so that they were exposed equally to heat and consequently dried uniformly and in the shortest possible time.

The process of soaking was performed by means of thorough immersion.

RESULTS AND ANALYSIS

The results of principal importance are shown in Figures 2 and 5. Figure 2 shows, through two curves, the variation of CBR strength with molding moisture content: Curve A shows samples A, B, C, etc., tested according to standard CBR methods (hereafter these samples are referred to as "A-samples"); curve 1 shows samples 1, 2, 3, etc., oven-dried and then tested according to standard CBR methods (referred to as "1-samples").

In spite of the relatively light heating conditions imposed on the samples it remains clear that the preliminary drying increases the bearing support of the soil. We can observe also that this increment tends to be smaller (around 6 percent) on the dry side and larger (around 15 percent or more) on the wet side of optimum moisture content.

It is a well-known and accepted fact that drying increases the effective pressure, even in nonsaturated compacted soil. Lambe (3) explains this phenomenon in terms of

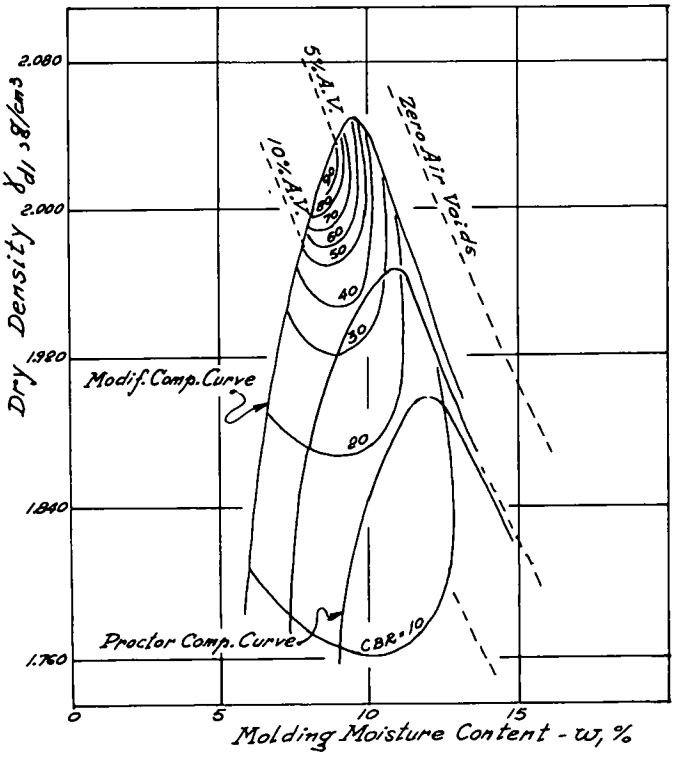

Figure 3. Variation of soaked CBR with the energy of compaction—after Kleyn (6), in Wooltorton (9).

increase of water deficiency involving, as a necessary circumstance, the negative increase of pore pressure. Structure of soil permitting, the drying process is accompanied by shrinkage and, consequently, increase in density.

The experience of Jervis and Eustis (4), Seed, Mitchell and Chan (5), and Kleyn (6) proves that—supercompaction excluded—the strength (after soaking) increases with the growth of energy of compaction when dealing with a given molding moisture content (Fig. 3). Therefore, the increase in strength caused by pre-heating corresponds to an increase in the original energy of compaction E_1 (55 blows, etc.) to E_2,

$$E_2 = E_1 + \Delta E \qquad (1)$$

where ΔE is the "heating effect" measured in terms of energy of compaction or compacting effort.

Figure 4 shows a schematic representation of the probable mechanism of the drying and wetting process for a nonsaturated soil, based on British experience at the Road Research Laboratory (7). A compacted sample of high degree of saturation (sample X, Fig. 4) tends, when submitted to drying, to follow a trajectory that approximately coincides with its corresponding line of constant degree of saturation (at least when the drying is of little intensity). A sample of low degree of saturation (sample Y, Fig. 4), in contrast, loses water and simultaneously lessens its degree of saturation; in other words, it shrinks less or may not shrink at all. On the other hand, when wetting, the curves for drying-wetting are not so steep, denoting that the absorbed volume of water is much bigger than the growth of the voids volume.

Taking into consideration both Figures 3 and 4, we must conclude that the representative points for preliminary drying have undergone a dislocation to a "new" curve of compaction (of energy $E_1 + \Delta E$), displaced upwards and to the left of the orginal curve (of energy E_1). Consequently, the soaked CBR values of the "new" curve are larger

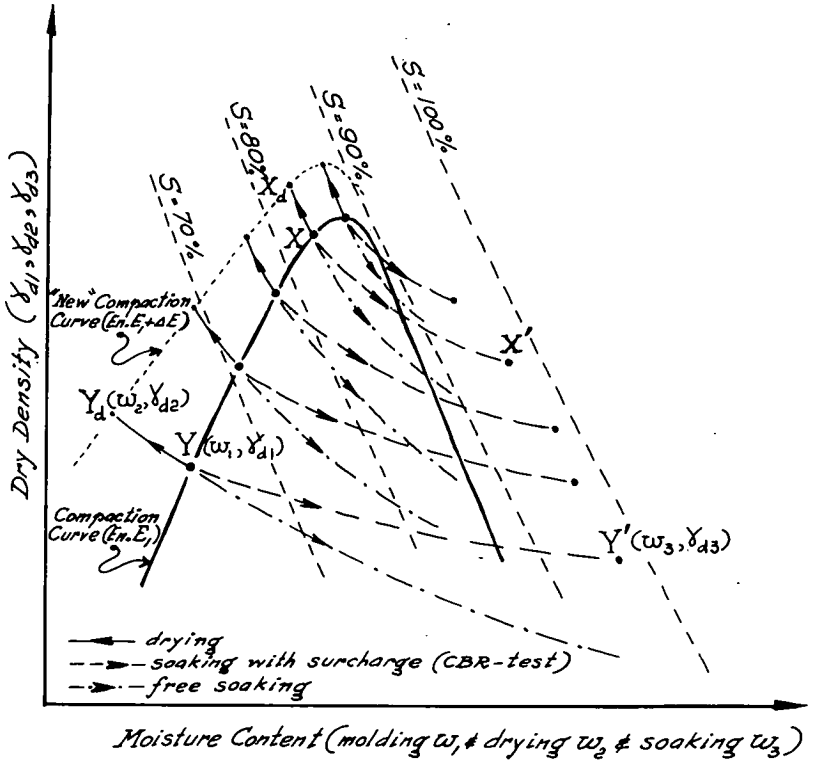

Figure 4. Schematic representation of drying and wetting mechanism of nonsaturated soil.

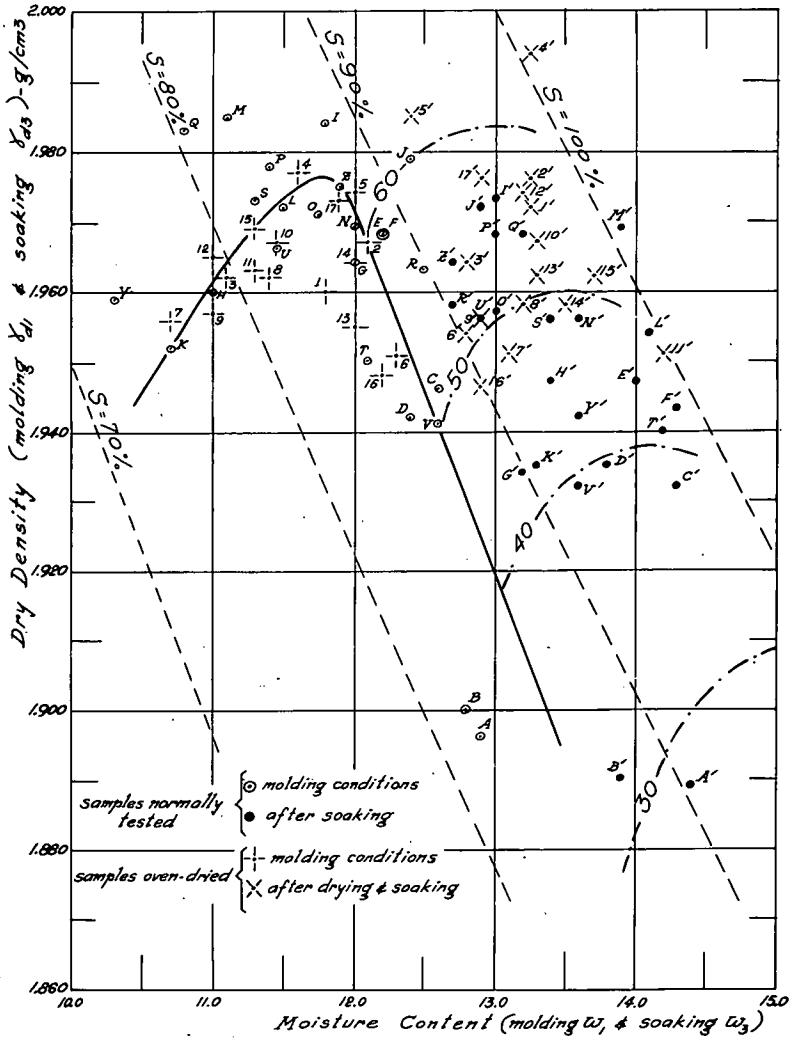

Figure 5. Conditions before and after soaking for normally tested samples and oven-dried samples—iso-CBR curves related to conditions after soaking.

than those from curve E_1. It is worth noting that the dislocation of the points mentioned varies in accordance with their initial degree of saturation. The increase ΔE of energy is not constant along the original curve—it varies with the original degree of saturation of each point. In other words, the "new" curve of compaction does not correspond exactly to a normal curve of constant energy.

If the following symbols are used:

	Molding Conditions	After Drying	After Soaking
Dry Density	γ_{d_1}	γ_{d_2}	γ_{d_3}
Moisture Content	w_1	w_2	w_3

Figure 5 shows (a) the compaction curve obtained for all samples investigated, i. e., the correlation curve of the dry density against the molding moisture content w_1, for A-samples and for 1-samples; (b) the location of points (γ_{d_3}, w_3) representing the conditions after the 4-day soaking, for A-samples and 1-samples (note that the moisture axis is valid for w_1 and w_3); and (c) iso-CBR curves related to the conditions after soaking (γ_{d_3}, w_3).

The dry density γ_{d_3} was calculated differently for A-samples and for 1-samples. For A-samples, γ_{d_3} was determined from the expansion E_S:

$$\gamma_{d_3} = \frac{\gamma_{d_1}}{1 + E_S} \tag{2}$$

For 1-samples, the calculation using the formula

$$\gamma_{d_3} = \frac{\gamma_{d_2}}{1 + E_S} \tag{3}$$

would require determination of the density γ_{d_2} resulting from drying and shrinkage. However, because the direct determination of γ_{d_2} was quite difficult due to the test conditions, the author decided to calculate γ_{d_2} from the consideration of tri-dimensional shrinkage:

$$\gamma_{d_2} = \frac{\gamma_{d_1} \cdot (1 + e_1)}{1 + e_1 - \frac{G_S \cdot \gamma_w}{w_d} \cdot \Delta V_v} \tag{4}$$

where e_1 is the initial (molding) void ratio, G_S is the specific gravity of solids, W_d is is the dry weight of the soil mass, γ_w is the unit weight of water, and ΔV_v is the change in volume of voids by shrinkage. Taking into account what has been said before about the probable mechanism of the drying process of nonsaturated soil, the author advanced the following hypotheses:

1. That the volume reduction (shrinkage by heating) is uniform throughout the sample. Such a hypothesis is acceptable if the drying period is compatible with the sample dimensions and type of soil tested. Only in the initial moment is there a tendency for the surface layers to dry faster than the center, because they are in more direct contact with the hot surroundings; as time goes by the moisture content tends toward homogeneity throughout the sample, since the moisture of the center flows toward the surface layers. Hallaire (8), in describing his experiments, says "desiccation starts throughout the sample as soon as the surface is subjected to evaporation." It is important to observe, moreover, that when the author opened at least two CBR samples (No. 14 and No. 50) immediately after oven-drying, he obtained the results given in Table 2, which indicate that the central part had dried and that there was reasonable homogeneity. However, in view of the small difference between W_2 and W_1 of these two samples, it is possible that the observed results could be a consequence of drying during the molding operation or an error in moisture determination. To clarify this point the author performed a different type of moisture determination (before compaction, from the tray; immediately after compaction, by quartering the CBR samples) on three samples (24, 29, and 56-A in Table 2). The moisture content of sample 56-A was smaller after the compaction than before it, which seems logical, although samples 24 and 29 showed just the opposite, which was difficult to explain.

TABLE 2

CBR TEST RESULTS

Samples No.	Time in Oven at 40 C (hours)	Molding Moisture Content Before Compaction[a] (w_1%)				Molding Moisture Content After Compaction[b] (w_1%)					Moisture Content After Drying (w_2%)					Loss of Water[c] (cm^3)
		First Layer	Second Layer	Third Layer	Average Value	T	MT	MB	B	Average Value	T	MT	MB	B	Average Value	ΔV_w
14	2	12.40 12.10	12.70 12.60	12.30 12.10	12.35 –	–	–	–	–	–	11.60	11.90	11.70	11.80	11.75	28
50	3	11.30 11.35	11.50 11.45	11.45 11.70	11.45	–	–	–	–	–	10.90	10.80	10.20	10.50	10.60	38
24	0	12.25 12.45	12.05 12.25	12.50 12.35	12.30	12.60	12.60	12.55	12.40	12.55	–	–	–	–	–	–
29	0	12.20 11.80	12.00 12.20	12.10 12.10	12.10	12.00	12.50	12.30	12.30	12.30	–	–	–	–	–	–
56-A	0	11.60 11.15	11.70 11.25	11.75 11.35	11.45	10.95	10.60	10.85	10.90	10.80	–	–	–	–	–	–

[a] Determined from the tray.
[b] Determined by quartering the sample.
[c] Calculated from $\Delta V_w = \frac{W_s}{\gamma_w} \cdot (W_1 - W_2)$.

2. That the volume reduction (shrinkage by heating) occurs with permanency of the initial degree of saturation S_1 (as molded). Such a hypothesis is valid exclusively for samples of high S_1 (above 70 percent, perhaps)—in which it is possible to admit that water is mainly in the void space around the contact points—and only under non-severe conditions of drying. This hypothesis implies that the relationship between the volume of water lost by drying and the corresponding change of void volume is equal to the initial degree of saturation, i. e.:

$$\frac{\Delta V_W}{\Delta V_V} = S_1 \tag{5}$$

and therefore, the change of voids is

$$\Delta V_V = \frac{\Delta V_W}{S_1} \tag{6}$$

or in other words, the reduction of voids is greater than the loss of water.

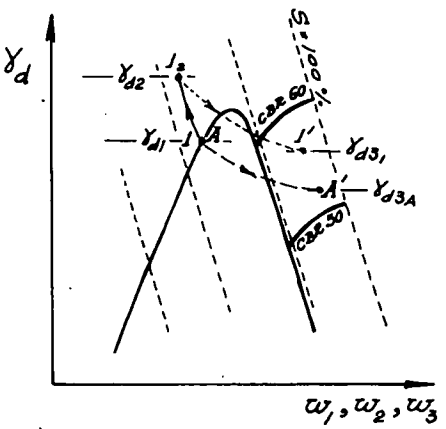

Figure 6. Schematic representation of heating effect.

Then, by weighing the samples before and after drying, ΔV_W was obtained, and it was possible to calculate ΔV_V (Eq. 6), γ_{d_2} (Eq. 4), and finally γ_{d_3} (Eq. 3).

It is worthwhile to consider that Eq. 3, when applied to the 1-samples is not entirely correct, since during the soaking the expansion of these samples is tridimensional in the initial phase. But the error is negligible and does not seriously affect the density.

Figure 6, which is a simplification of Figure 5, shows that, after soaking, the 1-sample tends toward a position in the graph corresponding to a higher CBR value. Therefore, Figure 5 explains why the 1-samples have CBR strengths higher than the A-samples. Furthermore, it allows moderating the results of Figure 2, clearing up whether the eventual scattering of points in this figure is due to intrinsic failure of the CBR test.

CONCLUSIONS

There is no doubt about the positive effect of preliminary heating ("dry curing") on soil strength. Since 1946, McDowell has called the attention of engineers to this matter. However, dry curing has not received the attention deserved and little research has been done on the subject.

It is evident that the problem of natural heating concerns mainly the countries having tropical climates. But the eventual application of moderate artificial heating is of interest to all soil engineers, from tropical countries (in general, less developed) and from temperate and cold countries (more developed) as well.

The present paper pertains to a given type of soil and to restricted conditions of heating (temperature and time of exposure). It seems to the author that it would be important to conduct a broader investigation with other soils and conditions of heating, searching for the benefits from such practice and for the exact limits of technical and economical feasibility.

It is reasonable to assume that sandy and gravelly soils do not show any influence from moderate heating. Otherwise, well-graded soils, with fines of medium to low plasticity, are probably best for preliminary heating to improve bearing support.

ACKNOWLEDGMENTS

The present investigation was performed under the auspices of the Conselho Nacional de Pesquisas (Technological Section) of Brazil, at the Laboratory of the Escola Nacional de Engenharia da Universidade do Brasil, in the years 1955-1956. The author is indebted to Professors A. J. da Costa Nunes and R. A. Pizarro, who made available the necessary facilities, and to his colleagues from the Highway Department of Guanabara State, J. Medina, N. N. Pereira, and F. Bolivar L. Carneiro, for their encouragement. Professor J. Medina reviewed the paper and presented helpful suggestions. The efficient collaboration of technicians A. B. Barcellos and J. F. Costa and typist O. Maciel deserves the sincere thanks of the author. Finally, the author wishes to acknowledge the support of the Instituto de Pesquisas Rodoviárias, associated with Conselho Nacional de Pesquisas, for aiding in preparation of the final manuscript.

REFERENCES

1. McDowell, C. Progress Report on Development and Use of Strength Tests for Subgrade Soils and Flexible Base Materials. HRB Proc., Vol. 26, p. 484-511, 1946.
2. Zalazar, L. M. Efecto del Curado a Seco en Suelos Y Estruturas no Tratadas de Pavimentos Flexibles. Proc. Second Panamerican Conf. on Soil Mech. and Found. Eng., Vol. 2, paper IV/3, Brazil, 1963.
3. Lambe, T. W. Residual Pore Pressure in Compacted Clay. Proc. Fourth ICOSOMEF, Vol. 1, p. 207-211, Paris, 1961.
4. Jervis, W. H., and Eustis, J. B. Accepted Procedure for the CBR Test. Symposium on Development of CBR-Flexible Pavement Design Method for Airfields. Trans. ASCE, Vol. 115, 1950.
5. Seed, H. B., Mitchell, J. K., and Chan, C. K. The Strength of Compacted Cohesive Soils. ASCE Research Conf. on Shear Strength of Cohesive Soils, Denver, 1960.
6. Kleyn, S. A. Methods of Soil Testing as Applied to the Design of Road Foundations Proc. South Africa S. C. E., Vol. 44, 1946.
7. Wooltorton, F. L. D. The Scientific Basis of Road Design. London, 1954, p. 134.
8. Hallaire, M. Soil Water Movement in the Film and Vapor Phase Under the Influence of Evapotranspiration. HRB Spec. Rept. 40, p. 88-105, 1958.
9. Wooltorton, F. L. D. Moisture Content and the CBR Method of Design. HRB Spec. Rept. 40, p. 268-297, 1958.

Expansion of Soils Containing Sodium Sulfate Caused by Drop in Ambient Temperatures

HAROLD D. BLASER, Federal Housing Administration, Sacramento, California, and OSCAR J. SCHERER, Nevada Testing Laboratory, Las Vegas, Nevada

•AS EARLY AS 1960 it was recognized that soils containing a high concentration of water-soluble sulfates exhibit an expansive phenomenon resembling that of expansive clays and frost heave. This condition was observed particularly in alluvial deposits in the flat arid areas of southern Nevada and southeastern California. The expansion of these soils occurs during ambient temperature drops from daytime temperatures of approximately 90 F to below 40 F at night. This expansion caused structural damage to lightweight single-story homes in particular and to interior concrete floors, exterior flat work, and asphalt driveways. This phenomenon, herein referred to as "salt heave," predominantly caused vertical expansion without many of the inherent swelling and shrinking characteristics of common clay soil.

The writers began as early as 1962 to isolate individual parameters of this phenomenon to obtain control of the condition. Only by early recognition of the presence of water-soluble sulfate salts in the soil was it possible to control or eliminate heaving and resultant structural damage.

The final test procedure described herein provides a method to evaluate soils containing sodium sulfate salts.

FIELD OBSERVATIONS AND EVALUATION

The swelling phenomenon of some surface soils in arid areas is due primarily to the characteristics of sodium sulfates and possibly other water-soluble salts.

Not all soils, however, that contain sodium sulfates exhibit expansive characteristics. It was noted by the writers that soils containing as little as 0.5 percent sodium sulfates may exhibit expansive qualities in greater proportion than soils containing up to 10 percent or more. Some soils containing high percentages of sodium sulfates show very little expansion.

Two major behavioral characteristics of sodium sulfate soils were noted by the writers:

1. Upon evaporation in warm weather, the moisture in the soils containing sodium sulfate deposits the salt on the ground surface; and
2. When subjected to low ambient temperatures, the moisture in the soils containing sodium sulfate forms crystals and increases the soil volume, causing vertical expansion. This expansion sometimes is incorrectly identified as expanding clay rather than salt heave.

Numerous attempts were made in the laboratory to determine the magnitude of the expansion taking place. Progress in the program did not occur until the natural conditions that cause the phenomenon were recognized and more closely studied. The final procedures were based on the condition that soils for laboratory testing should have a similar moisture content, density, sulfate content, etc., as in situ soils have at the time the heaving or expansion takes place. Prolonged testing indicated that, within a 30-day testing period, measured expansion would fluctuate with day and night variation of laboratory temperatures. As a result, a closer study of natural temperatures and soil moisture conditions was made.

It is believed that the following two characteristics of sodium sulfate cause expansion of the soil:

1. If Na_2SO_4 in solution is cooled below a temperature of 90 F, it tends to bind H_2O. One Na_2SO_4 molecule can bind up to 10 H_2O molecules, building the solid phase $Na_2SO_4 \cdot 10\ H_2O$, also known as Glauber's salt. When the temperature rises during periods of higher humidity, the sodium sulfate solid phase apparently dissolves in its own water of hydration and moves toward the surface in this liquid phase by capillary action.

2. Above 90 F, great quantities of Na_2SO_4 salts are in solution in the moisture of the natural soil. At a temperature of 90 F as much as 52 grams of Na_2SO_4 is soluble in 100 grams of water. As the temperature decreases, the solubility of sodium sulfate decreases rapidly and hydration increases. During this process, the salt crystals expand against the soil structure.

Although the principal laboratory and field test work reported herein pertains to the Glenwood Housing Tract, other similar problem soils were investigated and documented. This phenomenon, however, is found in most soils having certain common characteristics of classification, grain-size distribution, and sodium sulfate content.

Houses damaged by salt heave usually exhibited the following defects:

1. Interior floors, nominally 4 in. thick, cracked and raised in the middle of rooms and under non-load-bearing partitions;
2. Exterior concrete flat work, nominally 4 in. thick, cracked and raised as much as 4 in. or more;
3. Carport roof beams, supported on concrete flat work, raised the roof rafters and ceiling joists above the wall top plate;
4. Exterior walls of lightweight stucco frame construction were subject to damage, while block walls were not generally affected;
5. Six-in. concrete block fences were subject to damage when footings were placed less than 12 in. below finished grade.

From these observations, it was evident that salt heave affected relatively light structures and floors with less than 45-lb/sq ft dead loads.

In the Glenwood Tract, a salt heave or swell was predominantly parallel to and directly under the roof eaves or adjacent to lawns and planting areas.

The salt heave damage, in nearly every instance occurred in the late fall and early spring, and always during ambient temperature drops from daytime temperatures of 90 F to below 40 F at night.

This salt heave was generally confined to soils containing 0.5 percent sodium sulfate and in situ soil densities of 80 to 90 lb/cu ft. Although surface and near-surface sodium sulfate concentrations in pockets of up to 40 percent have been encountered in many areas, they generally do not exceed 1 to 2 percent over wide areas.

EARLY TREATMENT

An early method to counteract the effects of salt heave was accomplished by mechanically blending expanding soils with open-grained pit-run gravels in order to increase the void ratio, thereby permitting expansion and minimizing vertical displacement. Other methods of early control included chemical soil treatment by additives to stabilize the saline soils by chemical reaction converting hydrating salts to insoluble non-hydrating salts.

Calcium chloride ($CaCl_2$ as a stabilizing additive) was first used in laboratory research and subsequently in the field at three housing tracts. This produced a satisfactory restraining result when low sodium sulfate concentrations in soils were encountered. The additive was introduced to the mixing water during grading operations.

Phosphoric acid (H_3PO_4) was subsequently used, producing similar results. This procedure was used with good results on several projects where sodium sulfate contents were in the range of up to approximately 1.5 percent and where uniform soil classifications were ML and OL. The additive was also introduced to the mixing water during grading operations.

INITIAL LABORATORY TEST PROCEDURES AND FIELD DETERMINATIONS

Based on the understanding and knowledge of the salt heave phenomenon, laboratory work was initiated to attempt to duplicate natural field conditions. A special test chamber was developed where temperature variations could be induced and controlled between 35 and 120 F (Fig. 1).

The initial testing program, using the temperature-controlled chamber, was conducted with a 2½-in. diameter ring and a 2-in. diameter reaction plate (Fig. 2). Results were erratic because sample-to-ring friction influenced expansion. Using the same soils, it was determined that the expansion in the 2½-in. ring reached a maximum of 11.4 percent whereas in the subsequently adopted ring molds the same soil produced a 17.0 percent expansion (Fig. 3).

The field investigation included two studies of soil conditions. These tests were initiated on the basis of a preliminary outdoor soil temperature measurement during an ambient temperature of 32 F. The results indicated a soil temperature increase to 65 F at a depth of 18 in.

Two field investigations were conducted to obtain information necessary to evaluate the local salt heave problem; they consisted of the following:

1. A study, conducted inside a house, of the effects of simulated ambient temperature changes on in situ soils to depths of 24 in.; and
2. A study, conducted outdoors, of soluble sodium sulfate and soil moisture content vs depth.

The test arrangement for the temperature study included the installation of long-stem dial temperature gages to various depths and periodic readings for a term of 9 days during the heating cycle and various readings for a period of 15 days during the cooling cycle. The temperature measurements were conducted by circulating air at 110 F for a period of 7 days and subsequently cooled air at 50 to 55 F for 15 days. This test was carried out in an unoccupied house with a wood flooring system. The results of the tests are shown in Figure 4, which indicates the initial temperature rise and subsequent drop to approximately 61 F at a depth of 10 to 15 in., decreasing to approximately 51 F near the surface.

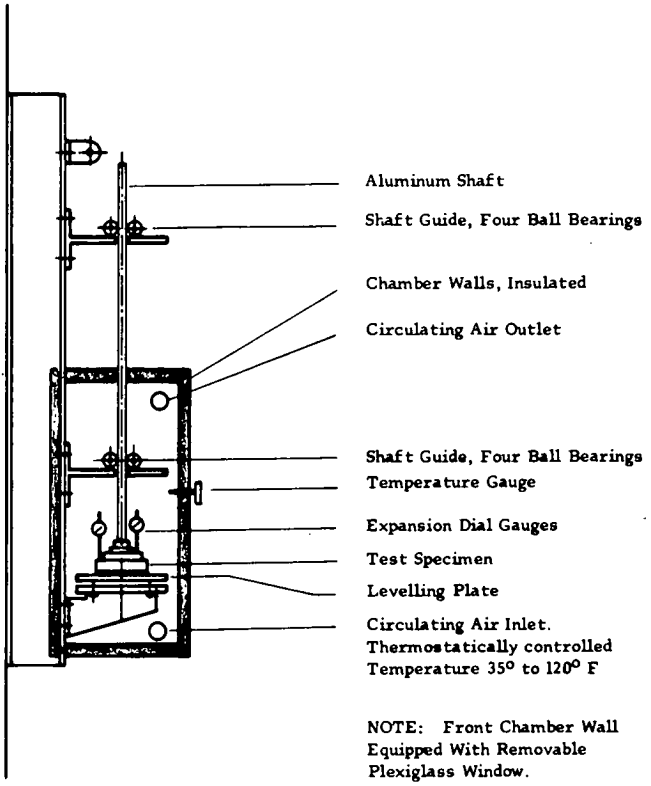

Figure 1. Test chamber arrangement.

The soluble sodium sulfate and soil moisture determinations were made to assist in the evaluation of the evidently important relation between sodium sulfate and moisture, and its effect on foundation depths. Data in Figure 5 indicate that the high sodium sulfate content decreases with depth and diminishes to approximately 0.4 percent below 5ft. The moisture increases to 10 percent at 2.5 ft and up to approximately 20 percent at 5 ft.

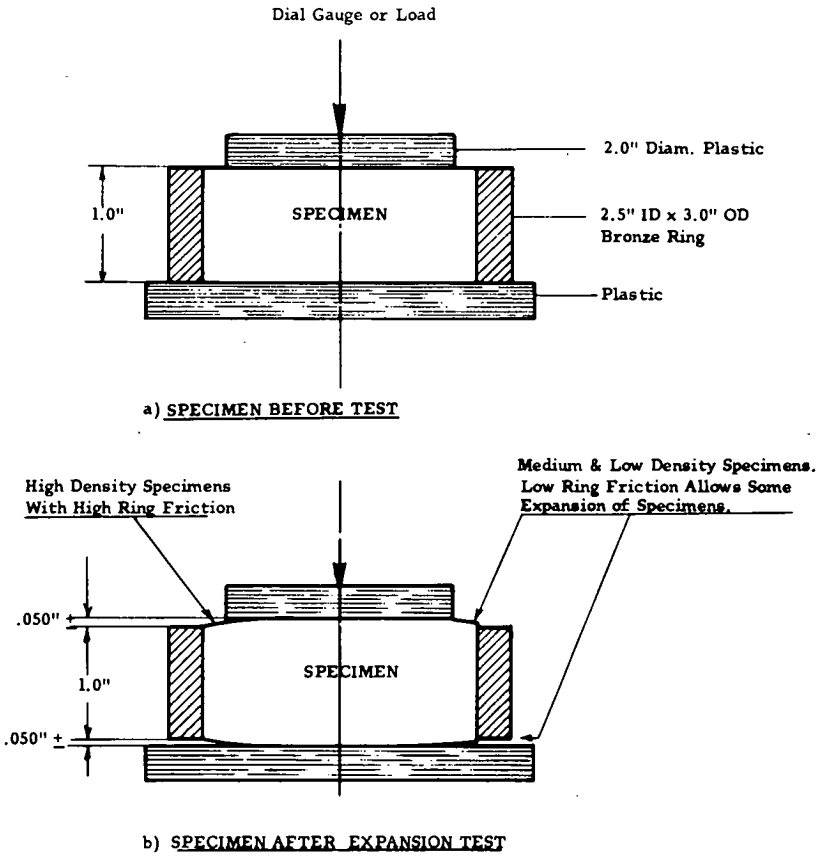

Figure 2. Test specimen arrangement, initial program.

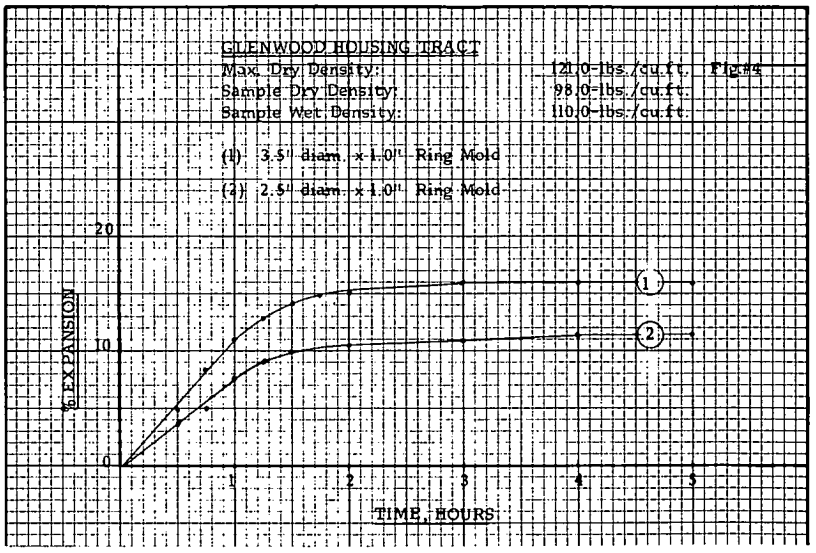

Figure 3. Comparison of final procedure (1) and initial procedure (2) results.

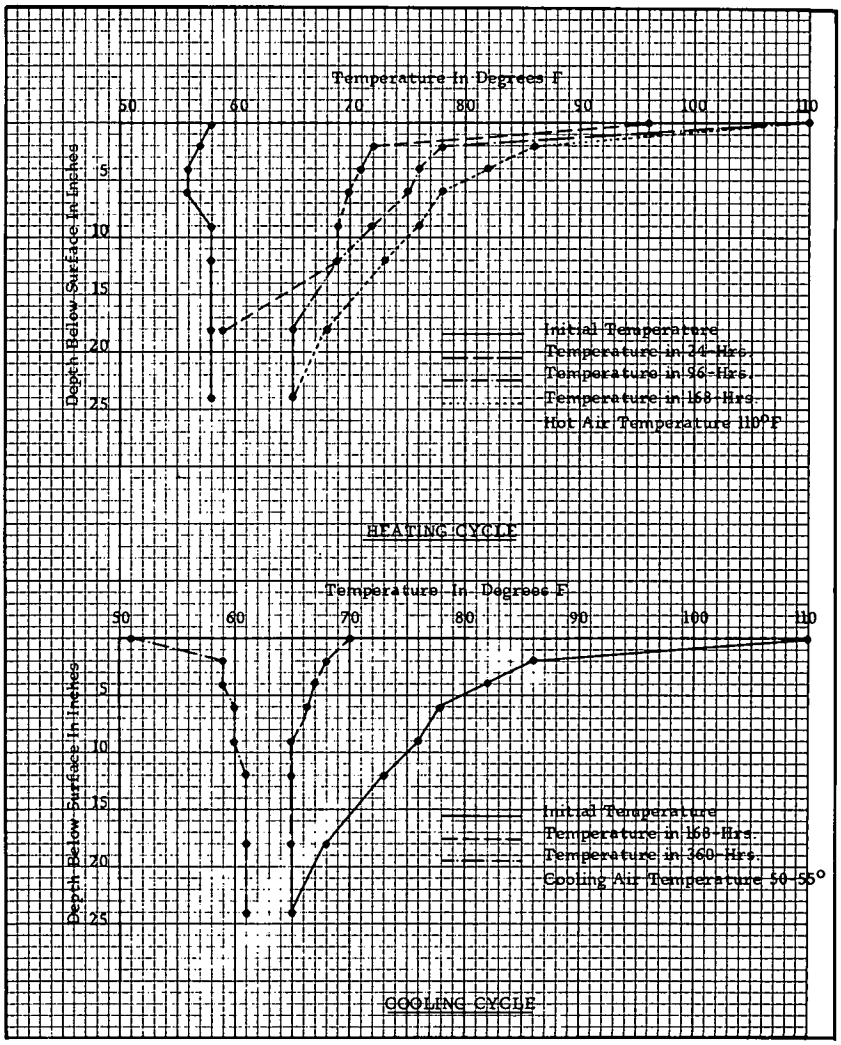

Figure 4. Temperature penetration into foundation soils due to artificial heat and cold cycles.

FINAL LABORATORY TESTING

Consistent test results suitable for correlations could not be obtained with various soils having different characteristics, grain size, Atterberg limits, and sulfate content, so all further testing was performed with a blended soil from the Glenwood Tract. This blending included soils from surface to 24 in. in depth and is hereafter identified as sample No. 3 (Figs. 6 and 7).

The final research was based on the following known factors affecting salt heave:

1. Soils that contain over 0.2 percent Na_2SO_4 in solution and over 15 percent of minus 0.005-mm fractions are subject to salt heave in varying degrees;
2. A change in ambient temperatures to below approximately 55 F causes crystallization of Na_2SO_4 solutions, and this crystallization in turn causes volume change or salt heave;
3. The volume change increases with an increase of the Na_2SO_4 content and an increase in minus 0.005-mm fractions; and

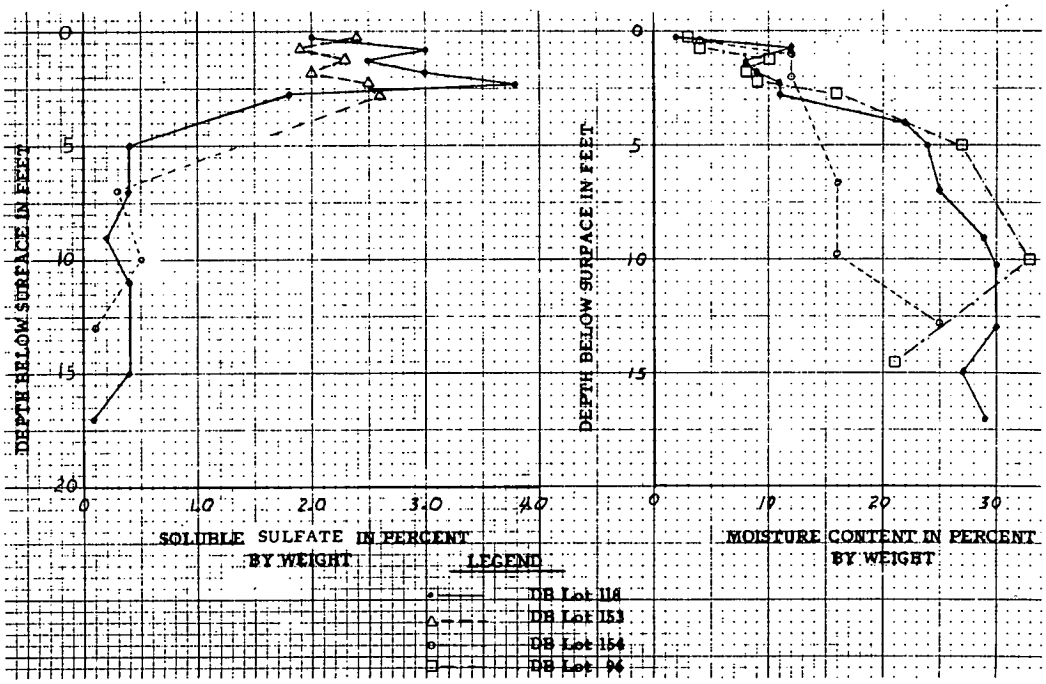

Figure 5. Soluble sulfate and moisture vs depth.

4. Sufficient free moisture must be present in the soil to sustain crystallization of the sodium sulfate.

The physical and chemical characteristics of sample No. 3 were as follows:

Soil classification:	Light brown silty clay, some fine to coarse sand CL.	
Grain-size analysis (hydrometer):	25 percent minus 5-micron fractions (Fig. 7)	
Atterberg limits and indices:		
Liquid limit	28.8	(Fig. 8)
Plastic limit	14.8	(Fig. 8)
Plasticity index	14.0	(Fig. 8)
Specific gravity	2.68	
Maximum dry density (ASTM Designation D 1557, Method C)	121.0 lb/cu ft	(Fig. 7)
Maximum wet density	135.0 lb/cu ft	(Fig. 7)
Optimum moisture	12.0 percent	(Fig. 7)
Chemical analysis:		
Total soluble salts	3.8 percent	

The minus 5-micron soils fractions were composed about equally of non-clay and clay minerals. The principal non-clay minerals were calcite, dolomite, quartz, and various hydration forms of gypsum, hemihydrate, and anhydrite. The clay minerals were mica, montmorillonite chlorite, and minor trace amounts of kaolinite, illite, and sepiolite. These determinations were from X-ray diffraction analysis.

Atterberg limits determinations, made in 1965 with various Glenwood soils (Fig. 8), indicated plasticity indices of 9.0 minimum and 18.8 maximum.

All tests referred to above were performed under dead load surcharge conditions varying between 0 and 75 lb/sq ft. Maximum expansion for sample No. 3, shown in

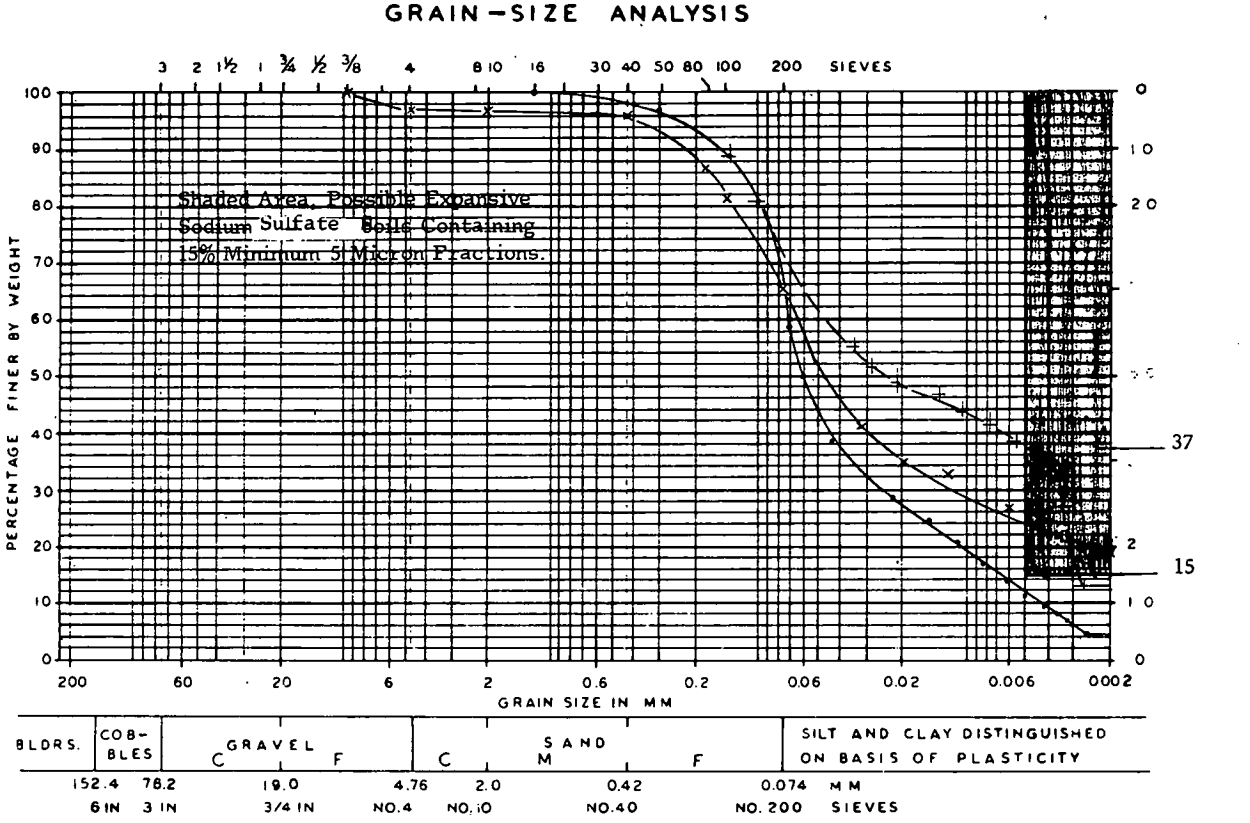

TEST PIT/BORING NO.		DESCRIPTION AND CLASSIFICATION		
#1 .	Desert Hills	0.0 to 0.6-ft. depth;	Natural Moisture = 9.0%;	Na_2SO_4 = 0.6%
#2 +	Glenwood Lot 153	1.5 to 2.0-ft. depth;	Natural Moisture = 16.0%;	Na_2SO_4 = 3.2%
#3 x	Glenwood - Blended Sample;	0.0 to 2.0-ft. depth;	Natural Moisture = 14.0%;	Na_2SO_4 = 3.8%

Figure 6. Description of soil samples 1, 2, and 3.

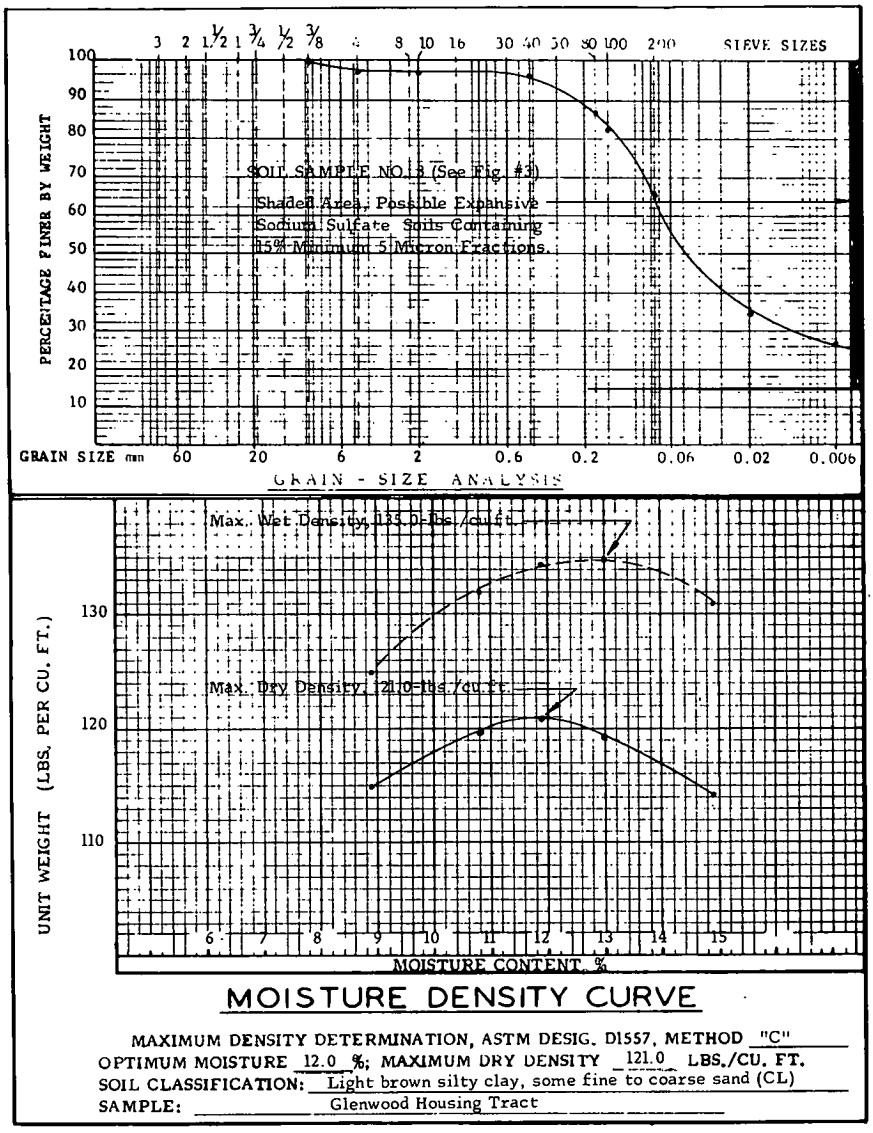

Figure 7. Analysis of blended soil sample No. 3.

Figure 9, was obtained with a dead load of 5.0 lb/sq ft. The total volume change did not materially change although the specimen height varied from 0.25 to 1.0 in.

Although various soil densities were used for the research work, the data given here are based on 98 lb/cu ft dry density or approximately 81 percent of maximum dry density.

TEST PROCEDURES

Soils for ring molds 0.25 to 1.0 in. high were weighed for each ring mold volume to produce the 98 lb/cu ft dry density and were compacted to substantially uniform conditions. A special mold compaction unit that produced uniform soil densities was developed and subsequently used. Soils were compacted to 81 percent of maximum dry density in 0.25, 0.50, 0.75 and 1.0-in. high rings 3½ in. in diameter. The weighed soil

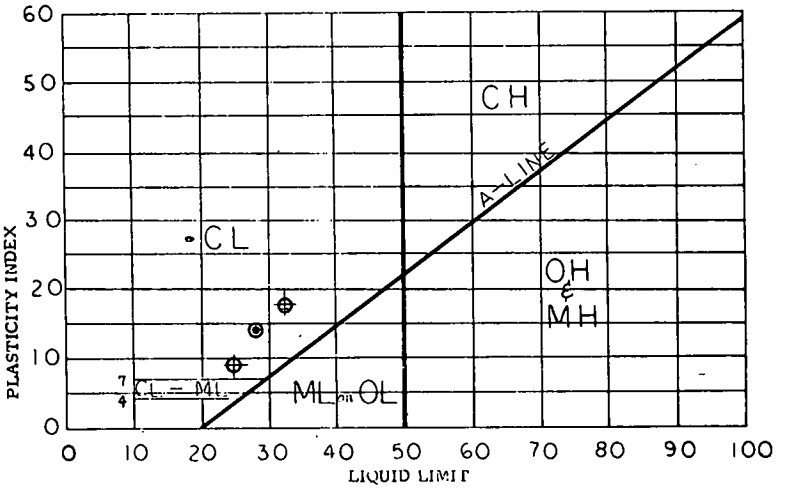

GLENWOOD HOUSING TRACT

Soil Classification: Light brown silty clay; some fine to coarse sand

Maximum Density Determination, ASTM Desig. D 1557, Method "C"

Maximum Dry Density:	121.0-lbs./cu.ft.
Optimum Moisture:	12.0%

◎ Atterberg Limits Determination

Liquid Limit:	28.8
Plastic Limit:	14.8
Plasticity Index:	14

Φ 1965 Determinations - Maximun & Minimum

Figure 8. Plasticity chart, unified soil classification system.

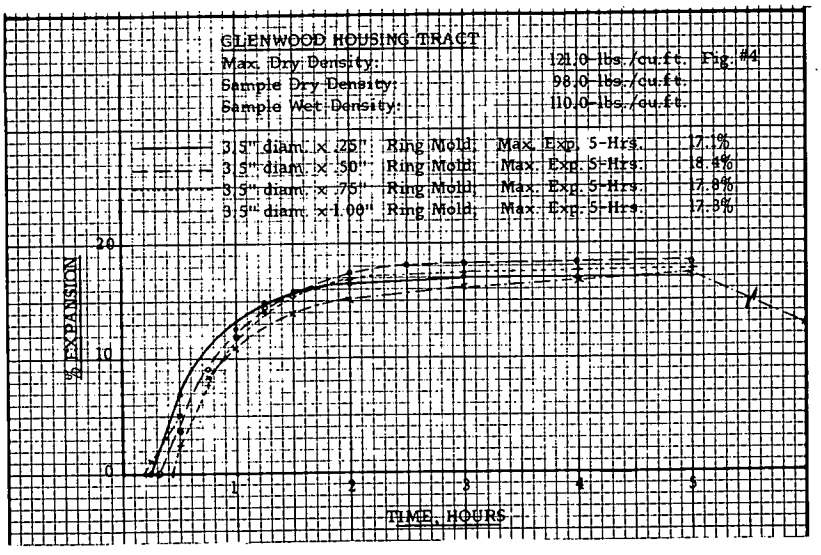

Figure 9. Results of final laboratory tests, sample No. 3.

sample was placed in layers and compacted manually with a ½-in. diameter brass rod or in a special apparatus with a static hydraulic pressure.

The sample was then placed in the test chamber (Fig. 1) at laboratory temperatures of 75 F. A plate (¼ x 2-in. diameter) was placed in the center of the test specimen.

When tests were conducted without surcharge loads, the dial gage stem was placed directly on the 2-in. diameter plate. When tests were conducted with surcharge loads from 0 to 30 lb/sq ft, weights were placed directly on the 2-in. diameter plate and the dial gage stem on either the plate or surcharge weight. The shaft with various additional weights was placed directly on the 2-in. plate to obtain surcharge loads from 30 to 75 lb/sq ft.

The sample remained in the test chamber for a period of 1 hour at laboratory temperature to allow for possible expansion due to overcompaction. If no measurable change occurred within this time period, as determined by the dial gage, the chamber was closed and the cooling cycle started.

Within 30 minutes (or as soon as the chamber temperature reached 54 to 55 F) the volume change was initiated and was continued to nearly peak expansion, which was reached within approximately 2 hours. Figure 9 shows the expansion in percent of the

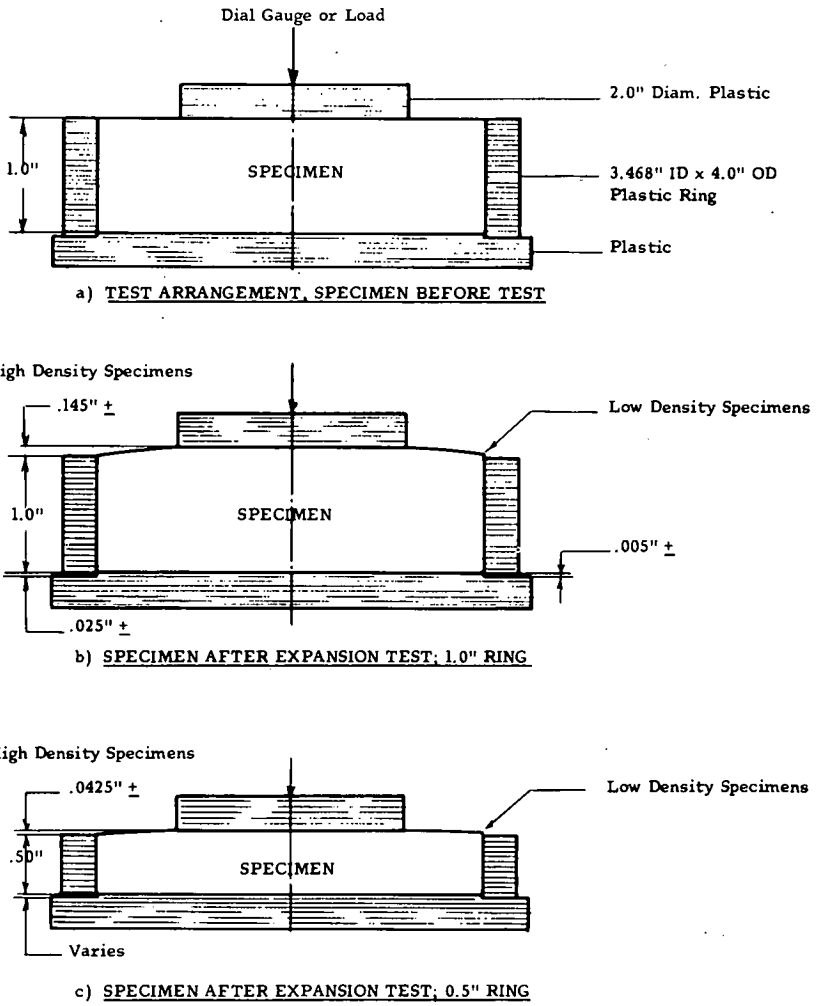

Figure 10. Test specimen arrangement, final laboratory procedure.

initial sample height. No appreciable volume change occurred after the initial 2-hour expansion period.

TEST RESULTS

Figure 2 shows the specimen reaction to the lowered temperature in the 2.5-in. ID ring. High vs lower soil density is illustrated by the final specimen height at the ring, a height which results from variable friction values.

Figure 10 illustrates similar specimen expansion at the ring, but due to the greater distance between pressure plate and ring, friction does not affect specimen expansion. This observation is based on the test data in Figure 9. No appreciable discrepancies in total expansion were noted, provided that the height of the sample and the distance between pressure plate and ring approximated a 1-to-1 ratio.

All specimens exhibited expansion by forming an arc on top and occasionally an arc on the bottom. Because it is not attached to the bottom plate, the ring has free vertical movement also.

During the expansion test no sodium sulfate, such as is deposited by evaporation, is visible on the specimen surface except small sodium sulfate crystals that form in the cooling process.

CONCLUSIONS

1. The salt heave phenomenon as it occurs in the southern Nevada area is due to temperature variations, which usually occur in the fall, late winter, or early spring.
2. Soils that contain over 0.2 percent of Na_2SO_4 in solution and 15 percent or more of minus 0.005-mm fractions should always be investigated for salt heave if ambient daily temperature variations range from 35 to 100 F and if ample soil moisture is available.
3. Although proven successful to date, calcium chloride or phosphoric acid treatment of soils that contain soluble sulfate do not completely eliminate the possibility that sulfates in the underlying soil may rise to the surface, ultimately creating the salt heave problem again. This condition would, however, be limited to areas exposed to hot climatic conditions, but could also be encountered in areas covered by concrete floors or asphalt pavement where adequate moisture is available.
4. Blending sulfate-laden soils with open-grained material would be a solution. As an alternative, finished structural pads should be built with imported salt-free open-grained fill material in order to eliminate cold temperature penetration into lower sulfate-laden soil. It should be noted that the streets in the Glenwood Housing Tract were not subject to damage. The principal reason for this is the fact that the high-sulfate-content soils were removed and replaced with the usually open-grained Type I or II base course material for a total thickness of 12 in. or more. The addition of $2\frac{1}{2}$-in. asphalt pavement placed the soils subject to salt heave beyond the influence of changing ambient temperatures and moisture source.
5. This phenomenon of expansion due to sulfate salts can occur separately or concurrently with other expansive characteristics of clay soils.
6. The expansion, which is due to high sulfate soils and which causes damage to lightweight structures and principally to concrete slabs, can be reduced with adequate surcharge loading. Laboratory testing showed swell reductions from 17 percent to 2 percent under 75 lb/sq ft loading.

Influence of Heat Treatment On the Pulverization and Stabilization Characteristics of Typical Tropical Soils

E. C. CHANDRASEKHARAN, S. BOOMINATHAN, E. SADAYAN, and
K. R. NARAYANASWAMY SETTY, College of Engineering, Guindy, Madras, India

Although laboratory investigations have established the feasibility of stabilizing highly plastic clays with stabilizers such as cement, the problem remains of pulverizing and obtaining a uniform mixture of the soils with the stabilizers in the field. The present work deals with an experimental study of (a) the influence of heat treatment on the pulverization characteristics of two typical tropical soils (lateritic and black cotton soils) with and without addition of salts, and (b) the influence of heat treatment and aggregate sizes on the stabilization characteristics of pulverized black cotton soils with 12 percent cement.

The pulverization characteristics were determined in terms of the energy required for the new surface area created due to disaggregation caused by low-velocity impact and cutting. The susceptibility to stabilization of black cotton soil with cement was analyzed from the unconfined compressive strengths of soil cement specimens immersed under water after moist-curing for seven days.

The investigations show that (a) heat treatment and addition of sodium chloride result in a reduction of the plasticity of the soils and in a significant improvement in their pulverization characteristics; (b) there exists an optimum sodium chloride content of 3 percent and heat treatment of 250 C for two hours, at which susceptibility to pulverization is maximum; (c) the smaller the aggregate sizes of the black cotton soil, the greater is its susceptibility to stabilization with cement; and (d) a minimum heat treatment up to 300 C is necessary to improve the stabilization characteristics of black cotton soil aggregates of sizes $^3/_8$ to $^3/_{16}$ in. and $^3/_{16}$ in. to 7 B. S. with cement.

•SOIL STABILIZATION is normally employed where the soils existing at a site are not entirely acceptable in their present state. Although granular soils and lean clays have been successfully stabilized with portland cement, lime, and other admixtures, attempts to stabilize fat clays in the field have not been very successful owing to difficulties in pulverizing them into sufficiently small aggregates and obtaining the desired soil-stabilizer mixtures. The stabilization of highly plastic clays involves adequate pulverization of the soil, optimum mixing of the soil with the stabilizer (and water if necessary) and compaction. At present the processes of pulverization (or comminution) and mixing are accomplished with large amounts of energy, and the final stabilization of the soil at the site may sometimes prove even more expensive than a complete replacement of the clay soil with imported granular materials.

Comminution involves several physical actions but perhaps the most important is the breaking apart of the monolithic soil surface, which has formed into a large, structurally continuous unit through cycles of wetting and drying. Because of the large amount of energy involved in breaking the field soil mass, even small economies de-

veloped in these processes have a significant value. This suggests determination of factors influencing pulverization, theories of size reduction, degree of pulverization, optimum aggregate sizes for economical stabilization, etc. Research by Nichols et al (8, 9, 10, 11), Vilenskii (17), Keen (6), Yoder (20), Shaw et al (15), Grimer and Hose (5), Uppal and Bhatia (16), Bose (3), Barbour (1), Chandrasekharan and Chandrasekhar (4), and Scott-Blair (14) permits the following observations:

1. A granular or lumpy structure is the most desirable characteristic necessary from the point of view of plant growth or successful incorporation of stabilizers into soils.
2. The moisture content of the soil is the principal controlling factor in the comminution and workability of cohesive soils. Normally a friable consistency between plastic and shrinkage limit is favorable.
3. The most stable soil-stabilizer system is obtained when certain optimum aggregate sizes are used.
4. Addition of granular materials or certain salts such as sodium chloride into natural soils improves their engineering characteristics and renders them more workable in stabilization processes because of greater ease of pulverization.
5. Adoption of proper techniques of size reduction, namely cutting action for moist soils and impact or attrition for dry soils, yields best results.
6. Effective machine design, with proper shape of cutting edges, tools, and mounting arrangements can save considerable power and improve the degree of pulverization with economy.
7. Depending on the consistency of the soil, operations at lowest possible speeds can minimize the energy required for comminution.
8. There is a definite need to develop theoretical concepts and laboratory techniques to determine the pulverization characteristics of cohesive soils and arrive at methods to improve their susceptibility to pulverization and hence stabilization.

The experimental investigations reported in this paper consist of two parts. The first part deals with the pulverization characteristics of two typical tropical soils (lateritic and black cotton soils) with and without heat treatment and addition of common salt, and the second part deals with the susceptibility to stabilization with cement of the black cotton clay, pulverized and subjected to heat treatment.

DETERMINATION OF PULVERIZATION CHARACTERISTICS OF LATERITIC AND BLACK COTTON SOILS

Soils Used

A lateritic soil from Mysore and a black cotton soil from Coimbatore were used in the investigation. The origin and occurrence of laterite soils and rocks have been described and discussed by Winterkorn and Chandrasekharan (18). These soils are formed in situ and are characterized by the leaching of silica and accumulation of iron and aluminum oxides. The lateritic soil used in this investigation contains 35 percent gravel, 48 percent sand, 13 percent silt, and 4 percent clay (M. I. T. classification) and falls under SC or SF in Casagrande's plasticity chart. The differential thermal analysis (Fig. 1) does not clearly reveal the kaolinite clay mineral, presumably due to the presence of impurities in the soil.

The Geological Survey of India (3) suggests that the black cotton soil may be derived from the products of continuous weathering of igneous rocks such as gneiss and trap. The black or grey color is due to the presence of titanium along with organic matter. In general the black cotton soils contain montmorillonite and illite minerals to a greater extent and are highly argillaceous and somewhat calcareous. They contain a high percentage of iron oxide and magnesium and calcium carbonates. The black cotton soil used in this investigation contains 4 percent gravel, 9.5 percent sand, 27 percent silt, 59.5 percent clay (M. I. T. classification), and 4 percent of organic matter and falls under the CH group in Casagrande's plasticity chart. The differential thermal analysis (Fig. 1) indicates the presence of montmorillonite with a very high endothermic reaction between 100 and 300 C, a small second endothermic reaction between 500 and

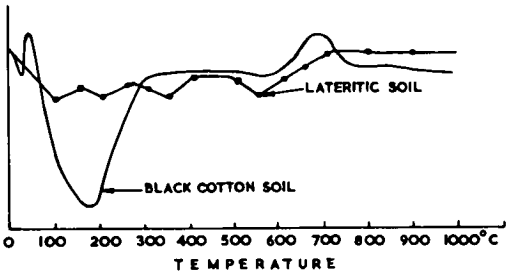

Figure 1. Differential thermal analysis curves for black cotton and lateritic soils.

600 C, and an exothermic reaction between 600 and 750 C.

Tests on Pulverization Characteristics

The two tests conducted to determine the pulverization characteristics were (a) low-velocity impact and (b) cutting. The former was performed on heat-treated black cotton and lateritic soils with and without the addition of sodium chloride and the latter was limited to the black cotton soil subjected to heat treatment alone.

Low-Velocity Impact Test—Various percentages by weight of sodium chloride (½, 1, 3, and 5) were dissolved in suitable quantities of water and the solutions were added to the soil aggregates passing a 3/16-in. sieve. The consistency of the soil-water-salt slurry was kept approximately at the respective liquid limits, namely 55 percent for the black cotton soil and 20 percent for the lateritic soil. The slurry was transferred into wooden molds, 1 in. in diameter and 2 in. high, and the sides of the molds were gently tapped in order to obtain a uniform density. The samples were allowed to remain in the molds at the laboratory temperature for 24 hours to allow possible physical and physicochemical changes to occur. A set of three samples for each combination thus obtained was placed in an electrical muffle furnace kept at specified constant temperatures of 100, 200, 300, and 400 C. The samples were heated for a duration of 2 hours. Similar samples were also prepared on the natural soils without salt.

All the samples were subjected to pulverization in a low-velocity impact test. A steel ball weighing 6¼ lb was dropped from a height of 15 in. to fall directly on the soil specimen. The fragments of the crushed specimen were sieved through B. S. sieve sizes of 3/8 and 3/16 in. and Nos. 7, 36, and 200 and the weight retained in each was determined. From the mean weighted diameter considerations, the new surface area created was calculated. The potential surface area present in 100 grams of soil was determined for the particle sizes as obtained in a mechanical analysis of the natural soil and this area was assumed to represent the basic standard of 100 percent pulverization. The degree of pulverization was defined as the newly formed surface area of aggregates of particles due to crushing divided by the original potential surface area of the soil particles. Assuming 100 percent efficiency for impact, the energy per degree of pulverization is

$$\frac{\text{Energy Input}}{\text{Degree of Pulverization}}$$

Cutting Tests—The black cotton soil passing a 3/16-in. sieve was heated at 100, 200, and 300 C for 24 hours and allowed to cool to room temperature. Samples of 200 grams of the heat-treated aggregates were mixed separately with 10, 15, 20, 25, 35, and 40 percent by weight of water and compacted in Dietert's compaction apparatus (22) suitably modified so that the same dry density of 1.5 g/cc was obtained. A cutting tool of mild steel 7 by 7 by 0.3 cm with the edge sharpened to 0.5 mm in a distance of 2 cm was attached to a proving ring in a compression testing machine and the compacted samples of 5.1 cm diameter and 5.1 cm high were cut at a rate of 1.27 cm per minute. The proving ring readings were noted for every 2.5 mm depth of cutting.

Discussion of Test Results

Effect of Sodium Chloride on Consistency—The results of the consistency tests with and without salt and heat treatment are given in Figure 2. In the case of the black cotton soil, for addition of 1 percent sodium chloride, there is an increase in the liquid

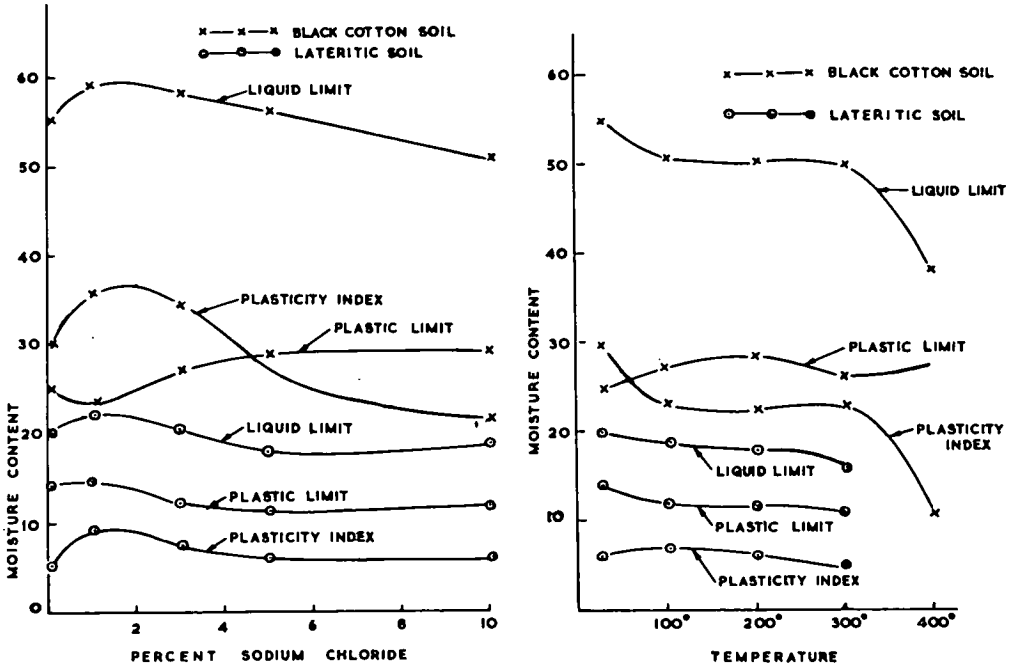

Figure 2. Influence of salt and heat treatment on consistency properties.

limit and a decrease in the plastic limit with a net increase in the plasticity index from 30 to 35. Further addition of sodium chloride reduces the plasticity index primarily due to reduction in the liquid limit. In the case of the lateritic soil, the same trend of increase in the plasticity index from 5.5 to 9 is revealed for addition of 1 percent sodium chloride. With progressive addition of sodium chloride up to 3 percent, the plasticity index is reduced to that of the natural soil and thereafter there is no further variation. The adsorption of sodium ions on the natural soil may explain the increase in the plasticity index due to dispersion effects and the decrease at the higher salt content may be attributed to some sort of a decrease in double layer repulsion (2). This effect is, however, not very conspicuous in the lateritic soil because of its poor activity.

Effect of Temperature on Consistency—The plasticity index for black cotton soil is reduced gently in the initial ranges of heat treatment between 25 and 200 C, and thereafter the reduction is rather fast and steady for the temperature range from 300 to 400 C. This may be attributed to the change in moisture adsorption characteristics of the predominant clay mineral of montmorillonite present in the soil. The temperature effect on the consistency properties of lateritic soil is not significant, because of the presence of the weakly active clay mineral kaolinite and oxides of iron and aluminum. The plasticity index also remains more or less the same for the ranges of heat treatment adopted in this investigation.

Effect of Sodium Chloride and Temperature on Pulverization—Figures 3 and 4 show the results of low-velocity impact tests. An increase in the temperature of the raw soil shows a decrease in the energy requirement. For the increase in temperature from 100 to 250 C the reduction in energy requirement is quite rapid. Heating the black cotton soils after treatment with sodium chloride results generally in a decrease in the energy for pulverization. However, the 3 percent combination shows less energy requirement than the 5 percent combination, although the plasticity index for the 5 percent combination is less than that for the 3 percent combination. The higher energy requirement for pulverizing the 5 percent combination may have to be attributed to the possible cementation effects due to crystallization of the greater amount of salt present. For a combination of 3 percent salt content and heat treatment at 250 C, the energy

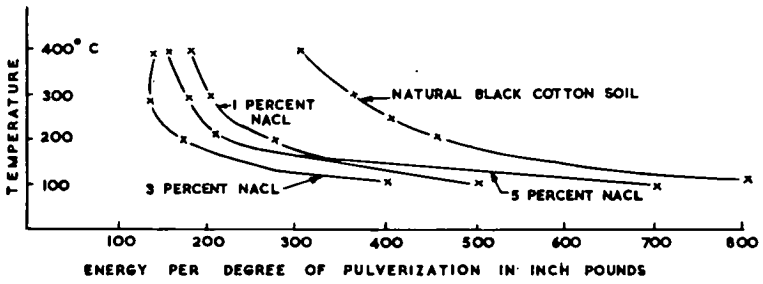

Figure 3. Variation of impact energy for unit degree of pulverization with heat treatment and salt content for black cotton soil.

requirement per unit degree of pulverization is the least. Addition of 3 percent salt and heat treatment up to 100 C has reduced the energy requirement from 800 to 400 in.-lb and this is comparable to the influence of heat treatment alone at 250 C on the natural soil.

The influence of addition of sodium chloride to the lateritic soil is more or less the same as that for the black cotton soil except that the range of energy variation per unit degree of pulverization is very small because of a lower activity of the lateritic soil. At 250 C there is a relative fall in the energy requirement and at 400 C the variation is negligible. The optimum salt content and optimum temperature for improving the susceptibility to pulverization of lateritic soil are 3 percent and 250 C respectively, the same as for the black cotton soil.

The energy spent in cutting the specimen was calculated from the curves correlating cutting load and depth of cutting (Fig. 5). The energy required to make the specimens fail was determined from the area enclosed by the curves up to the peak value and horizontal axis. Figure 6 shows a progressive decrease in energy requirement with increase in heat treatment and the existence of an optimum water content at which the cutting energy is a maximum. Close examination of Figure 6 also reveals that these curves are more or less a replica of the moisture-density curves obtained in conventional compaction tests. In the present series of tests, the dry density was maintained constant and a maximum energy of cutting was required for specimens compacted at a particular moisture content, which may be termed as the "optimum moisture for maximum energy." With progressive increase in temperature of treatment, the maximum cutting energy required reduces with a corresponding increase in the optimum moisture content. At the high ranges of moisture contents, the cutting energies are more or less the same irrespective of the temperature of treatment. For 15 percent moisture content the natural soil (25 C) shows the maximum resistance to cutting while the samples heated to 300 C show approximately the least energy of cutting. This leads to the obvious conclusion that the natural soil containing 15 percent of moisture content

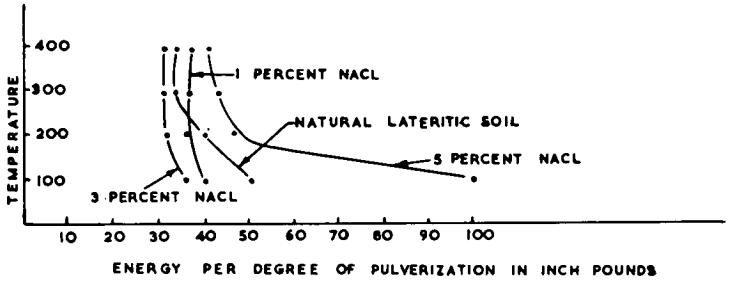

Figure 4. Variation of impact energy for unit degree of pulverization with heat treatment and salt content for lateritic soil.

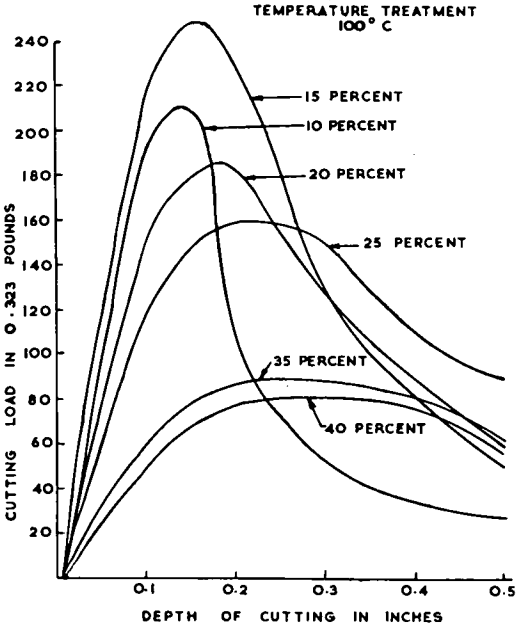

Figure 5. Variation in cutting load with depth of cutting.

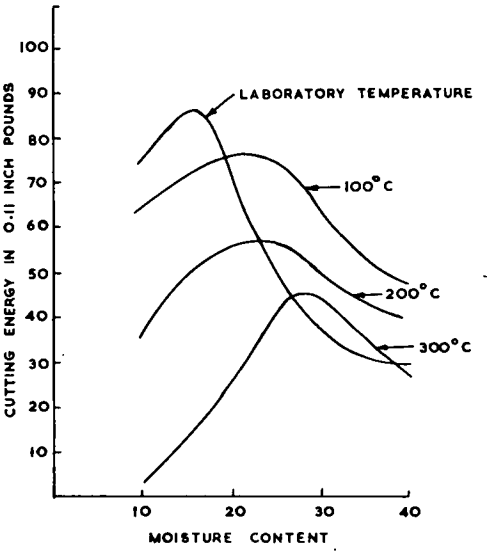

Figure 6. Variation in cutting energy with heat treatment and moisture content for black cotton soil.

is more difficult to cut than the same soil with higher moisture content. The latter condition may therefore seem to be easier for pulverization. From the practical point of view however, pulverization may involve a combination of crushing, impact, and cutting and as such the maximum energy required for cutting under a particular condition need not warrant a correspondingly higher energy for crushing or impact. On the contrary, samples at 15 percent moisture contents could be relatively more brittle, and would be more easily susceptible to pulverization by crushing or impact. A more comprehensive study would have to take into account all these processes affecting pulverization.

SUSCEPTIBILITY TO STABILIZATION OF HEAT-TREATED BLACK COTTON SOIL WITH CEMENT

The objective was the determination of the changes in grain size and physical properties of the black cotton soil of different aggregate sizes due to heat treatment and the susceptibility of the heat-treated soil to stabilization with cement. The intention of heat treatment was not to subject the black cotton soil to high temperatures and convert it into an absolutely non-plastic brick-like material but to spend the least possible heat energy on the black cotton soil and obtain a soil-cement material of requisite stability.

Test Procedure

The black cotton soil was pulverized to different aggregate sizes ($^3/_8$ to $^3/_{16}$ in., $^3/_{16}$ in. to B. S. 7, B. S. 7 to 14, B. S. 14 to 36, and B. S. 36 to 200) by means of a jaw crusher. Samples of different aggregate sizes were subjected to identification and classification tests such as grain size distribution, liquid limit, plastic limit, shrinkage limit, and moisture-density relationship in a Dietert's compaction apparatus. The consistency tests were conducted on the whole soils and not on their -36 (B. S.) fractions as normally done in the standard tests. The different soil aggregates were subjected to heat treatment at constant temperatures of 100, 175, 300, and 400 C for durations of 2 and 8 hours, and in certain cases for 24 hours also. The heat-treated samples were again

subjected to the identification and classification tests mentioned. The aggregates, with or without heat treatment, were mixed with 12 percent cement by weight, and six soil-cement specimens, 2 in. in diameter and 2 in. high, were prepared at their respective optimum water contents using Dietert's compaction apparatus and moist-cured for 7 days. One set of three specimens was tested for unconfined compressive strength immediately after the curing, and the other was immersed in water for a week and then tested for unconfined compressive strength. The rate of strain adopted was 0.05 in. per minute.

Discussion of Test Results

Influence of Heat Treatment on Grain Size—Typical results of mechanical analysis conducted on the black cotton soil of different aggregate sizes subjected to heat treatment are given in Table 1. With an increase in temperature there is a general tendency for a reduction in the colloidal content from 35 percent to 21 percent and hence the formation of non-plastic materials. The samples heated to 100 C have, however, shown a higher colloidal content of 45 percent and also a relatively higher percentage of small size fractions than the raw soil. This strange behavior is to be attributed to the possible hydrophilic nature of the organic content (4 percent) in the soil. The reduction in the colloid content, and also the increase in the particle sizes for higher temperature treatment, are to be attributed to the cementation of small particles and formation of stable aggregates called molecular aggregates by Puri (12).

Influence of Heat Treatment on Consistency—Typical results of consistency tests conducted on black cotton soil aggregates of different sizes heated to 100 C and 175 C for durations of 2, 8, and 24 hours, and 300 C and 400 C for durations of 2 and 8 hours, are given in Table 1. In general, with increased heat treatment there is a tendency for a decrease in liquid limit and an increase in shrinkage limit. The plastic limit does not vary appreciably. The net result is a decrease in the plasticity index values, and for the aggregate size of B. S. 36 to 200 heated to 8 hours at 400 C, the soil exhibits no plasticity at all because no plastic limit test was possible. In one or two in-

TABLE 1

MECHANICAL ANALYSIS OF HEAT-TREATED BLACK COTTON SOIL

Soil Properties	Sieve No.				
	B.S. 3/8-3/16 in.	B.S. 3/16 in.-7	B.S. 7-14	B.S. 14-36	B.S. 36-200
(a) Aggregates at Laboratory Temperature					
Percentage clay	59.5		58.5		52.5
Liquid limit	56.0		57.0		60.0
Plastic limit	27.0		28.0		24.0
Plasticity index	29.0		29.0		36.0
Shrinkage limit	6.3		7.0		6.0
Optimum moisture content	15.90	17.10	20.0	20.30	23.50
Maximum dry density, g/cc	1.750	1.660	1.720	1.710	1.600
Unconfined Compressive Strength, psi					
Moist curing	322.00	220.00	214.00	431.00	582.00
Immersion curing	39.00	57.10	323.00	415.00	441.00
(b) Aggregates Heated at 300 C for 8 Hours					
Percentage clay	47.50		40.00		35.50
Liquid limit	38.00		34.00		34.00
Plastic limit	29.00		24.00		25.00
Plasticity index	9.00		10.00		9.00
Shrinkage limit	15.10		15.70		16.20
Optimum moisture content	16.80	11.50	16.30	17.50	18.90
Maximum dry density, g/cc	1.76	1.65	1.80	1.79	1.68
Unconfined Compressive Strength, psi					
Moist curing	423.00	265.00	410.00	588.00	606.00
Immersion curing	224.00	188.00	282.00	468.00	439.00

stances the general trend of an increase in the shrinkage limit with increase in heat treatment has been reversed. The tendency for the liquid limit to decrease with an increase in heat treatment has also been reversed in some instances, particularly at low temperatures. For example, in the case of $^{3}/_{8}$ to $^{3}/_{16}$ in. aggregates the heat treatment up to 100 C results in an increase in the liquid limit with a net increase in the plasticity index from 28.0 from the natural soil to 33.0 for the heated soil. The shrinkage limit also confirms the higher plasticity characteristics. This anomaly could again be attributed to the presence of organic matter, the exact behavior of which is still unknown. Usually the presence of all types of organic materials destroys the plasticity; the reason for enhancing the plasticity probably depends on the nature of the organic material and one would suspect that such organic materials would provide particularly hydrophilic surfaces (12).

From a study of Table 1 and other data obtained during the investigation, it is seen that a minimum heat treatment up to 300 C seems essential for eliminating the hygroscopic moisture and rendering the material distinctly less plastic. This is also apparent from the initial endothermic reaction in the differential thermal curve up to 300 C in Figure 1. Bose (3) has reported the conversion of black cotton soil into a non-plastic material by heat treatment at 400 C for an hour. Uppal and Bhatia (16) indicated such a conversion by heat treatment of 500 C for 2 hours. The present work indicates a commencement of the change even at 300 C and completion at 400 C for the soil aggregates tested.

Moisture-Density Relationship—Table 1 shows typical results of tests on the influence of heat treatment on the moisture-density relationship of the soil-cement specimens. With decrease in the aggregate sizes, there is an increase in the optimum

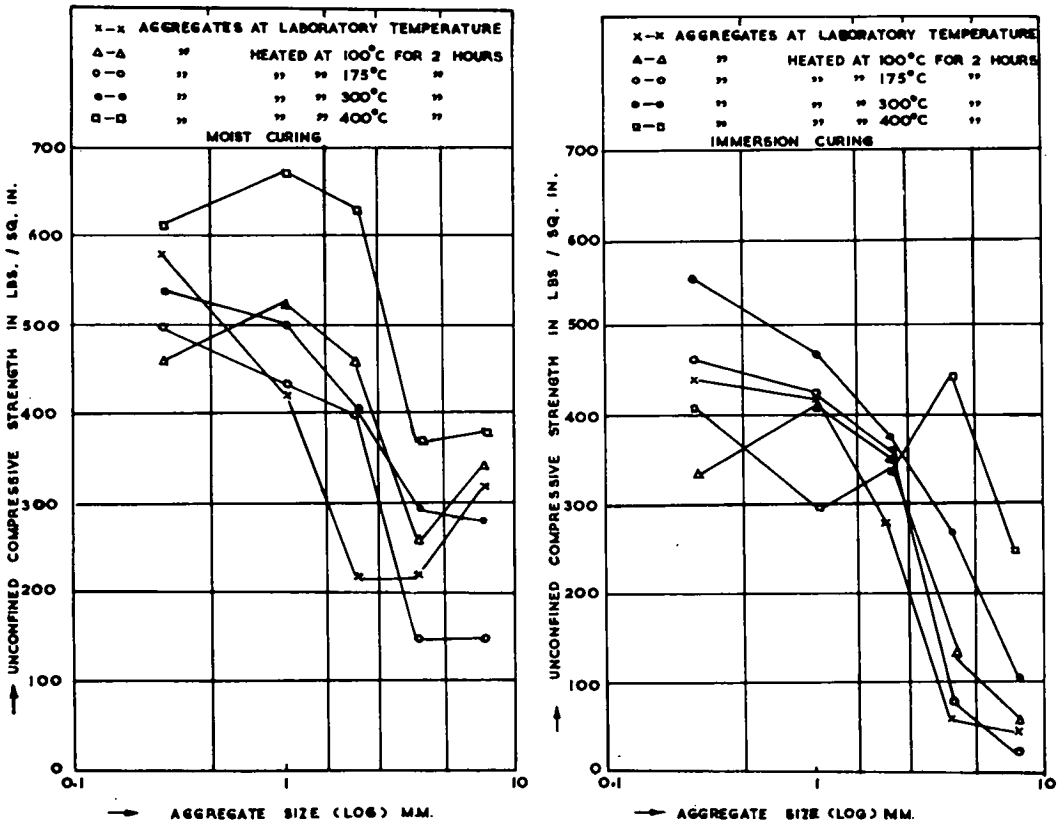

Figure 7. Variation in unconfined compressive strength of cement-stabilized black cotton soil of different aggregate sizes with heat treatment for 2 hours.

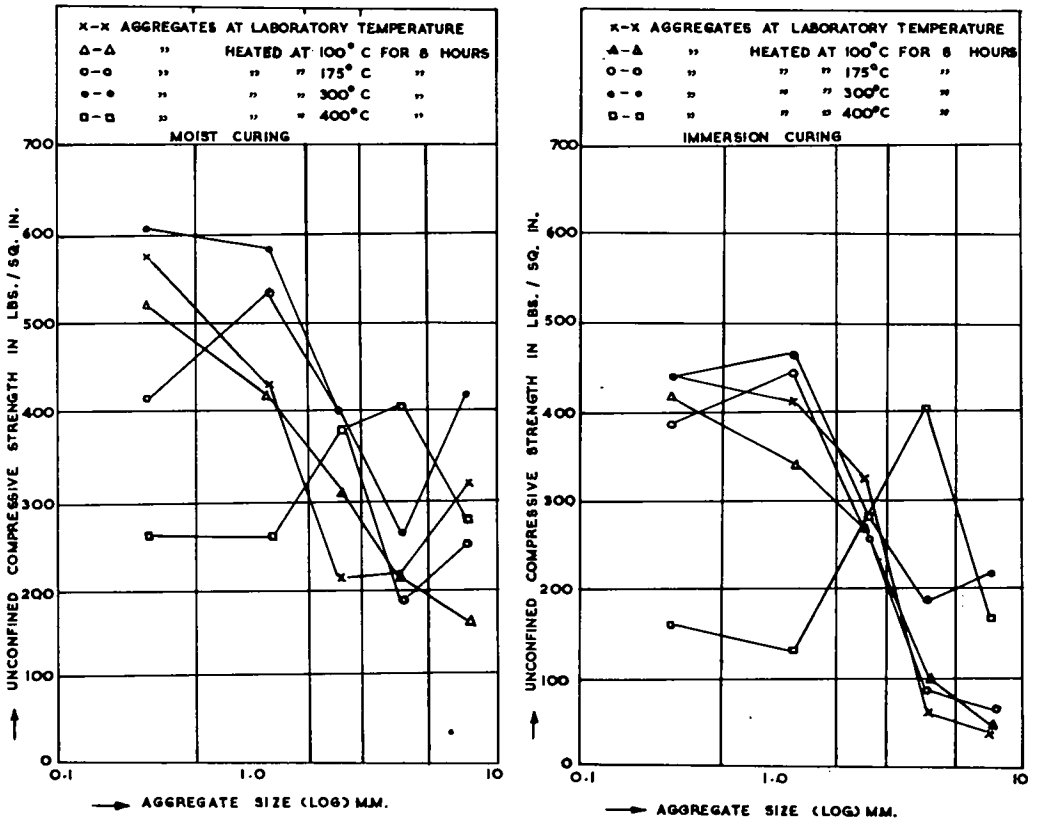

Figure 8. Variation in unconfined compressive strength of cement-stabilized black cotton soil of different aggregate sizes with heat treatment for 8 hours.

moisture content, which may be attributed to the progressively increased surface area to be covered by the water films. The maximum dry density shows a high value for aggregate sizes of $^3/_8$ to $^3/_{16}$-in., with a decrease for the next smaller size, then an increase, reaching a maximum value before finally decreasing for the aggregate size of B. S. 36-200. For higher temperatures of 300 and 400 C, there is a distinct tendency for a reduction in the optimum water content. The maximum dry density of 1.80 g/cc has been obtained for aggregates of size B. S. 7-14 heated at 300 C for 8 hours and $^3/_8$-$^3/_{16}$ in. heated at 400 C for 8 hours. The least value of 1.56 g/cc has been obtained for B. S. 14-36 aggregates heated at 400 C for 8 hours. This is the temperature range at which the material has exhibited very little plasticity and is evidently sandy in texture. This poor density value has to be attributed to the poor compactibility of the (poorly graded) sandy material obtained by heating, whereas the material which gave the maximum density might be considered to be fairly well graded with adequate fines to permit maximum compaction.

Influence of Heat Treatment on Strength—The results of unconfined compression tests on moist-cured and immersed soil-cement specimens are shown in Figures 7, 8, and 9. In general, a tendency for an increase in the unconfined compressive strength with a decrease in the aggregate sizes is noticed for both sets of specimens. However, the immersed samples show a more consistent and reliable trend than the moist-cured ones. A comparison of the influence of different degrees of heat treatment shows no significant improvement for the immersion-cured strength at 100 C and 175 C for the coarser aggregates ($^3/_8$ to $^3/_{16}$ in. and $^3/_{16}$ in. to B. S. 7). The position is, however, much improved for the same aggregates when treated at 300 C, and the best results are obtained for a heat treatment at 400 C. In the case of other small sizes the heat treat-

ment has not very much altered the immersion-cured strength except in the case of samples heated to 400 C for 8 hours. In most of the cases the smaller aggregate sizes of B. S. 7-14, 14-36, and 36-200 show much-reduced strength values for immersion-cured specimens, probably indicating the creation of too much of a non-plastic material such as sand or silty sand, which have smaller unconfined compressive strength values than the untreated clay soil of similar aggregate sizes. The decrease in strength, however, should not be taken as a deterioration in the quality of the resultant material, because a stabilized sand-cement may show higher strength values under confined conditions than a clay-cement under similar conditions (21). The importance of volume relationships in soil stabilization is also brought out in the results (19).

It is clear from the foregoing that the larger aggregates warrant higher heat energy and the smaller aggregates may lose strength and stability characteristics at certain temperatures higher than an optimum for which best results can be obtained. If unconfined compressive strengths as determined from these tests are taken as the criteria, over-heating may give rise to non-plastic materials, which may require higher cement content for best results to be obtained. The study reveals that the degree and duration of heat treatment will have to be tied down to the size of aggregates or clay clods that have to be rendered less plastic or workable. Further, it is seen that for a given percentage of cement (12 percent in this case), the optimum conditions for maximum unconfined compressive strength exist not when the soil is absolutely non-plastic, but when it contains certain poorly plastic fractions, which probably render the compacted material more dense and stable. The objective, therefore, should be to obtain the best possible structural arrangement of the soil-stabilizer system, which gives the requisite strength and stability at a minimum cost and which may involve various opera-

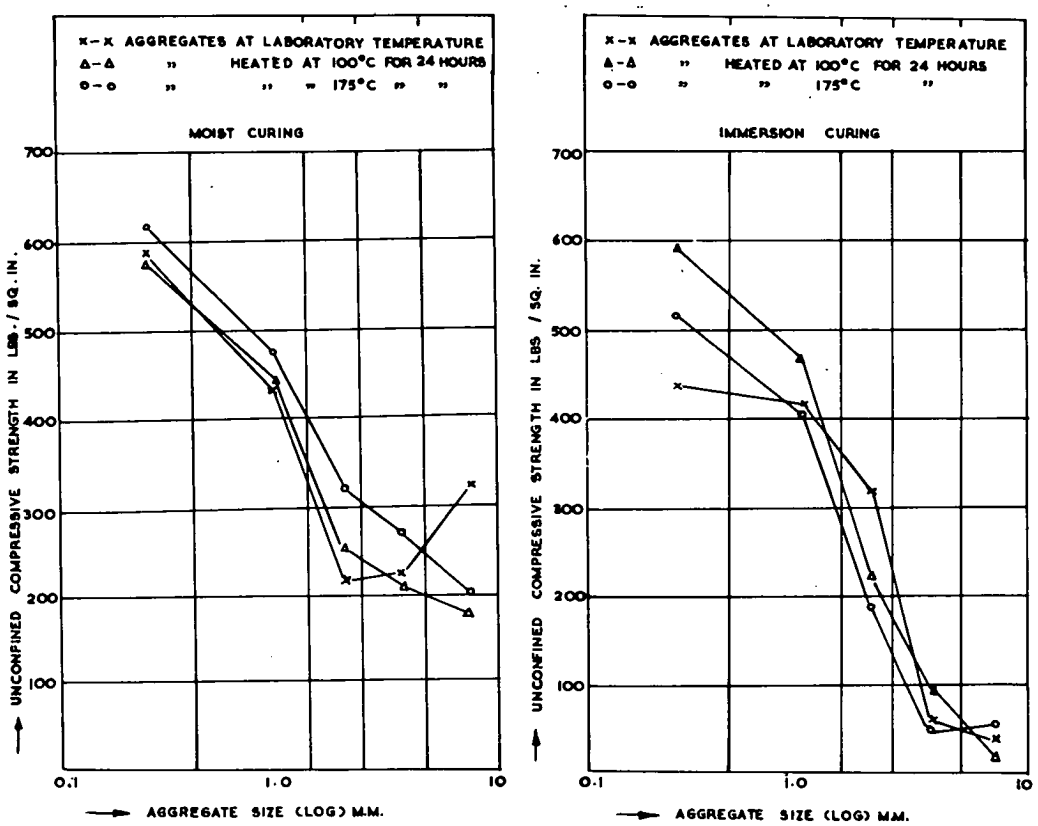

Figure 9. Variation in unconfined compressive strength of cement-stabilized black cotton soil of different aggregate sizes with heat treatment for 24 hours.

tions, namely conversion of the highly plastic clay into a poorly plastic material and processing it with a minimum amount of stabilizer. The poor stabilization characteristics of the non-plastic material obtained by high heat treatment have also been reported by Bose (3).

CONCLUSIONS AND RECOMMENDATIONS

This study on the pulverization and stabilization characteristics of clay soils due to heat treatment and addition of salt has led to the following conclusions and recommendations:

1. Addition of common salt (sodium chloride) improves the susceptibility of plastic soils to pulverization and the energy requirement is minimum for an optimum salt content of 3 percent.
2. For the test conditions and temperature ranges adopted, heat treatment at 250 C for two hours appears to be the desirable minimum to facilitate easy pulverization.
3. Optimum pulverization characteristics are obtained for a combination of a salt content of 3 percent and a heat treatment at 250 C.
4. Whereas the effect of heat treatment may be permanent, the addition of salt both on the pulverization and stability characteristics would need further investigation, since the salt may be susceptible to leaching and may adversely influence the setting of the stabilizer.
5. The energy per degree of pulverization as defined in this work forms a useful basis for comparing the energy requirements in the pulverization of soils. Although the expression for energy per degree of pulverization involves the use of the potential surface area of the individual particles of natural soils as obtained from mechanical analysis, a more appropriate expression would take into account the surface area of optimum aggregate sizes for the soils used and processes involved in a given stabilization work.
6. Heat treatment of pulverized black cotton soil at 300 C reduces the black cotton soil to a medium plastic material and that at 400 C to a poorly plastic or non-plastic one. The reduction in the plasticity characteristics improves the strength of the soil-cement specimens made of coarser aggregate sizes ($^3/_8$ to $^3/_{16}$-in. and $^3/_{16}$-in. to B. S. 7). In the case of the finer aggregates, their conversion into non-plastic material has not resulted in any increase in the unconfined compressive strength but only a decrease. The decrease in strength may not be taken as a reflection of the quality of the resulting material, because a stabilized sand-cement may show higher strength under confined conditions than a clay-cement under identical field conditions. Volume relationships seem to play a significant role in the stability of such soil-stabilizer systems.

ACKNOWLEDGMENT

The experimental investigation reported in this paper forms part of the theses submitted by K. R. Narayanaswamy Setty (7) and E. Sadayan (13) to the Madras University in partial fulfillment of the MSc degree from the College of Engineering, Guindy, Madras, in 1968.

REFERENCES

1. Barbour, A. O. The Comminution of Cohesive Soils and the Workability of Soil Bitumen Mixtures. MSE thesis, Princeton University, 1964.
2. Baver, L. D. Soil Physics. John Wiley and Sons, New York, 1956.
3. Bose, S. K. Stabilization of Certain Clayey Soils in India by Thermal Treatment. Jour. Indian Road Congress, New Delhi, Vol. 18, paper 168, 1953.
4. Chandrasekharan, E. C., and Chandrasekhar, T. S. Stabilized Soil Construction in the Formation of Tuticorin Thiruchendur Road. Jour. Indian Road Congress, Vol. 20, Part I, paper 180, Oct. 1955.
5. Grimer, F. J., and Hose, N. F. The Effect of Pulverization on the Quality of Clay Cement. Proc. Fourth Internat. Conf. on Soil Mech. and Found. Engineering, Vol. 2, p. 109-113, 1957.

6. Keen, B. A. The Physical Properties of the Soil. Longmans, Green and Co., New York, 1931.
7. Narayanaswamy Setty, K. R. Influence of Heat Treatment on Pulverized Black Cotton Soils for Stabilization. MSc (Eng.) thesis, Madras University, 1968.
8. Nichols, M. L., and Baver, L. R. An Interpretation of the Physical Properties of Soil Affecting Tillage and Implement Design by Means of the Atterberg-Consistency Constants. Proc. Second Internat. Conf. on Soil Science, No. 6, p. 175-188, 1930.
9. Nichols, M. L., Reed, I. R., and Reaves, C. A. Soil Reaction to Plow Ware Design. Agri. Eng., Vol. 39, p. 326-329, 1958.
10. Nichols, M. L. The Dynamic Properties of Soils, I. Agri. Eng., Vol. 12, p. 259-264, 1931.
11. Nichols, M. L. The Dynamic Properties of Soils, II. Agri. Eng., Vol. 12, p. 321-324, 1931.
12. Puri, A. N. Soils—Their Physics and Chemistry. Reinhold Publishing Corp., New York, 1949.
13. Sadayan, E. Influence of Heat Treatment and Chemicals on the Pulverization Characteristics of Clay Soils. MSc (Eng.) thesis, Madras University, 1968.
14. Scott-Blair, G. W. Measurement of the Plasticity of Clays. Jour. Physics Chem. No. 35, p. 374-382, 1931.
15. Shaw, B. T., Haise, H. R., and Farnesworth, R. B. Four Years Experience With Soil Penetrometer. Soil Science Soc. of Amer. Proc., No. 7, p. 48-55, 1937.
16. Uppal, H. C., and Bhatia, H. S. Stabilization of Black Cotton Soil for Use in Road Construction. Indian Road Congress Road Research Bull. No. 5, 1958.
17. Vilenskii, D. G. Soil Science. State Teachers College Publishing House, Ministry of Culture, Moscow, p. 213-215, 1957.
18. Winterkorn, H. F., and Chandrasekharan, E. C. Laterite Soils and Their Stabilization. HRB Bull. 44, p. 10-29, 1951.
19. Winterkorn, H. F., and Dutta Choudhury, A. N. Importance of Volume Relationships in Soil Stabilization. HRB Proc., p. 553-560, 1949.
20. Yoder, R. E. The Significance of Soil Structure in Relation to the Tilth Problem. Soil Science Soc. of Amer. Proc., No. 2, p. 21-33, 1937.
21. Annual Report of Highway Research Station, Madras, p. 174-175, 1960-1961.
22. Soil Mechanics for Road Engineers. Her Majesty's Stationery Office, London, 1955.

Influence of Temperature and Other Climatic Factors on the Performance of Soil-Pavement Systems

H. Y. FANG, Chairman, Soil Engineering Division,
Fritz Engineering Laboratory, Lehigh University

Typical climatic and environmental data obtained during the AASHO Road Test are summarized. A brief description of the instruments, methods of installation, and measuring techniques is presented. The influence of temperature and climatic factors on the performance of soil-pavement systems are examined, including the effect of the various cover conditions on the seasonal fluctuation of the groundwater level, on the depth of frost penetration, and on the temperature in different parts of the soil-pavement system. In addition, the influence of temperature on the soil-pavement performance as reflected in surface strains and deflections is discussed. Finally, the seasonal fluctuations of strength characteristics of pavement components and of subsurface conditions are evaluated. It is suggested that the data available from the AASHO Road Test can provide a useful basis on which to develop a more complete understanding of the performance of soil-pavement systems.

•THE IMPORTANCE of climatological factors related to the performance of highway pavements was pointed out by Eno in 1929 (15). These factors include temperature, frost, sunshine, wind, humidity, precipitation, runoff, and evaporation. In 1944 Winterkorn (31) used physicochemical concepts to explain how these factors affected the performance of highway structures. Since then, many investigators have attempted to develop measuring techniques and analysis methods that isolate each of these factors. Highway engineers believed that moisture content and temperature of pavement components, as well as depth of frost penetration and groundwater fluctuation, had the most significant effects on pavement performance (5, 13, 32, 33, 36). Ultimately, all these factors derive from the thermal regime on the earth surface (17, 31, 33, 35).

Guinnee (18) reported information concerning subgrade moisture content and its change with time under rigid pavements having various dimensions of the pavement components. Russam and Coleman (23) discussed the effect of climatic factors on subgrade moisture conditions. Croney, Coleman, and Black (13) showed how the distribution of water in soil is related to highway design and performance. Fang and Schaub (16) demonstrated that subsurface conditions influence deflection and strength characteristics of pavement components. Kolyasev and Gupalo (20) showed the relationship of thermal diffusivity and heat conductivity to soil moisture content and density.

Crabb and Smith (12) studied soil temperature under various vegetation covers. Carson (11) analyzed the time variation of soil and air temperature data by use of Fourier techniques and discussed the heat-transfer processes operating in soil.

Kersten and Johnson (10, 19) reported that, both from theoretical and field observations, frost penetration is greatest in soils with low moisture content and least in those with high moisture content. This, of course, is a consequence of the high specific heat of water. Turner and Jumikis (27) discussed the relationships between surface

temperature and moisture content and considered problems of drainage, frost heave, and moisture migration in soil upon freezing. Aldrich (4) discussed the fundamentals relating to the penetration of frost below highway and airfield pavements.

Studies of groundwater fluctuation related to climatic factors and soil conditions have been reported by several investigators (7, 21, 24, 30).

Winterkorn (32, 33, 34, 35) and Van Rooyen and Winterkorn (28, 29) investigated, both theoretically and experimentally, thermal conductivity and mass transport in moist soils and similar porous systems.

The major objectives of this paper are to summarize the typical climatic and environmental data obtained from the AASHO Road Test; to discuss the effect of the various cover conditions on the seasonal fluctuations of groundwater level and on the depth of frost penetration; to present temperature data for different parts of the soil-pavement system; to correlate strains and deflections of the system with temperature; and to study the influence of seasonal factors on the strength characteristics of pavement components. The systematic collection of such data is considered a prerequisite for comprehensive analyses of the effects of temperature and other climatological factors on soil-pavement systems.

DESCRIPTION OF THE AASHO ROAD TEST SITE

The location of the AASHO Road Test is northwest of Ottawa, La Salle County, Illinois. The annual precipitation at the site averages about 34 in., of which about 2.5 in. occur as 25 in. of snow. The area has an average mean summer temperature of 76 F and an average mean winter temperature of 27 F. Normally, the average depth of frost penetration is about 28 in. The soil usually remains frozen during the winter except for alternate thawing and freezing of the immediate surface.

The topography of the Road Test area is level to gently undulating with elevations varying from 605 to 635 ft above mean sea level. Drainage is provided by several small creeks, which drain into the Illinois River. Surface drainage, however, is generally slow.

Geologic information indicates that the area was covered by ice during several glacial periods and that the present-day subsurface soils were deposited or modified during these periods. Surface soils were subsequently derived from a thin mantle of loess deposited during a postglacial period. Bedrock, varying from sandstone at the west end of the test road to either a clay shale or shaley limestone at the east end, is found 10 to 30 ft below the surface.

The test facility was constructed along the alignment of Interstate Route 80 and consisted of four major loops (Loops 3 through 6) and two smaller loops (Loops 1 and 2). Loop 1 was not subjected to traffic.

The road test sections were constructed of one type each of soil, subbase, and base material considered typical of national practice. Both flexible and rigid pavements of various design thickness were included. Within the flexible pavement sections, four types of base were included: crushed stone; regular gravel; cement-treated gravel; and bituminous-treated gravel. The details of the construction procedure, field control, and variability of the test results are given in the AASHO Road Test reports (1, 26).

GROUNDWATER FLUCTUATION

Groundwater levels generally fall in the winter period and rise in the spring. Meyer (22) observed in both laboratory and field investigations that groundwater levels fell during the winter as the air temperature decreased and rose approximately the same amount in the spring as the air temperature increased. Schneider (24) also investigated the relationships of air temperature to groundwater levels. He attributed winter water table decline to upward movement of capillary moisture toward the frost layer. Willis et al (30) reported that water table lowering was associated with depth of frost and was accompanied by increased soil moisture in the frost zone about the water table. Benz et al (7) also demonstrated that changes in soil moisture content and water table elevation were associated with soil temperature. As the soil temperature decreased

during the winter, the water table fell and the soil moisture content increased in the surface horizons by migration of water from the subsoil.

The groundwater fluctuation study at the AASHO Road Test included three different cover conditions: under uncovered areas, under rigid pavements, and under flexible pavements. In addition, a comparison between nontraffic and traffic areas was undertaken.

A total of 26 water table measurement installations were made on the centerline of all the test loops. Four-inch diameter cores were taken from the pavement surface and holes were bored to a depth of 16 ft. A sand-gravel mulch was placed in the holes to form a base for the pipe through which water table elevations were to be measured. The pipe was lowered into the hole with the top of the pipe approximately ½ in. below the pavement surface. The sand-gravel mulch was compacted around the pipe and brought to within 1 ft of the surface. On the rigid pavement test sections, a concrete mix was placed level to the pavement surface around the top of the pipe. On the flexible pavement a hot-mix asphalt was compacted around the pipe. On the uncovered area the water table installations were placed along the fence line of the right-of-way. To measure the elevation of the water table at each installation, a portable electrical sounding device was designed. The details of the device and the test procedures have been reported by Leathers, Fang, and Donnelly (21).

Groundwater level readings were taken at each location approximately every two weeks from August 1958 to January 1961. Figure 1 shows the groundwater fluctuation with time for the various cover conditions. It may be seen that the groundwater fluctuations were significantly greater under the nontraffic loop (Loop 1) than under the traffic loop (Loop 6). However, under the same traffic conditions, the groundwater fluctuations for both rigid and flexible pavements were similar. For the uncovered area the groundwater level was closer to the ground surface then for the covered area because the rate of infiltration of the uncovered area was greater than for the covered area.

FROST PENETRATION

A device was developed at the Road Test by which determination of "depth of frost" could be made without disturbing the pavement. The system was based on the knowledge that the electrical resistance of a soil-water system changes rapidly upon freezing due to a large difference in resistivity between the solid and liquid phase of water. Pairs of electrodes buried in the soil at 1-in. intervals of depth were connected to leads that extended to the surface. Measurements of the resistance across these electrodes indicated the depth to which the soil-water system had frozen. The details of this system and test procedure are described by Carey and Andersland (9).

Frost depth indicators were installed in both flexible and rigid pavement test sections. There were 28 installations in the rigid pavement test sections and 16 installations in the flexible pavement test sections of Loop 1.

The installations in the rigid pavement tests sections were one per test section and were located at a point 1 ft from the pavement edge and 1 ft from a transverse joint. In sections with a base, the top of the indicator was placed 2 in. below the top of the subgrade. In those sections with no base, the indicator top was placed immediately beneath the concrete pavement surface.

The flexible pavement installations on Loop 1 were located in six test sections. Four of these sections had two indicators each, one in the shoulder material at the pavement edge and the other at the centerline of the section. The other two sections had four indicators each: one in the shoulder material, one at the pavement edge, one at the centerline of the section, and one at the centerline of the traffic lane.

In addition, a total of 20 frost indicators were installed in two test sections in each of the other five traffic loops (Loop 2 through Loop 6). These installations were made at the pavement edge and at the centerline of the traffic lane. In all installations the top of the indicator was placed 1 in. below the top of the embankment soil. Data were taken at least once each month during the frost period.

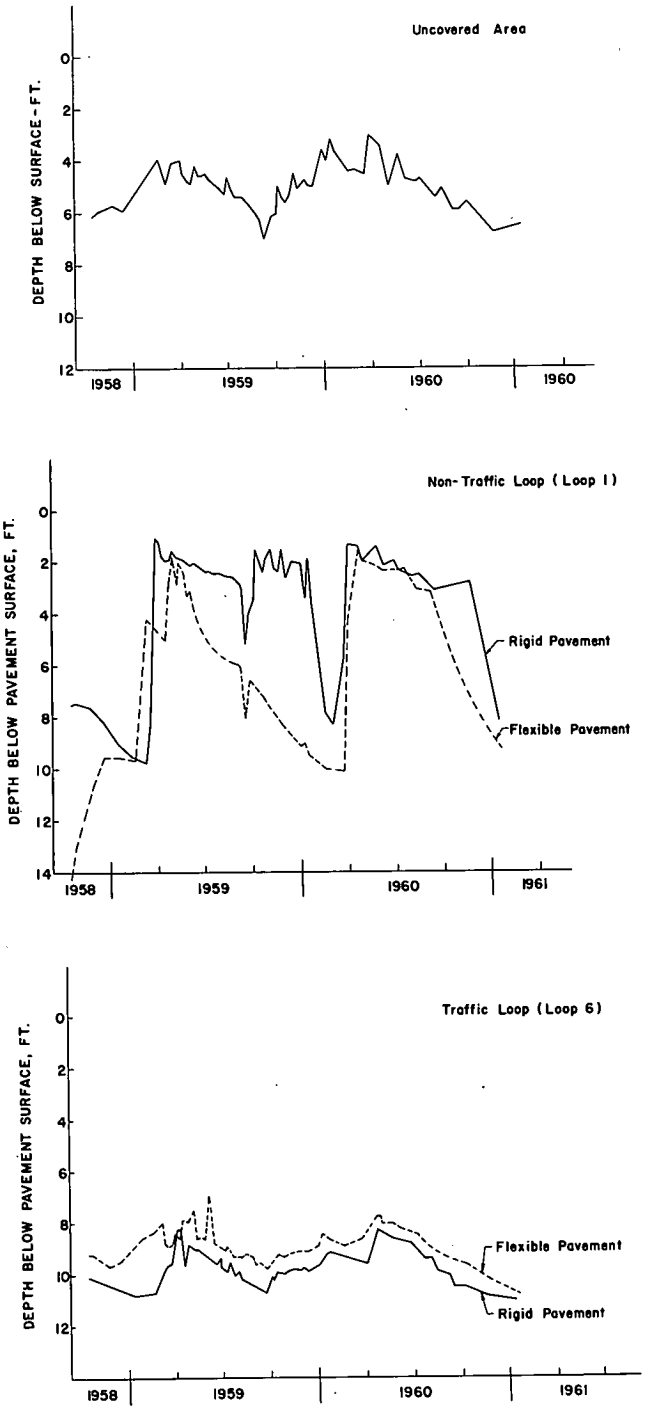

Figure 1. Groundwater fluctuation under various cover and traffic conditions.

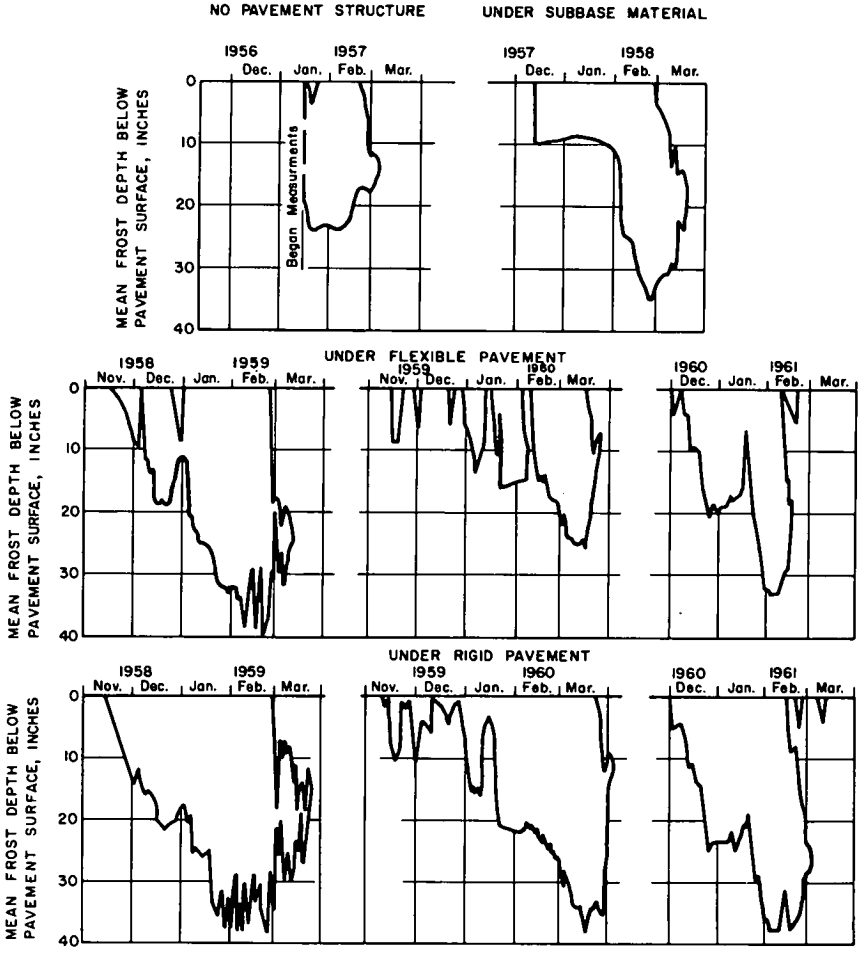

Figure 2. Frost depth under various cover conditions.

Figure 2 shows the mean frost penetration below the pavement surface for the four cover conditions studied: (a) no pavement structure; (b) under subbase material; (c) under flexible pavement; and (d) under rigid pavement.

It may be seen from Figure 2 that, in general, frost penetration was greater under rigid pavements than under flexible pavements, due to the greater heat conductivity of portland cement concrete. However, it should be noted that there was no subbase material in the case of rigid pavements. In fact, some rigid pavement test sections had neither subbase nor base material.

TEMPERATURE OF THE SOIL-PAVEMENT SYSTEM

Soil temperatures have been shown to vary in a somewhat regular pattern, reflecting both the annual and diurnal cycles of solar radiation. Superimposed on these regular cycles are fluctuations of variable duration and amplitude created by changing climatic conditions. Variation of air and soil temperatures have been reported by many investigators (11, 12, 13, 17, 25). Data are lacking, however, for the temperature variation within the pavement sections and for soil temperatures underneath various types of pavement covers. Data presented here show the temperature variation within the soil-pavement system for flexible pavements, rigid pavements, and their shoulders.

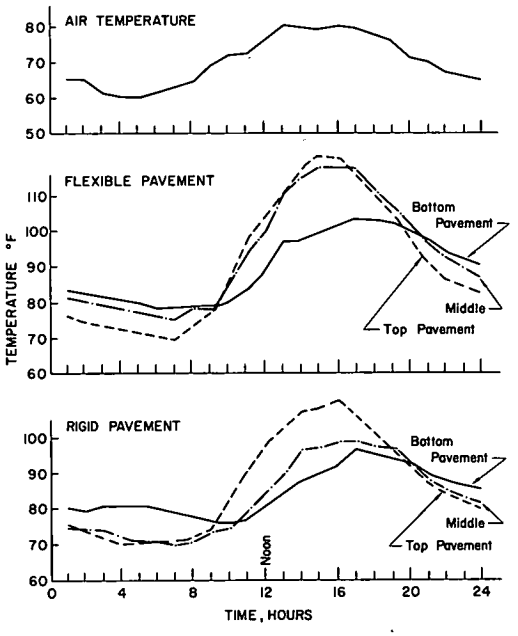

Figure 3. Twenty-four hour temperature study of pavement sections.

At the Road Test, thermocouple rods were used to measure temperatures. For the flexible pavements, thermocouples were located in both the nontraffic loop (Loop 1) and the traffic loops (Loops 2 through 6). Six indicators were placed at each test section: in both shoulder materials, at the pavement edge, at the centerline of the traffic lane, at the centerline of the pavement, and at the centerline of the passing lane. A code designation was given to each thermocouple in order to identify the test section, pavement component, hole number, and placement depth.

For the rigid pavements, thermocouples were located in Loop 1 with three indicators per test section. Two of these indicators were in the center of the section with one placed at the pavement edge and the other placed 1 ft from the centerline. The third indicator was located at a transverse joint, 2 in. from the pavement edge.

These thermocouples were read with a recording device capable of automatically reading 220 thermocouples consecutively at intervals of 5 minutes to 1 hour. Selected readings were made with a Bristol Recording Dynamaster (21).

Thermocouple data were used in the analysis of rigid pavement curl studies and in conjunction with pavement deflection studies for both rigid and flexible pavements. Other analyses were made including a study of 24-hour temperature variations, an investigation of frost depth-temperature relationships, and a study of temperature-depth effects. Typical temperature variation curves are shown in Figures 3 to 5.

Figure 3 shows the results of a 24-hour temperature study and indicates that although temperatures within both flexible and rigid pavement sections exhibited similar trends with time to those of the air temperature, the magnitude of variation of pavement temperature was much greater. Figure 3 also indicates that, in the early morning when the air temperature was low, the temperature of the pavement bottom was higher than that of the pavement surface. When the air temperature rose, the temperature at the top of the pavement surface rose sharply compared with that at the middle and bottom part of the pavement. This phenomenon is explained by the concept of heat conductivity or thermal diffusivity (17).

Figure 4 shows isotherms for the soil pavement system of Loop 1 (flexible pavement). The upper part of the figure was obtained when the air temperature was a maximum (80 F). The lower part was obtained the same day when the air temperature was a minimum (49 F). From these curves it may be seen that, when the air temperature was at its maximum level, the temperature of the underlying granular material decreased with increasing depth under the pavement centerline. When the air temperature was at a minimum level, the temperature of the underlying granular material increased with depth. In all cases, the "penetration" of a given temperature beneath the surfacing was significantly different from that beneath the crushed stone shoulders. When the air temperature was at its maximum level, heat penetrated into the granular material and embankment soil under the pavement surfacing to a greater depth than beneath the shoulders.

Temperature vs depth data for a 24-hour period are shown in Figure 5 for a soil-pavement section with rigid surfacing. It may be noted that, as in the case of Figure 4, the daily variation in air temperature had little influence on the temperature of the

3-0-16 DESIGN, LOOP I

MAY 25, 1960 2:00 PM

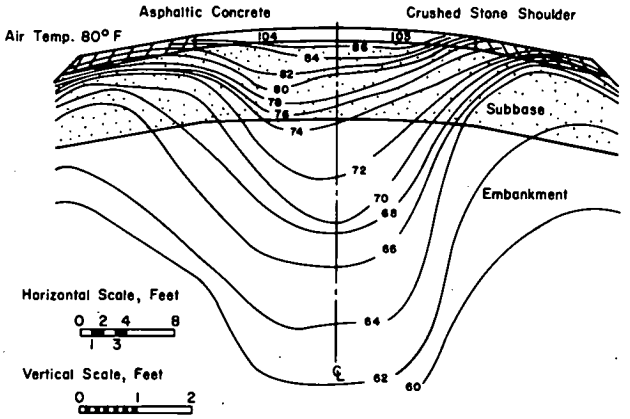

MAY 25, 1960 4:00 AM

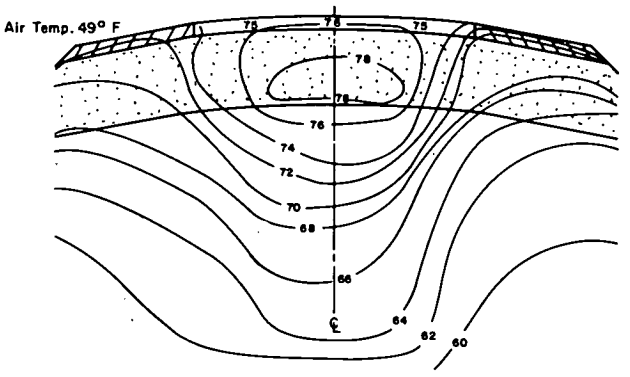

Figure 4. Soil-pavement system isotherms (flexible pavement).

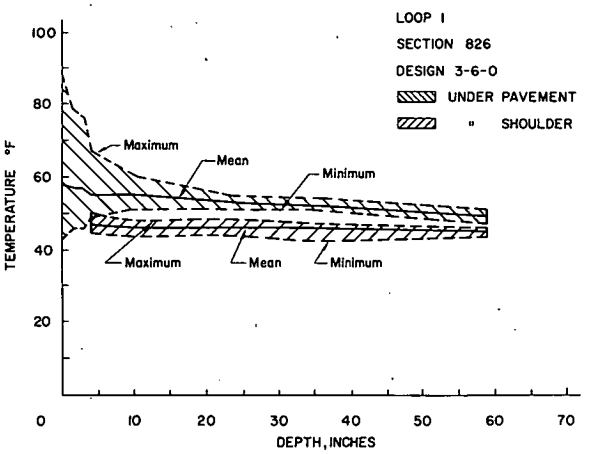

Figure 5. Temperature variations in soil-pavement system (rigid pavement).

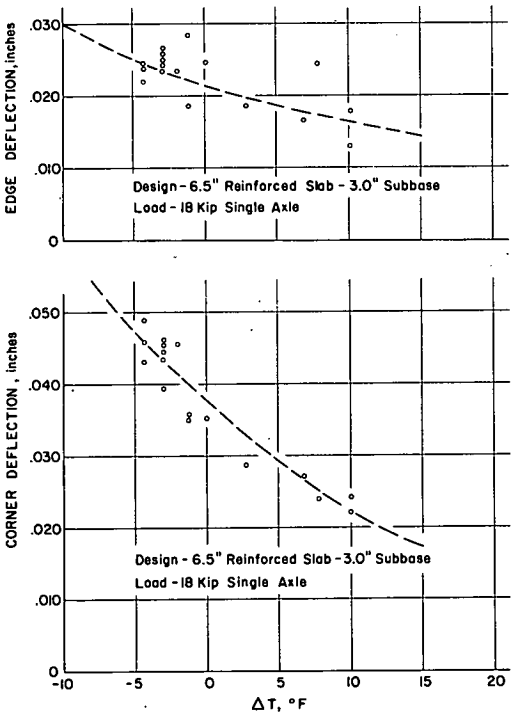

Figure 6. Effect of temperature on deflection of soil-pavement system (rigid pavement).

subgrade. However, the depth of influence may be expected to be a function of both thickness and heat capacity of the pavement materials.

INFLUENCE OF TEMPERATURE ON THE PERFORMANCE OF SOIL-PAVEMENT SYSTEMS

One useful measure of the performance of a soil-pavement system is the static and dynamic deflection of the pavement surface. Studies of the influence of temperature on surface deflections were conducted for both rigid and flexible pavement surfacings at the AASHO Road Test.

Rigid Pavements

Two devices were used for measuring the edge and corner deflections of the rigid pavement sections. The static rebound deflections were measured by means of a Benkelman beam deflection indicator (2, 6) having a probe length from pivot to tip of 10 ft. The Benkelman beam was placed on the shoulder and a standard measuring procedure was followed (2). The dynamic deflections were measured by use of linear variable differential transformers (LVDT) mounted in a $^3/_4$-in. diameter shell and installed at the pavement surface. The movable core foot of the LVDT rested on the top of a reference rod. This rod was anchored securely to a perforated plate located 6 to 8 ft below the pavement surface.

The pavement strain was measured by use of electrical resistance strain gages. The strain gages were cemented at the central transverse joint of each test section.

Deflection and strain measurements taken during the 24-hour studies are plotted (Figs. 6 and 7) against the temperature differential (ΔT) existing in a 6.5-in. slab selected as a standard. [Temperature differential is the temperature (F) at a point $^1/_4$ in. below the top surface of the 6.5-in. standard slab minus the temperature at a point $^1/_2$ in. above the bottom surface, determined at the time the strain or deflection was measured (2, p. 186).]

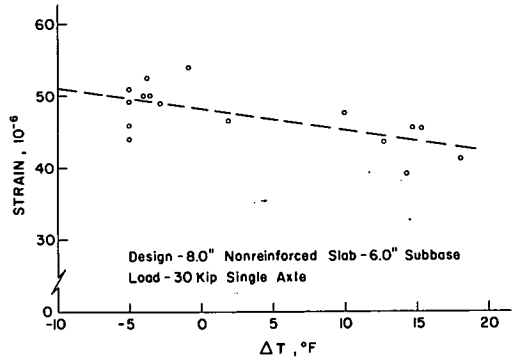

Figure 7. Effect of temperature on strain of soil-pavement system (rigid pavement).

When ΔT was positive, the top surface temperature of the standard 6.5-in. slab was higher than that at the bottom. It may be seen from Figure 6 that, as the temperature in the top of the slab increased relative to the bottom, the pavement strain or deflection decreased. A similar trend may be observed in all three cases shown in Figures 6 and 7.

Flexible Pavements

The influence of mat temperature on pavement deflection has been studied by

several investigators (6, 8, 14, 25). Sebastyan (25) pointed out that the rebound deflections of pavements are affected by the mat temperature. He suggested that an average deflection change of 0.002 in. per 10 F variation of temperature may be used to correct the pavement deflections to a standard temperature of 70 F.

A standard Benkelman beam deflection test procedure was used to establish the effect of temperature on the deflection of flexible pavement having different types of base and pavement thickness. Typical data are shown in Figure 8 in which each point shown in the left part of the figure represents the average of all measurements within each loop for test sections having the same surfacing thickness. Measurements were made at four locations in each test section, two in the inner wheelpath and two in the outer wheelpath of the traffic lane. A 12-kip single axle load was used on all loops. The average base and subbase thicknesses were the same for each surfacing thickness.

The right part of Figure 8 represents data from the special base wedge test sections of Loop 6 at the Road Test. The surfacing thickness over all base types was 4 in., the subbase thickness beneath the bituminous and cement base was 4 in., and beneath the stone base it was 8 in. A 30-kip single axle load was used in this special study.

The results of the tests indicate that considerable reduction in pavement deflection may result from a decrease in mat temperatures.

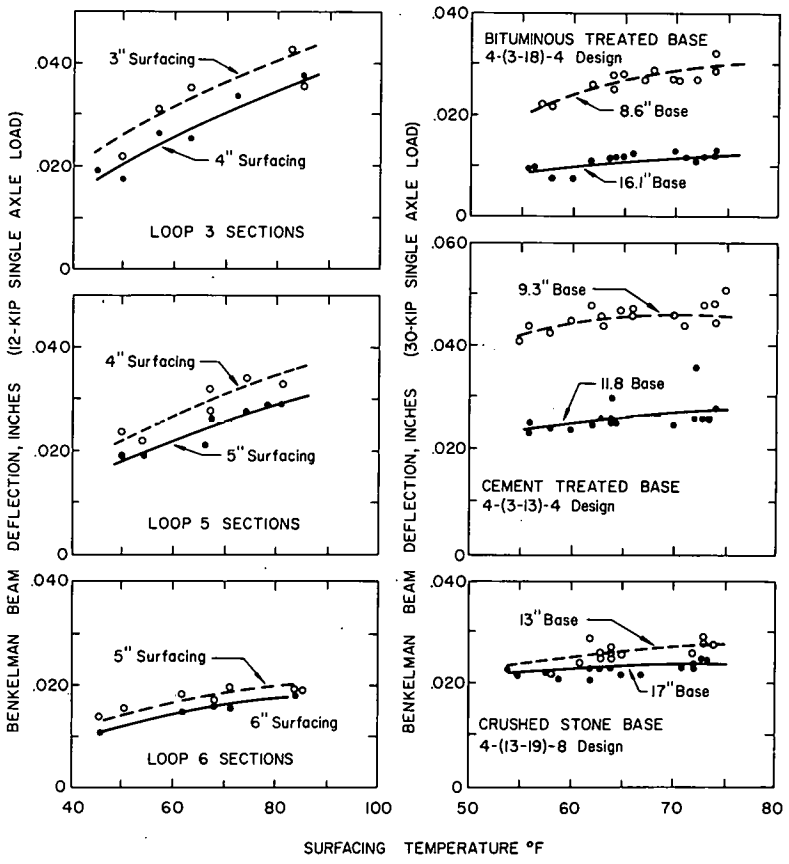

Figure 8. Effect of temperature on deflection of soil-pavement system (flexible pavement).

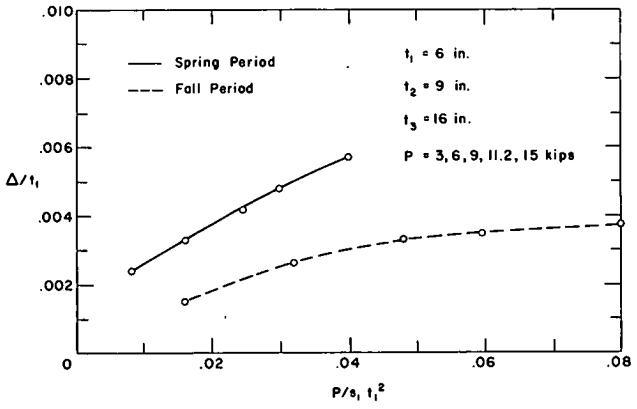

Figure 9. A nondimensional plot of the relationship between soil-pavement system deflection and wheel load (flexible pavement).

INFLUENCE OF SEASONAL FACTORS ON THE PERFORMANCE OF SOIL-PAVEMENT SYSTEMS

The influence of seasonal factors on the performance of soil-pavement systems is discussed in terms of the pavement surface deflections as well as the strength of the pavement components. Only data for flexible pavements are presented. However, similar information for rigid pavements may be found in the AASHO Road Test Report (2).

Deflection

The influence of seasonal factors on flexible pavement deflections have been reported by several investigators (8, 14, 25). The maximum deflection of a flexible pavement usually occurs immediately after the spring thaw and deflections then decrease to a minimum value by fall. It has been observed that a secondary increase in deflection may occur during the latter part of the initial thawing period. This is tentatively attributed to a readjustment in the thermal regime beneath the pavement when some frozen strata still exist at depth. Deflection may also increase in midsummer when pavement temperatures are highest. This increased deflection, however, is believed to result from temperature variations occurring in the bituminous surface course of the pavement and is usually insignificant when compared with the spring thaw deflections. The relationship between deflection and seasonal variation appears to be a function of subgrade soil type, total thickness and type of pavement structure, and rate and characteristics of the spring thawing. At the Road Test, comprehensive studies of this effect with various surface thicknesses were reported and similar conclusions were drawn (2, 6).

Fang and Schaub (16) used nondimensional techniques based on dimensional analysis to provide a rational basis for analyzing the Benkelman beam deflection data of flexible pavements. Data obtained from the AASHO Road Test have been successfully analyzed by such techniques.

Figure 9 shows a nondimensional plot of the pavement deflection (Δ/t_1) vs the wheel load parameter ($P/s_1 t_1^2$) for the spring and fall periods. The parameter P is the wheel load, s_1 is the strength of the surface, Δ is the pavement deflection, and t_1, t_2, and t_3 are the thicknesses of the surface, base course, and subbase respectively. It may be seen that for the spring period, for a given thickness of base or subbase, the pavement deflection increased sharply as the wheel load increased. For the fall period, there was a slight increase in pavement deflection as the wheel load was increased.

Figure 10 shows a nondimensional plot of the pavement surface deflection vs the thickness parameter under a given wheel

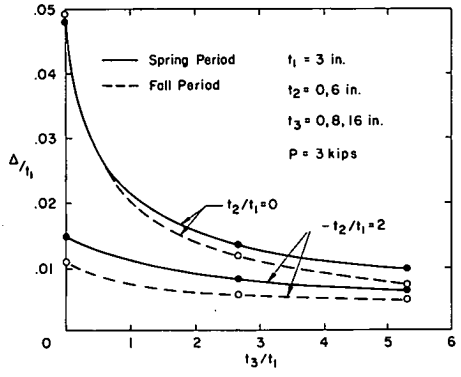

Figure 10. A nondimensional plot of the relationship between soil-pavement system deflection and thickness (flexible pavement).

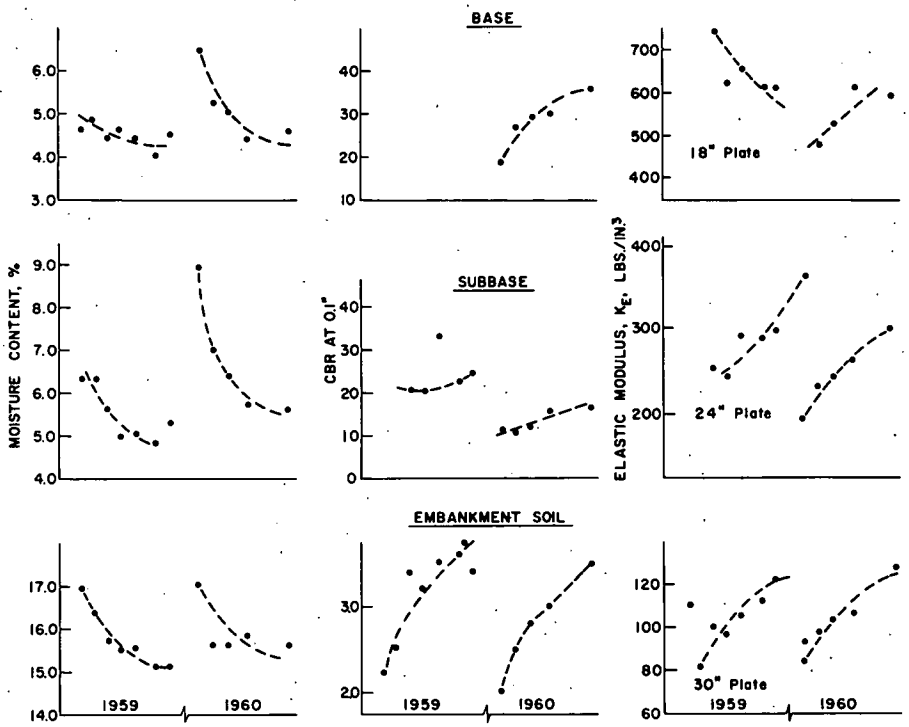

Figure 11. Seasonal variation in strength characteristics of soil-pavement system (flexible pavement) Loop 1.

load for different base thicknesses for both spring and fall periods. It may be seen that, for a given wheel load and strength of asphaltic concrete, the pavement deflection decreased as the subbase thickness increased. As the base thickness was increased from 0 to 6 in., the pavement deflection decreased markedly. The spring and fall variations of nondimensional deflection with thickness were similar.

Strength

The variation of moisture content, CBR, and elastic modulus over a period of two years is shown in Figure 11. All data were obtained from the nontraffic loop (Loop 1). It may be seen that, as may have been predicted, there was a tendency for the strength of the pavement components to increase as the moisture content decreased. It should be noted that tests on the traffic loops have yielded moisture content, CBR, elastic modulus, and density values that were different in magnitude from those obtained in Loop 1 studies. Normally, moisture contents were less, and CBR and elastic modulus values were greater on the traffic loops than on the non-traffic loops. This is believed to be a result of the additional compaction provided by traffic loads.

SUMMARY AND CONCLUSIONS

A brief description of the instruments, methods of installation, and measuring techniques used to obtain climatic and environmental data at the AASHO Road Test, conducted during the period 1958 to 1961, are presented.

The influence of temperature and other climatic factors on the performance of soil-pavement systems can be summarized as follows:

1. Groundwater fluctuations were significantly greater under the nontraffic loop than under traffic loops. Under the same traffic conditions, however, the groundwater

fluctuations for both rigid and flexible pavements were similar. For the uncovered area, the groundwater level was closer to the ground surface than for the covered area.

2. The data indicate that frost penetration was greater under rigid pavements than under flexible pavements, due in part to the greater heat conductivity of portland cement concrete.

3. The 24-hour temperature study indicated that temperatures within both flexible and rigid pavement sections exhibited trends similar to the air temperature, although the magnitude of variation of pavement temperature was much greater. Temperature vs depth data for both rigid and flexible pavements show that the daily air temperature variation had little influence on the temperature of subgrade soils.

4. Correlation of temperature conditions with soil-pavement performance as reflected in surface strains and deflections suggests that there is considerable reduction in pavement strains and deflections as the mat temperature decreases.

5. The influence of seasonal factors on the performance of the soil-pavement system is discussed in terms of the pavement surface deflections as well as in terms of the strength of pavement components. For illustration, only data for flexible pavements are presented. It is shown that there is a significant difference in both deflection and strength between spring and fall for both traffic and non-traffic loops.

ACKNOWLEDGMENTS

Sincere appreciation is extended to W. N. Carey, Jr., and R. C. Leathers, former Chief Engineer for Research and Engineer of Special Assignments of the AASHO Road Test, Highway Research Board, respectively, for their conception of the project and for their supervision of much of the work during the experimental phase.

Professor Hans F. Winterkorn of Princeton University provided constructive criticism and numerous suggestions. Professors J. W. Fisher and T. J. Hirst reviewed the manuscript.

The financial assistance provided by the Pennsylvania Highway Department and the Bureau of Public Roads is gratefully acknowledged.

REFERENCES

1. The AASHO Road Test, Report 2: Materials and Construction. HRB Spec. Rept. 61B, 1962.
2. The AASHO Road Test, Report 5: Pavement Research. HRB Spec. Rept. 61E, 1962.
3. The AASHO Road Test, Report 6: Special Studies. HRB Spec. Rept. 61F, 1962.
4. Aldrich, H. P., Jr. Frost Penetration Below Highway and Airfield Pavements. HRB Bull. 135, p. 124-149, 1956.
5. Barber, E. S. Effect of Water Movement on Soil. HRB Spec. Rept. 40, p. 212-225, 1958.
6. Benkelman, A. C., Kingham, R. I., and Fang, H. Y. Special Deflection Studies on Flexible Pavements. HRB Spec. Rept. 73, p. 102-125, 1962.
7. Benz, L. C., Willis, W. O., Sandoval, F. M., and Mickelson, R. H. Soil Water Translocation in a High Water Table Area. Water Resources Research, Vol. 4, No. 1, p. 95-101, Feb. 1968.
8. Canadian Good Roads Association. CGRA Benkelman Beam Procedure. CGRA Tech. Publ. No. 12, Ottawa, 1959.
9. Carey, W. N., Jr., and Andersland, O. B. Frost Depth Determination by Electrical Resistance Measurements. Highway Research Abstracts, Vol. 27, No. 4, April 1957.
10. Carlson, H., and Kersten, M. S. Calculation of Depth of Freezing and Thawing Under Pavements. HRB Bull. 71, p. 81-98, 1953.
11. Carson, J. E. Analysis of Soil and Air Temperatures by Fourier Techniques. Jour. of Geophysical Research, Vol. 68, No. 8, p. 2217-2232, April 15, 1963.
12. Crabb, G. A., Jr., and Smith, J. L. Soil-Temperature Comparisons Under Varying Covers. HRB Bull. 71, p. 32-80, 1953.

13. Croney, D., Coleman, J. D., and Black, W. P. M. Movement and Distribution of Water in Soil in Relation to Highway Design and Performance. HRB Spec. Rept. 40, p. 226-252, 1958.
14. Curtis, W. E., and Shields, B. P. Determination of Spring Load Carrying Capacity from Benkelman Beam Deformation. Symposium on Pavement Design and Evaluation, Canadian Good Roads Association, Ottawa, 1960.
15. Eno, F. H. The Influence of Climate on the Building, Maintenance, and Use of Roads in the United States. HRB Proc., Vol. 9, p. 211-249, 1929.
16. Fang, H. Y., and Schaub, J. H. Analysis of the Elastic Behavior of Flexible Pavement. Proc., Second Internat. Conf. on Structural Design of Asphalt Pavements, Univ. of Michigan, Aug. 1967.
17. Geiger, Rudolf. The Climate Near the Ground. Harvard Univ. Press, 1965, 611 pp.
18. Guinnee, J. W. Field Studies on Subgrade Moisture Conditions. HRB Spec. Rept. 40, p. 253-267, 1958.
19. Kersten, M. S., and Johnson, R. W. Frost Penetration Under Bituminous Pavements. HRB Bull. 111, p. 37-62, 1955.
20. Kolyasev, F. E., and Gupalo, A. I. On the Correlation of Heat and Moisture Properties of Soils. HRB Spec. Rept. 40, p. 106-133, 1958.
21. Leathers, R. C., Fang, H. Y., and Donnelly, D. E. Report on the AASHO Road Test Climatological Data. AASHO Road Test Field Office Report, HRB, Aug. 1961.
22. Meyer, A. F. Effect of Temperature on Groundwater Levels. Jour. of Geophysical Research, Vol. 65, No. 6, p. 1747-1752, 1960.
23. Russam, K., and Coleman, J. D. The Effect of Climatic Factors on Subgrade Moisture Conditions. Geotechnique, Vol. 11, No. 1, p. 22-28, March 1961.
24. Schneider, R. Correlation of Groundwater Levels and Air Temperatures in the Winter and Spring in Minnesota. U. S. Geological Survey, Water-Supply Paper 1539-D, 1961.
25. Sebastyan, G. Y. The Effect of Temperature on Deflection and Rebound of Flexible Pavements Subjected to the Standard CGRA Benkelman Beam Test. Symposium on Pavement Design and Evaluation, Canadian Good Roads Association, Ottawa, 1961.
26. Shook, J. F., and Fang, H. Y. Cooperative Materials Testing Program at the AASHO Road Test. HRB Spec. Rept. 66, p. 59-102, 1961.
27. Turner, K. A., Jr., and Jumikis, A. R. Subsurface Temperatures and Moisture Contents in Six New Jersey Soils, 1954-1955. HRB Bull. 135, p. 77-108, 1956.
28. Van Rooyen, M., Winterkorn, H. F. Theoretical and Practical Aspects of the Thermal Conductivity of Soils and Similar Granular Systems. HRB Bull. 168, p. 143-205, 1957.
29. Van Rooyen, M., and Winterkorn, H. F. Structural and Textural Influences on Thermal Conductivity of Soils. HRB Proc., Vol. 38, p. 576-621, 1959.
30. Willis, W. O., Parkinson, H. L., Carlson, C. W., and Hans, H. J. Water Table Changes and Soil Moisture Loss Under Frozen Conditions. Soil Science, Vol. 98, p. 244-248, 1964.
31. Winterkorn, H. F. Climate and Highways. Proc., American Geophysical Union, Part 3, p. 405-411, 1944.
32. Winterkorn, H. F. Water Movement Through Porous Hydrophilic Systems Under Capillary, Electrical and Thermal Potentials. American Society for Testing and Materials, Spec. Tech. Publ. No. 163, p. 27-35, 1954.
33. Winterkorn, H. F. Soil Water Interactions and Water Conduction in Soils. Princeton Univ. Conf. on Water Supply, p. 43-83, 1958.
34. Winterkorn, H. F. Mass Transport Phenomena in Moist Porous Systems as Viewed from the Thermodynamics of Irreversible Processes. HRB Spec. Rept. 40, p. 324-338, 1958.
35. Winterkorn, H. F. Behavior of Moist Soils in a Thermal Energy Field. Clay and Clay Minerals, Vol. 9, p. 85-103, 1962.
36. Yoder, E. J. Principles of Pavement Design. John Wiley, p. 123-143, 1959.

Effect of Temperature on Some Engineering Properties of Clay Soils

JOAKIM G. LAGUROS, Associate Professor of Civil Engineering, University of Oklahoma

The engineering properties of soils are generally measured in the laboratory at room temperature. However, seasonal changes modify the thermal environment of the soils in the field and therefore a concern as to the type and degree of influence of the temperature changes on the engineering properties of soils is justifiably expressed.

In an attempt to assess this influence, laboratory studies were conducted on four clay soils—a kaolinitic, an illitic, a montmorillonitic, and a montmorillonitic-illitic—at temperatures of 35, 70, and 105 F with ± 2 F deviation. The standard laboratory tests were run on remolded specimens of soils compacted at their maximum density and optimum moisture content, and included those tests necessary to evaluate the very fundamental properties of liquid limit, plasticity index, unconfined compressive strength, and consolidation.

In all four soils the liquid limit decreased with an increase in temperature. The plasticity index followed the same trend with the exception of the kaolinitic soil, in which the plasticity index showed a slight increase with temperature increase. The unconfined compressive strength data, contrary to other established data, indicated an increase in strength with an increase in temperature. The illitic soil, however, deviated from this tendency by showing a parabolic type behavior with the highest value at 72 F. The void ratio-pressure relationships resulted in a family of somewhat parallel curves. For the kaolinitic and montmorillonitic soils the curves at low temperature were found to be above those at high temperature. On the other hand, for the illitic and montmorillonitic-illitic soils the void ratio-pressure curve at 105 F was between the 72 F and 35 F curves, with the 72 F curve occupying the lowest level.

It is concluded that since slightly higher densities were observed with temperature increases, the thermal energy effects were overcompensated.

•IN ENGINEERING practice, design values used for soil properties are those determined either in the field or the laboratory without due regard to temperature. However, in testing for research into fundamental soil behavior, it has become apparent that temperature is an important parameter. To bridge this gap interest has recently (1, 2, 4, 5, 6, 7, 8, 9) been shown in assessing the influence of temperatue on soil engineering properties.

The present study is an attempt to further help in evaluating temperature effects on soils. It is limited to clay soils primarily because clay plays an especially energetic role in soil behavior.

METHODS OF INVESTIGATION

Materials

Four C-horizon soils varying primarily in type and amount of clay were selected. Their properties are given in Table 1.

Laboratory Tests

The standard laboratory tests performed on all four soils were the liquid limit, the plastic limit, the unconfined compressive strength, and the consolidation tests. All specimens were tested at 35, 70, and 105 F with ± 2 F deviation. While this selection seems rather arbitrary, it reflects the range within which construction in the field takes place. The two extreme values of the temperature range and control of temperature were maintained by a heating and cooling unit (Therm-o-Rite Products Co.).

As indicated in Figure 1, the liquid limit and plastic limit tests were run in a small chamber. The equipment and materials were placed in the chamber 3 hours in advance of testing to bring them to the desired temperature.

The unconfined compressive strength test was performed in a closed Lucite cylinder on remolded specimens compacted to maximum density at optimum moisture content using the Harvard miniature compaction apparatus. The soil, water, and equipment had been maintained at the respective desired temperature, but compaction took place at ro temperature. Consequently, it will be logical to assume that the 35 F specimens were prepared at a temperature slightly higher than 35 F and the 105 F specimens at a temperature slightly less than 105 F. As soon as the specimens were prepared, they were stored in the chamber having the desired temperature and kept for 2 hours prior to being tested. The test densities were also recorded.

The consolidation test was performed on remolded specimens compacted statically in the consolidometer ring (2.5 in. in diameter, 1 in. high) to maximum density at optimum moisture content. In the preparation of specimens, the same temperature control was exercised as in the unconfined compressive test with the exception that the compacting machine was at room temperature. As soon as the specimens were prepared, both the ring and the specimens were immersed and maintained in water for 24 hours to obtain saturation at the designated appropriate temperature. The standard consolidation test was run in a box (Figs. 2, 3), containing water whose temperature

TABLE 1

PROPERTIES OF SOILS

Sample designation	N. Carolina clay	Illinois clay	Texas clay	Oklahoma clay
Sampling location	Durham Co., N. C.	Livingston Co., Ill.	Harris Co., Tex.	Payne Co., Okla.
Soil series	White Store	Clarence	Lake Charles	Renfrow
Laboratory designation	A	B	C	D
Textural composition, percent				
Gravel (above 2 mm)	0.0	0.0	0.0	0.0
Sand (2-0.074 mm)	13.0	10.0	3.0	2.0
Silt (0.074-0.005 mm)	22.0	38.0	36.0	24.6
Clay (below 0.005 mm)	65.0	52.0	61.0	73.4
Clay (below 0.002 mm)	50.0	34.0	40.0	5.0
Physical properties				
Liquid limit, percent	54	32	65	50
Plastic limit, percent	25	17	18	22
Plasticity index	29	15	47	28
Chemical properties				
C.E.C.[a], m.e./100 g	36.2	10.8	27.3	18.5
Carbonates	0.9	22.5	16.6	10.2
pH	5.4	8.3	8.2	7.5
Organic matter	0.3	0.7	0.1	0.2
Non-clay minerals[b]	Quartz, feldspar	Quartz, feldspar	Quartz, feldspar	Quartz, feldspar
Clay minerals[b]	Kaolinite-halloysite	Illite	Montmorillonite	Montmorillonite-illite
Classification				
Textural	Clay	Clay	Clay	Clay
AASHO	A-7-6 (20)	A-6 (11)	A-7-6 (20)	A-7-6 (17)
Unified	CH	CL	CH	CL

[a]Cation exchange capacity determined by the ammonium acetate (pH = 7) method on soil fraction less than 0.42 mm.
[b]X-ray diffraction analysis.

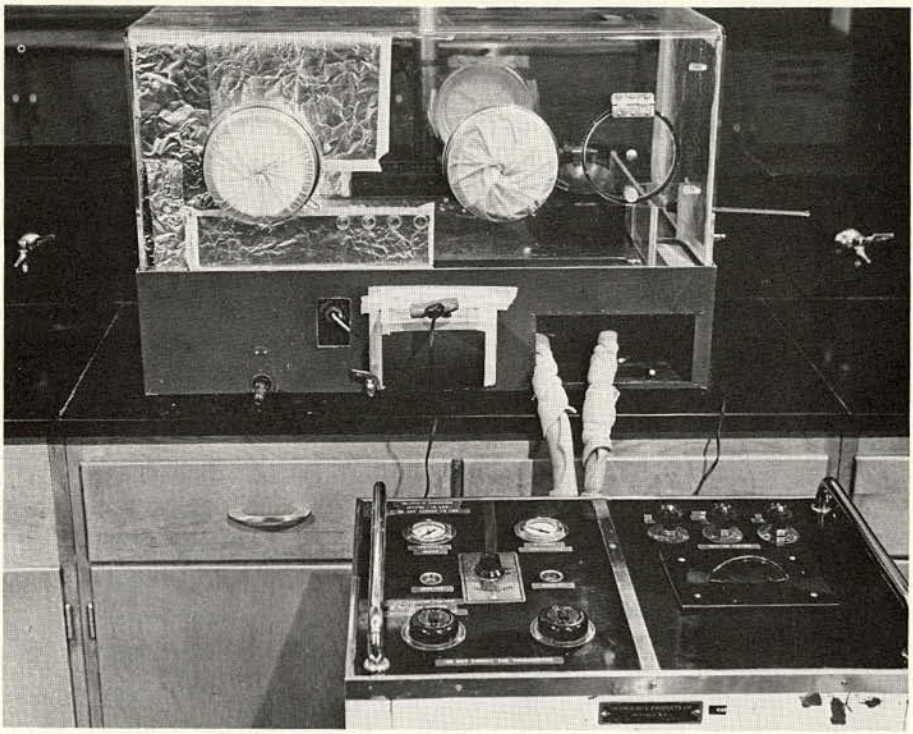

Figure 1. Incubator type chamber used for liquid limit and plastic limit test. Heating and cooling unit in the foreground.

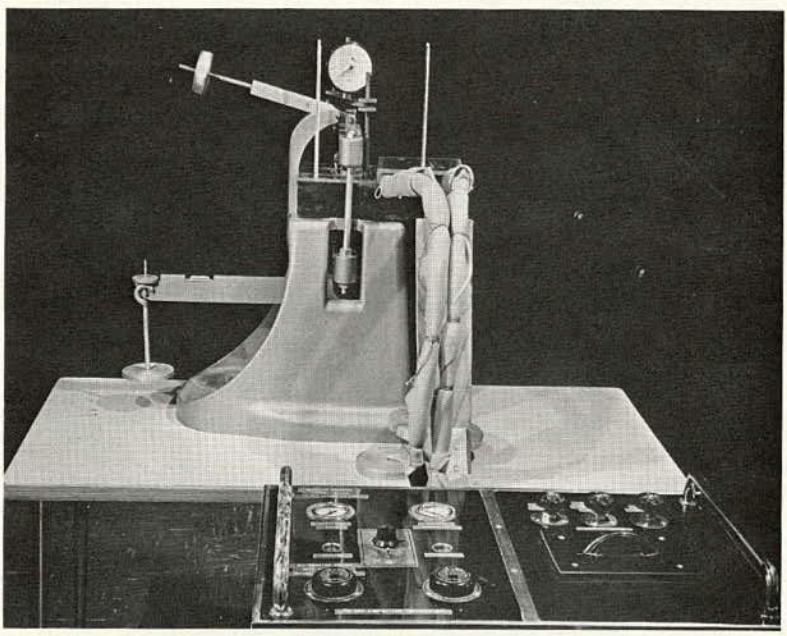

Figure 2. Consolidation test apparatus.

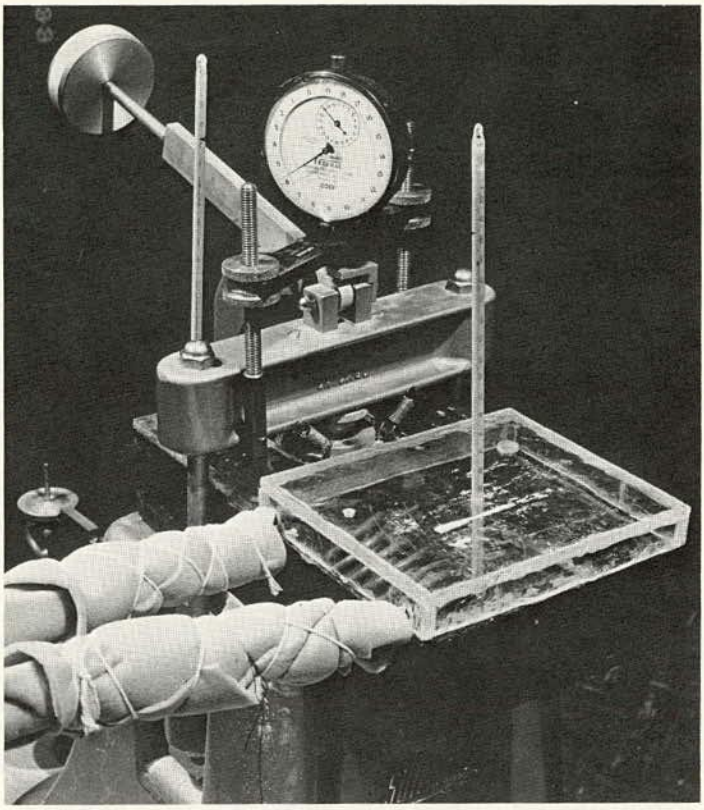

Figure 3. Temperature control during consolidation test.

was controlled by the heating unit. In the consolidation measurements the Levermatic soil test equipment (C-224) was used.

In following the one-dimensional two-way drainage procedure, 0.25, 0.50, 1.00, 2.00, 4.00, and 8.00 kg per sq cm load intensities were applied through a dead weight lever-type loading system. For each consolidation pressure, readings at total elapsed times of 0, 0.25, 0.50, 0.75, 1.00, 2.25, 4.00, 6.25, 9.00, 12.25, 16, 25, 36, 49 minutes, etc., were taken for a period of 24 hours. The consolidation response was measured in terms of the coefficient of consolidation, C_v, where

$$C_v = \frac{Th^2}{t}$$

and T = time factor, h = longest drainage path, and t = elapsed time. In calculating C_v, T_{90}, and t_{90}, the "square root of time" fitting method was used. For the liquid limit, plastic limit, and unconfined compressive strength tests, three determinations were used whereas only two were used for the consolidation test.

From the foregoing it becomes evident that the preparation of specimens did not take place at exactly the test temperatures specified. However, for the type of unsophisticated equipment used, thermometric measurements indicated that test temperature variation was limited to ± 2 F of the designated temperature of the test. Therefore, temperature effects should be interpreted with these limitations in mind and they should be looked upon as indicating a trend rather than exact quantified conclusions.

TABLE 2

SOIL ENGINEERING PROPERTIES AT VARIOUS TEMPERATURES

Soil Type Lab Designation	Temperature (F)	Liquid Limit (percent)	Plasticity Index (percent)	Uc[1] (psi)	Max. Dry Density[2] (pcf)	Optimum Moisture Content[2] (percent)	Cv[3] (10^{-4} cm^2/sec)
A	35	54	25	49	97.1		32.6
(kaolinitic)	70	54	29	52	97.7	25.8	30.7
	105	46	30	55	98.0		25.2
B	35	35	16	87	111.7		11.5
(illitic)	70	32	15	89	111.7	18.2	10.9
	105	31	5	83	111.5		11.2
C	35	80	54	60	102.2		4.1
(montmorillonitic)	70	65	47	64	102.9	22.3	2.5
	105	56	33	66	103.2		1.4
D	35	60	30	67	105.2		3.5
(montmorillonitic-illitic)	70	50	28	71	105.3	21.1	2.7
	105	48	26	72	106.1		2.9

[1]Unconfined compressive strength. [2]Harvard miniature compaction. [3]Coefficient of consolidation.

RESULTS

The summary of test results is given in Table 2.

In all four soils the liquid limit decreased with an increase in temperature (Fig. 4). Whereas in soils A and C the decrease was pronounced, in soils B and D the decrease was small, which, in view of the nature of the test, indicates a tendency rather than a decisive decrease. The plasticity index values (Fig. 5) show a definite decrease with temperature increase except for soil A; again it may be argued that this displays a tendency rather than a definite increase.

The unconfined compressive strength of the soils, as depicted in Figure 6, increased with increases in temperature. Soil B constitutes an exception in that it shows a parabolic tendency, the highest strength being observed at 70 F.

The consolidation e-log p curves for the four soils, shown in Figures 7 through 10, displayed two distinct patterns. At low temperature, soils A and C have curves above those at high temperature, whereas soils B and D deviated slightly from this trend in that the 105 F curve lies above the 70 F curve but below the 35 F curve. The same

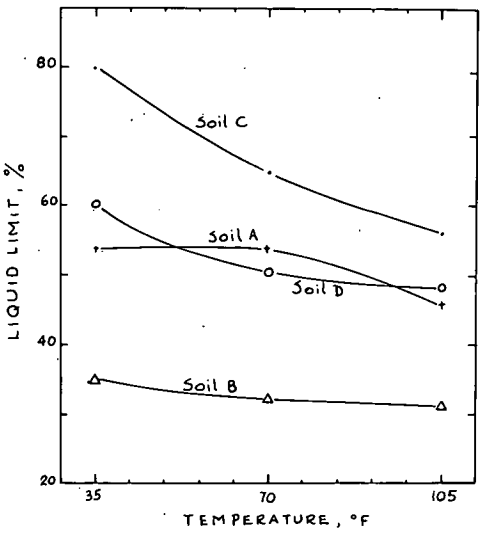

Figure 4. Effect of temperature on liquid limit.

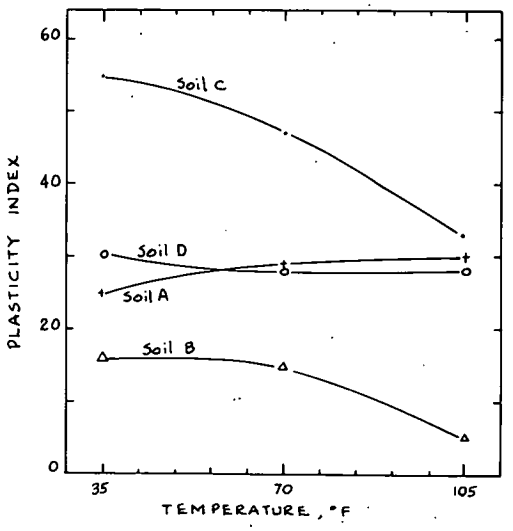

Figure 5. Effect of temperature on plasticity index.

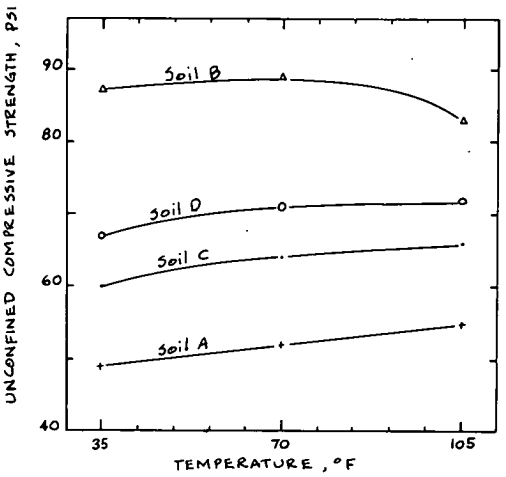

Figure 6. Effect of temperature on strength.

phenomenon was observed for the coefficient of consolidation, C_v, which decreased with higher temperatures for the A and C soils, whereas C_v values at 70 F were the lowest for the B and D soils (Fig.11).

In reviewing previous studies in this area, it is possible to summarize the temperature effects as in Table 3. The explanations for these changes are based on the Gouy-Chapman mechanism of double layer, the modification of water viscosity, and the accompanying effects on the geometric arrangement of the soil particles.

In this study the lowering of the liquid limit with high temperatures is a manifestation of the low void ratio and of the water easily draining out; the same reasoning holds true for the plasticity index. That soil A did not obey this rule, insofar as the PI is concerned, may be ascribable, if at all, to the plastic limit test during which there has probably taken place an exchange of heat between the soil and the operator's hand to such a degree that it upset equilibrium conditions.

The unconfined compressive strengths generally indicated an increase with temperature increases. This contradicts data from earlier work (1) wherein low strength at high temperatures was attributed to pore pressure increase and attendant effective stress decrease. The soils studied in this case displayed slightly higher densities (Table 2) at higher temperatures. Admittedly, the density variations are small and their dependability may be questioned in view of the experimental error. But the

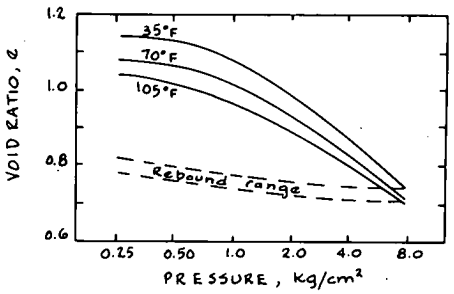

Figure 7. Consolidation curves for soil A.

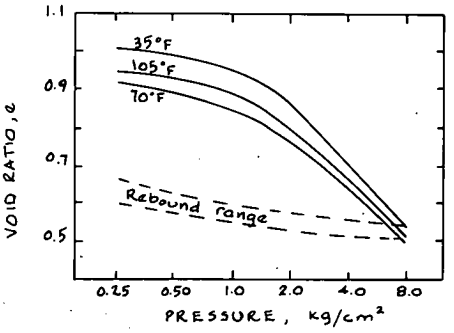

Figure 8. Consolidation curves for soil B.

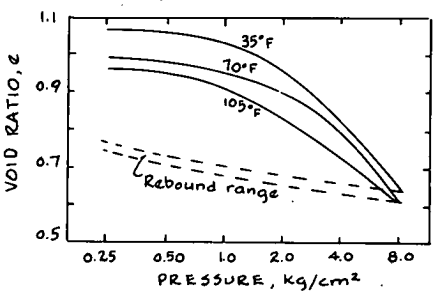

Figure 9. Consolidation curves for soil C.

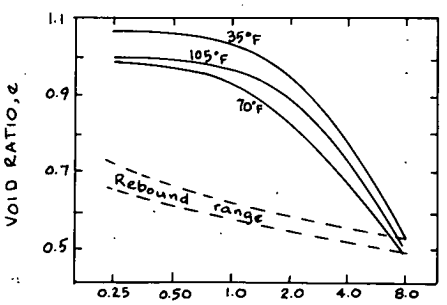

Figure 10. Consolidation curves for soil D.

TABLE 3
TEMPERATURE EFFECTS ON SOILS

Temperature	Diffuse Ion-Layer Thickness (net effect)	Soil Structure	Volume	Void Ratio	Pore Pressure	Water	Shear Strength
High	Increase	Dispersion	Compression	Low	Increase	Drains out	Low
Low	Decrease	Flocculation	Swelling	High	Decrease	Absorbed	High

density trend may be helpful in explaining the paradox of strength increase with temperature increase. The increase in thermal energy produces an interparticle bond strength decrease but at the same time there is a lowering of the void ratio. It is likely that, in the cases studied, the void ratio decrease overcompensated the bond strength decrease. That soil B behaved differently is not surprising because this illitic soil has shown peculiar behavior (3). Among the four soils used in this study, soil B had the lowest coefficient of hydraulic conductivity, 3.5×10^{-6} cm/sec (3); this may help account for the building up of uniform and nonuniform pore pressures at high temperatures that cannot be dissipated easily, and thus low shear strengths resulted.

The application of the criteria indicated in Table 3 to the consolidation characteristics of clay soils leads to two predictions. First, at high temperatures low pressures suffice to cause the same amount of consolidation as high pressures do at low temperatures; second, at low temperatures consolidation is more rapid than at higher temperatures. Both predictions seem to hold true for soils A and C. At high temperatures the occurrence of the lowering of the void ratio implies that consolidation begins at an initially lower void ratio, and it becomes evident that at high consolidating pressures the curves tend to converge, thereby minimizing the difference in temperature effects. Unfortunately, the test was not carried out beyond 8 kg/cm^2 and therefore it cannot be stated at this time whether or not the curves intersect. A similar, but somewhat less pronounced, relationship appears to exist among the coefficients of consolidation for the A and C soils. Implicit in the picture of voids ratio change is the change in soil structure. However, void ratio is not adequate to describe soil structure and it should be regarded as only a rough measure of soil structure. Soils B and D, which contain illite, departed slightly from the aforementioned description of consolidation behavior. To define what happens at 105 F is complex; it can only be traced to the peculiarity resulting from the presence of illite.

The rebound curves in all four soils present an interesting observation in that they fall, for all three temperatures, within a narrow band formed by intersecting lines. A possible explanation offered is that, once the soil is compressed to a pressure of 8 kg/cm^2, temperature effects in the decompression phase are so minimized that delineation becomes difficult.

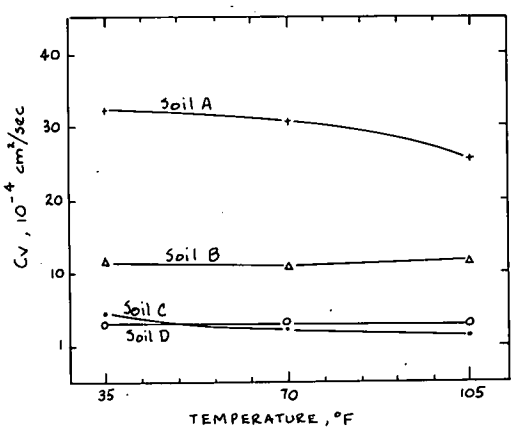

Figure 11. Effect of temperature on C_v.

To attempt to interpret and project the test data in terms of practical or field behavior of these clay soils, one is forced to accept that at high temperatures the soils display higher shearing strength and subside more, but the rate of consolidation is slower than at low temperatures. This, given the test conditions, should be looked upon as a tentative conclusion.

To substantiate and verify these findings, it will be necessary to dwell more extensively on density studies and on such other factors as activity, pH, and adsorbed

ions, in addition to the type and amount of clay mineral, in order to offer more precise explanations of the paradoxical behavior of the clays studied.

REFERENCES

1. Campanella, R. G., and Mitchell, J. K. Influence of Temperature Variations on Soil Behavior. Jour. Soil Mech. and Found. Div., ASCE, Vol. 94, No. SM3, May 1968.
2. Finn, F. M. The Effect of Temperature on the Consolidation Characteristics of Remolded Clay. Symposium on Consolidation Testing of Soils, ASTM Publ. No. 126, 1951.
3. Laguros, J. G. Response Differences in the Stabilization of Clayey Soils. Paper presented at the Second Highway Research Symposium, Rio de Janeiro, Sept. 1966.
4. Lambe, T. W. The Structure of Inorganic Soil. Proc. ASCE, Vol. 79, Proc. Sept. No. 315, Oct. 1953.
5. Lambe, T. W. Compacted Clay. Trans. ASCE, Vol. 125, 1960.
6. Lambe, T. W. Residual Pore Pressures in Compacted Clay. Proc. Fifth Internat. Conf. on Soil Mech. and Found. Engr., Vol. 1, 1961.
7. Mitchell, J. K., and Campanella, R. G. Creep Studies on Saturated Clays. Symposium on Laboratory Shear Testing of Soils, ASTM-NRC, Spec. Tech. Publ. No. 361, Ottawa, Sept. 1963.
8. Mitchell, J. K., Campanella, R. G., and Singh, A. Soil Creep as a Rate Process. Jour. Soil Mech. and Found. Div., ASCE, Vol. 94, No. SM1, Jan. 1968.
9. Paaswell, R. E. Temperature Effects on Clay Soil Consolidation. Jour. Soil Mech. and Found. Div., ASCE, Vol. 93, No. SM3, May 1967.

Effect of Temperature on Elasticity of Clays

SAKURO MURAYAMA, Disaster Prevention Research Institute, Kyoto University

•IN GENERAL, clays behave viscoelastically under external stress and, moreover, such behavior is affected by temperature. There is some type of clay whose stress-strain relation can be expressed by a linear relation with a parameter of time, as long as the applied external stress is less than a certain critical value or the upper yield value. The viscoelastic behavior of the clay skeleton can be analogized with the behavior of the mechanical model. The writer has previously proposed (1) a model that consists of an independent Hookean spring E_1 connected in series with a modified Kelvin element as shown in Figure 1. The latter element is composed of a Hookean spring E_2, a slider σ_2, and a dashpot whose coefficient is obtained from the following equation applying the theory of rate process:

$$\eta = \frac{\sigma_2}{d\epsilon_2/dt} = \frac{\sigma_2}{2A \cdot \sigma_{20} \cdot \sinh(B\sigma_2/\sigma_{20})} \tag{1}$$

where σ_2 is the axial compressive stress distributed on the dashpot, σ_{20} is the magnitude of σ_2 at the initial time when external stress is applied, and ϵ_2 is the axial strain produced in the dashpot. A and B are rheological constants expressed as the following relations:

$$\left.\begin{aligned} A &= A_0 \frac{\varkappa T}{h} \cdot \exp\left(\frac{-E_0}{\varkappa T}\right) \\ B &= \frac{B_0}{T} \end{aligned}\right\} \tag{2}$$

where A_0 and B_0 are constants dependent on soil structure, $\varkappa$ is Boltzmann's constant, h is Planck's constant, T is the absolute temperature of the clay, and E_0 is the free energy of activation. As represented by Eq. 1, this viscosity of clay is a non-Newtonian viscosity or a kind of structural viscosity. This model showed good agreement with the experimental results on undisturbed Osaka marine clay, but further adaptability for other types of clay will be checked in the future.

The influence of temperature on the mechanical behavior of clay has been theoretically explained by several investigators (2, 3), mostly from the point of view of the thermal dependence of the viscosity of clay, but that of the elasticity of clay does not seem to have been thoroughly investigated yet. In these circumstances, the purpose of this study is to investigate the thermal effect on the elasticity of clay, expressed as the independent Hookean spring E_1 and the Hookean spring E_2 in the Kelvin element, by applying the theoretical relations existing under the stress relaxation test.

In the process of mobilizing clay particles, the particles are subjected to the apparent elastic resistance due to the imbalance of the attractive and repulsive physicochemical forces induced by the surrounding particles as well as the viscous resistance due to the adsorbed water interposed between the particles. Therefore, the elasticity of a clay skeleton represented as the spring elements in the mechanical model may be partly due to the flexure of thin plate-like clay particles, but a more effective cause of such elasticity is rather supposed to be due to the physicochemical interparticle force. Moreover, according to the Gouy-Chapman theory, an increase in temperature reduces the double layer thickness and this in turn causes the reduction in the electric repulsion between clay particles (4). Therefore, it may be expected that the elasticity of clay or the elastic constants of the springs in the model can be influenced by temperature.

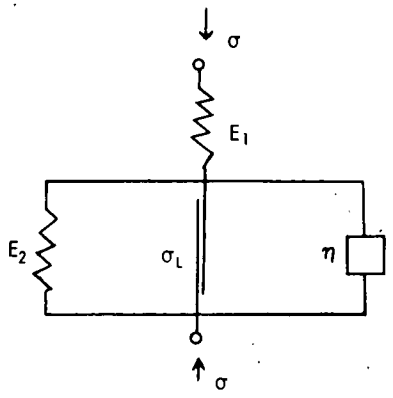

Figure 1. Mechanical model of clay skeleton.

THEORETICAL RELATION UNDER STRESS RELAXATION

The critical compressive stress below which a linear stress-strain relation holds is denoted as the upper yield value σ_u. The model shown in Figure 1 is valid when $\sigma < \sigma_u$. If $B \geq 2$, or

$$B > B\sigma_2/\sigma_{20} \geq 2 \tag{3}$$

the following approximation holds for Eq. 1 within an error of 2 percent:

$$2 \sinh (B\sigma_2/\sigma_{20}) \doteq \exp (B\sigma_2/\sigma_{20}) \tag{4}$$

Therefore the mechanical behavior of the model can be expressed by the following equations:

$$\left.\begin{aligned} \epsilon &= \epsilon_1 + \epsilon_2 \\ \epsilon_1 &= \sigma/E_1 \\ d\epsilon_2/dt &= A \cdot \sigma_{20} \cdot \exp (B\sigma_2/\sigma_{20}) \end{aligned}\right\} \tag{5}$$

where

$$\sigma_2 = \sigma - \sigma_\ell - E_2 \epsilon_2, \quad \sigma_{20} = \sigma - \sigma_\ell$$

The relaxation of stress in a clay skeleton under a constant axial initial strain ϵ_0 can be analyzed through solution of Eq. 5 under the following condition:

$$\epsilon = \epsilon_1 + \epsilon_2 = \epsilon_0 \tag{6}$$

Since ϵ_2 is zero at t = 0, stress in a clay skeleton at t = 0 is obtained as

$$\sigma_{t=0} = E_1 \epsilon_0 \tag{7}$$

Substituting the second equation of Eq. 5 and Eq. 6 into the fourth equation of Eq. 5 σ_2 becomes

$$\sigma_2 = [(E_1 + E_2)\sigma - E_1\sigma_\ell - E_1E_2\epsilon_0]/E_1 \tag{8}$$

Similarly, from Eqs. 5 and 7, σ_{20} becomes

$$\sigma_{20} = E_1\epsilon_0 - \sigma_\ell \tag{9}$$

By substitution of Eqs. 8 and 9 into Eq. 3, the validity condition for σ is transformed as

$$\epsilon_0 E_1 > \sigma \geq \frac{E_1E_2}{E_1 + E_2}\left[\epsilon_0\left(1 + \frac{2E_1}{BE_2}\right) + \frac{\sigma_\ell}{E_2}\left(1 - \frac{2}{B}\right)\right] \tag{10}$$

The fundamental equation of stress relaxation is obtained by eliminating ϵ_2 from the third equation of Eq. 5 as follows, provided that B is large and exp (– B) is negligibly small:

$$\left.\begin{aligned} \sigma &= \frac{E_1E_2}{E_1 + E_2}\left[\left(\epsilon_0 + \frac{\sigma_\ell}{E_2}\right) - \left(\epsilon_0 - \frac{\sigma_\ell}{E_1}\right)\frac{E_1}{BE_2}\log (Rt)\right] \\ R &= A \cdot B \cdot (E_1 + E_2) \end{aligned}\right\} \tag{11}$$

where

If σ is beyond the limit expressed by Eq. 10 and at $t \to \infty$, σ is obtained by substituting $\sigma_2 = 0$ into Eq. 8 as follows:

$$\sigma_{t \to \infty} = \frac{E_1 E_2}{E_1 + E_2} \left(\epsilon_0 + \frac{\sigma_\ell}{E_2} \right) \tag{12}$$

It is shown from Eqs. 11 and 12 that the stress σ decreases linearly with the logarithm of time until σ reaches the limiting value expressed by Eq. 10 and finally it relaxes to a finite value of $\sigma_{t \to \infty}$. Because this relation is valid only when $\sigma \leq \sigma_u$, the critical initial strain ϵ_{oc} beyond which the instantaneous axial stress exceeds σ_u is given by

$$\epsilon_{oc} = \sigma_u / E_1 \tag{13}$$

Eliminating ϵ_0 from Eqs. 7 and 12, we obtain

$$E_2 = \frac{\sigma_{t \to \infty} - \sigma_\ell}{\sigma_{t=0} - \sigma_{t \to \infty}} \cdot E_1 \equiv \alpha \cdot E_1 \tag{14}$$

By differentiation of Eq. 11, we obtain

$$-\frac{d\sigma}{d \log t} = \frac{E_1^2}{B(E_1 + E_2)} \left(\epsilon_0 - \frac{\sigma_\ell}{E_1} \right) \tag{15}$$

Substituting Eqs. 2, 7, and 14 into Eq. 15, we obtain

$$-\frac{d\sigma}{d \log t} = \frac{\sigma_{t=0} - \sigma_{t \to \infty}}{B_0} \cdot T = \frac{\sigma_{t \to \infty} - \sigma_\ell}{\alpha \cdot B_0} \cdot T \tag{16}$$

If a certain temperature T_a deg K is adopted as a standard, Eq. 16 is transformed as

$$\left.\begin{aligned} \sigma_{t \to \infty} &= \frac{k \cdot \alpha \cdot B_0}{T_a} \left(-\frac{d\sigma}{d \log t} \right) + \sigma_\ell \\ \text{where} \quad k &= T_a / T \,, \quad \alpha = E_2 / E_1 \end{aligned}\right\} \tag{17}$$

From Eq. 14, $\sigma_{t \to \infty}$ is given by

$$\sigma_{t \to \infty} = \frac{\alpha}{1 + \alpha} \sigma_{t=0} + \frac{1}{1 + \alpha} \sigma_\ell \tag{18}$$

When the second term $\sigma_\ell / (1 + \alpha)$ of the right-hand side of Eq. 18 is negligibly small compared with the term of the left-hand side, Eq. 18 can be written approximately as

$$\sigma_{t \to \infty} = \frac{\alpha}{1 + \alpha} \sigma_{t=0} \tag{19}$$

STRESS RELAXATION TESTS UNDER UNIAXIAL STRAIN

The specimens used for stress relaxation tests were of undisturbed clay obtained from the Osaka diluvial layer. The results of physical tests of the clay are as follows: specific gravity, 2.57; L. L., 76.2 percent; P. L., 30.7 percent; contents of clay, silt, and sand, 45, 38, and 17 percent respectively.

The maximum preconsolidation stress measured by oedometer tests is 3.8 kg/cm^2. The lower yield value σ_ℓ measured by flow tests is 0.01 kg/cm^2. The upper yield value σ_u is determined as the stress corresponding to the first inflection point of the stress-

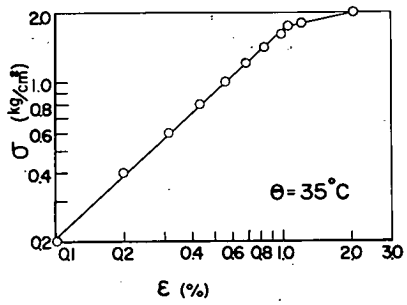

Figure 2. Logarithmic relation of stress vs strain in stress-controlled compression test to determine upper yield value.

strain curve on logarithmic paper, which is obtained by a stress-controlled undrained test whose load is added in equal increments at uniform time intervals. By this procedure σ_u is determined as 1.75 kg/cm^2 at 35 C, as shown in Figure 2. The cylindrical clay specimen (height 8.0 cm, diameter 3.57 cm) was covered by a thin rubber membrane and was placed in a triaxial compression cell of a plastometer. This plastometer (2) consists of a triaxial compression testing unit and a recording and controlling unit. In the case of the stress relaxation test, a constant axial deformation applied on the specimen can be read on the scale indicator of the plastometer and its response in the axial stress is automatically and continuously recorded by the recording unit. In the cell of the testing unit, water of definite temperature but of no pressure was circulated to keep the specimen at constant temperature. After the temperature of the specimen reached the equilibrium state, constant axial strain ϵ_0 was instantaneously applied on the specimen under undrained condition, then the axial stress σ was recorded electronically with the time by the plastometer.

Examples of the results of the stress relaxation tests at 30 C for various initial strains (ϵ_0 = 0.25, 0.5, 0.75, 1.00, 1.50, and 2.00 percent) reproduced from the recrods are shown in Figure 3. This figure shows that the axial stress σ decreases proportionately with the logarithm of time for some period and finally approaches a finite value $\sigma_{t\to\infty}$ as predicted by Eqs. 11 and 12. Therefore from the record of the plastometer

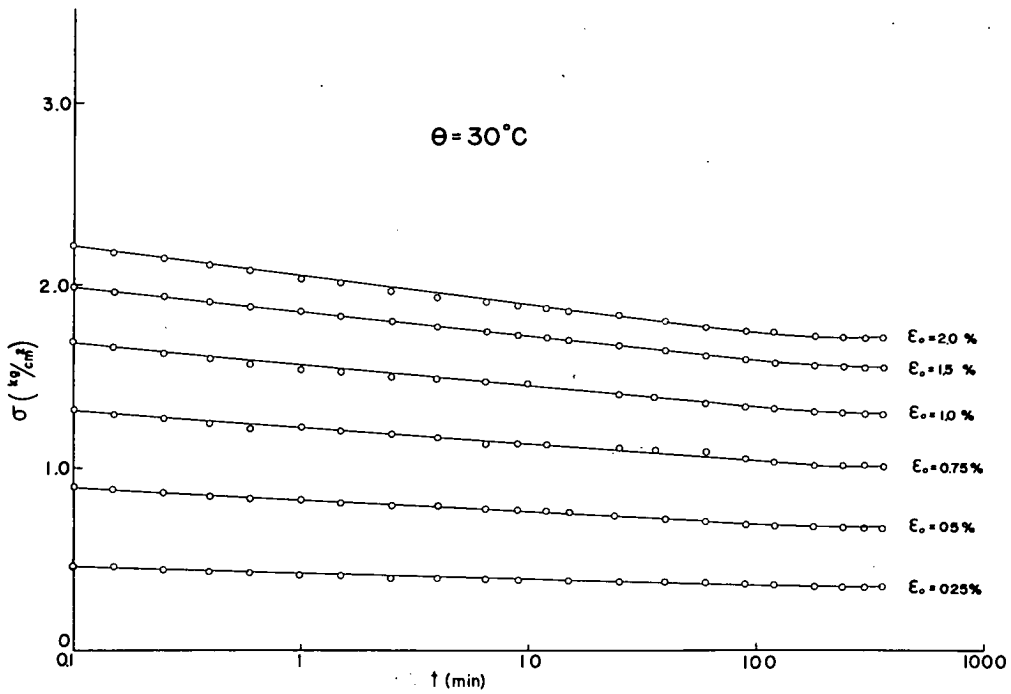

Figure 3. Curves representing axial stress vs elapsed time relation during stress relaxation.

the initial axial stress $\sigma_t = 0$ caused by the instantaneously applied strain can be read and from Figure 3 the rate of stress relaxation $d\sigma/d\log t$ and the final axial stress $\sigma_{t\to\infty}$ can be measured for each applied initial strain ϵ_0 and each temperature θ C.

EXPERIMENTAL RESULTS

The similar stress relaxation tests indicated in Figure 3 were performed under various temperatures, namely θ = 10, 20, and 40 C. From these tests, values of $\sigma_t = 0$, $\sigma_{t\to\infty}$, and $d\sigma/d\log t$ were observed in the various cases of ϵ_0 and θ. The following consideration will be developed on the basis of these values.

If the standard temperature T_a ($T_a = 273 + \theta_a$) defined in Eq. 17 is adopted as 313 (θ_a = 40 C, T_a = 273 + 40 = 313), the value of K in Eq. 17 is given by

$$K = \frac{T_a}{T} = \frac{313}{\theta + 273}$$

According to the theoretical consideration, the relation between $d\sigma/d\log t$ and $\sigma_{t\to\infty}$ and that between $\sigma_{t=0}$ and $\sigma_{t\to\infty}$ can be represented by Eqs. 17 and 19, as long as the applied initial strain ϵ_0 is less than the critical strain expressed by Eq. 13. Therefore if observed values of $K\left(-\frac{d\sigma}{d\log t}\right)$ and $\sigma_t = 0$ are plotted against $\sigma_{t\to\infty}$ on a natural scale, these relationships are expected to be represented by straight lines extending to a certain limit. Figure 4 shows these relationships obtained by plotting all the observed values. Since the plotted points within a certain limit will lie along two straight lines starting from the vicinities of the origin of axes as predicted by Eqs. 17 and 19, the experimental relations can be expressed by the following linear equations independent of temperature:

$$\left.\begin{aligned} \sigma_{t\to\infty} &= (2/3)\cdot\ \sigma_t = 0 \\ \sigma_{t\to\infty} - \sigma_\ell &\doteqdot 9.5\left[K\left(-\frac{d\sigma}{d\log t}\right)\right] \\ \sigma_\ell &\doteqdot 0.01\ \mathrm{kg/cm^2} \end{aligned}\right\} \qquad (20)$$

Referring the first equation in Eq. 20 to Eq. 19, α is given by

$$\alpha \doteqdot 2 \quad (\text{where } \alpha = E_2/E_1) \qquad (21)$$

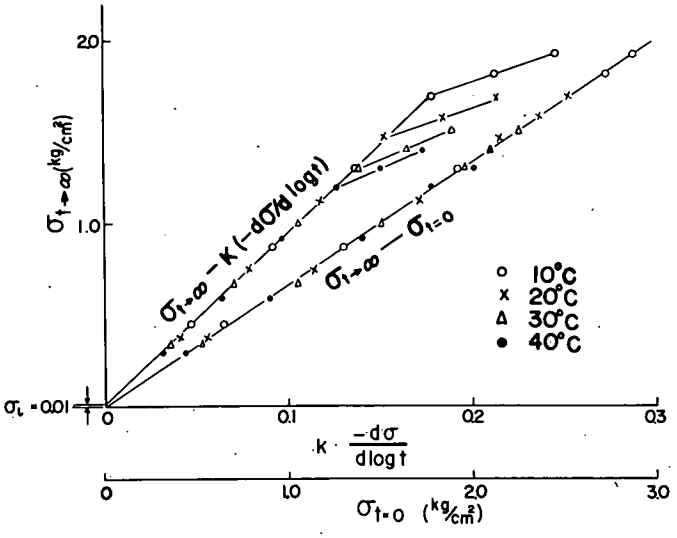

Figure 4. Relationship among $K\cdot(-d\sigma/d\log t)$, $\sigma_{t=0}$ and $\sigma_{t\to\infty}$ under various temperatures.

This relation shows that the values of elastic moduli E_1, E_2 are proportional to each other irrespective of temperature. Moreover, in Figure 4. the experimental relationship between t = 0 and $\sigma_{t\to\infty}$ is represented by a straight line for whole value of $\sigma_{t=0}$. From this result, therefore, the linear relation between E_1 and E_2 seems to be still valid even if ϵ_0 exceeds the critical strain ϵ_{oc}.

While the linear relationship between $K(-d\sigma/d \log t)$ and $\sigma_{t\to\infty}$ is valid only within a certain limit of the straight line as shown in Figure 4, in the region beyond this limit the relationship deviates from this straight line and is represented by a short, gently inclined line. Therefore the relation between $d\sigma/d \log t$ and $\sigma_{t\to\infty}$ seems to be affected by the applied initial strain ϵ_0

In order to investigate the effects of ϵ_0 on the values of $\sigma_{t=0}$, $\sigma_{t\to\infty}$, and $d\sigma/d \log t$, these experimental values are plotted against ϵ_0 as shown in Figures 5, 6, and 7. These figures show that these relationships are linear within the same strain range up to about 0.95 percent of ϵ_0, where they deflect to become a gentler gradient. Since the strain corresponding to the deflection point should be the critical initial strain ϵ_{oc}, it can be said that the value of ϵ_{oc} is kept constant independent of temperature.

In order to observe the influence of temperature on $\sigma_{t=0}$, $\sigma_{t\to\infty}$, and $d\sigma/d \log t$, Figures 5, 6, and 7 are rearranged as shown in Figures 8, 9, and 10, respectively.

From each set of $\sigma_{t=0}$ lines in Figure 5 and $\sigma_{t\to\infty}$ lines in Figure 6 corresponding to the same temperature, the elastic moduli E_1 and E_2 at this temperature can be computed through Eqs. 7, 19, and 21. In Figure 11 the elastic moduli thus computed are plotted against ϵ_0. From these figures, it is observed that E_1 and E_2 at a certain temperature are kept constant within the limit of ϵ_{oc}, but beyond this limit they decrease with the increase of ϵ_0. This suggests that the fracture in the clay skeleton proceeds with the applied strain exceeding the value of ϵ_{oc}. The effect of temperature on the elastic moduli is shown in Figure 12, in which the constant elastic moduli shown in Figure 11 are plotted against their respective temperatures. From these figures it can be concluded that the elasticity of clay decreases with the increase in temperature.

As stated, the value of ϵ_{oc} is kept constant independent of temperature and E_1 at a certain temperature is also kept constant as long as ϵ_0 is less than ϵ_{oc}, and therefore the value of E_1 at a certain temperature can be calculated by the data shown in Figure 2. In Figure 2, since the upper yield value of this clay is 1.75 kg/cm^2 at 35 C, the value of E_1 at this temperature

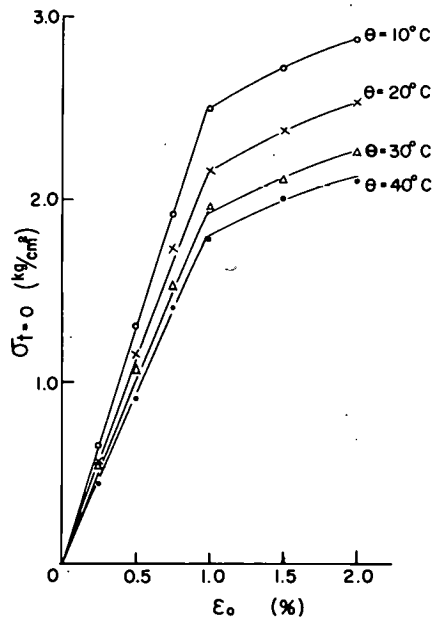

Figure 5. Relationship between initial axial stress $\sigma_{t=0}$ and initially applied axial strain ϵ_0.

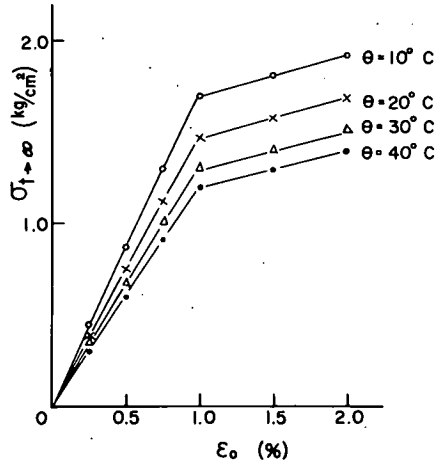

Figure 6. Relationship between final axial stress $\sigma_{t\to\infty}$ and initially applied axial strain ϵ_0.

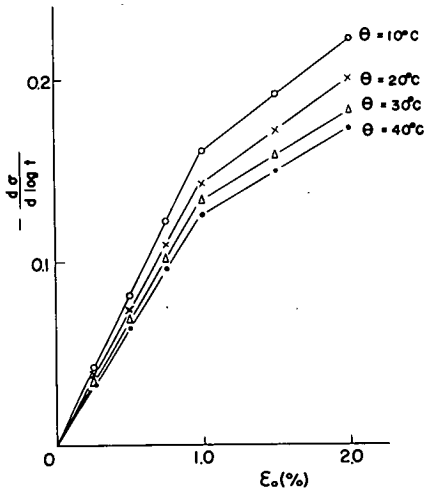

Figure 7. Relationship between rate of stress relaxation $d\sigma/d \log t$ and initially applied axial strain ϵ_0.

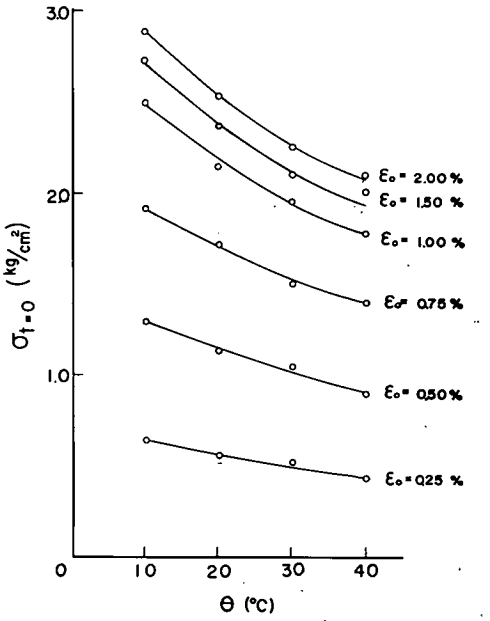

Figure 8. Relationship between initial axial stress $\sigma_{t=0}$ and temperature θ.

can be calculated by Eq. 13:

$$E_1 = \sigma_u/\epsilon_{oc} \doteq 1.75/0.0095 = 185 \text{ kg/cm}^2 \tag{22}$$

Referring the theoretical equation of Eq. 17 to the experimental relations of Eq. 21 and the second equation of Eq. 20, a rheological constant B_0 can be obtained as follows:

$$B_0 = \frac{9.5 \cdot T_a}{\alpha} = \frac{9.5}{2} T_a = 4.75\ T_a \tag{23}$$

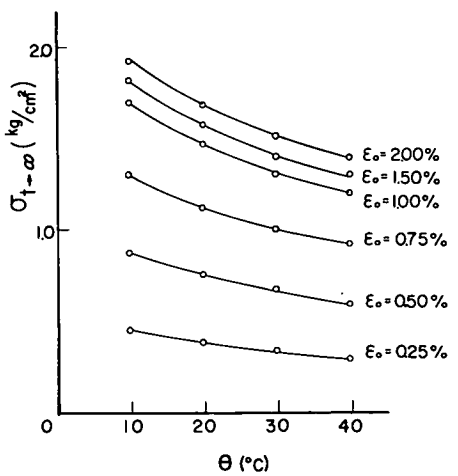

Figure 9. Relationship between final axial stress $\sigma_{t\to\infty}$ and temperature θ.

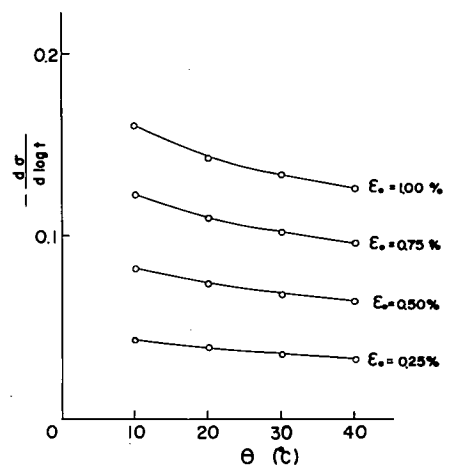

Figure 10. Relationship between rate of stress relaxation $d\sigma/d \log t$ and temperature θ.

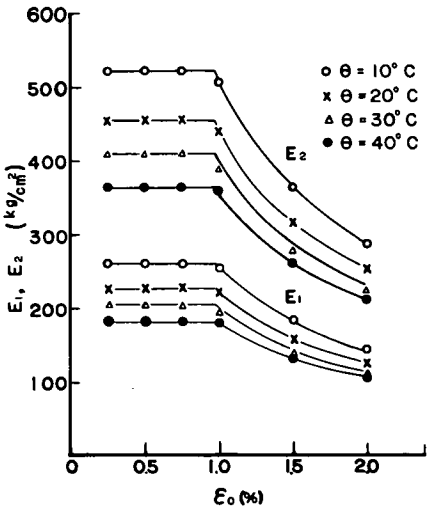

Figure 11. Elastic moduli related to initially applied strain under various temperatures.

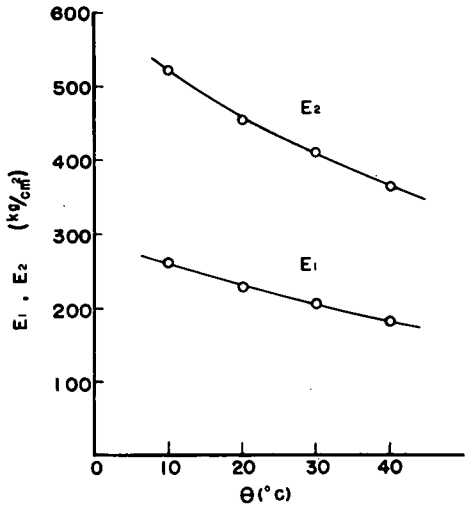

Figure 12. Relationship between elastic moduli of the mechanical model shown in Figure 1 and temperature.

Hence B is expressed as

$$B = B_0/T = 4.75 \cdot 313/(\theta + 273) \tag{24}$$

Computed values of B from Eq. 23 for θ = 10, 20, 30, and 40 C are 5.25, 5.07, 4.90, and 4.75 respectively. This relation is represented by a curve in Figure 13.

RELATION BETWEEN THE RESULTS OF STRESS RELAXATION TESTS AND FLOW TESTS

Solving Eq. 5 under the condition of σ = constant, the equation for normal flow is obtained as

$$\epsilon = \frac{\sigma}{E_1} + \frac{\sigma - \sigma_l}{E_2} + \frac{\sigma - \sigma_l}{BE_2} \log(A \cdot B \cdot E_2 \cdot t) \tag{25}$$

By the differentiation, we get

$$\frac{1}{BE_2} = \frac{d\epsilon}{d \log t} \cdot \frac{1}{\sigma - \sigma_l} \tag{26}$$

The uniaxial compression flow tests under undrained conditions were performed on the same clay sample used on the stress relaxation tests. Figure 14 is the relationship between $d\epsilon/d \log t$ and applied stress σ obtained by the flow tests at 20 C. From this figure, the lower yield value σ_l is read ad 0.01 kg/cm^2. Figure 15 shows curves representing the flow strain ϵ against time t relation obtained by the flow test of σ = 1 kg/cm^2 under various temperatures (θ = 10, 20, 30, and 40 C). Applying the value of $d\epsilon/d \log t$ in Figure 15 to Eq. 26, BE_2 can be computed.

In the flow test shown in Figure 15, the initial axial strain $\epsilon_{t=0}$ when the load is applied was also observed for each temperature condition. Measured values of $\epsilon_{t=0}$ for θ = 10, 20, 30, and 40 C were 0.393, 0.419, 0.623, and 0.705 percent, respectively. Applying these initial strains to Eq. 7, values of E_1 are obtained. Besides, since Eq. 21 may also be valid for this clay under the flow testing, E_2 can be obtained by multiplying the E_1 obtained above by α. From the values of BE_2 and E_2, B can be computed

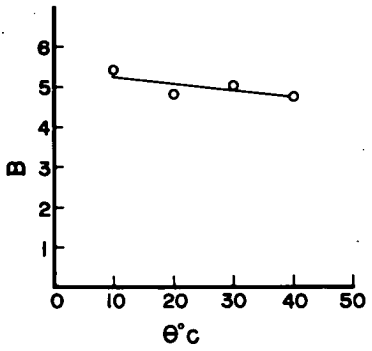

Figure 13. Relationship of rheological constant B vs temperature θ.

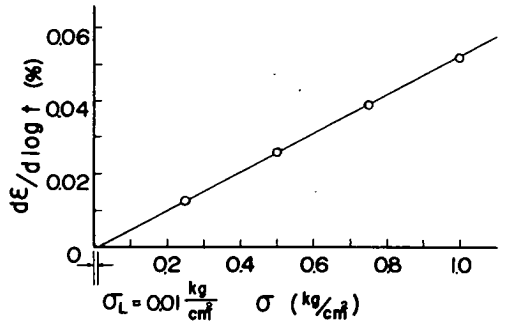

Figure 14. Relationship between rate of flow strain dε/d logt t and applied σ obtained by flow tests (20 C).

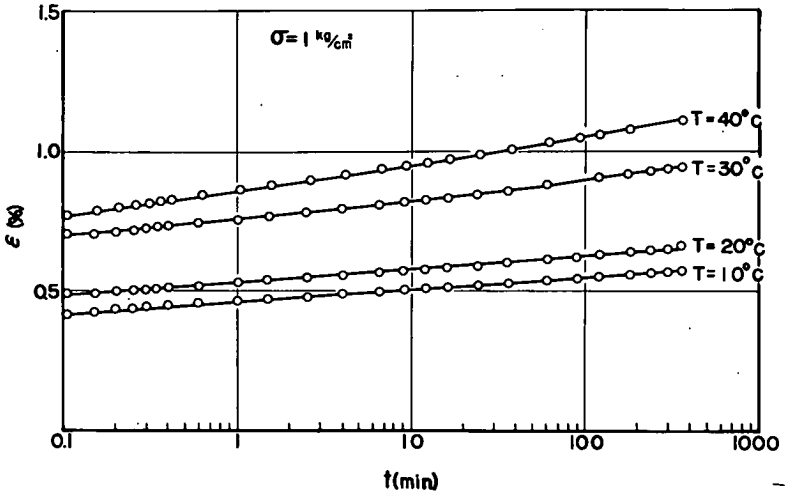

Figure 15. Curves representing axial strain ε vs time t relation during flow under various temperatures.

for each temperature condition, and the computed values of B are plotted in Figure 13 as points. In the figure, these points do not lie well on the line obtained by the stress relaxation tests. But this discrepancy may be supposed to be due mainly to the heterogeneity of the undisturbed diluvial clay sample.

CONCLUSIONS

Because clay is a viscoelastic material, it is necessary to investigate its mechanical behavior from the point of view of its elasticity as well as its viscosity. The mechanical behavior of the clay skeleton whose stress and strain are expressed by a linear relation with a parameter of time has been simulated by the model shown in Figure 1. The viscosity of clay is influenced by temperature as suggested in the flow behavior at various temperatures. Similarly, the effect of temperature on the elasticity of clay can be investigated by the behavior on the stress relaxation tests at various temperatures. In this study the effect of temperature on the elastic moduli in the model is investigated. The main results obtained are as follows:

1. The behavior of Osaka marine clay under the stress relaxation test is well predicted by the mechanical model proposed by the writer.

2. As the value of the rheological constant B obtained by flow tests practically concides with that obtained by stress relaxation tests, the equations of Eq. 5 are verified to express the behaviors in both testing procedures, irrespective of temperature.

3. Elastic moduli E_1 and E_2 are kept constant within the limit of a critical initial strain ϵ_{oc}, but beyond this limit they decrease with the increase of initial strain. The latter behavior suggests the occurrence of a fracture in a clay skeleton

4. The critical initial strain ϵ_{oc} is kept constant independent of temperature.

5. Ratio of E_1 to E_2 is constant independent of temperature and also seems to be constant independent of the magnitude of applied initial strain ϵ_0.

6. Elastic moduli E_1 and E_2 measured within the limit of ϵ_{oc} decrease with the increase in temperature.

ACKNOWLEDGMENT

The writer wishes to express his deep appreciation to Mr. Kunio Iida for his sincere cooperation in these experimental studies.

REFERENCES

1. Murayama, S., and Shibata, T. On the Rheological Characters of Clay, Part I. Bulletin No. 26, Disaster Prevention Research Inst., Kyoto Univ., 1958.
   Murayama, S., and Shibata, T. Flow and Stress Relaxation of Clays. Proc. Rheology and Soil Mech. Symposium of IUTAM, Grenoble, France, April 1964, p. 99-129.
2. Murayama, S., and Shibata, T. Rheological Properties of Clays. Proc. Fifth Internat. Conf. on Soil Mech. and Found. Eng., Paris, 1961, p. I-269-273.
3. Mitchell, J. K., Campanella, R. G., and Singh, A. Soil Creep as a Rate Process. Jour. Soil Mech. and Found. Div., ASCE, Vol. 94, No. SM1, Proc. Paper 5751, Jan. 1968, p. 231-253.
4. Lambe, T. W. The Structure of Compacted Clay. Jour. Soil Mech. and Found. Div. ASCE, Vol. 84, No. SM2, Proc. Paper 1954, May 1958, p. 1654-7.

Effect of Temperature on Strength Behavior of Cohesive Soil

CALVIN A. NOBLE and TURGUT DEMIREL,
Iowa State University

The objective of this study was to determine the effect of temperature on peak shearing strength and creep behavior of two cohesive soils and thus to characterize their behavior in terms of more fundamental parameters than is the current general practice. A simple model for soil based on bonds at interparticle contacts and an equation for rate of deformation of a stressed soil mass are proposed and shown to be consistent with observed soil behavior. The same model and equation were found to apply to soil behavior in both direct shear and creep tests.

The study was conducted on remolded, statically compacted specimens of a highly plastic clay and a low-plasticity silt using a direct shear machine. The machine was modified to permit control of specimen temperature and for use as a controlled stress apparatus as well as controlled rate of deformation.

•THE SOLUTION of engineering problems involving soils consists of three basic steps: (a) determination of soil properties, (b) determination of changes in stress or in other environmental conditions, and (c) prediction of the behavior of the soil when subjected to the changes. Of these, the weakest is the understanding of the properties of soils. Although testing methods have been refined to a high degree and behavior under known conditions can be observed, the reasons for the behavior are most often a matter of conjecture. In particular, the shearing strength of cohesive soils has been the subject of much controversy and study from the earliest consideration of soil as an engineering material. The late Donald W. Taylor (33) in 1948 wrote, ". . . no physical property of cohesive soil is more complex than the shearing strength. This property depends on many factors, and the individual factors are themselves complicated but, in addition, they are inter-related to such a degree that it is extremely difficult to understand their combined action."

One of the major reasons for the difficulty in understanding the behavior of cohesive soils is that they interact with water and show colloidal behavior. At low water contents clays exhibit high strength due to water films surrounding individual grains, but their strength rapidly decreases as water content increases. The nature of these water films and their influence on the strength behavior of clays is not well understood at present. Since the viscosity and density of water and the nature of the diffuse double layer vary with temperature, a study of the effect of temperature on the strength behavior of clays should aid in understanding fundamental properties of clays and in particular their shearing strength. The effect of temperature on the shearing strength of cohesive soils and its use to characterize their behavior has been considered relatively little to date.

THEORETICAL CONSIDERATIONS

A simple model of cohesive soil may be envisioned on the basis of bonds formed at interparticle contacts due to an oriented water structure in the adsorbed water layers adjacent to clay particles. Various concepts of the nature of the adsorbed water have been proposed (15, 18, 20, 27), and there is general agreement that at least the first

few layers of water are strongly bound to the mineral surfaces. The high energy of adsorption of water (30) seems to preclude any direct mineral-to-mineral contact but, when two particles are in close proximity, their adsorbed layers intermix and form a continuous structure in this zone causing the particles to be bonded. Similar concepts of bonding were suggested by Terzaghi (34). In a study of Lilla-Edet clay, Bjerrum and Wu (5) found a peak in the curve of cohesion vs consolidation stress for stresses below the preconsolidation pressure. They suggested rigid bonds between particles of the undisturbed clay similar to a chemical cementation. Low (19) stated that clay and other minerals affect the water molecules to give a quasi-crystalline structure which possesses greater rigidity or viscosity than ordinary water. He suggested that the orderliness of this water structure decreased with distance from the mineral surface but that the influence may be from 200 to 300 Å from the surface. Exchangeable ions tend to disrupt this structure to a degree depending on their charge, size, and degree of dissociation. This was investigated by Leonards and Andersland (16) by means of controlled freezing of soils. As more of the free water was frozen the ions were concentrated in the adsorbed layer causing greater disruption of the water structure and subsequently a decrease in strength.

There is evidence to suggest that the formation of these bonds is time-dependent. Leonards and Rahmiah (17) found a quasi-preconsolidation pressure in specimens after a period of rest under a load in the normally consolidated range. This is probably related to the gain in strength during secondary consolidation reported by Crawford (7). The phenomenon of thixotropy in clays (8, 29) also suggests time-dependence of bond formation which takes place through a gradual orientation of the water molecules into positions of least free energy under the influence of the surface energy of the particles and hydrogen bonding between the water molecules.

Stresses applied to the particulate system are transferred through these bonds and deformation of the system occurs by distortion and breaking of bonds. Deformation of a clay mass under low stresses probably occurs largely through deformation of the bonds but, in a completely random system, there will probably be some particles or domains in such an orientation that any virgin deformation will cause some bonds to break. It is, therefore, doubtful that truly elastic deformation can occur except in cases where the system has been prestressed under the same stress components. This condition is approached in preconsolidation but even then a hysteresis effect generally occurs. Higher stresses will cause disruption to most susceptible bonds first and, as stresses become higher, all bonds in the zone of stress will tend to be disrupted, giving rise to plastic deformation. With deformation, new bonds will tend to form at points of contact but, since formation is time-dependent and reorientation of particles tends to occur with deformation, the new bonds will be weaker than those existing prior to deformation. The process of shear deformation will then consist of bond deformation, bond breaking, and bond formation; the latter processes are similar to the "jumping of bonds" suggested by Tan (32). Immediately following the breaking of a bond, an unstable condition exists that may be referred to as the "activated state" in which the "contact zone" between particles consists essentially of oriented water. The resistance of deformation would be very low, depending only on the viscosity of the water. An increase in temperature increases the thermal energy of the water molecules forming the bonds and thereby effectively lowers the resistance of the system to deformation.

Since the particles in a soil mass exist in a large variety of orientations and spacings, a statistical approach is reasonable in considering the stress-deformation behavior of the mass based on a particulate model. The breaking of a bond involves overcoming an energy barrier and then reaching a new equilibrium state. Thus, the rate at which bonds are broken and reformed under a given stress condition should be related to an activation energy and should be a function of applied stress. This is illustrated in Figure 1. The energy barrier is expressed as activation free energy, which is ΔG in the unstressed mass. Application of a shearing stress tends to reduce the barrier height by an amount that is some function of the applied stress τ.

If deformation involves units surmounting an energy barrier, it may be assumed that the rate of deformation is given by an equation of the form of the Arrhenius equation,

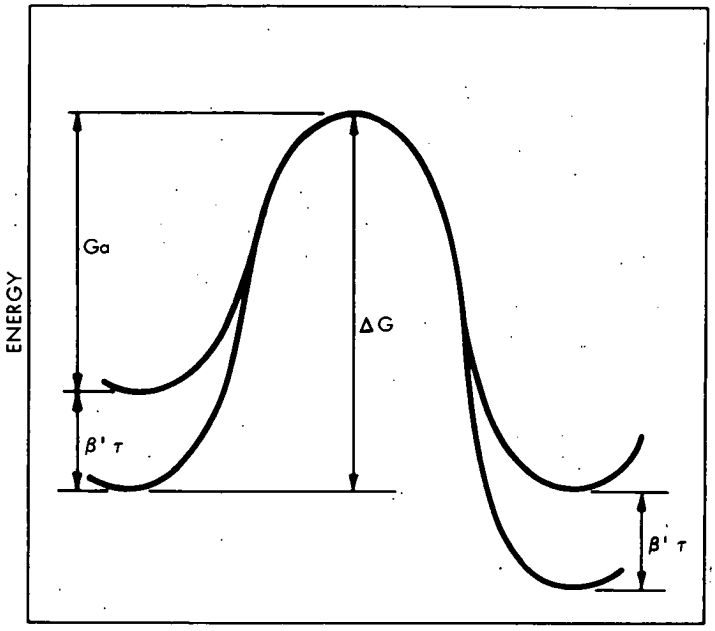

Figure 1. Energy barrier.

which suggests that the rate of deformation is proportional to the fraction of bonds with sufficient energy to surmount the energy barrier. Further, an applied shear stress, τ, will tend to decrease the effective barrier, and the amount of decrease may be represented by an energy term $\beta'\tau$. As illustrated in Figure 1, this gives

$$\Delta G = Ga + \beta'\tau \tag{1}$$

and the deformation rate may be expressed as

$$\dot{\delta} = A' \exp\left(\frac{-\Delta G + \beta'\tau}{kT}\right) \tag{2}$$

where $\dot{\delta}$ is the rate of deformation, A' is a frequency factor, and $\exp\left(\frac{-\Delta G + \beta'\tau}{kT}\right)$ is the Boltzmann factor representing the fraction of bonds with energy equal to or greater than Ga. From thermodynamics, the activation free energy may be written as

$$\Delta G = \Delta H - T\Delta S \tag{3}$$

where ΔH is the activation enthalpy, ΔS the activation entropy, and T the absolute temperature. If it is assumed that ΔS is independent of temperature, it may be included in the pre-exponential term. Further, letting

$$\frac{\beta'}{kT} = \beta \tag{4}$$

and combining Eqs. 2, 3, and 4 gives the basic equation for deformation rate,

$$\dot{\delta} = A \exp\left(\frac{-\Delta H}{kT}\right) \exp(\beta\tau) \tag{5}$$

where the pre-exponential term A includes the entropy. In the substitution of Eq. 4 it is assumed that β is independent of temperature and this assumption is substantiated by the experimental data.

Equation 5 is essentially the same as the relation suggested by Dorn in 1954 on phenomenological grounds as applying to creep of metals. Dorn was concerned about the limitation that Eq. 5 implied a finite creep rate under zero shearing stress, and to overcome this he assumed that for low stresses the exponential stress function could be replaced by a power function τ^n, thus implying different mechanisms at high and low stresses. It would appear more appropriate, based on the proposed model, to consider that the mechanism remains constant regardless of stress level. When $\tau = 0$, Eq. 5 becomes

$$\dot{\delta} = A \exp\left(\frac{-\Delta H}{kT}\right) \tag{6}$$

Substitution of experimental values of A, ΔH, and reasonable values of temperature for a clay-water system into Eq. 6 gives values of deformation rate so small as to be essentially zero. Further, when no stress is applied to the system, the deformation has no directionality and the meaning of Eq. 6 is probably related to bond changes in the system due to thermal agitation and may be related to thixotropic hardening of the material.

A similar approach to the problem of creep based on Eyring's rate process theory (9, 10, 11) has been proposed for metals (14), for bituminous materials (12), and for soils (2, 21, 23, 24, 25). In this approach, the rate of deformation is given by

$$\dot{\delta} = A \exp\left(\frac{-\Delta H}{kT}\right) \sinh\left(\frac{\beta'\tau}{kT}\right) \tag{7}$$

When shearing stress is zero, the hyperbolic sine is zero and thus the creep rate is zero. However, for stresses of engineering interest, $\beta'\tau/kT$ will have a value greater than one and therefore the hyperbolic sine is reasonably approximated by the exponential as in Eq. 5. Kauzmann (14) suggested that for some cases the exponential relation may be more valid even when stresses are relatively low.

The energy term $\beta'\tau$ introduced into Eq. 1 may be interpreted as the mechanical energy (free energy) absorbed by a bonding unit in surmounting the energy barrier. This energy is expended only if the barrier is surmounted; otherwise it is stored in deforming a bond. From the dimensionless group $\beta'\tau/kT$ it can be seen that β' has dimensions of volume. This is interpreted to be the average volume of material containing one bond. As the number of bonds per unit volume of soil increases, the size of the zone of influence of a bond decreases. This may occur as a result of increased confining pressure or a decrease in temperature. This interpretation agrees with that of Andersland and Akili (2) who refer to β' as the volume of a flow unit. In the derivations based on rate process theory (11, 21), the energy term $\beta'\tau$ arises as the product $f\lambda/2$ where f is the shearing force per interparticle contact and λ is the distance between successive equilibrium positions. This is also in essential agreement, since it is reasonable to assume that the distance between successive equilibrium positions would be the dimensions of one side of a flow unit. From the foregoing, β' and thus β may be expected to vary with mineralogy and confining stress. As stated earlier, β is independent of temperature and thus β' must vary directly with the absolute temperature in conformity with this interpretation.

The pre-exponential term A in Eq. 5 was assumed to include the entropy of activation and appears to be most related to the soil structure. The relation between entropy and order in a system is well established in statistical thermodynamics. Factors that affect structure in a soil include consolidation conditions and water content. The known behavior of clays (4, 13) indicates that strength varies approximately linearly with consolidation stress and normal stress during shear and exponentially with water content at failure. Since a small range of water content variation was used in the experimental program, it was assumed for simplicity that the relation with water content was linear. Before these variables are included in the relation for deformation rate, the relation between strength and deformation rate must be considered.

A convenient form of Eq. 5 is obtained by taking logarithms:

$$\ln \dot{\delta} = \ln A - \frac{\Delta H}{kT} + \beta\tau \tag{8}$$

For the case of direct shear tests, the shear stress is the dependent variable and Eq. 8 may be written in the form

$$\tau = \frac{1}{\beta}\left(\frac{\Delta H}{kT} + \ln \dot{\delta} - \ln A\right) \tag{9}$$

Because of the method of derivation, Eq. 9 does not necessarily express a failure criterion but rather states that a given level of shear resistance is afforded by the soil when subjected to given levels of the variables on the right side of the equation. However, justification for the assumption that Eq. 9 does express a failure criterion is obtained from the experimental results, which indicate that the stress τ is closely related to the peak failure stress obtained from direct shear tests. With this assumption the effects of normal stresses and water content can be introduced into Eq. 9 to give

$$\tau m = \frac{1}{\beta}\left(\frac{\Delta H}{kT} + \ln \dot{\delta} - \ln M'\right) + \rho Pc + \mu Pns - \gamma w \tag{10}$$

where τm, the shear strength, replaces the shear stress τ; M′ is a new constant; Pc is the consolidation stress; Pns is the normal stress during shear; w is the water content; and ρ, μ, γ are linear coefficients.

The effect of temperature of consolidation (as distinct from temperature of shear) on strength properties has apparently not been reported previously. Based on the experimental evidence, this variable was also considered to have a linear relation to strength. Introducing this into Eq. 10 gives the relation

$$\tau m = \frac{1}{\beta}\left(\frac{\Delta H}{kTs} + \ln \dot{\delta} + \alpha Tc - \ln M\right) + \rho Pc + \mu Pns - \gamma w \tag{11}$$

where Ts is the temperature of shear, Tc is the temperature of consolidation, and M is a constant.

The introduction of these variables into Eq. 9 may be considered a subdivision of the term A. The relationship for deformation rate may now be written in terms of all the variables by rearranging to give

$$\ln \dot{\delta} = \ln M - \frac{\Delta H}{kTs} + \alpha Tc + \beta\tau - \beta\rho Pc - \beta\mu Pns + \beta\gamma w \tag{12}$$

Equations 11 and 12 are the model equations proposed for soil deformation processes. It is reasonable to suppose that deformation of soil is governed by some mechanism (such as breaking of bonds) that is the same regardless of the method of stress application for the intensity of stress within reasonable limits. The equations cannot be proven correct but can be shown to fit the known facts of soil behavior as well as the observed experimental results.

The relationships of normal stresses and water content to shear strength were discussed when they were introduced. The undrained strength of soils has been shown to vary with the logarithm of time to failure while the drained strength variation with time to failure may be approximated by a logarithmic relation (4, 13, 21, 35). From the coefficients for shear temperature ($\Delta H/k$ for creep tests and $\Delta H/\beta k$ for direct shear tests), values for activation enthalpy may be determined.

The proposed model equation bears considerable similarity to that proposed by Mitchell (21). Although derived differently, their basis lies in chemical rate theory and their final form consists of a sum of linear terms, which accounts for the variables known to affect deformation strength behavior.

TABLE 1
SOIL PROPERTIES

Property	Clay	Silt
Specific gravity	2.74	2.68
Liquid limit	89	34
Plastic limit	30	24
Percent passing No. 200 sieve	99.4	98.2
Percent finer than 2 microns (by hydrometer analysis)	80.4	25
Mineralogical composition (by X-ray diffraction)	Calcium montmorillonite	Quartz Calcite Dolomite Montmorillonite Mica Kaolinite
AASHO classification	A-7	A-6

EXPERIMENTAL PROGRAM

Properties of Soils

The two Iowa soils used in the experimental program were an alluvial clay and a clayey silt. The properties of the soils were determined using standard procedures and are summarized in Table 1.

Soil Preparation

The soils were air-dried and pulverized to pass a No. 40 sieve, mixed with water to give compacted specimens of about 100 percent saturation, and stored for several weeks prior to testing.

Individual test specimens approximately ½ in. thick were formed by removing a predetermined weight of the stored soil, molding it by hand into the shear rings and statically compacting it.

A total load of 1,000 lb was applied to the highly plastic clay and 500 lb to the clayey silt. The load was applied at a rate of about 0.08 in. per minute, maintained for 1 minute in the case of the clay and ½ minute for the silt and then released at the same rate.

Shear Apparatus and Test Methods

The experimental study was conducted using a direct shear apparatus. Some of the advantages of this method of testing include simple temperature control, simple specimen preparation, rapid drainage during consolidation, and relatively simple laboratory techniques compared with triaxial testing. The direct shear apparatus provided a rapid means of obtaining a wide range of information.

The disadvantages include lack of drainage control during shear, nonhomogeneity of stress, and indeterminancy of stress components. Most of these factors are discussed in the ASTM Symposium on Direct Shear Testing of Soils (1) and by Sowers (31). It was suggested by Bishop (3) that the principal stress conditions at failure are not known precisely in shear boxes and that the error in undrained cohesion may be of the order of $(1 - \cos \varphi_e) \times 100$ percent, which is generally less than 5 percent for clay of high plasticity. The disadvantages of the method were well appreciated but were considered to be outweighed by the advantages.

Temperature control was achieved by constant-temperature water baths. The temperature of the sample was controlled by circulating the water through the shear rings, which were designed to permit circulation inside each ring. Specimen temperature was measured by a copper-constant thermocouple and a potentiometer recorder which could be read with a precision of 0.2 deg. After equilibrium was achieved, the temperature of the specimen could be maintained to within 0.25 C.

In all tests the shear temperature Ts was equal to or less than the consolidation temperature Tc. This was necessary because any increase in temperature above the

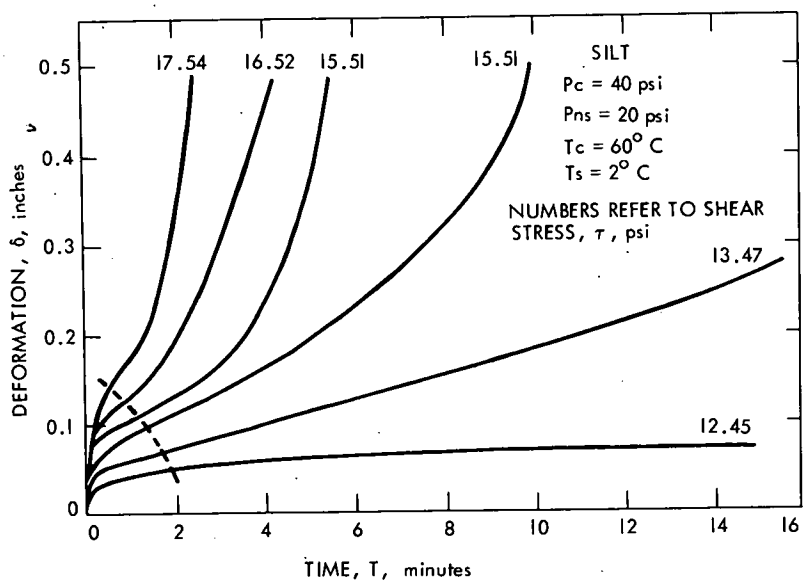

Figure 2. Sample deformation-time curves for silt.

consolidation temperature would result in further consolidation occurring under the higher temperature, with the result that strength would be the same as if the soil had been consolidated under the higher temperature.

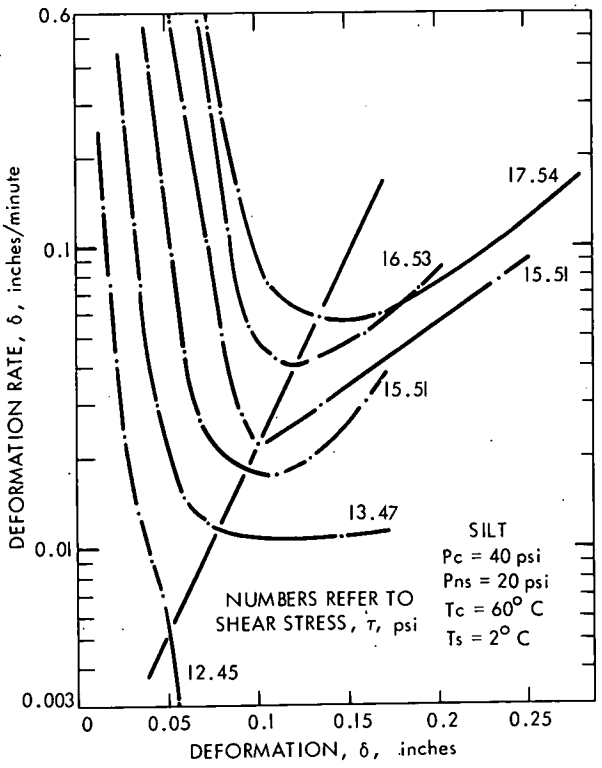

Figure 3. Sample deformation rate curves for silt.

The effect of temperature on the soil pore water pressure was illustrated by the behavior of the soil specimens subjected to temperature changes. On cooling, the volume of the specimen initially decreased and then, as the soil reached the new temperature and the rate of cooling decreased, the specimen reswelled about half of the original volume decrease. In all cases of cooling, negative pore pressure, measured with a transducer pore pressure device, was indicated and cavitation of the water occurred if the temperature change was larger and rapid. Conversely, heating the sample caused a volume increase and positive pore pressures that decreased with time. This behavior is similar to that reported by Mitchell and Campanella (22) and Campanella and Mitchell (6).

The laboratory tests performed in this investigation were of two basic types. The first type of test was a standard, controlled rate of strain, direct shear test. In this test, a given rate of deformation was imposed on the

specimen and the developed shear resistance was recorded at regular intervals of deformation. The second type of test was a creep test in which a given shear stress was applied to the specimen and the resulting deformation was recorded at regular time intervals and simultaneously by a strip-chart recorder. Each type of test was run on each soil type giving four series of tests. Within each series, the consolidation and shearing temperatures were varied in fixed increments.

ANALYSIS

In order to relate the results of the creep tests to the proposed model equation, it was necessary to choose some criterion for selection of the most significant value of deformation rate. The problem is complicated by the possibility of two different types of curves, as shown in Figure 2. Schoeck (28) stated that the basic equation for creep (Eq. 5) is valid ". . . only if there exists a unique and time independent relation between strain and structure." He further suggested that this condition can be satisfied in certain ranges of stress and temperature where (in metals) either no recovery takes place or the rate of recovery is fast compared to the rate of work hardening. In soils, these conditions are probably related to the rate of structure change and the rate of consolidation. An inspection of the basis of Eq. 5, i.e., the rate of passage of flow units over an energy barrier, indicates a validity only for the case of the second derivative with respect to time equal to zero, which is satisfied either for a steady-state condition or a point of inflection in the deformation-time curve. A second condition, which would seem necessary for the determination of valid parameters for soils, is that soil structure be the same for each specimen. For a given pretest history (consolidation temperature, stress, etc.), the structure of the soil at the beginning of the test should be essentially constant. Variations during the tests are probably related to deformation, shear stress, and temperature, with deformation having the primary influence. Mitchell et al (23) worked entirely with terminal creep curves and suggested that it was necessary to compare specimens at the same time after the start of creep. This approach appears inconsistent with the requirement of time-independence of Eq. 5.

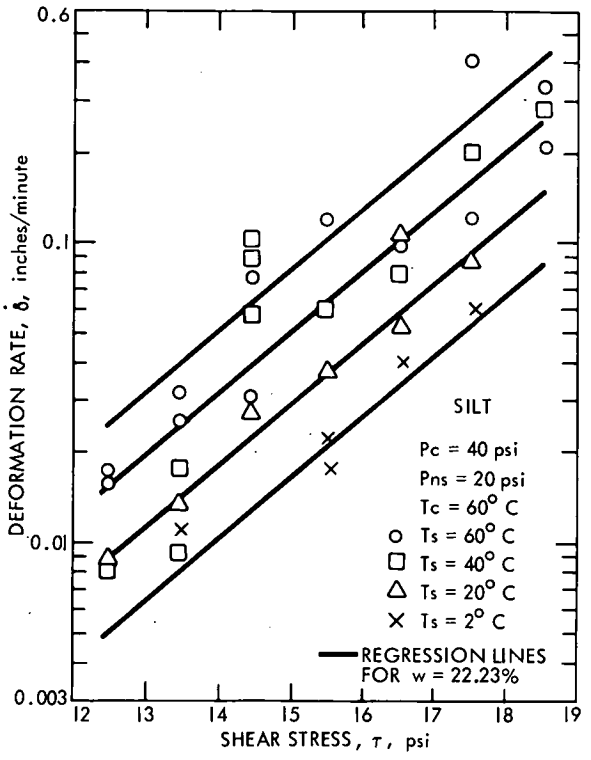

Figure 4. Deformation rate variable with shear stress for silt.

In this study, the minimum points of the rate of deformation vs deformation curves, which are equivalent to points of $\dot{\delta} = 0$, were joined by a straight line, which was then extrapolated to intersect the terminal creep curves and the points of intersection between the line, and the curves were assumed to satisfy the two criteria. These lines are shown in Figure 3 for silt. The points of intersection were transferred to the deformation time curves (Fig. 2) to show the relationship with these curves. For all the tests on clay the lines either were approximately vertical, indicating constant deformation, or had a large negative slope, indicating greater deformation at lower stresses. For all the tests on silt the intersecting line had

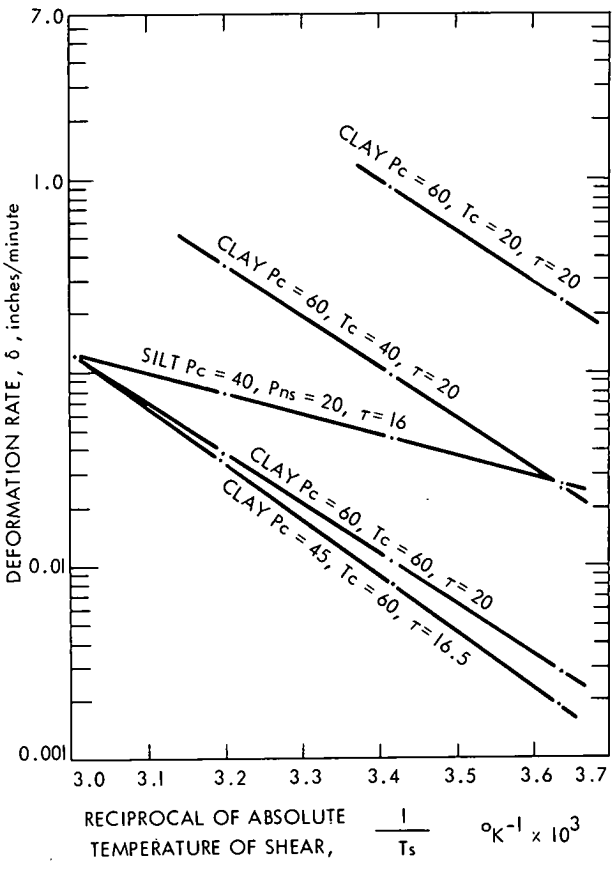

Figure 5. Deformation rate variable with shear temperature.

a positive slope in the order of 3: 1, as illustrated in Figure 3.

The points of intersection obtained from curves in Figure 3 gave the values of deformation rate plotted against shear stress, as in Figure 4 for silt. The slope of the straight lines on these plots is equal to the coefficient β while the differences in deformation rate for different shear temperatures at a given level of shear stress give the value of $\Delta H/k$. These relationships are plotted in Figure 5 for silt and clay.

The results of direct shear tests on clay are shown in Figure 6, where peak shear strength τm is plotted against the reciprocal of the absolute temperature of shear Ts. The different points show effects of different consolidation temperatures Tc.

Points on Figures 4 and 6 show considerable scatter from the expected straight lines. This scatter can be attributed to two main factors: general experimental errors including variations in initial water content and structure, and variations due to differences in water content during the test. The first factor could not easily be determined but may be due to differences in the internal structure of the soil specimens as a result of small differences in initial water content during compaction. Duplications of tests showed variations in shear strength that did not correlate well with the variations in density or water content, tending to confirm the hypothesis of variable internal structure. The water content of all specimens was determined at the end of the test. For given temperatures of consolidation and shear and a given normal stress, the variation of water content was generally less than 0.5 percent of the dry weight of soil, but variations over 1 percent occasionally occurred. However, differences in temperature of consolidation and, most particularly, of shear resulted in differences in water content of over 2 percent for the clay. A part of the variation may be attributed to nonuniform distribution of moisture in the stored batches of soil. Since the variation in water content was small, random, and partially masked by experimental variation, its effect was not readily distinguishable. However, as the proposed model equation had all linear terms, which were assumed to be independent, and there were a reasonable number of data points for most test series, the advantages of treating the data statistically were obvious and a multiple-regression program for an IBM 360 computer was used to treat all experimental data.

Regression Analysis

The dependent variables (τm in Eq. 11 and $\ln \dot{\delta}$ in Eq. 12) were regressed on the applicable independent variables to obtain values for the linear coefficients in the equations. It was possible to treat the test results by considering groups of tests in which

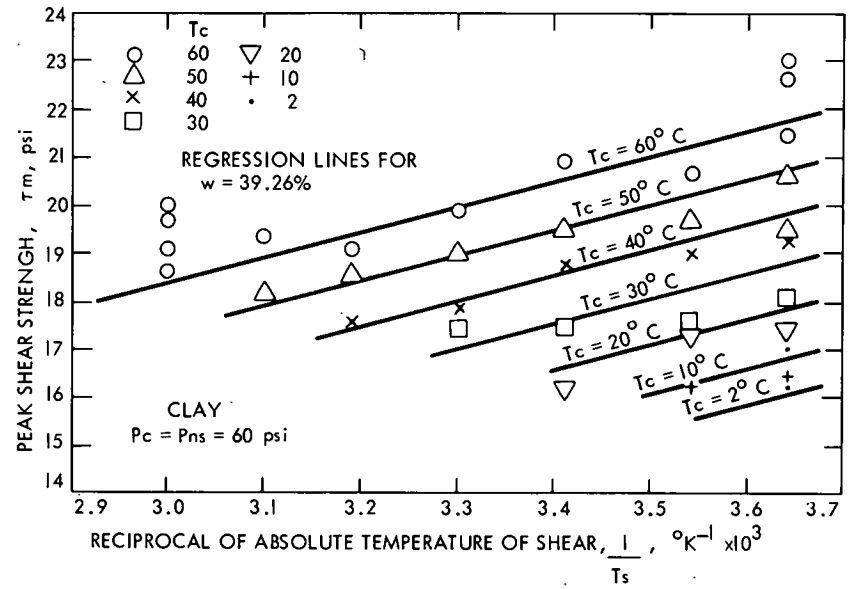

Figure 6. Variation in shear strength of clay with temperature of consolidation and shear for series B4.

TABLE 2

COMPARISON OF COEFFICIENTS OF EQUATION 11 OBTAINED BY REGRESSION FOR CREEP AND DIRECT SHEAR TESTS ON CLAY

Series	Tc (deg C)	Ts (deg C)	Pc (psi)	Intercept	$\frac{\Delta H}{\beta k}$	$\frac{1}{\beta}$	ρ	$\frac{\alpha}{\beta}$	γ	Avg. w	Avg. Gm
				(a) Expected Coefficients From Creep Tests							
A1	60 40 20	60 40 20 2	45	-22.629	4.843	0.739		0.084	0.595	40.70	1.287
A2	60 40 20	60 40 20 2	60	-25.290	5.321	0.894		0.099	0.636	39.86	1.324
A1 & A2	60 40 20	60 40 20 2	45 60	-14.771	5.089	0.829	0.182	0.093	0.625	40.36	1.307
				(b) Experimental Coefficients From Direct Shear Tests							
B1	14 59.5	14 58.8	15 120	-15.901	12.288	8.062	0.144	0.138	0.733	35.85	1.407
B2	65	1.5 65	45	-18.324	7.977				0.520	38.69	1.373
B1 & B3	14 60	2 60	15 120	- 5.022	7.361	1.173	0.148	0.074	0.467	38.21	1.370
B4	2 60	2 60	60	-16.258	5.303			0.098	0.501	39.26	1.346
B5	20 60	2 60	60	-30.714	6.366			0.094	0.936	39.26	1.340
B1-B5 incl.	2 65	1.5 65	15 120	-11.898	8.267	1.934	0.112	0.143	0.654	38.76	1.360

TABLE 3

COEFFICIENTS OF EQUATION 12 OBTAINED BY REGRESSION FOR CREEP TESTS ON SILT USING COMBINED GROUPS OF TESTS

Series	Tc (deg C)	Ts (deg C)	Pc (psi)	Pns (psi)	Intercept	$\frac{\Delta H}{k}$	β	$\beta\rho$	$\beta\mu$	$\beta\gamma$	Avg. w	Avg. Gm
C2	40	40 2	60	60	-13.354	3.975	0.236			0.864	20.76	1.684
C2	40	40 2	60 40	40	-32.120	4.152	0.206	0.016		1.866	21.50	1.650
C2	40	40 2	60 40 20	20	-35.088	3.752	0.348	0.038		1.825	22.41	1.644
C2	40	40 2	60 40 20	60 40 20	-22.876	3.555	0.308	0.043	0.003	1.294	21.81	1.659
C1	60 40 20	60 40 20 2	40	20	-14.257	2.460	0.464			0.547	22.23	1.690
C1 & C2	60 40 20	60 40 20 2	60 40 20	60 40 20	-13.465	2.663	0.407	0.067	0.047	0.749	22.00	1.676

some of the parameters were constant and regressing on the remaining variables. Further, all similar tests on a given soil could be treated as one group and regression carried out on all the variables. This leads to a large number of possible combinations and results, examples of which are given in Table 2 for clay and in Tables 3 and 4 for silt.

It was previously proposed that the deformation mechanism of soil should be consistent regardless of the method of stress application. This would be substantiated by agreement of the coefficients of Eq. 11 obtained from direct shear tests with those of Eq. 12 obtained from creep tests. The comparison can be made by multiplying the direct shear coefficients or by dividing the creep coefficients by their respective values of β. The latter method was used since the β values obtained from the creep tests were much better defined than those from direct shear tests, where a relatively small range of deformation rate was used, and these variations were largely related to other changes in procedure or technique. This comparison for clay is given in Table 2, which shows the converted coefficients for two series of creep tests run at different normal stresses and the coefficients for these two series combined. In the combination, the normal stress Pc was included as an additional variable. The lower part of the table gives the experimental coefficients obtained from five series of direct shear tests on clay and some combinations of these series. The tables include the range of variables used and average values of water content w and mass specific gravity Gm for the groups.

TABLE 4

COMPARISON OF COEFFICIENTS OF EQUATION 11 OBTAINED BY REGRESSION FOR CREEP AND DIRECT SHEAR TESTS ON SILT

Series	Tc (deg C)	Ts (deg C)	Pc (psi)	Pns (psi)	Intercept	$\frac{\Delta H}{\beta k}$	$\frac{1}{\beta}$	ρ	μ	γ	Avg. w	Avg. Gm
(a) Expected Coefficients From Creep Tests												
C1 & C2	60 40 20	60 40 20 2	60 40 20	60 40 20	-33.084	6.543	2.457	0.165	0.115	1.840	22.00	1.676
(b) Experimental Coefficents From Direct Shear Tests												
D1	60 40 20	60 40 20 2	60 40 20	60 40 20	-30.346	4.832	1.240	0.123	0.359	1.769	21.90	1.659

Table 3 gives the coefficients of Eq. 12 obtained by regression for creep tests on silt. The first three lines give coefficients for tests of series C2 combined according to normal stress during the shear phase of the test (Pns); the fourth line gives coefficients for all tests of series C2 combined; the fifth line gives coefficients for series C1 in which the consolidation pressure Pc was constant at 40 psi and the normal stress during shear Pns was constant at 20 psi; the sixth line gives coefficients for all creep tests on silt combined with the regression conducted on all independent variables.

Table 4 gives a comparison of coefficients of Eq. 11 for creep and direct shear tests on silt obtained similarly to those for clay. The expected coefficients from creep tests were obtained from the sixth line of Table 3.

Regression lines shown in Figures 4 and 6 were plotted using the coefficients obtained from the group of tests performed at the corresponding normal stresses and using the average water content for that group. Thus, water contents different from the average cause the points to fall above or below the regression lines and illustrate the effect of water content.

DISCUSSION OF RESULTS

The coefficient β, although somewhat variable for the smallest group of tests based on Tc and Ts, became quite constant for the larger groupings of tests on the clay and for the silt tests at fixed values of normal stresses. There was, however, a significant difference in the values for the two sets of tests performed on the clay at different normal stresses (Table 2) and in the values obtained at different normal stresses on silt (Table 3). In both cases the values of β were lower at the higher normal stresses. These results indicate a possible relationship between the coefficient β and the normal stress during shear Pns. However, tests on the clay were performed at only two levels of normal stress, which was the same for the consolidation and shear phases of the tests. The higher normal stresses used during shear for tests on the silt gave the poorest results in terms of variability. These tests appeared to be very sensitive to variation in water content and test techniques. Because of these limitations the relationship between the coefficient and normal stress during shear is not well defined. However, the decrease in β with increased normal stress is in agreement with the proposed interpretation of β' as the volume of a flow unit. An increase in normal stress would tend to increase the number of bonds and thus decrease the average volume of influence of a bond. A similar reasoning may be used to account for the observation that the value of β for silt is about one-fourth that for clay. The value of β' for clay under 60 psi normal stress is calculated to be 0.6711×10^{-18} cm^3, which is equivalent to the volume of a cube 87.6 Å on a side whereas, for silt under the same normal stress, the value of β' is 0.142×10^{-18} cm^3, or the volume of a cube 52.1 Å on a side. In the case of the clay, the volume is on the order of size of a clay particle while for the silt the volume is considerably smaller, which implies that the bonds and adjacent equilibrium positions occur between asperities on the surface of the silt particles.

The variation of β between the smallest groups of tests did not show any consistent relationship with variables other than normal stress. Specifically, no consistent relationship with temperature could be discerned and this observation substantiates the assumption made in deriving Eq. 5. Regardless of other possible functional relationships of the coefficient β, all the creep test results indicate a linear relation between the logarithm of deformation rate and shear stress, in accordance with Eq. 5.

Values of the coefficient $\Delta H/k$ or $\Delta H/\beta k$ (and hence activation enthalpy) determined from the regression analyses appear to be reasonably constant for each group of tests having the same normal stress. However, it does increase slightly with increased normal stress, indicating an increase in bond strength with a decrease in particle spacing. Mitchell et al (23) report a decrease in activation energy with increased deviator stress. The energy barrier should be related to bonds in the oriented water and the strength of these bonds would be expected to increase slightly with decreased particle spacing due to surface induction.

The value of activation energy was found, from the values of $\Delta H/k$ and $\Delta H/\beta k$ given in the tables, to range from 12 to 21 kilocalories per mole for the clay and from 5 to 8 kilocalories per mole for the silt. For both soils the higher values were obtained from the direct shear tests.

The magnitude of activation enthalpy obtained for the silt was about half that obtained for the clay. This gives an indication of the effect of particle size and, indirectly, of mineralogy. The bound water layer associated with calcium montmorillonite would be more oriented and relatively thicker than the layer associated with silt. This suggests a stronger bond and higher activation energy for the clay. It would be expected that activation energy for other minerals would reflect their relative surface activity. The activation enthalpy measured for the silt is only a little higher than that for unbound water, which suggests that the bonds are not strongly influenced by the surface energy of the particles.

Under a normal stress, such as during consolidation, the contact zones between particles or domains are probably subjected to localized shear stresses, and a breaking of bonds would then occur to permit particle reorientation accompanying the deformations of consolidation.

From this model it is reasonable to consider consolidation as a rate process having a mechanism similar to that proposed for shear deformation. This approach has been suggested by Wu et al (36), who considered consolidation on the basis of rate process theory. The effect of temperature on consolidation is related to an increase in thermal energy, which permits more rapid passage of flow units over the energy barrier and allows deformation to progress more rapidly. This increase in the rate of consolidation is also related to the decreased viscosity of the water, which permits more rapid drainage. These effects have been reported by Paaswell (26) and others. In the case of clay, the consolidation temperature shows the additional effect of increasing the bonding, as indicated by higher values of $\Delta H/k$ similar to the effect of increased normal stress. The silt, however, showed no significant effect due to temperature of consolidation. This behavior further supports the suggestion of a weak influence of particle surface energy in the case of silt.

The coefficient of water content $\beta\gamma$ varied quite erratically. This is not surprising in view of the small and random variation in water content between the samples, but unfortunately leaves the coefficient poorly defined. The average value of $\beta\gamma$ for the creep tests on clay with 45 psi normal stress was 0.8, and with 60 psi normal stress was 0.7; but the value of γ in both cases was approximately 0.6, which is of the same order as found from the direct shear tests. The creep tests on silt with Pc = 40 psi and Pns = 20 psi gave a value of $\beta\gamma$ of about 0.55, while the average for all creep tests on silt was 0.75, giving an average value of $\gamma = 1.8$, which was the value obtained as an average from all direct shear tests. From this it may be inferred that water content variations of a given magnitude have more effect on silt than on highly plastic clay, a fact that is well recognized and that may be explained on the basis of the large differences in specific surface area between these materials.

As previously discussed, the coefficient β is probably related to the normal stress during shear and the coefficient $\Delta H/k$ is probably related to consolidation stress; however, the results recorded (for example, in the top three lines of Table 2) indicate that these variations were of insufficient magnitude to account for the increased strength with increased normal stresses. Therefore, in the linear equation, significant coefficients for Pc and Pns where also obtained.

The general agreement between the values of the coefficients obtained from creep and direct shear tests tends to confirm the postulate that there is one consistent deformation mechanism for soils that is independent of method of load application. These confirmations were obtained as a result of performing the creep tests at stresses that were on the order of the peak shear strength of the soil. These stresses were higher than those generally used for creep testing and gave minimum points of deformation rate rather than terminal creep curves.

CONCLUSIONS

The experimental part of the study, consisting of 434 creep and direct shear tests on two different soil types, yielded the following observations:

- Creep tests show a linear relationship between the logarithm of deformation rate and shear stress, and the proportionality coefficient is linearly related to the volume of the flow unit and may be related to the normal stress.
- Activation energy values obtained from creep tests are approximately equal to those obtained from direct shear tests and for the clay are of the same order of magnitude as other reported values. The values of activation energy obtained for the silt are about 40 percent of those obtained for the clay.
- The coefficients relating deformation rate and shear strength to water content were also found to agree quite well. The values for silt were about three times larger than the values for clay, as would be expected due to the differences in specific surface area between these soils. Because of the narrow range of water content values used, the relationship was assumed to be linear and the coefficients were rather poorly defined for smaller groups of tests.
- The agreement between the coefficients obtained from the two test procedures tends to confirm the hypothesis of a single deformation mechanism that is independent of test procedure.

This study of the effect of temperature on the shear strength and creep behavior of soils has yielded a model equation in terms of simple parameters that reasonably characterizes the deformation and strength behavior of the soils. Modifications of the model equation may be required as further investigation reveals the interdependencies of some of the variables and, specifically, the functional relationship of water content. The test results were analyzed by multiple regression, which aided interpretation of the variability due to differences in water content.

ACKNOWLEDGMENTS

The research was conducted under the sponsorship of the Engineering Research Institute of Iowa State University. This support is gratefully acknowledged. The authors also wish to express their appreciation for the help and encouragement extended by Dr. Richard L. Handy, head of the Soil Section, and the other members of the Soil Research Laboratory.

REFERENCES

1. American Society for Testing and Materials. Symposium on Direct Shear Testing of Soils. ASTM Spec. Tech. Publ. 131, 1953.
2. Andersland, O. B., and Akili, W. Stress Effect on Creep Rates of a Frozen Clay Soil. Geotechnique, Vol. 17, p. 27-39, 1967.
3. Bishop, A. W. The Strength of Soils as Engineering Materials. Geotechnique, Vol. 16, p. 91-130, 1966.
4. Bishop, A. W., and Henkel, D. The Measurement of Soil Properties in the Triaxial Test, Second Ed. Edward Arnold Publ., Ltd., London, 1962.
5. Bjerrum, L., and Wu, T. H. Fundamental Shear-Strength Properties of Lilla-Edet Clay. Geotechnique, Vol. 10, p. 101-109, 1960.
6. Campanella, R. G., and Mitchell, J. K. Influence of Temperature Variations on Soil Behavior. ASCE Proc., Vol. 94, No. SM3, p. 709-734, 1968.
7. Crawford, C. B. Cohesion in an Undisturbed Sensitive Clay. Geotechnique, Vol. 13, p. 132-146, 1963.
8. Eichler, J., and Kazda, J. Two Studies of the Heterogeneous System of Clayey Soils. Proc. Sixth Internat. Conf. on Soil Mech. and Found. Eng., Vol. 1, p. 36-40, 1965.
9. Eyring, H. Viscosity, Plasticity and Diffusion as Examples of Absolute Reaction Rates. Jour. Chemistry and Physics, Vol. 4, p. 283-291, 1936.

10. Eyring, H., and Powell, R. E. Rheological Properties of Simple and Colloidal Systems. In Colloid Chemistry (Jerome Alexander, ed.), Vol. 5, p. 236-252, Reinhold, New York, 1942.
11. Glasstone, S., Laidler, K., and Eyring, H. The Theory of Rate Processes. McGraw-Hill, New York, 1941.
12. Herrin, M., and Jones, G. Behavior of Bituminous Materials From the Viewpoint of Absolute Rate Theory. Proc. AAPT, Vol. 32, p. 82-105, 1963.
13. Hvorslev, M. J. Some Considerations and Data Regarding the Shear Strength of Clays. Research Conf. on Shear Strength of Cohesive Soils, p. 169-273, ASCE, New York, 1960.
14. Kauzmann, W. Flow of Solid Metals From the Standpoint of the Chemical Rate Theory. Amer. Inst. of Mining and Metallurgical Engineers Trans., Vol. 143, p. 57-83, 1941.
15. Leonard, R. A., and Low, P. F. Effect of Gelation on the Properties of Water in Clay Systems. Proc. Nat. Conf. on Clays and Clay Minerals, Vol. 12, p. 311-325, 1964.
16. Leonards, G. A., and Andersland, O. B. The Clay-Water System and the Shearing Resistance of Clays. Research Conf. on Shear Strength of Cohesive Soils, p. 793-810, ASCE, New York, 1960.
17. Leonards, G. A., and Rahmiah, B. K. Time Effects in the Consolidation of Clays. ASTM Spec. Tech. Publ. 254, p. 116-130, 1960.
18. Low, P. F. Physical Chemistry of Clay-Water Interaction. Advances in Agronomy, Vol. 13, p. 269-327, 1960.
19. Low, P. F. Effect of Quasi-Crystalline Water on Rate Processes Involved in Plant Nutrition. Soil Science, Vol. 93, p. 6-15, 1962.
20. Martin, R. T. Adsorbed Water on Clay: A Review. Proc. Nat. Conf. on Clays and Clay Minerals, Vol. 9, p. 28-70, 1962.
21. Mitchell, J. K. Shearing Resistance of Soils as a Rate Process. ASCE Proc., Vol. 90, No. SM1, p. 29-61, 1964.
22. Mitchell, J. K., and Campanella, R. G. Creep Studies on Saturated Clays. ASTM Spec. Tech. Publ. 361, p. 90-110, 1964.
23. Mitchell, J. K., Campanella, R. G., and Singh, A. Soil Creep as a Rate Process. ASCE Proc., Vol. 94, No. SM1, p. 231-253, 1968.
24. Murayama, S., and Shibata, T. On the Rheological Characters of Clay: Part I. Disaster Prevention Research Institute, Kyoto University, Bulletin No. 26, p. 1-43, 1958.
25. Murayama, S., and Shibata, T. Rheological Properties of Clays. Proc. Fifth Internat. Conf. on Soil Mech. and Found. Eng., Vol. 1, 269-273, 1961.
26. Paaswell, R. E. Temperature Effects on Clay Soil Consolidation. ASCE., Vol. 93, No. SM3, p. 9-22, 1967.
27. Rosenqvist, I. Mechanical Properties of Soil-Water Systems. ASCE Proc., Vol. 85, No. SM2, p. 31-53, 1959.
28. Schoeck, G. Theory of Creep. Creep and Recovery, p. 198-226, Amer. Soc. for Metals, Cleveland, 1957.
29. Seed, H. B., and Chan, C. K. Thixotropic Characteristics of Compacted Clays. ASCE Proc., Vol. 83, No. SM4, p. 1427-1-35, 1957.
30. Senich, D., Demirel, T., and Handy, R. L. X-Ray Diffraction and Adsorption Isotherm Studies of the Calcium Montmorillonite-H_2O System. Highway Research Record 209, p. 23-54, 1967.
31. Sowers, G. F. Strength Testing of Soils. ASTM Spec. Tech. Publ. 361, p. 3-21, 1964.
32. Tan, T. K. The Fundamental Properties of Clays, Loess and Rocks and Their Application to Engineering Problems. Scientia Sinica, Vol. 14, p. 1169-1193, 1959.
33. Taylor, D. W. Fundamentals of Soil Mechanics. John Wiley, New York, 1948.

34. Terzaghi, K. V. Undisturbed Clay Samples and Undisturbed Clays. Contributions to Soil Mechanics: 1941-1953. Boston Society of Civil Engineers, Boston, 1941.
35. Whitman, R. V. Some Considerations and Data Regarding the Shear Measurements. Research Conf. on Shear Strength of Cohesive Soils, p. 581-614, ASCE, New York, 1960.
36. Wu, T. H., Resendiz, D., and Neukirchner, R. J. Analysis of Consolidation by Rate Process Theory. ASCE Proc., Vol. 92, No. SM6, p. 229-248, 1966.

Transient Temperature Influences on Soil Behavior

ROBERT E. PAASWELL, State University of New York at Buffalo

In cases where changes in temperature affect soil responses such as strength of compacted subgrades and embankments, changes in compaction properties during stabilization due to moisture migration, and changes in deformation of stressed clay soil layers, the ability to predict temperature profiles within the affected areas becomes highly desirable. This paper analyzes the temperature profile that is developed in soil samples for conditions of transient temperature changes at one boundary surface. The study is divided into two parts. The first is concerned with temperature distribution as affected by local inhomogeneities for nonsaturated soils. Close study is also made on moisture changes as affected by this surface temperature change. The second part is concerned with the pattern of temperature increase and decrease imposed on a stressed, saturated soil. For this case the theory of heat conduction was used to predict the temperature distribution within the soil sample.

For the study of the first part, a parabolic form of temperature increase was applied at the upper boundary surface of an insulated cylinder to an unsaturated sample of a clay soil compacted at varying moisture contents and density states. The resultant temperature-time-space distribution curves were analyzed and the resultant moisture content distribution curves were compared with the initial moisture content distribution curves. In the constant stress tests, a thermal pulse was applied at the upper surface of a saturated consolidated soil, and the resultant temperature-time-space distribution was determined.

The tests indicate that establishment of temperature profiles enables correlation to be made between surface temperature changes and moisture changes on a transient basis. Where surface boundary conditions can be accurately modeled, heat conduction theory, assuming a sample homogeneity, can be used to predict these temperature profiles.

•IN RECENT YEARS there has been a growing body of research on the physical and mechanical properties of soils and their dependence on or independence of temperature. The use and interpretation of laboratory models is the first step in the interpretation of field performance. The use of uniform thermal coefficients, for example, and the analysis of the influence of sample inhomogeneities on temperature changes within the sample caused by boundary changes can be closely analyzed in the lab and the findings transferred to the field. This would be useful in the analysis of field performance of compacted soils, where temperature changes might cause moisture migration and strength changes, altering the response of the soil to imposed stresses. Another occurrence could be the case of a confined soil layer subject to temperature increases that result in pore pressure fluctuations and subsequent deformation. Through the use of mathematical models and physical models, close study can be made of the influences of temperature changes on soil behavior.

In the study of the effects of temperature changes on soil behavior, much research has been made on various steady-state conditions, i. e., the properties of soil at one temperature vs the properties of the same soil at another higher, or lower, constant temperature. Field conditions, however, are far from steady-state, and it becomes

important to establish how soil characteristics change during temperature changes, i. e., the transient case.

The familiar and frequently used theory of heat conduction, when applied to soils, often includes the assumption that the soil is homogeneous. For soil of a consistent moisture density pattern throughout, this assumption may be used, by considering that this three-phase material has uniform thermal characteristics such as conductivity and diffusivity (1). Soil compacted to a given density at a specific site during the process of stabilization, or soil that exists naturally above the water table, is generally not uniformly homogeneous, and the nature of the actual heat transfer as measured by temperature patterns influenced by localized inhomogeneities represents a portion of the work studied herein. The warming cycle during the day causes temperature increases in the upper surfaces of the soil, and these temperature increases result in some moisture changes in the affected layers. One purpose of the first series of tests is to investigate the manner in which the measurable surface temperature pattern (here, increasing only) influences the temperature distribution pattern within the sample and the moisture pattern within the sample, and the extent to which this pattern is influenced by local inhomogeneities in moisture content.

In a saturated soil, the utilization of heat conduction theory becomes simplified due to the more homogeneous state of the soil. Field temperature conditions, however, are not steady-state, so the use of heat conduction theory, with time-dependent temperature boundary conditions to predict field temperature patterns, becomes desirable. By being able to predict subgrade temperatures, given surface distributions, it should then be possible to estimate changes in other temperature-dependent soil properties, such as strength, for a given environmental situation. The sinusoidal temperature pattern is a simplified approximation of a naturally occurring temperature pattern at ground surface. In the second series of tests reported here, a comparison is made between the temperature pattern predicted by the theory of heat conduction and the pattern as modeled in the laboratory on a stressed-saturated clay sample. In addition, some attention is given to the deformation induced in the sample due to the changing surface temperature.

TRANSIENT TEMPERATURE PROPAGATION

Recompacted soil cylinders were subjected to a pattern of increasing temperature at the upper boundary surface, with the remaining surfaces insulated. In these tests, the original moisture content distribution was established to ascertain the degree of homogeneity attained by compaction and the influence of this pattern of homogeneity on resultant temperature and moisture distributions.

Table 1 lists 16 samples of a soil indigenous to the Buffalo area, PI = 30, LL = 54, specific gravity = 2. 73, that were compacted at nominal moisutre contents as given. These samples were compacted in insulated cylinders 10 cm in diameter and 15. 6 cm in height. An embedded copper foil heater was placed at the upper axial surface, controlled by a variable power source, which enabled the surface temperature pattern to have the desired time history. Temperature records were maintained by thermocouples throughout the sample connected to a recording potentiometer (Fig. 1).

In order to show the temperature distribution and moisture redistribution during these increasing temperature tests, samples 3, 8, 9, and 13 are compared showing temperature-time and moisture content sample height distributions in Figures 1 and 2. The temperature tests consisted of increasing the temperature at the upper surface while the other surfaces remained insulated.

The surface temperature increase, nonlinear in form, was from ambient temperature (26 C ±) to 80 C ± in 240 minutes. This value was recorded by thermocouple No. 1 (TC 1). The temperature propagation throughout the interior of the sample is shown by the temperature-time profile for thermocouple locations TC 2 through TC 5. It has been noted (1) that thermal diffusivity increases with increasing moisture content and decreasing density. This is shown clearly in Figure 1 where, for example, the propagation of the 50 C isothermal line from the surface to TC 2 takes 52 minutes for sample 3, 50 minutes for sample 8, 40 minutes for sample 9 and 42 minutes for

TABLE 1

SAMPLE PROPERTIES—TRANSIENT TEMPERATURE TESTS

Sample No.	Nominal Initial Moisture Content, w_i percent	Void Ratio, e	Density, γ_s, g/cc
1	19.2	1.16	1.24
2	19.3	1.24	1.21
3	19.8	1.39	1.14
4	20.6	1.03	1.34
5	30.0	0.83	1.49
6	30.6	0.80	1.51
7	31.0	0.80	1.51
8	31.7	0.82	1.50
9	39.4	1.09	1.31
10	40.5	1.12	1.28
11	41.1	1.14	1.27
12	41.5	1.12	1.28
13	50.2	1.36	1.15
14	50.3	1.38	1.15
15	51.5	1.39	1.14
16	54.4	1.50	1.09

sample 13. Sample 15 has a greater moisture content but a smaller density than sample 9. It is also noted that in sample 3, the surface temperature rises to 81 C before there is a 1 C temperature rise at TC 5, whereas for the other samples noted the surface temperature was less than 75 C (surface temperature increase, ΔT = 49 C) before a 1 C temperature increase occurred at TC 5.

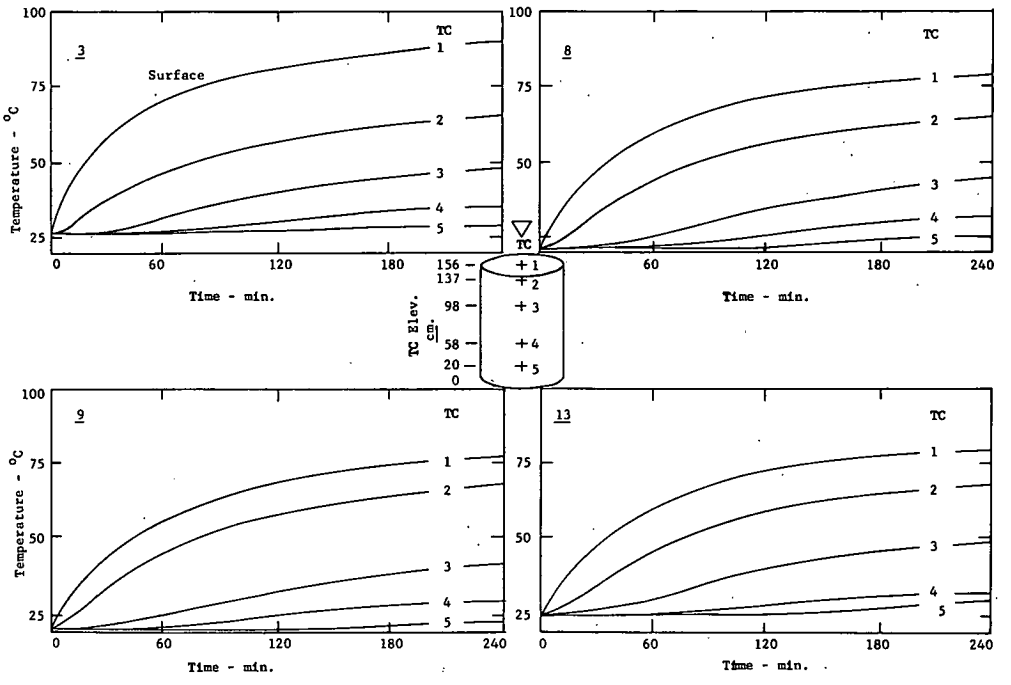

Figure 1. Temperature-time distribution in samples.

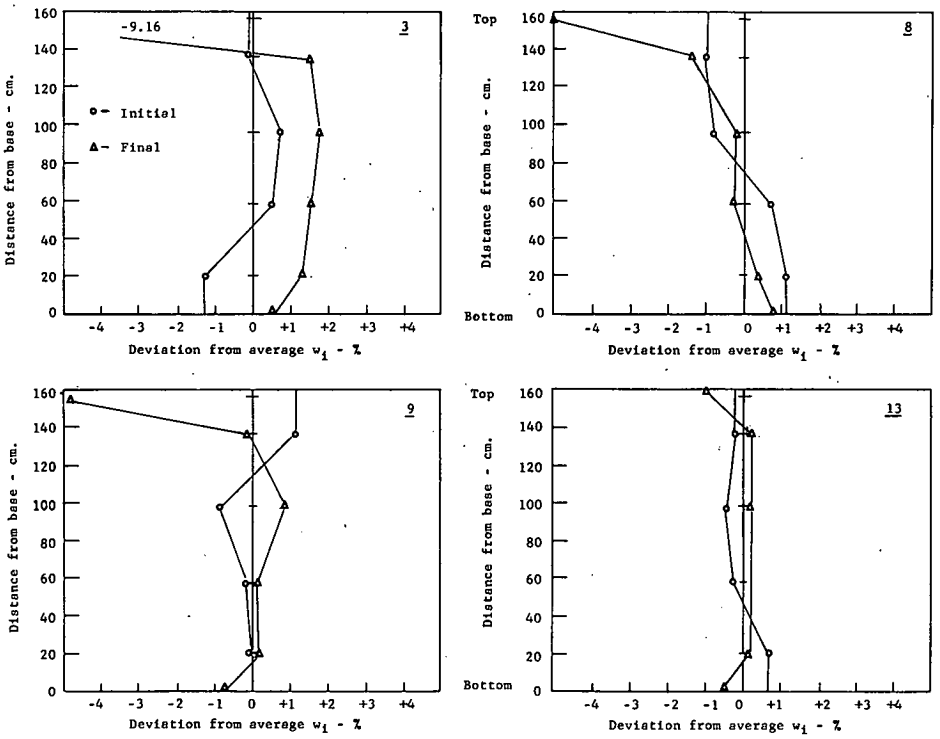

Figure 2. Initial and final moisture distribution in samples.

Of greater interest is the nature of the transmission of temperature through the soil as influenced by the moisture content. Figure 2 as noted shows the nominal initial moisture content w_i percent and the final moisture content w_f percent. The w_i percent is the average of the moisture contents taken as each of 4 layers was compacted into the container. There is a deviation of approximately 1 percent in no set pattern at the start of the test. It should be noted that, because there were initial moisture content gradients, however slight, throughout the sample, the natural process in the soil if no temperature tests were made would be some equilibrating moisture redistribution within the sample.

The most significant change in moisture content occurs near the heated surface, as noted in Table 2. The initial moisture content taken at the time of compaction is compared with the final moisture content near the surface taken immediately after completion of the test. It is seen that there is a substantial decrease in moisture content near the surface in every case. The moisture contents in Table 2 are also calculated as percent saturation for each sample in order to have a more uniform basis for comparison. The greatest decreases in percent saturation occur in samples 1 through 4. These also represent the greatest decrease in actual moisture content. Samples 1 through 4 were compacted at the smallest moisture contents (approximately 20 percent), and with the exception of sample 4, percent saturations less than 45 percent. The remaining samples were compacted at saturations near 100 percent.

This would indicate that as moisture contents increased significantly, the moisture movement near the points of maximum thermal gradient decreased. The least moisture movement occurred at the highest moisture contents (samples 13-16). Because the surface temperature was maintained at less than 100 C, and because the upper surface was covered by the heating cap, moisture change due to evaporation at the surface was minimized.

TABLE 2

CHANGES IN MOISTURE CONTENT AND SATURATION DUE TO TEMPERATURE INCREASES—UPPER SURFACE

Sample No.	Initial Moisture Content, w_i Percent	Initial Percent Saturation, S_i Percent[1]	Final Moisture Content, w_f Percent	Final Percent Saturation, S_f Percent	Net Change Moisture Content, percent	Net Change Percent Saturation
1	18.7	44.0	7.9	18.5	8.8	25.5
2	18.8	41.0	12.4	27.0	6.4	14.0
3	19.7	39.0	10.6	21.4	9.0	17.6
4	22.3	59.0	12.9	33.0	9.3	26.0
5	31.1	103.0	28.4	94.0	2.7	9.0
6	31.8	108.0	29.0	99.0	2.4	9.0
7	31.1	105.0	29.1	99.0	2.0	6.0
8	30.7	106.0	26.8	89.0	3.9	17.0
9	40.5	98.0	34.5	86.0	6.0	12.0
10	40.6	99.5	38.8	94.5	1.8	5.0
11	41.3	101.0	38.3	93.0	3.0	8.0
12	41.5	101.0	39.8	97.0	1.7	4.0
13	50.0	100.0	49.3	98.5	0.7	1.5
14	50.1	99.0	48.1	95.0	2.0	4.0
15	50.0	102.0	49.5	100.0	0.7	2.0
16	54.3	99.0	52.6	96.0	1.7	3.0

[1]Initial percent saturation was computed based on original nominal moisture content. Thus inhomogeneities may cause some to appear greater than 100. These are given here to emphasize change in percent saturation, rather than to give individual values of percent saturation.

Figure 2 illustrates further the somewhat erratic pattern of initial and final moisture content distributions throughout the sample. Combined with the moisture decrease near the surface of the sample, there is a general moisture increase in the middle third of the sample. This would further amplify the moisture flow in the direction of the decreasing temperature gradient, especially at points where the temperature gradient is highest. The tests were always concluded when the surface temperature was still increasing. This meant that steady-state conditions were never realized so that water flows never reached an equilibrium state. In the sample with the highest density (i. e., the lowest permeability) the moisture increase was limited to the upper half of the sample, whereas in the other samples illustrated the moisture flow propagated further into the sample in the direction of decreasing temperature. It should be noted again that the moisture flow due to heat would be coupled with a general redistribution of moisture within the sample prior to the temperature increase. This too would cause the somewhat erratic nature of the temperature distribution. In all cases as represented by Figure 1 the temperature flow was uniform and continuous, that is, there were no sudden jumps due to inhomogeneities in the sample. The temperature pattern at successively deeper thermocouples was one of offset parallelism, as would be predicted by general heat conduction behavior. This point in fact is amplified in the latter part of this paper.

The uniform pattern of the temperature distribution suggests that the temperature propagation throughout a soil sample is not substantially affected by localized inhomogeneities but nonetheless has great influence on the degree of moisture movement within the sample. These results suggest that the soil-water system can be approached as a homogeneous unit in making preliminary predictions of temperature distribution due to transient temperature boundary conditions.

SINE PULSE PROPAGATION

To compare temperature distribution patterns as predicted by heat conduction theory with patterns as established in soil, tests were performed on recompacted saturated

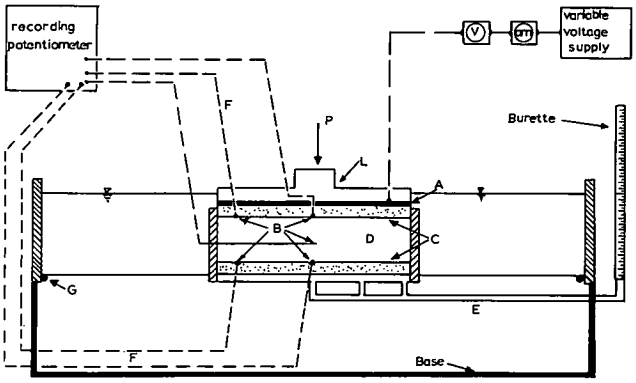

KEY:

A - Thermofoil heater
B - Thermocouples
C - Porous stones
D - Soil sample
E - Drains
F - Thermocouple lead wires
G - O-Ring
L - Brass loading cap
am - Ammeter
V - Voltmeter
P - Load

Figure 3. Sample test setup for sine pulse tests.

cylinders of the same soil. For these tests the temperature distribution is assumed sinusoidal at the upper boundary surface, with other surfaces remaining constant. In addition, these tests were used as preliminary tests in evaluating the influence of such a transient temperature pattern on deformation of a stressed soil.

The equipment used in these tests was described in some detail in a previous paper (3), but shall be described here briefly for clarity. A fixed-ring consolidometer, 6.34 cm in diameter, was adapted so that temperature increases could be made at the upper axial surface and temperature measurements made at the upper and lower surfaces and in the center of the sample (Fig. 3). The clay soil, premixed with distilled water at a moisture content greater than optimum, was compacted in the retaining ring to the desired density (Table 3). The soil was then saturated in distilled water under a seating load of 0.31 kg/cm^2. Drainage and saturation took place through the upper and lower surfaces. The heating element was contained within the loading cap and consisted of an etched upper foil heater surrounded by Kapton film and secured by an adhesive to the cap. The heating element was the same diameter as the ring, 6.24 cm, and was 0.0025 cm thick. Power was supplied through a variable voltage control. The loading cap also contained the upper

TABLE 3

PROPERTIES OF SAMPLES IN SINE PULSE TESTS

Sample	Dry Density, g/cc	Moisture Content at Compaction, percent	Max. Surface Temp., deg C	Max. Temp. Increase Above Ambient, deg C	Time to Attain T Max., minutes	Average Rate of Increase, deg C/minute	Max. Lower Surface Temp. Increase, ΔT_B, deg C	Time to Attain ΔT_B, minutes	Time Lag
1	1.39	36	71	46	16	2.9	11	18	2
2	1.36	38	71	46	16	2.9	14	16	0+
3	1.35	40	74	47	8	5.9	5	16	8
4	1.34	42	72	47	8	5.9	4	16	8
5	1.42	36	44	20	6	3.3	6	6	0+
6	1.47	32	72	49	10	4.9	7	16	6
7	1.47	32	73	40	6	6.7	1	6*	0+
8	1.47	32	43	20	6	3.3	1	8	2
9	1.47	32	45	19	6	3.2	1	6*	0+
10	1.47	36	42	19	4	4.7	1	12	8
11	1.47	33	42	15	4	3.8	1	6*	2
12	1.47	33	70	43	10	4.3	5	14	4
13	1.47	33	70	38	6	6.3	3	8	2

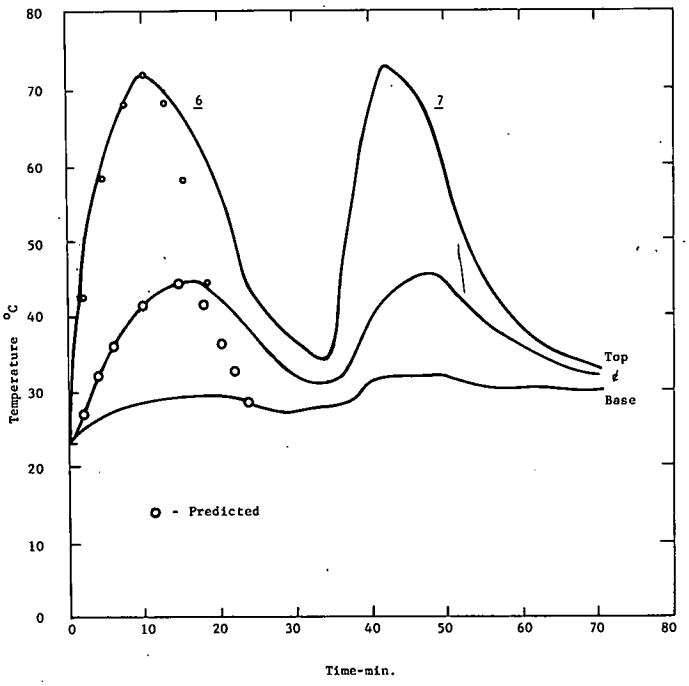

Figure 4. Temperature-time profiles, sine pulse tests, samples 6 and 7.

porous stone; thus there was a distance of 0.63 cm separating the heater and the upper sample surface. Fine wire copper-constantan thermocouples were placed at the surfaces of the upper and lower porous stones and in the center of the sample, permitting a temperature profile to be established across the thickness of the sample and in addition serving as a control on the temperature at the upper surface. To assume that no phase changes would take place within the sample, the maximum upper surface temperature was always less than 100 C. The shape of the upper surface temperature input was attained through control of the variable voltage supply, which was done manually for these tests. The sample was surrounded by a water bath at ambient temperature

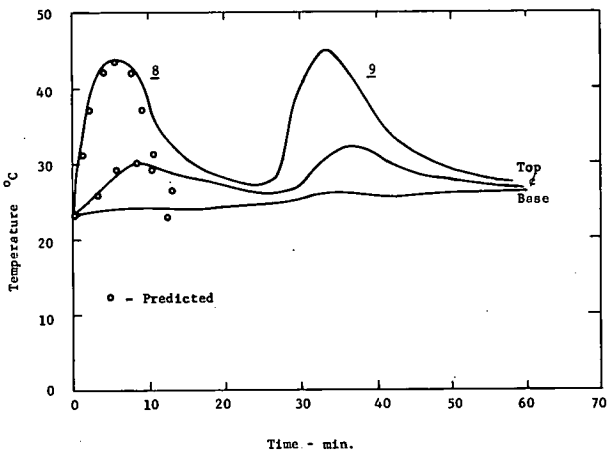

Figure 5. Temperature-time profiles, sine pulse tests, samples 8 and 9.

(25-30 C). The relative size of the water bath (15.24 cm diameter) and the small source of the temperature input were believed to be adequate to approximate the desired boundary conditions of constant temperature at all points except the upper surface. The relatively short time of the temperature increases was also believed to add to the stability of temperature at the boundary.

The temperature tests were begun 24 hours after the samples had been placed in the water bath. The tests are summarized in Table 3. Figures 4 and 5 show the temperature-time history for samples 6, 7, 8, and 9.

To provide an estimate of the rate of temperature flow through the sample the following boundary value problem (3) was solved for a cylinder of radius a and height L:

$$\nabla^2 T = \frac{1}{k}\frac{\partial T}{\partial t} \tag{1}$$

$$T(r,\ z = 0,\ t) = T^* f(t) \tag{2}$$
$$T(r,\ z = h,\ t) = 0$$
$$T(r = a,\ z,\ t) = 0$$
$$T(r,\ z,\ t = 0) = 0$$

where

$$f(t) = \sin \pi t/t^* \qquad 0 \leq t \leq t^*$$

and

$$f(t) = 0 \qquad t^* < t \tag{3}$$

Note that the zero temperature reference can be changed to an ambient, To, temperature reference by the addition of To. The solution to this problem was obtained as

$$\frac{T}{T^*} \sin \frac{\pi t}{t^*} \sum_{n=1}^{\infty} \frac{2}{\alpha n} \frac{J_o\left(\alpha_n \frac{r}{a}\right) \sin h\left[\alpha_n \left(\frac{L-z}{a}\right)\right]}{J_1(\alpha_n) \sin h\left(\alpha_n \frac{L}{a}\right)}$$

$$- 4 \sum_{n=1}^{\infty} \sum_{n=1}^{\infty} \frac{(m\pi)\, J_o\left(\alpha_n \frac{r}{a}\right) \sin\left(\frac{m\pi z}{L}\right)}{\left[m^2\pi^2 + \alpha_n^2 \left(\frac{L}{a}\right)^2\right] J_1(\alpha)_n\, \alpha_n} \cdot B \tag{4}$$

where

$$B = \frac{\pi\left[\lambda_{mn} t^* \cos\left(\frac{\pi t}{t^*}\right) + \pi \sin\left(\frac{\pi t}{t^*}\right)\right]}{(\lambda_{mn}\, t^*)^2 + \pi^2}$$

$$- \frac{\pi\, \lambda_{mn} t^* \exp(-\lambda_{mn} t)}{(\lambda_{mn} t^*)^2 + \pi^2} \qquad 0 \leq t \leq t^* \tag{5a}$$

or

$$B = \frac{-\pi\, \lambda_{mn} t^* \exp(-\lambda_{mn} t)\left[1 + \exp(\lambda_{mn} t^*)\right]}{(\lambda_{mn} t^*)^2 + \pi^2} \qquad t^* < t \tag{5b}$$

Values of thermal diffusivity based on density and saturated moisture content were computed using formulas given by Kersten. These values ranged from 0.21 to 0.23 cm^2/min. The theoretical solution for the temperature-time profile at the sample center and upper surface is shown as circular points in Figures 4 and 5. Where the actual time surface input resembles the theoretical sine input, the predicted results are quite accurate. However, the time input shows a temperature lag on the cooling part of the cycle that is due both to a slight heating of the water in the porous stone and a heating of the cap, which does not permit rapid cooling to the original ambient. This lag is reflected in the temperature profile throughout the sample and becomes more pronounced with depth in the sample, as can be seen by the figures.

As would be expected, the greater the period of the pulse, the greater the heat transferred into the sample, as manifested by greater temperature increases throughout. In samples 1 and 2, the time for the surface temperature to reach its maximum value was 16 minutes and the corresponding lower surface was between 11 and 14 C. From Table 3 it is seen that the maximum lower surface increase in all other cases was no greater than 7 C. It is also noted from repetitive cases that when a temperature decrease lag occurs, i.e., when there is a decay rather than a rapid drop-off followed by a rapid increase, there is a tendency for slight temperature increase throughout, as illustrated by the center and lower surface temperature profiles in Figures 4 and 5. Whereas the period of the pulse shows the relative insulating properties of the soil, the repetitive type pulse shows the net temperature buildup in the soil, which in actual field situations can be quite significant. The good agreement of the loading portion of the sine curve with predicted temperature distributions also suggests that the heat conduction equation can be used with some success in approaching the temperature distribution in the two-phase saturated soil by assuming that the material responds as a homogeneous solid. This assumption is made more valid by noting from the first test series that the moisture propagation decreases as the saturated moisture content increases.

In tests 1 through 4 deformation responses were noted together with the temperature profile. In all cases it was observed that there was a slight swelling initially coincident with the temperature increase, followed by a contraction with temperature decrease. To separate out the natural thermal expansion of the loading system due to temperature increases, calibrations were performed for the same pulses applied to the soil. These yielded, on the basis of a 2.54 cm height comparative brass sample, strains of 0.41 percent increase for a 20 C temperature increase above ambient and 0.82 percent for a 45 C temperature increase. These strains were then subtracted from the total expansion of the soil to determine the net strain, expansion or contraction of the soil system. These samples were subjected to a net stress of 0.31 kg/cm^2 applied at ambient temperature and the temperature tests were not commenced until consolidation under this stress had ceased (a value chosen as < 0.002 cm over a 4-hour period).

For tests 1 and 2, the temperature increase was applied over a 16-minute period, and the net change was 0.35 percent decrease in volume at peak strain. For tests 3 and 4, the maximum temperature increase was applied over half the time period in tests 1 and 2, and the net change at peak surface temperature ranged from 0.7 to 1.5 percent expansion. These strains were not completely recovered at the conclusion of the tests when the surface temperature was still somewhat above the original ambient temperature.

In a recent paper (4) Campanella and Mitchell have made a study of causes of this change in volume of soils due to various temperature increases. In their paper and in a previous paper by the author (5), it is noted that increases in temperature result in increases in pore pressure. Campanella and Mitchell further note that such increases lead, therefore, to a decrease in effective stress, which for undrained samples could result in natural swelling (unloading effect).

In the sine pulse tests, the temperature is applied rapidly to one surface of the sample. There is a significant difference in the resultant temperature propagation between this type of heating and a uniform heating of the entire soil sample. In the

latter, any increase in pore pressure would be reflected uniformly throughout the whole system, whereas in the former, pore pressure increases that are due to both thermal expansion of the saturating pore fluid and decrease of effective stress (total stress applied, external stress remaining constant) would increase at a decreasing rate in the direction of the decreasing temperature gradient. There are then two forces at work, somewhat opposing each other. As the sample swells due to heating of the pore fluid, the pore pressure increases, and the pressure can be dissipated by flow from the nearest drainage face. In this case the nearest drainage face is also the source of increasing temperature and the fluid would normally flow in the direction of decreasing temperature. Further, the rate of dissipation of pore pressure is controlled by the permeability of the system. If flow to the drainage face is limited while simultaneously the temperature is increasing, the result would appear temporarily as a net volume increase, as noted in samples 3 and 4. It is evident that further testing along these lines is necessary to confirm this.

The sine pulse tests, the tests by Campanella and Mitchell, and previous tests by the author (6) all show the importance of clearly delineating the boundary conditions in temperature tests in order to gain full understanding of the nature of temperature propagation and the resultant changes in deformation that may occur in a stressed sample.

CONCLUSIONS

The first test series on nonsaturated soils indicates that uniform temperature profiles with no discontinuities will be established in a recompacted soil when the initial moisture content variation throughout the sample depth varies as much as 2 percent in an erratic pattern. The soil can, then, be considered homogeneous with regard to its gross thermal properties. The increasing surface temperature causes moisture migration, as expected, with quantities of water (as evidenced by percent saturation) decreasing with increasing percent saturation.

The second test series indicated that, where boundary conditions can be modeled, heat conduction theory will predict temperature distributions within the sample. In addition, the sine temperature pulse applied to one surface of the stressed sample caused volume changes that result from a buildup and possible subsequent relief of pore pressure. These tests indicate that more research must be made into the interrelationship of the temperature boundary conditions, in the field and as modeled in the laboratory, and resulting subsequent deformation before more definite conclusions can be made.

It is known that the strength and density of compacted soil are dependent upon temperature. Because temperature changes in the field are continuous, establishment of continuous temperature profiles beneath the surface becomes desirable. By assuming homogeneity the ability to predict changes becomes simplified. Establishment of temperature profiles permits correlation to be made between surface temperature and moisture migration in a somewhat continuous, rather than steady-state, basis. Where recompacted soils are subject to stress, changing temperature patterns can create varying deformation patterns, depending on the boundary conditions (both flow and temperature) of the soil. While heat conduction theory can be used with some certainty, it becomes imperative to model the field conditions in the laboratory by proper choice of boundary conditions. Then, the use of heat conduction theory with proper laboratory testing should prove of great benefit in analyzing and predicting field soil performance under transient temperature conditions.

ACKNOWLEDGMENT

The research on the sine pulse was partially supported by a grant from the Research Foundation of the State University of New York. R. Eckerson carried out the experiments on the large cylinder tests.

REFERENCES

1. Kersten, M. Final Report, Laboratory Research for the Determination of Thermal Properties of Soils. Engineering Experiment Station, University of Minnesota, 1949.
2. Reno, W., and Winterkorn, H. Thermal Conductivity of Kaolinite Clay as a Function of Type of Exchange Ion, Density and Moisture Content. Highway Research Record 209, p. 79-85, 1968.
3. Paaswell, R., and Reismann, H. Transmission of a Thermal Pulse Through Soil. Paper T68 presented at American Geophysical Union, Washington, 1968.
4. Campanella, R., and Mitchell, J. Influence of Temperature Variations on Soil Behavior. Jour. Soil Mech. and Found. Div., ASCE, Vol. 94, No. SM3, Proc. Paper 5958, May 1968.
5. Paaswell, R. E. Thermal Influence on Flow From a Compressible Porous Medium. Water Resources Research, Vol. 3, No. 1, 1967.
6. Paaswell, R. E. Temperature Effects on Clay Soil Consolidation. Jour. Soil Mech. and Found. Div., ASCE, Vol. 93, No. SM3, Proc. Paper 5225, May 1967.

Some Temperature Effects on Soil Compressibility And Pore Water Pressure

ROBERT L. PLUM, Goldberg-Zoino and Associates, Cambridge, Mass., and
MELVIN I. ESRIG, Cornell University

Data are presented to show that heating a cohesive soil increases its compressibility at low levels of applied stress and also produces volume decreases. The volume changes associated with temperature increases are shown to be related to the degree of overconsolidation of the soil, decreasing as the overconsolidation ratio increases. Cooling the soil alters its stress-strain characteristics and causes it to behave as if it were overconsolidated. Secondary compression rates are shown to be affected only slightly by heating and significantly by cooling. Temperature-induced pore water pressures in undrained triaxial specimens are shown to be related to the stress history of the specimen and, for some materials, predictable from the results of triaxial consolidation tests.

•THE BEHAVIOR of soils under a particular stress system and at a constant temperature is governed by the stress (or strain) history of the material and by the applied effective stresses. Altering the temperature of a soil specimen can produce effects similar to changes in stress history (2, 5, 7, 12, 13) and can produce changes in the pore water pressures within the material (2, 5, 12, 15).

Clearly, any such changes, if unrecognized, may have important engineering implications. For example, a sample of a marine sediment may have been subjected to a temperature increase of 20 C between the time it was recovered from the ocean floor and was brought to the laboratory for testing. Temperature changes of this magnitude can be expected to alter the mechanical behavior of the soil and complicate, or make impossible, a proper engineering solution to a submarine problem.

Large temperature changes, frequently of a cyclic nature, also occur in more conventional circumstances. Samples obtained at a building site during the winter are subject to temperature decreases upon removal from the ground and then to temperature increases when they arrive in the laboratory, unless considerable care in handling is exercised. The reverse can occur in summer or in hot climates where the air temperature exceeds that of the ground and the laboratory. Thus, soil samples are frequently subjected to large temperature changes, and engineers must be in a position to evaluate the way these changes affect the mechanical behavior of the material.

SUMMARY OF LITERATURE

There is experimental evidence to indicate that the heating of a cohesive soil will cause it to decrease in volume (4, 12, 13), to decrease in undrained shear strength, and, perhaps, to exhibit a decrease in shear strength parameters obtained from an effective stress analysis (10). The observations suggest that temperature increases do not alter significantly the compressibility of soil upon continuous loading although its void ratio at a given pressure declines with increasing temperature (2, 3, 4).

Lambe (7) explained the decrease in volume of cohesive soils on heating using the double layer equations presented by Marshall (10). The development of these equations includes the assumption that the dielectric constant of the pore water is unaffected by temperature. In this form, the equations suggest that an increase in temperature depresses the electric double layer and permits the soil particles to move together.

TABLE 1

SOIL INDEX PROPERTIES

Index Property	Soil	
	Illite	Newfield Clay
Liquid limit, percent	112	25
Plastic limit, percent	28	14
Plasticity index, percent	84	11
Specific gravity	2.76	2.74
pH	5.1	7.9
Percent clay (<0.002 mm)	96	32
Primary clay minerals	Illite	Hydrous Mica Chlorite

Direct measurement of changes in particle spacing with variations in temperature in a montmorillonite slurry subjected to low stresses were reported by Yong et al (17). They observed volume increases in sodium montmorillonite subjected to temperature increases at constant externally applied stresses of less than one atmosphere. One might expect that the increase in energy associated with heating a soil would cause the expansion of the electric double layer in accordance with Yong's observations rather than the decrease in thickness suggested by Lambe.

The observation that temperature increases cause a decrease in soil volume as long as the drainage of pore water is permitted and the fact that, when heated, water will expand more than soil, leads to the conclusion that excess pore water pressures will develop whenever drainage is restricted. Temperature-induced pore water pressures have been reported by a number of investigators (2, 4, 12, 14, 15).

Several expressions have been developed to permit prediction of the temperature-induced pore water pressures (2, 14, 15). These expressions account for the volume changes in soil and water due to temperature changes but do not consider any changes in soil compressibility with temperature or the effects of secondary compression.

The research on temperature effects in cohesive soils has established that temperature increases cause volume decreases and has suggested that the volume change is somewhat dependent on rate of temperature increase (13). It is not yet clear how the stress history, perhaps as defined by the overconsolidation ratio, affects the observed volume changes. Nor is it clear why the heating of a soil temporarily increases its compressibility (i. e., causes the soil to decrease in volume while under a constant applied stress) but no change in compressibility from the preheating condition is observed when loading is continued at the new, higher temperature. The investigation reported herein was performed in an attempt to clarify some of these points and to gain insight into the phenomenon of pore water pressure development due to temperature change.

MATERIALS AND EXPERIMENTAL OBSERVATIONS

Two remolded soils were used in the testing program. One was a fractionated illitic material of high liquid limit and the other a glacial lake clay obtained from Newfield, New York. The properties of the soils are given in Table 1.

Submerged, $\frac{3}{4}$-in. thick soil specimens were tested in a fixed ring consolidometer around which water was circulated at a constant temperature. The tests were performed at temperatures of 50 and 24 C. About 3 hours were required to change the temperature of the circulating water by 26 C. Maximum variations of less than 2 C from these fixed temperatures occurred during the testing program and were found experimentally to have virtually no effect on the readings.

Temperature Effects on Volumetric Strain

Samples of illite and Newfield clay were poured into consolidometer rings as slurries and were consolidated to a pressure of 1. 7 psi at an initial temperature of 24 C before any heating was done. The initial water content of the illite was 180 percent and the initial water content of the Newfield clay was 44 percent. Consolidation was begun from a slurry in order to insure that the soil would be normally consolidated at very low pressure. Three tests were performed with each of the materials. In one test the soil was consolidated at a constant temperature of 24 C, in a second a temperature of 50 C was maintained, while in the third test the sample was loaded to 30 psi (New-

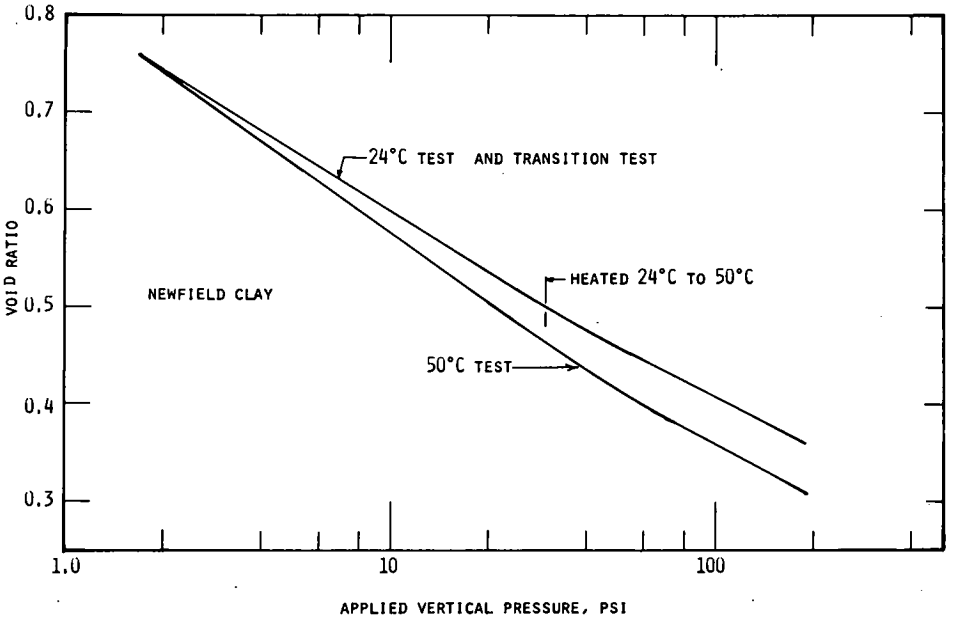

Figure 1. Consolidation test on Newfield clay.

field clay) or 40 psi (illite) at 24 C, then heated to 50 C and loading was continued. The results of these three tests on each of the materials are shown in Figures 1 and 2.

To facilitate comparison of the test results and to correct for small variations in the initial moisture content of the individual specimens, all of the test data have been normalized to a common void ratio at 1. 7 psi of pressure. The curves in Figures 1 and 2

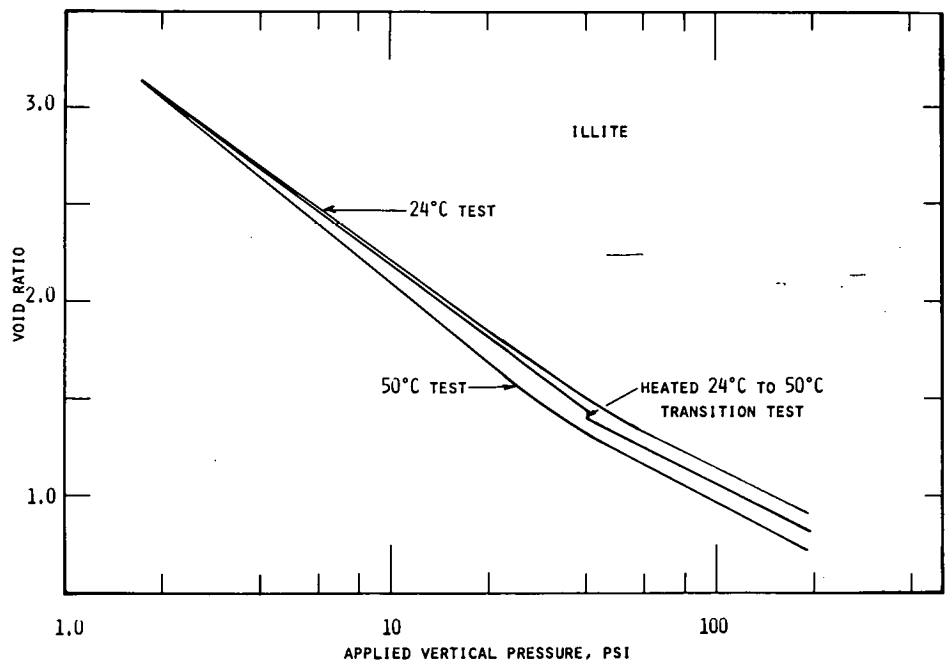

Figure 2. Consolidation test on illite.

TABLE 2

COMPRESSION INDEXES OF SOILS AT DIFFERENT TEMPERATURES

Test Temperature (deg C)	Illite		Newfield Clay	
	Low Pressure (<30 psi)	High Pressure (>30 psi)	Low Pressure (<30 psi)	High Pressure (>30 psi)
50	1.40	0.86	0.238	0.170
24	1.24	0.82	0.208	0.170
Transition Test				
50	–	0.84	–	0.170
24	1.23	–	0.204	–

indicate that at applied pressures smaller than about 30 psi both soils were more compressible when tested at 50 C than at 24 C. However, at pressures in excess of 30 psi, little difference in compressibility was apparent. In the transition tests, where the soil was first loaded to 30 psi before heating, the temperature change produced essentially no volume change of the inactive Newfield clay and about a 1 percent volumetric strain of the illite.

The slopes of the curves in Figures 1 and 2 are indicative of the compressibility of the soils and are defined as the compression indexes of the materials. Clearly, the compression index of each of the materials varies as a function of pressure and of temperature. This is in contrast with the observations of others (2, 3, 4). The compression indexes of the two materials at pressures above and below 30 psi and at temperatures of 50 and 24 C are given in Table 2.

The results of the transition tests (Figs. 1 and 2) showed that, after heating, both materials continued to behave as normally consolidated clays. The effect on the behavior of the material of heating to 50 C and then recooling to 24 C was investigated using the illitic material. Some of the results of this investigation are shown in Figure 3. Although recooling caused a slight expansion of the material, the volume change is too small to be shown on the figure. It can be seen that the cycle of heating and cooling

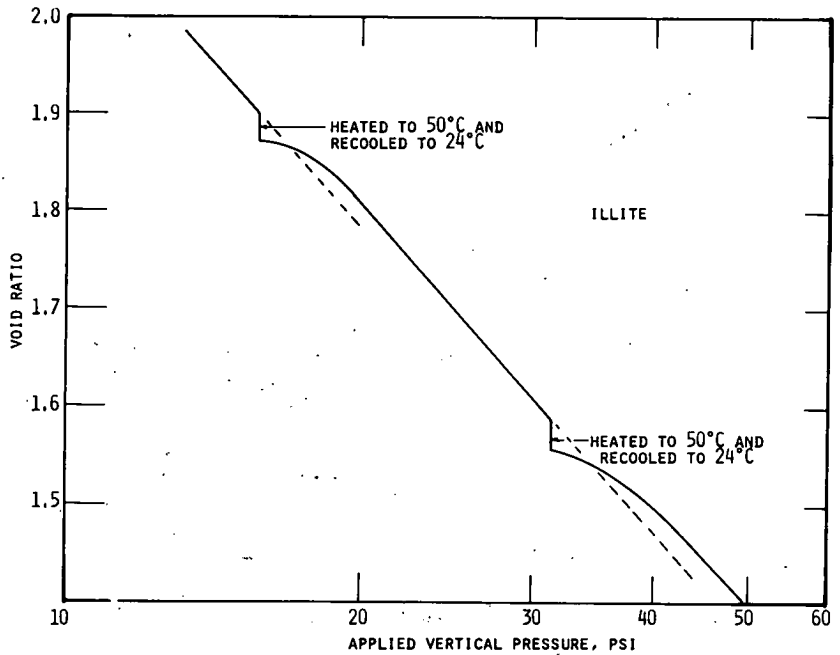

Figure 3. Effect on stress-strain behavior in consolidometer of heating and cooling illite.

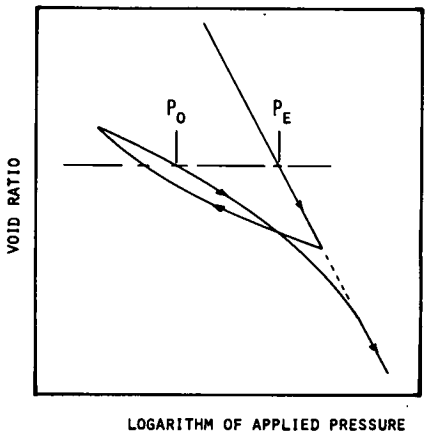

Figure 4a. Definition of overconsolidation ratio.

has caused the soil to behave as if it were overconsolidated. Furthermore, the new virgin portion of the consolidation curve, established by reloading after completing the cooling-reheating cycle, is displaced from the original virgin curve toward higher pressures. The reloaded soil appears to behave as if it were more overconsolidated than the volumetric strain associated with heating would suggest. Apparently a quasi-preconsolidation load similar to that found by Leonards and Rahmiah (8) was developed. This observation suggests that laboratory testing of natural soils that have been heated and recooled during the period of handling could lead to an incorrect evaluation of the maximum previous pressure to which the material had been subjected.

In assessing the effect of temperature changes on natural soils, it is of interest to investigate the relationship between the volumetric strain produced by heating and the overconsolidation ratio of material. When a soil is unloaded and then reloaded it arrives at the void ratio associated with the maximum previous pressure at a somewhat lower stress level and does not rejoin the virgin portion of the stress-strain curve until the maximum previous pressure has been exceeded. This is illustrated in Figure 4a. Because of this reloading behavior it is most convenient to define overconsolidation ratio as the ratio of the equivalent consolidating pressure p_e to the current pressure p_o at the time the soil is heated. The equivalent consolidation pressure is defined as the pressure required during the first cycle of loading to bring the material to the same void ratio it exhibited at the time it was heated. This definition is also illustrated in Figure 4a.

The relationship between the volumetric strain and the overconsolidation ratio p_e/p_o for the illitic material is shown in Figure 4b. It is evident that the volumetric strain associated with temperature increases decreases significantly as the soil is overconsolidated and is essentially zero at an overconsolidation ratio of the order of 1.7. These data suggest that volume change resulting from temperature cycling is considerably less important for overconsolidated soil than for normally consolidated soil.

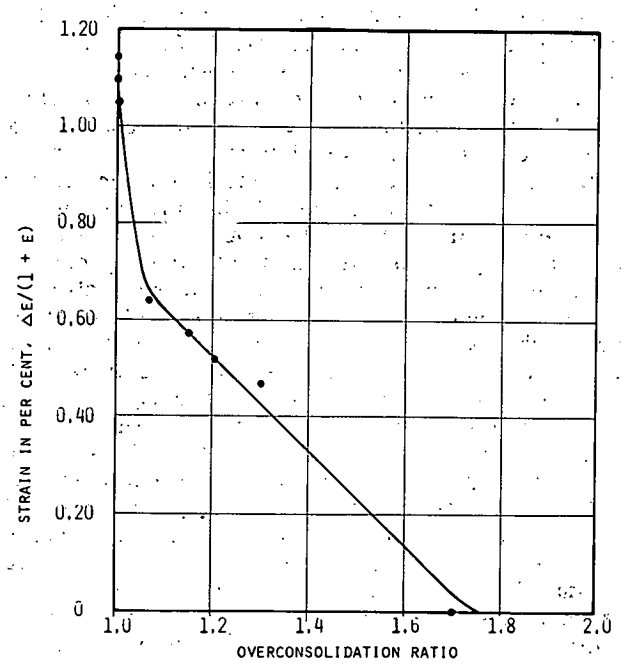

Figure 4b. Effect of overconsolidation ratio on volume change of illite heated from 24 C to 50 C.

Temperature Effects on Secondary Consolidation

Several investigators have reported that the heating of cohesive soils increases the rate of secondary consolidation (2, 9, 16). They also report thet secondary consolidation is of minor importance

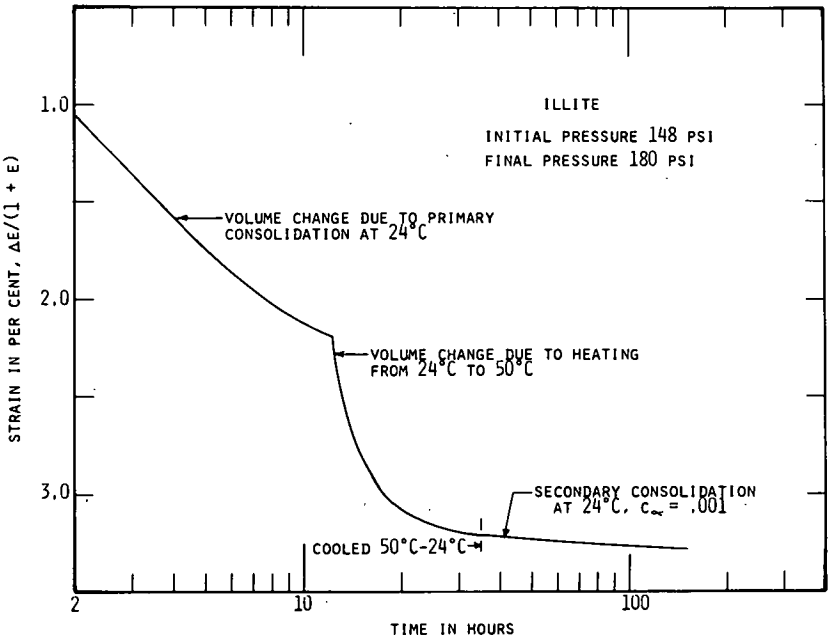

Figure 5. Effect of heating and cooling on secondary consolidation behavior of illite.

in overconsolidated soils. Two tests were performed with the illitic material in order to investigate these statements.

The illitic material exhibited a rate of secondary consolidation, defined by the slope of the consolidation curve on a plot of $\Delta e/(e + 1)$ vs logarithm of time in hours, of 0.005 when the temperature was 24 C. Figure 5 shows the results of a test in which a specimen of the same material was heated to 50 C after primary consolidation was completed and the volumetric strain due to heating was permitted to occur before the sample was cooled back to 24 C. After cooling, the volumetric strain of the specimen was observed for the next 5 days. It is important to note that about one day was required for the heating of the sample and for straining under the change in temperature. During the last 5 days, the relationship between volumetric strain and the logarithm of time was linear and had a slope c_α of 0.001. This is one-fifth of that exhibited by the normally consolidated material and suggests, once again, that the heating caused the sample to behave as if it were overconsolidated.

In a second test, the soil was consolidated at 24 C, heated to 50 C, and allowed to consolidate at this new temperature. As before, the heating caused a volumetric strain that required about one day to dissipate. Thereafter, the soil redefined a secondary consolidation curve with a slope c_α of 0.0053, which was only slightly larger than the slope of 0.0048 observed before heating.

It is of passing interest to note that the slopes of the secondary consolidation curves shown in Figure 6 increase by 10 percent due to heating and that the thermal energy, given by the ratio of the absolute temperatures of 323 C/297 C, was also increased by about 10 percent. Considered to be of greater significance, however, is the observation that increasing the temperature of the consolidating specimen of illitic material produced a rather small change in its secondary consolidation characteristics. However, this small change was only observable when the specimen was permitted to consolidate for a considerable time after the temperature change had occurred. It is considered possible, therefore, that the marked changes in secondary compression characteristics due to increases in temperature that have been reported by many investigators (2, 9, 16) have been confounded by the volumetric strains associated with heating. Further work in this area is apparently required.

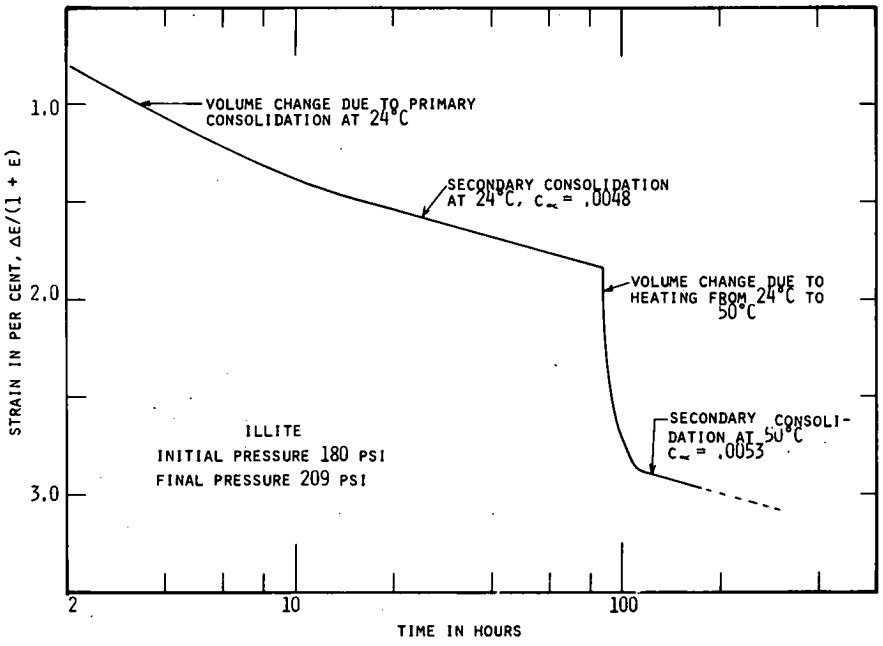

Figure 6. Effect of heating on secondary consolidation behavior of illite.

Temperature Effects on Pore Water Pressure

A lengthy discussion has been presented by Campanella and Mitchell (2) on whether or not the pore water pressures developed by changing the temperature of a soil specimen under undrained conditions should follow a closed hysteresis loop on temperature cycling as they observed (12) or should produce a pore water pressure that increases at a decreasing rate with each cycle to some maximum value. Their discussion indicated quite clearly that temperature cycling under undrained conditions was akin to repeated loading of the soil and suggests that in a soil like Newfield clay that exhibits no significant decrease in volume with increases in temperature, the pore water pressure developed by temperature changes should be directly predictable from the results of a triaxial consolidation test where the three principal stresses are equal.

Temperature cycling of Newfield clay remolded at a water content of 19 percent was done in a triaxial cell surrounded by a constant-temperature water bath. A backpressure of 30 psi was used to insure complete saturation of the soil, and pore water pressures were measured using a temperature-compensated pressure transducer. The temperature was varied between about 14 and 35 C, with some variation occurring in the actual end-points, at effective consolidating pressures of 20, 40, and 60 psi (cell pressures of 50, 70, and 90 psi). The results of the tests at 40 psi are shown in Figure 7 and indicated, as did the tests at 20 and 60 psi, that there was a gradual increase in pore water pressure for four cycles of temperature, after which no increase in pore pressure was observed with additional cycling.

The data in Figure 7 are similar to those presented by Campanella and Mitchell (2) for San Francisco Bay mud, Henkel and Sowa for Weald clay (5), and Sangrey for Newfield clay (15). They differ from the earlier data obtained by Mitchell and Campanella (12) in that they show the development of the hysteresis loop after four temperature cycles. This loop is not clearly defined in Figure 7 because the pore pressure measurements could only be obtained at the end of a temperature cycle after sufficient time had elapsed for temperature equalization throughout the system. The importance of these differences among the data can be discussed best after consideration is given to the results of a triaxial consolidation test to simulate temperature cycling.

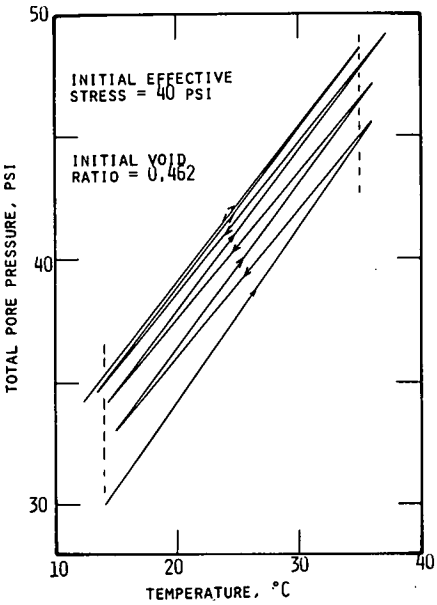

Figure 7. Pore water pressures resulting from undrained temperature cycling of Newfield clay.

Volume changes in the consolidation test were measured using a volume change gage that was calibrated and accurate to 0.0002 cc and was connected to the backpressure system and to the specimen. Stress cycling was done between two void ratios. The change in void ratio actually used corresponds to the volume expansion of the water in the sample when it is heated between 14 and 38 C. The results of this test in which cycling was done at effective consolidation pressures of 40 and 60 psi are shown in Figure 8. For clarity, only the unloading paths are shown in Figure 8 by single lines.

It required five stress cycles in the consolidation test to develop a closed hysteresis loop rather than the four cycles of temperature required before no further change in pore water pressure was observed. A portion of this difference may be the result of the nonuniformity of the temperature cycling, which is apparent from an inspection of Figure 7, and the rest may be associated with the somewhat too-large void ratio change used in the simulated temperature test (the consolidation test).

A comparison of the pore water pressures measured in the undrained tests (Fig. 7) with those predicted from the drained tests (Fig. 8) is given in Figure 9. The pore pressures given in Figure 8 were extrapolated or interpolated, as required, so that the comparison could be made for the temperature range of the consolidation test, i. e., for a temperature variation of 14 to 38 C.

The results of the triaxial consolidation and undrained triaxial tests in which the temperature was varied can be seen to be in good agreement when the specimen was reloaded or the temperature returned to its initial value and in poorer agreement at the higher pore pressures representing the unloading of the soil or the increasing of temperature. It is concluded that the drained consolidation test to simulate temperature cycling provides a reasonable representation of the stress changes produced by temperature changes, at least for materials that undergo minimal volume changes due to temperature increases.

The data in Figures 7 to 9 appear to substantiate the basic assumptions made in developing equations to predict pore pressure changes due to temperature fluctuations (2, 14, 15). Equally important, however, is the observation that it takes several cycles of loading and unloading or of temperature variation before a hysteresis loop can be expected.

The drained stress cycling of the Newfield clay between two fixed void ratios produced a material that was overconsolidated. It would appear that it is only when the material is somewhat overconsolidated that a closed hysteresis loop can and does develop. This could be the explanation for the observations of Campanella and Mitchell (2). The two materials they tested that exhibited a hysteresis loop almost immediately upon temperature cycling were overconsolidated. Their illitic soil and been overconsolidated by drained temperature cycling before the undrained tests were performed while their kaolinitic material was overconsolidated by initially cooling the sample before the temperature was raised and then cycling back to the cooled temperature.

Thus, the data included herein suggest an explanation for the hysteresis effect noted by some and not observed by others. They also suggest the validity of the approach used to predict pore water pressures in undrained specimens due to temperature changes (2). Newfield clay was an appropriate material to use in arriving at these conclusions because the test results reported earlier indicate that temperature increases cause

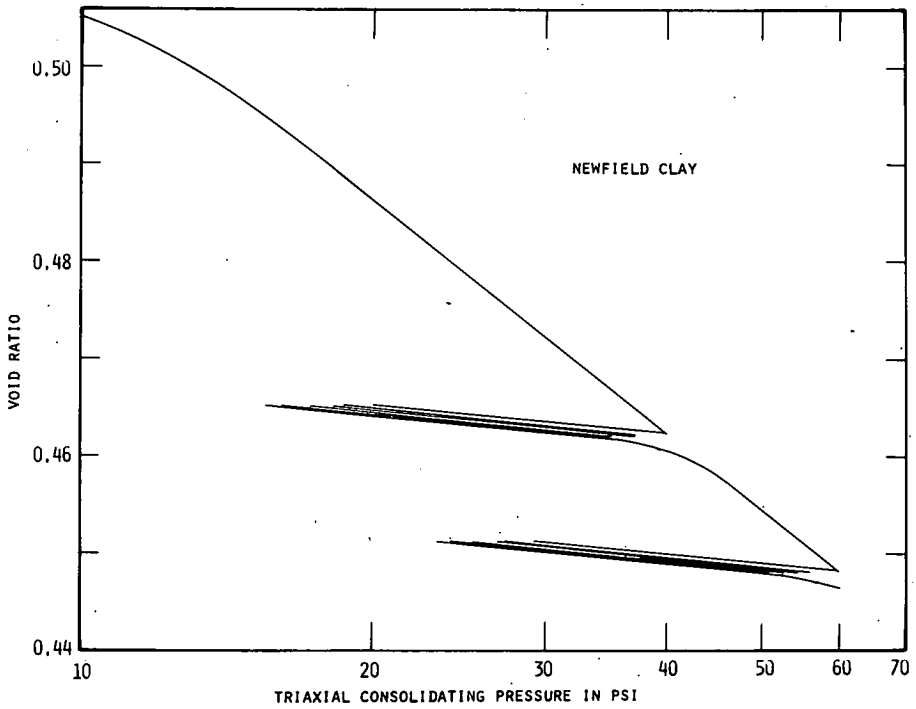

Figure 8. Triaxial consolidation test on Newfield clay to simulate temperature cycling.

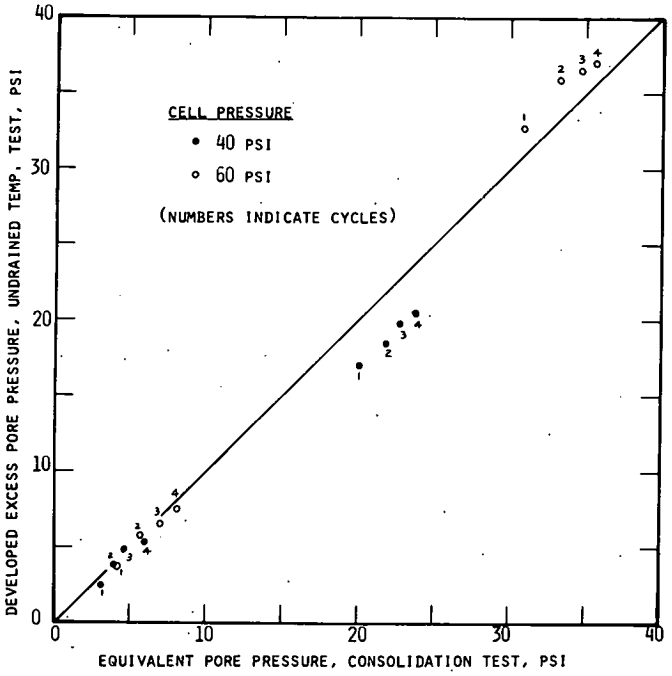

Figure 9. Comparison of undrained pore pressures and simulated pore pressure due to temperature cycling.

little volume change and virtually no change in compressibility within the pressure range of the investigation.

MECHANISTIC INTERPRETATION OF SOIL BEHAVIOR DUE TO HEATING

A cohesive soil may be considered to be composed of clay platelets of various shapes and sizes packed in some fashion dependent upon its manner of deposition (or artificial preparation) and its environment. Loads applied to the material externally are transmitted through the system at points of particle "contact." In this concept, the clay fabric is pictured as a complex three-dimensional truss with the contact points as the joints. The forces at the contacts are the Van der Waals forces of attraction, the repulsive forces due to the interaction of the electric double layers on the clay surfaces, and some portion of the externally applied forces. If the electric double layers are expanded and, as a result, the repulsive forces increased, readjustment of the soil structure under the applied loads can be expected.

Decreases in soil volume with expansion of the electric double layer have been reported by Kenney (6). While maintaining a constant, externally applied, axial force on a soil specimen in a consolidometer, Kenney leached salts from samples of noncemented Norwegian marine clays, thereby increasing the thickness of the electric double layer, and he observed a marked decrease in the volume of the specimen. The decrease in volume was pressure-dependent and was most pronounced at high pressures. Kenney explained this observation by reference to interparticle forces and to Lambe's (7) mechanistic model of soil behavior. He suggested that the expansion of the electric double layer decreased the effective stresses at the particle contacts, which permitted shear failures to occur at these contacts. Volume decrease (consolidation) is the manifestation of these shear failures.

By hypothesizing that heating expands the electric double layer, as the leaching of the salts is known to do, it is possible to explain the apparently contradictory observations of Lambe (7) and Yong (17), discussed earlier. The tests reported by Yong et al (17) were performed on sodium montmorillonite specimens consolidated from a slurry at pressures of less than 1 atmosphere. The concentrations of salts in the pore fluid were such that a reasonably dispersed structure (parallel clay plates) might be expected. Interparticle contact was probably small. Consequently, expansion of the electric double layer by heating would be expected to cause the observed volume increase.

The clays used in the tests reported by Lambe (7) and others were less active and interparticle contacts were important. Expansion of the electric double layer would, in this case, reduce the effective stresses at the points of contact and permit shear deformations and consolidation to occur. Mechanistically speaking, Lambe (7) and Kenney (6) suggested that the effective stress at the point of contact N' is related by Eq. 1 to the stress N associated with the externally applied loads, to the repulsion R of the electric double layers, and to the attraction A of the Van der Waals attractive forces:

$$N' = N - (R - A) \tag{1}$$

The resistance to sliding at the particle contact is assumed to be some function of N'. If some constant external force is assumed, then changes in interparticle effective stress are related to changes in the repulsive and attractive forces. It is commonly assumed that the respulsive forces decrease exponentially with interparticle distance while the attractive forces vary with the inverse third power of the interparticle spacing. In accordance with Eq. 1, an increase in the thickness of the electric double layer, which increases the interparticle repulsion when the particle spacing is essentially fixed, decreases N' and therefore decreases the shearing resistance at the particle contact. When the shearing resistance at the points of contact is reduced and the shearing stress is maintained sensibly constant, shear displacement can be expected. The displacement will continue until the particles are rearranged to a configuration that is stable under the new effective stresses.

The preceding argument suggests that the heating of a cohesive soil with a significant number of interparticle contacts should lead to the increase in compressibility observed at low pressures in the tests reported herein rather than produce no change as observed by others (2, 3, 4).

It is also of interest to note that Yossef et al (18) have shown that the liquid and plastic limits of soils decrease with increasing temperature. They explain their results by reference to the decreasing viscosity of water with increasing temperature. However, it is clear that both the liquid and plastic limit tests are measures of the shearing resistance of the soil and therefore their observations are considered to be in agreement with the mechanistic model proposed and to be explained better by reference to this model.

Tests by Burmister (1) also tend to confirm the foregoing hypothesis. Burmister's tests show that the maximum dry density that can be obtained from a Proctor compaction test is increased as the temperature increases. At 65 F, the dry density of a particular soil was found to be 104 pcf at the optimum moisture content. The same material achieved a dry density of only 90 pcf at 35 F.

The proposed model may also be used to explain the observation that decreasing the temperature of a consolidating soil mass causes it to behave as if it were overconsolidated. By decreasing the temperature, the electric double layer is compressed, the repulsive forces are reduced, and the shearing resistance at the points of contact is increased. Thus, a large increase in external stress is required before significant further consolidation is obtained.

SUMMARY AND CONCLUSIONS

Data have been presented to suggest that temperature increases do, indeed, cause changes in the compressibility of soils. However, the compressibility changes are most notable in soft soils consolidated under small stresses. At applied stresses in excess of about 30 psi, temperature increases appear to produce insignificant changes in compressibility.

Cooling a sample causes it to behave as if it were overconsolidated, as suggested by Campanella and Mitchell (2), and appears to produce a quasi-preconsolidation load. This temperature-induced alteration in stress history could be of consequence when the results of laboratory tests are applied to field problems.

The volume change of a specimen subjected to an increase in temperature is dependent on its degree of overconsolidation. At an overconsolidation ratio of 1.7, no apparent volume decrease occurred in the illitic material as a result of a temperature increase of 26 C.

Secondary compression rates appear to be only slightly affected by increases in temperature, provided that sufficient time is allowed for the volume change associated with the temperature increase to be dissipated. This conclusion is in sharp contrast to the conclusions reached by others (2, 9, 16). In agreement with the observations of others (2), the data indicate that overconsolidation of soil by decreasing its temperature reduces the rate of secondary consolidation dramatically. Consequently, for those soil problems in which secondary consolidation is an important consideration, great care must be exercised in obtaining, handling, and testing the specimens.

Temperature changes are known to induce pore water pressures in soils. The new data presented herein suggest that current techniques for the prediction of these temperature-induced pore water pressures are sound and that for some materials, at least, the pore water pressures can also be predicted from the results of consolidation tests in which the specimen is unloaded between two void ratios.

ACKNOWLEDGMENTS

This investigation was performed at Cornell University while one of the writers held a National Science Foundation Traineeship. This support is acknowledged and appreciated. The writers also wish to thank Dr. Dwight A. Sangrey for his interest and help during the early stages of the investigation.

REFERENCES

1. Burmister, D. M. Environmental Factors in Soil Compaction. Symposium on Compaction of Soils, ASTM Spec. Tech. Publ. 337, 1964.
2. Campanella, R. G., and Mitchell, J. K. Influence of Temperature Variations on Soil Behavior. Jour. Soil Mech. and Found. Div., ASCE, Proc. Paper 5958, Vol. 94, No. SM3, p. 709-734, 1968.
3. Finn, F. N. The Effect of Temperature on the Consolidation Characteristics of Remolded Clay. ASTM Spec. Tech. Publ. 126, p. 65-72, 1951.
4. Gray, H. Progress Report on Research on the Consolidation of Fine-Grained Soils. Proc. Internat. Conf. on Soil Mech. and Found. Eng., Harvard University, Vol. 2, p. 138-141, 1936.
5. Henkel, D. J., and Sowa, V. A. Discussion of paper by Mitchell and Campanella, Symposium on Laboratory Testing of Soils, ASTM Spec. Tech. Publ. 361, p. 104-107, 1963.
6. Kenney, T. C. Shearing Resistance of Natural Quick Clays. PhD thesis submitted to University of London, 1966.
7. Lambe, T. W. A Mechanistic Picture of Shear Strength in Clay. Proc. ASCE Research Conf. on Shear Strength of Cohesive Soils, Boulder, Colorado, p. 555-580, 1960.
8. Leonards, G. A., and Rahmiah, B. K. Time Effects in the Consolidation of Clay. Symposium on Time Rate of Loading in Soils, ASTM Spec. Tech. Publ. 254, p. 116-130, 1959.
9. Lo, K. Y. Secondary Compression of Clays. Jour. Soil Mech. and Found. Div., ASCE, Proc. Paper 2885, Vol. 87, No. SM4, p. 61-66, 1961.
10. Marshall, C. E. The Physical Chemistry and Mineralogy of Soils. John Wiley and Sons, New York, 1964.
11. Mitchell, J. K. Shearing Resistance of Soils as a Rate Process. Jour. Soil Mech. and Found. Div., Proc. Paper 3773, Vol. 90, No. SM1, p. 29-61, 1964.
12. Mitchell, J. K., and Campanella, R. G. Creep Studies on Satruated Clays. Symposium on Laboratory Shear Testing of Soils, ASTM Spec. Tech. Publ. 361, p. 90-103, 1963.
13. Paaswell, R. E. Temperature Effects on Clay Soil Consolidation. Jour. Soil Mech. and Found. Div., ASCE, Proc. Paper 5225, Vol. 93, No. SM3, p. 9-22, 1967.
14. Plum, R. L. The Effect of Temperature on Soil Compressibility and Pore Pressure. MS thesis submitted to Cornell University, 1968.
15. Sangrey, D. A. The Behavior of Soils Subjected to Repeated Loading. PhD thesis submitted to Cornell University, 1968.
16. Schiffman, R. L., Ladd, C. C., and Chen, A. T. Secondary Consolidation of Clay. Proc. Rheology and Soil Mech. Symposium, Grenoble. Springer-Verlag, Berlin, 1966.
17. Yong, R. T., Taylor, L., and Warkentin, B. P. Swelling Pressures of Sodium Montmorillonite at Depressed Temperatures. Proc. 11th Nat. Conf. on Clay and Clay Minerals, p. 268-281, 1962.
18. Youssef, M. S., Sabry, A., and El Ramli, A. H. Temperature Changes and Their Effects on Some Physical Properties of Soils. Proc. 5th Internat. Conf. on Soil Mech. and Found. Eng., Vol. 1, p. 419-421, 1961.

Soil Stabilization by Incipient Fusion

JAMES L. POST and JOSEPH A. PADUANA,
Department of Civil Engineering, Sacramento State College

A procedure is given for determination of the melt range of soil-additive mixtures using the phase equilibria approach, thus making possible the choice of a fluxing agent to bring the melt range of the mixtures within the capabilities of existing mobile downdraft heaters. The investigation includes the melt-temperature range of soils with respect to their composition, an analysis of soils representative of the various oxide combinations found in soil types comprising the surface of the earth, and the thermal stabilization of a soil by use of a common fluxing agent to lower the incipient fusion temperature.

The behavior of soils at high temperatures was investigated to predict phase changes and melt ranges for the mineral combinations existing in soils. A list of common clay and non-clay minerials is presented, including structural water contents, typical atomic proportions of dry melt, and melt-temperature ranges, and a method is described for estimating the full-melt temperatures of soils with these data. Some estimated and observed fusion ranges are given for soil aggregate material.

Mineralogy and oxide combinations of common soil types of the world are considered, and a list of representative soils is presented together with the soil mineral contents.

A typical soil from the Sierra Uplift was investigated for mineral content, and the reduction in soil full-melt temperature was estimated for increments of soda ash additive necessary to bring the temperature within usable range for practical thermal stabilization. Pyrometric cone tests, combining visual observation with thermo-electric recording, were used to determine the soil-additive incipient fusion temperatures.

Further research is needed on the effects of type and amount of fluxing agent on the properties of thermally stabilized soils.

•THE INITIAL investigation into high-temperature soil properties was undertaken because a space isotope power supply may eventually return to earth and become buried in a soil, and such a system is thermally very hot. The purpose of this investigation is to show how the approximate melt range of a soil may be determined using the phase equilibria approach, and to show how the soil melt range may be lowered by the addition of an appropriate fluxing agent to make possible the thermal stabilization of a typical soil for road construction with existing equipment.

SOIL MINERAL COMPONENTS

The entire soil horizon consists of in-place weathered rock or transported material comprised of certain mineralogical suites, which are primarily determined by source material, climate, and topography. There are ordinarily two or three colloidal-size minerals that predominate in a soil depending on the weathering stage of the soil.

The silicate minerals that form the predominant portion of most soils, along with carbonates, sulfates, and oxides, may be described in terms of constituent oxides when considering the melt range of any soil complex. The composition of the crust of

the earth has been estimated to consist of approximately the following oxide percentages: SiO_2, 59.8; Al_2O_3, 14.9; Fe_2O_3, 2.7; FeO, 3.4; MgO, 3.7; CaO, 4.8; Na_2O, 3.2; K_2O, 3.0; H_2O, 2.0; TiO_2, 0.8; CO_2, 0.7; P_2O_5, 0.3; remainder, 0.7. These twelve oxides, which form the predominant portion of the earth's crust, vary in melt temperature from 0 C for H_2O to 2800 C for MgO but have an average melt range of about 1300 C.

Certain components of soils were first investigated during the latter part of the 19th century by ceramists to determine their fluxing properties. The soil components of primary interest to the ceramists were the clays and feldspars, especially kaolinite and microcline. During this time research was also conducted on the high-temperature physical characteristics of silica-alumina refractory bricks for use in metallurgical processes.

Most of the soil mineral investigations undertaken in agriculture and mineralogy have involved reactions at ambient temperatures. The study of the formation and alteration of rocks and minerals at high temperatures and pressures has been undertaken primarily in geochemistry and geophysics and is far from being complete. Much work has also been done with the high-temperature phase relations of metals, alloys, and oxides in metallurgy.

SOLID PHASE REACTIONS

A soil mass consists of a network of solid particles enclosing voids filled with moisture and gas. The solid particles may consist of many different minerals, some of which contain water as an integral part of their crystal lattice structure (hydration compounds). Most solid particles also hold surface water layers by means of molecular attraction (adsorption). A soil mass may also contain carbonate and sulfate minerals which, when heated sufficiently, will degas with subsequent alterations in crystalline structure.

The clay minerals (hydrous layered silicates) may also contain layers of water that are bound to the clay mineral surfaces by the residual negative charges possessed by the clay mineral structures and the cations, such as Ca^{++} or Na^{+}, contained in the water. This "bound water" requires considerable heat energy to be separated from the solids. Many common soil minerals suffer a significant weight loss when the minerals are heated through their solid phase ranges. Nutting (1) and Grim (2) have given weight loss data for the more common clay minerals and the more common hydrous non-clay soil minerals.

When the temperature of the soil mass is first increased the free interstitial water is driven off, then the adsorbed water is driven off. The bound water held by the clay minerals may not be completely and irreversibly driven off until many of the hydrated soil minerals, such as gypsum, goethite, and gibbsite, are also dehydrated. As the soil mass is heated further the hydration water is driven off and new minerals are formed having different crystalline morphologies. Often several solid-state phase changes may ensue, with the hydration water being driven off in stages and then the anhydrous minerals going through several phase changes.

At higher temperatures the carbonate soil minerals, such as calcite and dolomite, begin to break down, the partial pressure of the carbon dioxide increases rapidly, even in calcite above 600 C, and at higher temperatures the solid-state phases of the oxides result (1, p. 216). The chlorides, sulfides, and sulfates are metastable when heated in air; the sulfides tend to become sulfates and the minerals melt without oxidizing when forming a predominant part of the soil mass. If a large part of the surface area of the soil mass is exposed to air the chlorides and sulfates will eventually oxidize with a resultant loss of chlorine and sulfur dioxide as the temperature is increased; however, the sulfates tend to be stable even in the molten state under some conditions. Of these chlorides and sulfates, halite and gypsum are the only two common soil minerals that are encountered in soils, and these minerals seldom comprise a predominant part of the soil masses except in hot arid playas, such as the bolsons of the southwest United States.

The figures and tables given by Nutting (1) may be used to estimate weight losses in soil masses when heated. It is only necessary to know the quantitative mineralogy of the soil mass to estimate the weight loss of the soil for any temperature. Most soil masses consist largely of quartz and feldspars and thus, when heated, will suffer weight losses mainly from the gassing of free pore water and adsorbed water.

LIQUID PHASE

The congruent melt point of a compound is the temperature at which the liquid phase of the compound is in equilibrium with the solid phase. When there is more than one compound present, each with different melt points, the mixture will melt incongruently. Most soils consist of mixtures of minerals comprised of several different oxides and therefore will exhibit incongruent melt ranges rather than a melt point.

A mixture of two or more solid compounds, when heated to the eutectic temperature, produces a certain amount of liquid by interaction or fusion, but the upper melt point of the combination of minerals will depend on the mixture ratio. A eutectic mixture will melt congruently. The temperature range in which there is a phase change from solidus to liquidus is dependent on the mixture of soil minerals and the rate of heating. The rate of heating in turn is dependent on several soil parameters, such as grain size distribution, absolute density, gas-phase conditions, and moisture content.

MELT POINT DETERMINATION

At a temperature of about 500 C the adsorbed water on the clay particles will be driven off irreversibly, and by 900 C the CO_2 will be driven off the calcium carbonate. The SO_3 of the sulfates and the organic content of the soil also will have been mostly driven off. The organic material may cause a reducing action when being burned off.

The typical composition of the more common soil minerals is listed in Tables 1 and 2 together with the atomic proportions of oxides present at dry melt conditions. The

TABLE 1

COMMON SOIL MINERALS (NON-CLAY)

Mineral	Structural Water (%)	Typical Atomic Proportions of Dry Melt									Melt Point (deg C)	
		CaO	K_2O	Na_2O	FeO	Fe_2O_3	TiO_2	MgO	Al_2O_3	SiO_2	Estim.	Observed
Feldspars:												
Albite	–	0.004	–	0.114	–	–	–	–	0.200	0.682	1115	1100-1200
Oligoclase	–	0.040	–	0.091	–	–	–	–	0.232	0.637	1200	1200-1300
Andesine	–	0.078	–	0.067	–	–	–	–	0.261	0.594	1305	1300-1355
Microcline	–	–	0.133	0.024	–	–	–	–	0.198	0.645	1355	1150-1530
Orthoclase	–	–	0.105	0.042	–	–	–	–	0.199	0.654	1305	1150-1530
Anorthoclase	–	0.012	0.042	0.080	–	–	–	–	0.207	0.659	1200	1100-1200
Amphiboles:												
Hornblende	1.9	0.124	–	0.010	0.101	0.034	0.009	0.150	0.073	0.499	–	1180-1220
Pyroxenes:												
Enstatite	0.3	0.008	–	–	0.046	0.006	–	0.353	0.010	0.577	–	1380-1500
Augite	0.5	0.193	–	–	0.094	0.019	0.008	0.142	0.035	0.509	–	1150
Carbonates:												
Calcite	44.4%CO_2	1.000	–	–	–	–	–	–	–	–	2550	2570
Dolomite	47.4%CO_2	0.579	–	–	0.025	–	–	0.396	–	–	2300	2100
Sulfates:												
Gypsum	20.6	1.000	–	–	–	–	–	–	–	–	2550	–
Zeolites:												
Analcite	8.3	–	–	0.147	–	–	–	–	0.254	0.599	1150	–
Iron oxides:												
Hematite	–	–	–	–	–	1.000	–	–	–	–	–	1594
Goethite	10.5	–	–	–	–	0.987	–	–	–	0.013	1585	–
Magnetite	–	–	–	–	0.309	0.691	–	–	–	–	–	1594
Alumina oxides:												
Gibbsite	33.7	–	–	–	–	–	–	–	0.979	0.021	2025	2020
Corundum	–	–	–	–	–	0.010	–	–	0.983	0.007	2025	2020
Others:												
Quartz	–	–	–	–	–	–	–	–	–	1.000	–	1720
Ilmenite	–	–	–	–	0.411	0.071	0.505	0.013	–	–	1390	1400
Halite	–	–	–	–	–	–	–	–	–	–	–	801

TABLE 2

COMMON CLAY MINERALS

Mineral	Structural Water (%)	Typical Atomic Proportions of Dry Melt									Melt Point (deg C)	
		CaO	K_2O	Na_2O	FeO	Fe_2O_3	TiO_2	MgO	Al_2O_3	SiO_2	Estim.	Observed
Kandites:												
Kaolinite	14.3	–	–	–	–	–	–	–	0.460	0.540	1810	1785
Halloysite	17.4	–	0.006	–	–	–	–	–	0.456	0.538	1800	1775
Smectites:												
Montmorillonite	21.2	0.030	–	–	–	0.029	–	0.041	0.236	0.664	1490	–
Nontronite	22.4	0.029	–	–	–	0.380	–	–	0.071	0.520	1580	–
Micas:												
Muscovite	4.8	–	0.106	0.009	–	–	–	–	0.395	0.490	–	1255-1290
Phlogopite	3.1	–	0.098	–	0.048	0.031	0.016	0.231	0.158	0.418	1200	–
Biotite	2.3	–	0.086	–	0.186	0.056	0.038	0.094	0.153	0.387	–	1155-1240
Others:												
Illite	7.2	–	0.071	–	–	0.041	–	0.019	0.279	0.600	1590	–
Vermiculite	19.1	–	–	–	0.012	0.065	–	0.291	0.197	0.435	1580	–
Rapidolite	11.3	–	–	–	0.255	0.034	–	0.185	0.231	0.295	1540	–
Attapulgite	19.9	–	0.006	–	–	0.044	–	0.131	0.129	0.690	1530	1380-1500
Serpentine	13.5	–	–	–	–	0.005	–	0.483	0.012	0.500	1800	–

estimated and observed melt ranges are given for non-clay minerals in Table 1 and clay minerals in Table 2. The typical mineral compositions are derived from data tabulated by Deer et al (3).

The most common minerals forming the rocks of the outer crust of the earth are feldspars, quartz, micas, amphiboles, and pyroxenes, the feldspars often comprising more than half of this combination. Because the soils are derived from the earth's rock crust, a large portion of soils will consist of feldspar, quartz, and micas, the amphiboles and pyroxenes being more susceptible to weathering. Clay minerals are largely of diagenetic origin and may be formed in place or be detrital; kaolinite, illite, and montmorillonite are the most common clay minerals.

To determine the melt range for any soil, the mineral constituents of the soil must be identified and the amount of each mineral present must be ascertained. The soil constituents may be expressed as oxides, as in Tables 1 and 2, and their atomic propor-

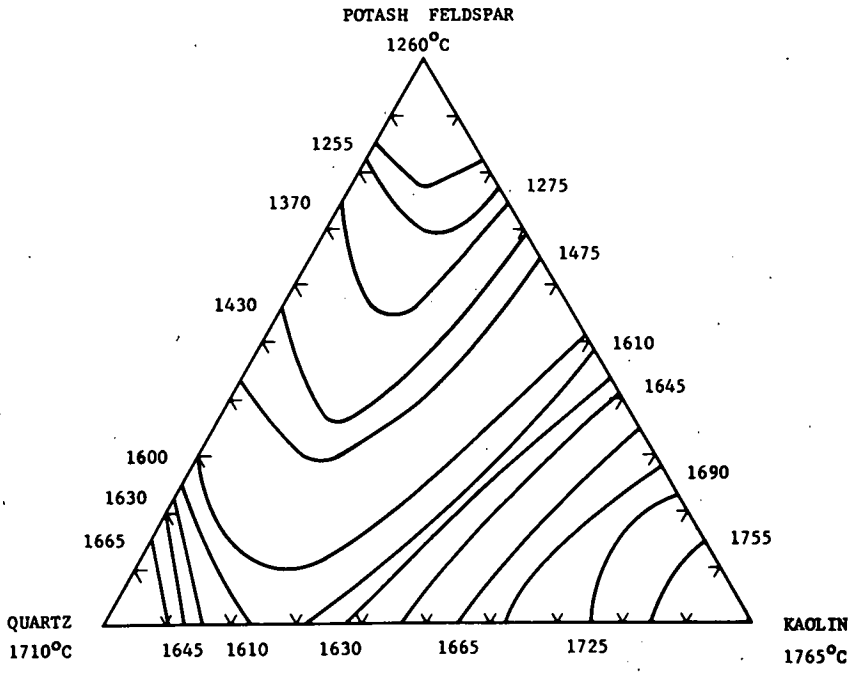

Figure 1. Feldspar-kaolin-quartz ternary phase diagram [after Wilson (6)].

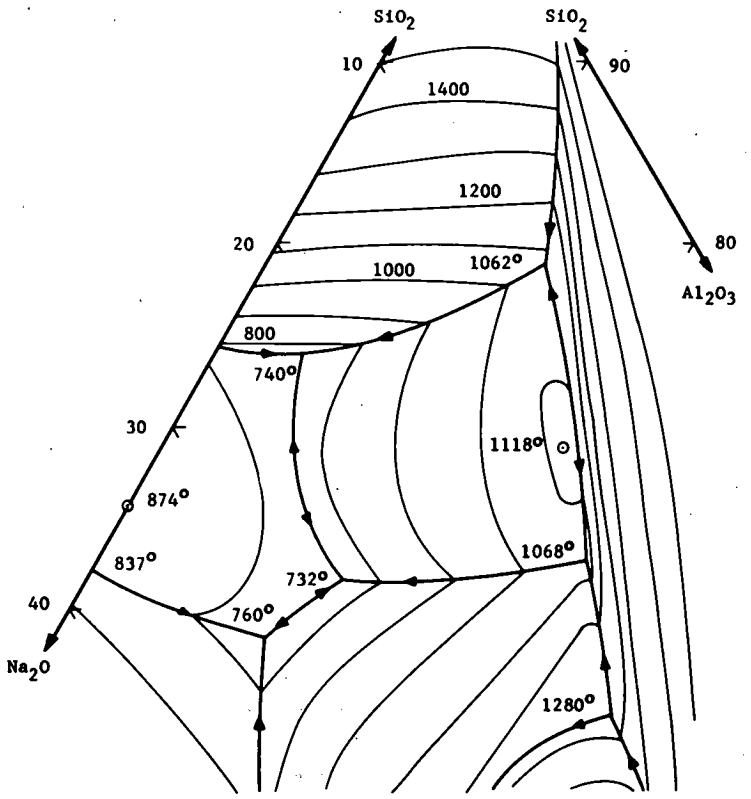

Figure 2. A portion of the system Na_2O-Al_2O_3-SiO_2; composite [after Levin et al (5)].

tions may then be computed. After the soil mineral composition is determined, a summation of the more predominant oxides must be made.

The upper melt range of the soil may be determined from oxide ternary phase diagrams. In general there will be only three or four predominant oxides in the soil. When more than three oxides are present, an interpolation must be made between phase diagram temperature values. This interpolation may be considered as linear in nature for purposes of estimating the soil melt range because a slight depression in melt point is ordinarily produced by the addition of another oxide. The amount of melt temperature depression is given by Raoult's law.

The most common phase system encountered in the study of refractories is the silica-alumina binary phase system, including the most common clay minerals. Refractory bricks made from these clays are in this binary phase system. A direct comparison may be made between estimated and observed melt temperatures for different silica-alumina ratios (4).

The most common rock minerals—the feldspar suite—contain a discontinuous solid-state series of mineral compositions consisting of lime, soda, and potash feldspars. Minor amounts of some other oxides may be present in the feldspars but are not common. The feldspar ternary phase diagram is given by Levin et al (5, p. 313) and shows that the potassium and sodium feldspars, as well as the potassium and sodium oxides, have similar melt ranges except for the formation of leucite from potash feldspar when more than about 75 percent of potash feldspar is present.

The fusion ranges for the potash feldspar-kaolin-quartz (flint) ternary phase system were determined before 1907, as shown by Wilson (6, p. 252). Soda feldspar gives melt ranges similar to the potash feldspars, so that the phase diagram (Fig. 1) may be used to estimate the melt ranges of mixtures when albite or perthite are used instead of the microcline.

Phase diagrams are given by Levin et al (5) and Muan and Osborn (7) for all of the more common soil mineral oxides that may be encountered. A portion of the Na_2O-Al_2O_3-SiO_2 ternary phase diagram is shown in Figure 2. Phase diagrams give full-melt temperatures for pure mineral systems in each case. Because there are always minor constituents and trace elements in soils, melt ranges for soils will nearly always be lower than those indicated by ternary phase diagrams. As an example, the fusion temperatures given in Figure 1 are generally about 100 C below those given by the comparable Al_2O_3-K_2O-SiO_2 ternary phase diagram. Some metal oxides, such as Na_2O, greatly depress the melt point of oxide mixtures, even when present in small quantities.

Additional ternary phase diagrams most relevant to soil minerals are the seven diagrams that include Al_2O_3 and SiO_2 as end points together with either CaO, FeO, Fe_3O_4, K_2O, MgO, Na_2O, or TiO_2 as a third end point, as well as composite systems CaO-MgO-SiO_2 and MgO-FeO-SiO_2. The quaternary phase diagrams (7) of CaO-MgO-SiO_2 for differing amounts of Al_2O_3 are also very helpful.

The ternary phase diagram, Figure 1, includes many of the common pedalfer soils of the humid temperate and subtropical zones of the world, potash-soda feldspars being considered together. The upper melt range of the potash feldspar-kaolin-quartz mixtures may be computed in the following manner, considering a mixture of 25 percent K-feldspar, 50 percent kaolin, and 25 percent quartz:

25% K-feldspar					
Formula (ideal)		K_2O	Al_2O_3	$6SiO_2$	
Atomic weight		94	102	360	= 556
Atomic proportion [A.P.]		0.163	0.184	0.647	
A.P. X 25%		4.2%	4.6%	16.2%	
50% Kaolin					
Formula (ideal)			Al_2O_3	$2SiO_2$	
Atomic weight			102	120	= 222
Atomic proportion			0.459	0.541	
A.P. X 50%			22.9%	27.1%	
25% Quartz					
Formula				SiO_2	
Atomic weight				60	= 60
Atomic proportion				1.000	
A.P. X 25%				25.0%	
Oxide ratio	Σ	4.2%	27.5%	68.3%	= 100.0%

The observed and estimated full-melt temperature (Figs. 1 and 2) may be compared for different proportions of feldspar, kaolin, and quartz comprising artificial soil mixtures. Generally, the estimated melt temperatures appear to be about 100 C higher than the observed melt temperatures. The minerals used to produce the data for Figure 1 were not chemically pure, and therefore a lower melt range is to be expected.

In fusion tests the high viscosity of the melted feldspar, the low rate of solution of the quartz, and the slow diffusion of the partially mixed and partially melted batch materials hinder the attainment of equilibrium and of homogeneity, so that the constituents not only differ from the equilibrium phases but the composition varies throughout the mixture.

The following is an example of the determination of the melt range of a calcareous sandy soil from the Rio Grande basin. The mineral composition was estimated from X-ray diffraction and chemical analyses, and, using the oxide constituent proportions given in Tables 1 and 2, the total oxide content was computed and adjusted for loss of water and carbon dioxide. The computed dry-melt oxide content, in percent, included: SiO_2, 73.4; Al_2O_3, 11.7; CaO, 9.8; Na_2O, 2.3; K_2O, 2.0; MgO, 0.5; and Fe_2O_3, 0.3.

TABLE 3

FUSION RANGE OF SOIL AGGREGATE MATERIAL

Soil No.	Material	Approximate Melt Range (deg C)	
		Estimated	Observed
	(a) Natural soils		
1	Black Hills bentonite	–	1340
2	Calcareous soil, Tijeras, N. M.	1950-2050	–
3	Coastal clayey soil, Texas	1600-1620	–
4	Estancia Playa soil, N. M.	1350-1400	1220-1260
5	Granitic detrital soil, N. M.	1200-1320	1310-1335
6	Hawaiian lateritic soil	1900-1950	–
7	Hayes, Kansas, soil	1250-1495	1235-1285
8	Magnesian soil, N. M.	1350-1435	1260-1310
9	Podzol soil, Wisc.	1350-1450	–
10	Rio Salado dune sand, N. M.	1300-1400	1330-1340
	(b) Aggregates		
	Basalt (and gabbro)	–	1140*
	Clays (North America)	–	1580-1800
	Clays (aluminous)	–	1800-1880
	Clays (carboniferous)	–	1605-1675
	Granite (and rhyolite)	–	800-1100
	Kaolins (southern)	–	1645-1765
	Silica sand	–	1700-1750
	(c) Artificial soils		
	Calcareous soil	1300-1325	1235-1300
	Clayey soil	1300-1390	1310-1340
	Organic calcareous soil	1275-1300	1220

*Basalt may have a melt range from 1100 to 1400 C.

With the given Al_2O_3-SiO_2 ratio of 11.7-73.4, the other oxides give approximately the following melt ranges (deg C): CaO, 1470; K_2O, 1050; Na_2O, 950; MgO, 1595; and Fe_3O_4, 1550. Using a linear interpolation based on the ratio of the other oxides present, the upper melt limit of the soil was found to be about 1340 C, the perthitic feldspar melting incongruently at about 1200 C.

The surface soil at Trinity Site in the Jornada del Muerto is similar in composition to the soil of the Rio Grande basin and displays a comparable melt range. The soil at Trinity Site was melted to a maximum depth of about one inch for about a 1500-ft radius from the nuclear detonation, the temperature of the soil surface probably approaching one million degrees centigrade for a fraction of a second and sustaining a melt temperature for several seconds. The X-ray diffraction analysis of the slag (trinitite) indicates that while the surface was completely melted the lower portion of the slag layer still contained much unmelted quartz, the feldspars having nearly all melted.

Lists of observed melt temperature data have been compiled for soil minerals by Norton (8) and Clark (9), but little melt temperature data are available on soil mineral-aggregate material. Some readily available data are listed in Table 3, including melt-temperature data for both rock and soil mineral aggregates. The soil samples used for melt range determinations were prepared by Post (4), and the fusion tests were conducted by R. W. Foster at the New Mexico Bureau of Mines and Mineral Resources for Sandia Corporation.

The artificial soils included the following minerals: calcareous soil containing 25 percent calcite, 15 percent kaolinite, 30 percent perthite, and 30 percent quartz; clayey soil containing 10 percent calcite, 30 percent kaolinite, 30 percent perthite, and 30 percent quartz; and organic calcareous soil containing 22.5 percent calcite, 13.5 percent kaolinite, 27.0 percent perthite, 27.0 percent quartz, and 10.0 percent carbon. The fusion range of granite and basalt were taken from data by Tuttle and Bowen (10), and the remainder of the aggregates, listed in Table 3, from Norton (8).

WORLD SOIL TYPES

Common Soil Constituents

The predominant soils that comprise the surface of the earth have been classified in terms of soil assemblages (11) and weathering stage (12). These classifications are very general and not always consistent. Although moisture content, grain-size distribution, and density are important parameters in the investigation of the fusion and heat conductance of soils, the mineralogical composition of soils is by far the most important factor in determination of soil fusion temperatures and reaction products.

A determination of soil samples that are characteristic of the majority of the land area of the world was made by correlating soil classification, weathering stage, and predominant mineralogy of the soil types and observing their common constituent characteristics (4). The soil type is primarily dependent on source material, topography,

and climate, while the weathering stage is primarily dependent on topography and climate. The soil type and the weathering stage of the soil are, of course, time-dependent.

The world distribution of soil and rock includes 12 kinds of soil assemblages, which were selected by Goldberg et al (11) as representative of the most common soils, where soil is considered to be the natural unconsolidated material overlying consolidated rock.

The weathering stage of the soil types was derived from the soil weathering classification proposed by Jackson et al (12) and was used to aid in determining the predominant mineralogy possible for each soil type.

The first five of the twelve soil types and lithosol have common constituent characteristics that comprise 46.7 percent of the total land area of the world. The next three soil types comprise another 9.0 percent of the land area and differ little in mineral content from the first five. It appears from these data that the mineralogical composition of a soil is largely dependent on source materials and, generally, only dependent on weathering where the climate is windy, hot, or humid, or some combination of the three conditions prevail.

The list of ten representative soils in Table 3 are comprised of common soil minerals that include ten of the most common oxides of the crust of the earth in various combinations. The majority of soil minerals are silicates, many of which contain significant amounts of alumina. Of the remaining mineral oxides, sodium and potassium tend to give low soil-melt ranges, as in granitic soils, and calcium and magnesium tend to give higher soil-melt ranges, as in limestones. Iron, aluminum, and titanium oxides tend to give intermediate-to-high melt ranges, as do the clay minerals.

Soil Mineral Analysis

The mineralogical analyses of the ten soil samples were accomplished by X-ray diffraction, using the spectrometric power technique, and by chemical test procedures. The soils were reduced in size to material passing a No. 140 sieve, and the mineral aggregates to material passing a No. 200 sieve.

The carbonate, gypsum, halite, and goethite mineral contents were determined by chemical test procedures and the other mineral contents were determined by X-ray diffraction. The estimated composition of the ten soil samples is given in Table 4. The soil samples were chosen to be representative of typical soil oxide assemblages found throughout the world soil types rather than typical soils.

The X-ray powder diffraction data that were used for the analyses of the soil samples were obtained mainly from the ASTM powder diffraction file. Many other sources were used, including data published by the British Mineralogical Society (13), the American Mineralogist, the Mineralogical Magazine, and Geochimica et Cosmochimica Acta.

TABLE 4

COMPOSITION OF REPRESENTATIVE WORLD SOILS

Mineral	Soil Constituents (percent) for Soil No. (see Table 3):									
	1	2	3	4	5	6	7	8	9	10
Quartz	5	8	45	8	45	—	50	—	60	50
Oligoclase	5	1	—	5	20	—	10	25	10	20
Microcline	—	—	—	—	10	—	10	—	15	25
Hornblende	—	—	—	—	—	—	—	—	5	2
Muscovite	—	—	—	—	—	—	—	—	—	—
Biotite	5	—	—	—	—	—	—	—	—	1
Kaolinite	—	—	25	—	—	—	5	—	—	—
Montmorillonite	80	8	25	5	7	—	5	—	—	—
Illite	—	2	—	—	3	—	5	—	—	—
Chlorite	—	—	—	—	3	—	—	30	5	—
Calcite	—	75	—	13	6	—	—	5	—	—
Dolomite	—	3	—	25	—	—	—	—	—	—
Gypsum	—	—	—	31	—	—	—	—	—	—
Geothite	—	1	—	—	—	55	—	—	—	—
Gibbsite	—	—	—	—	—	30	—	—	—	—
Others	5	2	5	13	6	15	15	40	5	2

Note: Sample 4 contains about 8 percent halite, sample 6 about 10 percent Fe_3O_4, sample 7 about 5 percent mixed-layer clays, and sample 8 about 35 percent talc.

THERMAL SOIL STABILIZATION

History

A discussion of the thermal stabilization of soils may include the production of pottery, ceramics, and bricks; however, the term is also applicable to the increase in stability and bearing capacity of soils by application of heat. Thermal stabilization of soils may also be effected by freezing (14).

The degree and type of thermal stabilization depend on the amount of heat energy used. The free water

may be driven out of the soil by temperatures up to 350 C (reversible) or temperatures up to 550 C (irreversible); the dried soil may be fired to a temperature of 600 C (bricking), or the dried soil may be heated above incipient fusion temperatures.

Thermal stabilization of soils was first used successfully for road construction in Australia nearly 30 years ago (14), and since then the method has also been used for other purposes, such as the stabilization of slopes and foundations (15). Equipment is now available for producing the amount of heat energy necessary for foundation stabilization (14) and surface stabilization (15).

Procedure

For effective thermal stabilization of soils it is only necessary to brick the soil or to reach incipient fusion temperatures. Most soils melt incongruently over a temperature range so that it is only necessary to reach the initial melt range to effectively cement the soil mass. The bricking of the soil is caused by loss of structural water by the soil minerals with the formation of new minerals.

Fluxing agents are commonly used to lower the melt range of mineral aggregates so that stable products can be more readily formed. Whereas limestone is commonly used as a fluxing agent for steelmaking, it is not suitable as a soil fluxing agent because of its moderately high melting range when included with soil oxides. Calcite, when added to a typical acidic granitic soil in amounts up to 45 percent, will actually increase the soil full-melt temperature slightly (4). Another common fluxing agent in metallurgical work is soda ash (sodium carbonate). Soda ash is readily available at low cost and causes low melt ranges when mixed with soils.

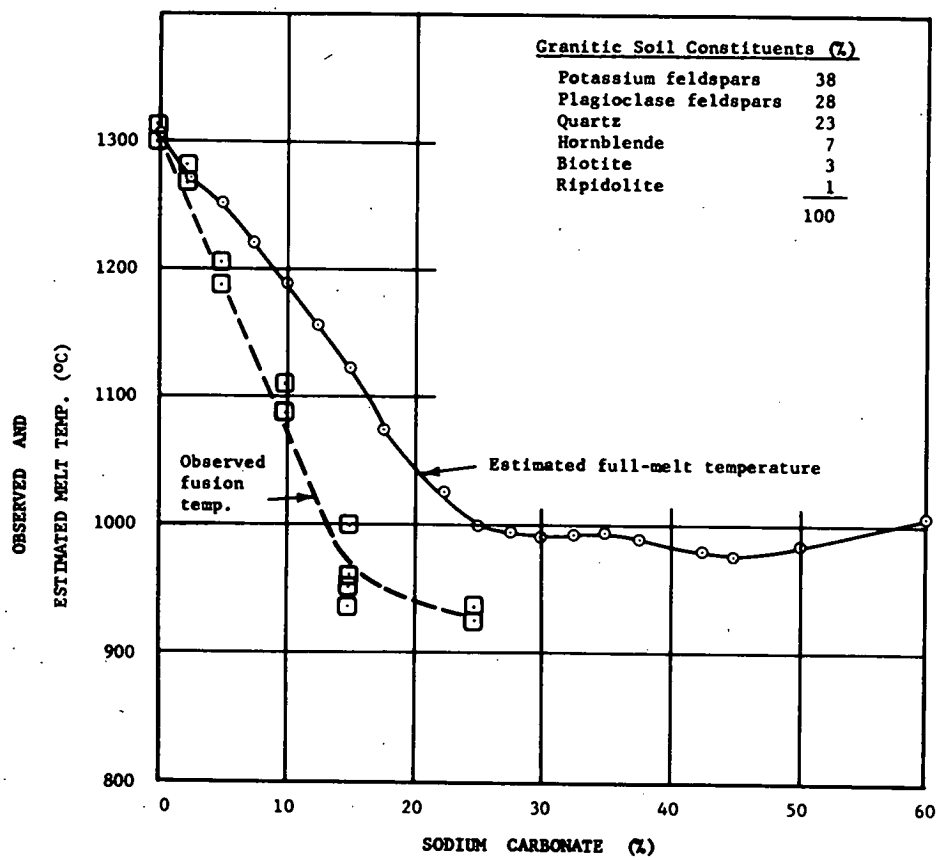

Figure 3. Effect of Na_2CO_3 additive on the melt temperature of a granitic soil.

Fusion Tests

A soil sample was obtained that is typical of the granitic detrital soils of the Sierra Uplift of California. The mineralogical composition of the soil was determined by X-ray diffraction and the dry-melt oxide constituents were computed using the data from Tables 1 and 2.

The soil mineral constituents are given in Figure 3 with the feldspar series in two parts. The potassium feldspars include 22 percent orthoclase, 10 percent microcline, and 6 percent anorthoclase (tentatively), and the plagioclase feldspars include 15 percent andesine, and 13 percent oligoclase. The percentage values represent the average of results from five soil mineral analyses.

The predominant dry-melt oxides in the soil (in percent) were: CaO, 2.7; K_2O, 4.1; Na_2O, 3.9; $FeO + Fe_2O_3$, 1.9; MgO, 1.6; Al_2O_3, 15.7; and SiO_2, 70.1. The effect of differing amounts of soda ash additive on the full-melt temperature of the soil was estimated using the ternary phase diagrams and the results were plotted (Fig. 3). The amount of additive is given in terms of percent of air-dry soil weight.

Pyrometric test cones were prepared from mixtures of the granitic soil and the sodium carbonate additive in accordance with a standard method (ASTM Designation C 24-56). The amount of additive expressed as a percent of the air-dry soil weight varied for different specimens from 0 to 25 percent. The test cones were mounted on plaques of refractory clay, and heating was conducted in an electric furnace. Instead of using standard pyrometric (PCE) cones to indicate approximate temperature equivalents corresponding to softening of the test cones, thermo-couples were installed in the furnace and connected to instrumentation for recording temperatures. This arrangement provided for a wider range of measurable temperatures and, it is believed, to more accurate determinations of furnace temperatures. The fusion (end-point) temperature or softening of a test cone was indicated by visual observation of the top bending over and the tip touching the plaque in accordance with the ASTM method. The experimental results are plotted in Figure 3 and indicated as observed fusion temperatures.

As expected, the observed fusion temperatures for the soil-additive mixtures are lower than the estimated melt temperatures because of impurities in the soil. More importantly, both the predicted and the observed values indicate clearly that the melt temperature of the granitic soil can be lowered when soda ash is mixed with the soil.

SUMMARY

Most soils apparently exhibit a melt range that varies between 1250 and 1750 C, the fat clay soils tending to melt at about 1700 C and the feldspar-rich soils tending to melt at about 1300 C. Soils with a high alumina or lime content tend to have a very high melt range, corundum melting at about 2000 C and calcite at about 2500 C. Soils consisting of detrital granite tend to have a very low melt range of about 1100 C because of the large proportion of potash and soda feldspars normally present in granite. After a soil has completely melted, the melt consists of a homogeneous mixture of oxides derived from the original constituent minerals if the soil is heated in an open-air environment. Theoretical and laboratory investigations indicate that the addition of soda ash lowers the melt temperature range of a typical soil from the Sierra Uplift to within a usable range for practical application.

The effect of other common fluxing agents on the melt range of soils should be investigated for ordinary types of soils. Because of the slowness of heat transmission in soils, the use of additives that include oxidants with fluxing agents should be considered in future research in this area.

Field tests for thermal stabilization of soils should be conducted using existing mobile down-draft heaters modified to treat prepared soil media. The effects of type and amount of fluxing agents on the bearing capacity of a stabilized soil should be investigated.

ACKNOWLEDGMENTS

The initial part of this study was conducted for Sandia Laboratories at the Eric H. Wang Civil Engineering Research Facility, University of New Mexico. Data from the initial investigation have not been used in their original form. The authors wish to express their appreciation to the staff of the School of Engineering at Sacramento State College for its effort in the preparation of this paper.

REFERENCES

1. Nutting, P. G. Some Standard Dehydration Curves of Minerals. Prof. Paper 197-E, Geol. Survey, U.S. Department of the Interior, 1943.
2. Grim, R. E. Clay Mineralogy. McGraw-Hill, N. Y., 1953.
3. Deer, W. A., Howie, R. A., and Zussman, J. Rock Forming Minerals, Vols. 1-5. John Wiley, N. Y., 1962.
4. Post, J. L. The Fusion of Soils. SC-CR-67-2688, U. S. AEC, Sandia Laboratories, Albuquerque, 1967.
5. Levin, E. M., Robbins, C. R., and McMurdie, H. F. Phase Diagrams for Ceramists. American Ceramic Society Pub., Columbus, Ohio, 1964.
6. Wilson, H. Ceramics-Clay Technology. McGraw-Hill, N. Y., 1927.
7. Muan, A., and Osborn, E. F. Phase Equilibria Among Oxides in Steelmaking. Addison-Wesley, Reading, Mass., 1965.
8. Norton, F. H. Refractories. McGraw-Hill, N. Y. 1949.
9. Clark, S. P. (ed.). Handbook of Physical Constants. Memoir 97, Geological Society of America, N. Y., 1966.
10. Tuttle, O. F., and Bowen, N. L. Origin of Granite in the Light of Experimental Studies in the System $NaAlSi_3O_8$-$KAlSi_3O_8$-SiO_2-H_2O. Memoir 74, Geological Society of America, N. Y., 1958.
11. Goldberg, J., Fosberg, F. R., Sachet, M. H., and Reimer, A. World Distribution of Soil, Rock, and Vegetation. USGS Pub., TEI 865, 1965.
12. Jackson, M. L., Tyler, S. A., Willis, A. L., Bourbeau, G. A., and Pennington, R. P. Weathering Sequence of Clay-Size Minerals in Soils and Sediments. Jour. Physical and Colloidal Chem., Vol. 52, No. 7, 1948.
13. Brown, G. (ed.). The X-ray Identification and Crystal Structures of Clay Minerals. Mineralogical Society, London, 1961.
14. Jumikis, A. R. Thermal Soil Mechanics. Rutgers Univ. Press, New Brunswick, N. J. 1966.
15. Day, D. E. Thermal Stabilization of Soils. Report 1, Tech. Report No. 6-706, U. S. Army Engr. Waterways Exper. Sta., Corps of Engineers, Vicksburg, Miss., 1965.

Pavement Temperatures and Their Engineering Significance in Australia

B. G. RICHARDS, Commonwealth Scientific and Industrial Research Organization, Syndal, Victoria

This paper describes the results of an Australia-wide investigation of seasonal temperatures in and beneath highway pavements. Outside the limited alpine areas, pavement temperatures varied from about 5 C to over 60 C. Thus frost action can be neglected in Australia, but the advantages and disadvantages of high temperatures should be considered in pavement design.

Only poor correlations were found between pavement and air temperatures and the results suggest that net radiation is not only important but extremely variable over the lateral dimensions of the roadway. Net radiation also caused significantly higher temperatures under the bituminous seal than the natural surface.

The temperature gradients were of insufficient magnitude and duration to cause a significant thermal transfer of moisture through the subgrade. This observation is also in agreement with conclusions based on the observed moisture conditions. It is suggested that any thermal transfer of moisture that does take place is more likely to lead to safer conditions than the reverse.

The results suggest that pavement subgrade temperatures observed in Australia have a significant effect on pavement performance, but only insofar as they affect the load-spreading properties of bituminous layers or cement- or lime-treated bases.

•THE INFLUENCE of temperature on pavement performance is now reasonably well documented, indicating that temperature is an important factor in pavement design. For example, if temperatures fall below freezing for sufficiently long periods, frost heave and the reduction of stability during the spring thaw can cause serious damage to road pavements.

In Australia frost action need not be considered, except in the limited and sparsely populated alpine areas. Aitchison and Richards (1) and Richards (2, 3) have shown how, in frost-free areas, the influence of environment (including climate) on subgrade stability and pavement performance can be included in practical design techniques. These techniques have followed the development of new soil suction instrumentation (4). This work suggests that moisture movement under temperature gradients is insignificant in the wide range of soil types and climatic zones investigated and that it is safe to assume isothermal conditions in predicting moisture changes and equilibria beneath sealed pavements.

The Australian investigation (1), undertaken by the Division of Soil Mechanics, Commonwealth Scientific and Industrial Research Organization (CSIRO), with the assistance of the National Association of Australian State Road Authorities, was primarily concerned with the observation of soil suction values under sealed pavements throughout Australia. However, to permit temperature corrections to be made to the gypsum block suction readings, and to provide data on temperature gradients should thermal transfer

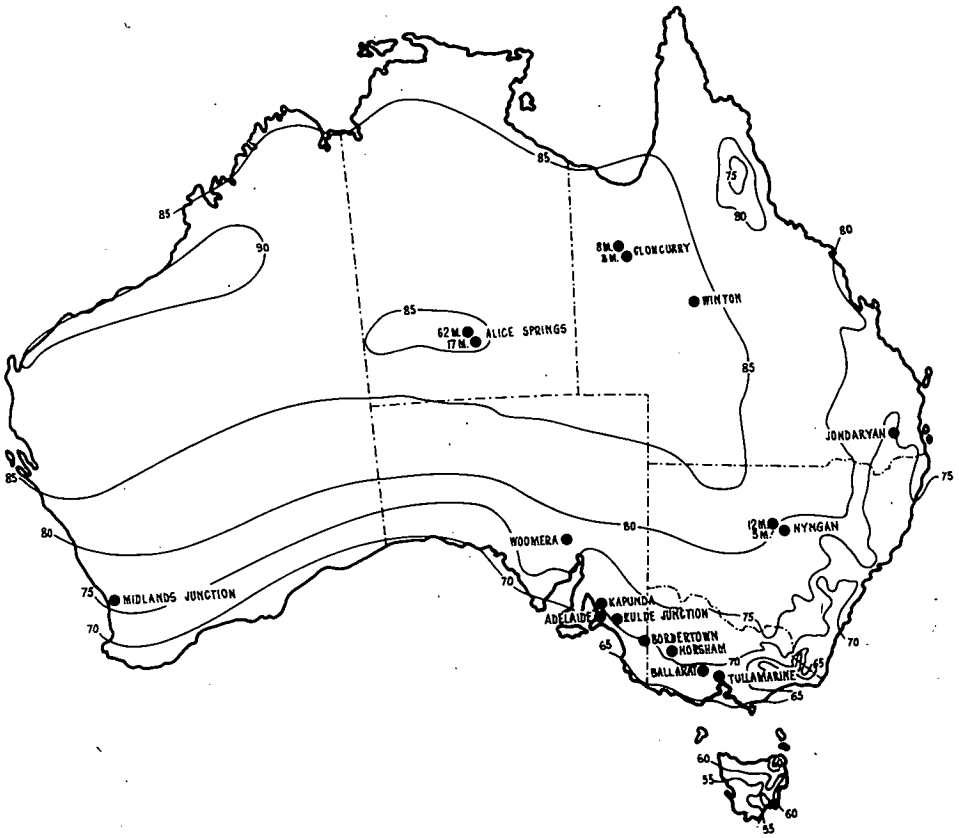

Figure 1. Maximum temperature isotherms (deg F) and location of field sites.

of moisture be evident, temperature measurements were also made. Consequently a large volume of temperature data under typical sealed pavements was amassed. No attempt was made initially to investigate pavement temperatures specifically, and the temperature instrumentation was not ideal, being chosen for convenience. In spite of this, the data do provide useful and interesting information. For instance, the temperature gradients measured permitted the assumption that thermal moisture transfer beneath sealed pavements is negligible under Australian conditions to be analyzed more critically.

In warm areas, such as in Australia, it is the high temperatures and the duration of these temperatures that are most important. The higher the temperature, the lower is the effective elastic modulus of bituminous layers, causing reduced time-dependent, load-spreading properties and lower stability of the pavement as a whole. High temperatures also increase loss of volatiles and oxidation, resulting in increased brittle behavior of bituminous materials and reduced fatigue life. The development of strength and elastic properties of cement- and lime-treated materials is also dependent on temperature and this has important practical significance in warmer areas.

SELECTION OF FIELD SITES

The 18 field sites were chosen to be representative of the wide range of soil and climatic conditions existing throughout Australia (1). The Great Soil Groups (5) provided a convenient and practical level of pedological classification of Australian Soils, in that the number of units was workable, while the morphological attributes of each Great Soil Group were sufficiently distinct to permit ready recognition with the as-

sistance of Soil Map of Australia (6). Furthermore, the chemical characteristics of representative profiles from each Great Soil Group have been defined (7). Another important characteristic of this classification is that most of the dominant soils are not unrelated to the current climate. Thus, frequently the selection of a site to represent a given soil meant that a specific climatic zone was studied. The range of climate covering the Australian continent is summarized in Figures 1 and 2.

The sites were therefore chosen on the basis of Great Soil Group and climate. No attempt was made to study all the major soils or climates, but a reasonable coverage of those conditions of interest to the moisture investigation was achieved. Attention was concentrated primarily on soils with a significant clay content occurring in environments such that some seasonal moisture deficiency of long duration might be expected. Consequently, sites were not selected in abnormally humid environments or on desert sand soils, which is unfortunately a limitation on the temperature data.

CHARACTERISTICS OF REPRESENTATIVE SITES

In order to ensure that each site was acceptable as representative of its region, several factors other than soil and climate were established as basic requirements. These defined the need for the installation site to reflect a modal or dominant soil in its characteristic environment with a pavement of standard form constructed in a manner least likely to introduce any local effects, particularly on moisture conditions (1).

When more than one site was chosen on the same Soil Group, climatic conditions were considered. Where possible an attempt was made to obtain the extremes of climatic conditions occurring in the mapped areas of the Group, e.g., summer rainfall and winter rainfall

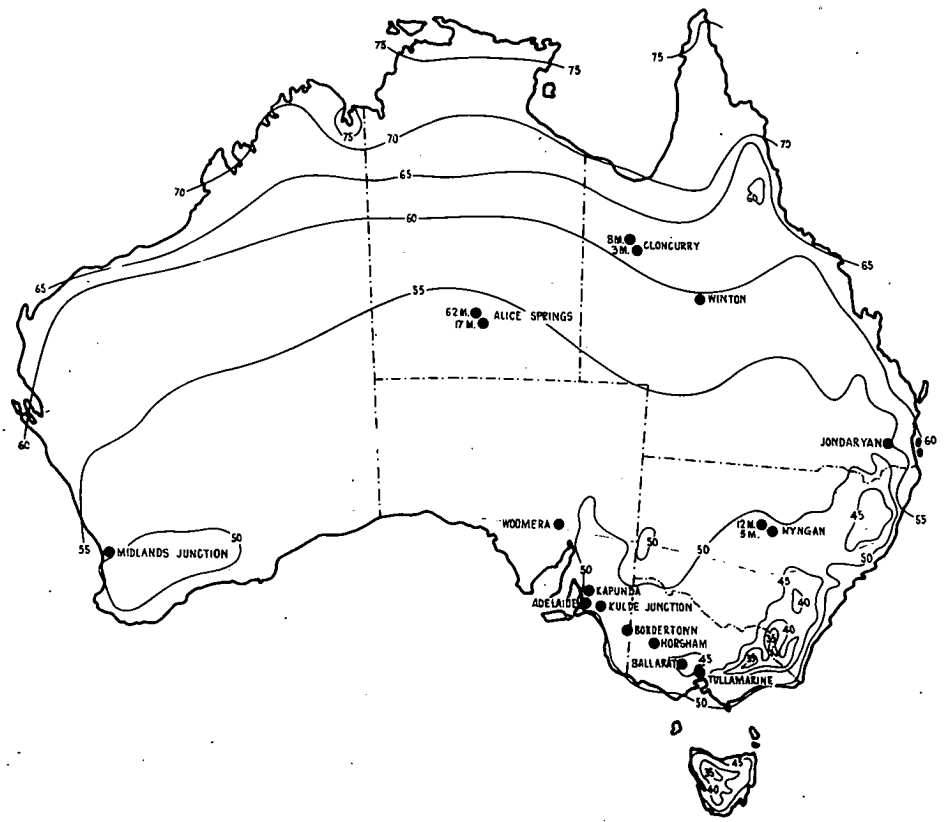

Figure 2. Minimum temperature isotherms (deg F) and location of field sites.

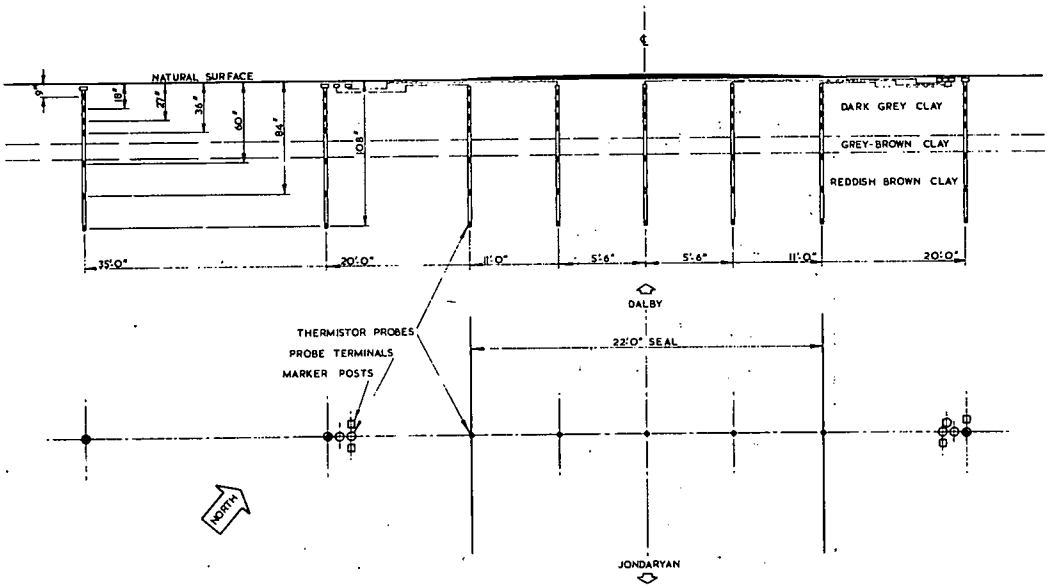

Figure 3. A typical field site.

or most arid and most humid. By the choice of such extremes it was planned not only to investigate the influence of rainfall on moisture conditions, but also to try and isolate any thermal influences on moisture transfer.

The details of each site have been described in detail elsewhere (1). The cross-sectional layout of the instrumentation was the same at each site as far as was practical, and a typical installation is shown in Figure 3. A brief summary of the climatic conditions at each site is given in Table 1, and the location of the sites is set out in Figures 1 and 2. Because the sites were identical in all respects, particularly in the seal type and width, with the exception of the soil type and climatic conditions, the differences in temperature should be strongly dependent on the soil and climatic conditions.

INSTRUMENTATION

The instrumentation and techniques employed in these installations have been described elsewhere (1) and a brief description of the temperature instrumentation is all that is considered necessary here.

The soil temperature was measured by means of thermistors incorporated in thermistor blocks (Fig. 4). These blocks were identical externally to the gypsum blocks for soil suction measurements and the "dummy" spacer blocks. The design of these blocks was chosen to overcome certain limitations in gypsum block design as well as for convenience in installation. These blocks could be mounted together axially in the form of a 2-in. diameter probe, the correct spacing of the gypsum and thermistor blocks being achieved by the insertion of "dummy" blocks. The spacing selected for temperature measurements was 6, 15, 24, 33, 57, 81, and 105 in. depth.

The thermistors used were STC type K5221. Considerable variation was found between thermistors, but it was such that the calibration curves remained parallel, as shown in Figure 5. This meant that the thermistors could be grouped into batches with an accuracy of ± 0.25 C by checking the resistance in a water bath at a set temperature (25 C). Each probe used thermistors of the same nominal resistance (at 25 C), which was noted so that the appropriate calibration curve could be used later. However, it cannot be claimed that the accuracy of reading is ± 0.25 C because long-term drift and insulation breakdown was apparent in a few cases. In general, an accuracy of ± 1.0 C is probably more correct, providing care is taken in disregarding those installations that develop spurious readings.

TABLE 1

SOILS AND CLIMATIC FACTORS AT INSTALLATION SITES

Great Soil Group	Area of Australia Dominated by Soils of Chosen Great Soil Group	Location of Installation	Climatic Factors[a]					Climatic Indices		
			Annual Rainfall P (in.)	Mean Temp. (deg F)	Evap. From Water Surface Ep (in.)	Drainage D (in.)	Deficit d (in.)	After Gentilli[b]	After Prescott[a] K	Thornthwaite Moisture Index[b] T
Red brown earth	2-3%	Adelaide, S. A.	25.3	61.3	31.8	2.0	8.5	CB'd'c	2.24	-18.2
		12 mi NW of Nyngan, N.S.W.	14.9	64.8	39.6	0	24.6	DB'd	1.16	-37.7
Grey and brown soils of heavy texture	5-10%	Horsham, Vic.	17.6	58.9	27.8	0	10.2	CB'dc	1.71	-22.1
		Bordertown, S. A.	18.8	58.8	23.8	0.6	5.6	CB'dc	2.04	- 9.7
		Tullamarine, Vic.	19.5	58.0	24.1	0	4.6	CB'dc	2.10	+ 5.3
		8 mi W of Cloncurry, Qld.	16.9	77.9	66.1	0	49.2	DA'd	0.90	-44.4
Desert sand plain soil	5%	62 mi N of Alice Springs, N. T.	9.9	69.1	54.3	0	44.3	EB'	0.60	-49.6
Arid red earth	5%	17 mi N of Alice Springs, N. T.	9.9	69.1	54.3	0	44.3	EB'	0.60	-49.6
Stony desert tableland soil	3-5%	Roadway at Woomera, S. A.	6.1	65.6	42.7	0	36.6	EB'	0.44	-51.6
		Aerodrome at Woomera, S. A.	6.1	65.6	42.7	0	36.6	EB'	0.44	-51.6
Meadow podzolic soil	<5%	2½ mi N of Midlands Junction, W. A.	34.5	65.0	44.5	12.5	22.5	BB's	2.42	+34.5
Black earth	1-2%	4½ mi NW of Jondaryan, Qld.	25.1	66.3	35.3	0	10.2	CB'dh	2.08	- 4.2
Kraznozem	<1%	2½ mi W of Gordon, Vic.	27.4	53.9	20.5	6.9	0	CB'r	3.31	+10.0
Brown soil of light texture	2-3%	5½ mi NW of Nyngan, N.S.W.	14.9	64.8	39.6	0	24.6	DB'd	1.16	-37.7
Lateritic red earth	1%	3½ mi W of Cloncurry, Qld.	16.9	77.9	66.1	0	49.2	DA'd	0.90	-44.4

[a] At nearest station. [b] From map.

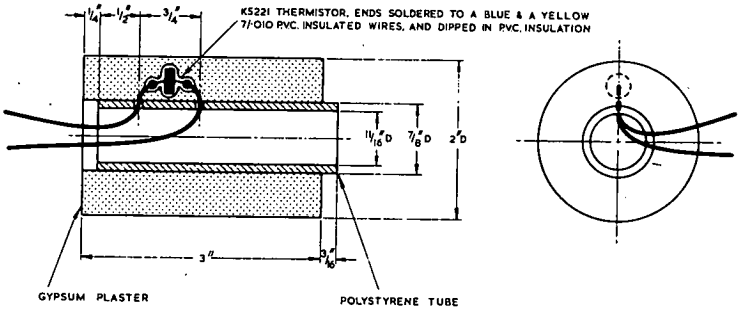

Figure 4. Thermistor block.

RESULTS

The data were produced from periodic observations (usually monthly) at the field installations in the form of resistance measurements at 56 points on a transverse section across the roadway, as shown in Figure 3. From each set of resistances from the thermistor readings, a temperature section across the roadway was produced such as in Figure 6. Because of the large volume of data, only a brief summary can be presented in this paper.

At those installations that gave good sets of data over a 2- to 4-year period, two sets of data were produced, viz., the mean temperatures at each depth beneath (a) the natural surface and (b) the bituminous seal.

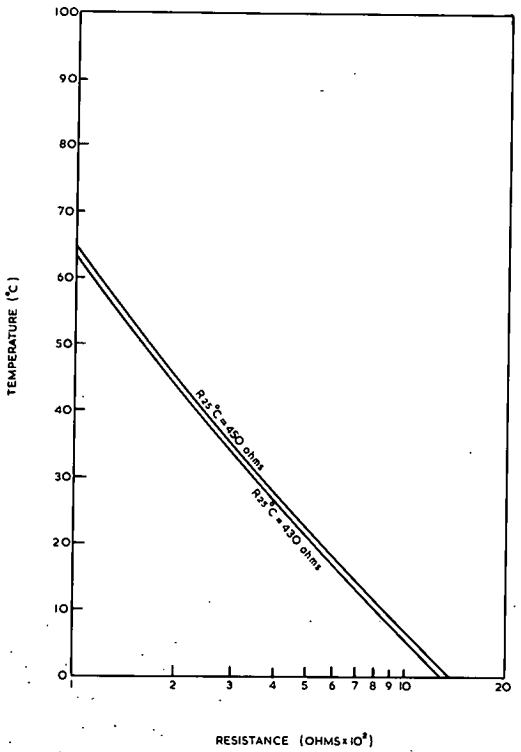

Figure 5. Calibration curves for STC type K5221 thermistors.

For those beneath the natural surface, the arithmetic mean of the temperatures at each depth was taken from the 3 probes away from the bituminous seal and for the corresponding month of the year during the period of observation. Similarly, for the temperatures beneath the bituminous seal, the readings from the 3 probes beneath the interior of the seal were used. This permitted plotting of annual variations in monthly mean temperatures, as shown in Figures 7 and 8. Also included in Figure 8 are the maximum and minimum temperatures that were observed at each depth.

Diurnal variations in temperature could not be investigated because of the nature of the research. Diurnal variations can be extremely high at the upper surface of bituminous layers in warmer areas (8, 9, 10). However, bituminous layers provide good thermal insulation and cause rapid decreases in diurnal temperature variations over depths of only a few inches below the exposed surface (10). This agrees with the theoretical results of the solution to the equation of heat conduction that describes the diurnal temperature variations in bituminous materials and soil (11). However, any influence of diurnal tempera-

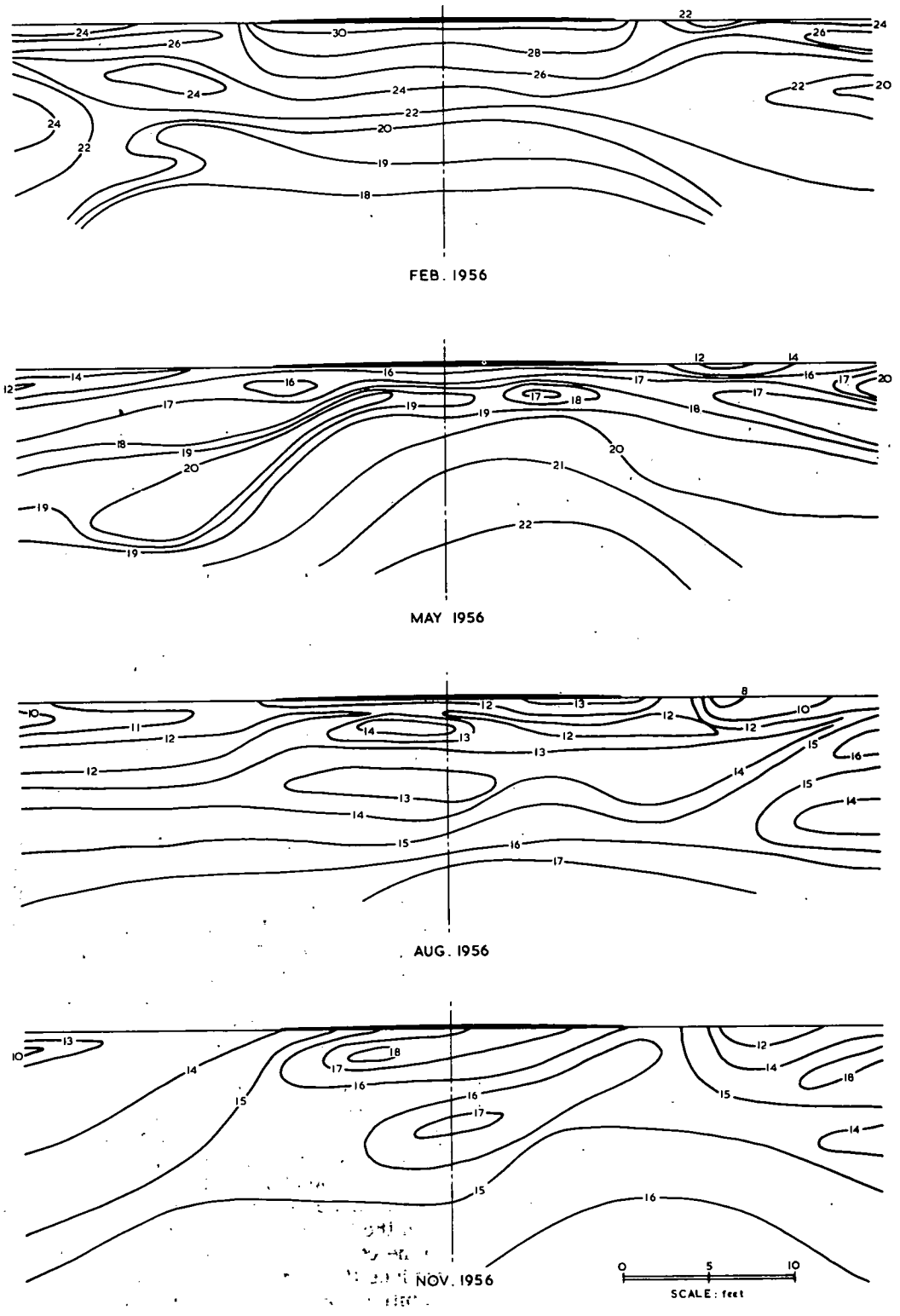

Figure 6. Typical temperature contours (°C) at the Horsham site.

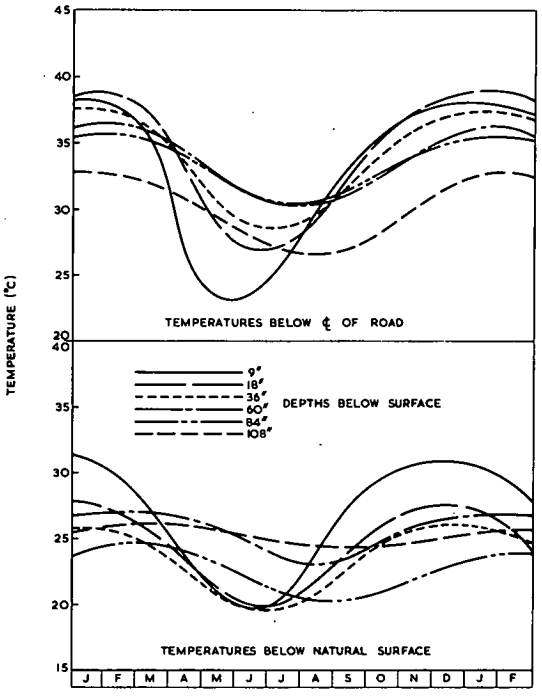

Figure 7. Typical seasonal temperature variations at various depths below centerline of road and natural surface (Jondaryan site).

ture was avoided as far as possible by making the observations at approximately the same time of day.

DISCUSSION OF RESULTS

An examination of all the temperature observations indicates that pavement temperatures over most of the Australian continent range from about 5 C to well over 60 C. The only possible exception to this would be in the limited alpine areas where temperatures below 0 C could be expected. This means that, in general, frost action need not be considered in pavement design (which is the practice of the Australian road authorities). However, the high temperatures observed are very widespread and can have considerable effect on pavement performance, as will be discussed below. These high temperatures are not always considered in pavement design under present Australian design practices.

The individual temperature readings often showed large variations laterally (of the order of ± 5 C near the surface) under the same surface and at the same depth and time. The nature of these variations suggested that they were due more to variations in heat gain or loss (e.g., net radiation) at the surface, rather than difference in the thermal diffusivity of the material. This means, therefore, that actual soil temperatures at the installations can vary considerably from the mean values shown in Figures 7 and 8 and that the mean values themselves are probably not very precise. This is one reason why a large scatter was obtained in the figures that follow. However, the results do show definite trends, which, because of the foregoing arguments, are probably as useful as could be obtained for practical purposes without carrying out a large-scale statistical investigation.

Climatic Trends

The climatic data available in the vicinity of each site included the 30-year averages for the average daily maximum, minimum, and mean temperatures for each month and the whole year. Because this information is available for more than 600 stations throughout Australia, it was considered that any trends between observed soil temperatures and available climatic data could be useful for practical purposes. Consequently, three relationships were examined:

1. Absolute maximum observed temperature at 6 in. depth vs the maximum average daily temperature (Fig. 9);
2. Mean maximum observed temperature at 6 in. depth vs the maximum average daily mean temperature (Fig. 10); and
3. Mean observed temperature at 9 ft depth vs yearly average daily mean temperature (Fig. 11).

These relationships are not considered to be necessarily the best, but they are suggested as possibilities by examination of the theoretical equation for heat conduction in soils.

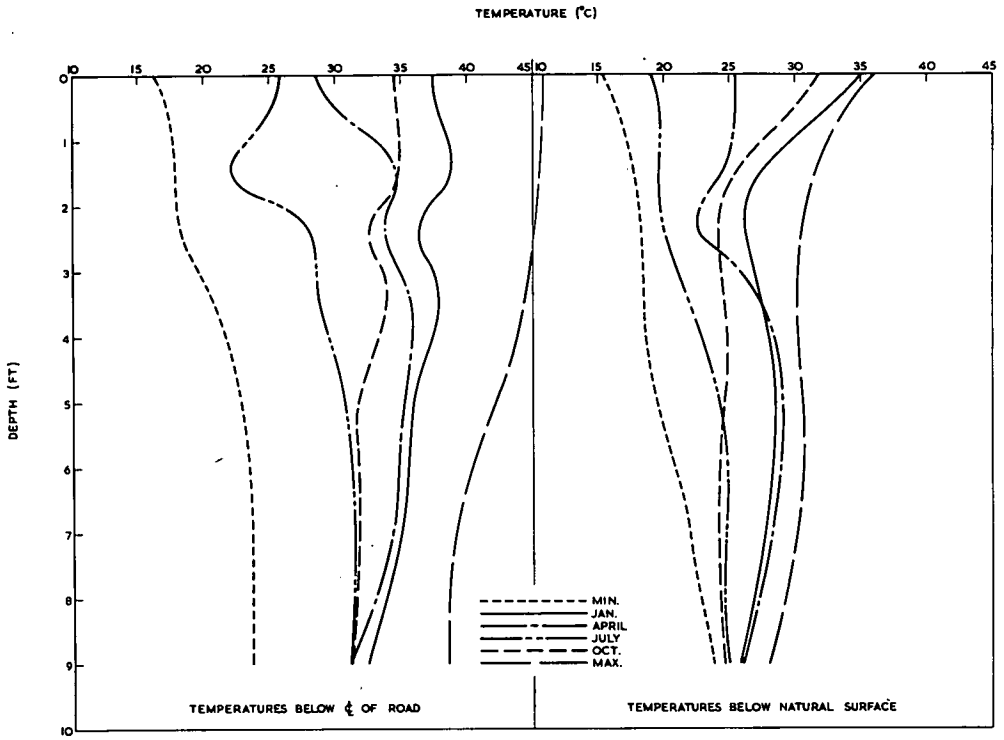

Figure 8. Typical temperature profiles at various months below centerline of road and natural surface (Jondaryan site).

Furthermore, the straight-line correlations shown in Figures 9, 10, and 11 are not very significant and are only shown to indicate trends.

These statistical trends, however, clearly indicate that the soil temperatures are strongly dependent on climate, as could be expected. Furthermore, the summer temperatures and the mean temperatures at all depths are significantly greater under the bituminous seal than under the natural surfaces. The winter temperatures (not shown because of very poor correlations) tend to be slightly higher under the bituminous seal in most cases, although not significantly. These results could again be expected due to the increased thermal absorption characteristics or the increased net radiation taking place at the black bituminous surface.

Thermal Gradients Likely To Cause Moisture Transfer

There is now considerable theoretical and experimental evidence that moisture flow can be set up in soil under temperature gradients (12, 13, 14, 15, 16). This flow, which occurs mainly in the vapor phase in the direction of decreasing temperature, can cause appreciable moisture transfer under certain conditions.

More information has become available on moisture flow under thermal gradients (17, 18). Cary (16), working with Columbia loam soil, obtained thermal moisture fluxes under thermal gradients, which suggest a coefficient of moisture transfer under thermal gradients of 1.4×10^{-6} cm^2/sec deg C at relatively low suctions. Rollins, Spangler, and Kirkham (13) obtained data for a silt loam giving coefficients of the order of 3×10^{-7} cm^2/sec deg C at unknown suctions, but relatively high air voids. Clays with low air voids, even at quite high suctions, should have coefficients no higher, and probably much less, than these, except perhaps in very dry areas. In dry areas, however, thermal moisture transfer is unlikely to have any significant effect on pavement thicknesses.

From the temperature profiles such as Figure 7, the maximum temperature gradient is only of the order of 0.3 C/cm over short distances (of the order of 10-15 cm). This

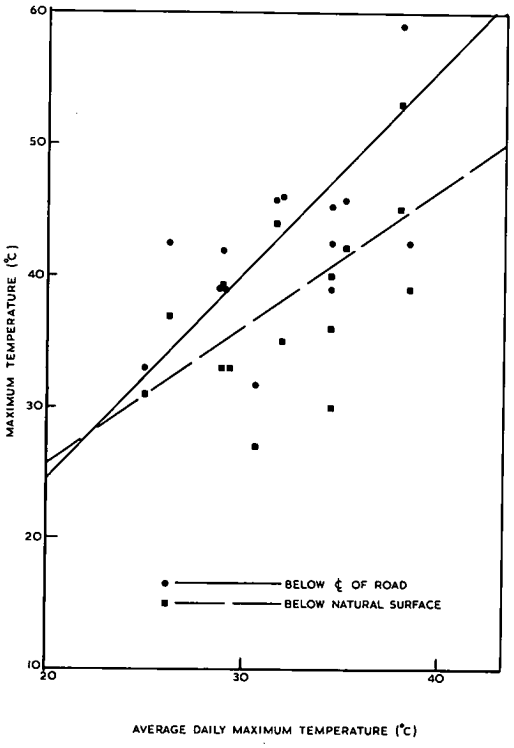

Figure 9. Absolute maximum temperature at 6 in. depth vs the maximum average daily maximum temperature.

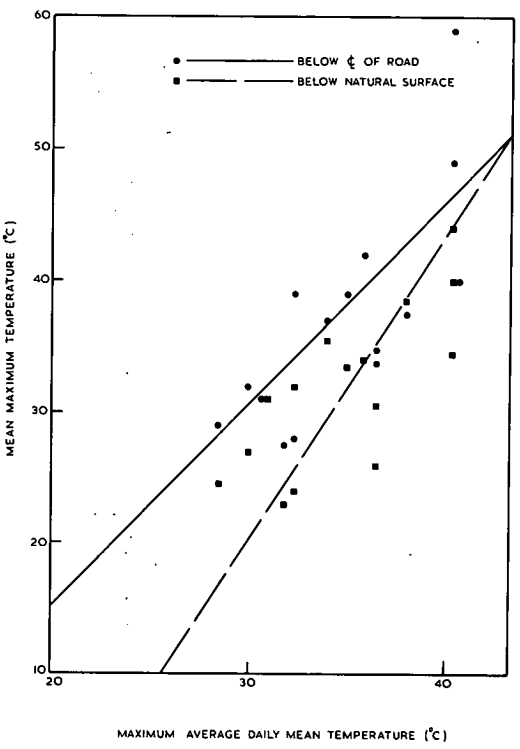

Figure 10. Mean maximum observed temperature at 6 in. depth vs the maximum average daily mean temperature.

gradient is unlikely to cause moisture flow in excess of 10^{-7} cm/sec. Not only does this flow take place over a very short distance, but the temperature gradient exists at any given depth for only a short time as the temperature wave moves vertically down the soil profile. Furthermore, the temperature gradients reverse seasonally, causing a reversal of thermal moisture transfer. However, as pointed out by Croney and Coleman (11), temperature variations are not sinusoidal, so that seasonal flows do not balance, resulting in a net vertical moisture transfer.

The largest average temperature gradient over the whole soil profile occurred at the Woomera road installation, where the gradient was 0.07 C/cm in January, decreasing with depth. Again, this gradient occurs only for a short duration, and to some extent reverses in the winter months. At all other sites the average temperatures were considerably less than this value. Consequently, thermal moisture flow will probably never exceed 2×10^{-8} cm/sec even for short periods.

Aitchison and Holmes (19) have analyzed the effect of vertical flow on suction profiles due to a net evaporative loss at the surface. These results for Waite loam, plus similar calculations by the author using permeability data for Syndal and Horsham clay (20), suggest that only small variations from isothermal conditions can occur due to permanent thermal moisture flow of this order and even smaller variations for the actual flow, which would occur over a short period.

It is also interesting to note that, in every case, the generally high temperatures immediately under the pavement resulted in small gradients in mean temperature with temperatures decreasing both vertically down the profile and laterally away from the centerline at all depths. Thus, if net thermal moisture flow has any effect at all, it would be to increase the subgrade suction, which would result in increased stability and safer conditions than predicted.

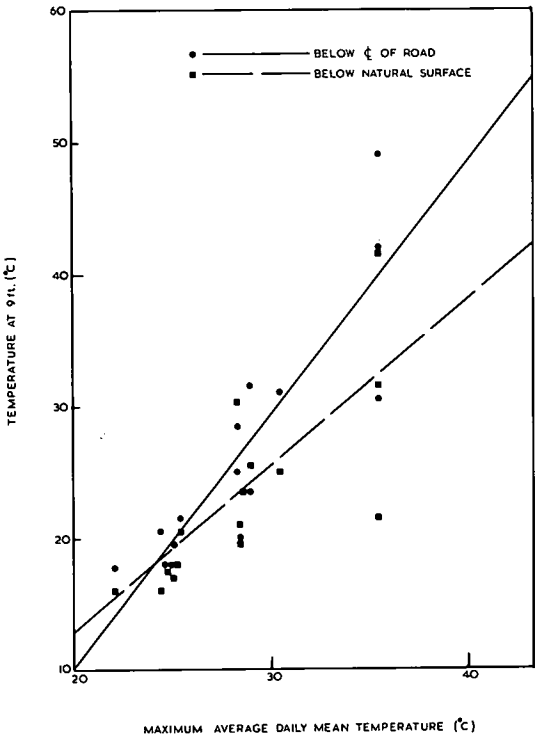

Figure 11. Mean observed temperature at 9 ft depth vs yearly average daily mean temperature.

Temperatures at the Surface of the Bituminous Layer

While no temperatures were measured at the surface, temperatures in excess of 60 C obviously occur in central and northern Australia, as seen from Figure 9. Whiffin and Lister (21) have clearly demonstrated that the load-spreading properties of bituminous roads deteriorate markedly with rise in temperature. The increased stresses and strains at high temperatures must therefore lead to higher pavement deflections and reduced life, apart from the deterioration of the bituminous materials themselves.

Temperatures in the Base Course

Temperatures were also very high in the pavement at a depth of 6 in. The mean maximum temperature probably exceeds 50 C, with localized temperatures probably exceeding 60 C. Maclean and Clare (22), Dumbleton (23), and Metcalf (24) have all demonstrated the increased rate of gain of strength of both lime- and cement-stabilized soils with increase in temperature. These results therefore indicate the fallacy of curing laboratory samples at, say, 25 C in those cases where the in situ temperatures may exceed 50 C for long periods.

CONCLUSIONS

The results of the Australian-wide investigation described are not very conclusive, but they indicate that, in normal areas, soil and pavement temperatures vary from about 5 C to over 60 C. Freezing conditions do not occur, and frost action is not a problem. However, very high temperatures do occur that can have a very significant effect on pavement performance.

There is a significant, but rather poor, correlation between soil and pavement temperatures and recorded air temperatures. The results suggest that net radiation is not only important, but extremely variable even over the lateral dimensions of the roadway. Net radiation is also the reason for the significantly higher temperatures under the bituminous seal than the natural surface.

The temperature gradients are of insufficient magnitude and duration to be likely to cause significant thermal transfer of moisture. This observation is in agreement with conclusions based on the observed moisture conditions. In fact, any thermal transfer of moisture that does take place is probably more likely to lead to safer conditions than the reverse.

Thus, in general, the soil and pavement temperatures observed in Australia have a significant effect on pavement performance, but only insofar as they affect the load-spreading properties of bituminous layers or cement- or lime-treated bases.

REFERENCES

1. Aitchison, G. D., and Richards, B. G. A Broad-Scale Study of Moisture Conditions in Pavement Subgrades Throughout Australia. In Moisture Equilibria and Moisture Changes in Soils Beneath Covered Areas (G. D. Aitchison, ed.). Butterworths, Sydney, 1965.
2. Richards, B. G. Moisture Flow and Equilibria in Unsaturated Soils for Shallow Foundations. Permeability and Capillarity of Soils, ASTM STP 417, p. 4-34, 1966.
3. Richards, B. G. Soil Water and Its Effect on Soil Engineering Parameters. In Land Evaluation (G. A. Steward, ed.). MacMillan of Australia, Melbourne, 1968.
4. Richards, B. G. Review of Measurement of Soil Water Variables and Flow Parameters. Proc. Symposium on Field Measurements in Soil Engineering, Fourth Conf. Aust. Rd. Res. Bd, 1968.
5. Stephens, C. G. A Manual of Australian Soils. CSIRO, Melbourne, 1956.
6. Stephens, C. G. The Soil Landscapes of Australia. CSIRO Soil Publ. No. 18, Melbourne, 1961.
7. Stace, H. C. T. The Morphological and Chemical Characteristics of Representative Profiles of the Great Soil Groups of Australia. Div. of Soils, CSIRO, Adelaide, 1961.
8. Strongman, F. S. The Materials Laboratory's Evaluation of Some Kenya Materials. Proc. Conf. Civ. Eng. Problems Overseas, London. Inst. of Civ. Eng., 1964.
9. James, J. G., and Millard, R. S. Plastic White Line Road Markings for the Tropics: A Full-Scale Experiment in Hong Kong. Dept. of Scientific and Industrial Research Lab. Note No. RN/3759/JGJ.RSM (unpublished), 1960.
10. Roberts, P. K., and Russam, K. Road Temperatures in the Tropics. Road Res. Lab., Ministry of Transport, RRL Report No. 29, 1966.
11. Croney, D., and Coleman, J. D. Moisture Movements in Road Subgrades Associated With Fluctuations of the Pavement Temperature. DSIR, Road Res. Lab. Note No. RN/842/DC. JDC, 1947.
12. Gurr, C. G., Marshall, T. J., and Hutton, J. T. Movement of Water in Soil Due to a Temperature Gradient. Soil Sci., Vol. 74, p. 335-345, 1952.
13. Rollins, R. L., Spangler, M. G., and Kirkham, D. Movement of Soil Moisture Under a Thermal Gradient. Proc. HRB, Vol. 33, p. 492-508, 1954.
14. Philip, J. R., and De Vries, D. A. Moisture Movement in Porous Materials Under Temperature Gradients. Trans. Amer. Geophys. Union, Vol. 38, p. 222-232, 1957.
15. Woodside, W., and Kuzmak, J. M. Effect of Temperature Distribution on Moisture Flow in Porous Materials. Trans. Amer. Geophys. Union, Vol. 39, No. 4, p. 676-680, 1958.
16. Cary, J. W. Water Flux in Moist Soil: Thermal versus Suction Gradients. Vol. 100, No. 3, p. 168-175, 1965.
17. Winterkorn, H. F. Mass Transport Phenomena in Moist Porous Systems as Viewed From the Thermodynamics of Irreversible Processes. HRB Spec. Rept. 40, p. 324-338, 1958.
18. Winterkorn, H. F. Behavior of Moist Soils in a Thermal Energy Field. Clay and Clay Minerals, Vol. 9, 1962.
19. Aitchison, G. D., and Holmes, J. W. Suction Profiles in Soils Beneath Covered and Uncovered Areas. Proc. Fifth Internat. Conf. on Soil Mech. and Found. Eng., Paris, 1961.
20. Richards, B. G. Determination of the Unsaturated Permeability and Diffusivity Functions From Pressure Plate Outflow Data With Non-Negligible Membrane Impedance. In Moisture Equilibria and Moisture Changes in Soils Beneath Covered Areas (G. D. Aitchison, ed.). Butterworths, Sydney, 1965.

21. Whiffin, A. C., and Lister, N. W. The Application of Elastic Theory to Flexible Pavements. Proc. Internat. Conf. on Struct. Design of Asphalt Pavements, p. 499-521, 1962.
22. Maclean, D. J., and Clare, K. E. Contribution to discussion on A Review and Evaluation of Soil-Cement Pavements. Proc. ASCE, No. SM3, p. 115-118, 1960.
23. Dumbleton, M. J. Investigations to Assess the Potentialities of Lime for Soil Stabilization in the United Kingdom. DSIR, Road Res. Tech. Paper No. 64, London, 1962.
24. Metcalf, J. B. The Effect of High Curing Temperature on the Unconfined Compressive Strength of a Heavy Clay Stabilized With Lime and With Cement. Proc. Fourth Aust.-N. Z. Conf. Soil Mech. and Found. Eng., p. 126-130, 1964.

Temperature Effects on the Unconfined Shear Strength of Saturated, Cohesive Soil

MEHMET A. SHERIF and CHESTER M. BURROUS
University of Washington

Temperature-controlled, undrained and unconfined compression tests were conducted on reconstituted clay. The reconstituted clay studied, one-half Champion and one-half Challenger (known by its trade name as C & C), had previously demonstrated a linear relationship between the logarithm of shear strength and moisture content at room temperature. The experiments were aimed toward studying the effect of temperature on this relationship.

The samples were consolidated at room temperature and were failed in undrained, unconfined compression at temperatures of 75, 100, 125, and 150 F. The results indicate that, for a soil of constant moisture content, an increase in temperature causes a reduction in shear strength, and for the same temperature difference, the absolute reduction in the original strength increases as the initial moisture content of the soil decreases. The relation between the logarithm of shear strength and moisture content appears to be linear for constant temperature over the range of temperatures tested.

Two different equations describing the shear strength of the clay as a function of both moisture content and temperature are proposed. The first relates an increase in temperature to an equivalent increase in moisture content by an experimentally determined factor. The second relates the decrease in strength to the ratio of absolute reference and test temperatures and to the densities of the pore fluid corresponding to these temperatures.

•IN 1936 Hogentogler and Willis (4) found that the stability or strength of a compacted cohesive soil decreases with increasing temperature. Their explanation of this phenomenon was based on Winterkorn and Baver's (16) concept, which postulated an increase in free water at the expense of adsorbed water with rising temperatures. In 1958 Lambe (7) believed that an increase in temperature should result in an increase in shear strength.

Leonard (8) believed that an increase in temperature should cause a reduction in shear strength and supported his point of view by citing the work of Hogentogler and Willis (4), Rosenqvist (12), and Trask and Close (15), which show that an increase in temperature tends to cause reduction in shear strength. Ladd (5) conducted cone-penetration tests on Buckshot clay at various temperatures (5, 22 and 50 C) and found that hot samples gave slightly higher strength at a given mositure content and cold samples gave a higher strength at a given consolidation pressure. Semchuk (14) performed undrained triaxial tests on two soils (both consolidated and sheared at test temperatures of 35 and 77 F) and found practically no temperature influence on shear strength for both soils. Seed, Mitchell, and Chan (13) found that pore pressures in undrained triaxial samples vary with temperature and that an increase in temperature causes an increase in pore pressure. This result was varified by Ladd (5) and others.

From undrained triaxial tests conducted on compacted San Francisco Bay mud, Mitchell (10) found that higher temperatures produce lower shear strength and higher pore-pressure buildup during the shear. The data obtained by Duncan and Campanella (3) on soils consolidated at 68 F and sheared in undrained triaxial tests (at 68, 95. 8, and 119. 8 F) indicated that an increase in temperature causes a reduction in strength,

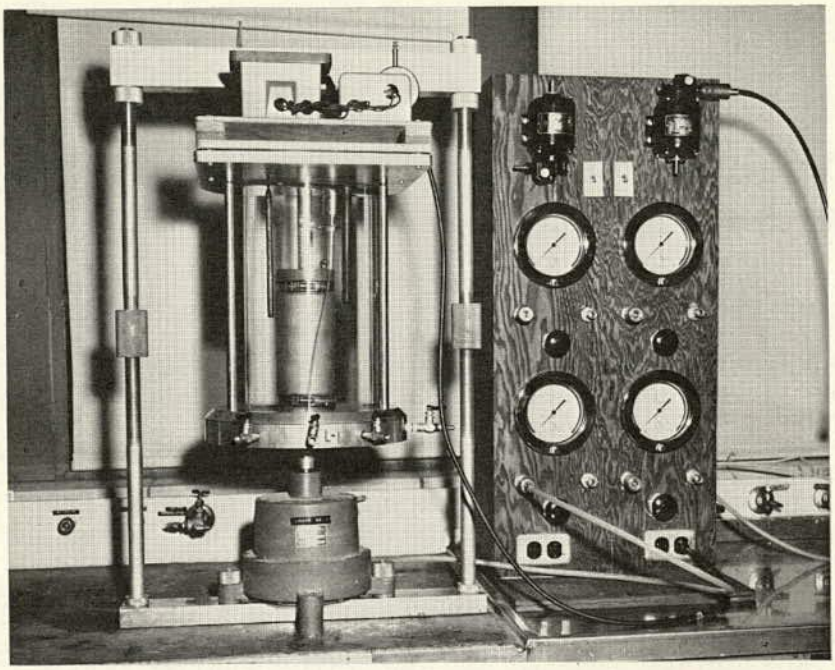

Figure 1. Temperature-controlled triaxial cell.

an increase in initial pore pressure, and a decrease in pore-pressure buildup during the shear testing.

In view of the importance of temperature effects on the engineering properties of soil and because of the apparent lack of complete agreement among previous researchers, it was decided to further enrich the existing body of knowledge on this subject by conducting additional studies at the University of Washington.

TABLE 1

COMPRESSIVE STRENGTH OF C & C CLAY

Test Designation	Temperature (deg F)	Failure Moisture Content (percent)	Compressive Strength (psi)
75-1	75	40.8	12.4
75-2	75	40.3	15.1
75-3	75	38.6	19.5
75-4	75	37.7	26.4
75-5	75	37.4	28.4
75-6	75	34.7	50.2
75-7	75	34.4	52.7
100-1	100	39.2	15.3
100-2	100	38.7	17.2
100-3	100	37.5	23.2
100-4	100	37.1	27.4
100-5	100	35.5	35.0
100-6	100	34.9	42.2
125-1, 2[1]	125	41.5	9.1
125-3	125	38.6	13.9
125-4, 5[1]	125	36.9	25.7
125-6, 7[1]	125	34.65	41.4
150-1, 2[1]	150	40.35	9.85
150-3	150	38.0	18.0
150-4	150	37.1	19.8
150-5	150	35.0	31.9
150-6	150	33.5	46.0

[1]Average of two tests.

SOIL TYPE AND EXPERIMENTAL PROCEDURE

The clay tested was a powdered dry commercial kaolinite clay produced by the Spinks Clay Company (Paris, Tenn.) and known by the trade name C & C. It was selected because previous test data (11) showed a linear relationship between the logarithm of strength and the moisture content at room temperature. Fifty pounds of the dry clay (85 percent finer than 0.005 mm) was mixed with distilled, de-aired water to a moisture content of 47 percent and stored in a plastic container in a humid room for approximately one year before use. The physical properties of the sample, determined just before starting the experiments, are as follows: liquid limit, 68

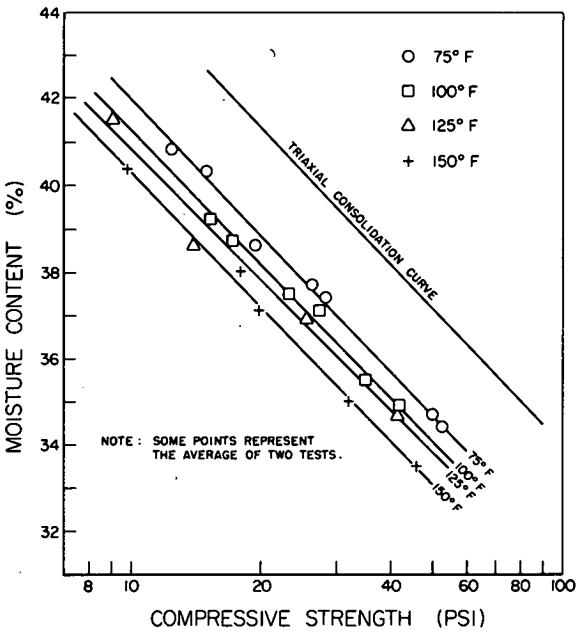

Figure 2. Failure envelopes for C & C clay as a function of moisture content and temperature.

percent; plastic limit, 35 percent; shrinkage limit, 22 percent; specific gravity, 2.58.

The clay was molded and trimmed into test cylinders 2.8 in. in diameter and 6.5 in. in height, then enclosed in a single layer of slit filter paper and two rubber membranes. The samples were placed in triaxial cells and consolidated for 7 days at room temperature (approximately 75 F) under hydrostatic stresses ranging from 20 to 98 psi. At the end of the consolidation period, the samples were taken out of the triaxial cells and their diameter, height, and moisture content were determined. The samples were then placed in heat-controlled triaxial cells over a plastic-covered pedestal to prevent any "communication" between the sample and the drainage outlets; thus no pore pressures were measured. Each cell was subsequently filled with glycerine, which was continuously circulated by propellers to insure a uniform temperature within the cell. Each cell was heated by a 500-watt electric-resistance heater element submerged in the cell fluid. A thermostat kept the temperature range to ±2 F. Several checks proved the effectiveness of the propellers. Figure 1 shows one of the temperature-controlled triaxial cell assemblies during the shearing operation. Each experiment was conducted at a constant cell temperature of 75, 100, 125, and 150 F. The cell was maintained at the test temperature for at least 8 hours prior to shear to insure a uniform temperature throughout the soil. At the end of this period, the change in the height of the sample was measured and the change in the volume of the sample was calculated. The calculation was based on the assumption that the temperature expansion of the pore water is the same as that of ordinary water and that the temperature expansion of the individual soil particles is negligible. With this information, the average cross-sectional area of the sample was estimated.

Following the 8-hour heating period, the soil was loaded in unconfined compression in a stress-controlled loader at the rate of 5.07 lb per 2 minutes (approximately 0.8 psi per 2 minutes) until failure. No drainage was permitted and no lateral stresses were applied during the 8-hour heating and during the actual shear. At the end of failure, the samples were taken out for moisture content determination. When the moisture content of the sample, just before heating, exceeded that of the sample at failure by more than 0.1 percent the test data were not included in the calculation. Likewise, the test data were rejected when the moisture content of the soil in the immediate vicinity of the failure plane differed from that of other parts of the sample by 0.2 percent.

The degree of saturation was calculated from

$$S \text{ percent} = \frac{W_w}{\gamma_w \left(V - \frac{W_s}{\gamma_s} \right)} \times 100 \qquad (1)$$

where S is the degree of saturation; W_w and W_s are the weight of the water and solids, respectively; V is the total volume of the soil-water system; and γ_w and γ_s are the density of water and solids. (Since the measurement of volume is subject to some error, a sample was not rejected as being unsaturated unless the calculated degree of saturation was less than 98 percent.)

For each test, the true compressive stress was plotted against the Henkey strain, e^H (also referred to as the true strain), defined as

$$e^H = - \int_{L_i}^{L_f} \frac{dL}{L} = - \ln (1 - e^c) \qquad (2)$$

where e^c is the Cauchy or engineering strain. (The compressive strength at failure was defined as the peak compressive stress.)

EXPERIMENTAL RESULTS

The results obtained from this experimental series are given in Table 1. In Figure 2, a plot of the moisture content of the soil and the logarithm of compressive strength at each test temperature is shown. The lines in Figure 2 are obtained by a least squares fit (at each test temperature) of the unconfined compressive strength as a function of percent moisture content. It is apparent from this figure that an increase in temperature causes a decrease in the compressive strength of the soil. This result is only logical because the adsorbed water around the individual clay particles assumes a less rigid state as the temperature rises (16), thereby increasing pore pressures and reducing the effective stresses and, therefore, the shear strength of the soil. The increase in entropy of the soil-water system and the increase in Brownian movements (within the liquid occupying the pore interstices) with rising temperatures also contribute to the reduction of strength by preventing the system from assuming the state of least potential energy, where it can reach a stable condition that is most favorable to improved bond-formation among the particles.

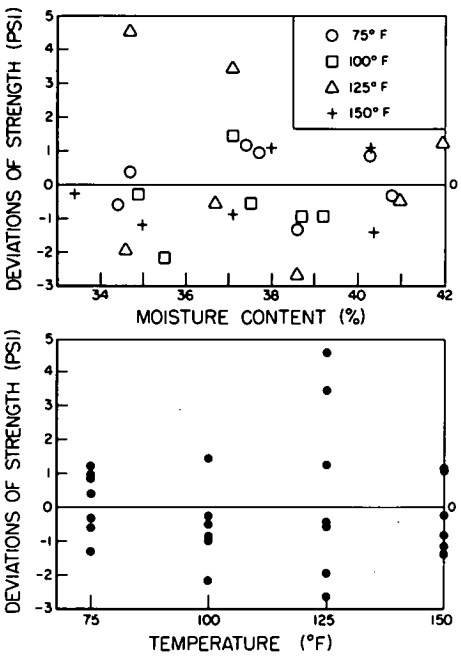

Figure 3. Statistical deviations in strength, or the differences between experimentally predicted (Eq. 4) values of the compressive strength.

Figure 2 further indicates that the soil samples of lower moisture content undergo greater reduction in strength (for the same rise in temperature) than those of higher moisture content, since an increase of 75 F in temperature at w = 41 percent decreases the compressive failure stress by only about 4 psi, while at w = 34 percent the soil loses about 17 psi in strength.

The samples that failed at 75 F were considered to be "reference" samples since this was also the consolidation temperature. As previously mentioned, at the reference temperature there is a linear relationship between the logarithm of the compressive strength and the moisture content. This can be expressed as

$$\sigma_o = \exp (A - Bw) \qquad (3)$$

where σ_o is the compressive strength at the reference temperature, w is the moisture content in percent, and A and B are material constants that must be determined experimentally.

Two different equations describing the compressive strength of C & C clay as a function of both moisture content and temperature have been derived from the data. The first relates an increase in temperature to an equivalent increase in moisture content:

$$\sigma_T = \exp (A - Bw - C\Delta T) = \sigma_o \exp (-C\Delta T) \quad (4)$$

where σ_T is the compressive strength at reference temperature, w is the moisture content, ΔT is the difference between the test and reference (or consolidation) temperature, and A and B are the same material constants as in Eq. 3. The soil parameter C is characteristic of temperature-induced changes in the clay and must be determined by testing at a temperature other than the reference temperature.

Equation 4 indicates that the strength of the soil decreases with both increasing moisture content and temperature, and that the increase in temperature is analogous to an increase in moisture content. Consequently, $C\Delta T/B$ might be regarded as being equal to w', an equivalent moisture content.

A least squares fit of Eq. 4 to the data is shown in Figure 4 by solid lines. The statistical deviations in strength with respect to moisture content and temperature changes are shown in Figure 3. It is seen from Figure 3 that the deviations are relatively random and evenly scattered about line 0-0, thus indicating that the parameter C appears to be independent of both moisture content and temperature (2).

The second proposed equation, shown below, relates the change in compressive strength to the ratio of the reference and test temperatures and to the ratio of the densities of the pore fluid at these respective temperatures. This equation eliminates the need for experimental determination of the constant C:

$$\sigma_T = \frac{T_o}{T} \exp \left[A - B \left(\frac{\gamma_{wo}}{\gamma_w} \right) w \right] \quad (5)$$

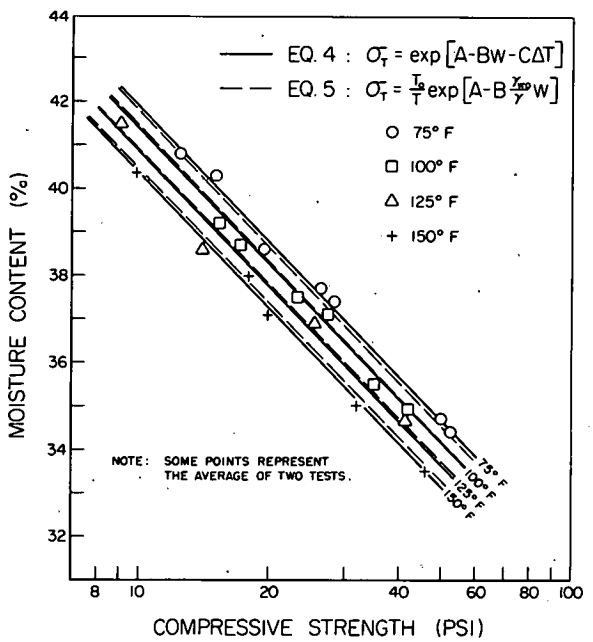

Figure 4. Least squares fit of Eq. 4 and Eq. 5 to the data.

where γ_{wo} and γ_w are the water densities at reference and test temperatures, T_o and T, respectively.

The least squares fit of Eq. 5 is shown in Figure 3 by dashed lines and can be compared with the least squares fit of Eq. 4, shown by solid lines. Over the temperature and moisture content range considered, Eqs. 4 and 5 predict nearly the same values. These equations become the same as Eq. 3 when the test temperature is the same as the reference (consolidation) temperature.

Further research is being conducted at the University of Washington to determine if the foregoing relationships are applicable to other soils, and if so, how well the parameters discussed can be related to some easily determinable soil properties such as LL, PL, or PI.

CONCLUSIONS

The following conclusions can be made about C & C clay consolidated at 75 F and sheared at 75, 100, 125, and 150 F in unconfined and undrained compression:

1. An increase in temperature causes a decrease in compressive strength, as indicated in Figure 2. Moreover, an increase in temperature is analogous to an increase in moisture content, as revealed by Eq. 4.
2. A linear relationship exists between the logarithm of compressive strength and the moisture content at all test temperature levels. The failure lines at constant temperatures appear to be almost parallel to the consolidation curve, as shown in Figure 2.
3. Soil samples of lower moisture contents undergo greater absolute reduction in strength with rising temperatures than those of higher moisture content levels. This is in agreement with Campanella and Mitchell's recent finding in which they state that, at small values of effective stress, temperature-induced pore pressures decrease (1).

REFERENCES

1. Campanella, R. G., and Mitchell, J. K. Influence of Temperature Variations on Soil Behavior. Jour. of Soil Mech. and Found. Div., ASCE, Vol. 94, No. SM3, May 1967.
2. Drapier, N. R., and Smith, H. Applied Regression Analysis. John Wiley, New York, 1966, 407 p.
3. Duncan, J. M., and Campanella, R. G. The Effect of Temperature Changes During Undrained Tests. Report TE-65-10 to U. S. Army Engineers Waterways Experiment Station. Soil Mechanics and Bituminous Materials Research Laboratory, Univ. of California, Berkeley, Nov. 1965.
4. Hogentogler, C. A., and Willis, E. A. Stabilized Soil Roads. Public Roads, Vol. 17, No. 3, May 1936.
5. Ladd, C. C. Physico-Chemical Analysis of the Shear Strength of Saturated Clays. DSc dissertation, M. I. T., Cambridge, 1961.
6. Ladd, C. C. Discussion, Jour. Soil Mech. and Found. Div., ASCE, Vol. 90, No. SM6, p. 181-185, Nov. 1964.
7. Lambe, T. W. The Structure of Compacted Clay. Trans. ASCE, Reprint Paper 3041, Vol. 125, 1960.
8. Leonards, G. A. Discussion, Trans. ASCE, Reprint Paper No. 3041, Vol. 125, 1960.
9. Leonards, G. A., and Andersland, A. M. The Clay-Water System and the Shearing Resistance of Clays. Research Conf. on Shear Strength of Cohesive Soils, ASCE, Boulder, Colorado, 1960.
10. Mitchell, J. K. Shearing Resistance of Soils as a Rate Process. Jour. Soil Mech. and Found. Div., ASCE, Vol. 90, No. SM1, Proc. Paper 3773, Jan. 1964.
11. Rieder, G. U. The Shear Strength of Clays as a Function of Moisture Content and Rate of Shear. MS thesis, Univ. of Washington, 1964.
12. Rosenqvist, I. Th. Investigations in the Clay-Electrolyte-Water System. Publication No. 9, Norwegian Geotechnical Inst., Oslo, 1955, p. 107.
13. Seed, H. B., Mitchell, J. K., and Chan, C. K. The Strength of Compacted Cohesive Soils. Research Conf. on Shear Strength of Cohesive Soils, ASCE, Boulder, Colorado, 1960.
14. Semchuk, W. Effect of Temperature on the Shear Strength of Two Edmonton Clay Soils. MS thesis, Univ. of Alberta, Edmonton, 1962.
15. Trask, P. D., and Close, J. E. H. Effect of Clay Content on Strength of Soils. Proc. Sixth Conf. on Coastal Engineering, Council on Wave Research, The Engineering Foundation, 1958.
16. Winterkorn, H., and Baver, L. D. Sorption of Liquids by Soil Colloids. Soil Science, Vol. 40, No. 5, Nov. 1935.

Influence of Seepage Stream on the Joining of Frozen Soil Zones in Artificial Soil Freezing

TSUTOMU TAKASHI, Seiken-Reiki Co., Osaka, Japan

In artificial soil freezing, the presence of a seepage stream disturbs the development and joining of frozen soil zones around the freezing pipes due to heat gain from the seepage stream. In order to obtain the mutual quantitative relationships among velocity of seepage stream, representative length of freezing zone, permeability coefficient of soil, temperature of seepage stream and coolant, and distance between freezing pipes and radius of the pipe, a theoretical study has been performed. The study consists of two parts. In the first part, the author has investigated by hydraulics theory and Darcy's law how to estimate the amount of dam-up in front of the frozen zones as freezing of the soil progresses. In the second part, the critical dam-up head, below which it is possible to achieve the joining of frozen zones under the presence of seepage stream as intensified by dam-up head, is solved mathematically.

•AT PRESENT, in the application of artificial freezing of soils, the ice-soil curtain can be achieved by cooling the freezing pipes laid under the ground. In the absence of seepage, it is obvious that the frozen-soil cylinders around the freezing pipes grow until they join, and the planned frozen-soil curtain is achieved. In the presence of seepage, however, the heat carried by it may often cause difficulties in joining of the ice-soil cylinders (1). These phenomena are frequently experienced with the spread of the freezing region (2). For instance, Khakimov (3) noted that when the method of artificial freezing of soils was carried out on the Irtysh riverside in the Soviet Union in 1952, the seepage flow caused difficulties in the joining of the frozen-soil cylinders and the freezing time was delayed about four months.

This paper tries to establish a criterion for determining whether the joining of frozen-soil cylinders can be achieved in spite of the above-mentioned influence from seepage flow. This phenomenon is the consequence of complicated hydrodynamics and heat transfer, and so the result depends on several assumptions. However, the result itself has a definite form and is considered to represent the process of the phenomenon sufficiently as the first approximation, and to be useful in practice.

In this paper the author describes, when an obstacle is formed by soil freezing in a uniform seepage, how large a dam-up arises before and behind it, and then derives a criterion for determining whether the frozen-soil curtain can be achieved in the presence of the seepage flow caused by the hydraulic gradient accompanied by the dam-up.

CHARACTERISTICS OF THE PHENOMENON

First we consider the following case. As shown in Figure 1, a finite number of freezing pipes have been arranged in a row in order to form a frozen curtain, and the seepage flow, having a uniform velocity u_∞ (natural velocity), is perpendicular to the line in which the pipes are arranged. After freezing, frozen-soil areas grow around the freezing pipes, an obstacle against the seepage flow appears, and the velocity u_∞ varies.

In our experience in cases like this, after sufficient freezing time, almost frozen soil cylinders join to the ice-curtain, but the areas of large dam-up or high permeability coefficient often do not join. Here, dam-up is the greatest at the central part (the

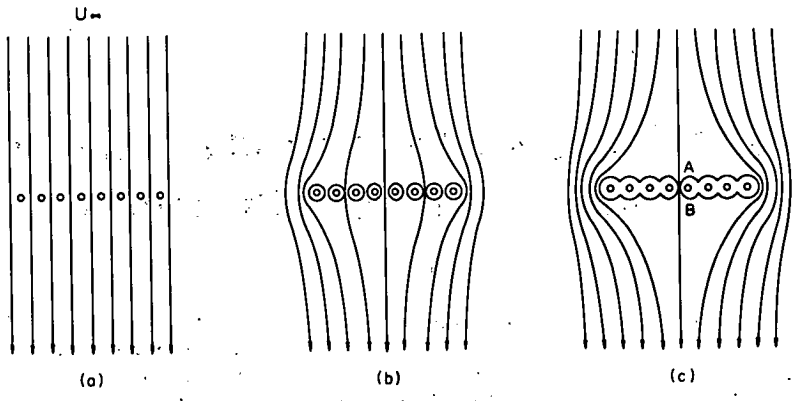

Figure 1.

point A, B), so we will calculate the quantity of dam-up at the point A, B and investigate the influence of the seepage flow caused by dam-up between A and B on the joining of the frozen-soil cylinders.

QUANTITY OF DAM-UP ACCOMPANYING THE FREEZING PROCESS

When groundwater moves among soil particles, the flow is laminar in the case of small hydraulic gradients, and it is well known that the following formula represents the velocity caused by the gradient according to Darcy's law:[1]

$$U_x = -\lambda \frac{dp}{dx} \tag{1}$$

where

U_x = the flow velocity in the direction of x, in m/h;
λ = the permeability coefficient, in m/h; and
$\frac{dp}{dx}$ = the hydraulic gradient in the direction of x, in m/m.

In the case where soils are uniform and homogeneous, it is known from this equation that the velocity distribution around the frozen soil is equal to that of the incompressible perfect fluid by regarding λp as a velocity potential Φ, i.e.,

$$\Phi = \lambda p \tag{2}$$

Thus, if the velocity potential Φ of the incompressible perfect fluid is known, the pressure p in the groundwater can be calculated as

$$p = \frac{\Phi}{\lambda} \tag{3}$$

In the case of two dimensions, the velocity potential Φ around the several forms of obstacles in the incompressible perfect fluid is often solved by means of conformal representation. For example, where the flow is perpendicular to a flat plate, as shown in Figure 2, the velocity potentials at the point A, B are respectively (4)

[1]In this paper the author treats only the case in which seepage flow follows Darcy's law. Where the seepage flow is turbulent, no application of the method of artificial freezing of soils can be done.

$$\left.\begin{aligned} \Phi_A &= \frac{1}{2}\,\ell\, U_\infty \\ \Phi_B &= -\frac{1}{2}\,\ell\, U_\infty \end{aligned}\right\} \tag{4}$$

Therefore, the head of dam-up between A and B is

$$p_A - p_B = \frac{1}{\lambda}(\Phi_A - \Phi_B) = \frac{\ell}{\lambda} U_\infty \tag{5}$$

where

ℓ = the width of frozen curtain perpendicular to the direction of seepage flow, and
U_∞ = the velocity of seepage flow before freezing.

As an example, when we assume that, in a uniform soil layer with permeability coefficient $\lambda = 10^{-1}$ cm/sec = 3.6 m/hr, seepage rate U_∞ = 8 m/day = 0.33 m/hr flow, and the frozen-soil curtain with a width 100 meters perpendicular to the flow as shown in Figure 2, the quantity of dam-up head at the center of that curtain is

$$p_A - p_B = \frac{100}{3.6} \times 0.33 = 9.26\,\text{m}$$

In order to examine the details, we study the section C-D in Figure 2(a). The head of groundwater of section C-D is as shown in Figure 2(b). The line CD is the groundwater level before formation of the obstacle. After that the level on the upstream side turns to CA and on the downstream side to BD and the water level between B and A becomes $(p_A - p_B)$. Then, if the ice-soil curtain is not attained at the area around A, the stream pours through that part, and in such a condition the ice-soil cylinders may remain open permanently.

Now, knowing the permeability coefficient λ and the natural velocity U_∞ or the hydraulic gradient dp/dx of the region where the method of artificial freezing of soils is to be applied, we can assume the maximum head of dam-up at the time the frozen-soil cylinders join to the ice-soil curtain is the above-mentioned relation. We thus try to establish a criterion for completing the ice-soil curtain in spite of the concentration of flow in the part of the curtain being frozen.

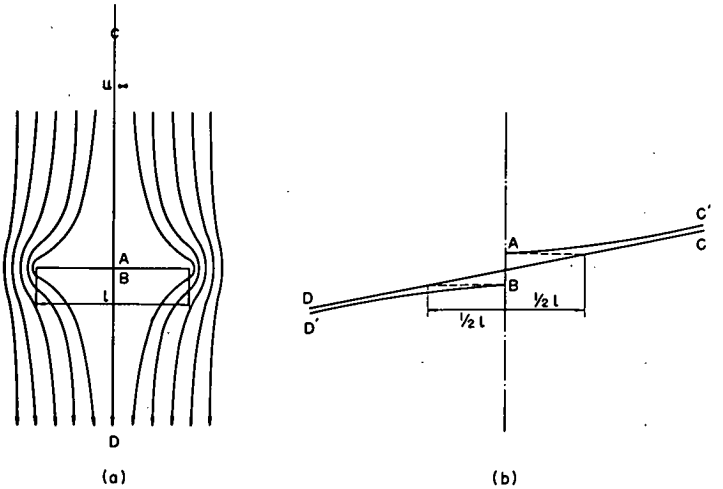

Figure 2.

MODEL OF THE STREAM BETWEEN THE FREEZING PIPES CAUSED BY DAM-UP

As already mentioned, we experienced that the frozen-soil cylinders did not join at that area where the dam-up is large or the permeability coefficient is relatively large from the ground disturbance at the time of boring to set the freezing pipes. To simplify the problem, this section treats the simplest model of ice-soil cylinders left open and the assumptions for getting it. Figure 3(a) represents the incomplete part of the frozen-soil curtain. At this time, the other part is already finished, and the thickness of the curtain is almost equal to L (the distance between the freezing pipes). The flow pours in the part A, B and the difference of dam-up head, $p_A - p_B$, mentioned in the previous paragraphs, arises between the point A and B.

The flow between A and B is considered to be like Figure 3(a); however, it is very complicated for mathematical analysis. Therefore, the following assumptions are proposed:

1. The section of the ice-soil cylinder is assumed to be circular, as shown in Figure 3(b). Research by Yoshinobu (5) and field measurements by Khakimov (3) show that this assumption diverges only slightly from the real condition. Strictly the section is oval toward downstream, but it can be considered to be a circle.
2. The seepage flow between the freezing pipes flows fast around the frozen-soil cylinders and slow in the center, as indicated in Figure 3(a), but is assumed to have a uniform velocity profile as in Figure 3(b).
3. The head of dam-up is the value adopted when the ice-soil curtain is completed as shown previously, and is also assumed to occur at point A and B at a distance between the freezing pipes, in front of and behind the frozen-soil curtain, as shown in Figure 3(b).

In developing the theory on the basis of these assumptions, we must take care of some additional points. In the limiting case of the freezing radius R approaching $\frac{1}{2}$ L in the model, as in Figure 3(b), the induced velocity just before the achievement of the ice-soil curtain is infinite. This is considered to actually happen, but the quantity of the flow between freezing pipes is finite, and so the ice-soil cylinders grow together, forming the ice-soil curtain.

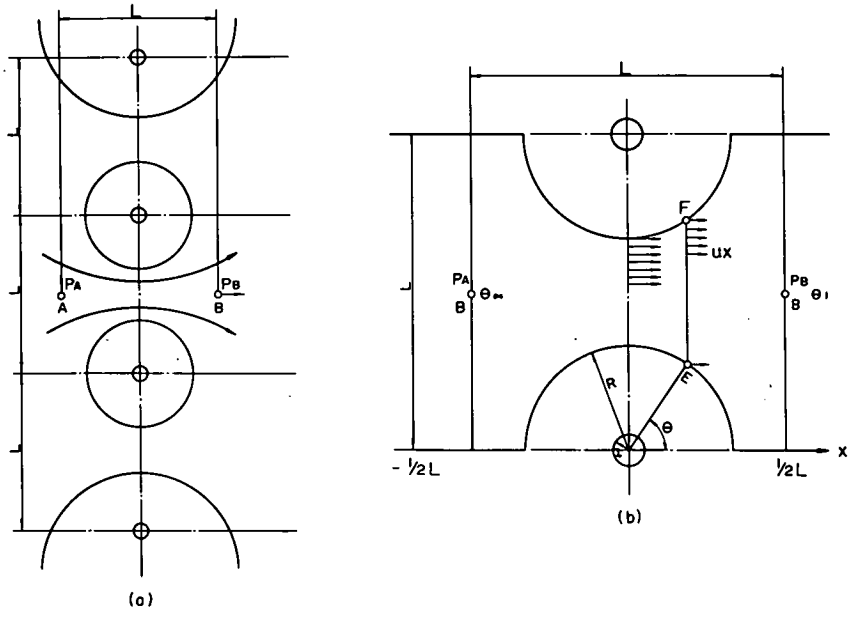

Figure 3.

THE QUANTITY OF INDUCED FLOW BETWEEN ICE-SOIL CYLINDERS

According to assumption 2, the quantity of water flowing between E and F in Fiugre 3(b) is, for $-R < x < R$,

$$V = \overline{EF} \times U_x = -(L - 2R \sin\theta)\,\lambda \frac{dp}{dx} \tag{6}$$

and for $-L/2 < x < -R$ and $R < x < L/2$,

$$V = L \times U_x = -L\lambda \frac{dp}{dx} \tag{7}$$

where

L = the distance between the freezing pipes,
R = the freezing radius, and
λ = the permeability coefficient.

Taking account that, for $-R < x < R$, $x = R\cos\theta$ and $dx = -R\sin\theta \cdot d\theta$, the transformation of Eqs. 6 and 7 is, for $-R < x < R$,

$$dp = \frac{V}{\lambda} \cdot \frac{R\sin\theta}{L - 2R\sin\theta} \cdot d\theta$$

and for $-L/2 < x < -R$ and $R < x < L/2$,

$$dp = -\frac{V}{\lambda}\frac{dx}{L}$$

Consequently, the resistance against flowing between A and B can be obtained by integration of that function about x from $-L/2$ to $L/2$, and its value must be equal to the dam-up head,

$$-(p_A - p_B) = \int_{x=-\frac{L}{2}}^{x=\frac{L}{2}} dp = \int_{x=-\frac{L}{2}}^{x=-R} dp + \int_{\theta=\pi}^{\theta=0} dp + \int_{x=R}^{x=\frac{L}{2}} dp$$

$$= \int_{x=-\frac{L}{2}}^{x=-R} \frac{V}{\lambda} \cdot \frac{dp}{L} - \int_{\theta=0}^{\theta=\pi} \frac{V}{\lambda} \frac{R\sin\theta}{L - 2R\sin\theta}\, d\theta - \int_{x=R}^{x=\frac{L}{2}} \frac{V}{\lambda}\frac{dx}{L}$$

and thus

$$(p_A - p_B)\frac{\lambda}{V} = \int_{\theta=0}^{\theta=\pi} \frac{R\sin\theta}{L - 2R\sin\theta}\, d\theta + \frac{2}{L}\int_{x=R}^{x=\frac{L}{2}} dx$$

$$= 1 - b + \frac{1}{\sqrt{1-b^2}}\left\{\frac{\pi}{2} - \tan^{-1}\frac{b}{\sqrt{1-b^2}}\right\} - \frac{\pi}{2}$$

where

$$b = \frac{2R}{L} \tag{8}$$

Thus the quantity of the flow can be obtained in the expression,

$$\frac{V}{\lambda (p_A - p_B)} = \frac{1}{1-b + \frac{1}{\sqrt{1-b^2}} \left\{ \frac{\pi}{2} - \tan^{-1} \frac{b}{\sqrt{1-b^2}} \right\} - \frac{\pi}{2}} = \frac{1}{f(b)} \tag{9}$$

The right-hand side of Eq. 9 is a function of b only, and variation of b from 0 to 1 shows the condition of varying flow between the freezing pipes from the beginning of the freezing to the completion of the ice-soil curtain.

The value of $1/f(b)$ is shown by curve 1 in Figure 4. According to Eq. 9, the quantity of the flow is

$$V = \frac{\lambda(p_A - p_B)}{f(b)}$$

and U_{max}, the fastest velocity in the center of the distance between freezing columns, is

$$\frac{V}{L - 2R} = \frac{\lambda(p_A - p_B)}{f(b)\, L(1-b)} = U_{max}$$

Thus

$$\frac{U_{max} \times L}{\lambda(p_A - p_B)} = \frac{1}{f(b) \times (1-b)} \tag{10}$$

Equation 10 represents a ratio in which the flow velocity increases in proportion to the freezing radius R during the process of freezing development. Taking b into the abscissa and $1/f(b)(1-b)$ into the ordinate, curve 2 of Figure 4 is plotted, and it shows that, at $b \to 1$, i.e., just before completion of the ice-soil curtain, the velocity tends to infinity. But as shown in Figure 4, curve 1, the quantity V of the flow is finite. [Khakimov, (3) tried to analyze this problem, but his analysis does not satisfy a boundary condition of the flow around the freezing pipes, and so his result is far from the real state, especially when $b \to 1$, and the velocity is finite.]

Finally, the pressure distribution between A and B according to Figure 3(b) can be obtained as

$$p_A - p = \int_{x=-L}^{x} dp \tag{11}$$

Figure 5 shows how the hydraulic gradient between the freezing pipes changes with increasing freezing radius R. Notice the rapid increase of hydraulic gradient as R approaches L/2.

THE HEAT EQUILIBRIUM EQUATION

In the previous section we calculated the quantity of flow between frozen-soil cylinders in a stationary state on the basis of three assumptions. In this section we will

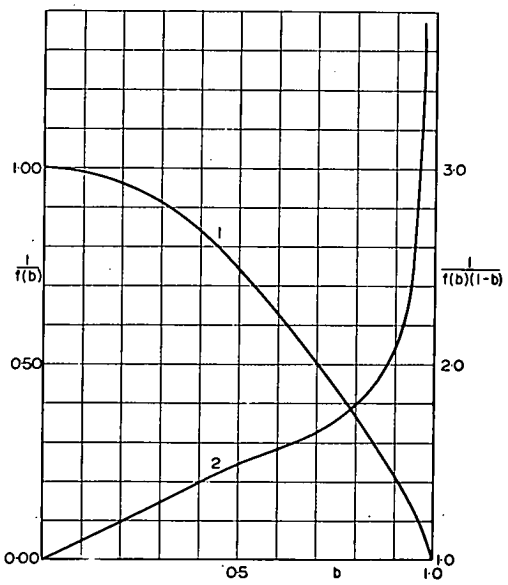

Figure 4.

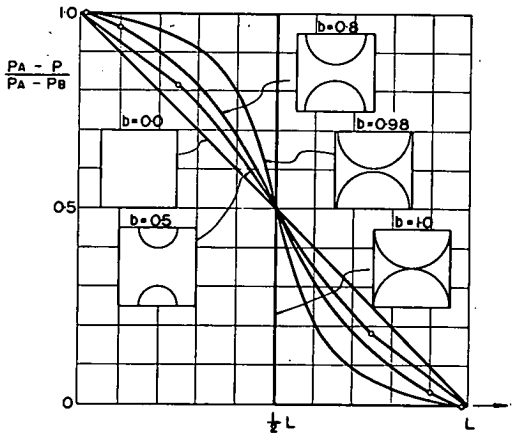

Figure 5.

calculate the temperature of the groundwater flowing downstream as the result of heat exchange.

If θ_∞ is the temperature of water from upstream and θ_1 is that of the water passed between the freezing columns to the downstream in Figure 3(b), the seepage is cooled from θ_∞ to θ_1 by passing between the freezing columns. Therefore the quantity of seepage flow in unit length perpendicular to the face of the paper in Figure 3(b) is

$$V = \frac{\lambda(p_A - p_B)}{f(b)}$$

and the heat quantity that cooled the flow is

$$q_1 = V\gamma c\,(\theta_\infty - \theta_1) = \frac{\lambda\gamma c\,(p_A - p_B)\,(\theta_\infty - \theta_1)}{f(b)} \qquad (12)$$

where

γ = the specific gravity of the groundwater in kg/m^3, and
c = the specific heat of the groundwater in kcal/kg deg C.

Then, as shown in Figure 3(b), around the freezing pipes the frozen-soil cylinders grow to radius R, and the temperature of the face of the freezing pipes is kept at θ_c and of the freezing boundary at θ_f, and so the heat quantity transferred to the freezing pipes is

$$q_2 = 2\pi k_1\,(\theta_f - \theta_c)\,\frac{1}{\ell n\,\frac{R}{a}} = 2\pi k_1\,\frac{\theta_f - \theta_c}{\ell n\,\frac{L}{2a} - \ell n\,\frac{L}{2R}} \qquad (13)$$

where

k_1 = the thermal conductivity of the frozen-soil in kcal/m.h. deg C;
θ_f = the freezing temperature of the groundwater, usually = 0 C; and
a = the outside radius of the freezing pipe in m.

Because there is no heat exchange except the two terms mentioned, the Eqs. 12 and 13 are equal together, and the following formula is thus obtained:

$$\theta_1 = \theta_\infty - \frac{2\pi k_1 (\theta_f - \theta_c)}{\lambda \gamma c (p_A - p_B)} \times \frac{f(b)}{\ell n \frac{L}{2a} - \ell n \frac{L}{2R}} \tag{14}$$

Here, putting

$$F\left(\frac{2a}{L}, b\right) = \frac{f(b)}{\ell n \frac{L}{2a} - \ell n \frac{L}{2R}}$$

$$= \frac{1 - b + \frac{1}{\sqrt{1-b^2}} \left\{ \frac{\pi}{2} - \tan^{-1} \frac{b}{\sqrt{1-b^2}} \right\} - \frac{\pi}{2}}{\ell n \frac{L}{2a} - \ell n \frac{L}{2R}} \tag{15}$$

then

$$\theta_1 = \theta_\infty - \frac{2\pi k_1 (\theta_f - \theta_c)}{\lambda \gamma c (p_A - p_B)} \times F\left(\frac{2a}{L}, b\right) \tag{16}$$

THE CRITICAL DAM-UP HEAD

The physical meaning of Eq. 16 is that the temperature of seepage passed through the unfrozen part is θ_1, when the frozen-soil curtain except for some unfrozen parts is achieved and a stationary state with freezing radius R around the freezing pipe is kept in the unfrozen part after a long lapse of freezing time in the situation in Figure 1. And it does not show when such a stationary state appears in the development of R. The radius R can be obtained only from the limit of the unsteady-state solution.

However, because we do not aim at computing R or θ_1 in a stationary state, but at deciding whether the ice-soil curtain is formed or not, we must investigate the character of Eq. 16. On the right-hand side of Eq. 16 the second term

$$\frac{2\pi k_1 (\theta_f - \theta_c)}{\lambda \gamma c (p_A - p_B)}$$

is a positive constant number given by the dam-up head $p_A - p_B$ and the cooling temperture θ_c. Accordingly, θ_1 can be obtained from inspection of the character during the variation of b from 0 to 1 in Eq. 15. Both the numerator and the denominator of Eq. 15 are always positive, as shown in Figure 4, and thus

$$F\left(\frac{2a}{L}, b\right) > 0, \text{ for } \frac{2a}{L} < b < 1 \tag{17}$$

When b tends to 2a/L, the denominator tends to zero and the numerator to one:

$$F\left(\frac{2a}{L}, b\right) \to +\infty, \text{ for } b \to +\frac{2a}{L} \tag{18}$$

Moreover, when b tends to 1, the numerator tends to infinity:

$$F\left(\frac{2a}{L}, b\right) \to +\infty, \text{ for } b \to 1 \tag{19}$$

and thus, for $2a/L < b < 1$, F (2a/L, b) must have a minimum value at least. Practically, we see by the numerical calculation that it is a function with a minimum value as in Figure 6.

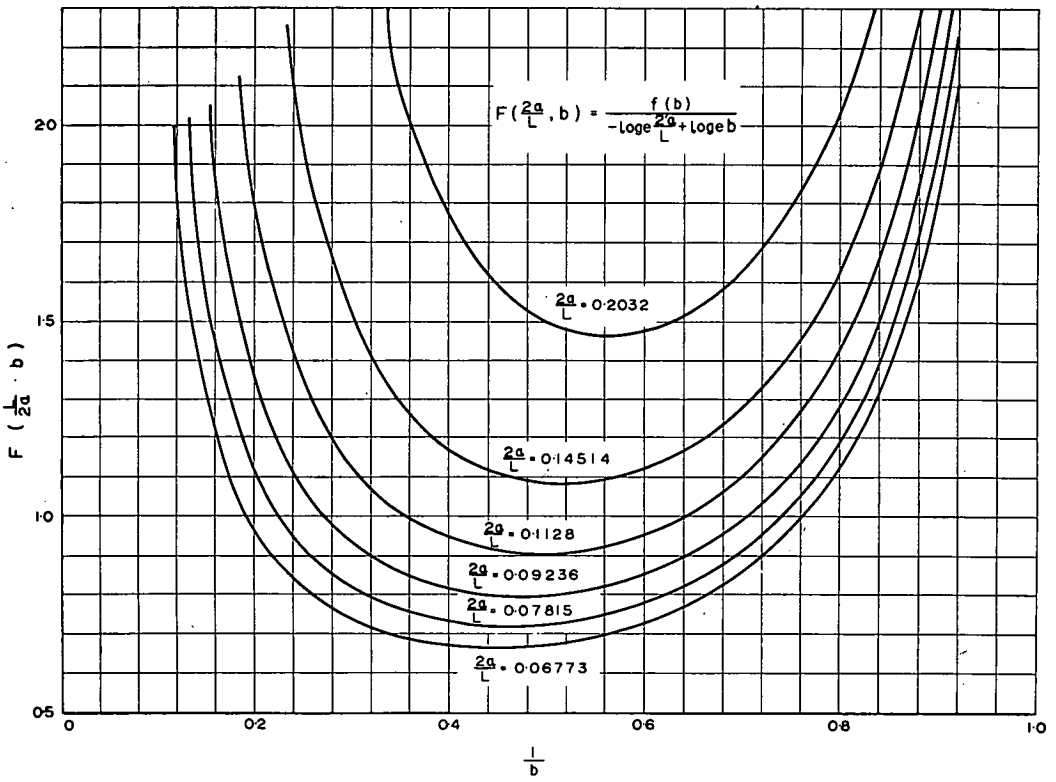

Figure 6.

This means that, for $2a/L < b < 1$, θ_1 has the only maximum value.

By supposing that b_{crit} represents b and that θ_1 is maximum, the following equation can be obtained:

$$\theta_{1\,max} = \theta_\infty - \frac{2\pi k_1 (\theta_f - \theta_c)}{\lambda\gamma c\,(p_A - p_B)} \cdot F\left(\frac{2a}{L},\ b_{crit}\right) \tag{20}$$

Because the groundwater flows, $\theta_{1\,max}$ is larger than the freezing temperature θ_f, i.e., $\theta_{1\,max} > \theta_f$. And when the dam-up head $p_A - p_B$ properly becomes small, $\theta_{1\,max}$ approaches and finally equals θ_f. Hence, we call such a dam-up head a critical dam-up head, $(p_A - p_B)_{crit}$. The value $(p_A - p_B)_{crit}$ is obtained by transformation of Eq. 20 by substituting θ_f for θ_1:

$$(p_A - p_B)_{crit} = \frac{2\pi k_1}{\lambda\gamma c} \frac{\theta_f - \theta_c}{\theta_\infty - \theta_f} \times F\left(\frac{2a}{L},\ b_{crit}\right) \tag{21}$$

This is the relationship we ask for, i.e., when the dam-up head $(p_A - p_B)$ expected to arise ahead of and behind the frozen-soil curtain is smaller than the critical dam-up head $(p_A - p_B)_{crit}$ given by Eq. 21, the following condition must be satisfied in order to complete the ice-soil curtain, namely, the temperature of the seepage across the unfrozen window cannot be higher than the freezing point θ_f. In other words, Eq. 21 is the sufficient condition for achievement of the ice-soil curtain.

EXAMINATION OF THE SOLUTION

The expression for the critical dam-up head consists of the product of three factors, as seen in Eq. 21. The first, $(2\pi k)/(\lambda \gamma c)$, is a factor determined from the property of the soils and the groundwater; the second, $(\theta_f - \theta_c)/\theta_\infty - \theta_f)$, is determined from the temperature of the ground before freezing and the surface of the freezing pipes; the third $F(2a/L, b_{crit})$ is determined from the radius of the freezing pipe and the distance between the pipes.

In this section we will examine the influence of these factors on the formation of the ice-soil curtain.

Influence of Properties of Soils

We will try the order estimation of Eq. 21. The order of $(\theta_f - \theta_c)/(\theta_\infty - \theta_f)$ and $F(2a/L, b_{crit})$ are 1, as indicated later. In the first factor, k is the thermal conductivity of the frozen soil $\fallingdotseq$ 2 kcal/m.h. deg C; γ is the specific gravity of the groundwater $\fallingdotseq$ 1000 kg/m^3; and c is the specific heat of the seepage $\fallingdotseq$ 1.0 kcal/kg deg C.

In urban civil engineering, dam-up head caused by the formation of a frozen curtain is not over 10 meters. If the dam-up head is over 10 meters, groundwater will overflow on the earth's surface. Accordingly, a frozen-soil curtain is achieved when the following condition of the permeability coefficient λ is satisfied:

$$\lambda < \frac{2\pi k}{\gamma c\,(p_A - p_B)_{crit}} \cdot \frac{\theta_f - \theta_c}{\theta_\infty - \theta_f} \cdot F\left(\frac{2a}{L}, b_{crit}\right)$$

$$\fallingdotseq \frac{10}{1000 \times 1 \times 10} \times 1 \times 1 = 10^{-3}\ \text{m/h} \fallingdotseq 10^{-4}\ \text{cm/sec} \qquad (22)$$

In other words, neglecting seepage has no noticeable influence when applying the method of artificial freezing of soil in uniform silt and clay in urban civil engineering.

However, when applying the method in a tunnel or deep pit in an impervious stratum where the dam-up head can be very large, the influence of seepage must be taken into account even in the case of permeability coefficients less than 10^{-4} cm/sec.

By the foregoing analysis we know that, when soil property improvement is necessary for lowering the permeability coefficient, it is efficient to use freezing pipes. The soil properties between the freezing pipes are, however, liable to be disturbed by boring and other factors.

Influence of Temperature of Ground and Coolant

The freezing point of groundwater θ_f in the second factor on the right-hand side of Eq. 21 is 0 C, if salts are not present. Thus, substituting $\theta_f = 0$, the following is obtained:

$$\frac{\theta_f - \theta_c}{\theta_\infty - \theta_f} = -\frac{\theta_c}{\theta_\infty} \qquad (23)$$

Consequently, we see that the critical dam-up head is inversely proportional to the initial temperature of the ground θ_∞. The nearer θ_∞ is to 0 C, the larger is the critical dam-up head, and at 0 C the ice-soil curtain is achieved however large the seepage. Jumikis (7) points out the difficulty of formation of a frozen-soil curtain in the case where the velocity of the seepage flow is faster than 2 m/day as the weak point of the artificial freezing of soils, but he does not indicate the condition of the dam-up and the temperature of the ground in that case. His suggestion is thereby limited in special cases. We also see that the critical dam-up head is in proportion to the temperature of the surface of the freezing pipes θ_c, and thus the freezing method by liquified nitrogen refrigerant ($\theta_c \fallingdotseq$ - 180 C) is nine times more effective than the usual brine (θ_c = -20 C).

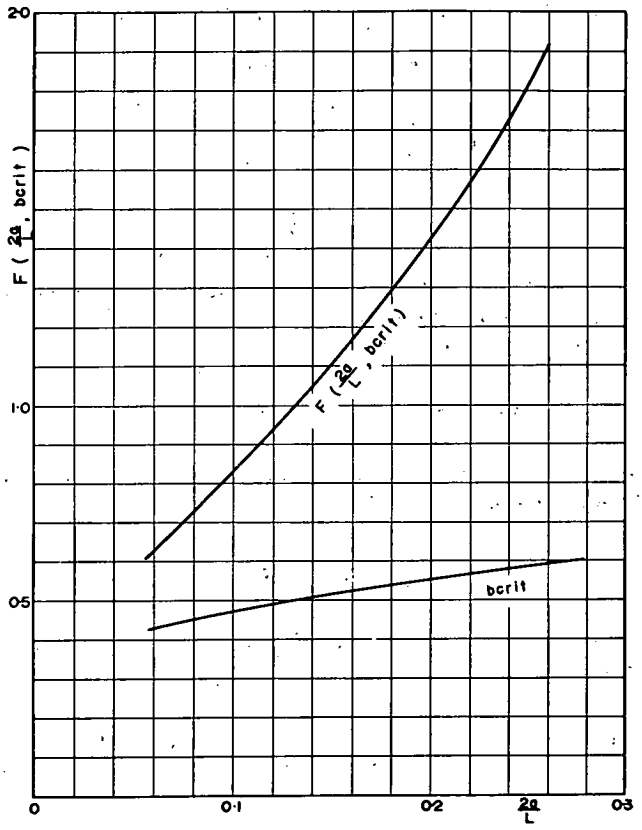

Figure 7.

Influence of Radius of Freezing Pipes and Distance Between Them

The third factor in the right-hand side of Eq. 21, $F(2a/L, b_{crit})$, is the minimum of Eq. 15. This factor has a parameter 2a/L, and enlarges with an increase of its value.

Figure 7, in which the abscissa is 2a/L and the ordinate $F(2a/L, b_{crit})$, shows that the relationship between them has a direct proportionality, and so at the same radius of pipes and half the interval, the critical dam-up head doubles, and at the same interval and half the radius, it becomes half.

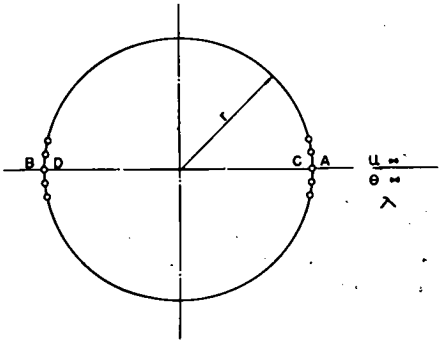

Figure 8.

EXAMPLES OF THE CALCULATION

In the case of comparatively simple forms of ice-soil curtain, we can calculate a dam-up head by the method of Eq. 5 when the value of seepage velocity U_∞ and permeability coefficient λ before freezing are known. In this section we make practical computations for two specific cases.

The Case of a Circular Shaft

In the case where the freezing pipes are set around a circle with the radius r as shown in Figure 8, if we write the velocity of the seepage flow before freezing U_∞ the difference of the

velocity potential at points A and B is, as shown earlier,

$$\Phi_A - \Phi_B = 4rU_\infty \tag{24}$$

Note that if the seepage velocity U is measured directly by a dyestuff or method of electric conductivity, it must be corrected as follows:

$$U_\infty = \frac{A\nu}{A} U$$

where $A\nu$ is the effective section-area of the pore and A is the apparent flowing-section area. Although the porosity n is commonly used for $A\nu/A$, it should be measured accurately. Using Eq. 3, we obtain

$$p_A - p_B = \frac{1}{\lambda}(\Phi_A - \Phi_B) = \frac{4r}{\lambda} U_\infty \tag{25}$$

When the frozen curtain is almost completed, the dam-up head at point A, C is considered to be half that described:

$$p_A - p_C = \frac{2r}{\lambda} U_\infty$$

Now, when $(p_A - p_C)$ is equal to the critical dam-up head given by Eq. 21, the critical velocity $U_{\infty crit}$ appears; i.e.,

$$\frac{2r\, U_{\infty crit}}{\lambda} = (p_A - p_C)_{crit} = \frac{2\pi k}{\lambda \gamma c} \frac{\theta_f - \theta_c}{\theta_\infty - \theta_f} F\left(\frac{2a}{L}, b_{crit}\right)$$

$$\therefore\ U_{\infty crit} = \frac{\pi k}{r\gamma c} \frac{\theta_f - \theta_c}{\theta_\infty - \theta_f} F\left(\frac{2a}{L}, b_{crit}\right) \tag{26}$$

When we insert the numerical values that are generally used in the formula, i.e., $k = 2.414$ kcal/m.h. deg C; $\gamma = 1{,}000$ kg/m^3; $c = 1$ kcal/kg deg C; $\theta_f = 0$ C; $\theta_c = -20$ C; $\theta_\infty = 18$ C; $2a/L = 0.1270$; and from Figure 7, $F(2a/L, b_{crit}) = 0.983$, we obtain

$$U_{\infty crit} = \frac{\pi \times 2.414}{r \times 1000 \times 1} \times \frac{20}{18} \times 0.983 \times 24 = \frac{0.2}{r} \text{ m/day}$$

In the case of comparatively rough soils that induce a seepage flow,

$$\frac{A\nu}{A} = 0.1 \sim 0.2$$

and so for the directly measured velocity we obtain

$$U_{crit} = \frac{1}{r} \sim \frac{2}{r} \text{ m/day}$$

We observe that the ice-soil cylinders can join in the freezing area with a radius of 2 m or so in the application of the method of artificial freezing of soils, even if the seepage velocity by direct measurement is 0.5 ~ 1.0 m/day, but the velocity of even 0.2 m/day causes difficulties when the radius r is enlarged to 10 m.

The Case of a Plane Ice-Soil Curtain

As another simple example, we will consider the case where the seepage flows perpendicular to the frozen-soil curtain as shown in Figure 2(a). In this case, because

the dam-up head is represented by Eq. 5, by the same viewpoint as previously, the critical velocity $U_{\infty crit}$ is obtained in the form

$$U_{\infty crit} = \frac{2\pi k}{\ell \gamma c} \frac{\theta_f - \theta_c}{\theta_\infty - \theta_f} \cdot F\left(\frac{2a}{L}, b_{crit}\right) \tag{27}$$

These two instances are the simplest ones in the case of forming an ice-soil curtain in uniform soils, and every critical flow velocity $U_{\infty crit}$ is in inverse ratio to the representative length of the frozen-soil curtain r, and ℓ. In other words, the larger the area of freezing soils is, the more difficult formation of an ice-soil curtain becomes.

CONCLUSION

Although this analysis depends on many assumptions, it nevertheless clarifies the mutual relationship between critical velocity, representative length of freezing zone, permeability coefficient of soils, temperature of stream and coolant, distance between freezing pipes, and radius of freezing pipe. This makes it possible by preliminary investigation to decide more precisely whether an ice-soil curtain can be achieved at a site of previous soil strata where the permeability coefficient is more than 10^{-3} cm/sec, knowing the permeability coefficient in the region and the hydraulic gradient or the velocity.

In the case where freezing temperature and the distance between the freezing pipes is normal and the critical velocity (or the critical dam-up head) is smaller than the seepage velocity (or the dam-up head), by changing the freezing temperature and the distance to the economical limit, we can make the critical velocity larger. But if the purpose is still not accomplished, we must try four methods as follows for countermeasures:

1. Make the permeability coefficient smaller by improving the soil properties between the freezing pipes, and enlarging the critical dam-up head (8);
2. Make the dam-up head smaller by installing a well for observation of water level and for pumping on both the upstream and downstream side (3);
3. Lower the freezing temperature θ_c temporarily by using liquified nitrogen refrigerant on the part of the frozen-soil curtain that remains open;
4. Accelerate the formation of the ice-soil curtain by adding a row of freezing columns.

The fourth of these countermeasures is more efficient than shortening the distance between the pipes or enlarging their radius. This is because the critical dam-up head is in inverse ratio to the distance and proportional to the radius of pipes, and by adding the row of freezing pipes, the path resistance of the seepage increases and the quantity decreases and, moreover, θ_∞ of the second row becomes small.

ACKNOWLEDGMENTS

In performing this analysis, I thank Sakuro Murayama, of the Kyoto University Disaster Prevention Research Institute, who gave me constant useful instruction; Tomomasa Tatsumi, of the Kyoto University Department of Physics, Setsuo Okuda, of the Kyoto University Disaster Prevention Research Institute, and Hirowo Yoshinobu, of the Osaka Prefecture University Department of Technology, who gave me appropriate comment and suggestion in developing the theory; Masamitsu Sumiyoshi and Tomimatsu Yasuda, members of the Seiken-Reiki Co., Ltd., Department of Freezing of Soils, who cooperated with me on numerical computations; and those members of the Seiken-Reiki Co., Ltd., Department of Freezing of Soils who gave me motivation and stimulation in the work.

REFERENCES

1. Takashi, Matsuwura, and Taniguchi. Artificial Freezing of Soils, 3. Reito, Vol. 36, No. 441, p. 1-15, 1962.

2. Murayama, Okamoto, Ikehara, Ito, and Takashi. Theory and Practice of Artificial Freezing of Soils. Japan Society of Civil Engineers, 22nd Annual Academic Lecture Meeting, Sec. 3, p. 107.
3. Khakimov, Kh. R. Artificial Freezing of Soils: Theory and Practice (1957). Translated into English by Israel Program for Scientific Translations, Jerusalem, 1966.
4. Susumu Tomochika. Hydrodynamics, p. 158-161.
5. Hirowo Yoshinobu. Frozen Region Formed Around a Line Heat Sink Under a Uniform Stream of an Incompressible Fluid. Jour. of the Physical Society of Japan, Vol. 19, No. 11, p. 2223-2231, Nov. 1964.
6. Takashi and Wada. About Artificial Freezing of Soils. Reito, Vol. 36, No. 408, p. 1-15, 1961.
7. Jumikis, A. R. Thermal Soil Mechanics. Rutgers Univ. Press, New Brunswick, N.J., 1966, p. 162.
8. Murayama, Endo, and Murata. Several Points of Artificial Freezing of Soils. Summary of Japan Society of Civil Engineers, 21st Annual Academic Lecture Meeting, Sec. 3, p. 3.

Effect of Preliminary Heat Treatment on the Shear Strength of Kaolinite Clay

HERBERT WÖHLBIER and DIETER HENNING
Department of Mining Engineering, Technical University Clausthal

•BECAUSE OF their mechanical properties some rocks are classified in the region between soils and rocks. Natural rocks of this kind, such as clay shale, conglomerate, or lignite, and artificially treated rocks such as stabilized soils, are of great interest in experimental and applied rock mechanics in mining engineering. This paper deals with some results of fundamental investigations concerning the mechanism of stabilization of cohesive soils. It is a part of a research program at the Department of Mining Engineering, Technical University Clausthal (Germany).

Thermal stabilization is here defined as an irreversible and effective increase of the shear strength of soil or rocks. Earlier papers report on the fundamentals of stabilization by heat treatment and the possibilities of application (2, 3). Heat treatment is the only procedure known till now to stabilize cohesive soils successfully in situ in the way the stabilization has been defined. Cohesive soils are aggregations of minerals or rocks with a higher percentage of fine-grained particles ($< 2\mu$) consisting largely of clay minerals. Cohesive soils are plastic within certain limits of water content. They are determined by a characteristic tensile strength. Their hydraulic permeability is relatively low ($k < 10^{-4}$ cm/sec).

When the experimental program was determined the aim was to work under reproducible testing conditions. This principle was of particular influence when the cohesive soil, the method of preliminary treatment, and the testing procedure were selected. Besides the stabilization, another aim of the investigation was to produce and characterize the change from a cohesive soil to a quasi-rock.

DETERMINATION OF SHEAR STRENGTH OF ROCKS

The shear strength of soils and rocks depends on physical and physicochemical properties of the rock (i.e., mineral content, structure, porosity, filling of voids, and related boundary effects), the initial conditions, and the dynamic and geometric limiting conditions. The influence of different factors, especially with regard to the shear strength of soils, has been described by others (5, 9).

The shear strength of samples in laboratory tests in most cases is determined by compression tests with multiaxial external loading and uniaxial tension tests. Best-known are triaxial tests on cylindrical specimens with axially symmetrical external loading, which were applied in this investigation program, too.

In soil mechanics it is common in the region of relatively low loading to plot Mohr's envelope of soils as a straight line. This simplification is no longer possible when the triaxial tests reach a wider part of the failure curve. Normally Mohr's envelope of soils or rocks is slightly curved. Therefore a different method was used to analyze the triaxial tests and to describe the envelope; it is discussed in the following.

When σ_{1i} and σ_{3i} (respectively σ_{1i}' and σ_{3i}' as effective stresses) are defined as maximum or minimum principal stresses under failure conditions it is possible to construct the corresponding stress-circles in $\sigma - \tau$ coordinates with $1/2\ (\sigma_{1i} + \sigma_{3i}) = \sigma_{oi}$ as coordinates of the centers and $1/2\ (\sigma_{1i} - \sigma_{3i}) = r_i$ as radii. By approximation the function (Fig. 1)

$$r = r\ (\sigma_o) \qquad (1)$$

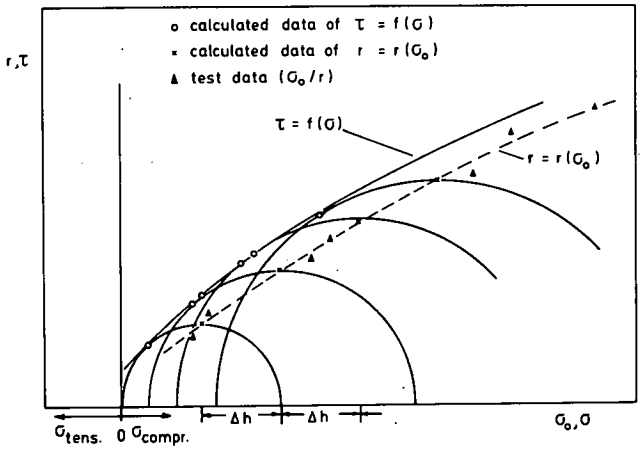

Figure 1. Construction of Mohr's envelope.

is formed. The equation of Mohr's envelope,

$$\tau = f(\sigma) \tag{2}$$

delivers

$$G(\sigma, \tau, \sigma_0) = (\sigma - \sigma_0)^2 + \tau^2 - r^2(\sigma_0) = 0 \tag{3}$$

and

$$\frac{\partial G}{\partial \sigma_0} = (\sigma - \sigma_0) + r \frac{\partial r}{\partial \sigma_0} = 0 \tag{4}$$

when σ_0 has been eliminated.

From Eq. 4 follows

$$\sigma_0 = g(\sigma) \tag{5}$$

The general equation of Mohr's envelope is now

$$\tau = \pm \left\{ r^2 [g(\sigma)] - [\sigma - g(\sigma)]^2 \right\}^{0.5} \tag{6}$$

Because of the relationship $r = r(\sigma_0)$, Eq. 6 is to be found in equations of different degrees of difficulty. Several solutions have been analyzed (4).

If Eq. 1 is written in the mathematical form of a straight line,

$$r = a + b\sigma_0 \tag{7}$$

the equation of the envelope (Coulomb's equation) changes to

$$\tau = \pm (a + b\sigma) \left(\frac{1}{1 - b^2} \right)^{0.5} \tag{8}$$

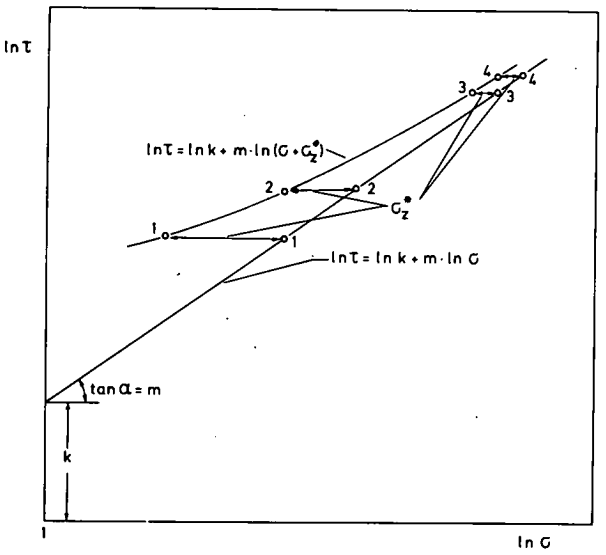

Figure 2. Determination of the parameters k, m, and σ_Z^*.

While analyzing the triaxial tests, which will be discussed later, the data σ_{0i} and r_i were equalized by an approximate polynomial. Within each measuring range (Fig. 1) the envelope consists of finite segments, which are plotted by steps of Δh with $r = r(\sigma_0)$. The envelopes have been calculated by a computer.

To describe the curved envelope an exponential equation of the form

$$\tau = \pm k \left(\sigma + \sigma_Z^*\right)^m \qquad (9)$$

is useful. If m = 1 the equation is identified by a straight line. In log-log coordinates the parameters k and m can be determined easily; σ_Z^* marks theoretically calculated data of the triaxial tensile strength of rock. From Figure 2 it follows that σ_Z^* can be calculated approximately only from the run of the failure line in the region of compressive loading (4, 10). Plotting Mohr's envelope in log-log coordinates, the line runs slightly curved as σ_Z^* was randomly equalized to zero. The real envelope referring to Eq. 9, however, has to be a straight line having the distance σ_Z^* from the corresponding curved line. Therefore it is possible to define the parameters k, m, and σ_Z^* with a good approximation. These results were also calculated by using a computer. As in soil mechanics, the parameter cohesion c, angle of internal

TABLE 1

PROPERTIES OF UNTREATED KAOLIN Ia FROM ZETTLITZ

Procedure	Constituent	Percent
Chemical analysis	SiO_2	47.37
	Al_2O_3	37.50
	Fe_2O_3	0.85
	TiO_2	0.20
	CaO	0.65
	MgO	0.15
	K_2O, Na_2O	0.65
	Loss on ignition	12.63
Analysis by Berdel method	Clay	95.5
	Quartz	1.0
	Feldspar	1.5
Analysis by Kallauner method	Clay	93.0
	Quartz	4.0
	Feldspar	3.0
Unit weight of solid constituents	2.629 g/cm^3	
Index of pH	8-8.5	
Grain-size distribution	< 1μ	57
	< 2μ	16
	< 3μ	12
	< 5μ	11
	<10μ	2
	<15μ	0.5
	>15μ	1
Liquid limit	0.529	
Plastic limit	0.346	
Plasticity index	0.183	

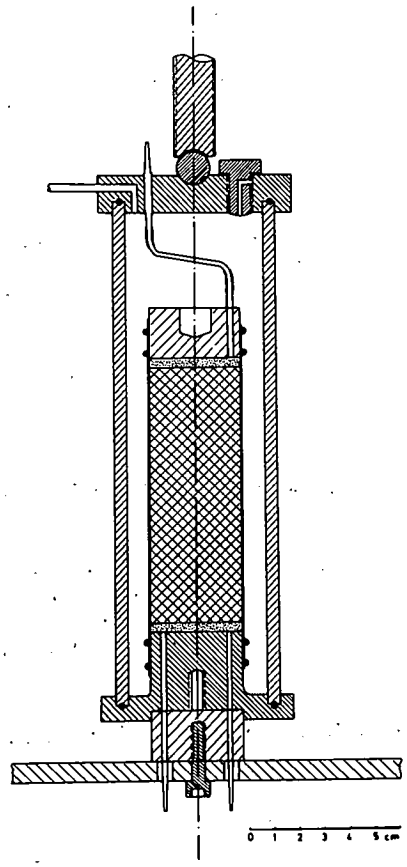

Figure 3. Consolidation cell.

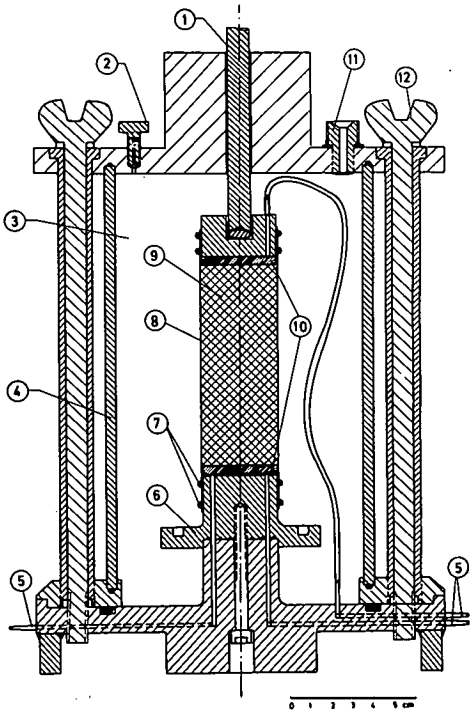

Figure 4. Triaxial cell: 1—piston; 2—air release valve; 3—water; 4—Perspex cylinder; 5—drainage or pore pressure connection; 6—lower part of consolidation cell; 7—rubber O-ring; 8—rubber membrane; 9—sample; 10—porous disc; 11—connection to pressure supply; 12—tightening screw.

friction ϕ, m, and k, and to some extent σ_z^*, too, can be expressed only as mathematical parameters of an equation, by which the run of the envelope and hence the shear strength of a rock can be described with sufficient accuracy.

TESTING PROCEDURE

For the investigation a standard material (Kaolin Ia from Zettlitz, CSSR) was selected that is characterized by optimal properties of drying and heating. The thermal reactions are well known (7). Table 1 shows some of the most important mineralogical data and index properties of the kaolin. For 14 days the kaolinite clay was kept with an initial water content of 48 to 50 percent. After that, samples that were to a great extent homogeneous and de-aired were prepared by a vacuum-extrusion press (diameter 40 mm, length 120 mm). The samples were dried for about 28 days, and then were heated for 48 hours in an electric furnace with temperatures up to 600 C. The increase of temperature by which the samples were heated was 60 C/hour. The treated samples were kept for 14 days in a desiccator and after that the dry and water-saturated specimens were tested with regard to their shear strength.

Wetting the specimens and the preconsolidation were performed in special consolidation cells (Fig. 3). Lowe and Johnson (6) described a similar method that was used after wetting the samples in order to get as high a saturation as possible. When water had passed the specimen at the upper porous stone, reduced pressure was brought to both ends of the sample. At the same time that the triaxial pressure outside of the partly de-aired specimen was taken, a pore water pressure was obtained. This action was repeated several times every 3 hours. Using the back-pressure method it was possible to get a saturation of more than 96 percent. The specimens in the cells were

consolidated at a pressure of 1, 3, 7, 12 or 25 kp/sq cm, i.e., at the same confining pressure applied on the triaxial tests. Because of the special construction of the consolidation cells it was possible to install the lower part of the consolidation cell together with the preconsolidated specimen in the triaxial cell (Fig. 4) so that the triaxial tests could be carried out after 1 or 2 days.

To achieve constant cell pressures up to 25 atm, special units were used that were developed by the second author (Fig. 5). The pressure pistons are moved by a back-geared motor to decrease the friction between piston and cylinder. This causes a fast automatic adaptation of the pressure system to volume changes in the cell.

With regard to water-saturated samples, the consolidated undrained (CU) triaxial tests were performed with measurement of pore water pressure. To measure the pore water pressure two specially designed and constructed devices were used that work automatically with null indicator controlled by a photoelectric tube (Fig. 6). The pump is driven by an electric motor combined with a solenoid brake. The system, because of its photoelectric control, is characterized by high operating reliability and small deviation.

The triaxial tests were performed using Geonor cells up to 7 atm and Farnell cells up to 25 atm, three each, as well as two testing machines with a screw jack operated by an electric motor and gearbox for tests with a controlled rate of strain. All data were registered photographically.

The same testing equipment was used when triaxial tests were performed on pre-treated dry specimens, but the porous stones were exchanged for metal plates. In addition to the triaxial tests, uniaxial compression and tension tests were made (Fig. 7).

Preliminary investigations concerning the influence of all different factors on water-saturated samples showed that a feed motion of 0.005 mm/min of the testing machine

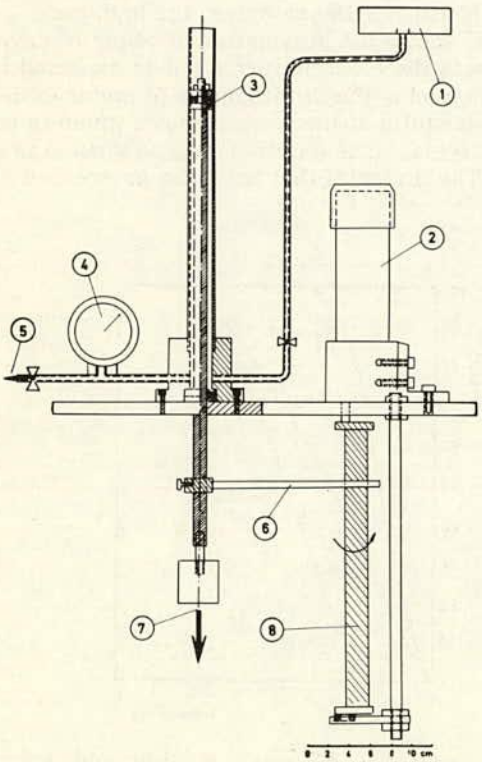

Figure 5. Apparatus for controlling cell pressure.

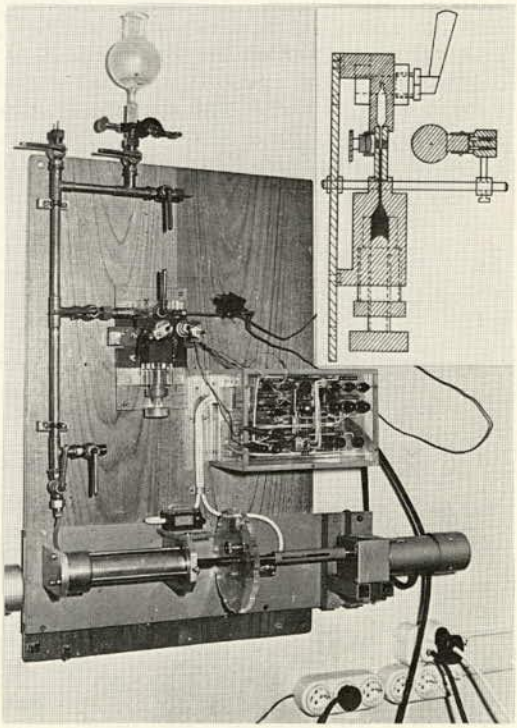

Figure 6. Apparatus for measuring pore pressure.

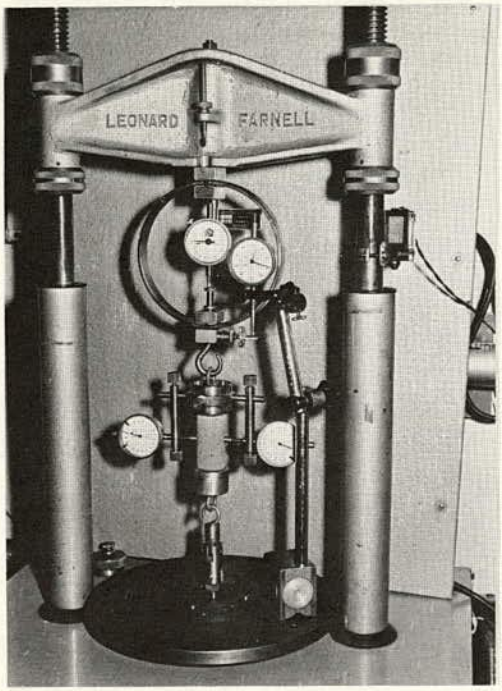

Figure 7. Apparatus for tensile tests.

was necessary, while for compression and tension tests of dry samples a maximum rate of strain of 0.01 mm/min was best.

The testing program was as follows: At least ten single tests at different confining pressures were carried out to define Mohr's envelope at every step of pretreatment (i.e., temperature of heating, dry, and water-saturated). Besides those tests necessary in determination of shear strength, several additional investigations were run that are discussed in the following section.

TEST RESULTS

The thermal reactions of the kaolinite, and especially those of the kaolin from Zettlitz, are known from numerous publications in ceramics research (7). Figure 8 gives an idea of the drying process of the samples that had an initial water content of 48 to 50 percent. The differential heating curve of kaolin (Fig. 9) shows a weak endothermal reaction in the region between 100 and 300 C that results from the dissipation of the residual adsorption water. Because of the relatively high velocity of heating of the samples, the high endothermal effect starts around 500 to 600 C, and shows the dissipation of water of crystallization. While heating the samples slowly in the electric furnace it is expected that destruction of the crystalline structure and beginning the development of metakaolin lie around 440 to 450 C. The modification to metakaolin at the temperatures given is confirmed by the results of X-ray diffraction analysis. The kaolin shows no change in the crystalline structure up to 400 C (Fig. 10). The material that has been pretreated at

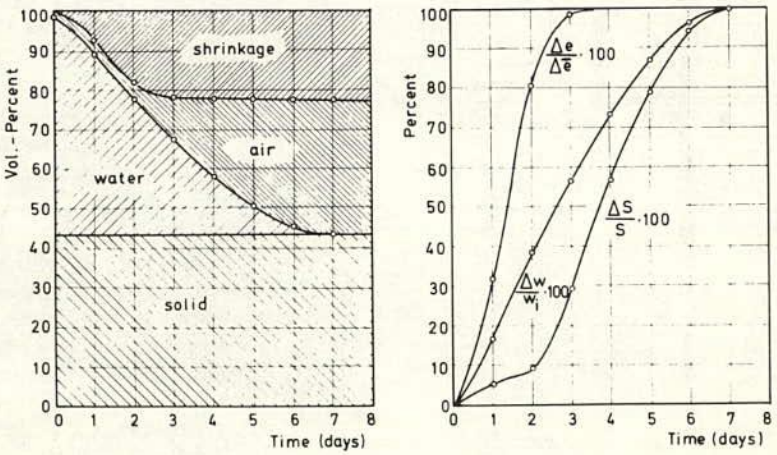

Figure 8. Drying process of the kaolin samples: e—void ratio; $\Delta\bar{e}$—total change of void ratio; S—degree of saturation; w_i—initial water content; Δw—change of water content.

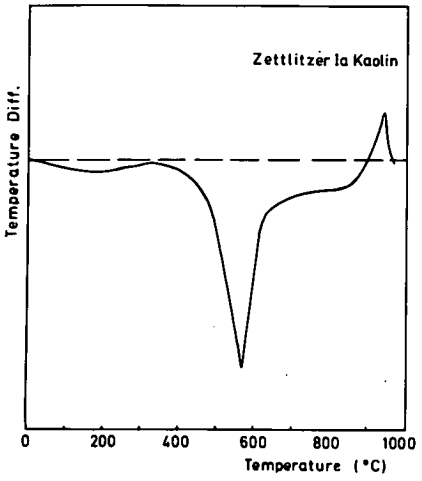

Figure 9. Differential thermal analysis of Kaolin Ia from Zettlitz.

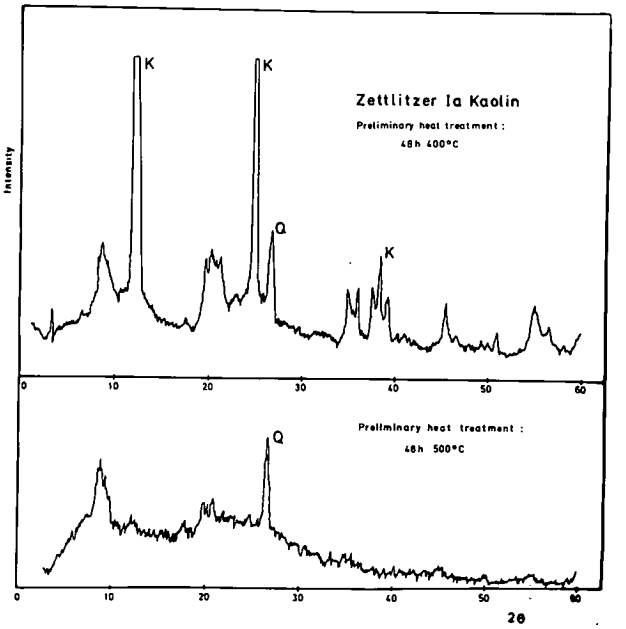

Figure 10. Structural analysis by X-ray diffraction of Kaolin Ia from Zettlitz.

500 C, however, has a clearly visible destroyed crystalline structure. In the diagram only the quartz is obvious.

Further investigations had to answer the question of how far any other characteristic data of the kaolin besides shear strength change in dependency on thermal pretreatment. Table 2 gives the results of those investigations. Except for the void ratio of the dry specimen, which shows the shrinkage of kaolin, these results, too, demonstrate that the specific gravity, flow limit, plastic limit, and plasticity definitely change after a treatment of more than 500 C. It is of great importance to the ensuing strength tests that the kaolin treated at more than 400 C no longer has a plasticity and does not swell when water is delivered.

TABLE 2

RESULTS OF HEAT TREATMENT

Preliminary Heat Treatment	Unit Weight of Solid Const. (g/cm^3)	Void Ratio e of Dry Samples	Liquid Limit	Plastic Limit	Plasticity Index
Untreated	2.629	–	0.529	0.346	0.183
48 hr 105 C	2.629	0.800	0.530	0.340	0.190
48 hr 200 C	2.622	0.814	0.525	0.336	0.189
48 hr 300 C	2.622	0.819	0.520	0.351	0.169
48 hr 400 C	2.620	0.815	0.522	0.378	0.144
48 hr 500 C	2.456	0.860	–	–	–
48 hr 600 C	2.485	0.848	–	–	–

TABLE 3

UNIAXIAL TENSILE STRENGTH OF DRY SAMPLES

Preliminary Heat Treatment	Uniaxial Tensile Strength (kp/cm^2)
48 hr 105 C	4.71
48 hr 200 C	5.06
48 hr 300 C	5.24
48 hr 400 C	5.43
48 hr 500 C	3.05
48 hr 600 C	4.68

Table 3 gives the results of uniaxial tensile tests run with dry pretreated samples. Figure 11 shows the failure line as a result of triaxial compression tests. In order to plot the graph in a distinct manner only the equalized curves are given. Because of the curved run of the envelope it is described by an exponential equation (Eq. 9). The theoretically calculated part of the failure line for tensile strength and small compres-

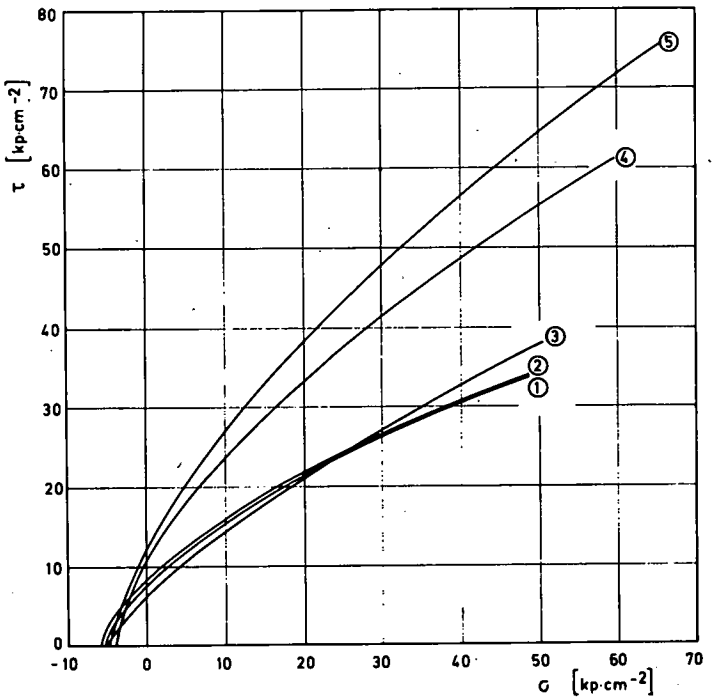

Figure 11. Mohr's envelopes of preliminary heat-treated dry samples (testing temperature 20 C). Equations of Mohr's envelopes:

(1) $\tau = \pm 2.50\ (\sigma + 5.3)^{0.66}$; pretreatment, 48 hr 200 C
(2) $\tau = \pm 2.95\ (\sigma + 5.8)^{0.61}$; pretreatment, 48 hr 300 C
(3) $\tau = \pm 1.73\ (\sigma + 5.0)^{0.78}$; pretreatment, 48 hr 400 C
(4) $\tau = \pm 4.38\ (\sigma + 4.0)^{0.64}$; pretreatment, 48 hr 500 C
(5) $\tau = \pm 4.29\ (\sigma + 4.65)^{0.68}$; pretreatment, 48 hr 600 C

sive strength correspond fairly well with the results of the experimentally found uniaxial tensile strength.

While the failure lines of the samples pretreated at temperatures of 200, 300, and 400 C show a similar run, it is to be recognized that the specimens treated at 500 and 600 C show a higher increase of shear strength in the region of compressive strength. Compared with the results of the tensile tests, it may be concluded that the change from kaolin to metakaolin at more than 400 C refers at the beginning to a higher decrease of uniaxial tensile strength. However, the specimens pretreated at 600 C develop a higher tensile strength corresponding to their increasing shear strength. The influence of thermal treatment at temperatures above 400 C on dry samples of kaolinite clay may be described in the way that the specimens achieve more and more the character of brittle rocks.

Because the kaolin keeps its plasticity up to 400 C, it is expected that the influence of water on the shear strength of pretreated samples up to that temperature is notable. Because the shear strength of rocks depends to a great extent on the void ratio and deformation conditions, these parameters were examined carefully in connection with the triaxial tests of the water-saturated specimen. The results of the CU tests in the form of the equalized and theoretically extrapolated failure lines are shown in Figure 12. The shear strength curves for samples at 105, 200, and 300 C are largely identical, so that Figure 12 only shows the failure lines for the untreated material and that which has been treated at temperatures ranging from 300 to 600 C.

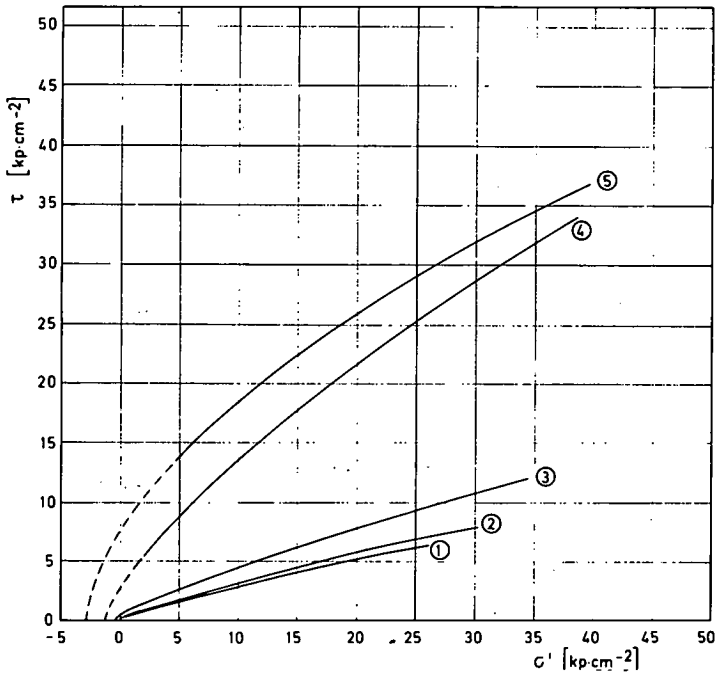

Figure 12. Mohr's envelopes of preliminary heat-treated water-saturated samples (testing temperature 20 C). Equations of Mohr's envelopes:

(1) $\tau = \pm 0.41\ (\sigma' + 0.10)^{0.84}$; untreated
(2) $\tau = \pm 0.49\ (\sigma' + 0.27)^{0.82}$; pretreatment, 48 hr 300 C
(3) $\tau = \pm 0.61\ (\sigma' + 0.61)^{0.83}$; pretreatment, 48 hr 400 C
(4) $\tau = \pm 2.38\ (\sigma' + 1.22)^{0.72}$; pretreatment, 48 hr 500 C
(5) $\tau = \pm 4.26\ (\sigma' + 2.80)^{0.58}$; pretreatment, 48 hr 600 C

It is recognized that the higher, durable stabilization increasing influence of the thermal treatment does not occur except above 400 C. The increase of shear strength up to 300 C is only due to the capillary tensile stress and when the sample is water-saturated due to the lasting initial stress, while in a specimen pretreated at 400 C first changes in the crystalline structure may occur. By referring to pressure-void ratio diagrams (Fig. 13) and stress-deformation properties of the samples (Figs. 14a-e), the influence of pretreatment may be shown more distinctly than relating to the failure lines. The pressure-void ratio lines show that the mobility of the solid skeleton decreases when the temperature of the pretreatment increases. The void ratio at the end of consolidation, which is of essential influence on the shear strength when CU tests are performed, is a function of the rigidity of the grain skeleton and also defines the stress-deformation behavior of the samples in triaxial tests.

In Figures 14a-e the specific axial strain ϵ_1 of the samples is plotted against the deviator stress. Looking at the untreated samples, the maximum of the deviator stress runs with increasing confining pressure σ_3 to a smaller axial strain ϵ_1. This result refers to the widely varying void ratio at different consolidation stresses σ_{3k} after consolidation has ended. On the other hand the samples pretreated at 400 C (Fig. 14c) show very clearly the typical stress-strain behavior of a quasi-rock. When σ_3 increases the maximum of the deviator stress moves to a higher axial deformation.

The increased rigidity of the solid skeleton is also noted quantitatively in a corresponding decrease of the specific axial strain up to the state of failure. That is especially distinct when Figures 14c-e are compared. In spite of the basic similarity,

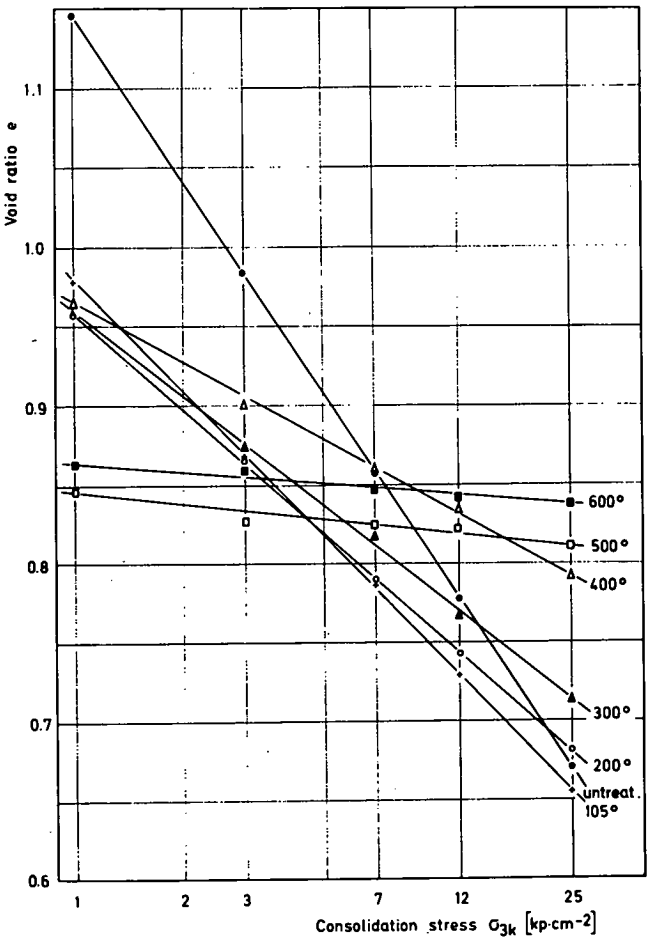

Figure 13. Pressure-void ratio lines of water-saturated samples.

the samples treated at 500 and 600 C show in comparison to those at 400 C an increased shear strength that is connected with a very much decreased axial deformation.

The mechanical properties of the stabilized specimen are to be recognized from the results of triaxial tests in addition from the dependency on the deformation in direction of the major principle stress. Investigations of that kind, although with a different testing technique, have been carried out by Schmertmann and Osterberg (8) and Broms (1). In both publications the failure line of rocks is described by a straight line, and it follows that the mobilization of the shear strength is defined with the aid of the mobilized shear strength parameters c and ϕ. It is indicated that the cohesion c of a rock is already mobilized at a much lower axial strain than the angle of internal friction.

Cohesion and internal friction, however, are first of all mathematical parameters of an equation describing a straight line, and secondly an index of soil mechanics data. Regarding curved failure lines as a result of triaxial tests at porous soils or rocks within a wider stress distribution, it is not very advantageous to use the parameters c and ϕ to characterize the failure line. It would be of much more sense to indicate the mobilization of shear strength at a certain normal stress σ or σ' in dependency on ϵ_1 in percent of the corresponding maximum shear strength of a rock to each normal stress. In Figure 15 Mohr's envelopes of the mobilized shear strength are plotted in σ-τ coordinates. It is easy to construct from the diagrams the percentage mobilized

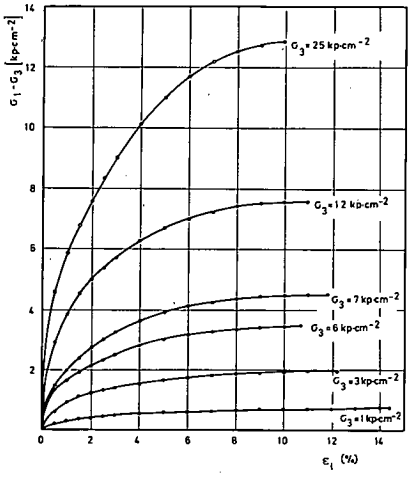

(a) Untreated samples.

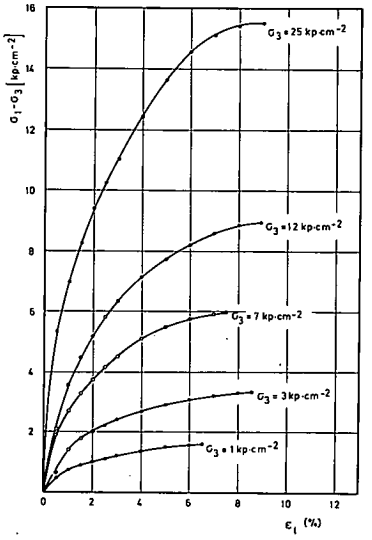

(b) Preliminary heat treatment 48 hr 300 C.

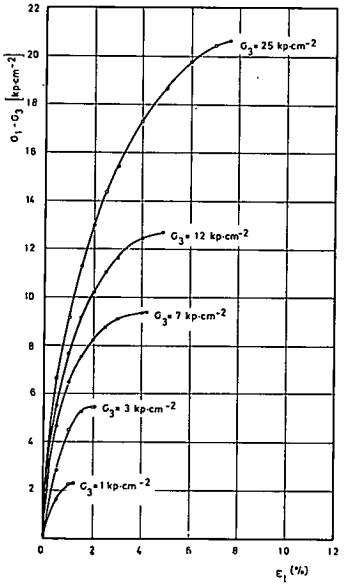

(c) Preliminary heat treatment 48 hr 400 C.

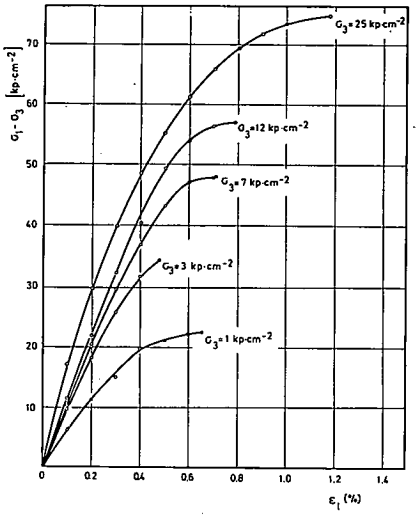

(d) Preliminary heat treatment 48 hr 500 C.

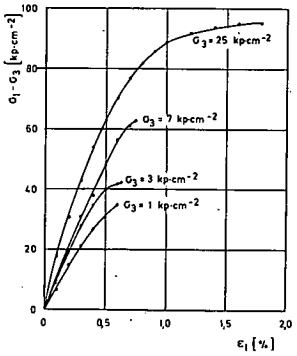

(e) Preliminary heat treatment 48 hr 600 C.

Figure 14. Stress-strain curves of preliminary heat-treated and water-saturated samples (testing temperature 20 C).

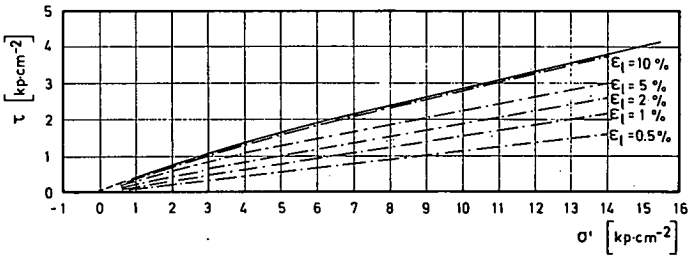

(a) Untreated samples.

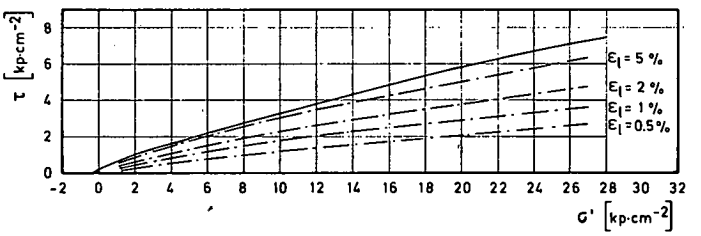

(b) Preliminary heat treatment 48 hr 300 C.

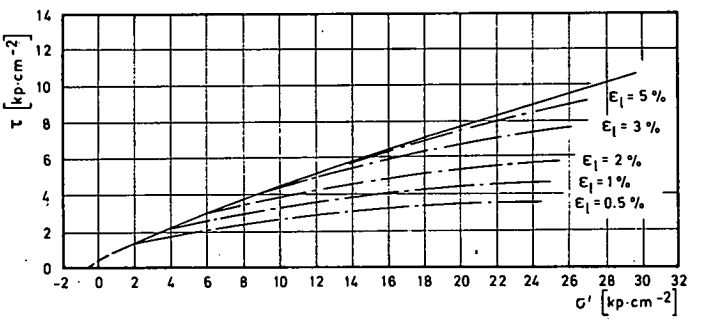

(c) Preliminary heat treatment 48 hr 400 C.

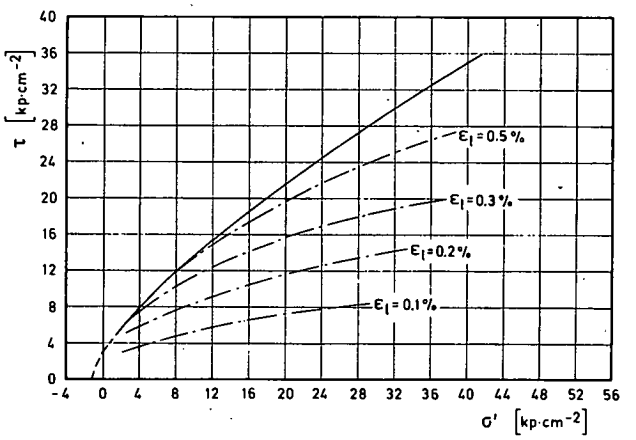

(d) Preliminary heat treatment 48 hr 500 C.

Figure 15. Mobilization of shear strength with axial strain ϵ_l on preliminary heat-treated water-saturated samples.

shear strength. The run of the curves shows from the stress-strain behavior the difference in the strength behavior of a rock that has been changed by stabilization artificially.

CONCLUSIONS

The results of experiments concerning the shear strength of preliminary heat-treated samples of kaolin from Zettlitz described in this paper permit the following conclusions:

1. The preliminary heat treatment of kaolinite clay, especially of kaolin from Zettlitz, provides effective stabilization, i.e., a permanent increase of the shear strength.
2. The successful stabilization can be characterized by Mohr's envelope of the material. This presentation can be improved by the mobilization of the shear strength in relation to axial strain in the direction of the major principal stress.
3. The slightly curved envelope can be described with sufficient accuracy by an exponential equation. The triaxial tensile strength that is to be calculated theoretically represents a characteristic factor. If the envelope is described in that way it is not necessary to use the normal parameters, cohesion and angle of internal friction, and to give them a different physical meaning. Because of the great number of factors influencing the shear strength and thus the stabilization, it cannot be expected that the influence of these factors can be noticed in the amount or in the mobilization of the parameters of shear strength. The reason is that these factors are only mathematical parameters of a certain approximated equation for the envelope.
4. Concerning the shear strength of preliminary heat-treated samples of a cohesive soil, the water as a void filling is of special importance. In the case of a material in which the increasing strength is only due to its capillary tension and not to changing structure, the effect of stabilization when reducing this capillarity by adding water is irreversible with a small amount. The increasing strength and with it the alteration of the mechanical properties mentioned is of less influence on the run of the envelope than on the stress-strain properties. For a better understanding of the mechanism of stabilization, other methods to determine stress-strain relation than those described here should be used. The influence of other polar and also apolar liquids on the same solid should especially be investigated.
5. Earlier investigations in this field have shown that several simplifying presumptions and suitable methods with regard to the preparation, pretreatment, and testing of the samples are necessary to keep the number of variable factors within a certain limit. In the case of an in situ treatment of the soil or rock, many additional influences are to be expected that will change considerably the picture concerning the effect of stabilization by heat treatment of kaolinite clays. To answer certain questions further investigations are necessary.
6. The results discussed here should have shown that it is possible to investigate and to characterize artificially modified rocks in the region between soils and rocks in a similar way. Therefore it seems justified to perform similar investigations on natural soils and rocks that are of great interest in civil and mining engineering.

ACKNOWLEDGMENTS

This investigation was performed in the Soil and Rock Mechanics Research Laboratory of the Department of Mining Engineering, Technical University Clausthal, under direction of the first author. The work is a part of the doctoral thesis of the second author. The authors gratefully acknowledge the assistance of the employees of the Research Laboratory, who performed many of the tests.

REFERENCES

1. Broms, B. B. A Note on Strength Properties of Rock. Proc. First Cong. Internat. Soc. Rock Mechanics, Vol. 2, Lisboa 1966, p. 69-71.

2. Henning, D. Möglichkeiten und Grenzen der Anwendung elektrochemischer und thermischer Verfestigungsverfahren. Bergbauwissenschaften, Vol. 12, p. 440-446, 1965.
3. Henning, D., and Lochte, J. Einige Grundlagen der Verfestigung bindiger Lockergesteine. Bergbauwissenschaften, Vol. 14, p. 279-287, 1967.
4. Henning, D., and Zimmermann. Über die Ermittlung der Bruchhüllkurve von Gesteinen auf der Grundlage von Messergebnissen. Bergbauwissenschaften, Vol. 15, p. 129-133, 1968.
5. Lambe, T. W. A Mechanistic Picture of Shear Strength in Clay. Research Conf. on Shear Strength Cohes. Soils, Univ. of Colorado, 1960, p. 555-614.
6. Lowe, J., and Johnson, T. C. Use of Back Pressure to Increase Degree of Saturation of Triaxial Test Specimens. Research Conf. on Shear Strength Cohes. Soils, Univ. of Colorado, 1960, p. 819-836.
7. Salmang, H. Die physikalischen und chemischen Grundlagen der Keramik. Springer-Verlag, Berlin-Göttingen-Heidelberg, 1954.
8. Schmertmann, J. H., and Osterberg, J. O. An Experimental Study of the Development of Cohesion and Friction With Axial Strain in Saturated Cohesive Soils. Research Conf. on Shear Strength Cohes. Soils, Univ. of Colorado, 1960, p. 643-694.
9. Seed, M., Mitchell, J. K., and Chan, C. K. The Strength of Compacted Cohesive Soils. Research Conf. on Shear Strength Cohes. Soils, Univ. of Colorado, 1960, p. 877-964.
10. Wöhlbier, H., and Henning, D. Untersuchungen über den Verlauf der Bruchhüllkurve von Gesteinen. Beitrag zum 10. Ländertreffen des Internationalen Büros für Gebirgsmechanik, Leipzig, 1968.

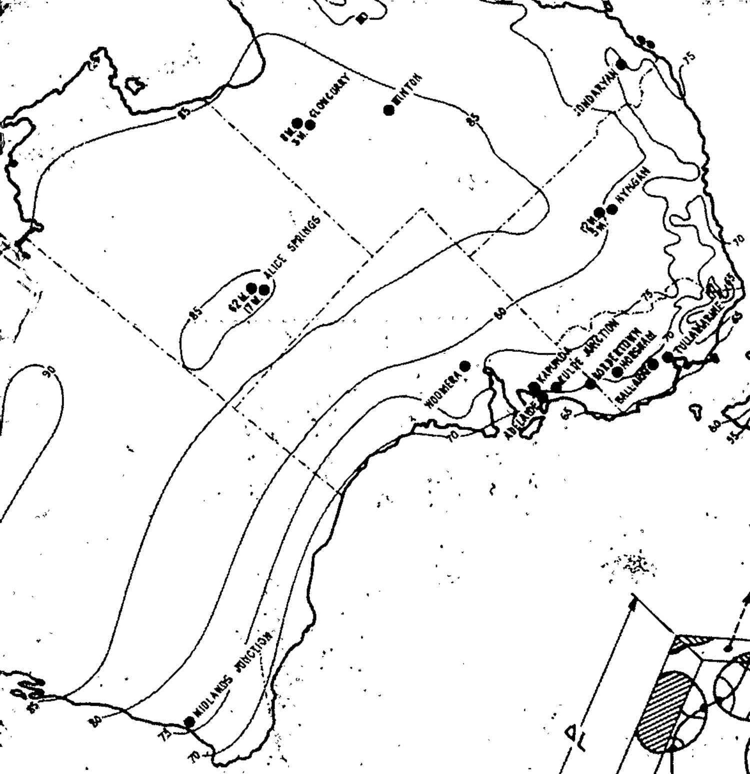
CLONCURRY
WINTON
JONDARYAN
NYNGAN
ALICE SPRINGS
WOOMERA
BORDERTOWN
HORSHAM
BALLARAT
TULLAMARINE
ADELAIDE
MIDLANDS JUNCTION

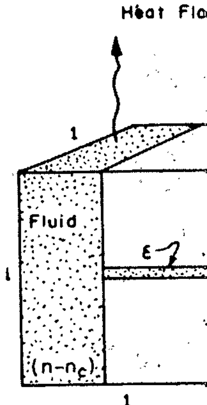
Heat Flo
Fluid
(n-n_c)

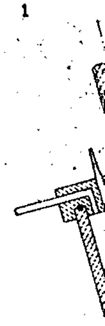

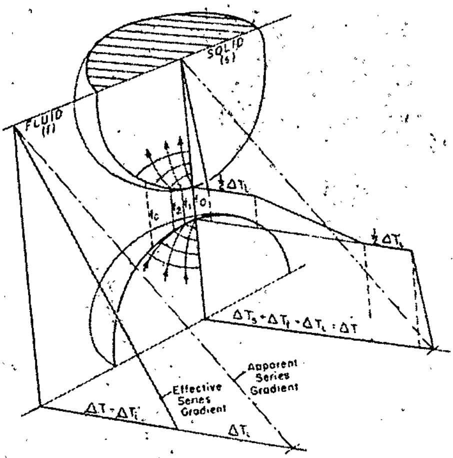
SOLID (s)
FLUID (f)
ΔT_s + ΔT_f + ΔT_L = ΔT
Apparent Series Gradient
Effective Series Gradient
ΔT - ΔT_i
ΔT_i

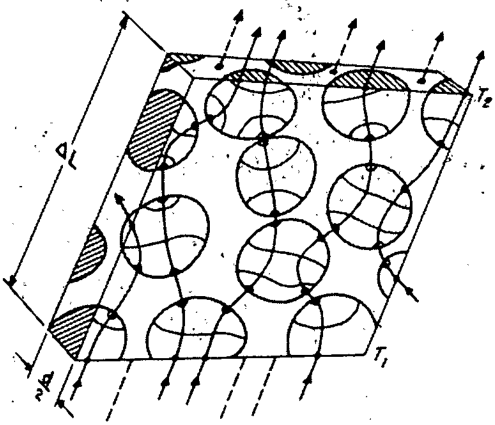
T_2
T_1

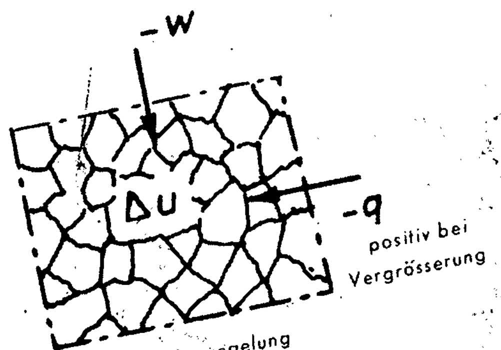
-W
Δu
-q
positiv bei Vergrösserung
Vorzeichenregelung

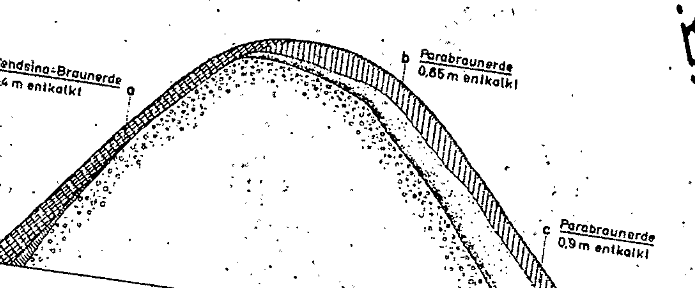
b Parabraunerde 0,65 m entkalkt
c Parabraunerde 0,9 m entkalkt

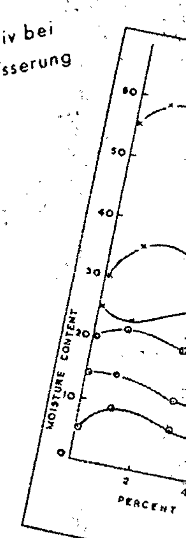
MOISTURE CONTENT
PERCENT

THE NATIONAL ACADEMY OF SCIENCES is a private, honorary organization of more than 700 scientists and engineers elected on the basis of outstanding contributions to knowledge. Established by a Congressional Act of Incorporation signed by Abraham Lincoln on March 3, 1863, and supported by private and public funds, the Academy works to further science and its use for the general welfare by bringing together the most qualified individuals to deal with scientific and technological problems of broad significance.

Under the terms of its Congressional charter, the Academy is also called upon to act as an official—yet independent—adviser to the Federal Government in any matter of science and technology. This provision accounts for the close ties that have always existed between the Academy and the Government, although the Academy is not a governmental agency and its activities are not limited to those on behalf of the Government.

The NATIONAL ACADEMY OF ENGINEERING was established on December 5, 1964. On that date the Council of the National Academy of Sciences, under the authority of its Act of Incorporation, adopted Articles of Organization bringing the National Academy of Engineering into being, independent and autonomous in its organization and the election of its members, and closely coordinated with the National Academy of Sciences in its advisory activities. The two Academies join in the furtherance of science and engineering and share the responsibility of advising the Federal Government, upon request, on any subject of science or technology.

The NATIONAL RESEARCH COUNCIL was organized as an agency of the National Academy of Sciences in 1916, at the request of President Wilson, to enable the broad community of U.S. scientists and engineers to associate their efforts with the limited membership of the Academy in service to science and the nation. Its members, who receive their appointments from the President of the National Academy of Sciences, are drawn from academic, industrial and government organizations throughout the country. The National Research Council serves both Academies in the discharge of their responsibilities.

Supported by private and public contributions, grants, and contracts, and voluntary contributions of time and effort by several thousand of the nation's leading scientists and engineers, the Academies and their Research Council thus work to serve the national interest, to foster the sound development of science and engineering, and to promote their effective application for the benefit of society.

The DIVISION OF ENGINEERING is one of the eight major Divisions into which the National Research Council is organized for the conduct of its work. Its membership includes representatives of the nation's leading technical societies as well as a number of members-at-large. Its Chairman is appointed by the Council of the Academy of Sciences upon nomination by the Council of the Academy of Engineering.

The HIGHWAY RESEARCH BOARD, an agency of the Division of Engineering, was established November 11, 1920, as a cooperative organization of the highway technologists of America operating under the auspices of the National Research Council and with the support of the several highway departments, the Bureau of Public Roads, and many other organizations interested in the development of highway transportation. The purposes of the Board are to encourage research and to provide a national clearinghouse and correlation service for research activities and information on highway administration and technology.